Teză de abilitare: Utilizarea metodelor moderne de lucru în vederea estimării susceptibilității la viituri rapide și inundații
Domeniul: Inginerie Civilă și Instalații
Autor: CS Dr. Romulus-Dumitru Costache

PORTOFOLIU LUCRĂRI ȘTIINȚIFICE

1. **Costache R.** (2025) *Flood susceptibility estimation using randomization-based machine learning models. A case study at the Putna river basin, Romania*, Geomatics, Natural Hazards and Risk, 2548505. DOI: https://doi.org/10.1080/19475705.2025.2548505. **ISI I.F. = 4.6 (Q1).**
2. **Costache R.**, Pal S.C., Pande C.B., Islam A.R.M.T., Alshehri F., Abdo H.G. (2024) *Flood mapping based on novel ensemble modeling involving the deep learning, Harris Hawk Optimization algorithm and stacking based machine learning*, Applied Water Science, 14(4): 78. DOI: https://doi.org/10.1007/s13201-024-02131-4. **ISI I.F. = 5.7 (Q1).**
3. **Costache R.,** Alireza A., Costache I., Crăciun A., Pham B.T. (2022) *New machine learning ensemble for flood susceptibility estimation,* Water Resources Management. 36(12), 4765-4783. DOI: https://doi.org/10.1007/s11269-022-03276-0. **ISI I.F. = 4.3 (Q1).**
4. **Costache R.,** Arabameri A., Costache I., Crăciun A., Islam A.R.M.T., Abba S.I., Sahana M., Pham B.T. (2022) *Flood susceptibility evaluation through deep learning optimizer ensembles and GIS techniques*, Journal of Environmental Management, 316, 115316. DOI: https://doi.org/10.1016/j.jenvman.2022.115316. **ISI I.F. = 8.7 (Q1).**
5. **Costache R.,** Tin T.T., Arabameri A., Crăciun A., Ajin R.S., Costache I., Islam A.R..M.T., Abba S.I., Sahana M., Avand M., Pham B.T. (2022) *Flash-flood hazard using Deep Learning based on H2O R package and fuzzy-multicriteria decision-making analysis*, Journal of Hydrology, 609, 127747. DOI: https://doi.org/10.1016/j.jhydrol.2022.127747. **ISI I.F. = 6.4 (Q1).** – **Highly Cited paper – Included in the Top 1% of the academic field of Engineering according to Web of Science (Clarivate Analytics) (January/February 2023).**
6. **Costache R.,** Popa M.C., Tien Bui D., Diaconu D.C., Ciubotaru N., Minea G., Pham Q.B. (2020) *Spatial predicting of flood potential areas using novel hybridizations of fuzzy decision-making, bivariate statistics, and machine learning*, Journal of Hydrology, 585, 124808, DOI: https://doi.org/10.1016/j.jhydrol.2020.124808. **ISI I.F. = 5.722 (Q1).** – **Highly Cited paper – Included in the Top 1% of the academic field of Environment/Ecology according to Web of Science (Clarivate Analytics).**
7. **Costache, R.,** Hong, H., & Pham, Q. B. (2020) *Comparative assessment of the flash-flood potential within small mountain catchments using bivariate statistics and their novel hybrid integration with machine learning models*. Science of the Total Environment, 711, 134514. DOI: https://doi.org/10.1016/j.scitotenv.2019.134514. **ISI I.F. = 7.963 (Q1).** – **Highly Cited paper – Included in the Top 1% of the academic field of Environment/Ecology according to Web of Science (Clarivate Analytics).**
8. **Costache R.** (2019) *Flash-Flood Potential assessment in the upper and middle sector of Prahova river catchment (Romania). A comparative approach between four hybrid models.* Science of The Total Environment, 659, 1115 – 1134. DOI: https://doi.org/10.1016/j.scitotenv.2018.12.397. **ISI I.F. = 6.551 (Q1).**
9. **Costache R.** (2019) *Flash-flood Potential Index mapping using weights of evidence, decision Trees models and their novel hybrid integration,* Stochastic Environmental Research and Risk Assessment, 33(7), 1375 – 1402. DOI: https://doi.org/10.1007/s00477-019-01689-9. **ISI I.F. = 2.237 (Q1).**

Data, Candidat,

20.04.2026 CS Dr. Romulus-Dumitru COSTACHE

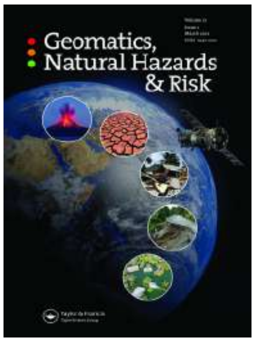

Geomatics, Natural Hazards and Risk

ISSN: 1947-5705 (Print) 1947-5713 (Online) Journal homepage: www.tandfonline.com/journals/tgnh20

Flood susceptibility estimation using randomization-based machine learning models. A case study at the Putna river basin, Romania

Romulus Costache

To cite this article: Romulus Costache (2025) Flood susceptibility estimation using randomization-based machine learning models. A case study at the Putna river basin, Romania, Geomatics, Natural Hazards and Risk, 16:1, 2548505, DOI: 10.1080/19475705.2025.2548505

To link to this article: https://doi.org/10.1080/19475705.2025.2548505

Published online: 20 Aug 2025.

GEOMATICS, NATURAL HAZARDS AND RISK
2025, VOL. 16, NO. 1, 2548505
https://doi.org/10.1080/19475705.2025.2548505

Taylor & Francis
Taylor & Francis Group

Flood susceptibility estimation using randomization-based machine learning models. A case study at the Putna river basin, Romania

Romulus Costache

Department of Civil Engineering, Transilvania University of Brasov, Brasov, Romania

ABSTRACT
Floods represent the natural hazards that generate the most damage at the international level. A very important stage in the flood risk management activity is the mapping of areas susceptible to these hazards. In this context, in the present study, the following 3 hybrid models were applied to determine flood susceptibility in Putna river basin, Romania: Randon Committee-Weights of Evidence (RC-WOE), Random SubSpace-Weights of Evidence (RSS-WOE) and Randomizable Filtered Classifier – Weights of Evidence (RFC – WOE). 14 flood predictors and 192 flood locations (divided into 70% training sample and 30% validating sample) were used as input data in the 3 models. The applied models confirmed the fact that the most important flood predictors are: slope angle, distance from rivers and elevation. At the same time, around 24% of the study area shows a high and very high susceptibility to floods. The ROC Curve method along with other statistical metrics, used to validate the applied models, showed that the accuracy of the models generally exceeded 80%, which represents a very good performance. The obtained results provide useful information for the authorities responsible for reducing the flood risk. Also, the future planning of the territory can obviously take into account the zoning of flood susceptibility.

ARTICLE HISTORY
Received 2 April 2025
Accepted 10 August 2025

KEYWORDS
Flood susceptibility; putna river basin; machine learning; bivariate statistics; hybrid models

1. Introduction

Floods are among the most destructive natural hazards worldwide, causing extensive damage to infrastructure, ecosystems, and human life (Duwal et al. 2023; Liao et al. 2024). The global vulnerability to flooding has increased by more than 40% over the past 2 decades (Wahba et al. 2024). These events account for significant economic losses annually, with global figures exceeding $20 billion and affecting millions of people (Abbass et al. 2022). Romania is one of the European countries most affected by floods. The year 2024 was marked by massive floods that affected Romania in September. According to the General Inspectorate for Emergency Situations from Romania, the floods affected 15,000 people, dozens of localities in 2 counties and caused a number of six deaths. The frequency and intensity of floods are projected to increase in the coming decades due to the combined effects of climate change (Roohi et al. 2024), urbanization, and socio-economic developments (Sesana et al. 2021). This situation shows how important it is to identify flood-prone areas and how great the need is to mitigate risks, reduce damage and increase resilience (Bhattarai et al. 2024).

Traditional methods for assessing flood susceptibility, such as hydrological and hydraulic modeling, have provided valuable insights but face limitations when addressing the multifactorial and dynamic nature of flood occurrences (Karim et al. 2023). In recent years, there has been a significant increase in advances in technologies associated with geographic information systems and remote sensing that allow rapid assessment and mapping of flood susceptibility (Bentivoglio et al. 2022; Zhu et al. 2024). It is now possible to integrate and analyze different data sets, such as topographic, hydrological, and land use factors, in geographic information systems (GIS) and remote sensing, which are crucial to

CONTACT Romulus Costache romuluscostache2000@yahoo.com, romulus.costache@unitbv.ro
This article has been corrected with minor changes. These changes do not impact the academic content of the article.

predicting flood-prone areas (Pourzangbar et al. 2025). The integrated use of these methods with new artificial intelligence techniques (Support Vector Machines (SVM), Artificial Neural Networks (ANN), Adaptive Neuro-Fuzzy Inference Systems (ANFIS), Decision Trees (DT), etc.) has rapidly increased the accuracy of flood susceptibility estimates (Hinge et al. 2024; Al-Sheriadeh and Daqdouq 2024). Thus, these methods generally require as input a set of flood predictors as independent variables along with a dependent variable represented by flood historical locations.

The effectiveness of machine learning models is also increased by using them together with bivariate statistical techniques such as frequency ratio (FR), index of entropy (IOE) (Kader et al. 2024). Also, Multicriteria Decision Making Analysis (MCDM) is another category of models that are used very successfully together with artificial intelligence models for estimating flood susceptibility (Hasan et al. 2023). These approaches help quantify the influence of each factor, such as slope, elevation, precipitation and proximity to water bodies, on flood risk.

According to the Floods Directive 2007/60/EC, mapping of flood-prone areas is a crucial step in order to improve the management of these risks and to support the authorities in charge of this task (Santos et al. 2024). These maps can provide emergency management teams with critical information for the development of early warning systems, evacuation plans and community preparedness plans (Arosio et al. 2024). In this way, material and human losses can be significantly reduced (Dyca et al. 2024).

A very important step in this process of creating flood maps is the selection of the factors conditioning the floods of this phenomenon (Varra et al. 2024). This is a key point in the entire procedure because flood predictors help to understand the characteristics of the land surface that can favor the formation of these hazards (Hoang and Liou 2024). In general, in this type of studies, the main predictors are the slope of the relief, the altitude, the hydrological factors, such as the proximity to rivers and the intensity of precipitation and the way of using the lands that influence the retention and runoff of water (Qasimi et al. 2024). For this reason, it is very important that the spatial data sets from which these factors are extracted have a high precision.

Taking into account all the exposed elements, the present research work aims to evaluate the flood susceptibility on Putna river basin from Romania using a number of 14 flood predictors that will represent input data for the hybrid models: Randon Committee-Weights of Evidence (RC-WOE), Random SubSpace-Weights of Evidence (RSS-WOE) and Randomizable Filtered Classifier – Weights of Evidence (RFC – WOE). Certainly, these models will have as input data the locations of historical floods that occurred in the Putna River basin. To validate the results, the ROC Curve method and several statistical metrics will be used. The three combinations of the three randomizable models with WOE were chosen over other ensemble models because they have a better generalization capacity given the following characteristics: (i) Random Committee creates a set of classifiers of the same type, but with different parameters, thus reducing overfitting; (ii) Random Subspace operates on subsets of features, increasing the diversity of classifiers and the stability of the prediction; iii) Randomizable Filtered Classifier (RFC) applies preprocessing to the data before learning, reducing the influence of noisy data. Other examples of ensemble models for assessing flood susceptibility are: Bagging (Saikh and Mondal 2023); Rotation Forest – Deep Learning (Li and Hong 2023); XGBoost-Boruta (Habibi et al. 2023); Bagging-Best First Decision Tree (Pham et al. 2021); CatBoost; Stacking ensemble (Ilia et al. 2022).

2. Study area

Putna River Basin, is situated in the central-eastern part of Romania. The surface of the study area has approximately 2,499 square kilometers. From the global location point of view, this is framed by the following coordinates: latitudes 45°31'N and 46°2'N, and longitudes 26°22′"E and 27°29'E (Figure 1). The study zone covers three major geographical regions of Romania: the Eastern Carpathians, the Subcarpathians, and the Romanian Plain (Costache and Bui 2019). The high variability in terms of altitude (from 14 to 1786 meters) significantly influences the hydrological processes in the area. From a climatic point of view, an average of 800 mm of precipitation per year is noted. Of major concern for floods and flash floods are the intense precipitation events that occur mainly during spring and early summer (Grecu et al. 2017). These can cause rapid runoff on slopes and further potential flooding in

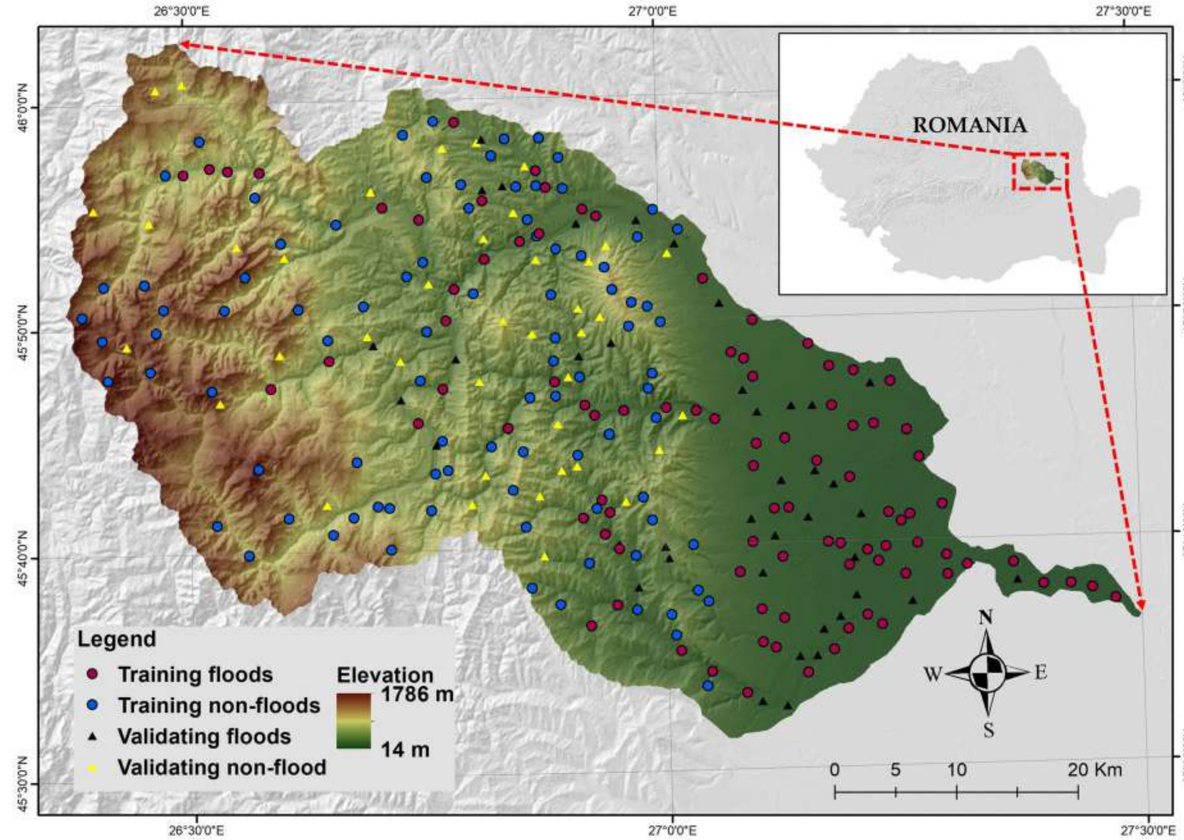

Figure 1. Study area location.

areas where the slope of the relief allows stagnation and accumulation of water. From a land use perspective, the river basin is covered in a proportion of 53.3% by forest. Agricultural areas account for about 18.1%, while pastures represent 10.2%.

Over time, the study area was seriously affected by floods. From this point of view, the year 2005 remains a reference because very large economic losses were recorded (Costache et al. 2022). According to the National Inspectorate for Emergency Situation from Romania, in that year (2005) there were material losses of about eight million euros. Approximately 14 localities were flooded, with a total population of about 21,000 people. Citizens from 41 communes and 3 cities felt the effects of the disaster. About 3,700 people were evacuated. Another 20,000 were isolated due to destroyed roads, bridges and access roads. Approximately 170 km of main roads were affected, while 26,000 hectares of agriculture areas were devastated (Figure 2).

Such events show how important preliminary hazard assessments are so that appropriate measures can be taken to reduce the risk and vulnerability to these disasters.

3. Data

3.1. Flood inventory

The flood inventory for the Putna River Basin was based on the locations collected from various sources, most of them being taken from the General Inspectorate for Emergency Situations of Romania. Therefore, a number of 132 locations were identified that were affected by the floods. These locations are randomly distributed on the study area taking into account a uniform location on the three major relief units. In order to ensure the objectivity of the study, but also to increase the accuracy of the results, a second set of data was additionally generated, numbering 132 locations that were not affected by floods (non-floods). The entire data set was further divided into two distinct sub-sets. Thus, 70% of the total locations were included in the training dataset, while 30% of them were assigned to the

Figure 2. (a) Effects of flood occurred on Putna river in Nereju locality in July 2005; (b) Effects of flood occurred on Putna river in Vadu Roșca locality in July 2005 (Source: National Inspectorate for Emergency Situation from Romania).

validation dataset. In training, 70% of the data samples are used for learning patterns, while 30% is used for validation to test performance on unknown data. This minimizes overfitting and ensures the model generalizes to other areas or periods (Tehrany et al. 2014).

3.2. Flood conditioning factors

The identification of the most suitable environmental factors for flood susceptibility assessment is a critical step in the modeling process (Al-Kindi and Alabri 2024). These geographical factors can be classified into several categories such as: topographical factors, hydrological factors, climatic factors and factors related to land use. Each of these factors has a determining role regarding the characteristics of floods (Al-Juaidi et al. 2018). The topographic or morphometric factors were obtained by derivation from the Digital Terrain Model taken from the SRTM database at 30 m.

3.2.1. Morphometric predictors

Morphometric features strongly influence runoff, water retention, and flow pathways.

3.2.1.1. Slope angle. The slope angle significantly influences, through the action of gravity, both the volume of water that drains to the surface and the retention capacity of the various areas (Liu et al. 2025). In the present case study, the values of slope are classified into the next classes: <3°, 3°–7°, 7°–15°, 15°–25°, and >25° (Figure 3f). Surfaces with slopes below 3° are very frequently prone to flooding due to poor drainage.

3.2.1.2. Elevation. Lower elevation areas are generally more prone to flooding, as they are closer to river systems and accumulate surface water. Elevation is typically divided into altitude classes, such as <200 m, 200–400 m, 400–600 m, 600–800 m, 800–1000 m, 1000–1200 m, 1200–1400 m, and >1400 m (Figure 3e). These categories allow for precise mapping of flood-prone lowland regions (Al-Juaidi et al. 2018).

3.2.1.3. Aspect. The aspect of slopes generates a huge influence on some parameters like soil moisture and surfaces temperature which can further influence the snow melting process. Aspect values are categorized into directional classes, including north, northeast, east, southeast, south, southwest, west, northwest, and flat zones (Figure 4e), each influencing water retention differently (Nachappa et al. 2020).

3.2.1.4. Topographic position index (TPI). By comparing the altitude of a cell with the altitude of the other cells in the surroundings, TPI can very precisely identify the areas corresponding to the river valleys. Common TPI classes include ranges such as (–35.39)–(–4.79), (–4.79)–(–1.57), (–1.57)–1.32, 1.32–4.86, and 4.86–46.73 (Figure 4b). Depressions indicated by lower values are more likely to accumulate water (Costache and Bui 2019).

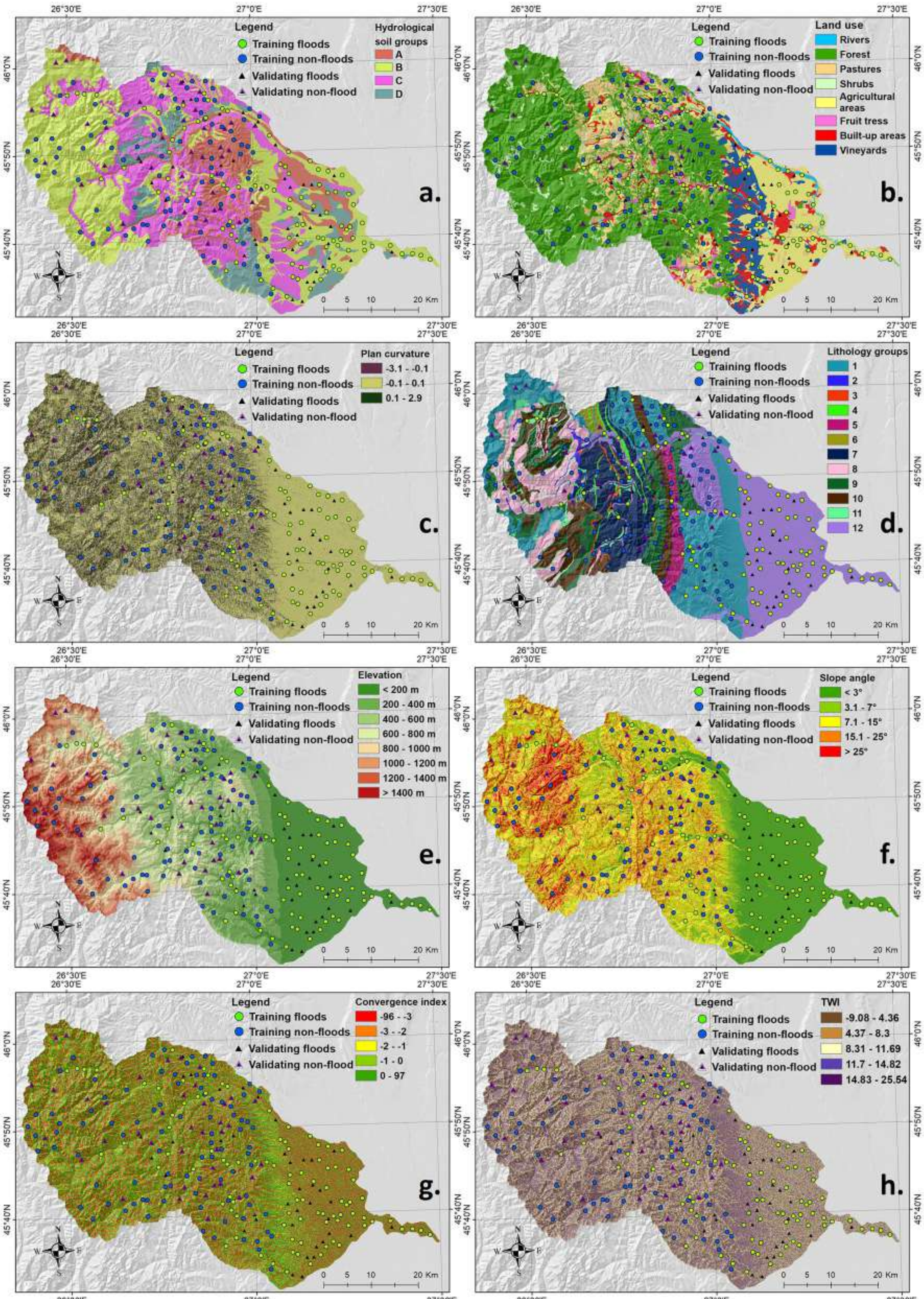

Figure 3. Percentage of flood pixels within classes/categories (a. Lithology; b. Slope angle; c. Plan curvature; d. Hydrological Soil Groups; e. TWI; f. Land use; g. Convergence Index; h. Elevation) (source: Costache and Bui (2019)).

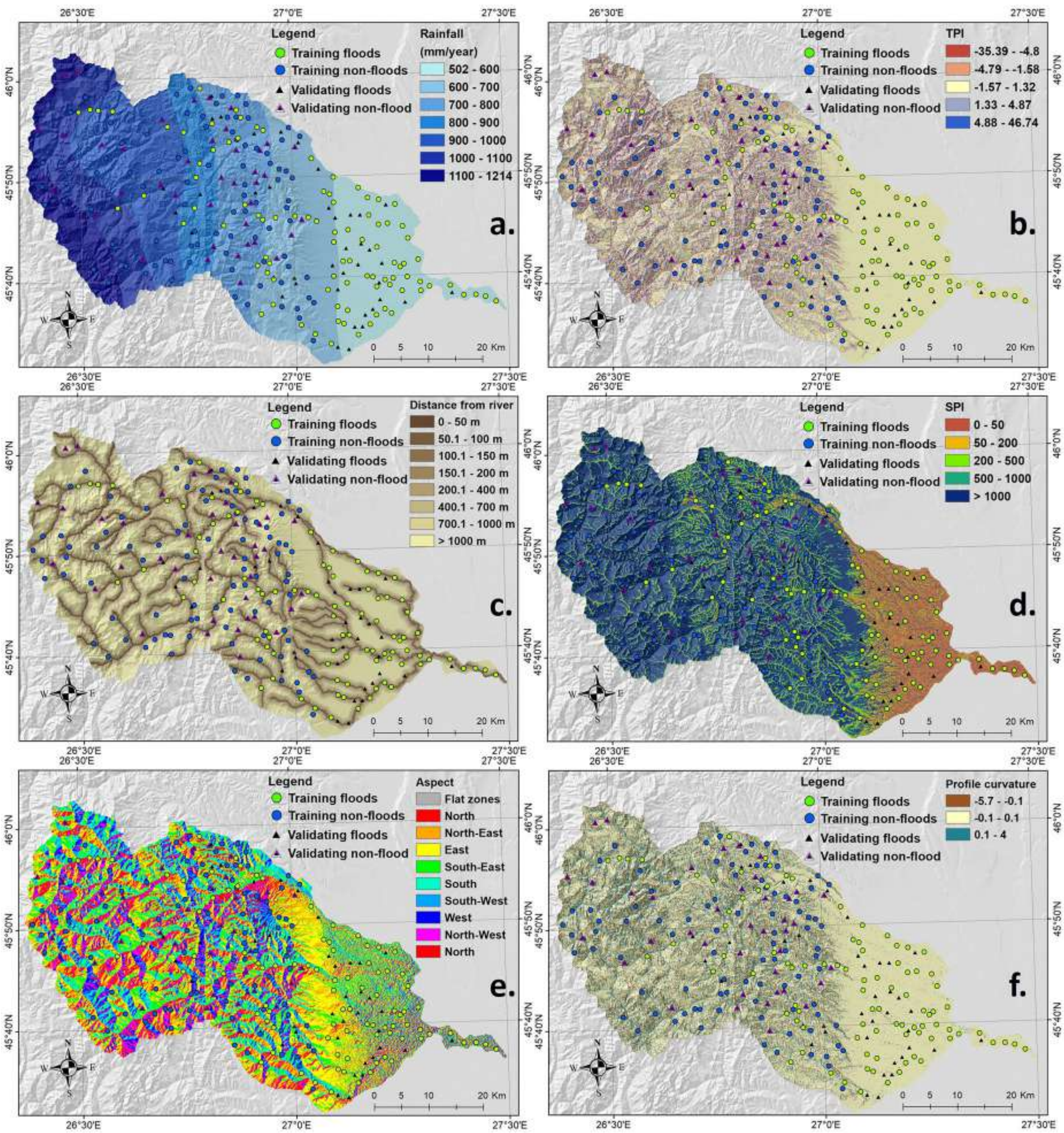

Figure 4. Percentage of flood pixels within classes/categories (a. Distance from river; b. Profile curvature; c. Rainfall; d. Aspect; e. SPI; f. TPI) (source: Costache and Bui (2019)).

3.2.1.5. Stream power index (SPI). SPI measures the erosive power of flowing water and is calculated from slope and upstream area. It is divided into classes such as 0–50, 50–200, 200–500, 500–1000, and >1000 (Figure 4d). Higher SPI values suggest stronger water flow and increased susceptibility to erosion and flooding.

3.2.1.6. Topographic wetness index (TWI). TWI highlights areas where water is likely to accumulate, combining slope and catchment area. It is classified into ranges such as (−9.07) − 4.36, 4.36–8.29, 8.29–11.69, 11.69–14.81, and 14.81–25.54 (Figure 3h). Higher TWI values indicate regions with greater water retention potential.

3.2.1.7. Profile curvature. The speed of water flow is decisively influenced by the direction of the vertical slope. This direction of the slope is captured by the Curvature values in the profile. The positive values of the curvature in the profile show the areas with decelerated leakage, while the negative values highlight the surfaces on which the leakage manifests itself in an accelerated manner. In our case study, the values of profile curvature were grouped into three classes: (−5.65)–(−0.1), (−0.1)–0.1, and 0.1–3.97 (Figure 4f).

3.2.1.8. Plan curvature. The contour line formed by the intersection of a horizontal plane with the terrain surface defines plan curvature, a morphometric quantity. Plan curvature values highlight locations with divergent and convergent runoff. Using expert judgment, three classes were established: (−3.07) – (−0.1), (−0.1)–0.1, and 0.1–2.89 (Figure 3c). Convergent zones are exposed to water accumulation.

3.2.1.9. Convergence index. Many research employed the convergence index, which is obtained from DEM, to measure flood or flash-flood risk. The positive values highlight the presence of interfluvial surfaces, whilst the negative values demonstrate a notable degree of hydrographic convergence. The next five classes were established for this index: **(−96) to (−3)** – highlighting convergent zones, exposed to water accumulation and high flood risk; **(−3) to (−2)** – highlighting some medium convergent areas; **(−2) to (−1)** – highlighting the slightly convergent zones; **(−1) to 0** – showing the Near-neutral zones from the convergence point of view; **0 to 95** (Figure 3g), representing minimal convergence or divergence.

3.2.2. Hydrological predictors

Hydrological attributes are fundamental to flood susceptibility, shaping water movement and accumulation patterns.

3.2.2.1. Distance to rivers. Proximity to rivers is a critical factor, as areas closer to watercourses are more vulnerable. The Euclidean distance to rivers is divided into classes such as 0–50 m, 50–100 m, 100–150 m, 150–200 m, 200–400 m, 400–700 m, 700–1000 m, and >1000 m (Figure 4c). Regions within 50 m of rivers exhibit the highest flood risks (Nachappa et al. 2020).

3.2.2.2. Hydrological soil groups (HSG). HSG categorizes soils based on their infiltration capacity, influencing runoff. Soils are classified into four groups: A, B, C, and D. Group A soils have high infiltration rates and low runoff potential, while Group D (Figure 3a) soils exhibit low infiltration and high runoff.

3.2.2. 3. Climatic predictors

Climatic factors, especially precipitation, play a significant role in flooding events.

3.2.2.4. Rainfall. Rainfall intensity and distribution drive surface water flow. The spatial variation of annual average rainfall is often interpolated using methods like spline. Typical classes include 502–600 mm/year, 600–700 mm/year, 700–800 mm/year, 800–900 mm/year, 900–1000 mm/year, 1000–1100 mm/year, and 1100–1214 mm/year (Figure 4a). Higher rainfall values correspond to higher flood susceptibility (Bannari et al. 2017).

3.2.2.5. Land use and geological predictors

Human activities and geological properties play significant roles in shaping flood dynamics.

3.2.2.6. Land use/Land cover. Land use impacts runoff and water retention. Categories include built-up areas, agricultural zones, forests, pastures, fruit orchards, shrubs, rivers, and vineyards (Figure 3b). Urban areas with impervious surfaces are particularly flood-prone.

3.2.2.7. Lithology. Geological characteristics influence water infiltration. Impermeable rocks like clay promote surface runoff, while permeable rocks like sand facilitate infiltration. Lithological units include loess deposits, sandstone and schists, clay and marls, conglomerates, and others (Figure 3d).

The percentage of flood pixels within classes/categories can be seen in Figures 5 and 6.

The data source and scale/resolution for each predictor are included in Table 1.

The percentage distribution of flood pixels over the classes/categories of flood predictors are represented in Figure 4(a-h) and Figure 5(a-f).

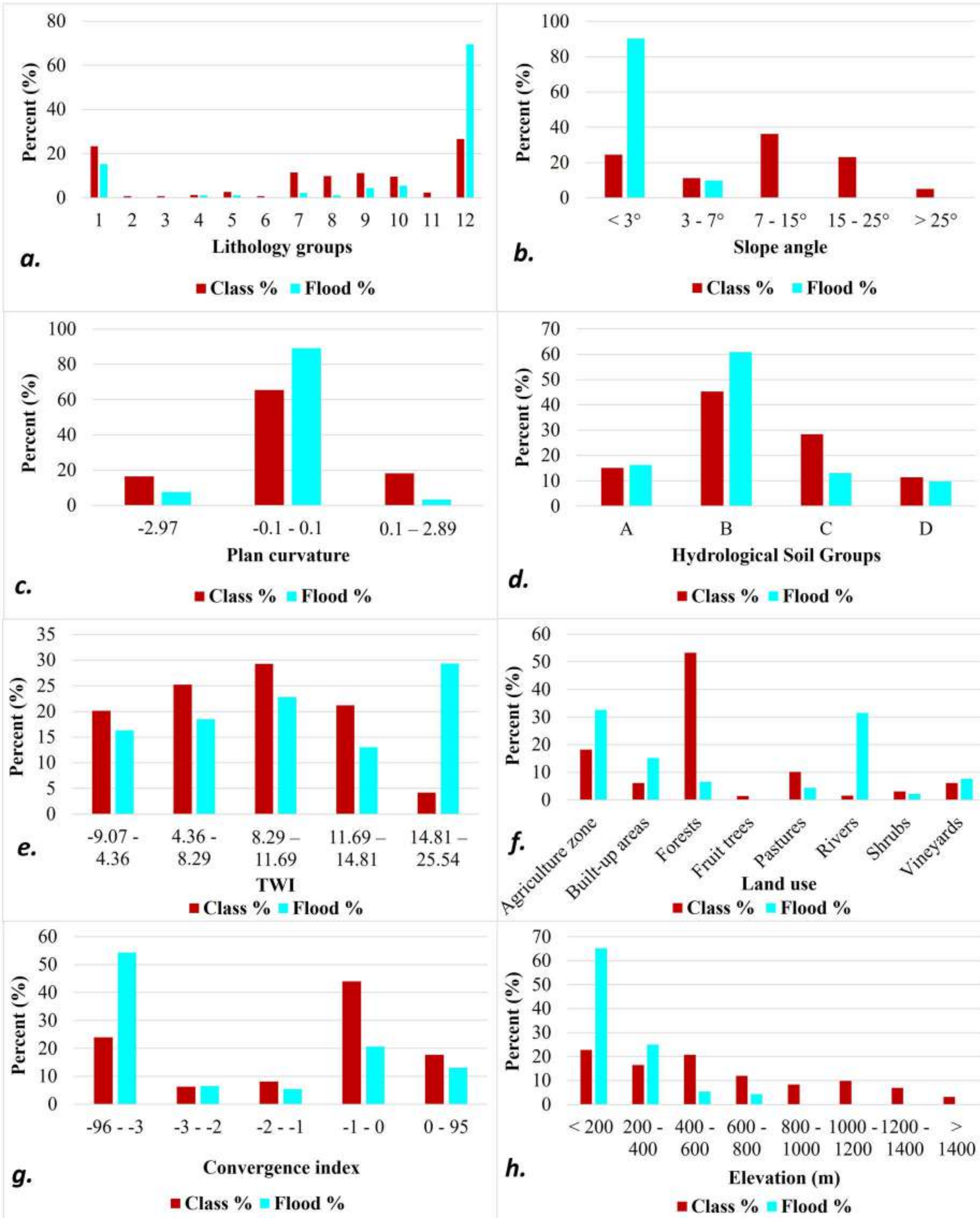

Figure 5. Percentage of flood pixels within classes/categories (a. Lithology; b. Slope angle; c. Plan curvature; d. Hydrological Soil Groups; e. TWI; f. Land use; g. Convergence Index; h. Elevation) (source: Costache and Bui (2019)).

4. Methods

4.1. OneR attribute Evaluation for feature selection

OneR (One Rule) is a simple yet effective attribute evaluation method used for feature selection in machine learning tasks (Parsania et al. 2014), including flood susceptibility mapping. The method is based on the idea of selecting the most predictive single feature (attribute) that can classify the target variable with the lowest error rate. In the context of flood susceptibility mapping, OneR helps identify

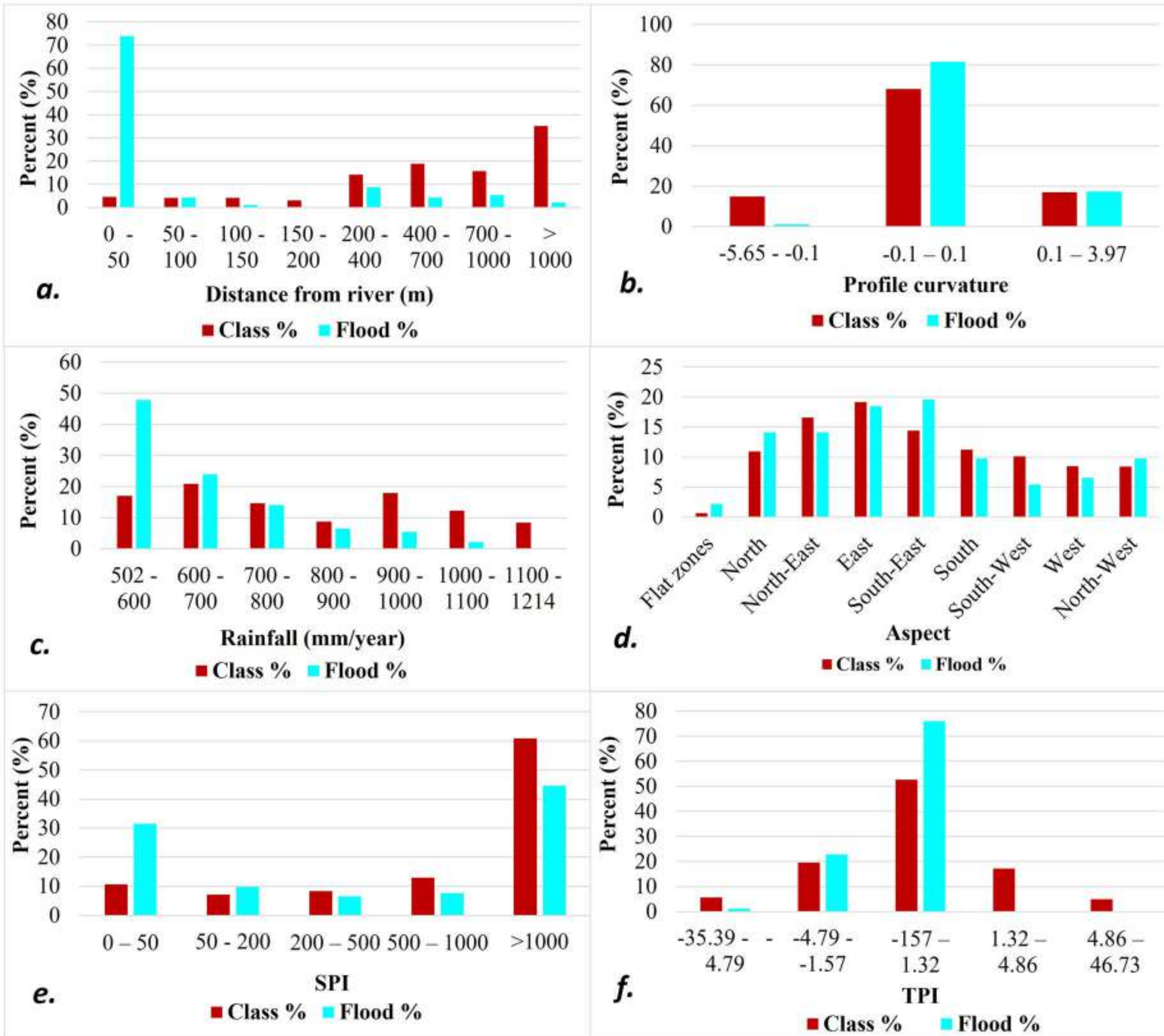

Figure 6. Percentage of flood pixels within classes/categories (a. Distance from river; b. Profile curvature; c. Rainfall; d. Aspect; e. SPI; f. TPI) (source: Costache and Bui (2019)).

Table 1. Flood predictors, scale/resolution, and the source of data.

Flood predictor	Scale	Resolution	Source
Lithology	1:200,000		Digital Geological Map of Romania
Slope angle	–	30 m	Shuttle Radar Topographic Mission (SRTM), 30 m
Plan curvature	–	30 m	Shuttle Radar Topographic Mission (SRTM), 30 m
HSG	1:200,000		Digital Soil Map of Romania
TWI		30 m	Shuttle Radar Topographic Mission (SRTM), 30 m
Land use	–	100 m	Corine Land Cover, 2018 database
Convergence index	–	30 m	Shuttle Radar Topographic Mission (SRTM), 30 m
Elevation	–	30 m	Shuttle Radar Topographic Mission (SRTM), 30 m
Distance from river	–	30 m	
Rainfall	–	30 m	
Profile curvature	–	30 m	Shuttle Radar Topographic Mission (SRTM), 30 m
Aspect	–	30 m	Shuttle Radar Topographic Mission (SRTM), 30 m
SPI	–	30 m	Shuttle Radar Topographic Mission (SRTM), 30 m
TPI	–	30 m	Shuttle Radar Topographic Mission (SRTM), 30 m

the most influential predictors (e.g. rainfall, slope, elevation, soil type, etc.) that are strongly associated with the occurrence of floods. The OneR method evaluates the predictive power of each feature (attribute) by constructing a single rule based on that feature and calculating its error rate. The general process can be summarized mathematically as follows:

For a given feature X, OneR constructs a rule that maps each value or range of values of X to the most frequent class C in the target variable Y (Muda et al. 2011).

Let X be a feature with m distinct values/ranges: $X = \{x_1, x_2, \ldots, x_n\}$.

Let Y be the target variable with 2 classes: $Y = \{y_1, y_2\}$ (flood and non-flood).

For each value x_i of X, the rule assigns the class C_i that appears most frequently in the dataset for that value:

$$C_i = \arg\max_{y_i} \text{ Count } (Y = y_i | X = y_i) \tag{1}$$

The OneR method was chosen for feature selection because, compared to other methods such as Information Gain Ratio, it directly tests the classification ability and prioritizes the practical effectiveness and not just the theoretical one of the predictors. Also, OneR does not combine variables, but evaluates them individually. Also, OneR can automatically eliminate redundant or collinear variables (Bagherzadeh-Khiabani et al. 2016).

4.2. Weights of Evidence

The Weights of Evidence (WoE) method is a model related to bivariate statistical techniques. This method is based on Bayes' conditional probability theorem and quantifies the spatial relationship between floods and their predictors. For this reason, this method is a widely used tool in studies of susceptibility to natural hazards. It assigns positive weights (W^+) for factors favoring flood occurrence and negative weights (W^-) for those linked to the absence of floods. These weights are then used to create susceptibility maps by integrating spatial relationships across multiple factors. The negative and positive weights are calculated as follows (Costache 2019a):

$$W^+ = ln \frac{\frac{Npix_1}{Npix_1 + Npix_2}}{\frac{Npix_3}{Npix_3 + Npix_4}} \tag{1}$$

$$W^- = ln \frac{\frac{Npix_2}{Npix_1 + Npix_2}}{\frac{Npix_4}{Npix_3 + Npix_4}} \tag{2}$$

where $Npix_1$ is the number of pixels with torrentiality in the class; $Npix_2$ is the number of pixels with torrentiality from outside the class; $Npix_3$ is the number of pixels in the class without torrentiality; $Npix_4$ is the number of pixels without torrentiality from outside of the class; W^+ is the positive weight and W^- is the negative weight.

The final coefficients values determined through WoE model, can be computed with the above formula (Costache 2019a):

$$Wf = Wplus + Wmin\,total - Wmin \tag{3}$$

where *W*plus is the positive weight of a class factor, *W*min is the negative weight of a class factor, *W*min total is the total of all negative weights in a multiclass map.

4.3. Random Committee (RC) model

Random Committee is an ensemble machine learning algorithm that builds multiple instances of a base learning model (often decision trees or other classifiers) on the same dataset with different random seeds. The final output is produced by averaging the predictions (for regression tasks) or voting (for classification tasks) of all the individual models in the ensemble (Niranjan et al. 2018). This algorithm is part of the ensemble learning family, where the primary objective is to improve model performance by combining the predictions of several individual models. The strength of the RC model lies in its ability to reduce variance and enhance predictive accuracy, particularly in datasets with high complexity or noise. This method is particularly effective for flood susceptibility assessments as it reduces prediction variance and improves generalization.

In the following rows the training and prediction phases are described (Lira et al. 2007).

Training phase: let $D = \{X, Y\}$ represent the dataset, where $X = \{x_1, x_2, \ldots, x_n\}$ is a set of flood predictors (e.g. slope, rainfall, TWI), and $Y = \{y_1, y_2, \ldots, y_n\}$ is the corresponding flood susceptibility classification or index. Then, RC trains k base models $\{M_1, M_2, \ldots, M_n\}$, each initialized with a unique random seed r_i:

$$M_i = \text{Train}\,(D, r_i), \quad i = 1, 2, \ldots, k \tag{4}$$

Here r_i introduces diversity in the models by affecting how they learn relationships between flood predictors and flood susceptibility.

Prediction phase: For a new input x (e.g. a location with predictor values like slope and rainfall), each base model M_i generates a prediction $y_i(x)$. Thus, the outputs $y_i(x)$ are categorical flood susceptibility classes (e.g. very low, low, medium, high, very high). The final prediction y^* is determined by majority voting:

$$y* = \text{ Mode } \left(y_1(x), y_2(x), \ldots, y_k(x)\right) \tag{5}$$

where Mode(•) identifies the most frequently predicted class.

Flood susceptibility models often assign weights to predictors (w_j) to determine their influence on the final susceptibility index. The formula for the flood susceptibility index (FSI) using the Random Committee ensemble can be expressed as:

$$FSI(x) = \frac{1}{k}\sum_{i=1}^{k}\left(\sum_{j=1}^{m} w_j x_j\right) \tag{6}$$

Where: k is the number of base models in the ensemble; m is the number of flood predictors; w_j is the weight assigned to the j-th predictor by the base models; x_j is the value of j-th predictor for the location x.

4.4. Random SubSpace (RSS)

The Random SubSpace (RSS) algorithm is an ensemble learning method that builds robust predictive models by training multiple classifiers on randomly selected subsets of features (subspaces) (Talukdar et al. 2021). This approach enhances the diversity of the ensemble and reduces the risk of overfitting, making it particularly suitable for flood susceptibility assessment, where feature-rich spatial and hydrological datasets are common. In the following rows are presented the main algorithm principles and equations (Swarna et al. 2022).

RSS first step is represented by the Random Feature Subsampling. Given a dataset with N observations and M features ($X = \{x_1, x_2, \ldots, x_M\}$), the RSS algorithm generates T base classifiers. For each base classifier, a subset of m features ($m < M$) is selected randomly without replacement. The selected feature set for the t-th classifier is:

$$\mathrm{X_t} = \{x_1, x_2, \ldots, x_{\mathrm{im}}\}, \text{ where } i_j \in \{1, 2, \ldots, M\}, \text{ and } |\mathrm{X}t| = \mathrm{m}.$$

The value of m is often a hyperparameter, typically chosen as:

$$m = \sqrt{M} \quad \text{or} \quad = \log_2(M) + 1,$$

depending on the dataset's dimensionality and the chosen base classifier.

RSS second step resides in the training base classifiers. Thus, each base classifier h_t is trained on the dataset using only the selected feature subset X_t. For an observation x_i (a vector of features), the output of the t-th classifier is:

$$h_t(x_i) = \text{ClassLabel or } h_t(x_i) = p(c_k|x_i),$$

where c_k is the probability of class k (e.g. flood-prone or non-flood-prone) for observation x_i.

The predictions of all T base classifiers are combined to produce the final prediction. For classification tasks like flood susceptibility, majority voting is commonly used:

$$H(x_i) = \arg\max_{c_k} \sum_{t=1}^{T} \mathrm{II}(h_t(x_i) = c_k) \tag{7}$$

where II is an indicator function:

$$\mathrm{II}(h_t(x_i) = c_k) = \begin{cases} 1, & if\ \ h_t(\mathrm{x}_i) = c_k \\ 0, & otherwise. \end{cases} \tag{8}$$

For probabilistic outputs, the predictions are averaged:

$$H(x_i) = \arg\max_{c_k} \frac{1}{T} \sum_{t=1}^{T} p(c_k|x_i) \tag{9}$$

After training, the model predicts flood susceptibility for all spatial units (e.g. pixels in a GIS grid). Each location is classified into susceptibility classes (e.g. low, moderate, high) based on the aggregated output $H(x_i)$.

Input Data: A flood susceptibility dataset with M features, such as: x_1 – Elevation; x_2 – Slope; x_3 – Rainfall; x_4 – Distance to rivers; x_5 – Soil type, etc. The target variable (y) represents flood susceptibility as a binary classification (e.g. 1: flood-prone, 0: not flood-prone) or multi-class (e.g. low, moderate, high).

4.5. Randomizable filtered classifier (RFC)

The Randomizable Filtered Classifier is a machine learning model based on feature preprocessing and classification by using some filters. By means of this approach, the framework necessary for the application of data conversion or filtering techniques is created (Alam et al. 2021). Thus, this model becomes very useful in terms of improving the performance of flood susceptibility assessment (Shahdad and Saber 2022).

Let $X = \{x_1, x_2, \ldots, x_\mathrm{n}\}$ represent the input dataset with n samples, where each sample x_i has m features $x_i = \{x_{i1}, x_{i2}, \ldots, x_{i\mathrm{m}}\}$, and $y = \{y_1, y_2, \ldots, y_\mathrm{n}\}$ represent the corresponding class labels.

The Randomizable Filtered Classifier combines four main components:

4.5.1. Filter (preprocessing step)

A filter is applied to transform the input data before training. Common preprocessing filters in flood susceptibility assessments include attribute selection (e.g. Principal Component Analysis or ReliefF), normalization (scaling data to a consistent range), and noise removal (e.g. smoothing spatial data).

The filtering process applies a transformation $\varphi(\cdot)$ to the dataset:

$$X' = \varphi(X) \tag{10}$$

Here, $\varphi(\cdot)$ could represent normalization, principal component analysis, or attribute selection. For example:

- Normalization:

$$x'_{\mathrm{ij}} = \frac{(x_{\mathrm{ij}} - \min(x_\mathrm{j}))}{(\max(x_\mathrm{j}) - \min(x_\mathrm{j}))} \tag{11}$$

- Principal Component Analysis (PCA):

$$\mathrm{X}' = \mathrm{XW} \tag{12}$$

where, W is a matrix of eigenvectors corresponding to the top k principal components.

4.5.2. Base classifier

The filtered data is then passed to a base classifier, which could be any machine learning algorithm such as Decision Trees, Random Forest, Support Vector Machines, or Naive Bayes. The classifier learns the relationship between flood-related features and flood susceptibility.

The transformed dataset X' is used to train the base classifier f(·), which maps the features to the target class:

$$\hat{y}_i = f(x_i'; \theta) \tag{13}$$

where θ represents the parameters of the base classifier (e.g. decision thresholds in decision trees or weights in logistic regression).

4.5.3. Randomization

Randomization is introduced at various stages, such as random sampling of features or instances, randomized parameter selection for the filter or the classifier, and random initialization of model weights or parameters.

Random Feature Subset Selection: A random subset of features x'_i, subset is used for training, ensuring diversity:

$$x_i', \text{ subset} \subseteq x_i' \tag{14}$$

Parameter Randomization: Parameters of the base classifier θ are initialized or sampled randomly from a predefined distribution:

$$\theta \sim \mathcal{D}(\mu, \sigma) \tag{15}$$

Random Instance Sampling (Bootstrapping): The dataset X′ is bootstrapped to train each iteration of the classifier:

$$\mathrm{X'}_{\mathrm{sample}} \sim \mathrm{X'} \tag{16}$$

4.5.4. Prediction

The final output of the model is a prediction of flood susceptibility classes for each location, which could be binary (flood-prone or non-flood-prone) or multi-class (e.g. low, moderate, high susceptibility).

For a classification task, the final prediction $\hat{y}$ is determined by the trained classifier. In some cases, ensemble methods may aggregate predictions:

$$\hat{y}_i = \text{MajorityVote}\left(f_1(x_i'), f_2(x_i'), \ldots, f_k(x_i')\right) \tag{17}$$

It should be noted that all the three randomization ensembles were configured, run and evaluated using Weka 3.9 software.

4.6. Results validation methods

4.6.1. ROC curve

The Receiver Operating Characteristic (ROC) curve is a graph used to quantify the accuracy of a classification model (Mangkhaseum et al. 2024). It shows the ability of the model to distinguish the different classes. The 2 elements are represented on the curve – the true positive rate (sensitivity) on the y-axis and the false positive rate (specificity 1) on the x-axis (Al-Juaidi et al. 2018). The measurable element resulting from the application of the ROC Curve is the area under the curve (AUC), depending on which a general performance of the model can be established. An AUC value closer to 1 indicates a highly effective model, whereas a value around 0.5 suggests performance equivalent to random chance.

The AUC can be derived using the next equation (Costache 2019b):

$$\mathrm{AUC} = \frac{(\sum TP + \sum TN)}{(\mathrm{P} + \mathrm{N})} \tag{18}$$

where TP (true positive), TN (true negative) are the sums of flood and non-flood locations correctly classified.

4.6.2. Statistical metrics

Statistical measures have an extremely important role in order to estimate the accuracy of the prediction power of the calculation models of the susceptibility to natural hazards. These methods produce quantitative results regarding the performance of a model by comparing the predicted results with the observed data (Costache et al. 2022). Below are presented the indices that will be used in this study, along with their equations:

$$\text{Sensitivity} = \frac{\text{TP}}{\text{TP} + \text{FN}} \tag{19}$$

$$\text{Specificity} = \frac{\text{TN}}{\text{FP} + \text{TN}} \tag{20}$$

$$\text{Accuracy} = \frac{\text{TP} + \text{TN}}{\text{TP} + \text{FP} + \text{TN} + \text{FN}} \tag{21}$$

$$\text{k} = \frac{p_{\text{o}} - p_{\text{e}}}{1 - p_{\text{e}}} \tag{22}$$

where P is the sum of flood locations, N is the sum of non-flood locations, FP (false positive) and FN (false negative) are the number of flood and non-flood locations erroneously classified, k is kappa coefficient, p_o is the observed flood locations, and p_e is the estimated flood susceptibility locations.

The flowchart of the methodological steps applied in the present research is showed in Figure 7.

5. Results

5.1. Feature selection

The first stage of the processing was represented by the evaluation of the ability to predict the geographical factors regarding the flood hazard using OneR Attribute Evaluation model. The highest predictive ability was achieved by the distance to river (0.198), followed by slope angle (0.16), elevation (0.14), SPI (0.123), convergence index (0.113), profile curvature (0.112), land use (0.09), TPI (0.085), TWI (0.082), lithology (0.067), aspect (0.053), hydrological soil group (0.04), rainfall (0.034) and plan curvature (0.023) (Figure 8).

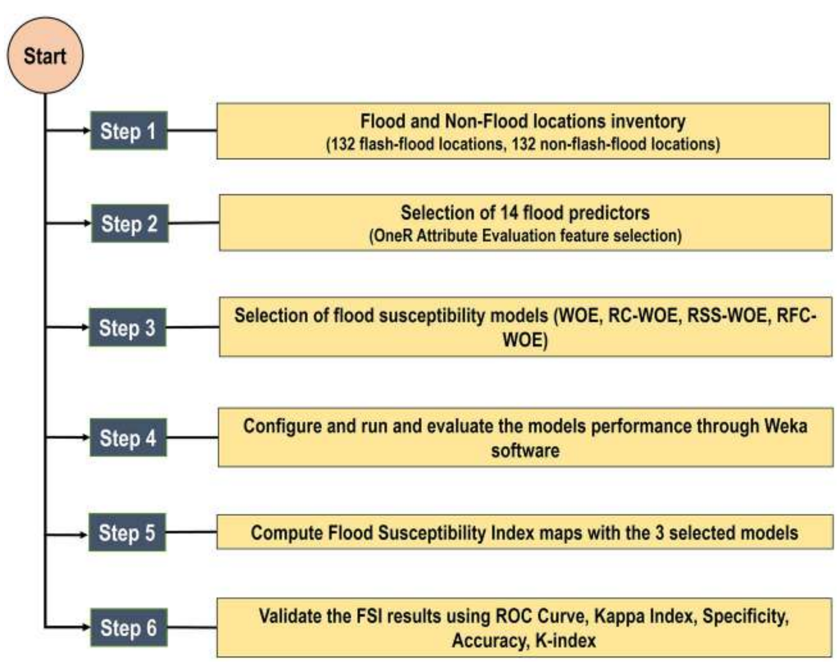

Figure 7. Flowchart of the methodological steps applied in the present research.

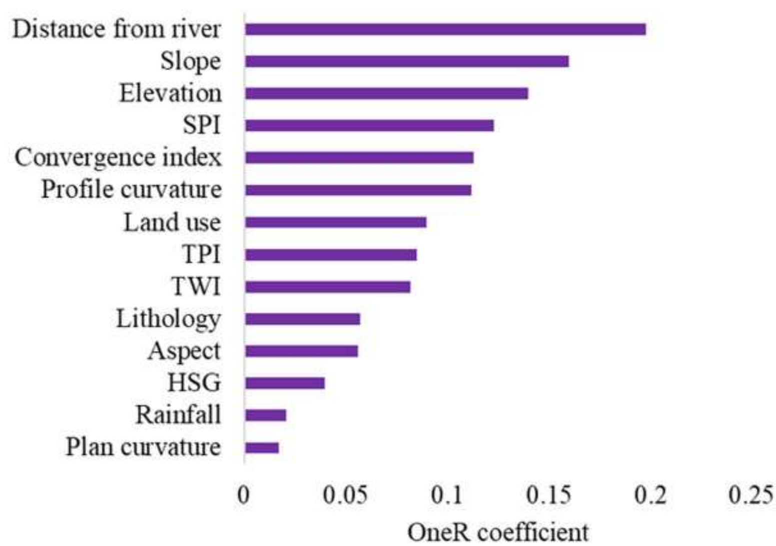

Figure 8. Prediction ability of flood conditioning factors.

5.2. Weights of evidence (WOE) coefficient

Following the derivation of the WOE coefficients, it was found that the highest value resulted for the category of lands represented by Rivers (WOE = 3.56). In second place is the class below 200 m of the factor represented by Elevation (WOE = 3.1). Next, the value of 2.9 attributed to the class under 50 m of the factor represented by Distance to river is noteworthy (Table 2). The calculation of the normalized values of the Weights of Evidence (WOE) coefficients was necessary to bring within the same range the values of all the geographical factors involved in the procedure for determining the susceptibility to floods. The normalized values of the WOE were assigned to the grids associated with the 14 factors and then brought to each point of the flood and non-flood locations. These values assigned to flood and non-flood locations constituted input data (independent variable) within the three machine learning models used in the present study.

5.3. RC-WOE

A ten-fold cross-validation procedure was involved in the training process of RC-WOE combined model. It should be noted that the Base Classifier was represented by Random Forest algorithm, while the Discretize method was employed as filter. Also, the number of iterations was set at 100. The performances of this training process were revealed by the following statistics scores: *k-statistic* = 1; *Mean absolute error* = 0.0161; *Root mean squared error* = 0.0505; *Relative absolute error* = 3.2204%; *Root relative squared error* = 10.097%. After evaluating the performance of the model training process, it was used to determine the importance values of the 14 factors regarding the flood hazard. Thus, the hierarchy was established for the flood predictors importance: Slope (0.132), Distance to rivers (0.098), Elevation (0.093), Land use (0.090), SPI (0.079), Convergence index (0.073), Profile curvature (0.070), Rainfall (0.066), Lithology (0.06), TPI (0.056), Plan curvature (0.053), HSG (0.05), TWI (0.042) and Aspect (0.038) (Figure 9).

The importance values were further used to calculate flood susceptibility by means of Map Algebra from ArcGIS 10.8. Thus, each importance value was multiplied by the raster related to each predictor so that the products resulting from the multiplication could then be integrated in a mathematical addition operation. The FSI RC-WOE values were thus derived and were divided into five classes by means of the Natural Breaks classification (Figure 10a). As can be seen in the central and western part of the study area, the Very low and Low values of FSI RC-WOE predominate. This is explained by the fact that the respective area is dominated by high altitudes and very steep slopes of the relief that do not allow the accumulation and stagnation of water on the surface.

Table 2. Weights of evidence coefficients.

Factor	Class	Class pixels	Flood pixels	W^+	W^-	Wf	Wf_N
Lithology	1	651309	14	−0.43	0.10	−0.40	0.48
	2	19032	0	0.00	0.01	−2.50	0.10
	3	19510	0	0.00	0.01	−2.50	0.10
	4	32990	1	−0.08	0.00	0.05	0.55
	5	72392	1	−0.87	0.02	−0.75	0.41
	6	17319	0	0.00	0.01	−2.50	0.10
	7	318729	2	−1.66	0.10	−1.63	0.26
	8	274930	1	−2.21	0.09	−2.17	0.16
	9	312505	4	−0.95	0.07	−0.89	0.39
	10	264690	5	−0.56	0.04	−0.47	0.46
	11	65548	0	0.00	0.02	−2.50	0.10
	12	739634	64	0.96	−0.88	1.98	0.90
Slope angle	<3°	684268	83	1.30	−2.04	2.08	0.90
	3–7°	310480	9	−0.13	0.02	−1.41	0.12
	7–15°	1011262	0	0.00	0.45	−1.50	0.10
	15–25°	643813	0	0.00	0.26	−1.50	0.10
	> 25°	138765	0	0.00	0.05	−1.50	0.10
Plan curvature	−3.07 to −0.1	460577	7	−0.78	0.10	−1.77	0.34
	−0.1 to 0.1	1822918	82	0.31	−1.16	0.58	0.90
	0.1–2.89	505093	3	−1.71	0.17	−2.77	0.10
HSG	A	419321	15	0.08	−0.02	−0.04	0.63
	B	1261176	56	0.30	−0.34	0.49	0.90
	C	790380	12	−0.78	0.19	−1.11	0.10
	D	317711	9	−0.15	0.02	−0.31	0.50
TWI	−9.07 to 4.36	560674	15	−0.21	0.05	−0.24	0.19
	4.36–8.29	704169	17	−0.31	0.09	−0.39	0.15
	8.29–11.69	816550	21	−0.25	0.09	−0.32	0.17
	11.69–14.81	590353	12	−0.48	0.10	−0.57	0.10
	14.81–25.54	116006	27	1.95	−0.30	2.27	0.90
Land use	Agriculture zone	507087	30	0.58	−0.19	0.99	0.59
	Built–up areas	172094	14	0.90	−0.10	1.21	0.61
	Forests	1486366	6	−2.10	0.69	−2.59	0.15
	Fruit trees	40743	0	0.00	0.01	−3.00	0.10
	Pastures	283144	4	−0.85	0.06	−0.70	0.38
	Rivers	44150	29	2.99	−0.36	3.56	0.90
	Shrubs	84452	2	−0.33	0.01	−0.13	0.45
	Vineyards	170552	7	0.22	−0.02	0.44	0.52
CI	−96 to −3	669022	50	0.82	−0.51	1.25	0.90
	−3 to −2	174471	6	0.04	0.00	−0.04	0.48
	−2 to −1	226342	5	−0.40	0.03	−0.51	0.32
	−1 to 0	1225291	19	−0.76	0.35	−1.18	0.10
	0–95	493462	12	−0.31	0.05	−0.44	0.34
Elevation (m)	<200	634620	60	2.87	−0.80	3.10	0.90
	200–400	458363	23	1.52	−0.11	1.07	0.47
	400–600	577977	5	0.26	0.18	−0.47	0.14
	600–800	332487	4	0.36	0.08	−0.28	0.18
	800–1000	231078	0	0.00	0.09	−0.65	0.10
	1000–1200	272860	0	0.00	0.10	−0.66	0.10
	1200–1400	193243	0	0.00	0.07	−0.63	0.11
	>1400	87960	0	0.00	0.03	−0.59	0.12
Distance from river (m)	0–50	128055	68	2.78	−1.30	2.90	0.90
	50–100	117809	4	0.03	0.00	−1.14	0.49
	100–150	115397	1	−1.34	0.03	−2.54	0.35
	150–200	85907	0	0.00	0.03	−5.00	0.10
	200–400	394637	8	−0.49	0.06	−1.72	0.43
	400–700	528655	4	−1.47	0.17	−2.81	0.32
	700–1000	437196	5	−1.06	0.11	−2.35	0.37
	> 1000	980932	2	−2.78	0.41	−4.37	0.16
Rainfall (mm/year)	502–600	475654	44	1.03	−0.46	1.16	0.90
	600–700	582608	22	0.14	−0.04	−0.16	0.61
	700–800	407731	13	−0.03	0.01	−0.37	0.56
	800–900	243309	6	−0.29	0.02	−0.65	0.50
	900–1000	500904	5	−1.20	0.14	−1.67	0.28
	1000–1100	343781	2	−1.74	0.11	−2.18	0.17
	1100–1214	234601	0	0.00	0.09	−2.50	0.10
Profile curvature	−5.65 to −0.1	415130	1	−2.62	0.15	−3.17	0.10
	−0.1 to 0.1	1900510	75	0.18	−0.54	0.32	0.90
	0.1–3.97	472948	16	0.03	−0.01	−0.37	0.74
Aspect	Flat zones	17844	2	1.22	−0.02	1.16	0.90
	North	305682	13	0.25	−0.04	0.21	0.31
	North–East	462325	13	−0.16	0.03	−0.27	0.19
	East	534831	17	−0.04	0.01	−0.12	0.22

(*continued*)

Table 2. Continued.

Factor	Class	Class pixels	Flood pixels	W^+	W^-	Wf	Wf_N
	South–East	401355	18	0.31	−0.06	0.29	0.33
	South	312528	9	−0.14	0.02	−0.23	0.19
	South–West	281582	5	−0.62	0.05	−0.75	0.10
	West	236970	6	−0.26	0.02	−0.36	0.16
	North–West	235471	9	0.15	−0.01	0.09	0.27
SPI	0–50	297174	29	1.08	−0.27	1.48	0.90
	50–200	199799	9	0.31	−0.03	0.47	0.50
	200–500	232501	6	−0.25	0.02	−0.13	0.26
	500–1000	361552	7	−0.53	0.06	−0.46	0.13
	>1000	1697562	41	−0.31	0.35	−0.53	0.10
TPI	−35.39 to −4.79	158589	1	−1.65	0.05	−2.14	0.19
	−4.79 to −1.57	545984	21	0.15	−0.04	−0.24	0.68
	−.157 to 1.32	1467093	70	0.37	−0.68	0.61	0.90
	1.32–4.86	477919	0	0.00	0.19	−2.50	0.10
	4.86–46.73	139003	0	0.00	0.05	−2.50	0.10

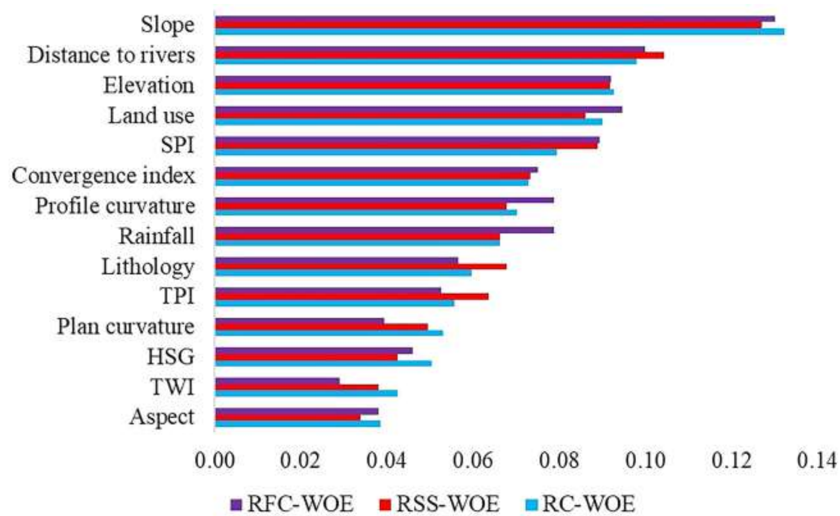

Figure 9. Flood predictors importance in 3 ensemble models.

A transition zone can then be observed in which the average FSI RC-WOE values predominate, while the low zone of the studied region is dominated by High and Very high values. This fact is primarily due to the angle of the slope, which is almost equal to 0, allowing an intense accumulation of water and favoring the occurrence of floods. From the point of view of the weights of the five classes within the study area, we can observe the following situation: Very low (19%), Low (28%), Medium (29%), High (12%) and Very high (12%) (Figure 11).

5.4. Rss-WOE

Also, in this case a ten-fold cross-validation procedure was involved in the training process of RSS-WOE combined model, having as Classifier the REPTRee algorithm. Further, the number of execution slots or threads that were used for constructing the ensemble was established to five. The next parameter represented by the number of iterations was set at 10, while the value of 1 was assigned to the random number seed to be executed. The size of each SubSpace involved in the training procedure is set to 0.5. Like in the above case, the training performance was highlighted by the next statistics scores: *k-statistic* = 1; *Mean absolute error* = 0.0487; *Root mean squared error* = 0.0852; *Relative absolute error* = 9.7405%; *Root relative squared error* = 17.047%. The training process was followed by the determination of importance values for all the 14 flood predictors in the next order: Slope (0.127), Distance to rivers (0.104), Elevation (0.092), SPI (0.089), Land use (0.086), Convergence index (0.073), Profile curvature (0.068), Lithology (0.068), Rainfall (0.066), TPI (0.063), Plan curvature (0.049), HSG (0.042), TWI (0.038) and Aspect (0.034) (Figure 9). These values were used, according to the steps described at

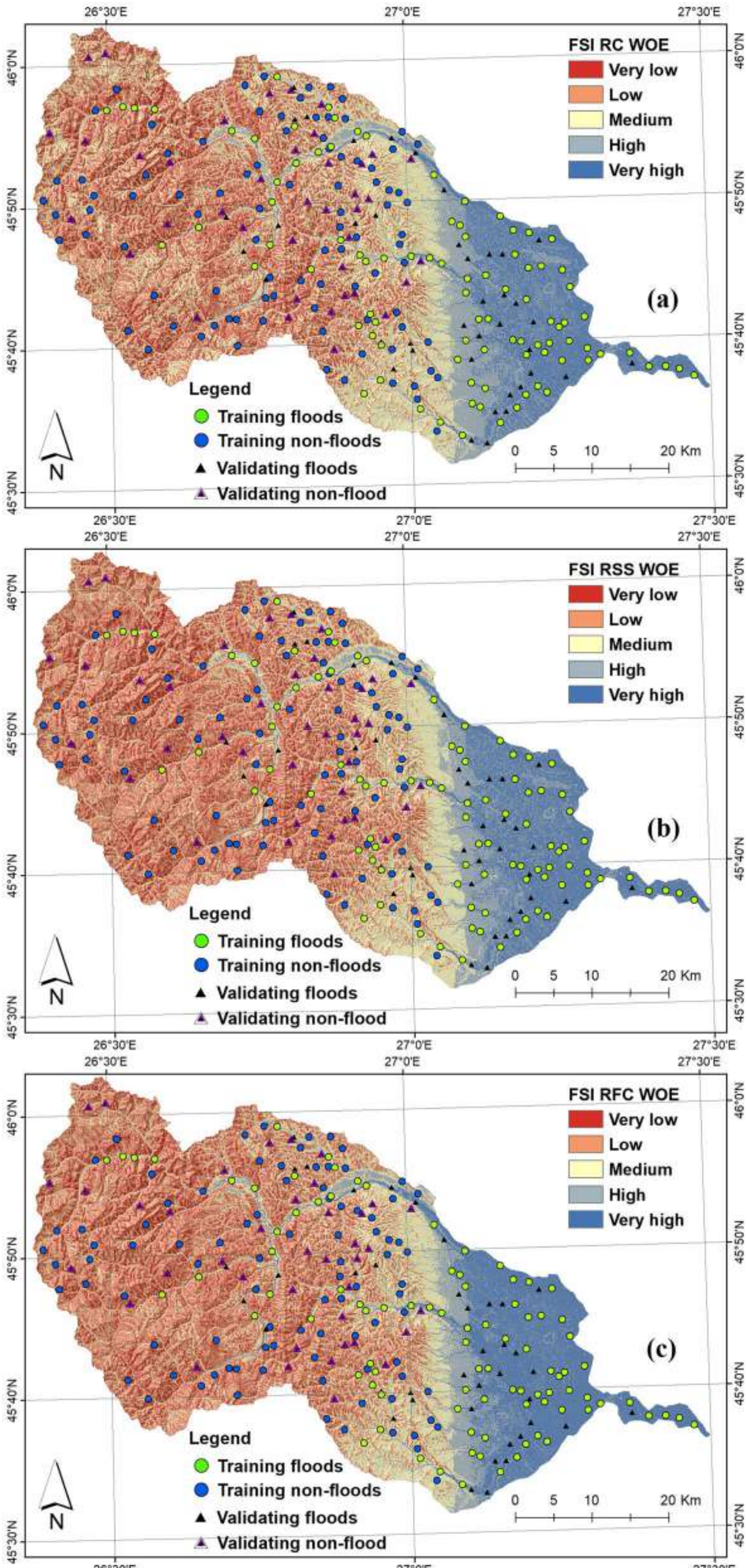

Figure 10. Flood susceptibility index (a. RC-WOE; b. RSS-WOE; c. RFC-WOE).

5.3, in the GIS environment for the derivation of the FSI RSS-WOE. As in the previous case presented, the FSI RSS-WOE (Figure 10b) values were divided into the five classes by using the Natural Breaks classification method. A similar pattern of the distribution of values can be observed on the surface of the study area, with the lowest susceptibility in its western part and the most prone surfaces to the

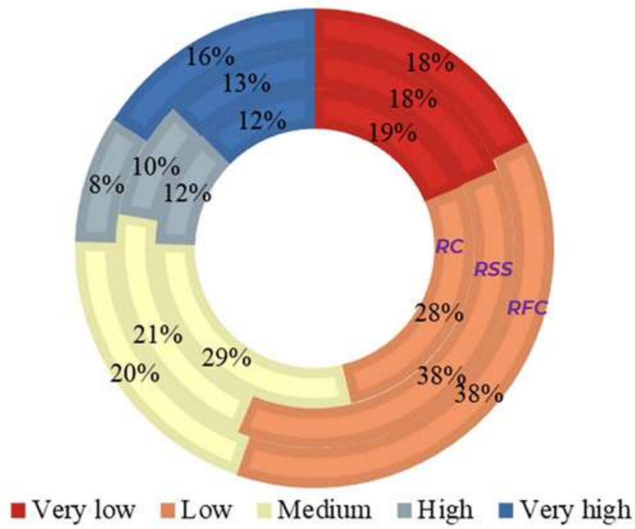

Figure 11. Percentage of FSI classes for each model applied.

phenomenon of flooding in the eastern part. If we analyze the weights occupied by the 5 classes of values, we can observe the following situation: Very low (18%), Low (38%), Medium (21%), High (10%) and Very high (13%) (Figure 11).

5.5. Rfc-WOE

Again, the ten-fold cross-validation process was involved to train RFC-WOE ensemble. In our case study the RandomProjection was used as filter and IBk as classifier. The base learner was selected the BatchPredictor, while the Batch size was set to 100. The performance statistical metrics revealed the next values: *k-statistic* = 0.9674; *Mean absolute error* = 0.0221; *Root mean squared error* = 0.1271; *Relative absolute error* = 4.4148%; *Root relative squared error* = 25.409%. In the case of this 3rd ensemble used to derive the flood susceptibility the next 14 importances for flood predictors were determined: Slope (0.13), Distance to rivers (0.1), Land use (0.095), Elevation (0.092), SPI (0.089), Profile curvature (0.079), Rainfall (0.079), Convergence index (0.075), Lithology (0.057), TPI (0.053), HSG (0.046), Plan curvature (0.039), Aspect (0.038), TWI (0.029). It should be mentioned that in the case of FSI RFC-WOE, the derivation of the final values was possible by following the steps described in section 5.3. Also, as in the case of the two previous derived indices the values were grouped with Natural Breaks method. Also, we can remark the presence of low and very low values in the western area (high and with steep slopes) and high and very high values in the eastern area (low and with reduced slopes) can be observed. The weights achieved by each class value within the study area revealed the next situation: Very low (18%), Low (38%), Medium (20%), High (8%) and Very high (16%) (Figure 11).

5.6. Results validation

5.6.1. ROC curve

In the case of verification and validation of the results offered by the three models, both Success Rate and Prediction Rate were used. Success Rate was graphically represented by considering flood susceptibility values and flood and non-flood points from the training sample (Figure 12a). From this point of view, the RFC-WOE model (AUC = 0.938) exceeded the performances of the other two models that reached an AUC = 0.926 (RC-WOE), respectively AUC = 0.916 (RSS-WOE). To build the graph represented by Prediction Rate, flood and non-flood locations from the validation sample were used. In this case, the best performances were achieved by the RFC-WOE model (AUC = 0.917), followed by RC-WOE (AUC = 0.877) and RSS-WOE (AUC = 0.872) (Figure 12b).

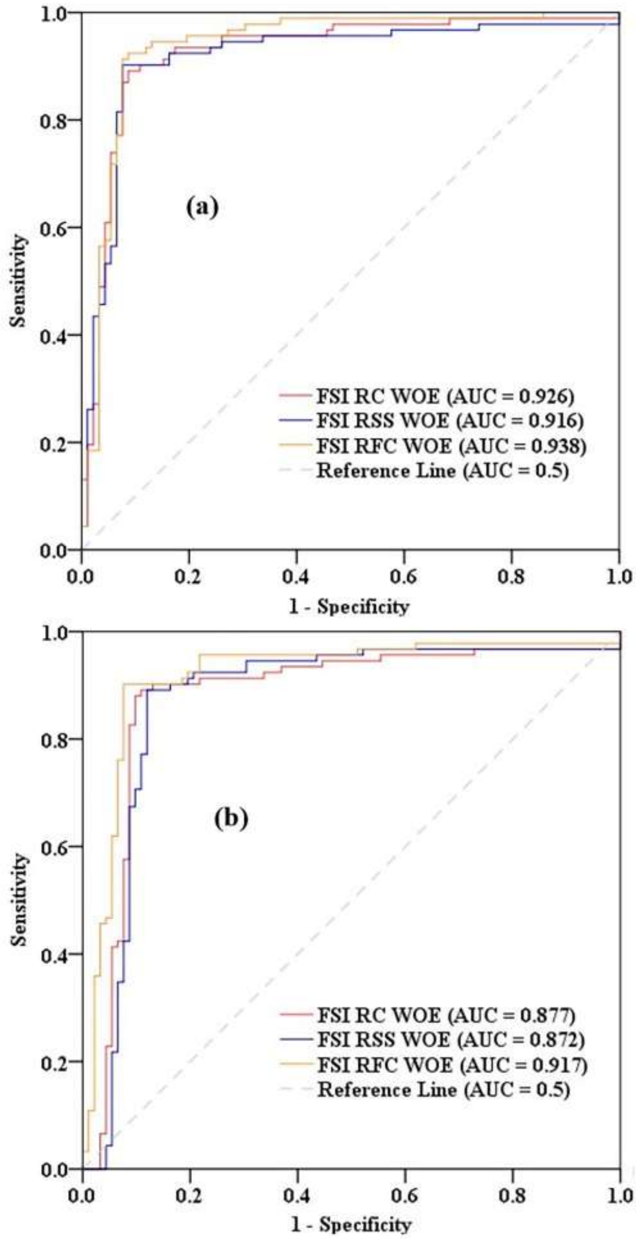

Figure 12. ROC curve (a. Success Rate; b. Prediction Rate).

5.6.2. Statistical metrics

The second stage in the validation and verification of the obtained results was represented by the calculation of metric statistics. Thus, in the case of the training sample, from the Accuracy perspective, the highest value was attributed to the RFC-WOE model (0.957). It was followed by RC-WOE (0.951) and RSS-WOE (0.946). For the same training sample, the k-index values were also composed which highlight the same hierarchy as follows: RFC-WOE (0.913), RC-WOE (0.902) and RSS-WOE (0.891). In the case of the validating sample, from the Accuracy perspective, the highest value was attributed to the RFC-WOE model (0.938). It was followed by RC-WOE (0.925) and RSS-WOE (0.913). For the same training sample, the k-index values were also composed which highlight the same hierarchy as follows: RFC-WOE (0.875), RC-WOE (0.85) and RSS-WOE (0.825) (Table 3).

Table 3. Statistical metrics for the applied flood susceptibility models.

	Training sample			Validating sample		
Metrics	RC-WOE	RSS-WOE	RFC-WOE	RC-WOE	RSS-WOE	RFC-WOE
TP	87	86	89	37	38	39
TN	88	88	87	37	35	36
FP	5	6	3	3	2	1
FN	4	4	5	3	5	4
Sensitivity	0.956	0.956	0.947	0.925	0.884	0.907
Specificity	0.946	0.936	0.967	0.925	0.946	0.973
Accuracy	0.951	0.946	0.957	0.925	0.913	0.938
k-index	0.902	0.891	0.913	0.850	0.825	0.875

6. Discussions

In the present period, the entire globe is talking more and more about the climate changes that are taking place and which are expected to be irreversible. Thus, together with these climate changes, more and more severe manifestations of meteorological phenomena appear, among which we also find intense precipitation in a very short period of time (Soria et al. 2025). This pattern of precipitation consequently determines the occurrence of severe flooding phenomena. One such highly publicized episode was represented by the floods produced in the area of the city of Valencia on 29 October 2024, causing the death of over 220 people. A similar event also occurred in Romania in an area very close to the region studied in this article on the night of 13–14 September 2024. In this case were also recorded a number of six casualties. Therefore, the quick and precise assessment of areas with high potential for flash floods and floods is very important in the current context.

In this study, results were obtained regarding flood susceptibility using three hybrid models formed by combining three machine learning techniques with the Weights of Evidence (WOE) method. Thus, the three models involved in the workflow (RC-WOE, RSS-WOE and RFC-WOE) managed to obtain very good performances in the flood susceptibility modelling process. Their predictive capacity is confirmed by the accuracy of over 0.9 both in the case of the validation station and in the case of the training station. This performance confirms once again the predictive power of machine learning models in terms of flood susceptibility mapping, this fact being confirmed in previous works that used machine learning algorithms (Tehrany et al. 2015; Chapi et al. 2017; Khosravi et al. 2019).

Another result worthy of consideration for the scientific works related to flood hazard is represented by the ranking of geographical factors according to their influence on the floodability process. Thus, in the present study it was established that the greatest influences are exerted by factors such as slope angle, distance to rivers and elevation. These results are similar to those published in the specialized literature by several authors (Fang et al. 2021; Islam et al. 2021; Demissie et al. 2024). Also, the areas and those covered by agricultural crops are noted as having a high influence, a fact confirmed by the results of Pradhan et al. (2023). The way in which the flood susceptibility values are spatially distributed within the study area can also be discussed. Thus, low areas with very low slopes can be noted, which are very exposed to the formation of floods. Areas with similar characteristics were classified as the most susceptible to such phenomena in other works that addressed the subject of susceptibility to floods (Tehrany et al. 2015; Seydi et al. 2022).

Overall, the current study offers some results that clearly show the effectiveness of machine learning models in terms of the potential of mapping areas exposed to floods, being in agreement with most of the studies carried out in the specialized literature that address the same subject.

Also, it is worth to note that this flood susceptibility study is useful for planners, policymakers, the scientific community, and other stakeholders. Thus, the planners from the study area can be helped by the present results in order to avoid the new developments in high flood-prone area. Also, by taking into account the present study, they can have a guide regarding the infrastructure reinforcement. The policymakers can use the present results in order to develop the flood risk legislation and for the improvement of flood risk management plan. The local authorities can use the present research in order to define the most efficient evacuation routes. From the scientific point of view, the present study establishes new three benchmark hybrid models that can be successful used in other study areas.

Insurance companies, local people and companies from the study area represent other important stakeholders that can be interested by the present research outputs.

7. Conclusions

The present study presents a successful application of a number of three hybrid machine learning models, integrating the Weights of Evidence (WOE) method with ensemble classifiers, in order to estimate flood susceptibility. The study area of the present research was the hydrographic basin of the Putna river located in the central-eastern area of Romania. It should be noted that the best performances among the three applied models were obtained by the RFC-WOE ensemble. Overall, all the models have achieved very high performance, so it can be concluded that the hybrid use of machine learning with bivariate statistics has a very high efficiency in this kind of studies. A number of 14 flood predictors were used to derive the three flood susceptibility maps. The most important ones turned out to be distance to rivers, slope and altitude. Since there is no reference system at the level of specialized literature, the flood susceptibility values were classified into 5 classes by means of the Natural Breaks method. The classes with high and very high flood potential are noteworthy, with weights between 23% and 24% of the entire area under research. The validation of the results was possible by applying ROC Curve and statistical metrics. A conclusion of the application of the 2 methods is that in all cases the scores exceeded 0.8, showing a good and very good performance of the applied models. In the current global context, future studies on this subject should also incorporate climate projections of rainfall amounts so that there is also a temporal and not just spatial prediction of the evolution of flood susceptibility values.

Ethical approval

This article does not contain any studies with human participants or animals performed by any of the authors.

Author contributions

CRediT: **Romulus Costache**: Conceptualization, Data curation, Formal analysis, Funding acquisition, Investigation, Methodology, Project administration, Resources, Software, Supervision, Validation, Visualization, Writing – original draft, Writing – review & editing.

Disclosure statement

No potential conflict of interest was reported by the author(s).

Funding

This work was supported by a grant of the Ministry of Research, Innovation and Digitization, CNCS/CCCDI - UEFISCDI, project number PN-IV-P8-8.1-PRE-HE-ORG-2023-0135, within PNCDI IV. Also this work received support from the European Union under the Horizon Europe Research & Innovation Programme (Grant Agreement no. 101123467 MultiCare).

Data availability statement

The data that support the findings of this study are available on request from the corresponding author.

References

Abbass K, Qasim MZ, Song H, Murshed M, Mahmood H, Younis I. 2022. A review of the global climate change impacts, adaptation, and sustainable mitigation measures. Environ Sci Pollut Res Int. 29(28):42539–42559. doi: 10.1007/s11356-022-19718-6.

Alam MT, Ubaid S, Sohail SS, Nadeem M, Hussain S, Siddiqui J, Shakil. 2021. Comparative analysis of machine learning based filtering techniques using MovieLens dataset. Procedia Comput Sci. 194:210–217. doi: 10.1016/j.procs.2021.10.075.
Al-Juaidi AEM, Nassar AM, Al-Juaidi OEM. 2018. Evaluation of flood susceptibility mapping using logistic regression and GIS conditioning factors. Arab J Geosci. 11(24):765. doi: 10.1007/s12517-018-4095-0.
Al-Kindi KM, Alabri Z. 2024. Investigating the role of the key conditioning factors in flood susceptibility mapping through machine learning approaches. Earth Syst Environ. 8(1):63–81. doi: 10.1007/s41748-023-00369-7.
Al-Sheriadeh MS, Daqdouq MA. 2024. Robustness of machine learning algorithms to generate flood susceptibility maps for watersheds in Jordan. Geomat Nat Hazards Risk. 15(1):2378991. doi: 10.1080/19475705.2024.2378991.
Arosio M, Arrighi C, Bonomelli R, Domeneghetti A, Farina G, Molinari D, Monteleone B, Scorzini AR, Martina M. 2024. Unveiling the assessment process behind an integrated flood risk management plan. Int J Disaster Risk Reduct. 112:104755. doi: 10.1016/j.ijdrr.2024.104755.
Bagherzadeh-Khiabani F, Ramezankhani A, Azizi F, Hadaegh F, Steyerberg EW, Khalili D. 2016. A tutorial on variable selection for clinical prediction models: feature selection methods in data mining could improve the results. J Clin Epidemiol. 71:76–85. doi: 10.1016/j.jclinepi.2015.10.002.
Bannari A, Ghadeer A, El-Battay A, Hameed NA, Rouai M. 2017. Detection of Areas Associated with Flash Floods and Erosion Caused by Rainfall Storm Using Topographic Attributes, Hydrologic Indices, and GIS. In: Pirasteh S, Li J, editors. Glob Chang Nat Disaster Manag Geo-Inf Technol. Cham: Springer International Publishing; p. 155–174. doi: 10.1007/978-3-319-51844-2_13.
Bentivoglio R, Isufi E, Jonkman SN, Taormina R. 2022. Deep learning methods for flood mapping: a review of existing applications and future research directions. Hydrol Earth Syst Sci Discuss. 2022:1–50.
Bhattarai Y, Duwal S, Sharma S, Talchabhadel R. 2024. Leveraging machine learning and open-source spatial datasets to enhance flood susceptibility mapping in transboundary river basin. Int J Digit Earth. 17(1):2313857. doi: 10.1080/17538947.2024.2313857.
Chapi K, Singh VP, Shirzadi A, Shahabi H, Bui DT, Pham BT, Khosravi K. 2017. A novel hybrid artificial intelligence approach for flood susceptibility assessment. Environ Model Softw. 95:229–245. doi: 10.1016/j.envsoft.2017.06.012.
Costache R. 2019a. Flash-flood Potential Index mapping using weights of evidence, decision Trees models and their novel hybrid integration. Stoch Environ Res Risk Assess. 33(7):1375–1402. doi: 10.1007/s00477-019-01689-9.
Costache R. 2019b. Flood susceptibility assessment by using bivariate statistics and machine learning models – a useful tool for flood risk management. Water Resour Manage. 33(9):3239–3256. doi: 10.1007/s11269-019-02301-z.
Costache R, Arabameri A, Costache I, Crăciun A, Pham BT. 2022. New machine learning ensemble for flood susceptibility estimation. Water Resour Manage. 36(12):4765–4783. doi: 10.1007/s11269-022-03276-0.
Costache R, Bui DT. 2019. Spatial prediction of flood potential using new ensembles of bivariate statistics and artificial intelligence: a case study at the Putna river catchment of Romania. Sci Total Environ. 691:1098–1118. doi: 10.1016/j.scitotenv.2019.07.197.
Demissie Z, Rimal P, Seyoum WM, Dutta A, Rimmington G. 2024. Flood susceptibility mapping: integrating machine learning and GIS for enhanced risk assessment. Appl Comput Geosci. 23:100183. doi: 10.1016/j.acags.2024.100183.
Duwal S, Liu D, Pradhan PM. 2023. Flood susceptibility modeling of the Karnali river basin of Nepal using different machine learning approaches. Geomat Nat Hazards Risk. 14(1):2217321. doi: 10.1080/19475705.2023.2217321.
Dyca B, Hartmann T, Tempels B. 2024. Land use planning and management for flood risk management. In Res Handb Flood Risk Manag. Glos, UK: Edward Elgar Publishing; p. 71–85. https://www.elgaronline.com/edcollchap/book/9781839102981/book-part-9781839102981-13.xml.
Fang Z, Wang Y, Peng L, Hong H. 2021. Predicting flood susceptibility using LSTM neural networks. J Hydrol. 594:125734. doi: 10.1016/j.jhydrol.2020.125734.
Grecu F, Zaharia L, Ioana-Toroimac G, Armaș I. 2017. Floods and flash-floods related to river channel dynamics. In: Radoane M, Vespremeanu-Stroe A, editors. Landf Dyn Evol Rom. Cham: springer International Publishing; p. 821–844. doi: 10.1007/978-3-319-32589-7_33.
Habibi A, Delavar MR, Sadeghian MS, Nazari B, Pirasteh S. 2023. A hybrid of ensemble machine learning models with RFE and Boruta wrapper-based algorithms for flash flood susceptibility assessment. Int J Appl Earth Obs Geoinformation. 122:103401. doi: 10.1016/j.jag.2023.103401.
Hasan MH, Ahmed A, Nafee KM, Hossen MA. 2023. Use of machine learning algorithms to assess flood susceptibility in the coastal area of Bangladesh. Ocean Coast Manag. 236:106503. doi: 10.1016/j.ocecoaman.2023.106503.
Hinge G, Hamouda MA, Mohamed MM. 2024. Flash flood susceptibility modelling using soft computing-based approaches: from bibliometric to meta-data analysis and future research directions. Water. 16(1):173. doi: 10.3390/w16010173.
Hoang D-V, Liou Y-A. 2024. Assessing the influence of human activities on flash flood susceptibility in mountainous regions of Vietnam. Ecol Indic. 158:111417. doi: 10.1016/j.ecolind.2023.111417.

Ilia I, Tsangaratos P, Tzampoglou P, Chen W, Hong H. 2022. Flash flood susceptibility mapping using stacking ensemble machine learning models. Geocarto Int. 37(27):15010–15036. doi: 10.1080/10106049.2022.2093990.
Islam ARMT, Talukdar S, Mahato S, Kundu S, Eibek KU, Pham QB, Kuriqi A, Linh NTT. 2021. Flood susceptibility modelling using advanced ensemble machine learning models. Geosci Front. 12(3):101075.
Kader Z, Islam MR, Aziz MT, Hossain MM, Islam MR, Miah M, Jaafar WZW. 2024. GIS and AHP-based flood susceptibility mapping: a case study of Bangladesh. Sustain Water Resour Manag. 10(5):170. doi: 10.1007/s40899-024-01150-y.
Karim F, Armin MA, Ahmedt-Aristizabal D, Tychsen-Smith L, Petersson L. 2023. A review of hydrodynamic and machine learning approaches for flood inundation modeling. Water. 15(3):566. doi: 10.3390/w15030566.
Khosravi K, Shahabi H, Pham BT, Adamowski J, Shirzadi A, Pradhan B, Dou J, Ly H-B, Gróf G, Ho HL, et al. 2019. A comparative assessment of flood susceptibility modeling using multi-criteria decision-making analysis and machine learning methods. J Hydrol. 573:311–323. doi: 10.1016/j.jhydrol.2019.03.073.
Li Y, Hong H. 2023. Modelling flood susceptibility based on deep learning coupling with ensemble learning models. J Environ Manage. 325(Pt A):116450. doi: 10.1016/j.jenvman.2022.116450.
Liao M, Wen H, Yang L, Wang G, Xiang X, Liang X. 2024. Improving the model robustness of flood hazard mapping based on hyperparameter optimization of random forest. Expert Syst Appl. 241:122682. doi: 10.1016/j.eswa.2023.122682.
Lira MM, De Aquino RR, Ferreira AA, Carvalho MA, Neto ON, Santos GS. 2007. Combining multiple artificial neural networks using random committee to decide upon electrical disturbance classification. In: 2007 Int Jt Conf Neural Netw. New York, USA: IEEE; p. 2863–2868. https://ieeexplore.ieee.org/abstract/document/4371414/.
Liu J, Zhao X, Chen Y, Sun H, Gu Y, Xu S. 2025. A novel flood conditioning factor based on topography for flood susceptibility modeling. Geosci Front. 16(1):101960. doi: 10.1016/j.gsf.2024.101960.
Mangkhaseum S, Bhattarai Y, Duwal S, Hanazawa A. 2024. Flood susceptibility mapping leveraging open-source remote-sensing data and machine learning approaches in Nam Ngum River Basin (NNRB), Lao PDR. Geomat Nat Hazards Risk. 15(1):2357650. doi: 10.1080/19475705.2024.2357650.
Muda Z, Yassin W, Sulaiman MN, Udzir NI. 2011. Intrusion detection based on k-means clustering and OneR classification. In: 2011 7th Int Conf Inf Assur Secur IAS. New York, USA: IEEE; p. 192–197. https://ieeexplore.ieee.org/abstract/document/6122818/.
Nachappa TG, Piralilou ST, Gholamnia K, Ghorbanzadeh O, Rahmati O, Blaschke T. 2020. Flood susceptibility mapping with machine learning, multi-criteria decision analysis and ensemble using Dempster Shafer Theory. J Hydrol. 590:125275.
Niranjan A, Nutan DH, Nitish A, Shenoy PD, Venugopal KR. 2018. ERCR TV: ensemble of random committee and random tree for efficient anomaly classification using voting. In: 2018 3rd Int Conf Converg Technol I2CT. New York, USA: IEEE; p. 1–5. https://ieeexplore.ieee.org/abstract/document/8529797/.
Parsania V, Jani NN, Bhalodiya N. 2014. Applying Naïve bayes, BayesNet, PART, JRip and OneR algorithms on hypothyroid database for comparative analysis. Int J Darshan Inst Eng Res Emerg Technol. 3(1):1–6.
Pham BT, Jaafari A, Phong TV, Yen HPH, Tuyen TT, Luong VV, Nguyen HD, Le HV, Foong LK. 2021. Improved flood susceptibility mapping using a best first decision tree integrated with ensemble learning techniques. Geosci Front. 12(3):101105. doi: 10.1016/j.gsf.2020.11.003.
Pourzangbar A, Oberle P, Kron A, Franca MJ. 2025. Analysis of the utilization of machine learning to map flood susceptibility. J Flood Risk Management. 18(2):e70042. doi: 10.1111/jfr3.70042.
Pradhan B, Lee S, Dikshit A, Kim H. 2023. Spatial flood susceptibility mapping using an explainable artificial intelligence (XAI) model. Geosci Front. 14(6):101625. doi: 10.1016/j.gsf.2023.101625.
Qasimi AB, Isazade V, Berndtsson R. 2024. Flood susceptibility prediction using MaxEnt and frequency ratio modeling for Kokcha River in Afghanistan. Nat Hazards. 120(2):1367–1394. doi: 10.1007/s11069-023-06232-2.
Roohi M, Ghafouri HR, Ashrafi SM. 2024. Developing an ensemble machine learning approach for enhancing flood damage assessment. Int J Environ Res. 18(5):90. doi: 10.1007/s41742-024-00647-w.
Saikh NI, Mondal P. 2023. GIS-based machine learning algorithm for flood susceptibility analysis in the Pagla river basin, Eastern India. Nat Hazards Res. 3(3):420–436. doi: 10.1016/j.nhres.2023.05.004.
Santos PP, Pereira S, Zêzere JL, Reis E, Oliveira SC, Garcia RAC, Ferreira TM. 2024. Understanding flood risk in urban environments: spatial analysis of building vulnerability and hazard areas in the Lisbon metropolitan area. Nat Hazards. 24. doi: 10.1007/s11069-024-06731-w.
Sesana E, Gagnon AS, Ciantelli C, Cassar J, Hughes JJ. 2021. Climate change impacts on cultural heritage: a literature review. WIREs Clim Change. 12(4):e710. doi: 10.1002/wcc.710.
Seydi ST, Kanani-Sadat Y, Hasanlou M, Sahraei R, Chanussot J, Amani M. 2022. Comparison of machine learning algorithms for flood susceptibility mapping. Remote Sens. 15(1):192. doi: 10.3390/rs15010192.
Shahdad M, Saber B. 2022. Multistep-ahead forecasting for maximum and minimum air temperatures using a new hybrid intelligence tree-based filter classifier. Model Earth Syst Environ. 8(4):5449–5465. doi: 10.1007/s40808-022-01424-4.
Soria JM, Muñoz R, Campillo-Tamarit N, Molner JV. 2025. Flash-flood-induced changes in the hydrochemistry of the Albufera of Valencia Coastal Lagoon. Diversity. 17(2):119. doi: 10.3390/d17020119.

Swarna KSV, Vinayagam A, Ananth MBJ, Kumar PV, Veerasamy V, Radhakrishnan P. 2022. A KNN based random subspace ensemble classifier for detection and discrimination of high impedance fault in PV integrated power network. Measurement. 187:110333. doi: 10.1016/j.measurement.2021.110333.

Talukdar S, Eibek KU, Akhter S, Ziaul SK, Islam ARMT, Mallick J. 2021. Modeling fragmentation probability of land-use and land-cover using the bagging, random forest and random subspace in the Teesta River Basin, Bangladesh. Ecol Indic. 126:107612. doi: 10.1016/j.ecolind.2021.107612.

Tehrany MS, Pradhan B, Jebur MN. 2014. Flood susceptibility mapping using a novel ensemble weights-of-evidence and support vector machine models in GIS. J Hydrol. 512:332–343. doi: 10.1016/j.jhydrol.2014.03.008.

Tehrany MS, Pradhan B, Mansor S, Ahmad N. 2015. Flood susceptibility assessment using GIS-based support vector machine model with different kernel types. Catena. 125:91–101. doi: 10.1016/j.catena.2014.10.017.

Varra G, Della Morte R, Tartaglia M, Fiduccia A, Zammuto A, Agostino I, Booth CA, Quinn N, Lamond JE, Cozzolino L. 2024. Flood susceptibility assessment for improving the resilience capacity of railway infrastructure networks. Water. 16(18):2592. doi: 10.3390/w16182592.

Wahba M, Sharaan M, Elsadek WM, Kanae S, Hassan HS. 2024. Examination of the efficacy of machine learning approaches in the generation of flood susceptibility maps. Environ Earth Sci. 83(14):429. doi: 10.1007/s12665-024-11696-x.

Zhu K, Lai C, Wang Z, Zeng Z, Mao Z, Chen X. 2024. A novel framework for feature simplification and selection in flood susceptibility assessment based on machine learning. J Hydrol Reg Stud. 52:101739. doi: 10.1016/j.ejrh.2024.101739.

Applied Water Science (2024) 14:78
https://doi.org/10.1007/s13201-024-02131-4

ORIGINAL ARTICLE

Flood mapping based on novel ensemble modeling involving the deep learning, Harris Hawk optimization algorithm and stacking based machine learning

Romulus Costache[1,2,3,4] · **Subodh Chandra Pal**[5] · **Chaitanya B. Pande**[6,7,8] · **Abu Reza Md. Towfiqul Islam**[10,9] · **Fahad Alshehri**[8] · **Hazem Ghassan Abdo**[11]

Received: 5 September 2023 / Accepted: 5 February 2024 / Published online: 14 March 2024

Abstract
Among the various natural disasters that take place around the world, flood is considered to be the most extensive. There have been several floods in Buzău river basin, and as a result of this, the area has been chosen as the study area. For the purpose of this research, we applied deep learning and machine learning benchmarks in order to prepare flood potential maps at the basin scale. In this regard 12 flood predictors, 205 flood and 205 non-flood locations were used as input data into the following 3 complex models: Deep Learning Neural Network-Harris Hawk Optimization-Index of Entropy (DLNN-HHO-IOE), Multilayer Perceptron-Harris Hawk Optimization-Index of Entropy (MLP-HHO-IOE) and Stacking ensemble-Harris Hawk Optimization-Index of Entropy (Stacking-HHO-IOE). The flood sample was divided into training (70%) and validating (30%) sample, meanwhile the prediction ability of flood conditioning factors was tested through the Correlation-based Feature Selection method. ROC Curve and statistical metrics were involved in the results validation. The modeling process through the stated algorithms showed that the most important flood predictors are represented by: slope (importance ≈ 20%), distance from river (importance ≈ 17.5%), land use (importance ≈ 12%) and TPI (importance ≈ 10%). The importance values were used to compute the flood susceptibility, while Natural Breaks method was used to classify the results. The high and very high flood susceptibility is spread on approximately 35–40% of the study zone. The ROC Curve, in terms of Success, Rate shows that the highest performance was achieved $FPI_{\text{DLNN-HHO-IOE}}$ (AUC = 0.97), followed by $FPI_{\text{Stacking-HHO-IOE}}$ (AUC = 0.966) and $FPI_{\text{MLP-HHO-IOE}}$ (AUC = 0.953), while the Prediction Rate indicates the $FPI_{\text{Stacking-HHO-IOE}}$ as being the most performant model with an AUC of 0.977, followed by $FPI_{\text{DLNN-HHO-IOE}}$ (AUC = 0.97) and $FPI_{\text{MLP-HHO-IOE}}$ (AUC = 0.924).

Keywords Artificial intelligence · Optimization algorithm · Flood potential · Buzău river basin · Romania

Introduction

The effects of natural disasters such as floods on the environment and human lives are severe, which impedes the growth of the economy in many regions across the world. There has been an increase in major flood events in recent years, which indicates that the frequency of major floods will continue to rise over the next couple of years (Abdo HG 2020; Tarasova et al. 2023). There is a direct correlation between this fact and the changes in the climate around the world (Qazi et al. 2023; Rizwan et al. 2023). Therefore, there will inevitably come a time when flood events will occur more frequently and with greater severity, which will lead to exponential growth in terms of economic damage as well as loss of human life (Endendijk et al. 2023). There are more than 3000 casualties caused by floods across the globe each year, and their economic losses amount to more than $20 billion (Dai et al. 2023; Lan et al. 2022). By the year 2050, flood damage is expected to increase by five times in Europe, and by the year 2080, it is expected to increase by 17 times (Costache et al. 2020c). There are many countries in Europe that are affected by floods, but Romania is one of the worst affected ones. It has been documented those numerous areas across Romania were affected by floods throughout the course of the 20th and early twenty-first centuries. Examples of the floods that occurred during these times include those that occurred in 1912, 1932, 1969, 1970, 2005, 2006 and 2010 (Costache et al. 2022b). Over a hundred-million-euro worth of material losses are caused by floods in Romania

Extended author information available on the last page of the article

every year. Since Romania became a member of the European Union in 2007, Romania was compelled to align its legislative system with the directives of the European Parliament, such as Directive 2007/60/EC. In accordance with this directive, flood risk management activities are included in the list of activities. Generally speaking, floods have a hard time being prevented, and their devastating effects are often amplified by a wide range of human activities and also by climate changes, which make it harder to prevent flooding (Wei et al. 2023; Kanani-Sadat et al. 2019). Although it is possible to greatly reduce the amount of damage caused by floods through the implementation of certain measures by the responsible authorities, it is also possible to reduce the loss of human life as well. Identifying the areas that have a high risk of flooding is the first step to reducing flood vulnerability, and the key to all measures that are meant to reduce flood vulnerability. An element that can increase the flood vulnerability is the groundwater characteristics (Paneerselvam et al. 2023; Sankar et al. 2023). This issue was approached in several studies during the last years (Balamurugan et al. 2020a; Panneerselvam et al. 2023b). The hydraulic modeling method is one of the most effective means of quantifying the extent of floodplains that are at risk from severe flooding. Through hydraulic modeling, the extent of floodplains is directly related to certain discharge values with various probability of exceeding them. While hydraulic modeling is time-consuming, it is also expensive to obtain the necessary data, like high-resolution Digital Elevation Model data, which is required for the hydraulic modeling (Popescu and Bărbulescu 2023). There has been an increasing number of studies in the last few years focusing on flood susceptibility assessment that have been using state-of-the-art methods that are capable of integrating flood predictors into geographical information systems (Xie et al. 2021; Hategekimana et al. 2018). In addition, it has been possible to quantify the influence certain flood predictors have on the amount of water accumulated at the soil surface. As a result, there are a number of different models that are used in the category of bivariate statistics, including the Certainty Factor, the Statistical Index, Index of Entropy, Weights of Evidence and Frequency Ratio (Costache et al. 2022a). Among the machines learning algorithms are: the Artificial Neural Network, the *K*-Nearest Neighbor, the Logistic Regression, the Adaptive Neuro-Fuzzy Inference System, the Support Vector Machine and the Decision Tree (Zhang 2024; Li et al. 2023; Arora et al. 2021; Shafizadeh-Moghadam et al. 2018). In the last years, there is also an important increase in the use of Deep Learning techniques like: Convolutional Neural Networks, Recurrent Neural Networks or Deep Learning Neural Networks (Guan et al. 2023; Wang et al. 2020; Bui et al. 2020). An ensemble of two or more stand-alone models combines into a hybrid model, which is sometimes considered to be more advanced, providing much more accurate results when compared to two or more stand-alone models (Costache et al. 2020b). A key component of machine learning and statistical models that are utilized in flood prediction is the use of input data from areas where flood phenomena have already occurred. Although there have been numerous hybrid or ensemble methods applied to determine flood susceptibility (Fenglin et al. 2023; Li and Hong 2023), there is no international consensus on a model or combination of models that gives the best results. For this reason, in order to fill the research gaps, the need is felt for the combined application of the most advanced Deep Learning and optimization techniques in order to carry out case studies for flood susceptibility.

Considering the elements exposed above, the present research work proposes a complex and state-of-the-art methodological workflow to derive the flood susceptibility mapping across a highly affected area from Romania. Thus, the Deep Learning, Multilayer Perceptron and a Stacking ensemble, all three models improved through Harris Hawk Optimization (HHO) technique, will be involved in the procedure of deriving the flood susceptibility maps. The stacking ensemble will be derived by the combination of the following machine learning models: Logistic Regression, Classification and Regression Tree, Naïve Bayes and Support Vector Machine. There were five statistical indicators used for the validation of results, including the ROC Curve, as well as several statistical indices.

Study area

This study area covers 5350 km^2 of land in the region of south-east Romania, which is located in the center of the country. A significant relief energy exists in the study area, which is evident at altitudes that range between 1 and 1925 m, reflecting a relatively high range of elevation, which facilitates the propagation of floods from high altitudes to areas at low altitudes (Fig. 1). Moreover, the presence of a slope that exceeds 25° in the upper area of the basin, as well as a flat surface in the lower area of the basin, thereby verifying the possibility of flood propagation and flow accumulation in the upper area of the basin. In accordance with the geological classification of the study area, deposits of internal Cretaceous flysch can be encountered in the mountain region of the area, whereas in the hilly area there is more predominance of Miocene and Sarmato-Pliocene deposits. Clays, gravels, and sands are some of the sedimentary rocks that are common in the plain region. Several geomorphological phenomena, such as gully erosion and landslides,

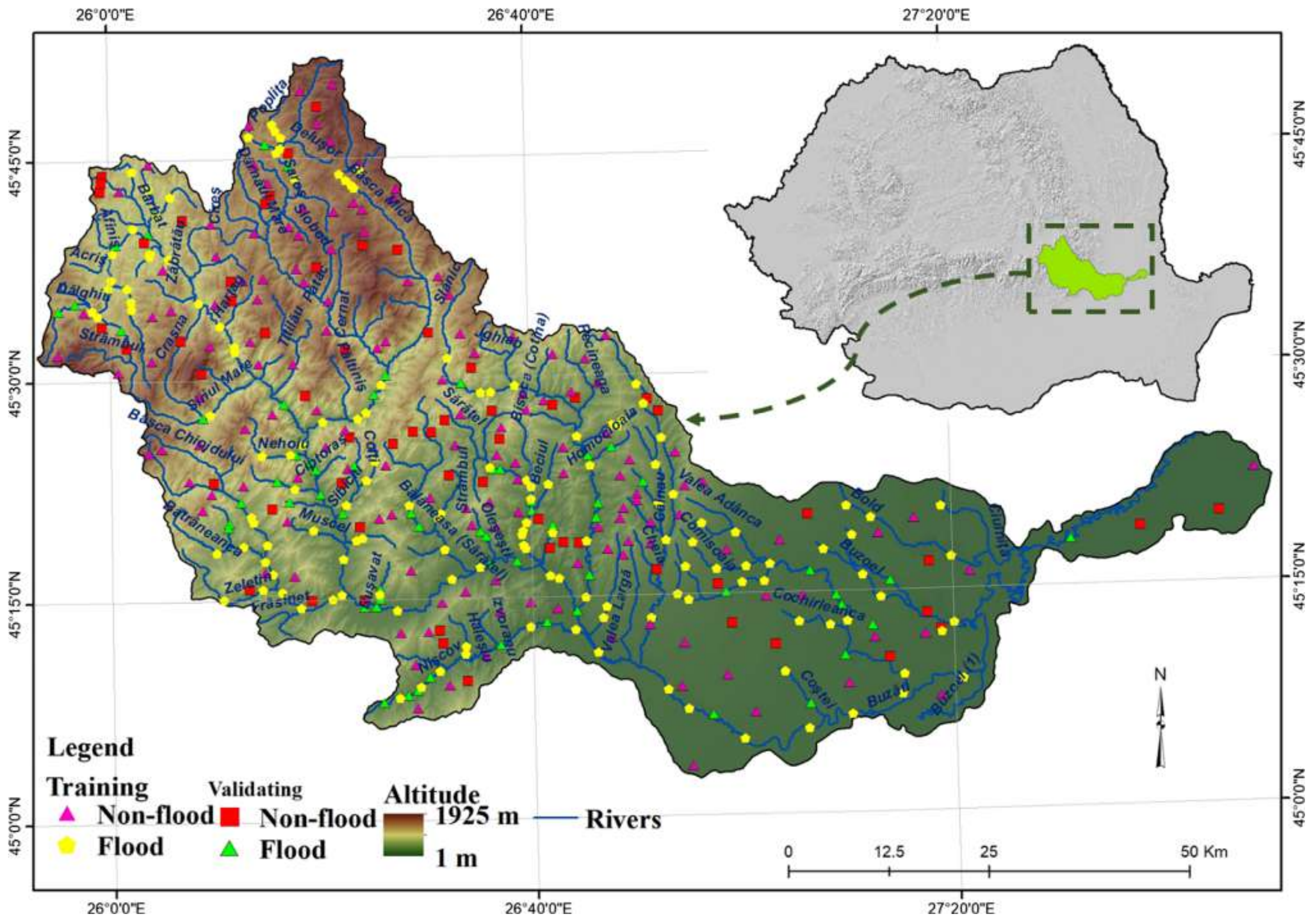

Fig. 1 Study area location

have emerged because of the geological structure of the area and the influence of exogenous factors, which are closely related to flash floods because of the influence of geological factors. There was an average annual precipitation of about 750 mm/year within the study area, but for a 24 h period, the maximum precipitation of 115.4 mm occurred at the meteorological station of Lăcăuți on 12 July 1969 (Minea 2013). From a hydrological perspective, the most important event to remember in 1975 was the increase in discharge of the Buzău river, the main collector in the hydrographic basin, following a heavy rainfall when, at the Măgura hydrometric station, the discharge reached to 2100 m^3/s after a heavy rainfall. It should be noted that one of the most important flood events that occurred on all the main tributary rivers occurred in 2005 when the maximum discharge values for the Câlnău and Slănic rivers reached 56.2 m^3/s and 54 m^3/s, respectively (Costache et al. 2021). Another environmental variable that heavily affects flood potential across the study area is the land use of the area, whether it be forest (40.7%), arable land (30.9%), or built-up areas (4.6%).

Data

Flood inventory

It is common knowledge that in order to predict accurately what areas will be affected by a phenomenon in the future, factors that have favored the production of that phenomenon in the past need to be considered in determining the characteristics of the factors that will drive that phenomenon in the future. In order to perform this study, the location of the locations affected by floods within the time period 1990–2020 have been surveyed and a list of the floods affected has been generated, taking into account only those events that have caused damage within the socio-economic segment (Fig. 1). The flood locations over the research zone were quantified to a total of 205 locations. The National Administration of Romanian Waters, General Inspectorate for Emergency Situations, as well as the Archives of the General Inspectorate for Emergency Situations were consulted in order to create the flood inventory in the study area. We generated another set of data that represents 205 non-flood locations as a means of improving the performance of the applied models. We divided the two data sets into two groups according to how they would be used for training (70%) and validating (30%).

Flood conditioning factors

During the process of estimating flood susceptibility, the flood locations will be the dependent variable; as explanatory variables, 12 flood predictors will be distributed spatially according to flood exposure values. Based on a very careful review of the literature, the next conditioning factors were involved in the analysis (Ozturk et al. 2018): altitude, slope, TPI, aspect, convergence index, TWI, hydrological soil groups, land use, plan curvature, lithology, distance from rivers and rainfall. The first seven flood predictors from the above, which represents morphometric indices, were found to be obtained from the processing of Digital Elevation Model (DEM). The DEM was achieved from the dataset represented by world Shuttle Radar Topographic Mission (SRTM) 30 m. It has also been shown that by using the DEM extracted from the SRTM 30 m database, previous studies focusing upon the same research topic have been able to achieve a high-quality solution in their results (Zhao et al. 2022).

It is very important to recognize that the gradient of the slope is one of the most important characteristics of the ground surface that contributes significantly to surface runoff and flow accumulation (Senanayake et al. 2022). This slope factor was obtained by the DEM processing, and its values are located between the range 0–55.9° (Fig. 2a). As a matter of fact, the Hydrological Soil Group (HSG) has an important influence on the velocity of water infiltration over the soil profile and thus the accumulation potential (Liu et al. 2023). Within the study area there is a presence of all four HSGs, with HSG B (55%) covering most of the surface area (Fig. 2b). According to the plan curvature measurement, hillslopes are subdivided into concave, convex, and planar regions based on the plan curvature measurement of 0 (Xu et al. 2022). A range of − 4.032 to 4.48 surface curvature values can be found in our study area (Fig. 2c). Using the convergence index, one can determine the perimeters of valleys with negative values and the interfluvial areas with positive values from a morphometric perspective (Fig. 2d). In terms of environmental factors, rainfall is a key factor in determining the genesis of floods (Lu et al. 2024; Yin et al. 2023; Lin et al. 2023). The average rainfall over a multiannual period ranged from 469 to 716 mm in the study area (Fig. 2e). Defining exposure to floods also involves defining the elevation of the land as another very important factor, as it reveals the different levels of water runoff in high and low areas, and thus the differences in exposure to flooding. There are a range of altitudes in the study area, ranging from 1 to 1925 m (Fig. 2f). Aspect is another factor that can have a significant influence on the occurrence of floods. The Eastern and South–Eastern slopes of the study area cover a total area of 30%, and the Eastern slopes cover a total area of 30%, according to (Costache et al. 2020c) (Fig. 3a). Furthermore, along with having a direct effect on the amount of water that is able to infiltrate into valleys, lithology also has a considerable impact on the shape of river valleys (Du & Wang, 2013). Among the twelve lithological categories in the Buzău river basin, the flysch accounts for the largest proportion (25% of the total lithology) (Fig. 3b). There are many flood predictors which use land use information as one of the most important factors because it influences the velocity of surface runoff by changing the Manning roughness coefficients that are used in the model (Singh and Pandey 2021). Nearly seventy-five percent of the study area is covered by arable lands and forests (Fig. 3c). Two other important morphometric factors are TWI (Fig. 3d) and TPI (Fig. 3e). In the Buzau River catchment, the maximum distance between the river and the highest point of the catchment is 10,648 m. As a result, the areas in the catchment are increasingly at risk of flooding due to their proximity to rivers (Fig. 3f).

There is a morphometric variable called Topographic Position Index (TPI) that measures the difference in elevation between the cells of a particular raster with those of its neighbors. The maximum value of the TPI as it pertains to the present research area is equivalent to 153.8, whereas the minimum value is equal to − 122.8 (Fig. 3e). It should be noted that TWI values indicate morphometrically that the flow accumulation is favored above the ground surface in these areas. We found a range of TWI values between 0 and 19.89 in the current study (Fig. 3d).

Methods

Correlation-based feature selection (CFS)

In addition to its fast ability to identify redundant, noisy and irrelevant information, Correlation-based Feature Selection (CFS) has many other important properties (Hall 1999). There can be a high degree of redundancy in a variable when it is correlated with other variables, resulting in a high degree of redundancy. This is due to the fact that the predictors with the highest CFS coefficient values are uncorrelated with each other and have a high degree of correlation to flood locations, which is a result of the fact that they are uncorrelated with other predictors. In order to calculate the CFS, we will use the formula below (Ozcift and Gulten 2011):

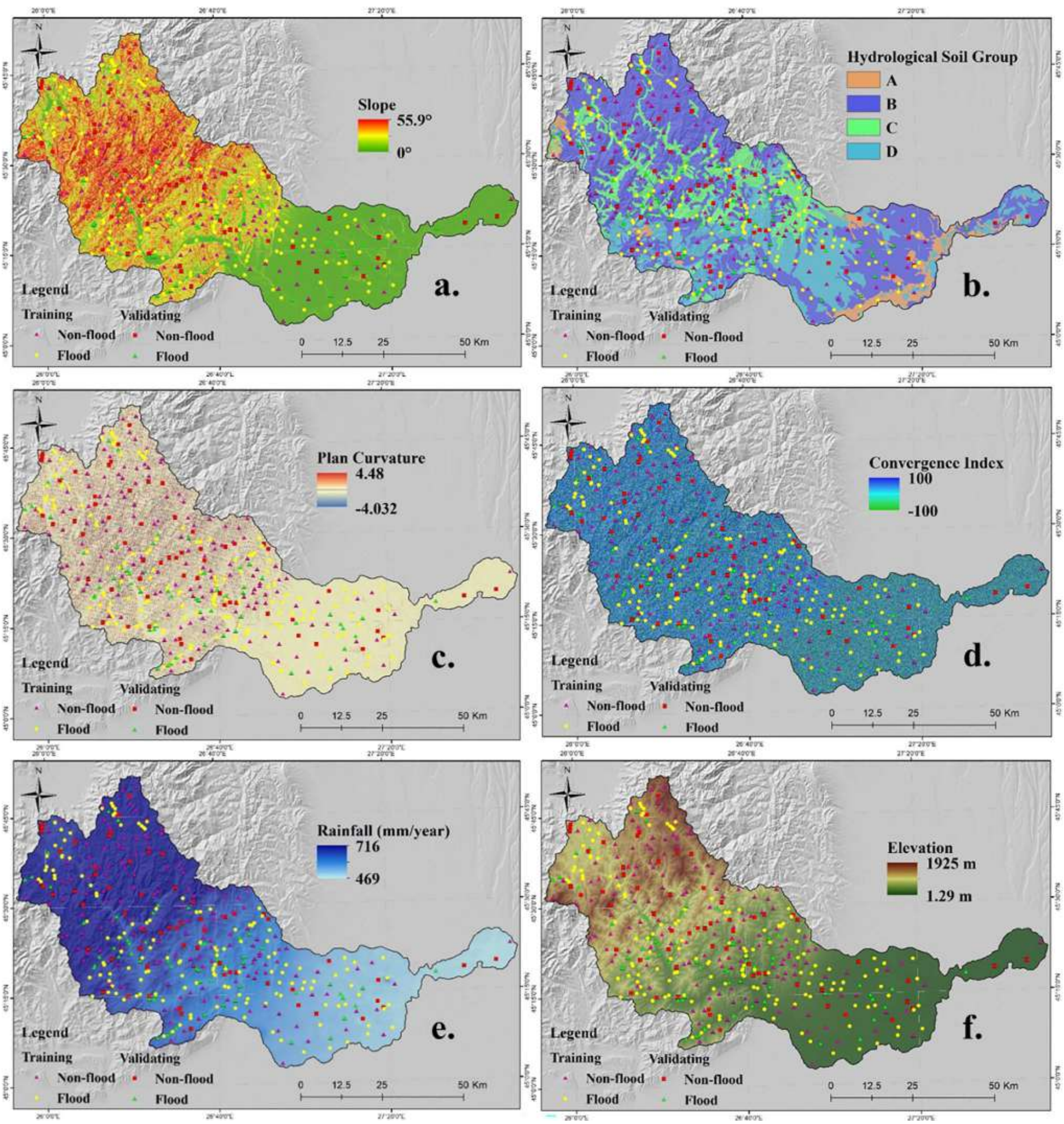

Fig. 2 Flood conditioning factors (**a** slope; **b** hydrological soil group; **c** plan curvature; **d** convergence index; **e** Rainfall; **f** elevation)

$$\mathrm{CFS} = \frac{kr_{\mathrm{cf}}}{\sqrt{k + k(k-1)r_{\mathrm{ff}}}}, \tag{1}$$

where *CFS* represents the Correlation between the conditioning factors and flood points, k represents the amount of conditioning factors, r_{cf} represents the average value of Correlation among the predictors and zones with torrentiality, and r_{ff} is the mean intercorrelation among the flood conditioning factors.

In order to derive the CFS, Weka software was used.

Index of entropy

The entropy of a system is a measure of the degree of disorder and instability, the amount of imbalance and uncertainty within it (Pourghasemi et al. 2012). The Boltzmann principle has been used to describe how the thermodynamic status of

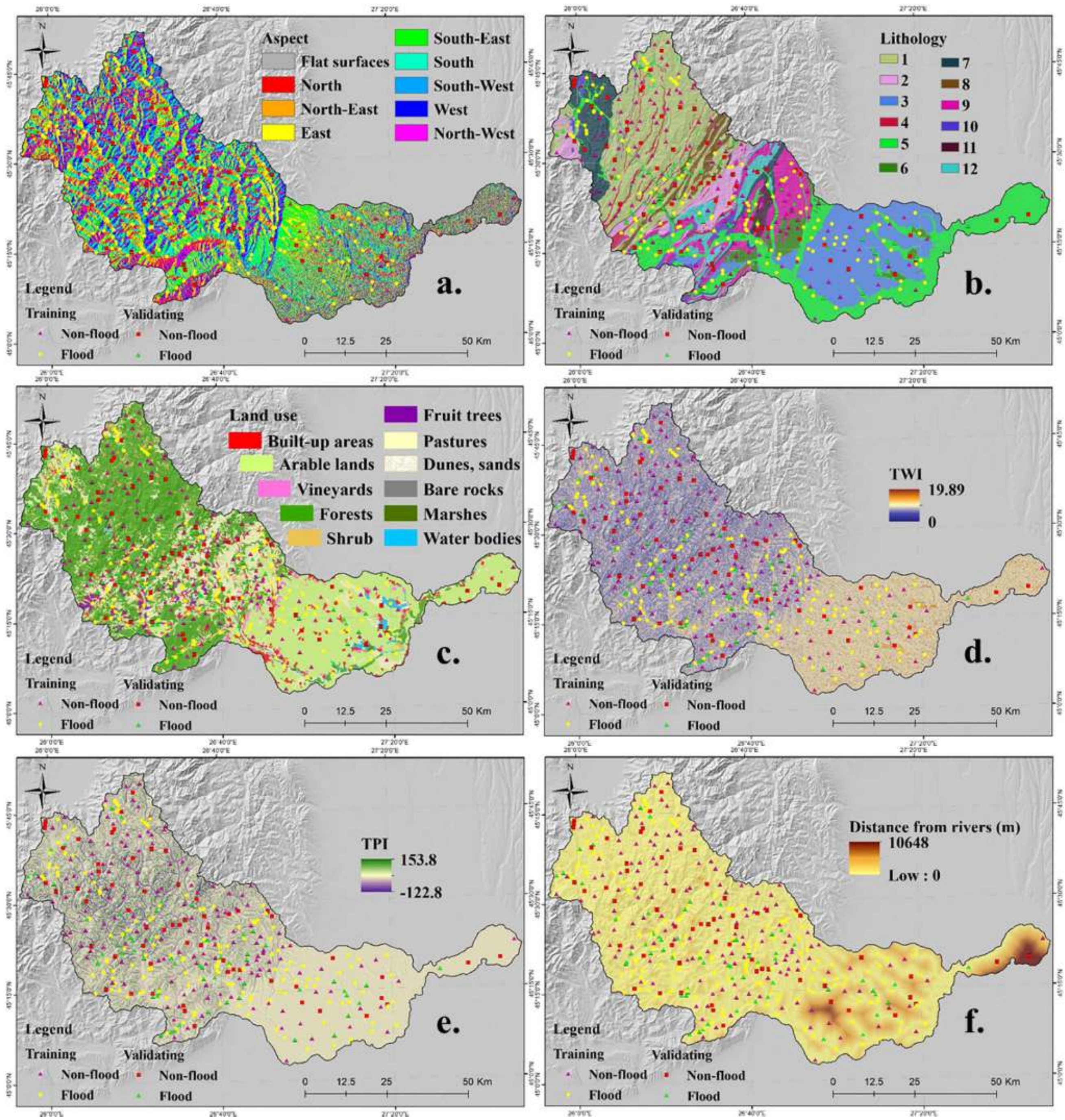

Fig. 3 Flood conditioning factors (**a** aspect; **b** lithology; **c** land use; **d** TWI; **e** TPI; **f** distance from rivers)

a system is determined by the quantity of entropy in the system that demonstrates a one-to-one relationship between the degree of disorder and the quantity of entropy. The Boltzmann principle was improved and the entropy model was introduced to the information theory in Shannon's time. It has been widely accepted that the information entropy method can be used to determine hazard weight indices and to assess natural hazards, such as sand storms, droughts, and debris flows, within an integrated environmental assessment. The degree of entropy of a flood can be defined as the extent to which various factors influence how the flood develops over time (Chen et al. 2015). As a result of a number of important factors, the index system provides an additional degree of entropy. As a result, an objective weight can be determined for the index system by using the entropy value as a basis for the calculation. The next equations will be used to derive the index of entropy coefficients that will be involved as input data in the machine learning models:

$$(P_{ij}) = \frac{FR_{ij}}{\sum_{j=1}^{S_j} FR_{ij}} \tag{2}$$

where FR_{ij} is the Frequency Ratio coefficient for each class or category, S_j is the number of classes and (P_{ij}) is the probability density.

$$H_j = -\sum_{i=1}^{S_j}(P_{ij})\log_2(P_{ij}),\ j = 1, 2, \ldots, n \tag{3}$$

$$H_{j\max} = \log_2(S_j) \tag{4}$$

$$I_j = \frac{H_{j\max} - H_j}{H_{j\max}},\ I = (0,1), j = 1, \ldots, n \tag{5}$$

$$P_j = \frac{1}{S_j}\sum_{i=1}^{S_j} P_{ij} \tag{6}$$

where H_j and $H_{j\max}$ represent the entropy values, I_j is the information coefficient and P_j is the IOE coefficient for each class.

Deep learning neural network (DLNN)

As a machine learning (ML) algorithm, the deep learning neural network (DLNN) has been shown to be efficient at working with large unstructured data sets of all sizes. As part of the studies which are related to the assessment of susceptibility to natural hazards in social communities, the DLNN is a version of the multilayer perceptron neural network. It has a higher number of hidden neurons, which has made it very popular in studies related to the assessment of susceptibility to natural hazards (Yang et al. 2022; Bui et al. 2019a). There are several layers in DLNN when it comes to the input layers which consist of independent variables, and several layers in the hidden layer which transfer the information from the input layer to the output layer (Zhou et al. 2022). It was decided to use the DLNN model to estimate an individual's susceptibility to floods in the current research. It follows that, according to the input layer in the model, the flood conditioning factors simulate the input data, whereas the flood and non-flood data sets simulates the output data in the output layer (Costache et al. 2020b). It was determined that the following sigmoid estimation function $E(Y = 1/x)$ could be used to classify the input data set into torrential pixels (1) and non-torrential pixels (0). In the output layer, there is one neuron per class i. This information provides an approximation of the equation $E(Y = i/x)$ that can be derived from the output layer (Costache et al. 2020b). After summing all the values up, there will be a value equal to one as a result. The following function has been used for the purpose of the present case study:

$$\text{softmax}(a_i) = \frac{\exp(a_i)}{\sum_k \exp(a_i)} \tag{7}$$

where a_i is *softmax* function layer.

The next mathematical relationships are associated to a deep learning neural network having multiple hidden layers (h):

For $h = 1, \ldots, H$ (hidden layers),

$$a^{(h)}(x) = b^{(h)} + W^{(h)}p^{(h-1)}(x) \tag{8}$$

$$p^{(h)}(x) = \varnothing(a^{(h)}(x)) \tag{9}$$

where, $\varnothing$ and is the activation function.

DLNN was applied using a dedicated script in Python language which was written with the help of Keras and Tensorflow packages.

Multilayer perceptron

In the field of artificial neural networks, Multilayer Perceptron (MLP) is one of the most widely used ANNs and it is a multilayer feed-forward network with one-way error propagation. This algorithm is capable of solving a wide range of problems, such as pattern recognition, time series prediction, and so on (Huang 2023; Li et al. 2019). Besides the fact that a flood is a physically complex process, it is also a nonlinear system that is affected by a number of natural factors as well as man-made elements. It thus follows that the MLP model has an excellent nonlinear mapping capability when compared with other techniques for mapping flood susceptibility, such as deterministic models or general linear statistical methods (Kia et al. 2012).

In order for the MLP model to work, it consists of three layers, or input, hidden, and output, which are all composed of the same types of neurons. A weight value is a calculation that determines how the connections are made between the hidden and input layers, as well as between the hidden and output layers. In order to form an orderly and stable structure, neural networks must be trained and tested with these weight values in order for them to be capable of making decisions. In this paper, we mainly examined the MLP model with a single hidden layer, since the MLP with a single hidden layer is able to approximate any nonlinear system with arbitrary accuracy. Specifically, two neurons will be positioned in the output layer representing flood and non-flood points. Input neurons in the input layer will be equal to flood predictor neurons, but output neurons will be equal to flood predictor neurons. The number of hidden neurons will be established according to the lowest RMSE value which will be obtained after the MLP optimization with the help of Harris Hawk Optimization (HHO) algorithm. The RMSE values can be determined using the next equation:

$$\mathrm{RMSE} = \sqrt{\frac{1}{n}\sum_{i=1}^{n}(c_i - \hat{c}_i)^2}, \tag{10}$$

where, n is the number of the flood sample, c_i and $\hat{c}_i$ are the observed flood data and the computed flood susceptibility values, respectively.

Logistic regression

The logistic regression method is one of the most commonly used methods for forming multidimensional regression relationships involving a dependent variable and a number of independent variables (Bai et al. 2010). There is an advantage to logistic regression that is that it can be applied to both continuous and discrete data, and may be a combination of both. The variables are not required to have normal distributions either, due to the addition of a link function to the usual linear regression model. As a result of taking the logit function of the dependent variable (a natural logarithm of the odds of the dependent occurring or not) into consideration, the algorithm of logistic regression utilizes maximum likelihood estimation of the dependent variable (Ali et al. 2020). Using logistic regression, you can estimate the probability of an event occurring on a given day in this way. In logistic regressions, the dependent variables are binary, with their two classes being defined as the presence (1) or absence (0) of the phenomenon being analyzed. The logistic regression model makes a spatial prediction of the susceptibility to this phenomenon based on the spatial relationship between the phenomenon and the factors classes/categories that are considered. According to this study, areas affected by flood locations have been assigned a value of 1 and non-flood locations have been assigned a value of 0. It is possible to calculate the generalized linear regression model using the following equation, which is based on the logistic regression method:

$$p = \frac{1}{1 + e^{-z}} \tag{11}$$

where p represents the likelihood (probability) of an event. Z represents a ranging from $-\infty$ to $+\infty$, which are defined using the next equation:

$$z = b_0 + b_1x_1 + b_2x_2 + \cdots + b_nx_n \tag{12}$$

where b_0 is the intercept of the model, the b_i ($i = 0, 1, 2, \ldots, n$) are the slope coefficients of the logistic regression model, and the x_i ($i = 0, 1, 2, \ldots, n$) are the independent variables.

Classification and regression tree (CART)

Using a recursive partitioning method, Classification and Regression Tree (CART) can be used to predict categorical predictor variables (classification) and continuous dependent variables (regression) by creating a classification tree. Using a CART method, you can present information intuitively and easily to yourself in a visual format that helps you understand what the information means. It is possible to use three types of independent variables to analyze the data (number, binary, and categorical), which makes this technique one of the most powerful and versatile tools available today. For the process of creating trees, each predictor must be selected in such a way that the data errors can be reduced in the process. An entropy value is a measure of how much a particular predictor is preferred over another when compared with other predictors. If a particular predictor's value is missing, the optimal ramification of a tree cannot be determined based on the value of that predictor. Using CART to predict new data, missing values will be handled in a way that is similar to substituting (surrogates) for those values (Breiman et al. 1984). There is an average of the response values within a terminal node when we calculate a predicted value for that node. A sampling rule known as modified towing is part of the CART algorithm, and it is based on comparing the target attribute between two child nodes to determine the optimal sampling rule. Following is the equation that describes how this process is carried out (Costache et al. 2020a):

$$I(\mathrm{Split}) = \left[0.25(q(1-q))^u \sum_k |PL(k) - PR(k)|\right]^2 \tag{13}$$

where: k represents the classes that are targeted, PL(k) and PR(k) are equal to the distribution of probability regarding the target in the left and right child nodes, respectively. The power term represented by u means a user-trollable penalty on splits generating unequal-sized child nodes.

Support vector machine

There are several supervised learning methods based on statistical theory that have been developed in conjunction with structural risk minimization theory. Support vector machine (SVM) is one of them (Ashrafzadeh et al. 2020). There is a decision surface that separates the classes based on the margin between the classes, which is maximized by the decision surface. As a result, the data points closest to the optimal hyperplane are called the support vectors, while the closest

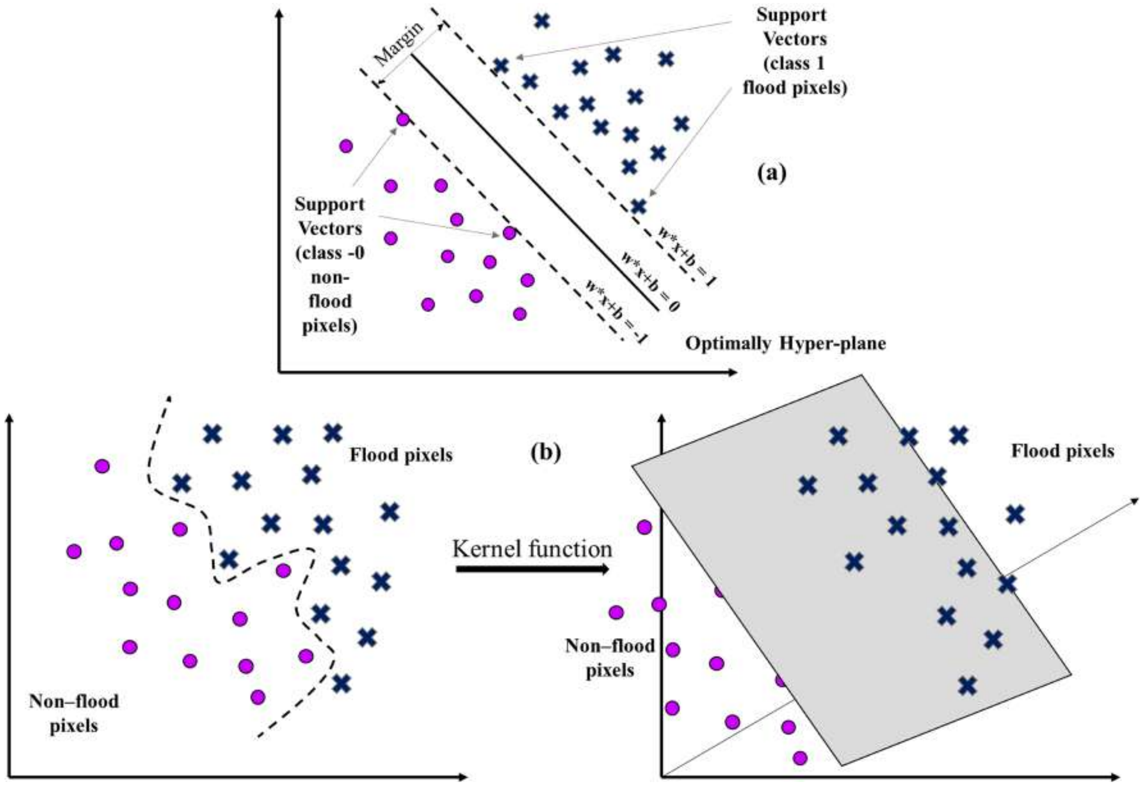

Fig. 4 Optimally hyper-plane (**a** linearly separable; **b** non-linearly separable)

points to the ideal hyperplane are called the optimal hyperplane. There are several critical elements of a training set which are the support vectors (Wei et al. 2022). As a rule of thumb however, SVMs are usually used for two-class classification purposes, where one aims to maximize the margin between the two classes; however, they may also be used for one-class classification purposes, where one tries to identify one of the classes and reject the rest. After that, in order to derive the optimal hyper plane for the feature space, a maximization of the margins of the class boundaries is performed. A support vector is the representation of the training points closest to the optimal hyperplane that are extracted from the training data. In order to classify new data, it is required that the decision surface is generated (Fig. 4a and b).

In the present research work, the support vector machine will contribute to the stacking ensemble along with another 3 models.

Naïve Bayes

Naïve Bayes (NB) is the last model that will be involved in the creation of the stacking ensemble algorithm. Naïve Bayes classifiers are regarded as a classifier based on the Bayes' theorem, which is a highly accurate classification system. The conditional independence assumption is made by the NB classifier when determining the output class (Zhou & Liu, 2022). This is called the assumption that all attributes are totally independent of the output class (Dai et al. 2024; Jiang et al. 2016). Among the many advantages associated with this method, the main one is that it is easy to construct, and complicate iterative parameter estimation schemes are not required as a result of the method (Tien Bui et al. 2012). There is also a high degree of robustness with regards to noise and irrelevant attributes in the NB classifier. In addition to the research field of flood susceptibility mapping, this method has also been applied to the areas of other natural hazards. NB simplifies the learning process significantly due to the assumption that features may be applied to any type of class (Jiang et al. 2016). This is done by using the following relation $P(x, c) = \prod_{i=1}^{n} P\left(x_i|c\right)$, where c is the class while x is the feature vector $x_i = (x_1, x_2, \ldots x_n)$. The variables x_i typically correspond to the predictors of floods, whereas the variables y referred to as the responses to flood points. It is therefore necessary to use Bayes's theorem in order to find the simplest equation which makes the best prediction in order to locate the class with the highest log-posterior probability (Costache et al. 2022c):

$$t_{\mathrm{NB}} = \underset{t_i \in [\text{torrential, no-torrential}]}{\operatorname{argmax}} P\left(t_i\right) \prod_{i=1}^{n} P\left(\frac{f_i}{t_i}\right) \tag{14}$$

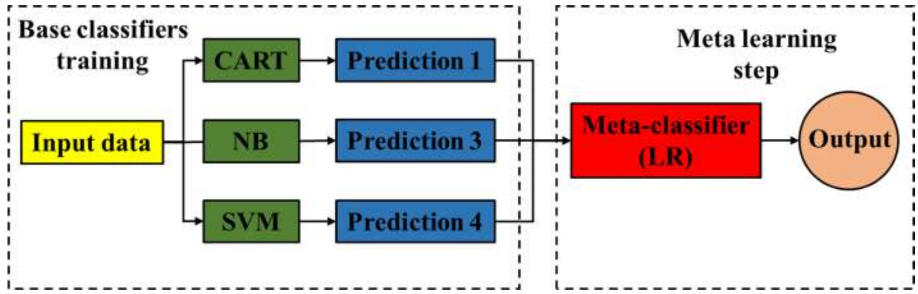

Fig. 5 Stacking ensemble structure

in which, $P(t_i)$ represents the value of t_i prior probability that can be calculated using the proportion of the observed cases with output class.

Stacking ensemble

One of the most popular methods of heterogeneous ensemble learning is the stacking technique, in which metamodels are used that can combine multiple subclassifies in order to produce a prediction that is more accurate based on the combinations of those subclassifies (Fang et al. 2021). It is necessary to point out that in the present case, there are three stages involved in the creation and application of the stacking ensemble (Fig. 5). They are (Costache et al. 2022c): (i) the training of the base classifier models, CART, CART, and SVM; (ii) the collection of the features in the outputs of the base classifiers for generating one new set of training data; (iii) the training of the meta-classifier model, with the help of the Logistic Regression. It is possible to estimate the calculated errors of all the base classifiers simultaneously using stacking ensembles, using the basic learning steps, and then to reduce these residual errors again using the meta-learning steps.

Harris Hawk optimization

Among the swarm-based algorithms, Harris Hawk Optimization was one of the algorithms that was discovered by Heidari et al. (2019). In an effort to satisfy its objectives, the HHO algorithm implements strategies to optimize its goals, which can be compared to the predatory behavior of hawks. It includes two main steps: exploration and exploitation. A Harris Hawk explores its prey from a perch at the feet of another hawk at a random place on the ground. They can then apply a soft or a hard besiegement in order to capture the prey (exploitation step). Accordingly, the HHO algorithm is a procedure inspired by the predatory behavior of hawks and is comprised of two main phases: exploration and exploitation. These two phases are important for optimizing the algorithm's objectives. In the exploration phase a mathematical algorithm determines what it is going to wait for, search for, and discover in order to find the desired hunt. Thus, the iter + *1* (representing the Harris Hawk position) can be determined using the next expression (Cao et al. 2021a; Bui et al. 2019b):

$$X(\text{iter}+1) = \begin{cases} X_{\text{rand}}(\text{iter}) - r_1 \left| X_{\text{rand}}(\text{iter}) - 2r_2 X(\text{iter}) \right. & \text{if } q \geq 0.5 \\ \left(X_{\text{rabit}}(\text{iter}) - X_m(\text{rabit}) \right) - r_3 \left(LB + r_4 (UB - LB) \right) & \text{if } q \geq 0.5 \end{cases} \tag{15}$$

where X_{rabit} is the position of rabbit, iter represent the iteration, X_{rand} is the hawk which was selected randomly from the entire population, r_i, I = 1, 2, 3, 4, q represent the numbers randomly created in the range [0, 1], while X_{m} revealed the mean position for all hawks and can be generated as following:

$$X_m(\text{iter}) = \frac{1}{N} \sum_{i=1}^{N} X_i(\text{iter}) \tag{16}$$

where X_i highlights the place where the hawks are located, while N is the size of hawk.

In the phase of transition between exploration and exploitation, T will be considered as maximum size regarding the repetitions, while E_0 will belong the interval (− 1, 1) and is the initial energy consumed along with each step. In this case HHO will calculate the energy associated to the escape of rabbit (E) using the next equation:

$$E = 2E_0 \left(1 - \frac{\text{iter}}{T} \right) \tag{17}$$

Then, if $|E| \geq 1$, the exploration stage will be started. If not, the solution neighborhood will be intended to be exploited.

In the exploitation phase, a certain parameter "r" is considered as being a measure of the chance that the prey to escape. A value of "r" lower than 0.5 is a successful escape situation. However, if $|E| \geq 0.5$, then then HHO takes soft surround, while is it lower than 0.5 a hard surround is applied (Bui et al. 2019b). In terms of the attack mechanism, the evasion and pursuit strategies of the prey animals, as well as the hawks, play an important role. The Fig. 6 highlights the different stages of HHO.

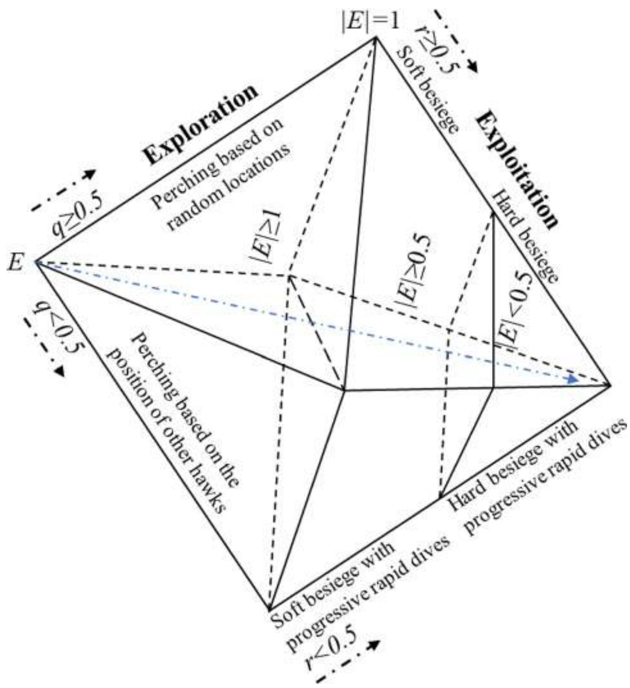

Fig. 6 Different phases of Harris Hawks optimization

Results validation

ROC curve

Two distinct methods were utilized to evaluate the performance of the applied models, namely the ROC Curve in conjunction with the density of flood pixels within each of the flood maps classes. An ROC curve is a graphic that depicts the specificity of a diagnostic test while the sensitivity of the test is represented by the other axis (Cao et al. 2021b). Based on the total number of predicted non-flood locations, specificity refers to the number of flood locations that have been classified incorrectly as flood locations, whereas sensitivity refers to the number of flood locations that have been classified correctly as flood locations as compared to all flood locations. The next equation will be implied for AUC-ROC Curve values calculation:

$$\mathrm{AUC} = \frac{\left(\sum \mathrm{TP} + \sum \mathrm{TN}\right)}{(P + N)} \tag{18}$$

where TP (true positive) is the flood points number that were correctly classified as being floods, TN (true negative) represents the non-flood locations that were classified as being non-floods in a correct manner, P represents number flood locations within the entire study area, while N represents all non-flood locations within the study zone.

Statistical metrics

To validate the results obtained through the four applied models, the 2nd approach that has been taken is to calculate several statistical measures to provide insight into the results obtained through the 3 models. It was already described in the previous subsection about the Sensitivity and Specificity of the test. As part of the current study, a mathematical inference was made about the overall accuracy of the flood susceptibility analysis, in order to determine its relative effectiveness (Panneerselvam et al. 2023a). The Kappa Index is an indicator of the degree of agreement between two raters who create two exclusive categories for both floods and non-floods based on their categorization of the total number of flood and non-flood locations. Below are represented the equations for the statistical metrics:

$$\mathrm{Specificity} = \frac{\mathrm{TN}}{\mathrm{TN} + \mathrm{FP}} \tag{19}$$

$$\mathrm{Sensitivity} = \frac{\mathrm{TP}}{\mathrm{TP} + \mathrm{FN}} \tag{20}$$

$$\mathrm{Accuracy} = \frac{\mathrm{TP} + \mathrm{TN}}{\mathrm{TP} + \mathrm{FP} + \mathrm{TN} + \mathrm{FN}} \tag{21}$$

$$k = \frac{p_{\mathrm{o}} - p_{\mathrm{e}}}{1 - p_{\mathrm{e}}} \tag{22}$$

where FP (false positive) and FN (false negative) are the floods and non-floods pixels not correctly classified, k is kappa coefficient, p_{o} is the observed flood pixels and p_{e} is the estimated flood pixels.

Figure 7 contains the schematically representation of the methodological steps followed in this research.

Results

Feature selection

The results of CFS method revealed that the highest average merit was achieved by slope angle (0.667), followed by Land use (0.632), Plan curvature (0.576), TWI (0.521), Hydrological Soil Group (0.452), Distance to rivers (0.421), TPI (0.394), Elevation (0.377), Lithology (0.332), Convergence index (0.314), Rainfall (0.212) and Aspect (0.182) (Fig. 8).

Taking into account these results, all flood predictors will be considered for the further analysis.

IOE coefficients

In order to encode the classes and categories of flood predictors the Index of Entropy (P_{ij}) coefficients were

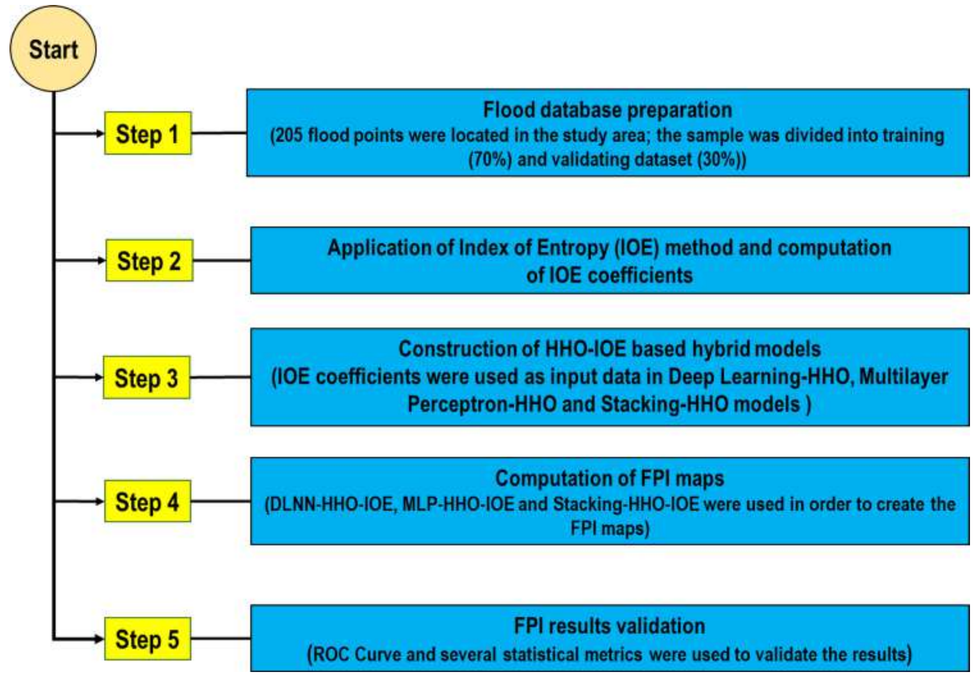

Fig. 7 Flowchart of the methodological workflow

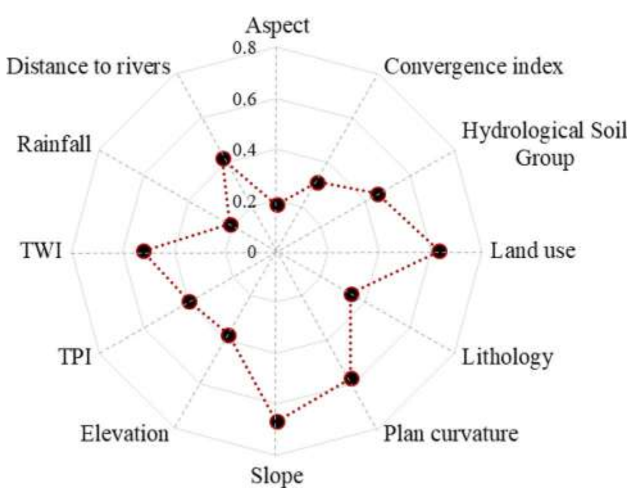

Fig. 8 Average merit of flood predictors calculated using CFS method

calculated. The highest IOE coefficient of 0.7, was achieved by TWI class between 10.68 and 19.89, followed by: slope class between 3.1 and 7° ((P_{ij}) = 0.57), TPI class between – 122.8 and – 34.2 ((P_{ij}) = 0.53), distance from river class between 0 and 50 m ((P_{ij}) = 0.53), land use category of water bodies ((P_{ij}) = 0.5) and plan curvature class between – 0.09 and 0.1 ((P_{ij}) = 0.49) (Table 1). The lowest values of this bivariate statistic were equal to 0 and was obtained by 11 flood predictor class/categories in which the flood points are missing. These IOE coefficients were further inserted as input data in the machine learning models in order to derive the flood susceptibility.

DLNN-IOE-HHO

The HHO algorithm was able to optimize the performances of DLNN model determining the loss and accuracy to reach very good values after the application of 100 epochs. Thus, the minimum loss, in terms of training sample was equal to 0.168 and was reached after 82 epochs, while in terms of validating data sample the minimum loss was 0.155 and was obtained after 91 epochs (Fig. 9a). If we discuss about the accuracy, it can be observed that the maximum value in terms of training sample was obtained after 63 epochs, while for validating dataset the optimum accuracy of 0.97 was achieved after 38 epochs (Fig. 9b). The architecture established based on a batch size of 100, a validation rate of 0.3 and a dropout rate of 0.3, is characterized by a number of 3 hidden layers, each of them with 89 hidden neurons. Obviously, the input layer contains 12 neurons and the output layer a number of 2 neurons (Fig. 9c).

In the last step, before the flood susceptibility computation for each of the flood predictors the importance was determined as following: Slope (19.35), Distance from river (17.63), Land use (12.1), TPI (10.3), Lithology (9.54), Plan curvature (8.32), Rainfall (6.53), Aspect (6.42), Elevation (5.32), Convergence Index (3.98), HSG (3.55) and TWI (1.96) (Fig. 10).

All the importance values were used in Map Algebra from ArcGIS software in order to create the flood susceptibility map through DLNN-HHO-IOE model. The $FPI_{DLNN\text{-}HHO\text{-}IOE}$ values were classified into 5 classes using Natural Breaks (Fig. 11a). According to the results provided, the very low

Table 1 Frequency ratio and index of entropy coefficients value distribution within flood conditioning factors classes/category

Factor	Class	Flood pixels	Class pixels	FR, P_{ij}	(P_{ij})	H_j	$H_{j\max}$	I_j	P_j
Plan curvature	(−4.03)–(−0.1)	22	813760	1.12	0.47	0.36	1.58	0.77	0.79
	(−0.09)–0.1	120	4229391	1.17	0.49				
	0.11–4.48	2	902090	0.09	0.04				
Slope (°)	0–3	98	2096422	1.93	0.40	0.34	2.32	0.85	0.96
	3.1–7	40	606526	2.72	0.57				
	7.1–15	6	1946782	0.13	0.03				
	15.1–25	0	1093638	0.00	0.00				
	25–55	0	201873	0.00	0.00				
TPI	(−122.8)–(−34.2)	32	389408	3.39	0.53	0.41	2.32	0.82	1.29
	(−34.1)–(−11.5)	59	1025382	2.38	0.37				
	(−11.4)–10.1	53	3214449	0.68	0.11				
	10.2–37.1	0	935266	0.00	0.00				
	37.2–153.8	0	380736	0.00	0.00				
C.I	(−100)–(−3)	78	1721674	1.87	0.46	0.61	2.32	0.74	0.81
	(−2.9)–(−2)	3	247790	0.50	0.12				
	(−1.9)–(−1)	2	336023	0.25	0.06				
	(−0.9)–0	12	644210	0.77	0.19				
	0.1–100	49	2995542	0.68	0.17				
Hydrological soil group	A	7	341746	0.85	0.22	0.60	2.00	0.70	0.95
	B	83	3242969	1.06	0.28				
	C	26	1071383	1.00	0.26				
	D	28	1289141	0.90	0.24				
Aspect	Flat surfaces	1	72784	0.57	0.08	0.99	3.17	0.69	0.93
	North	6	524887	0.47	0.06				
	North–East	20	694741	1.19	0.16				
	East	26	903945	1.19	0.16				
	South–East	24	899875	1.10	0.15				
	South	21	793016	1.09	0.15				
	South–West	18	737885	1.01	0.13				
	West	16	742253	0.89	0.12				
	North–West	12	575855	0.86	0.11				
Land use	Built-up areas	30	273759	4.52	0.26	0.46	3.17	0.86	1.97
	Agriculture areas	46	1840323	1.03	0.06				
	Vineyards	1	53415	0.77	0.04				
	Fruit trees	0	90234	0.00	0.00				
	Pastures	34	983962	1.43	0.08				
	Forests	11	2421852	0.19	0.01				
	Shrub	4	186818	0.88	0.05				
	Inland marshes	0	11138	0.00	0.00				
	Water bodies	18	83580	8.89	0.50				
Distance from river (m)	0–50	81	526369	6.35	0.53	0.55	3.00	0.82	1.49
	50–100	25	416254	2.48	0.21				
	100–150	16	454203	1.45	0.12				
	150–200	12	367919	1.35	0.11				
	200–400	9	1285190	0.29	0.02				
	400–700	1	1185694	0.03	0.00				
	700–1000	0	593507	0.00	0.00				
	> 1000	0	1115667	0.00	0.00				

Table 1 (continued)

Factor	Class	Flood pixels	Class pixels	FR, P_{ij}	(P_{ij})	H_j	$H_{j\max}$	I_j	P_j
Elevation (m)	2–200	48	1951514	1.02	0.16	0.72	3.00	0.76	0.79
	200–400	46	884762	2.15	0.34				
	400–600	17	803057	0.87	0.14				
	600–800	20	602552	1.37	0.22				
	800–1000	2	647751	0.13	0.02				
	1000–1200	10	611209	0.68	0.11				
	1200–1400	1	332459	0.12	0.02				
	> 1400	0	111937	0.00	0.00				
Rainfall (mm/year)	460–500	16	985015	0.67	0.09	0.72	3.00	0.76	0.88
	500–600	12	695309	0.71	0.10				
	600–700	43	909395	1.95	0.28				
	700–800	24	818862	1.21	0.17				
	800–900	32	832149	1.59	0.22				
	900–1000	12	801234	0.62	0.09				
	1000–1100	5	668968	0.31	0.04				
	1100–1160	0	233051	0.00	0.00				
Lithology	1	17	1517652	0.46	0.05	1.00	3.58	0.72	0.77
	2	5	404793	0.51	0.06				
	3	14	484363	1.19	0.13				
	4	1	57639	0.72	0.08				
	5	5	302091	0.68	0.07				
	6	3	194118	0.64	0.07				
	7	71	1218,884	2.40	0.26				
	8	2	260019	0.32	0.03				
	9	1	98442	0.42	0.05				
	10	2	178269	0.46	0.05				
	11	2	141858	0.58	0.06				
	12	21	1087113	0.80	0.09				
TWI	−0.37–3.05	6	2013896	0.12	0.01	0.41	2.32	0.82	3.05
	3.06–4.8	46	2421166	0.78	0.05				
	4.81–7.02	51	1023282	2.06	0.13				
	7.03–10.67	15	386558	1.60	0.10				
	10.68–19.89	26	100339	10.7	0.70				

flood potential values appear on around 17.44% of the study area, while the low flood potential is present on 19.43% of the entire territory. Medium class of flood potential has a percentage equivalent with 27.56%, while, together, the high and very high flood susceptibility is spread on 35.57% Buzău river basin (Fig. 12).

MLP-IOE-HHO

By the optimization procedure of MLP model, using HHO algorithm, the final results proved to be very performant This situation is highlighted by the metrics like pseudo-probability (Fig. 13a) which confirm the performance of classification the flood and non-flood points. Also, the Lift chart (Fig. 13b), ROC Curve (Fig. 13c) and Gain chart (Fig. 13d) emphasize the very good quality of flood and non-flood pixels classification. Additionally, very low value of RMSE (0.019) is corresponding with an architecture containing 35 hidden neurons (Fig. 13e). The importance assigned to the flood predictors revealed the next situation: Distance from river (18.3), Slope (17.93), Land use (14.32), TPI (13.24), Lithology (11.23), Rainfall (7.72), Convergence Index (6.04), HSG (5.67), Plan curvature (5.21), TWI (4.37), Aspect (4.2) and Elevation (3.21) (Fig. 10).

Fig. 9 IOE-DLNN-HHO properties (**a** loss; **b** accuracy; **c** architecture)

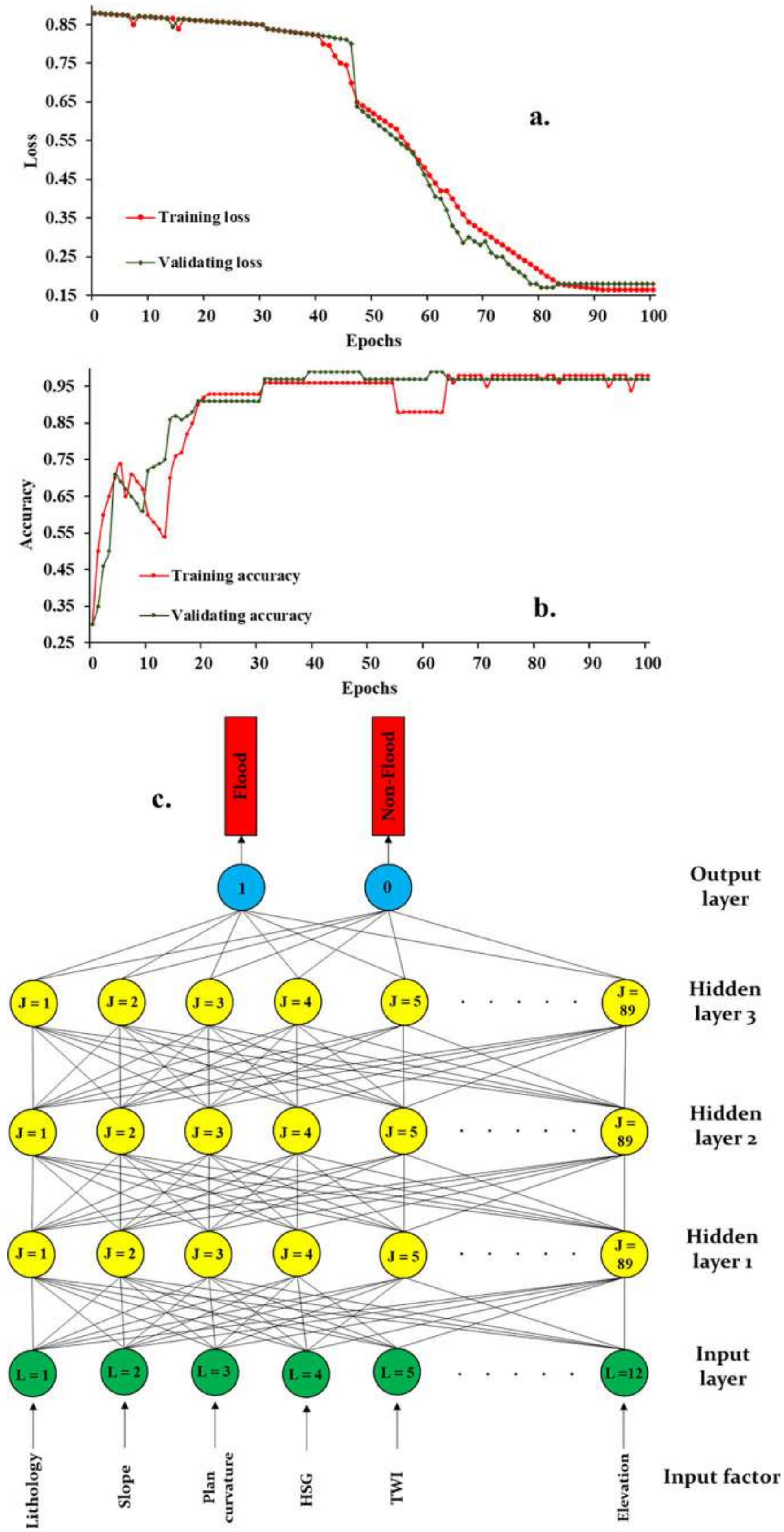

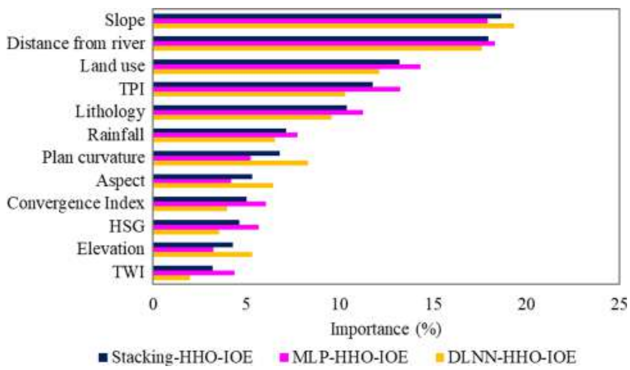

Fig. 10 Importance of flood predictors in terms of flood susceptibility

Like in the previous case, the $FPI_{MLP\text{-}HHO\text{-}IOE}$ was calculated by including the importance of each flood predictor into Map Algebra capabilities. Also, its values were split into 5 classes using the Natural Breaks method. The very low flood potential accounts 22.41% of Buzău river basin, while the low flood potential spans on 21.77% of the same area. Further, it can be seen that medium values of flood potential appears on around 19.72%, while the high and very high flood potential appear on 36.2% (Fig. 11b).

Stacking-HHO-IOE

In a first stage, the Stacking ensemble was created by the combination of of CART, NB and SVM models, having as meta-classifier the Logistic Regression (LR) model. The Stacking ensemble performances were further improved with the help of HHO algorithm. In terms of Stacking-HHO-IOE hybrid combination the highest importance was assigned to Slope angle (18.64), followed by Distance from river (17.965), Land use (13.21), TPI (11.77), Lithology (10.385), Rainfall (7.125), Plan curvature (6.765), Aspect (5.31), Convergence Index (5.01), Hydrological Soil Group (4.61), Elevation (4.265) and TWI (3.165) (Fig. 10).

The obtaining process of $FPI_{Stacking\text{-}HHO\text{-}IOE}$ values assumes the involvement of flood predictors importance into the Map Algebra application (Fig. 11c). Its values, split into 5 class with the Natural Breaks method, revealed that

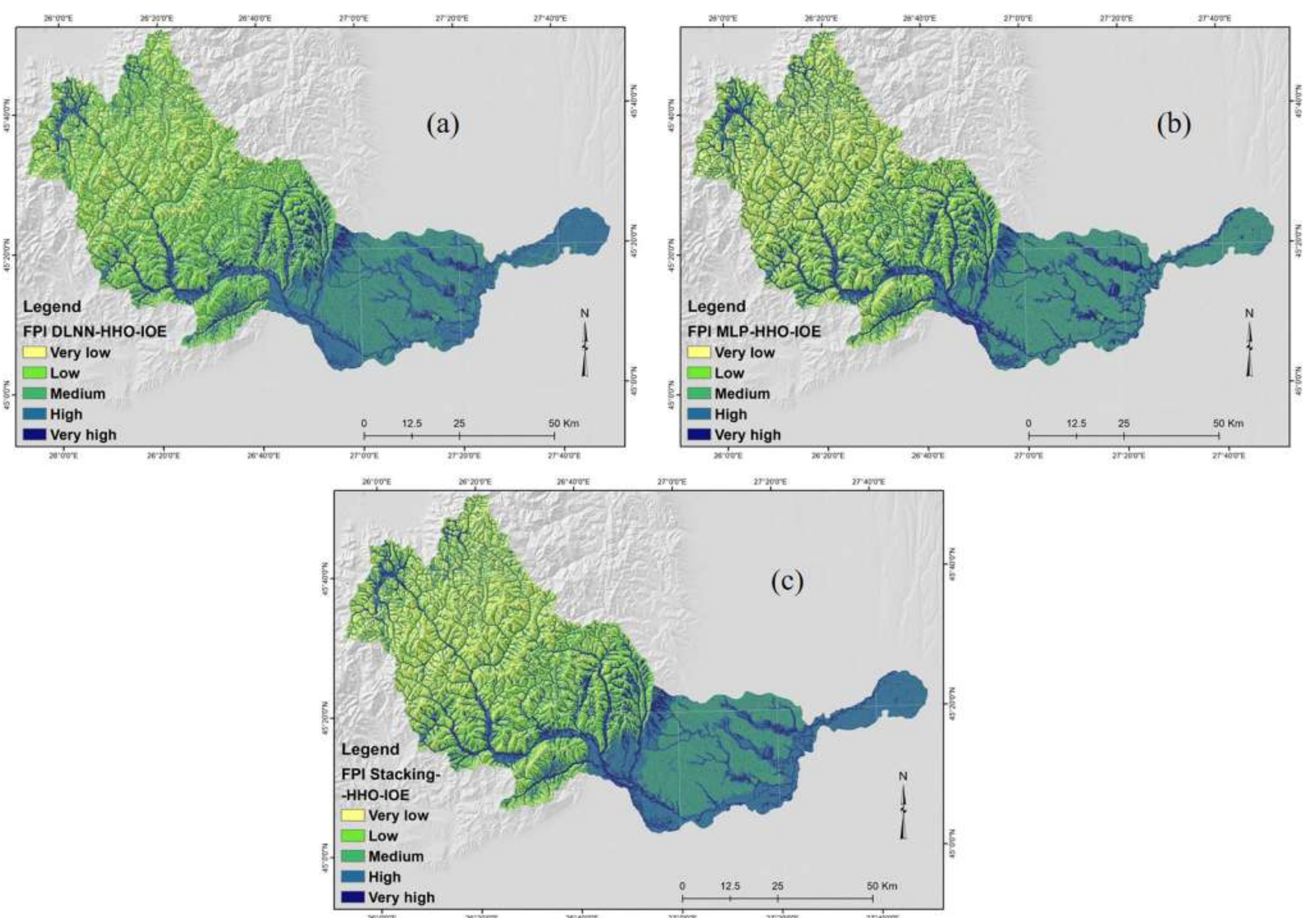

Fig. 11 Flood Potential Index (**a** FPI DLNN-HHO-IOE; **b** FPI MLP-HHO-IOE; **c** FPI Stacking-HHO-IOE)

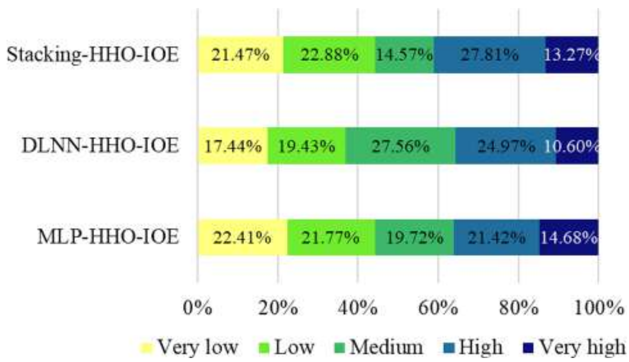

Fig. 12 Weights of FPI classes

very low potential is spread on 21.47% of Buzău river basin. The same index shows that low flood potential appears on 22.88% of the study zone, while the medium values are located on a percentage of 14.57%. Taken together the high and very high flood potential cover 41.08% of the study area.

Results validation

ROC Curve method implied the construction of both Success and Prediction Rate. According to the Success Rate AUC values, the highest performance was achieved $FPI_{DLNN\text{-}HHO\text{-}IOE}$ (AUC = 0.97), followed by $FPI_{Stacking\text{-}HHO\text{-}IOE}$ (AUC = 0.966) and $FPI_{MLP\text{-}HHO\text{-}IOE}$ (AUC = 0.953) (Fig. 14a). Figure 14b highlights the $FPI_{Stacking\text{-}HHO\text{-}IOE}$ as being the most performant model with an AUC of 0.977, followed by $FPI_{DLNN\text{-}HHO\text{-}IOE}$ (AUC = 0.97) and $FPI_{MLP\text{-}HHO\text{-}IOE}$ (AUC = 0.924).

The second stage of results validation procedure was accomplished with the help of several statistical metrics. Thus, in terms of training sample, the highest accuracy of 0.941 was achieved by DLNN-HHO-IOE, followed by Stacking-HHO-IOE (0.934) and MLP-HHO-IOE (0.927). The use of the same sample revealed a *K*-index equal to 0.882 for DLNN-HHO-IOE model, 0.868 for Stacking-HHO-IOE and 0.854 for MLP-HHO-IOE. In terms of validating data set, the best value of accuracy was attributed to DLNN-HHO-IOE (0.926), followed by Stacking-HHO-IOE (0.918) and MLP-HHO-IOE (0.91). The highest K-index was assigned to DLNN-HHO-IOE (0.852), followed by Stacking-HHO-IOE (0.836) and MLP-HHO-IOE (0.82) (Table 2).

Discussions

In today's society, floods are considered to be one of the most dangerous and complex natural disasters due to their short occurrence time, high-speed water runoff, as well as great sediment transportation, which can lead to severe damage to property and the loss of human life in a matter of seconds (Ruidas et al. 2022). Also, if there are some specific characteristics like groundwater level very close to the terrain altitude, the damages will be higher due to the fact that the amount of water will last more time at the ground surface (Balamurugan et al. 2020b; Panneerselvam et al. 2020). There is, however, no method that can completely prevent its occurrence. Due to this need, the development of flood prediction and mitigation strategies is crucial to reducing the risk of human deaths from floods and reducing the socioeconomic impacts of these events, which present several challenges for local authorities. Researchers have attempted to develop a proper mitigation strategy for floods in several different ways (Huang et al. 2022); among them is the Flood Susceptibility Mapping, which is one of the most crucial flood mitigation strategies available to help identify flood prone areas and to implement appropriate structural and nonstructural procedures that will minimize the impact of flooding in these areas (Mehryar and Surminski 2022). It has been discovered that there are several methods and modeling approaches that can be utilized to determine flood areas (Zhang et al. 2022). However, it is also very important to identify those methods that have more predictability and liability so that flooding can be prevented in the future. In the recent era, the field of Artificial Intelligence and Machine Learning algorithms has attracted considerable attention, particularly for the purpose of predicting environmental hazards (Pande et al. 2021); this is due to the accuracy of their predictions and the ability to work with very large datasets which are less costly. The results produced by each of these methods have been optimal on the basis of appropriate flood affecting factors in the region concerned. The Flood Susceptibility Mapping (FSM) has undergone substantial improvements over the last decade; however, improvements are still needed to improve the capability of the system to map flash floods. Machine Learning algorithms have been found to achieve similar accuracy compared to a number of existing methods of modeling flood probability, as well as differentiating the relationship between the environment effect and flooding incidence (Zhao et al. 2022). In a flood, geological conditions, hydrological conditions, morphological conditions, and topographical features play an important part in the entire phenomenon. Although, it is widely accepted that only a small number of factors contribute significantly to causing flood events in a particular area, thus choosing the right factors is an essential step in the Flood Susceptibility Mapping. In this study a number of 12 flood predictors were selected to be involved in the modeling procedure. From them, the most important factors revealed to be the Slope angle, Distance from river, Land use and Lithology (Chowdhuri et al. 2020). These factors achieved

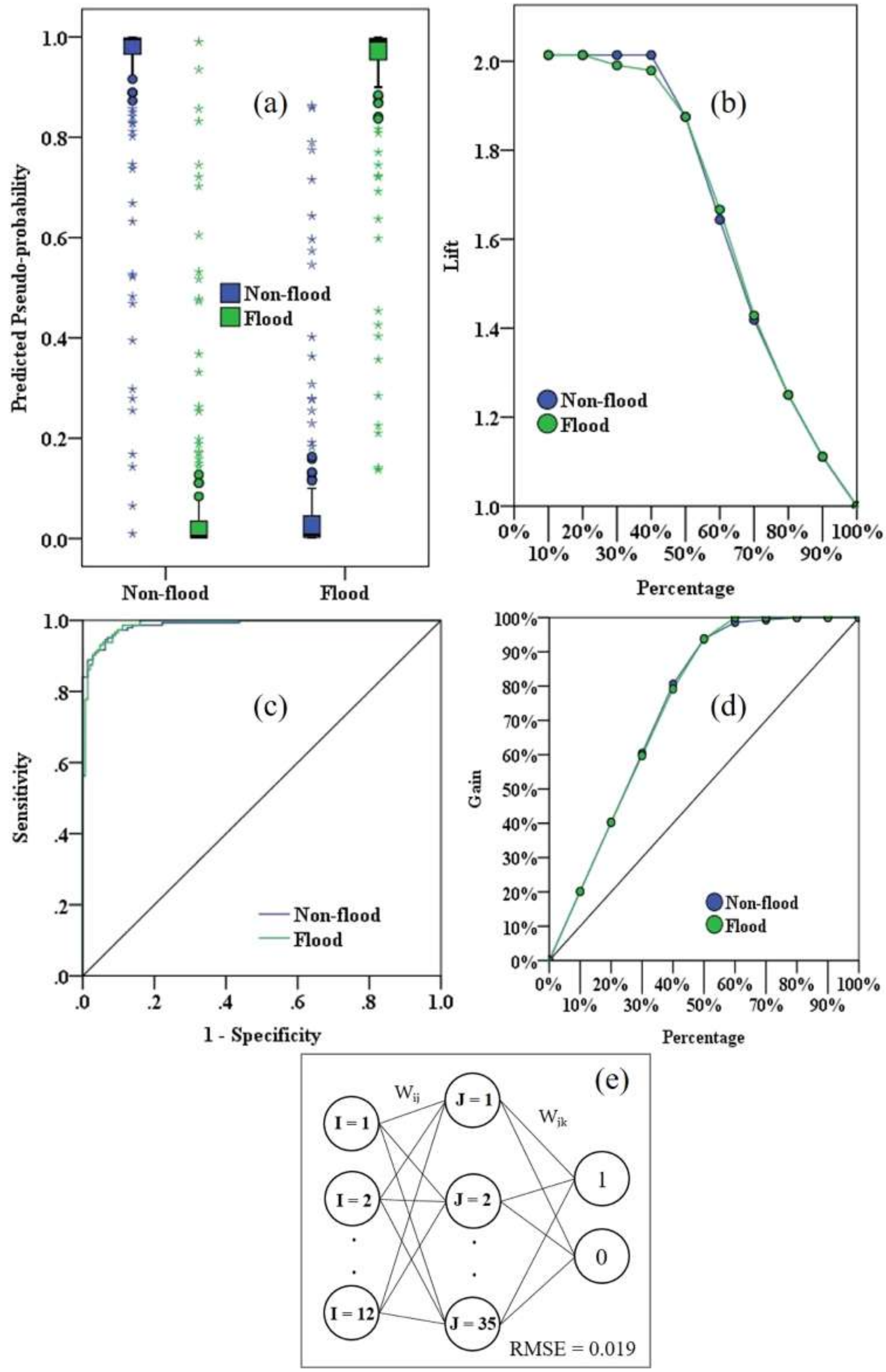

Fig. 13 Multilayer perceptron outputs (**a** pseudo-probability; **b** lift chart; **c** ROC curve; **d** gain chart; **e** architecture)

the highest importance values in terms of all the three complex models that were applied in this research work. The results is in a partially agreement with those achieved by Costache et al. (2020b). In the aforementioned research work, the application of Support Vector Machine (SVM)—IOE ensemble showed that distance from river obtained the highest importance, followed by slope angle, land use and lithology. The use of Harris Hawk Optimization algorithm

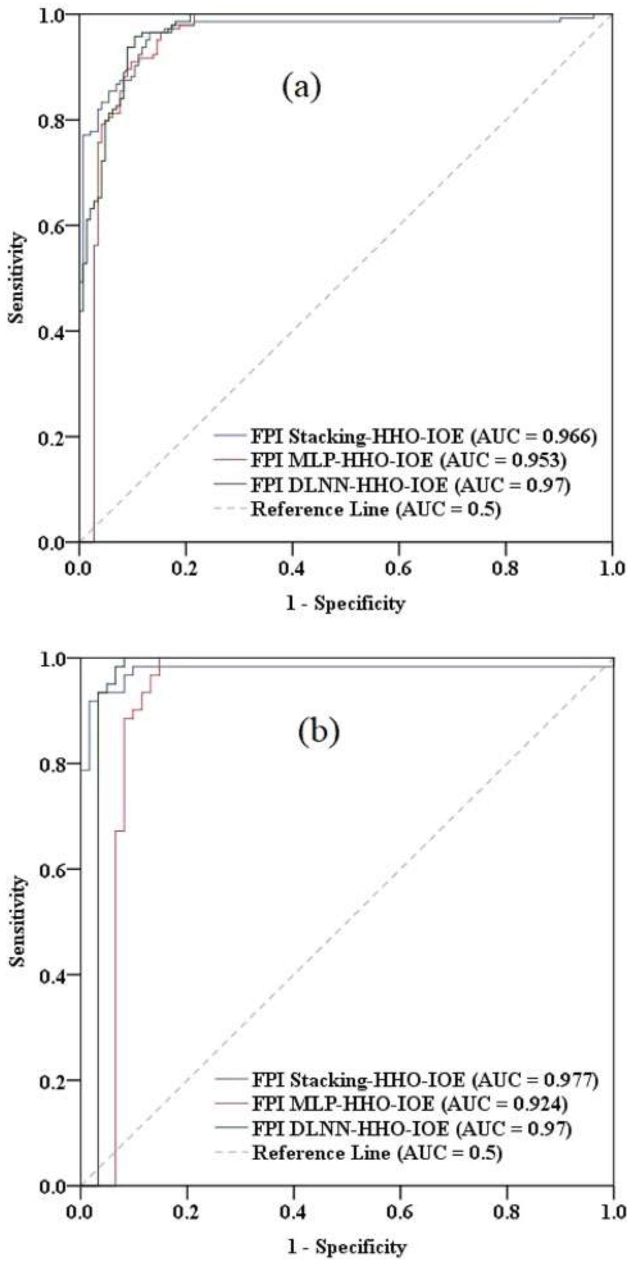

Fig. 14 ROC curves (**a** success rate; **b** prediction rate)

in the present study played a crucial role in the improvement of model's prediction accuracy. The same optimization algorithm was also successfully used by Paryani et al. (2021) that estimated the landslide susceptibility in Middle Zagros Mountain Range. The results of flood potential estimated over the Buzău river basin from Romania, shows that the most prone regions to flood occurence are located along the main river valleys and also within the main hilly and mountain depressions from the study zone.

There is always a possibility of uncertainty in any scientific model, which may induce some limitations to the results of a specific analysis. Input data or model parameters may be the source of limitation. The spatial representation of flood conditioning factors can lead to inherent errors in the present study, as well as in similar studies. Although the models used for flood susceptibility prediction performed very well, these results make it clear that any errors in input data or model parameters are minimal.

Conclusions

The present research aimed to propose three new optimized ensembles to evaluate the flood susceptibility within Buzău river basin from Romania. The study area represents a complex region that equally covers the mountain hilly and plain zones. In a first phase of the study, a number of 205 locations were collected where floods occurred in the past within the study area. At the same time, 12 flood predictors were selected as input data in the artificial intelligence models, whose ability to predict floods was tested by the Correlation-based Feature Selection method. By applying the prediction capacity evaluation method, all factors proposed were found to be important to some extent for the occurrence of flooding. Following the calculation of the index of entropy coefficients, the flood potential calculation models were developed based on their values. The highest performances, in terms of modeling procedure, was achieved by DLNN-HHO-IOE and Stacking-HHO-IOE models with values of AUC equal to 0.97 and 0.977, respectively. It should be noted also the coverage of high and very high flood potential that range from 35.57%, in the case of DLNN-HHO-IOE, to 41.09% in the case of Stacking-HHO-IOE.

The main novelty of the present research is represented by the combination of artificial intelligence models like DLNN, MLP and Stacking ensemble with Harris Hawk Optimization algorithm. The very high quality of the results makes this research a benchmark for the future studies related to the natural hazards susceptibility. Moreover, the results of this study can be very useful to the local and central authorities which are in charge with the flood mitigation measures.

Table 2 Statistical metrics involved in the evaluation of models' performance

	Training sample			Validating sample		
	DLNN-HHO-IOE	MLP-HHO-IOE	Stacking-HHO-IOE	DLNN-HHO-IOE	MLP-HHO-IOE	Stacking-HHO-IOE
TP	135	133	135	57	55	56
TN	136	134	134	56	56	56
FP	9	11	9	4	6	5
FN	8	10	10	5	5	5
Sensitivity	0.944	0.930	0.931	0.919	0.917	0.918
Specificity	0.938	0.924	0.937	0.933	0.903	0.918
Accuracy	0.941	0.927	0.934	0.926	0.910	0.918
K	0.882	0.854	0.868	0.852	0.820	0.836

Acknowledgements The authors extend their appreciation to Abdullah Alrushaid Chair for Earth Science Remote Sensing Research for funding.

Author contributions RC contributed to Methodology, RC, SCP, CBP, ARMTI, FA and HGA contributed to Formal analysis and investigation, RC, SCP, CBP, ARMTI, FA and HGA contributed to Writing—original draft preparation, RC, SCP, CBP, ARMTI, FA and HGA contributed to Writing—review and editing, RC, ARMTI, FA and HGA contributed to Supervision. All authors have read and agreed to the published version of the manuscript.

Funding This research was funded by Abdullah Alrushaid Chair for Earth Science Remote Sensing Research at King Saud University, Riyadh, Saudi Arabia.

Data availability The data that support the findings of this study are available on request from the corresponding author.

Declarations

Conflict of interest The authors have no conflicts of interest to declare.

Research involving Human Participants and/or Animals Not applicable.

Informed consent Not applicable.

References

Abdo HG (2020) Evolving a total-evaluation map of flash flood hazard for hydro-prioritization based on geohydromorphometric parameters and GIS–RS manner in Al-Hussain river basin Tartous Syria. Nat Hazards 104(1):681–703. https://doi.org/10.1007/s11069-020-04186-3

Ali SA, Parvin F, Pham QB, Vojtek M, Vojteková J, Costache R, Linh NTT, Nguyen HQ, Ahmad A, Ghorbani MA (2020) GIS-based comparative assessment of flood susceptibility mapping using hybrid multi-criteria decision-making approach, naïve Bayes tree, bivariate statistics and logistic regression: a case of Topľa basin. Slovakia Ecol Indic 117:106620. https://doi.org/10.1016/j.ecolind.2020.106620

Arora A, Arabameri A, Pandey M, Siddiqui MA, Shukla U, Bui DT, Mishra VN, Bhardwaj A (2021) Optimization of state-of-the-art fuzzy-metaheuristic ANFIS-based machine learning models for flood susceptibility prediction mapping in the middle Ganga Plain, India. Sci Total Environ 750:141565

Ashrafzadeh A, Kişi O, Aghelpour P, Biazar SM, Masouleh MA (2020) Comparative study of time series models, support vector machines, and GMDH in forecasting long-term evapotranspiration rates in northern Iran. J Irrig Drain Eng 146:04020010

Bai S-B, Wang J, Lü G-N, Zhou P-G, Hou S-S, Xu S-N (2010) GIS-based logistic regression for landslide susceptibility mapping of the Zhongxian segment in the Three Gorges area, China. Geomorphology 115:23–31

Balamurugan P, Kumar PS, Shankar K (2020a) Dataset on the suitability of groundwater for drinking and irrigation purposes in the Sarabanga river region, Tamil Nadu. India Data in Brief 29:105255. https://doi.org/10.1016/j.dib.2020.105255

Balamurugan P, Kumar PS, Shankar K, Nagavinothini R, Vijayasurya K, Balamurugan P, Kumar PS, Shankar K, Nagavinothini R, Vijayasurya K (2020b) Non-carcinogenic risk assessment of groundwater in southern part of Salem district in Tamilnadu, India. J Chil Chem Soc 65:4697–4707. https://doi.org/10.4067/S0717-97072020000104697

Breiman L, Friedman JH, Olshen RA, Stone CJ (1984) Classification and regression trees. Wadsworth International Group, Belmont, CA, pp 151–166

Bui DT, Hoang N-D, Martínez-Álvarez F, Ngo P-TT, Hoa PV, Pham TD, Samui P, Costache R (2019) A novel deep learning neural network approach for predicting flash flood susceptibility: a case study at a high frequency tropical storm area. Sci Total Environ 701:134413

Bui DT, Moayedi H, Kalantar B, Osouli A, Pradhan B, Nguyen H, Rashid ASA (2019b) A novel swarm intelligence—Harris hawks optimization for spatial assessment of landslide susceptibility. Sensors 19:3590

Bui Q-T, Nguyen Q-H, Nguyen XL, Pham VD, Nguyen HD, Pham V-M (2020) Verification of novel integrations of swarm intelligence algorithms into deep learning neural network for flood

susceptibility mapping. J Hydrol 581:124379. https://doi.org/10.1016/j.jhydrol.2019.124379
Cao B, Zhao J, Lv Z, Yang P (2021a) Diversified personalized recommendation optimization based on mobile data. IEEE Trans Intell Transp Syst 22(4):2133–2139. https://doi.org/10.1109/TITS.2020.3040909
Cao B, Gu Y, Lv Z, Yang S, Zhao J, Li Y (2021b) RFID reader anticollision based on distributed parallel particle swarm optimization. IEEE Internet Things J 8(5):3099–3107. https://doi.org/10.1109/JIOT.2020.3033473
Chen W, Li W, Hou E, Bai H, Chai H, Wang D, Cui X, Wang Q (2015) Application of frequency ratio, statistical index, and index of entropy models and their comparison in landslide susceptibility mapping for the Baozhong region of Baoji, China. Arab J Geosci 8:1829–1841
Chowdhuri I, Pal SC, Chakrabortty R (2020) Flood susceptibility mapping by ensemble evidential belief function and binomial logistic regression model on river basin of eastern India. Adv Space Res 65:1466–1489
Costache R, Hong H, Pham QB (2020a) Comparative assessment of the flash-flood potential within small mountain catchments using bivariate statistics and their novel hybrid integration with machine learning models. Sci Total Environ 711:134514. https://doi.org/10.1016/j.scitotenv.2019.134514
Costache R, Ngo PTT, Bui DT (2020b) Novel ensembles of deep learning neural network and statistical learning for flash-flood susceptibility mapping. Water 12:1549
Costache R, Popa MC, Bui DT, Diaconu DC, Ciubotaru N, Minea G, Pham QB (2020) Spatial predicting of flood potential areas using novel hybridizations of fuzzy decision-making, bivariate statistics, and machine learning. J Hydrol 585:124808
Costache R, Arabameri A, Elkhrachy I, Ghorbanzadeh O, Pham QB (2021) Detection of areas prone to flood risk using state-of-the-art machine learning models. Geomat Nat Haz Risk 12:1488–1507
Costache R, Pham QB, Arabameri A, Diaconu DC, Costache I, Crăciun A, Ciobotaru N, Pandey M, Arora A, Ali SA (2022a) Flash-flood propagation susceptibility estimation using weights of evidence and their novel ensembles with multicriteria decision making and machine learning. Geocarto Int 37:8361–8393
Costache R, Tin TT, Arabameri A, Crăciun A, Ajin R, Costache I, Islam ARMT, Abba S, Sahana M, Avand M (2022b) Flash-flood hazard using deep learning based on H2O R package and fuzzy-multicriteria decision-making analysis. J Hydrol 609:127747
Costache R, Tin TT, Arabameri A, Crăciun A, Costache I, Islam ARMT, Sahana M, Pham BT (2022) Stacking state-of-the-art ensemble for flash-flood potential assessment. Geocarto Int 37:1–24
Dai Z, Li X, Lan B (2023) Three-dimensional modeling of Tsunami waves triggered by submarine landslides based on the smoothed particle hydrodynamics method. J Mar Sci Eng 11(10):2015. https://doi.org/10.3390/jmse11102015
Dai H, Liu Y, Guadagnini A, Yuan S, Yang J, Ye M (2024) Comparative assessment of two global sensitivity approaches considering model and parameter uncertainty abstract key points. Water Resour Res 60(2):e2023WR036096. https://doi.org/10.1029/2023WR036096
Du W, Wang G (2013) Intra-event spatial correlations for cumulative absolute velocity arias intensity and spectral accelerations based on regional site conditions. Bull Seismol Soc Am 103(2A): 1117–1129. https://doi.org/10.1785/0120120185
Endendijk T, Botzen WW, de Moel H, Aerts JC, Slager K, Kok M (2023) Flood vulnerability models and household flood damage mitigation measures: An econometric analysis of survey data. Water Resour Res 59:e2022WR034192
Fang Z, Wang Y, Peng L, Hong H (2021) A comparative study of heterogeneous ensemble-learning techniques for landslide susceptibility mapping. Int J Geogr Inf Sci 35:321–347
Fenglin W, Ahmad I, Zelenakova M, Fenta A, Dar MA, Teka AH, Belew AZ, Damtie M, Berhan M, Shafi SN (2023) Exploratory regression modeling for flood susceptibility mapping in the GIS environment. Sci Rep 13:247
Guan H, Huang J, Li L, Li X, Miao S, Su W, Ma Y, Niu Q, Huang H (2023) Improved Gaussian mixture model to map the flooded crops of VV and VH polarization data. Remote Sens Environ 295:113714. https://doi.org/10.1016/j.rse.2023.113714
Hall MA (1999) Correlation-based feature selection for machine learning (PhD Thesis). University of Waikato Hamilton
Hategekimana Y, Yu L, Nie Y, Zhu J, Liu F, Guo F (2018) Integration of multi-parametric fuzzy analytic hierarchy process and GIS along the UNESCO world heritage: a flood hazard index, Mombasa County, Kenya. Nat Hazards 92:1137–1153
Heidari AA, Mirjalili S, Faris H, Aljarah I, Mafarja M, Chen H (2019) Harris hawks optimization: algorithm and applications. Futur Gener Comput Syst 97:849–872
Huang Y, Chen X, Zou Y-A, Zhang P, Li F, Hou Z, Li X, Zeng J, Deng Z, Zhong J (2022) Exploring the relative contribution of flood regimes and climatic factors to Carex phenology in a Yangtze River-connected floodplain wetland. Sci Total Environ 847:157568
Huang H, Huang J, Wu Y, Zhuo W, Song J, Li X, Li L, Su W, Ma H, Liang S (2023) The improved winter wheat yield estimation by assimilating GLASS LAI into a crop growth model with the proposed bayesian posterior-based ensemble kalman filter. IEEE Trans Geosci Remote Sens 611:1–18. https://doi.org/10.1109/TGRS.2023.3259742
Jiang L, Li C, Wang S, Zhang L (2016) Deep feature weighting for naive Bayes and its application to text classification. Eng Appl Artif Intell 52:26–39
Kanani-Sadat Y, Arabsheibani R, Karimipour F, Nasseri M (2019) A new approach to flood susceptibility assessment in data-scarce and ungauged regions based on GIS-based hybrid multi criteria decision-making method. J Hydrol 572:17–31
Kia MB, Pirasteh S, Pradhan B, Mahmud AR, Sulaiman WNA, Moradi A (2012) An artificial neural network model for flood simulation using GIS: Johor River Basin, Malaysia. Environmental Earth Sciences 67:251–264
Lan T, Hu Y, Cheng L, Chen L, Guan X, Yang Y, Guo Y, Pan, J (2022) Floods and diarrheal morbidity: evidence on the relationship effect modifiers and attributable risk from Sichuan Province China. J Global Health 12:1100712. https://doi.org/10.7189/jogh.12.11007
Li B, Guan T, Dai L, Duan G (2023) Distributionally robust model predictive control with output feedback. IEEE Trans Autom Control 1:8. https://doi.org/10.1109/TAC.2023.3321375
Li Y, Hong H (2023) modeling flood susceptibility based on deep learning coupling with ensemble learning models. J Environ Manage 325:116450
Li D, Huang F, Yan L, Cao Z, Chen J, Ye Z (2019) Landslide susceptibility prediction using particle-swarm-optimized multilayer perceptron: comparisons with multilayer-perceptron-only, bp neural network, and information value models. Appl Sci 9:3664
Lin X, Zhu G, Qiu D, Ye L, Liu Y, Chen L, Liu J, Lu S, Wang L, Zhao K, Zhang W, Li R, Sun N (2023) Stable precipitation isotope records of cold wave events in Eurasia. Atmos Res 296:107070. https://doi.org/10.1016/j.atmosres.2023.107070
Liu J, Wang Y, Li Y, Peñuelas J, Zhao Y, Sadans J, Tetzlaff D, Liu J, Liu X, Yuan H, Li Y, Chen J, Wu J (2023) Soil ecological stoichiometry synchronously regulates stream nitrogen and phosphorus concentrations and ratios. CATENA 231:107357. https://doi.org/10.1016/j.catena.2023.107357
Lu S, Zhu G, Meng G, Lin X, Liu Y, Qiu D, Xu Y, Wang Q, Chen L, Li R, Jiao Y (2024) Influence of atmospheric circulation on the stable isotope of precipitation in the monsoon margin region. Atmos Res 298:107131. https://doi.org/10.1016/j.atmosres.2023.107131

Mehryar S, Surminski S (2022) Investigating flood resilience perceptions and supporting collective decision-making through fuzzy cognitive mapping. Sci Total Environ 837:155854
Minea G (2013) Assessment of the flash flood potential of Bâsca river catchment (Romania) based on physiographic factors. Open Geosci 5:344–353
Ozcift A, Gulten A (2011) Classifier ensemble construction with rotation forest to improve medical diagnosis performance of machine learning algorithms. Comput Methods Programs Biomed 104:443–451
Ozturk U, Wendi D, Crisologo I, Riemer A, Agarwal A, Vogel K, López-Tarazón JA, Korup O (2018) Rare flash floods and debris flows in southern Germany. Sci Total Environ 626:941–952
Pande CB, Moharir KN, Panneerselvam B, Singh SK, Elbeltagi A, Pham QB, Varade AM, Rajesh J (2021) Delineation of groundwater potential zones for sustainable development and planning using analytical hierarchy process (AHP), and MIF techniques. Appl Water Sci 11:186. https://doi.org/10.1007/s13201-021-01522-1
Paneerselvam B, Ravichandran N, Li P, Thomas M, Charoenlerkthawin W, Bidorn B (2023) Machine learning approach to evaluate the groundwater quality and human health risk for sustainable drinking and irrigation purposes in south India. Chemosphere 336:139228. https://doi.org/10.1016/j.chemosphere.2023.139228
Panneerselvam B, Karuppannan S, Muniraj K (2020) Evaluation of drinking and irrigation suitability of groundwater with special emphasizing the health risk posed by nitrate contamination using nitrate pollution index (NPI) and human health risk assessment (HHRA). Hum Ecol Risk Assess Int J 27:1324–1348. https://doi.org/10.1080/10807039.2020.1833300
Panneerselvam B, Muniraj K, Duraisamy K, Pande C, Karuppannan S, Thomas M (2023a) An integrated approach to explore the suitability of nitrate-contaminated groundwater for drinking purposes in a semiarid region of India. Environ Geochem Health 45:647–663. https://doi.org/10.1007/s10653-022-01237-5
Panneerselvam B, Muniraj K, Pande C, Ravichandran N (2023b) Prediction and evaluation of groundwater characteristics using the radial basic model in semi-arid region, India. Int J Environ Anal Chem 103:1377–1393. https://doi.org/10.1080/03067319.2021.1873316
Paryani S, Neshat A, Pradhan B (2021) Improvement of landslide spatial modeling using machine learning methods and two Harris hawks and bat algorithms. Egypt J Remote Sens Space Sci 24:845–855
Popescu C, Bărbulescu A (2023) Floods simulation on the Vedea river (Romania) using hydraulic modeling and GIS software: a case study. Water 15:483
Pourghasemi HR, Mohammady M, Pradhan B (2012) Landslide susceptibility mapping using index of entropy and conditional probability models in GIS: Safarood basin. Iran Catena 97:71–84
Qazi A, Singh K, Vishwakarma DK, Abdo HG (2023) GIS based landslide susceptibility zonation mapping using frequency ratio information value and weight of evidence: a case study in Kinnaur District HP India. Bull Eng Geol Environ 82(8):332. https://doi.org/10.1007/s10064-023-03344-8
Rizwan M, Li X, Chen Y, Anjum L, Hamid S, Yamin M, Chauhdary JN, Shahid MA, Mehmood Q (2023) Simulating future flood risks under climate change in the source region of the Indus River. J Flood Risk Manag 16:e12857
Ruidas D, Chakrabortty R, Islam ARM, Saha A, Pal SC (2022) A novel hybrid of meta-optimization approach for flash flood-susceptibility assessment in a monsoon-dominated watershed, eastern India. Environ Earth Sci 81:1–22
Sankar K, Karunanidhi D, Kalaivanan K, Subramani T, Shanthi D, Balamurugan P (2023) Integrated hydrogeophysical and GIS based demarcation of groundwater potential and vulnerability zones in a hard rock and sedimentary terrain of southern India. Chemosphere 316:137305. https://doi.org/10.1016/j.chemosphere.2022.137305
Senanayake S, Pradhan B, Alamri A, Park H-J (2022) A new application of deep neural network (LSTM) and RUSLE models in soil erosion prediction. Sci Total Environ 845:157220
Shafizadeh-Moghadam H, Valavi R, Shahabi H, Chapi K, Shirzadi A (2018) Novel forecasting approaches using combination of machine learning and statistical models for flood susceptibility mapping. J Environ Manag 217:1–11
Singh G, Pandey A (2021) Flash flood vulnerability assessment and zonation through an integrated approach in the Upper Ganga Basin of the northwest Himalayan region in Uttarakhand. Int Journal Disaster Risk Reduct 66:102573
Tarasova L, Lun D, Merz R, Blöschl G, Basso S, Bertola M, Miniussi A, Rakovec O, Samaniego L, Thober S (2023) Shifts in flood generation processes exacerbate regional flood anomalies in Europe. Commun Earth Environ 4:49
Tien Bui D, Pradhan B, Lofman O, Revhaug I (2012) Landslide susceptibility assessment in Vietnam using support vector machines, decision tree, and Naive Bayes models. Math Probl Eng. https://doi.org/10.1155/2012/974638
Wang X, Huang J, Feng Q, Yin D (2020) Winter wheat yield prediction at county level and uncertainty analysis in main wheat-producing regions of China with deep learning approaches. Remote Sens 12(11):1744. https://doi.org/10.3390/rs12111744
Wei W, Gong J, Deng J, Xu W (2023) Effects of air vent size and location design on air supply efficiency in flood discharge tunnel operations. J Hydraul Eng 149(12). https://doi.org/10.1061/JHEND8.HYENG-13305
Wei W, Xu W, Deng J, Guo Y (2022) Self-aeration development and fully cross-sectional air diffusion in high-speed open channel flows. J Hydraul Res 60(3):445–459. https://doi.org/10.1080/00221686.2021.2004250
Xie X, Xie B, Cheng J, Chu Q, Dooling, T (2021) A simple Monte Carlo method for estimating the chance of a cyclone impact. Nat Hazards 107(3):2573–2582. https://doi.org/10.1007/s11069-021-04505-2
Xu J, Zhou G, Su S, Cao Q, Tian Z (2022) The development of a rigorous model for bathymetric mapping from multispectral satellite-images. Remote Sens 14(10):2495. https://doi.org/10.3390/rs14102495
Yang M, Wang H, Hu K, Yin G, Wei Z (2022) IA-Net an inception–attention-module-based network for classifying underwater images from others. IEEE J Oceanic Eng 47(3):704–717. https://doi.org/10.1109/JOE.2021.3126090
Yin L, Wang L, Keim BD, Konsoer K, Yin Z, Liu M, Zheng W (2023) Spatial and wavelet analysis of precipitation and river discharge during operation of the three Gorges Dam China. Ecol Indic 154:110837. https://doi.org/10.1016/j.ecolind.2023.110837
Zhang Y, Li Z, Wang J, Ge W, Chen X (2022) Environmental impact assessment of dam-break floods considering multiple influencing factors. Sci Total Environ 837:155853
Zhang J, Ren J, Cui Y, Fu D, Cong, J. (2024) Multi-USV task planning method based on improved deep reinforcement learning. IEEE Internet Things J 1–1. https://doi.org/10.1109/JIOT.2024.3363044
Zhao M, Liu Y, Wang Y, Chen Y, Ding W (2022) Effectiveness assessment of reservoir projects for flash flood control, water supply and irrigation in Wangmo Basin, China. Sci Total Environ 851:157918
Zhou G, Liu W, Zhu Q, Lu Y, Liu Y (2022) ECA-MobileNetV3(Large)+SegNet model for binary sugarcane classification of remotely sensed images. IEEE Trans Geosci Remote Sens 60:1–15. https://doi.org/10.1109/TGRS.2022.3215802
Zhou G, Liu X (2022) Orthorectification model for extra-length linear array imagery. IEEE Trans Geosci Remote Sens 60:1–10. https://doi.org/10.1109/TGRS.2022.3223911

Authors and Affiliations

Romulus Costache[1,2,3,4] · **Subodh Chandra Pal**[5] · **Chaitanya B. Pande**[6,7,8] · **Abu Reza Md. Towfiqul Islam**[10,9] · **Fahad Alshehri**[8] · **Hazem Ghassan Abdo**[11]

✉ Hazem Ghassan Abdo
hazemabdo@tartous-univ.edu.sy

Romulus Costache
romuluscostache2000@yahoo.com

Subodh Chandra Pal
geo.subodh@gmail.com

Abu Reza Md. Towfiqul Islam
towfiq_dm@brur.ac.bd

Fahad Alshehri
Falshehria@ksu.edu.sa

1 Department of Civil Engineering, Transilvania University of Brasov, 5, Turnului Str, 500152 Brasov, Romania

2 Danube Delta National Institute for Research and Development, 165 Babadag Street, 820112 Tulcea, Romania

3 National Institute of Hydrology and Water Management, București-Ploiești Road, 97E, 1st District, 013686 Bucharest, Romania

4 Research Institute of the University of Bucharest, 90-92 Sos. Panduri, 5th District, 050107 Bucharest, Romania

5 Department of Geography, The University of Burdwan, Bardhaman, West Bengal 713104, India

6 New Era and Development in Civil Engineering Research Group, Scientific Research Center, Al-Ayen University, Nasiriyah, Thi-Qar 64001, Iraq

7 Institute of Energy Infrastructure, Universiti Tenaga Nasional, 43000 Kajang, Malaysia

8 Abdullah Alrushaid Chair for Earth Science Remote Sensing Research, Collage of Science, King Saud University, Riyadh, Saudi Arabia

9 Department of Disaster Management, Begum Rokeya University, Rangpur 5400, Bangladesh

10 Department of Development Studies, Daffodil International University, Dhaka 1216, Bangladesh

11 Geography Department, Faculty of Arts and Humanities, Tartous University, Tartous, Syria

Water Resources Management (2022) 36:4765–4783
https://doi.org/10.1007/s11269-022-03276-0

New Machine Learning Ensemble for Flood Susceptibility Estimation

Romulus Costache[1,2] · **Alireza Arabameri**[3] · **Iulia Costache**[4] · **Anca Crăciun**[2] · **Binh Thai Pham**[5]

Received: 22 April 2022 / Accepted: 27 July 2022 / Published online: 25 August 2022

Abstract

Floods are among the most severe natural hazard phenomena that affect people around the world. Due to this fact, the identification of zones highly susceptible to floods became a very important activity in the researcher's work. In this context, the present research work aimed to propose the following 3 novel ensembles to estimate the flood susceptibility in Putna river basin from Romania: UltraBoost-Weights of Evidence (U-WOE), Stochastic Gradient Descending-Weights of Evidence (SGD-WOE) and Cost Sensitive Forest-Weights of Evidence (CSForest-WOE). In this regard, a sample of 132 flood locations and 14 flood predictors was used as input datasets in the 3 aforementioned models. The modeling procedure performed through a ten-fold cross-validation method revealed that the SGD-WOE ensemble model achieved the highest performance in terms of ROC Curve-AUC (0.953) and also in terms of Accuracy (0.94). The slope and distance from river flood predictors achieved the highest importance in terms of flood susceptibility genesis, while the aspect, TPI, hydrological soil groups, and plan curvature have the lowest influence in terms of flood occurrence. The area with high and very high susceptibility represents between 21% and 24% of the Putna river basin from Romania.

Keywords Flood susceptibility · Romania · Machine learning · Bivariate statistics · Putna river basin

1 Introduction

As part of the hydrological cycle, flooding has always been a natural part of the system, however, over the past decade, a gradual increase has been observed in the frequency and magnitude of flooding (Vojtek and Vojteková 2019; Zhang et al., 2022). In Romania, this has been a challenging task because many countries have found it difficult to develop effective flood prevention measures. As climate and land-use changes continue, flooding is expected to increase. This can largely be attributed to an increase in the occurrence of flood events (Pistrika et al. 2014; Afriyanie et al. 2020). As a result of these anthropogenic

Extended author information available on the last page of the article impacts, basins in which there has been substantial anthropogenic activity often experience increased runoff resulting in rapid erosion or increased evaporation processes (Chen et al. 2009; Chakrabortty et al. 2021). The mapping of flooding susceptibility is essential element of early warning systems intended to prevent and mitigate future flood risks since they identify the most prone zones based on the physical factors determining how much flooding will occur (Vojtek and Vojteková 2019; Janizadeh et al. 2021). Therefore, vulnerability assessment may also incorporate the notion of susceptibility. There is a series of conditions that have been recognized as necessary to construct flood susceptibility mapping techniques as they reflect the physical characteristics of the area under investigation (Arnell and Gosling 2016). These physical characteristics refer to several geographical components like lithology, land use, slope angle, river density, and other morphometric variables and hydrological soil groups. In selecting the appropriate conditioning factors for an assessment of flood susceptibility, one has to take into consideration the spatial scale of that analysis. For example, if the study zone is large (for example, the nation's territory), then using fewer variables would be reasonable. This is because it is more challenging to achieve the same data (thought at the same resolution or scale) for the whole area (Dodangeh et al. 2020). Some studies contend that fewer factors are possibly more likely to reduce the possibility of your receiving some overrated factors if there is a limited number of them. Local- scale (e.g., catchment) studies may integrate a variety of data and factors that are location-specific, allowing for an accurate description of flood predispositions because they utilize local data and variables.

Geographical information systems (GIS) have emerged as powerful tools to facilitate the synthesis of multiple input data sources (Zhao et al. 2020; Wang et al. 2021; Zhou et al. 2021a, 2021b), variables (Gao et al. 2021; Liu et al. 2021a, 2021b; Quan et al., 2022), and ensuing logical and mathematical relationships to generate flood susceptibility maps, as flooding has both spatial and temporal aspects. There have been several methods developed over the years which have been used to identify and assess flood-prone areas in different geographic areas of the world. It should be noted the very strong development after 2010 of machine learning techniques (Chao et al. 2021; Zhang et al. 2020; Zhang et al. 2021; Yin et al. 2022a; Zhan et al. 2022a, 2022b). Thus, they began to be used on a large scale in almost all scientific fields (Jafari-Asl et al. 2021; Rad et al. 2022). One of the factors that determined the accelerated increase in the degree of use of these modern techniques is represented by the development of software and the implementation of machine learning algorithms with the help of programming languages (Mehta and Devarakonda 2018). There were many advances in machine learning techniques used for mapping flood susceptibility in recent years, and several have revealed powerful features and demonstrated favorable results (Zhang et al. 2019; Liu et al. 2020; Liu et al. 2022; Li et al. 2022). These techniques include decision trees (Chen et al. 2020), artificial neural networks (Hong et al. 2018), random forest (Lee et al. 2017), Naive Bayes (Costache et al. 2019), logistic regression or support vector machine (Tehrany et al. 2015; Allahbakhshian-Farsani et al. 2020). Several studies have recently attempted to build flood susceptibility models by using hybrid strategies to determine their strengths and weaknesses. For example, machine learning was used to combine bootstrapping and subsampling methods (Dodangeh et al. 2020). Moreover, there were attempts to estimate the flood susceptibility using some advanced hybrid models that were generated by the combination of Dagging and Random Subspace algorithms (Tian et al. 2021), on the one hand, with the random forest, support vector machine and artificial neural network, on the other hand (Islam et al. 2021). Other authors compute the flood susceptibility using the functional trees hybridized with bagging and rotational forest(Arabameri et al. 2020). A common practice in the assessment of flood-prone areas is to combine the bivariate statistics methods, like frequency ratio or weights of evidence, with models from the machine learning category like classification and regression tree, deep learning neural network, random forest, or support vector machine (Costache and Bui 2019; Bui et al. 2020). Hybrid machine learning algorithms provide excellent results for modeling natural hazards and many natural hazard models have been applied to hybrid machine learning algorithms for implementation and creation. While there was an agreement among the scientists that some tools would be useful to evaluate various hazards more effectively (Chen et al. 2021), there was no universal agreement on which tools were best suited to stimulate natural hazards such as floods. Flood susceptibility and other ways of stimulating natural hazards are among the research topics being discussed by researchers.

Therefore, in the present research work, the main scope of the developed workflow was to estimate the flood susceptibility across the Putna river basin from Romania, with the help of novel ensemble algorithms which were generated by the combination of Weight of Evidence bivariate statistics and the next three machine learning models: UltraBoost, Stochastic Gradient Descending and Cost Sensitive Forest.

The accuracy of the results was demonstrated with the Receiver Operating Characteristic (ROC) Curve method and by the computation of several statistical metrics. It should be also mentioned that the following sections are structured as follows: Study area; Data; Methods; Results; Discussions; Conclusions and future directions.

2 Study Area

The Putna river basin in Romania is the subject of this case study (Fig. 1). There are 2509 km^2 in this catchment, and its boundaries have the following coordinates: 26° 22’ 13.08” and 27° 29’ 57.84” E longitude, and 46° 2’ 44.16” and 45° 31’ 23.16” N latitude (Costache and Bui, 2019).

It is verified by government data in Romania that the worst flooding event which can be attributed to the Putna river catchment took place in 2005, and this catastrophe caused the death of a total of 15 people (Romanescu and Nistor 2011). A total of approximately €150 million was also generated by flooding that year as a result of the floods (Tîrnovan et al. 2014). Supplementary aspects of the Study area are provided in Sect. 1 (S1) of Online Supplementary Material.

3 Data

3.1 Flood Inventory

As part of this study, a map of flood risk was created using information collected from the General Inspection for Emergency Situations of Romania. The study zone was subsequently found to have 132 flood events, as a result of this investigation procedure. It was determined that an additional sample with 132 non-flood locations should be created since flood suscep-

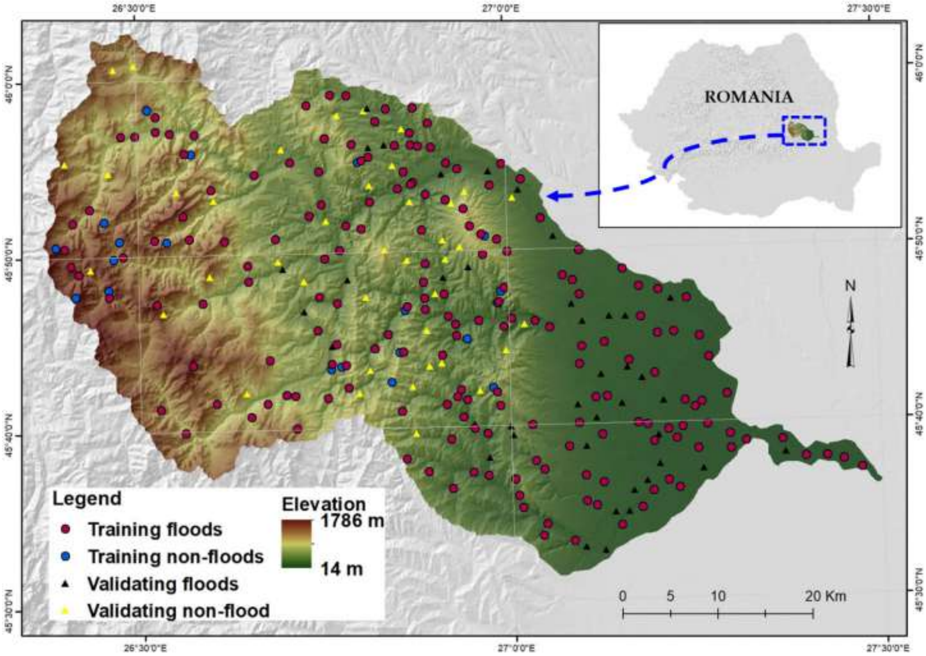

Fig. 1 Study area location

tibility mapping is a process related to the binary classification topic. Furthermore, to ensure that we have the opportunity to test the model's performance and to verify the accuracy of the prediction results, the flood and non-flood database samples were split into the training data set of 70% and the validation data set of 30%. Supplementary aspects of flood inventory are included in the Sect. 2 (S2) of the Online Supplementary File.

3.2 Flood Predictors

The flood predictors we chose to calculate the flood susceptibility for the entire region under study were comprised of 14 flood prediction models after careful consultation of the literature and taking into account the specific characteristics of the Putna River Basin. In order to create the Digital Elevation Model (DEM) across the area on which the study is focused, it was crucial to use the Shuttle Radar Topographic Mission at a resolution of 30 m. As a result, the DEM was used to derive the following nine morphometrical flood predictors, namely: slope angle (Fig. 2a), topographic position index (TPI) (Fig. 3a), elevation (Fig. 2 h), convergence index (Fig. 2c), plan curvature (Fig. 3b), stream power index (SPI) (Fig. 3c), profile curvature (Fig. 2b), topographic wetness index (TWI) (Fig. 2 g) and aspect (Fig. 3e). The rest of 5 conditioning factors (land use (Fig. 2d), lithological groups (Fig. 2e), distance from river (Fig. 3f), hydrological soil groups (Fig. 2f) and rainfall (Fig. 3d)) were derived using vectorial database such as: Corine Land Cover, 2018 used for land use; Geological Map of Romania 1:20000 used for lithology; National River Cadastre for Romania that was used as database for distance to river factor; Soil Map of Romania, 1:200000 used to extract hydrological soil groups; mean annual sum of precipitation for period 1980–2015

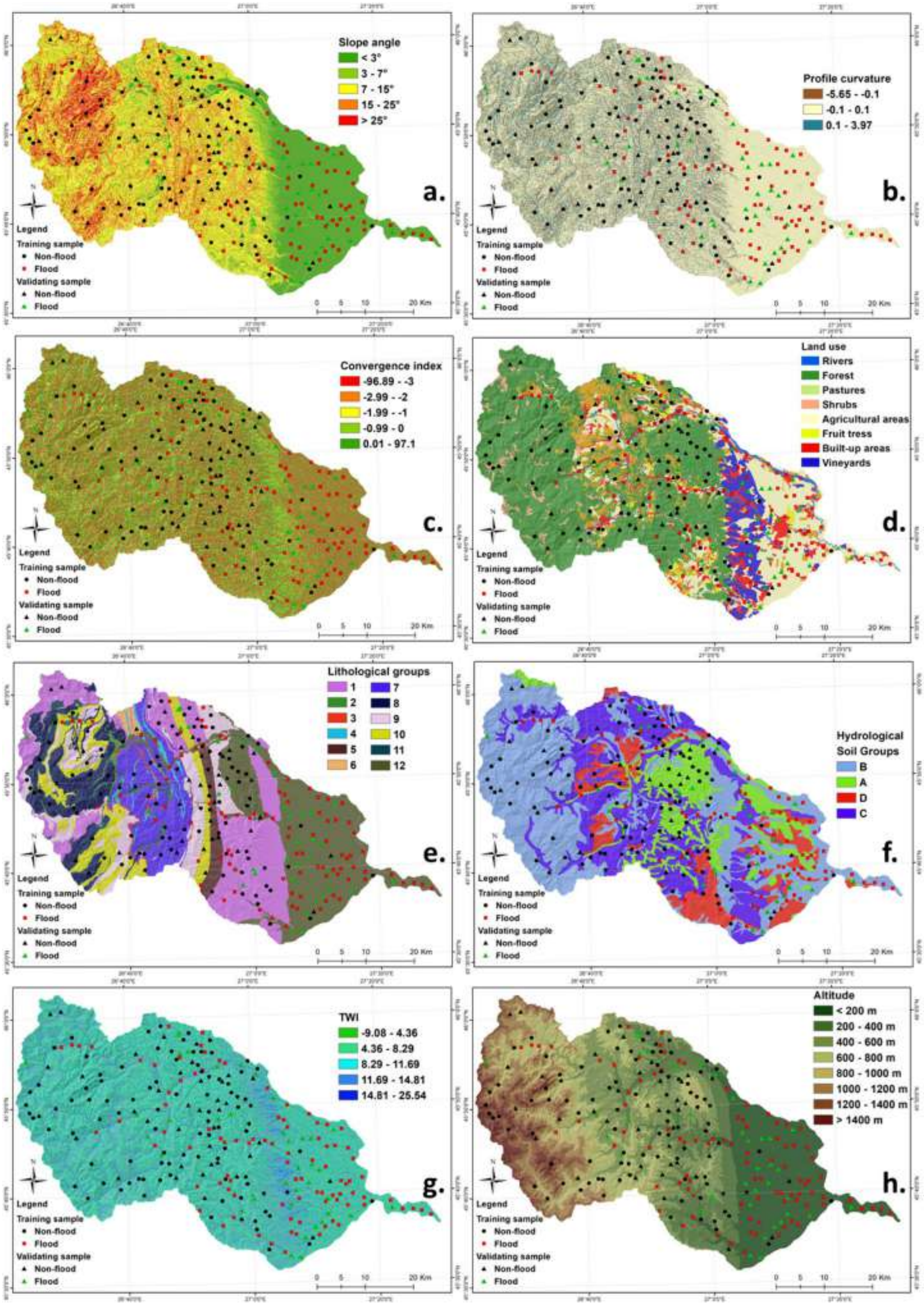

Fig. 2 Flood conditioning factors (a. Slope angle; b. Profile curvature; c. Convergence Index; d. Land use; e. Lithology; f. Hydrological Soil Groups; g. TWI; h. Elevation)

which was used to generate the rainfall map for the study area. A short description of the predictors is provided in Sect. 3 (S3) and Table S1 of the Online Supplementary Material.

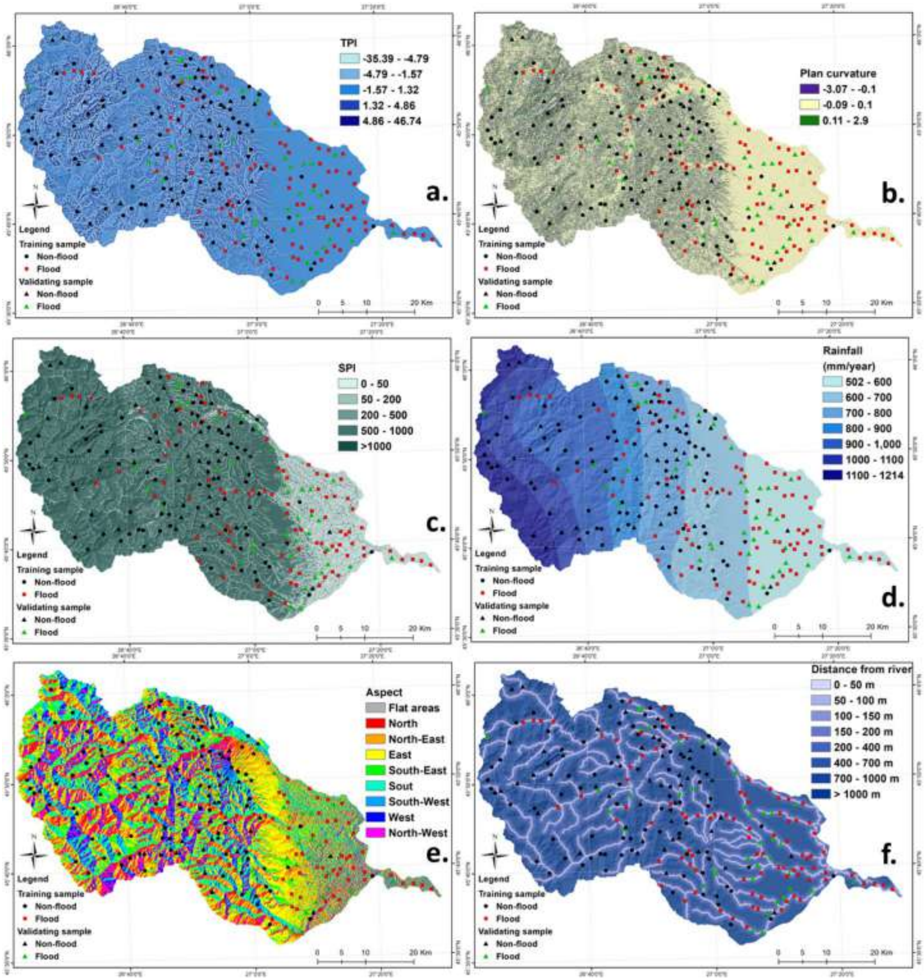

Fig. 3 Flood conditioning factors (a. TPI; b. Plan curvature; c. SPI; d. Rainfall; e. Aspect; f. Distance from river)

4 Methods

4.1 ReliefF Method

By using the ReliefF method, we will be able to make a preliminary evaluation of the predictive potential of the variables used as inputs to estimate flood susceptibility (Costache et al. 2021). Furthermore, it is important to emphasize that the ReliefF algorithm is capable of operating with continuous and discrete data. It is considered that the attribute value is assigned to the nearest instance of the same or a different class of the given attribute value (Costache et al. 2021). ReliefF was used in the present study as an analysis tool using Weka 3.9 software. Additional aspects of ReliefF method are included in Sect. 4 (S4) of Online Supplementary Material.

4.2 Weights of Evidence

To provide information as to how the Weights of Evidence method can be implemented in GIS environment, it is necessary to establish the following relationships (Armaş 2012):

$$W^{+} = \ln(\left[\frac{Npix_1}{Npix_1 + Npix_2}\right] / [\frac{Npix_3}{Npix_3 + Npix_4}]) \tag{1}$$

$$W^{-} = \ln(\left[\frac{Npix_2}{Npix_1 + Npix_2}\right] / [\frac{Npix_4}{Npix_3 + Npix_4}]) \tag{2}$$

where N_{pix1} is the number of flood pixels within a class; N_{pix2} is the number of flood pixels outside the specific class; N_{pix3} is the number of pixels in a class without flood locations; N_{pix4} is the number of non-flood pixels outside a class; W^+ is equal to the positive weight, while W^- represents the negative weight.

The final values of WOE coefficients (*Wf*) will be calculated using the next relation (Dahal et al. 2008):

$$Wf = Wplus + Wmintotal - Wmin \tag{3}$$

where *W*plus is the positive weight of a class/category from a factor, *W*min is the negative weight of a category belonging to a specific factor, *W*min total represents the sum of all the negative weights in a multiclass map.

The weights of evidence values were used as input data in the data mining models used in the present research. More aspects of Weights of Evidence can be found in Sect. 5 (S5) of Online Supplementary Material.

4.3 UltraBoost (U)

UltraBoost classifier represents a method used to boost heterogeneous learners. In the present research work, the UltraBoost algorithm is trained so as for each case to be assigned a specific probability of flooding (Moustafa et al. 2020). The attribute class forecast with the help of model is flood=1 for the areas highly exposed to flood and 0 for non-flood — so the output probabilities of flood genesis is ranging between 0 and 1. Additional aspects of UltraBoost model are inserted in Sect. 6 (S6) of Online Supplementary Material.

4.4 Stochastic Gradient Descending (SGD)

The stochastic gradient descent method is a stochastic approximation of the gradient descent method, which is an iteration-based method for generating a derivative function (Hoang 2019). In addition to its high efficiency, and ease with which it can be implemented for datasets with redundant samples, this algorithm is very popular. In the flood susceptibility analyses, SGD is seldom applied, which is something that needs to be investigated more in-depth. The application of SGD in the present research work was possible through Weka 3.9 software. Additional aspects of the Stochastic Gradient Descending (SGD) model are presented in Sect. 7 (S7) of Online Supplementary Material.

4.5 Cost Sensitive Forest (CSForest)

The CSForest can be applied through the mean of the Classification Cost Reduction (CCR) function which replaces the Gain Ratio that was used as a splitting criterion (Siers and Islam 2015). The tree built by CSForest, before pruning, is deeper than that by CSTree. CSForest, by contrast, builds an ensemble of trees and then uses CSVoting for classifying records/modules whereas the CSTree builds a single tree. In the present case study, the CSForest, for flood susceptibility modelling, was run in Weka 3.9 software. Additional aspects of Cost Sensitive Forest (CSForest) algorithm are included in Sect. 8 (S8) of Online Supplementary Material.

4.6 Results Validation

4.6.1 Receiver Operating Characteristic (ROC) Curve

ROC Curve suggests that a model can accurately predict flood susceptibility. Area Under Curve (AUC) measures the value of a curve of ROCs which is helpful for the user in getting the most important information (Xie et al., 2021a). The range of the AUC is between 0 and 1 (Xie et al., 2021b). Using the following mathematical relationship, we can estimate the AUC:

$$\mathrm{AUC} = \frac{\left(\sum TP + \sum TN\right)}{(\mathrm{P} + \mathrm{N})} \tag{4}$$

where TP (true positive), TN (true negative) are the sums of flood and non-flood locations correctly classified.

Additional aspects of ROC Curve are included in Sect. 9 (S9) of Online Supplementary Material.

4.6.2 Statistical Metrics

The next 5 statistical indicators were involved also in the results validation procedure: Accuracy, Specificity, Sensitivity, Kappa Index, and Precision. In order to calculate the statistical metrics, we will be using the following equations (Canbek et al. 2017):

$$\mathrm{Sensitivity} = \frac{\mathrm{TP}}{\mathrm{TP} + \mathrm{FN}} \tag{5}$$

$$\mathrm{Specificity} = \frac{\mathrm{TN}}{\mathrm{FP} + \mathrm{TN}} \tag{6}$$

$$\mathrm{Precision} = \frac{\mathrm{TP}}{\mathrm{TP} + \mathrm{FP}} \tag{7}$$

$$\mathrm{Accuracy} = \frac{\mathrm{TP} + \mathrm{TN}}{\mathrm{TP} + \mathrm{FP} + \mathrm{TN} + \mathrm{FN}} \tag{8}$$

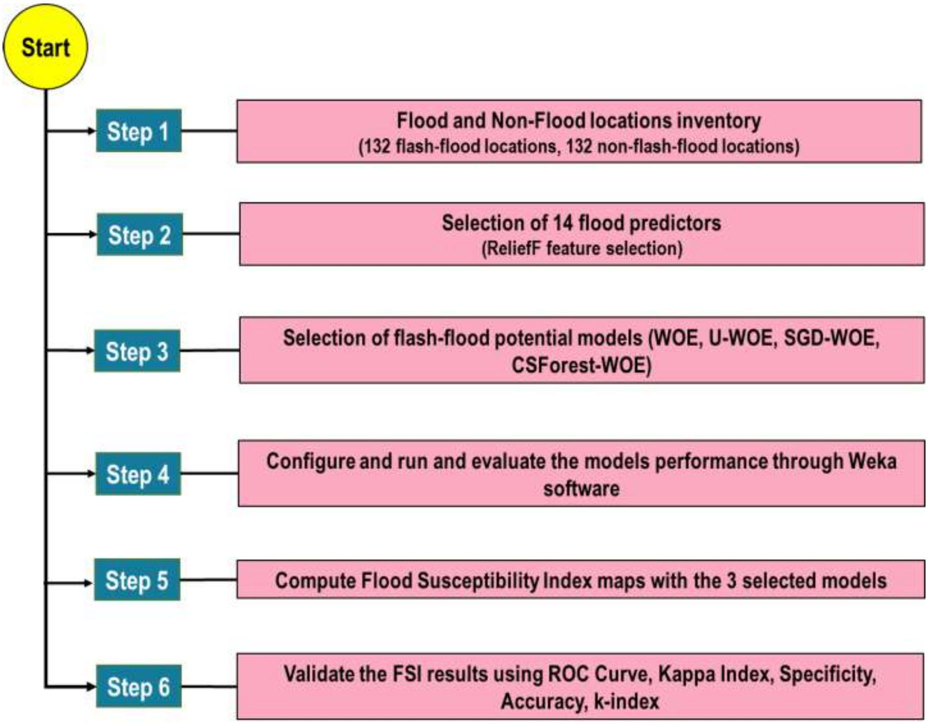

Fig. 4 Flowchart of the methodological steps applied in the present research

$$k = \frac{p_o - p_e}{1 - p_e} \tag{9}$$

where P is the sum of flood locations, N is the sum of non-flood locations, FP (false positive) and FN (false negative) are the numbers of flood and non-flood locations erroneously classified, k is the kappa coefficient, p_o is the observed flood locations, and p_e is the estimated flood susceptibility locations.

A short description of the workflow followed in the present study is represented in Fig. 4.

5 Results

5.1 Feature Selection Using ReliefF Method

The application of ReliefF method provided the following outcomes: Slope (0.653), Land use (0.390), Distance from river (0.354), Elevation (0.32), Plan curvature (0.318), Rainfall (0.246), SPI (0.22), HSG (0.207), TWI (0.161), Profile curvature (0.140), Lithology (0.138), TPI (0.048), Convergence Index (0.021) and Aspect (0.01) (Fig. S1). According to the obtained values, all the flood predictors have an influence on the flood triggering process, and therefore, all of them were considered in the workflow analysis.

5.2 Weights of Evidence Coefficients

The WOE value is also a positive value as well as a negative value, and consequently, this procedure was necessary. The WOE of 3.56 assigned to the river land use class was the highest value and was followed by elevation below 200 m (3.1) and the class of distance from river lower than 50 m (2.9) (Table S2). The WOE was used as an input dataset in the three machine learning models.

5.3 Ultraboost-Weights of Evidence (U-WOE)

The U-WOE ensemble model was trained through a ten-fold cross-validation method in Weka software. Following the training process, the Mean Absolute Error (MAE) was equal to 0.187, while the Root Mean Squared Erroe (RMSE) was 0.1991. The Precision revealed after the training procedure was equal to 0.989. A very important output of the training procedure is represented by the flood predictors importance which have the next values: Slope (0.162), SPI (0.115), Convergence index (0.105), Elevation (0.102), Rainfall (0.091), Distance from rivers (0.09), HSG (0.078), TPI (0.077), Plan curvature (0.072), Aspect (0.049), Lithology (0.027), Profile curvature (0.02), Land use (0.007) and TWI (0.004) (Fig. S2).

The importance values were imported in ArcGIS Map Algebra and the Flood Susceptibility Index (FSI) was calculated by the multiplication with WOE coefficients. The results of FSI_{U-WOE}, were reclassified into 5 classes through the help of Natural Breaks method. The first class, that indicates the very low flood susceptibility values, appears on around 21% of the study area (Fig. 5a). Further, another 35.38% of the research area is covered by low FSI_{U-WOE} values, while medium flood susceptibility has a total percentage of 19.41%. The high and very high flood susceptibility zones account for approximately 16% of the Putna river basin.

5.4 Stochastic Gradient Descending – Weights of Evidence (SGD-WOE)

The SGD-WOE model was also run in Weka software using the ten-fold cross-validation procedure. The next parameters were established in order to train the SGD-WOE ensemble: batch Size – 100; epochs – 100; epsilor – 0.01; lambda – 1.04E-4; learning rate – 0.01; seed – 1. The training procedure revealed the achievement of a Mean Absolute Error (MAE) of 0.131, while the Root Mean Squared Erroe (RMSE) was 0.145. The model Precision reached 0.991. The final step in the training of SGD-WOE model was the determination of the next values of flood predictors importance: Slope (0.305), Distance from rivers (0.127), TWI (0.094), SPI (0.087), Convergence index (0.079), Lithology (0.078), Elevation (0.074), Profile curvature (0.061), Land use (0.034), Rainfall (0.032), Aspect (0.012), TPI (0.007), HSG (0.006), Plan curvature (0.002).

These values were used in the GIS environment through Map Algebra in order to estimate the flood susceptibility index. The very low flood susceptibility is presented on 41.62% of the Putna river catchment (Fig. 5b). The low flood susceptibility is spread on 33.04% of the study zone, while the medium values of flood exposure have only 4.28% of the Putna river basin. A total of 21% of the study area is characterized by high and very high flood susceptibility values.

5.5 Cost Sensitive Forest – Weights of Evidence (CSForest-WOE)

In order to train the CSForest-WOE model, a ten-fold cross-validation algorithm was applied. The structure that provides the best performance for CSForest was formed by 5 trees (Fig. S3). The value of Mean Absolute Error (MAE) was 0.095, while the Root Mean Squared Error (RMSE) was equal to 0.127. The very high performance of the CSForest-WOE algorithm was revealed by the Precision of 0.993.

Further, the next hierarchy was revealed among the flood predictors: Slope (0.158), Distance from river (0.119), Elevation (0.108), SPI (0.094), Rainfall (0.086), Convergence index (0.082), Land use (0.068), Lithology (0.062), HSG (0.05), TWI (0.049), TPI (0.042), Plan curvature (0.04), Aspect (0.026) and Profile curvature (0.016).

The flood susceptibility values were split into 5 classes through the mean of Natural Breaks method. The very low values of $FSI_{CSForest-WOE}$ occupy around 26.51% of the Putna river basin, while the low flood susceptibility characterizes 34.31% of the research zone (Fig. 5c). Medium flood susceptibility has a total percentage of 14.93%, while the high class of $FSI_{CSForest-WOE}$ covers 7.67% of the area on which the present study is focused. The very high class reaches a total percentage of 16.57% of the study zone.

5.6 Results validation

5.6.1 ROC Curve

The Success Rate associated with flood susceptibility maps shows that $FSI_{SGD-WOE}$ has the highest performance with an AUC of 0.953, followed by FSI_{U-WOE} (AUC=0.951) and $FSI_{CFSorest}$ (AUC=0.95) (Fig. 6a). The results related to the Prediction Rate revealed that the best flood susceptibility maps were associated to the $FSI_{SGD-WOE}$ and FSI_{U-WOE} both of them having an AUC of 0.947. The $FSI_{CSForest-WOE}$ has the lowest performance being characterized by an AUC of 0.945 (Fig. 6b).

5.6.2 Statistical Metrics

In terms of the training sample, the highest accuracy was achieved by SGD-WOE (0.94), followed by U-WOE (0.935) and CSForest-WOE (0.929). Regarding the results for k-index, it should be noted that the best value was obtained by SGD-WOE (0.88), followed by U-WOE (0.87) and CSForest-WOE (0.859). In regards to the validating sample, it should be seen that the maximum accuracy of 0.938 was attributed to SGD-WOE model, followed by U-WOE (0.925) and CSForest (0.913). The k-index revealed the same hierarchy with SGD-WOE in the first place with 0.875, followed by U-WOE (0.85) and CSForest-WOE (0.825) (Table 1).

6 Discussions

There is no doubt that atmospheric emissions of greenhouse gases have been increasing in the past few decades, and these emissions have become increasingly pronounced because of the occurrence of weather-related and climate-related events such as flooding, droughts,

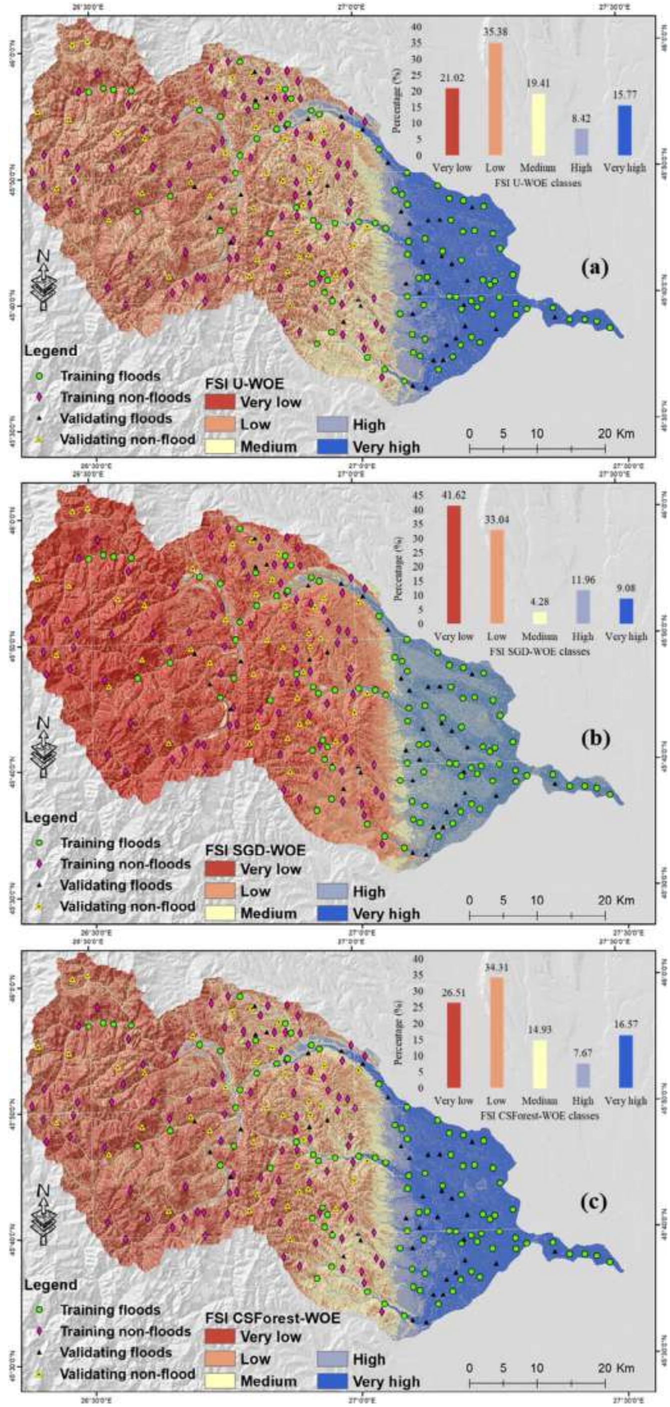

Fig. 5 Flood Susceptibility Index (a. U-WOE; b. SGD-WOE; c. CSForest-WOE)

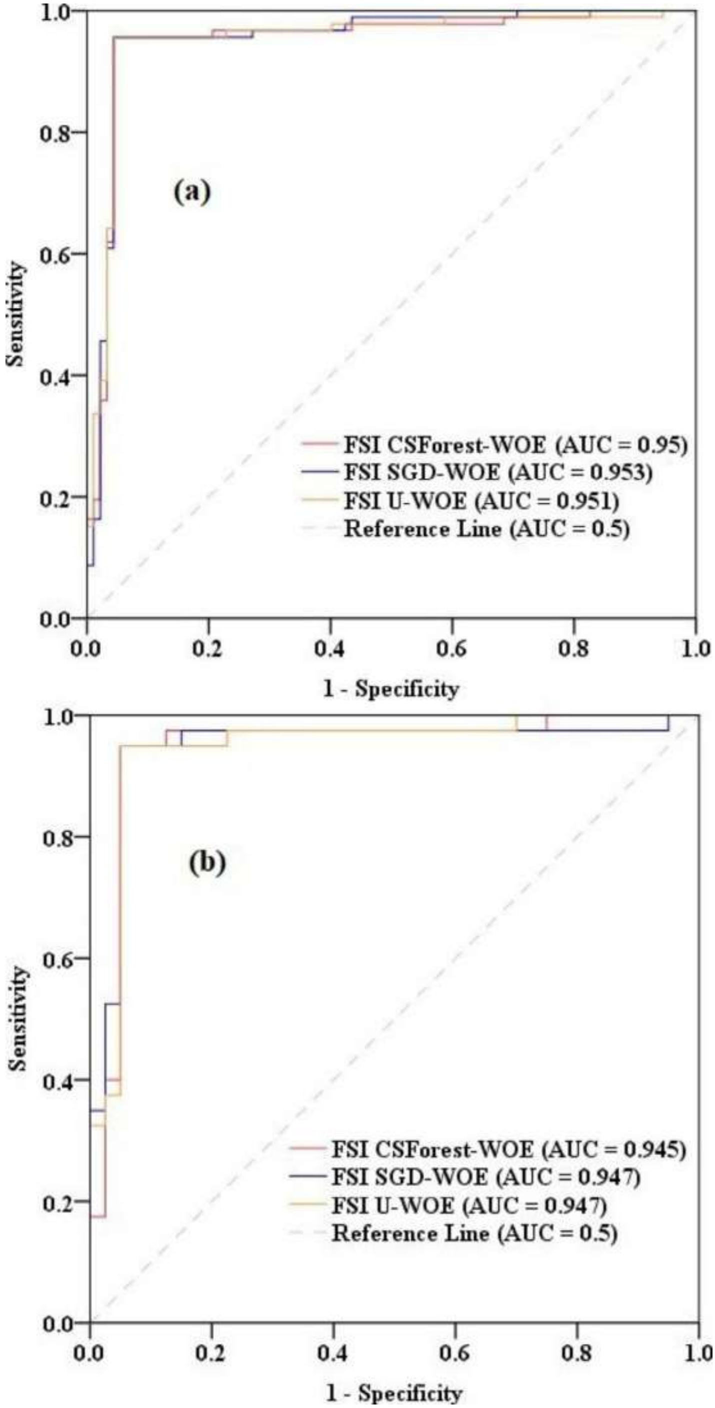

Fig. 6 ROC Curves (a. Success Rate; b. Prediction Rate)

Table 1 Statistical metrics for the applied flood susceptibility models

	Training sample			Validating sample		
Metrics	CSForest-WOE	SGD-WOE	U-WOE	CSForest-WOE	SGD-WOE	U-WOE
TP	85	87	88	36	37	38
TN	86	86	84	37	38	36
FP	7	5	4	4	3	2
FN	6	6	8	3	2	4
Sensitivity (%)	0.934	0.935	0.917	0.923	0.949	0.905
Specificity (%)	0.925	0.945	0.955	0.902	0.927	0.947
Accuracy (%)	0.929	0.940	0.935	0.913	0.938	0.925
k-index	0.859	0.880	0.870	0.825	0.875	0.850

storm surges, and sea-level rises (Dimeyeva et al. 2015; Yin et al. 2022b). Natural risk evaluation research works also include the flood susceptibility models, which are among the most challenging. Flood susceptibility prediction accuracy is strongly influenced by the effects of particular conditions relevant to the study area(s) and by the method used in making the prediction (Islam et al. 2021). As in many other similar studies, in this paper, the authors wanted to estimate the susceptibility to floods by comparative use of 3 machine learning models. These were also combined with a bivariate statistical method, the latter allowing uniform input data to be obtained for all flood predictors. The ensemble approach used in flood susceptibility mapping between researchers has been quite useful in some cases. An ensemble model was applied for bivariate and multivariate statistical analysis by Bui et al. (2019), and they found the ensemble model to be better than the individual models. The 3 machine learning models are represented by UltraBoost, Stochastic Gradient Descending and Cost Sensitive Forest, while the bivariate statistics method was represented by Weights of Evidence. The performance of the 3 models of flood susceptibility was performed using the ROC curves, the Area Under the Curve (AUC) and several statistical metrics (sensitivity, specificity, accuracy and k-index) results. All the results showed that the models were able to perform reasonably well in assessing flood-prone areas. All 3 models had associated AUC values greater than 0.945, which indicates a very high performance and a high accuracy of flood susceptibility maps. These performances far exceeded the performance obtained by Nachappa et al. (2020), in which ensemble methods between machine learning and bivariate statistics were also used and in which all AUC values were below 0.9. The aforementioned study focused on the Salzburg province from Austria which has a multitude of common climatic and relief characteristics as in the high and middle altitude regions of the present study area. Another study whose central topic was the determination of flood susceptibility using machine learning combined with bivariate statistics was conducted by Liuzzo et al. (2019) in Devon County, in the United Kingdom. And in this case, the AUC values obtained by the authors of the previously mentioned study were generally more than 0.91, being, therefore, lower than those obtained in the present study. This demonstrates once again that the use of the 3 algorithms in the present study may be more efficient than other machine learning models used in the literature. Another example of a study on flood susceptibility calculated by state-of-the-art algorithms was conducted by Wang et al. (2020). The authors of the study used a combination of Support Vector Machine (SVM) and Convolutional Neural Network (CNN) to estimate flood exposure in Shangyou County from China. In this case, the highest AUC value was 0.937 and was associated with the 2D-CNN algorithm. Even in this situation where very powerful computational algorithms were used in estimating flood susceptibility, the performance of the models applied in the present study was not exceeded.

The findings of the present study are generally expected to have a significant impact on refining flood risk management plans and activities as well as the principles in the region for making certain that additional damages caused by flooding are avoided.

7 Conclusions and Future Directions

The central topic of this scientific article is the estimation of flood susceptibility through 3 advanced machine learning models in the hydrographic area of the Putna River Basin in Romania. The combination of the bivariate statistical method represented by Weights of Evidence with the following 3 machine learning models allowed the generation of ensemble models that provided very good results: UltraBoost, Stochastic Gradient Descendent and Cost Sensitive Forest. The application of ROC Curve and Area Under Curve showed that the best performance was obtained by SGD-WOE ensemble whose AUC value was 0.953. Also, statistical metrics showed that the same model obtained the highest Accuracy, equal to 0.94. According to the flood susceptibility maps generated by the three ensemble models, the surfaces with a high and very high degree of flood exposure are found on surfaces that fall between 21.04% ($FSI_{SGD-WOE}$) and 24.24% ($FSI_{CSForest-WOE}$). These areas with high and very high exposure to floods are spread mainly in the plain area of the study area but also along the main valleys in this region.

The main novelty of the present study is the application for the first time in the literature of the three ensemble models in order to estimate the susceptibility to floods. Their very high performance is a strong reason for these three ensemble models to be taken over in other research papers and applied to other study areas. At the same time, the authors of the study consider, as future research directions, the integration of the methodology for estimating the susceptibility to floods within a wider methodology for estimating the risk of these phenomena. Thus, in future works, the socio-economic objectives of the studied area will also be taken into account. It is also considered to carry out detailed case studies on floodplains through hydraulic modeling and the use of digital land models with high spatial resolution.

Supplementary Information The online version contains supplementary material available at https://doi.org/10.1007/s11269-022-03276-0.

Author Contributions Conceptualization, R.C., I.C., A.C. and B.T.P.; methodology, R.C., A.A. and I.C.; software, R.C., I.C., and B.T.P.; validation, R.C., I.C., A.C. and B.T.P.; formal analysis, R.C., A.A., A.C. and I.C.; investigation, R.C., A.A. and I.C.; resources, R.C., I.C. and B.T.P.; data curation, R.C., I.C. and B.T.P.; writing—original draft preparation, R.C., I.C. and B.T.P.; writing—review and editing, R.C., A.A. and I.C.; visualization, R.C. and B.T.P.; supervision, R.C., A.A. and I.C.; project administration, R.C.; funding acquisition, R.C. and B.T.P. All authors have read and agreed to the published version of the manuscript.

Funding This work was supported by a grant of the Romanian Ministry of Education and Research, CNCS – UEFISCDI, project number PN-III-P1-1.1-PD-2019-0424-P, within PNCDI III.

Availability of Data and Materials The data used in this research are available by the corresponding author upon reasonable request.

Declarations

Ethics Approval The authors confirm that this article is original research and has not been published or presented previously in any journal or conference in any language (in whole or in part).

Consent to Participate and Consent to Publish Not applicable.

Competing Interests The authors have no conflict of interest.

References

Afriyanie D, Julian MM, Riqqi A, Akbar R, Suroso DS, Kustiwan I (2020) Re-framing urban green spaces planning for flood protection through socio-ecological resilience in Bandung City. Indonesia Cities 101:102710

Allahbakhshian-Farsani P, Vafakhah M, Khosravi-Farsani H, Hertig E (2020) Regional flood frequency analysis through some machine learning models in semi-arid regions. Water Resour Manage 34:2887–2909

Arabameri A, Saha S, Chen W, Roy J, Pradhan B, Bui DT (2020) Flash flood susceptibility modelling using functional tree and hybrid ensemble techniques. Journal of Hydrology 587:125007 https://doi.org/10.1016/j.jhydrol.2020.125007

Armaş I (2012) Weights of evidence method for landslide susceptibility mapping. Prahova Subcarpathians Romania Natural Hazards 60:937–950

Arnell NW, Gosling SN (2016) The impacts of climate change on river flood risk at the global scale. Clim Change 134:387–401

Bui DT, Tsangaratos P, Ngo P-TT, Pham TD, Pham BT (2019) Flash flood susceptibility modeling using an optimized fuzzy rule based feature selection technique and tree based ensemble methods. Sci Total Environ 668:1038–1054

Bui Q-T, Nguyen Q-H, Nguyen XL, Pham VD, Nguyen HD, Pham V-M (2020) Verification of novel integrations of swarm intelligence algorithms into deep learning neural network for flood susceptibility mapping. J Hydrol 581:124379. https://doi.org/10.1016/j.jhydrol.2019.124379

Canbek G, Sagiroglu S, Temizel TT, Baykal N, Science, Engineering (2017) (UBMK), IEEE, pp. 821–826

Chakrabortty R, Pal SC, Janizadeh S, Santosh M, Roy P, Chowdhuri I, Saha A (2021) Impact of climate change on future flood susceptibility: an evaluation based on deep learning algorithms and GCM model. Water Resour Manage 35:4251–4274

Chao L, Zhang K, Wang J, Feng J, Zhang M (2021). A comprehensive evaluation of five evapotranspiration datasets based on ground and grace satellite observations: Implications for improvement of evapotranspiration retrieval algorithm. Remote Sens 13(12): 2414.

Chen Y, Xu Y, Yin Y (2009) Impacts of land use change scenarios on storm-runoff generation in Xitiaoxi basin, China. Quatern Int 208:121–128

Chen W, Li Y, Xue W, Shahabi H, Li S, Hong H, Wang X, Bian H, Zhang S, Pradhan B (2020) Modeling flood susceptibility using data-driven approaches of naïve bayes tree, alternating decision tree, and random forest methods. Sci Total Environ 701:134979

Chen X, Quan Q, Zhang K, Wei J (2021) Spatiotemporal characteristics and attribution of dry/wet conditions in the Weihe River Basin within a typical monsoon transition zone of East Asia over the recent 547 years. Environ Model Softw 143:105116.

Costache R, Bui DT (2019) Spatial prediction of flood potential using new ensembles of bivariate statistics and artificial intelligence: A case study at the Putna river catchment of Romania. Sci Total Environ 691:1098–1118

Costache R, Hong H, Wang Y (2019) Identification of torrential valleys using GIS and a novel hybrid integration of artificial intelligence, machine learning and bivariate statistics. CATENA 183:104179

Costache R, Pham QB, Arabameri A, Diaconu DC, Costache I, Crăciun A, Ciobotaru N, Pandey M, Arora A, Ali SA (2021) Flash-flood propagation susceptibility estimation using weights of evidence and their novel ensembles with multicriteria decision making and machine learning.Geocarto International1–33

Dahal RK, Hasegawa S, Nonomura A, Yamanaka M, Masuda T, Nishino K (2008) GIS-based weights-of-evidence modelling of rainfall-induced landslides in small catchments for landslide susceptibility mapping. Environ Geol 54:311–324

Dimeyeva L, Sitpayeva G, Sultanova B, Ussen K, Islamgulova A (2015) High-altitude flora and vegetation of Kazakhstan and climate change impacts. Climate Change Impacts on High-Altitude Ecosystems. Springer, pp 1–48

Dodangeh E, Choubin B, Eigdir AN, Nabipour N, Panahi M, Shamshirband S, Mosavi A (2020) Integrated machine learning methods with resampling algorithms for flood susceptibility prediction. Sci Total Environ 705:135983

Gao C, Hao M, Chen J, Gu C (2021) Simulation and design of joint distribution of rainfall and tide level in Wuchengxiyu Region, China. Urban clim. 40:101005.

Hoang N-D (2019) Automatic detection of asphalt pavement raveling using image texture based feature extraction and stochastic gradient descent logistic regression. Autom Constr 105:102843

Hong H, Panahi M, Shirzadi A, Ma T, Liu J, Zhu A-X, Chen W, Kougias I, Kazakis N (2018) Flood susceptibility assessment in Hengfeng area coupling adaptive neuro-fuzzy inference system with genetic algorithm and differential evolution. Sci Total Environ 621:1124–1141

Islam ARMT, Talukdar S, Mahato S, Kundu S, Eibek KU, Pham QB, Kuriqi A, Linh NTT (2021) Flood susceptibility modelling using advanced ensemble machine learning models. Geosci Front 12:101075

Jafari-Asl J, Seghier MEAB, Ohadi S, van Gelder P (2021) Efficient method using Whale Optimization Algorithm for reliability-based design optimization of labyrinth spillway. Appl Soft Comput 101:107036

Janizadeh S, Vafakhah M, Kapelan Z, Dinan NM (2021) Novel Bayesian additive regression tree methodology for flood susceptibility modeling. Water Resour Manage 35:4621–4646

Lee S, Kim J-C, Jung H-S, Lee MJ, Lee S (2017) Spatial prediction of flood susceptibility using random-forest and boosted-tree models in Seoul metropolitan city, Korea. Geomatics, Natural Hazards and Risk 8, 1185–1203

Li X, Li X, Wang Y, Hu Y, Zhou C, Zhang H (2022) Numerical Investigation on Stratum and Surface Deformation in Underground Phosphorite Mining Under Different Mining Methods. Front Earth Sci 10:831856. https://doi.org/10.3389/feart.2022.831856

Liu Y, Zhang K, Li Z, Liu Z, Wang J, Huang P (2020) A hybrid runoff generation modelling framework based on spatial combination of three runoff generation schemes for semi-humid and semi-arid watersheds. J Hydrol 590:125440.

Liu S, Liu Y, Wang C, Dang X (2022) The Distribution Characteristics and Human Health Risks of High-Fluorine Groundwater in Coastal Plain: A Case Study in Southern Laizhou Bay, China. Front Environ Sci 10:901637. https://doi.org/10.3389/fenvs.2022.901637.

Liuzzo L, Sammartano V, Freni G (2019) Comparison between different distributed methods for flood susceptibility mapping. Water Resour Manage 33:3155–3173

Liu Y, Zhang Z, Liu X, Wang L, Xia X (2021a) Efficient image segmentation based on deep learning for mineral image classification. Adv Powder Technol 32(10): 3885-3903.

Liu Y, Zhang Z, Liu X, Wang L, Xia X (2021b) Ore image classification based on small deep learning model: Evaluation and optimization of model depth, model structure and data size. Miner Eng 172:107020.

Mehta N, Devarakonda MV (2018) Machine learning, natural language programming, and electronic health records: The next step in the artificial intelligence journey? J Allergy Clin Immunol 141:2019–2021

Moustafa AF, Cary TW, Sultan LR, Schultz SM, Conant EF, Venkatesh SS, Sehgal CM (2020) Color doppler ultrasound improves machine learning diagnosis of breast cancer. Diagnostics 10:631

Nachappa TG, Piralilou ST, Gholamnia K, Ghorbanzadeh O, Rahmati O, Blaschke T (2020) Flood susceptibility mapping with machine learning, multi-criteria decision analysis and ensemble using Dempster Shafer Theory.Journal of Hydrology125275

Pistrika A, Tsakiris G, Nalbantis I (2014) Flood depth-damage functions for built environment. Environ Processes 1:553–572

Quan Q, Liang W, Yan D, Lei J (2022) Influences of joint action of natural and social factors on atmospheric process of hydrological cycle in Inner Mongolia, China. Urban clim. 41:101043.

Rad MJG, Ohadi S, Jafari-Asl J, Vatani A, Ahmadabadi SA, Correia JA (2022) GNDO-SVR: An efficient surrogate modeling approach for reliability-based design optimization of concrete dams. Presented at the Structures, pp 722–733

Romanescu G, Nistor I (2011) The effects of the July 2005 catastrophic inundations in the Siret River's Lower Watershed, Romania. Nat Hazards 57:345–368

Siers MJ, Islam MZ (2015) Software defect prediction using a cost sensitive decision forest and voting, and a potential solution to the class imbalance problem. Inform Syst 51:62–71

Tehrany MS, Pradhan B, Jebur MN (2015) Flood susceptibility analysis and its verification using a novel ensemble support vector machine and frequency ratio method. Stoch Env Res Risk Assess 29:1149–1165

Tian J, Liu Y, Zheng W, Yin L (2021) Smog prediction based on the deep belief-BP neural network model (DBN-BP). Urban Clim. 41:101078

Tîrnovan A, Cojoc GM, Romanescu G, Obreja F (2014) Predicting the potential index of major floods production in the Suha river basin (Suha Bucovineana). Water resources and wetlands

Vojtek M, Vojteková J (2019) Flood susceptibility mapping on a national scale in Slovakia using the analytical hierarchy process. Water 11:364
Wang Y, Fang Z, Hong H, Peng L (2020) Flood susceptibility mapping using convolutional neural network frameworks. J Hydrol 582:124482
Wang S, Zhang K, Chao L, Li D, Tian X, Bao H, Chen G, Xia Y. (2021) Exploring the utility of radar and satellite-sensed precipitation and their dynamic bias correction for integrated prediction of flood and landslide hazards. J Hydrol 603: 126964.
Yin L, Wang L, Keim BD, Konsoer K, Zheng W (2022a) Wavelet Analysis of Dam Injection and Discharge in Three Gorges Dam and Reservoir with Precipitation and River Discharge. Water 14(4):567.
Zhan C, Dai Z, Soltanian MR, Zhang X (2022a) Stage-Wise Stochastic Deep Learning Inversion Framework for Subsurface Sedimentary Structure Identification. Geophys Res Lett 49(1):e2021GL095823. https://doi.org/10.1029/2021GL095823
Yin L, Wang L, Huang W, Tian J, Liu S, Yang B, Zheng W (2022b) Haze Grading Using the Convolutional Neural Networks. Atmosphere 13(4):522.
Xie W, Li X, Jian W, Yang Y, Liu H, Robledo LF, Nie W (2021a) A Novel Hybrid Method for Landslide Susceptibility Mapping-Based GeoDetector and Machine Learning Cluster: A Case of Xiaojin County, China. ISPRS Int J Geo-Inf 10(2):93.
Xie W, Nie W, Saffari P, Robledo LF, Descote P, Jian W (2021b) Landslide hazard assessment based on Bayesian optimization–support vector machine in Nanping City, China. Nat Hazards 109(1):931-948.
Zhan C, Dai Z, Samper J, Yin S, Ershadnia R, Zhang X, Wang Y, Yang Z, Luan X, Soltanian MR (2022b) An integrated inversion framework for heterogeneous aquifer structure identification with single-sample generative adversarial network. J Hydrol 610:127844.
Zhang K, Wang S, Bao H, Zhao X (2019) Characteristics and influencing factors of rainfall-induced landslide and debris flow hazards in Shaanxi Province, China. Nat Hazards Earth Syst Sci 19(1):93-105.
Zhang Z, Luo C, Zhao Z (2020) Application of probabilistic method in maximum tsunami height prediction considering stochastic seabed topography. Nat Hazards 104:2511-2530.
Zhang X, Ma F, Yin S, Wallace CD, Soltanian MR, Dai Z, Ritzi RW, Ma Z, Zhan C, Lü X (2021) Application of upscaling methods for fluid flow and mass transport in multi-scale heterogeneous media: A critical review. Appl Energy, 303:117603.
Zhang K, Shalehy MH, Ezaz GT, Chakraborty A, Mohib KM, Liu L (2022). An integrated flood risk assessment approach based on coupled hydrological-hydraulic modeling and bottom-up hazard vulnerability analysis. Environ Model Softw 148:105279.
Zhao T, Shi J, Lv L, Xu H, Chen D, Cui Q, Jackson TJ, Yan G, Jia L, Chen L, Zhao K, Zheng X, Zhao L, Zheng C, Ji D, Xiong C, Wang T, Li R, Pan J, Wen J, Yu C, Zheng Y, Jiang L, Chai L, Lu H, Yao P, Ma J, Lv H, Wu J, Zhao W, Yang N, Guo P, Li Y, Hu L, Geng D, Zhang Z (2020). Soil moisture experiment in the Luan River supporting new satellite mission opportunities. Remote Sens Environ 240:111680.
Zhou G, Li C, Zhang D, Liu D, Zhou X, Zhan J (2021a) Overview of Underwater Transmission Characteristics of Oceanic LiDAR. IEEE J Sel Top Appl Earth Obs Remote Sens 14:8144-8159.
Zhou G, Long S, Xu J, Zhou X, Song B, Deng R, Wang C (2021b) Comparison Analysis of Five Waveform Decomposition Algorithms for the Airborne LiDAR Echo Signal. IEEE J Sel Top Appl Earth Obs Remote Sens 14:7869-7880.

Authors and Affiliations

Romulus Costache[1,2] · Alireza Arabameri[3] · Iulia Costache[4] · Anca Crăciun[2] · Binh Thai Pham[5]

✉ Alireza Arabameri
alireza.ameri91@yahoo.com

Romulus Costache

romuluscostache2000@yahoo.com

Iulia Costache
iulia.elena.costache@gmail.com

Anca Crăciun
anca.craciun@ddni.ro

Binh Thai Pham
binhpt@utt.edu.vn

[1] Department of Civil Engineering, Transilvania University of Brasov, 5, Turnului Str, 500152 Brasov, Romania

[2] Danube Delta National Institute for Research and Development, 165 Babadag Street, 820112 Tulcea, Romania

[3] Department of Geomorphology, Tarbiat Modares University, 36581-17994 Tehran, Iran

[4] Faculty of Geography, University of Bucharest, 010041 Bucharest, Romania

[5] University of Transport Technology, 54 Trieu Khuc, Thanh Xuan, 100000 Ha Noi, Vietnam

Journal of Environmental Management 316 (2022) 115316

Contents lists available at ScienceDirect

Journal of Environmental Management

journal homepage: www.elsevier.com/locate/jenvman

Research article

Flood susceptibility evaluation through deep learning optimizer ensembles and GIS techniques

Romulus Costache [a,b,*], Alireza Arabameri [c], Iulia Costache [d,**], Anca Crăciun [b,***], Abu Reza Md Towfiqul Islam [e], S.I. Abba [f], Mehebub Sahana [g], Binh Thai Pham [h]

[a] Department of Civil Engineering, Transilvania University of Brasov, 5, Turnului Str, 500152, Brasov, Romania
[b] Danube Delta National Institute for Research and Development,165 Babadag Street, 820112, Tulcea, Romania
[c] Department of Geomorphology, Tarbiat Modares University, Tehran, 36581-17994, Iran
[d] Faculty of Geography, University of Bucharest, Bucharest, 010041, Romania
[e] Department of Disaster Management, Begum Rokeya University, Rangpur, 5400, Bangladesh
[f] Interdisciplinary Research Center for Membrane and Water Security, King Fahd University of Petroleum and Minerals, Dhahran, 31261, Saudi Arabia
[g] Department of Geography, University of Manchester, United Kingdom
[h] Geotechnical Engineering and Artificial Intelligence research group (GEOAI), University of Transport Technology, 54 Trieu Khuc, Thanh Xuan, Ha Noi, 100000, Viet Nam

ARTICLE INFO

Keywords:
Flood susceptibility
Romania
Iterative classifier optimizer
Neural networks
Decision tree

ABSTRACT

It is difficult to predict and model with an accurate model the floods, that are one of the most destructive risks across the earth's surface. The main objective of this research is to show the prediction power of three ensemble algorithms with respect to flood susceptibility estimation. These algorithms are: Iterative Classifier Optimizer – Alternating Decision Tree – Frequency Ratio (ICO-ADT-FR), Iterative Classifier Optimizer – Deep Learning Neural Network – Frequency Ratio (ICO-DLNN-FR) and Iterative Classifier Optimizer – Multilayer Perceptron – Frequency Ratio (ICO-MLP-FR). The first stage of the manuscript consisted of the collection and processing of the geodatabase needed in the present study. The geodatabase comprises a number of 14 flood predictors and 132 known flood locations. The Correlation-based Feature Selection (CFS) method was used in order to assess the prediction capacity of the 14 predictors in terms of flood susceptibility estimation. The training and validation of the three ensemble models constitute the next stage of the scientific workflow. Several statistical metrics and ROC curve method were involved in the evaluation of the model's performance and accuracy. According to ROC curves all the models achieved high performances since their AUC had values above 0.89. ICO-DLNN-FR proved to be the most accurate model (AUC = 0.959). The outcomes of the study can be used to guide future flood risk management and sustainable land-use planning in the designated area.

1. Introduction

Every year, many parts of the world are affected by natural disasters related to excess water resources. Among all types of natural disasters, floods are the risk phenomenon that causes the greatest economic loss and death. It can be noted that on a global scale, these hazards affect about 200 million people every year (Ali et al., 2020). Due to global climate change, the number of such disasters recorded in the past few decades has increased (Alfieri et al., 2018). The amount of damage caused by floods is expected to increase substantially in the next few years (Arabameri et al., 2019).

Taking into account the economic loss and loss of life caused by the flood, Romania is one of the worst-hit European countries, along with Italy, Germany, Spain, and France (Vinke-de Kruijf et al., 2015). Thus, research work in the domain of vulnerability to flooding is mandatory in order to develop preventive measures to reduce the effects of floods. In

* Corresponding author. Department of Civil Engineering, Transilvania University of Brasov, 5, Turnului Str, 500152, Brasov, Romania.
** Corresponding author.
*** Corresponding author.
E-mail addresses: romulus.costache@icub.unibuc.ro (R. Costache), alireza.ameri91@yahoo.com (A. Arabameri), iulia.elena.costache@gmail.com (I. Costache), anca.craciun@ddni.ro (A. Crăciun), towfiq_dm@brur.ac.bd (A.R. Md Towfiqul Islam), saniisaabba86@gmail.com (S.I. Abba), mehebub.sahana@manchester.ac.uk (M. Sahana), binhpt@utt.edu.vn (B.T. Pham).

https://doi.org/10.1016/j.jenvman.2022.115316
Received 19 January 2022; Received in revised form 24 March 2022; Accepted 12 May 2022
Available online 19 May 2022

this respect, the identification of flood risk zones with high precision is very important (Bui et al., 2019). Therefore, all measures intended to mitigate the impact of floods should be based on previously identified areas that are highly vulnerable to flood risk. Therefore, the high-precision flood sensitivity map can be regarded as a non-structural measure and should be considered in flood risk management.

The number of research papers that address the topic of flood susceptibility evaluation has greatly increased in the last few years (Islam et al., 2021; Pham et al., 2021; A. Saha et al., 2021). As the number of papers on this topic has increased, the models used to assess the spatial variability of flood susceptibility have also diversified. Therefore, a large number of papers are based on bivariate statistical methods, like: weights of evidence (S. Saha et al., 2021b), frequency ratio (Natarajan et al., 2021), index of entropy (Wang et al., 2021), certainty factor (Cao et al., 2020), evidential belief function (Chowdhuri et al., 2020) and statistical index (Akay, 2021). An important role in the methodologies developed for this type of studies is also owned by algorithms like: artificial neural networks (Khoirunisa et al., 2021), support vector machine (Liu et al., 2022), classification and regression trees (Choubin et al., 2019), random forest (Chen et al., 2020), Naïve Bayes (Tang et al., 2020), rotation forest (Costache and Bui, 2019), adaptive neuro-fuzzy inference system (Ahmadlou et al., 2019) or deep learning neural network (Ahmadlou et al., 2021). It is very important to mention that all the listed models require as a dependent variable the locations where the flood took place in the past. Also, the independent variable or the flood predictors are used in these types of models as explanatory factors. The possibility of evaluating model performance and verifying the results is a very important strength that characterizes these methods involved in the evaluation of flood susceptibility.

It should be mentioned that there is not a general consensus among the researchers regarding the most performant model in terms of flood susceptibility assessment. This is one of the reasons why new hybrid models are generated and applied to improve the results. In this regard, we can mention the hybrid integration of bivariate statistics with machine learning (Costache, 2019b), the ensembles of bivariate statistics with multicriteria decision-making analysis methods (Costache and Bui, 2020), the ensembles of multicriteria decision-making analysis methods with machine learning (Nachappa et al., 2020), or the hybrid models generated by the combination of multiple machine learning models (Prasad et al., 2021). Therefore, a novel ensemble approach is crucial for filling the above research gaps.

Taking all the above aspects into consideration, the purpose of this research is to estimate the flood susceptibility in a highly affected area from Romania, using 3 novel ensemble algorithms represented by: Iterative Classifier Optimizer – Alternating Decision Tree – Frequency Ratio (ICO-ADT-FR), Iterative Classifier Optimizer – Deep Learning Neural Network – Frequency Ratio (ICO-DLNN-FR) and Iterative Classifier Optimizer – Multilayer Perceptron – Frequency Ratio (ICO-MLP-FR). The integration of these models is explained by the fact that an optimization algorithm like ICO can be able to improve the performance of the three machine learning models in terms of flood susceptibility assessment. To the best of the authors' knowledge, these ensemble algorithms have not been used together to examine any natural hazard, such as flood susceptibility maps. The confusion matrix and other statistical indices like sensitivity, specificity, accuracy, and k-index will be involved in testing the model's performance, while the ROC Curve will be used in order to estimate the accuracy of the results. The novel aspect of this paper is that it integrates three new ensembles e.g., ICO-ADT-FR, ICO-DLNN-FR and ICO-MLP-FR for the first time for mapping flood susceptibility. It is hoped that the proposed novel ensemble approach is not limited to flood susceptibility studies but can be employed in other environmental disasters such as gully erosion, landslides, forest fires and avalanches.

2. Study area and data used

2.1. Study area

The present case study is focused on Putna river basin from Romania (Fig. 1). This catchment has a surface of 2509 km^2 and his extreme limits have the following coordinates: 26° 22′ 13.08″ and 27° 29′ 57.84″ E longitude, and 46° 2′ 44.16″ and 45° 31′ 23.16″ N latitude.

The study area covers the following 3 distinct relief regions: the Romanian Plain Region, Subcarpathian Region and Carpathian Region. Putna river catchment is distributed into three different topographical units, represented by mountain (Carpathian region), hilly (Subcarpathian region) and plain zones (Romanian Plain), which are prominently manifested in the elevation range from 14 m in the lowlands to 1786 m in the mountains. Another morphometric indicator that reveals the differences between the specific regions is the slope angle which is close to 60°, in the mountain area, while the main feature of the plain area is the slope angle close to 0°. Therefore, the slope distribution can offer a first indication regarding the spatial variability of flood susceptibility. Therefore, in mountainous and hilly areas the surface runoff is likely to occur, besides in plain areas that have higher water storage potential and are more likely to be affected by floods. The climatic conditions are characterized by frequent heavy rainfall events, while the annual sum of precipitation on average is about 800 mm/year, which varies according to relief units and altitude. The forests account for about 53.3% of the study area, being followed by agricultural areas (18.1%), pastures (10.2%), built-up areas (6.2%), vineyards (6.1%), shrubs (3%), rivers (1.6%) and fruit trees (1.5%) (Costache and Bui, 2019).

The data from the Romanian Government certifies that the most devastating flood events within the Putna river catchment occurred in 2005, a disaster that caused a total of 15 fatalities. Also, in that year, the total economic losses generated by floods were quantified at €150 million (Romanescu and Nistor, 2011).

2.2. Flood locations inventory

In the process of flood susceptibility computation, a very important input variable is represented by the locations of the past flood events. This is explained by the fact that the floods will be more likely in areas that have the same characteristics as those where they have already produced flood in the past (Arabameri et al., 2019). In this case, the sources for flood inventory locations can be: governmental archive databases, newspaper articles, past scientific articles, or field surveys (Costache and Bui, 2019). In this study, the flood inventory map was created based on the information from the General Inspectorate for Emergency Situations in Romania. Therefore, a total of 132 flood events occurred in the study zone. According to the authorities, these locations were placed in the most representative points of the flooded zones and therefore we consider that these locations are also representative for the present research work. Moreover, the high majority of the flood susceptibility studies in the literature are using as dependent variable the flood locations as points (Ahmadlou et al., 2019, 2019, 2019; Chowdhuri et al., 2020). Because of the fact that flood susceptibility mapping is a binary classification procedure, another sample with 132 non-flood locations was created. Moreover, in order to ensure the possibility to test the models' performances and to check the accuracy of the results, the total sample comprising the flood and non-flood locations was split in a first stage into 70% - training data set and 30% - validating data set. Furthermore, the training dataset was divided again into 70% - training data sets and 30% - testing data sets. It is worth to mention that the sampling process was done, in a random way, using the Subset tool of ArcGIS 10.8 software. The random sampling procedure was involved in order to ensure that the results are as objectives as possible and are not influenced by a subjective sampling process.

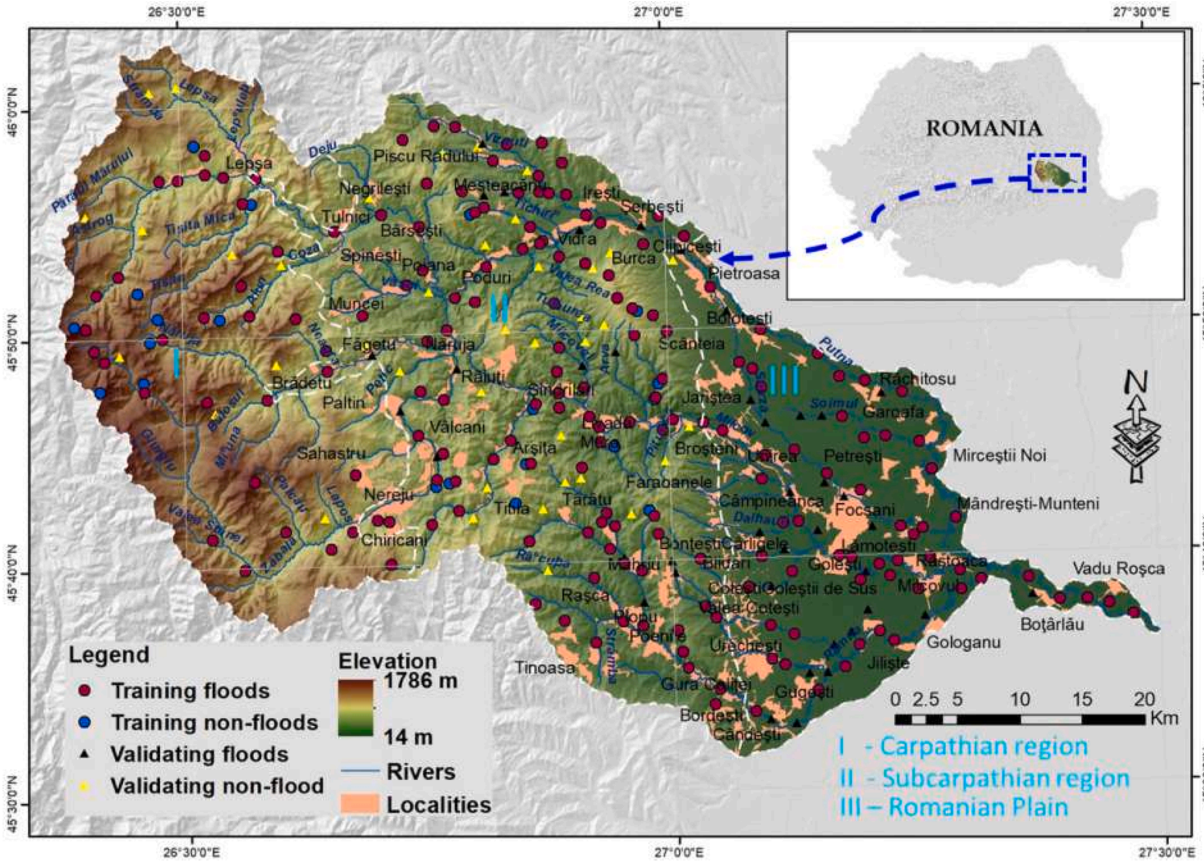

Fig. 1. Study area location.

2.3. Flood predictors

In all research papers where the main goal is to detect and quantify the flood-prone surfaces, the selection of predictors that have a great influence on the flood process is a crucial step. After a careful consultation of the literature (Chen et al., 2020; Nachappa et al., 2020; Tehrany et al., 2013) and giving specific conditions for the characteristics of the Putna River Basin, a total of 14 flood predictors were initially selected to calculate the flood susceptibility of the entire study area. The Shuttle Radar Topographic Mission (SRTM) at a spatial resolution of 30 m was an important data source from which the Digital Elevation Model (DEM) for the study area was extracted. Further, the DEM was involved in the derivation of the next 9 morphometrical flood predictors: slope angle, elevation, topographic position index (TPI), stream power index (SPI), plan curvature, topographic wetness index (TWI), profile curvature, convergence index, and aspect. The other 5 flood predictors were derived from specific databases like: Geological Map of Romania 1:200000 for lithology, Soil Map of Romania 1:200000 for hydrological soil group, Corine Land Cover 2018 data base for land use, and National River Cadaster of Romania for distance to river. The rainfall was achieved by the interpolation of the mean sum of multiannual precipitation values recorded within the period 1980 and 2015. The flood predictors are as follows:

Slope angle is an important morphometric factor which have a major influence in flooding phenomenon (Dahri and Abida, 2017). It is well-known that a flat area is more prone to flooding than an area with a high slope angle that leads to surface runoff manifestation. The slope angle was split into the following categories in order to create the slope angle map: < 3°; 3–7°; 7–15°; 15–25°; >25° (Fig. 2b). Elevation is a second morphometric factor that has a crucial role in the evaluation of flood susceptibility because of the fact that the flood events are more likely in low altitudes areas (Tehrany et al., 2013). For the present case study, the next 8 altitude classes were applied in order to generate the elevation map: < 200 m; 200–400 m; 400–600 m; 600–800 m; 800–1000 m; 1000–1200 m; 1200–1400 m; >1400 m (Fig. 2h). Topographic Position Index (TPI) manage to differentiates a cell from its surrounding cells was taken into account their elevation (Jenness, 2000). In the present research the next classes were defined for TPI map: 35.39 – (−4.79); (−4.79) – (−1.57); (−1.57) – 1.32; 1.32–4.86; 4.86–46.73 (Fig. 3f). Based on the slope angle values and the specific catchment area, topographic wetness index (TWI) is calculated (Ali et al., 2020). This indicator highlights the effect that topography has on the water accumulation phenomenon. In order to draw the TWI map, the following classes were established using the Natural Breaks method: (−9.07) – 4.36; 4.36–8.29; 8.29–11.69; 11.69–14.81; 14.81–25.54 (Fig. 2e). Stream Power Index (SPI) represents another morphometric indicator that will be used as flood predictor. Water's erosive power and transport capacity are considered in determining its values (Sharma et al., 2015). The next expert judgment-based classes were established for SPI map: 0–50; 50–200; 200–500; 500–1000; >1000 (Fig. 3e). Several studies have used the Convergence Index, derived from DEM, to assess flood and flash flood susceptibility (Zaharia et al., 2015, 2017). Interfluvial surfaces are highlighted by positive values, while hydrographic convergence is demonstrated by negative values (Costache, 2019a). Convergence Index map was generated based on the intervals used in the literature (Costache and Bui, 2020): (−96) – (−3); (−3) – (−2); (−2) – (−1); (−1) – 0; 0–95 (Fig. 2g). Profile curvature is a function of the slope direction in the vertical plan (Abedini et al., 2019). Enhanced surface runoff is indicated by values higher than 0, while decelerating surface runoff is indicated by negative values (Arabameri et al., 2020). Based on the following 3 classes, the profile curvature map was created: (−5.65) - (−0.1); (−0.1) - 0.1; 0.1–3.97 (Fig. 2c). The Aspect was found to be a predictor of flooding because it is mainly related to the variability of soil moisture (Dahri and Abida, 2017). An

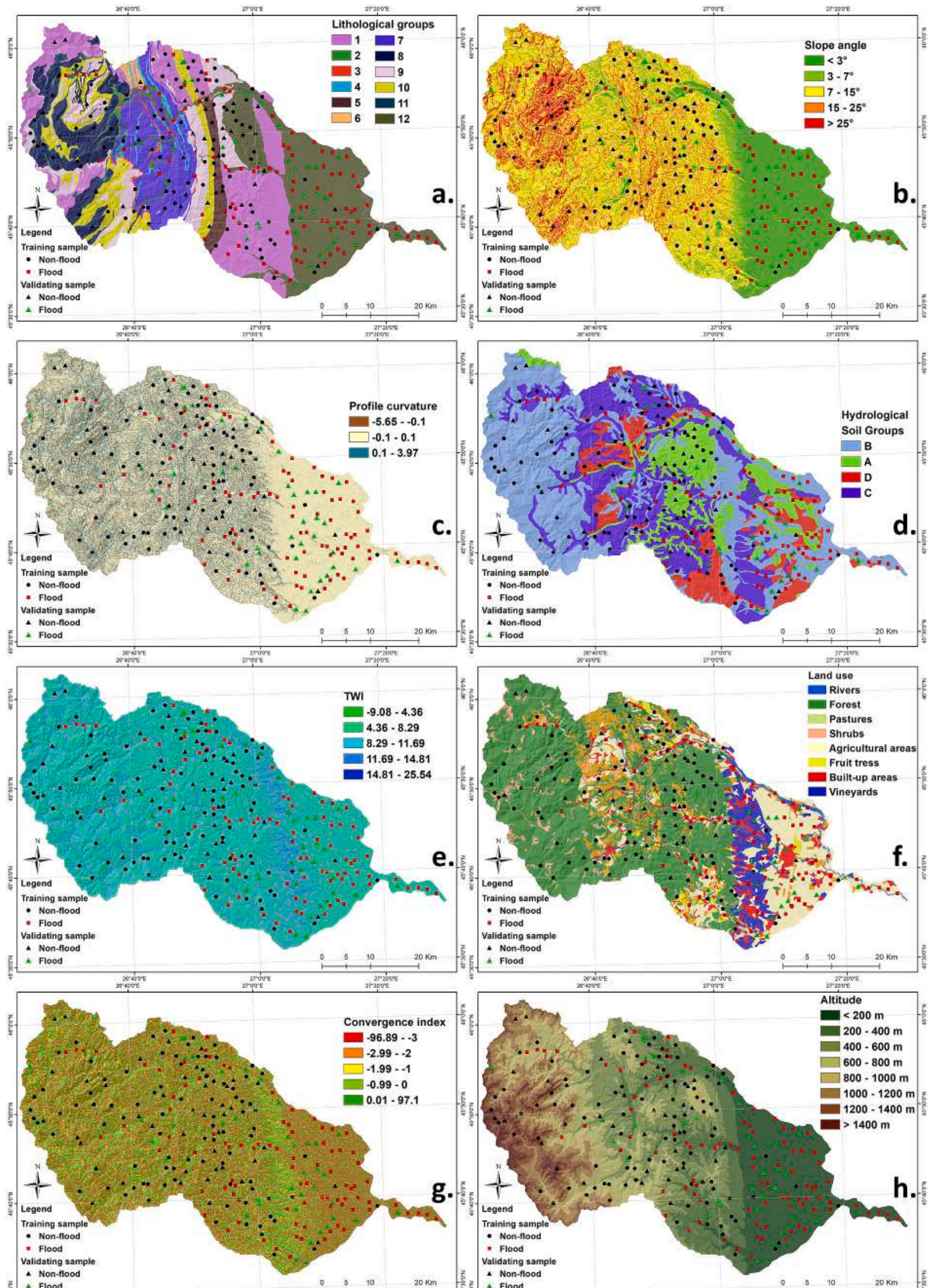

Fig. 2. Flood conditioning factors (a. Lithology; b. Slope angle; c. Profile curvature; d. Hydrological Soil Groups; e. TWI; f. Land use; g. Convergence Index; h. Elevation).

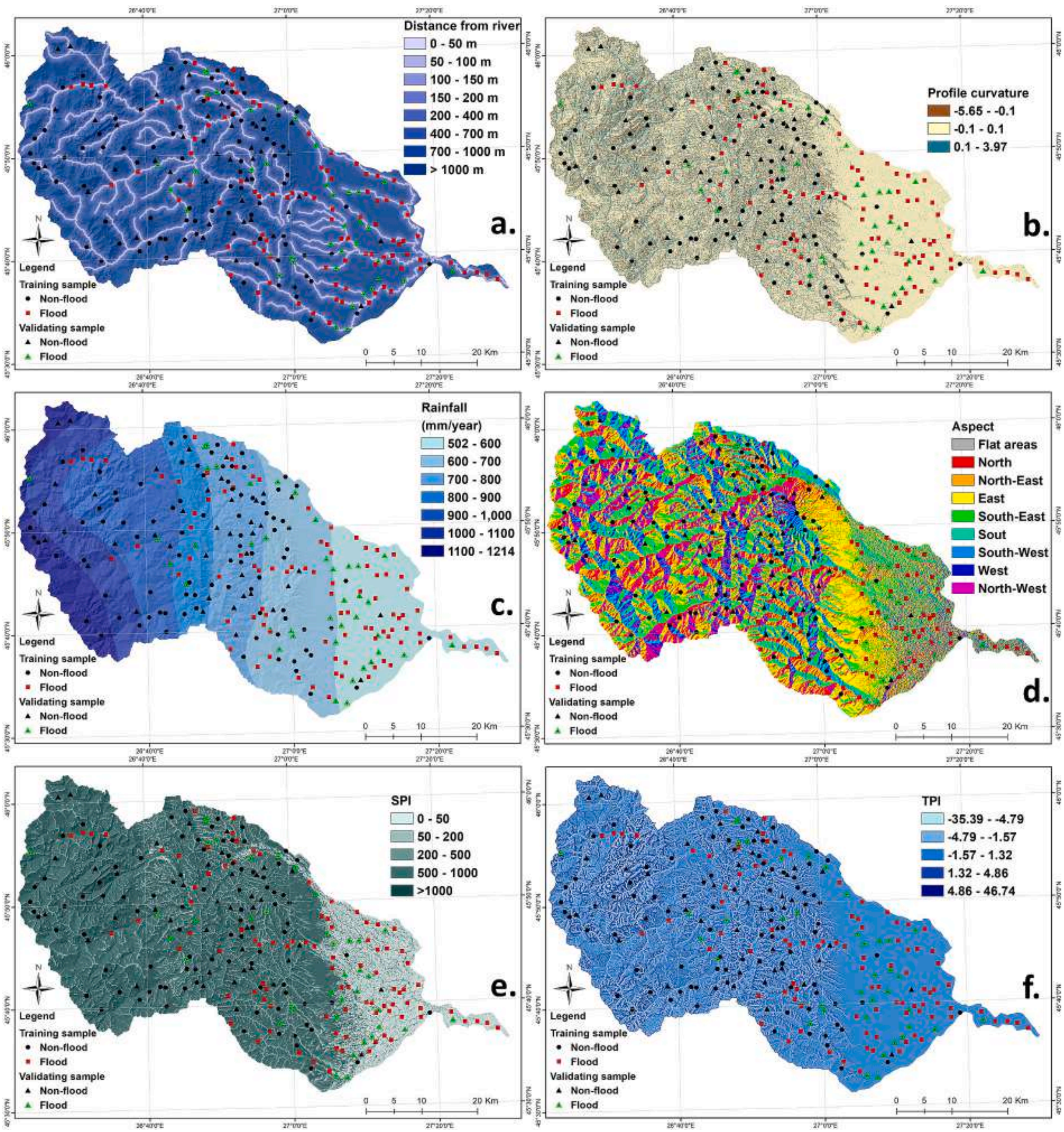

Fig. 3. Flood conditioning factors (a. Distance from river; b. Plan curvature; c. Rainfall; d. Aspect; e. SPI; f. TPI).

intersection between a horizontal plane and a terrain surface produces a contour line that defines the plan curvature. This value differentiates convergent runoff regions from divergent runoff ones. The next 3 classes were used to create the plan curvature map: (−3.07) – (−0.1); (−0.1) – 0.1; 0.1–2.89 (Fig. 3b). The Aspect raster values were grouped into one flat zone and the following 8 directions: flat zone, north, north-east, east, south-east, south, south-west, west, north-west (Fig. 3d). Land use is a flood prediction factor, which has a great influence on surface runoff and water storage processes. The following 8 land-use categories are defined in the Putna River catchment area: built-up areas, agriculture zone, forests, pastures, fruit trees, shrubs, rivers, and vineyards (Fig. 2f). Due to the permeability of the rock, lithology mainly controls the infiltration process of water, which in turn affects the flooding phenomenon (Costache and Bui, 2019). A total of 12 lithological categories were found in the study area (Fig. 2a). In Table 1, the rocks associated with the 12 categories are listed.

Table 1
Lithological categories located across the Putna river catchment (after Costache and Bui (2019)).

Lithological Categories	Coding
Loess deposits	1
Sandstone, schists	2
Gypsum, salt, clay	3
Sandstone, marls, tuffs	4
Marls, clay, sands	5
Clay, marls	6
Schists, gypsum	7
Conglomerates, breccia	8
Tuffs, salt, shale	9
Sandstones, clay	10
Sandy Flysch, marls	11
Sands, gravels	12

Rainfall plays a crucial role in the occurrence of flooding (Cao et al., 2016). Using the data of 14 weather stations and 15 hydrological stations, the spatial variation of the annual average rainfall value is obtained. It should be noted that the annual average rainfall value was used in the high majority of the studies related to the flood susceptibility assessment (Khosravi et al., 2018; Rahmati et al., 2020; Shafizadeh-Moghadam et al., 2018). Spline method was involved to interpolate all rainfall values. This algorithm is recommended when the number of data points is relatively small, as in the case of this analysis (Kourgialas and Karatzas, 2011). Once obtained, the rainfall values have been divided into the following 7 classes, established using a threshold of 100 mm/year: 502–600 mm/year; 600–700 mm/year; 700–800 mm/year; 800–900 mm/year; 900–1000 mm/year; 1000–1100 mm/year; 1100–1214 mm/year (Fig. 3c). Water infiltration is heavily influenced by the Hydrological Soil Group, a flood control parameter (Costache and Bui, 2019). Specifically, the soil texture controls hydraulic conductivity, and this influence directly impacts infiltration (Costache and Zaharia, 2017). According to Fig. 2d all 4 hydrological soil groups are inside the Putna river basin. There is a difference between flood-prone areas that are located near rivers, and areas that are further away from rivers that are less susceptible to floods. As a result, a large number of studies considered the distance from rivers as a flood conditioning factor (Nachappa et al., 2020). The Euclidean distance was used in order to derive the distance from river raster. In order to create the map of this predictor, its values were divided into the next 8 classes: 0–50 m; 50–100 m; 100–150 m; 150–200 m; 200–400 m; 400–700 m; 700–1000 m; > 1000 m (Fig. 3a).

All the classes/categories are also presented in Table S1.

3. Methods

The methodological steps are schematically represented in Fig. 4. In the next sub-sections are described the methods used in the present research.

3.1. Correlation-based feature selection (CFS)

The CFS method is employed in order to select the flood predictors which have a good correlation with the flood presence. In order for a factor to be of major significance, it must be highly correlated with the observed phenomenon and uncorrelated with the other factors (Costache, 2019a). A strong correlation between each flood predictor and flood locations indicates that factor has a superior ability to predict flood phenomena than the other factors. In correlation-based feature selection, fast and redundant information is displayed and the irrelevant and redundant information is filtered out. When a factor is highly correlated with another, it is usually redundant (Hall et al., 2009). The CFS scores associated to the flood predictors will therefore be higher for those which are directly correlated with the flood locations. The next relation is used to derive the CFS scores:

$$CFS = \frac{\mathrm{k}r_{cf}}{\sqrt{\mathrm{k} + \mathrm{k}(\mathrm{k}-1)r_{ff}}} \tag{1}$$

where *CFS* represents the correlation between each flood predictor with the presence/absence of flood locations, k is the number of flood predictors, r_{cf} the average correlation between flood predictos and flood locations, and r_{ff} the average intercorrelation between flood predictors.

3.2. Frequency ratio

An environment modelling procedure frequently involves the Frequency Ratio (FR), a bivariate statistical technique (Costache and Zaharia, 2017; Mohammady et al., 2012). The FR method was used in

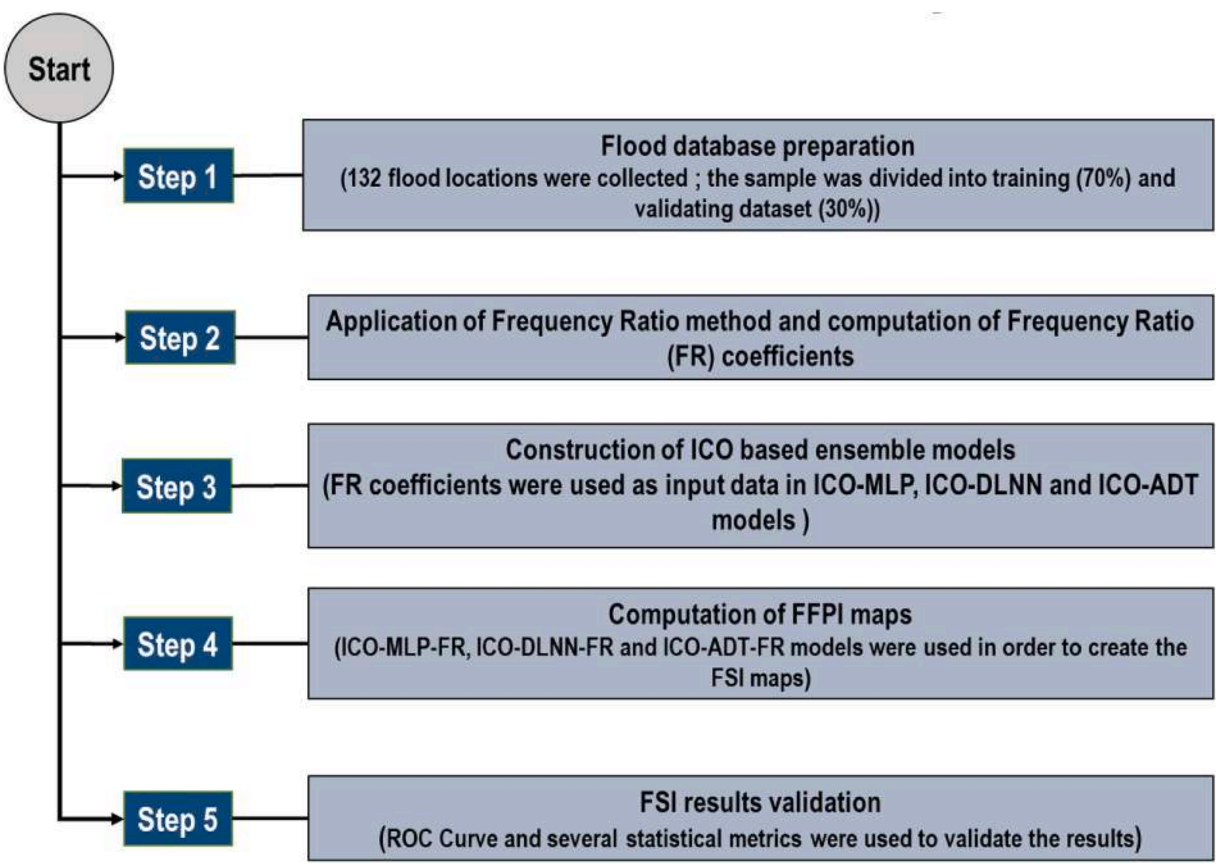

Fig. 4. Methodological flowchart.

this research work in order to encode the classes and categories of flood predictors. By analyzing spatial overlaps between the flood locations and the predictor's category and class, this method reveals the correlation between flood locations and flood conditioning factors. The following formula can be used to compute each class's FR coefficients (Rahmati et al., 2016):

$$FR = \left(\frac{Np(LXi)}{\sum_{i=1}^{m} Np(LXi)}\right) \Big/ \left(\frac{Np(Xj)}{\sum_{j=1}^{n} Np(Xj)}\right) \tag{2}$$

where *FR*-frequency ratio value attributed to a class/category *i* of parameter *j*, *Np(LXi)* is the number of flood locations within a class *i* of a flood conditioning factor *X*, *Np(Xj)* is the number of flood locations within the predictor *Xj*, *m* is the number of classes within a flood predictor *Xi*, and *n* is the number of flood predictors.

According to the literature it is recommended to avoid a high variation of flood conditioning factors in terms of its range values (Tehrany et al., 2014). Therefore, one of the most efficient solutions to solve this issue, which is very popular in the literature, is to compute the bivariate statistics coefficients for the classes/categories of flood predictors (Shafizadeh-Moghadam et al., 2018). Thus, in the present case the Frequency Ratio bivariate statistic model was used in this regard.

3.3. Multilayer Perceptron (MLP)

The Multilayer Perceptron (MLP) represents a multilayer feed-forward network algorithm having one-way propagation error. In addition, the MLP can handle a variety of pattern recognition problems and time series prediction issues (S. Saha et al., 2021a). Floods are complex physical processes that behave as nonlinear systems influenced by the natural human activities (Prasad et al., 2021). Consequently, the MLP model has an efficient nonlinear mapping capability compared to general linear statistical models or deterministic algorithms (Pham et al., 2017).

Generally, the MLP architecture is formed by an input layer containing input neurons, a hidden layer containing more hidden neurons and, in the case of the present research, an output layer with 2 output neurons. The weights values are used to process the connections between the neurons from all the three component layers (Pham et al., 2017). By training these weight values allows neural networks to have a stable and orderly structure with the capacity to make decisions. A technique called error backpropagation associated with a conventional gradient descent method, employed as rule for the training process of MLP, allows weight values to be adjusted between neurons according to the rate of error between the actual values and the MLP predicting values (Hassanien et al., 2014). With the gradient descent algorithm, an iterative solution can be used to calculate the minimal value of the root mean squared error (RMSE) of the objective function, as well as the optimal weights of neural network architecture. The RMSE can be determined by applying the next equation (Li et al., 2007):

$$RMSE = \sqrt{\frac{1}{n}\sum_{i=1}^{n}(c_i - \hat{c}_i)^2} \tag{3}$$

where, *n* represents the date number, c_i are the measured data, and $\hat{c}_i$ the calculated values.

3.4. Deep learning neural network (DLNN)

In machine learning, deep learning (DL), which is based on artificial neural networks, is a rapidly growing area of research that uses multi-dimensional representations of data patterns for classification and detection (Jung et al., 2020). The word 'deep' in this context refers to the transformation of data representations at one level into representations at another level through a chain of layers (Van Dao et al., 2020). A data transformation allows the extraction of the best hierarchical representation of data as the number of layers (depth of network) increases. In addition to the multiple hidden layers, there will also be 2 neurons which represent flood and non-flood pixels representing the effects of floods in the output layer. Since the flood susceptibility assessment, in essence, represents a binary classification process, flood location will receive the value of 1 and non-flood locations the value of 0 (Bui et al., 2020). In the DLNN training the sigmoid function, having the form E (Y = i/x), will be involved. The information that resides on a single output neuron that is associated with class i will allow to approximate the sigmoid function. Additionally, a softmax function of the following form will be used in this study (Costache et al., 2020):

$$softmax(a_i) = \frac{\exp(a_i)}{\sum_k \exp(a_i)} \tag{4}$$

where a_i is the term designing the *softmax* function.

In the next relation the activation function is present in order to express a deep neural network with many hidden layers (Costache et al., 2021b):

For $h = 1, \ldots,$ H (hidden layers),

$$a^{(h)}(x) = b^{(h)} + W^{(h)} p^{(h-1)}(x) \tag{5}$$

$$p^{(h)}(x) = k\left(a^{(h)}(x)\right) \tag{6}$$

where, *k* is associated to the activation function.

3.5. Alternating Decision Tree (ADT)

The Alternating Decision Tree (ADT) represents an ensemble method formed by the combination of boosting algorithm and decision trees method (Lei et al., 2020). This is a less complex method than other decision trees like Random Forest, Classification and Regression Trees or Rotation Forest. Based on multiple prediction alternate layers and nodes, the ADT model extends traditional decision trees and voted-stumps (Costache et al., 2021a). The prediction nodes in the ADT algorithm provide a single identifying number whereas the decision nodes specify a condition. Let c_1 represent a precondition, c_2 represent a base condition, and *a* and *b* represent two real numbers (Chen et al., 2017). Then *a* and *b* will be calculated with the next relations (Pham et al., 2016):

$$a = 0.5 * \ln\frac{W_+(c_1 \cap c_2)}{W_-(c_1 \cap c_2)}, \; b = 0.5 * \ln\frac{W_+(c_1 \cap \overline{c_2})}{W_-(c_1 \cap \overline{c_2})} \tag{7}$$

where W is equal to the sum of the values provided by the prediction node, and the optimal c_1 and c_2 are calculated by minimizing the Z_t (c_1, c_2), obtained with the following relation:

$$z_t(c_1 c_2) = 2\sqrt{W_+(c_1 \cap c_2) * W_-(c_1 \cap c_2)} + \sqrt{W_+(c_1 \cap \overline{c_2}) * W_-(c_1 \cap \overline{c_2})} + W(\overline{c_2}) \tag{8}$$

3.6. Iterative Classifier Optimizer (ICO)

Cross-validation is used as part of the Iterative Classifier Optimization (ICO) process to optimize the number of iterations (Meshram et al., 2021). Classes and attributes such as numeric, nominal, binary and empty nominal can be handled by ICO (Khosravi et al., 2021). After constructing the model, by the comparation of the observed values with the measured ones, the ICO algorithm then optimizes the model by introducing information from the observed and measured values into the model to adjust the output (Saad, 2018). ICO algorithms will be applied in the present research in order to optimize the training procedure of the three machine learning algorithms above presented. Thus, in the case of MLP model, ICO will be used to optimize hyperparameter represented by the number of hidden neurons in the hidden layer, and eventually, the weights between different layers of neurons that will help to reach the lowest RMSE value. Also, in terms of DLNN, the ICO algorithm will help to optimize the number of hidden layers and also the number of hidden neurons in each hidden layer. Thus, the architecture of deep neural network will be optimized and the loss and accuracy values will be adjusted. In the case of ADT model, the ICO algorithm will be involved to optimize hyperparameter represented by the maximum depth of decision tree so as the model to reach the maximum accuracy. It should be noted that maximum depth hyperparameter is able to control the entire tree complexity (Hong et al., 2020).

All the three ensembles were run in Weka 3.9 software.

3.6. Results validation

3.6.1. Statistical measures

We validated the results using the following statistical indices: Specificity, Sensitivity, Kappa Index, Accuracy and Precision. Statistical indices are regarded as significant if they indicate a spatial correlation between the observed flood and non-flood locations and the estimated flood susceptible zone (Costache, 2019b). The following equations will be involved in the statistical metrics calculation (Canbek et al., 2017):

$$\text{Sensitivity} = \frac{\text{TP}}{\text{TP} + \text{FN}} \quad (9)$$

$$\text{Specificity} = \frac{\text{TN}}{\text{FP} + \text{TN}} \quad (10)$$

$$\text{Precision} = \frac{\text{TP}}{\text{TP} + \text{FP}} \quad (11)$$

$$\text{Accuracy} = \frac{\text{TP} + \text{TN}}{\text{TP} + \text{FP} + \text{TN} + \text{FN}} \quad (12)$$

$$\text{k} = \frac{\text{p}_\text{o} - \text{p}_\text{e}}{1 - \text{p}_\text{e}} \quad (13)$$

where P is the sum of flood locations, N is the sum of non-flood locations, FP (false positive) and FN (false negative) are the number of flood and non-flood locations erroneously classified, k is kappa coefficient, p_o is the observed flood locations, and p_e is the estimated flood susceptibility locations.

3.6.2. ROC curve

In studies concerning the susceptibility to floods, the receiver operating characteristic (ROC) curve is a popular way to validate results (Chen et al., 2020; Nachappa et al., 2020; Tehrany et al., 2013). A ROC graph shows the relationship between sensitivity on the Y axis and 1-Specificity on the X axis. According to our study, this method demonstrates the capability of a model to accurately predict the flood susceptibility. The Area Under Curve (AUC) of ROC Curve enables the user to achieve the most valuable information. It ranges from 0 to 1. Next mathematical relation is used to estimate the AUC:

$$\text{AUC} = \frac{(\sum TP + \sum TN)}{(\text{P} + \text{N})} \quad (14)$$

where TP (true positive), TN (true negative) are the sums of flood and non-flood locations correctly classified.

In the present case study, both the Success Rate and Prediction Rate were constructed. The Success Rate that provides a measure of how well the flood points are classified by the flood susceptibility maps, while the Prediction Rate shows how well the generated maps can predict the flood phenomena (Vakhshoori and Zare, 2016).

4. Results

4.1. Application of CFS for predictors selection

Through the CFS method, the 14 flood conditioning factors have been evaluated for their predictive capacity. The Average Merit (AM) values were used to express their predictive capacity (Fig. 5). The following hierarchy was achieved after the application of CFS model: Slope (0.283), Distance from river (0.252), Land use (0.231), Lithology (0.183), Profile curvature (0.175), TWI (0.158), Rainfall (0.152), Hydrological Soil Group (0.148), Plan curvature (0.141), Elevation (0.134), Convergence index (0.115), SPI (0.081), Aspect (0.069) and TPI (0.041).

Given the fact that all the flood predictors achieved an CFS score higher than 0 it should be concluded that all of them can influence in a specific measure the flood phenomena, and therefore, all the flood predictors will be involved in the modelling process.

4.2. Frequency ratio results

The normalized FR values were used as input data in ICO-MLP, ICO-DLNN and ICO-ADT models. Regarding the FR values, it should be noted that a number of 16 classes of factors have this coefficient equal to 0 (Table S1). Due to the fact that almost all the floods' phenomena take place near the rivers, the highest FR values were obtained by River land use category (19.91) and Distance from rivers class between 0 and 50 m (16.1).

4.3. Establishment of flood susceptibility maps through ICO-based ensembles

4.3.1. ICO-DLNN-FR

By implementing the ICO-DLNN-FR ensemble, the optimum number of hidden layers was established to 3, while the optimum number of hidden neurons in each hidden layer was established to 100. Moreover, the values of loss and accuracy during the training procedure were adjusted. Thus, a number of epochs ranging from 1 to 100 were used in order to reach the optimum number of these two statistics values. Therefore, according to Fig. 6a, the loss value of training dataset decreases from 0.6931 in the first epoch, to 0.2477 in the last epoch. In terms of validating dataset, the loss value decrease from 0.693 to 0.2178. The oscillation of accuracy value during the 100 epochs is highlighted in Fig. 6b. Thus, in terms of training data set accuracy in the first epoch was 0.5 while in the final epoch was 0.9804. At the same time, the accuracy in terms of validating dataset started from 0.7556 in the first epoch and reach to 0.9778 in the last epoch. In this case, the highest performances were obtained using a number of 3 hidden layers with 100 hidden neurons (Fig. 6c). Also, during the training process was

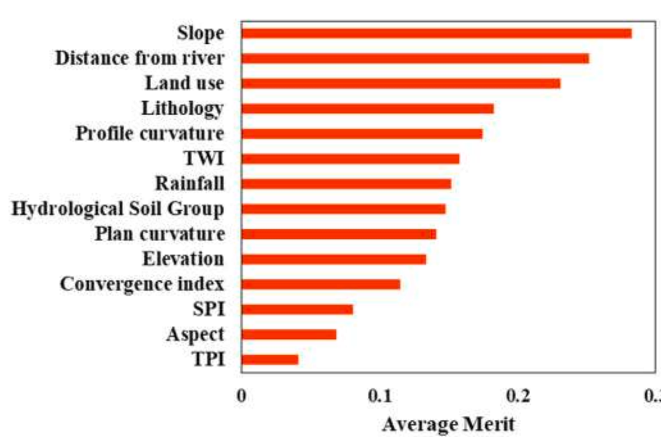

Fig. 5. Predictive capacity of flood conditioning factors using CFS model.

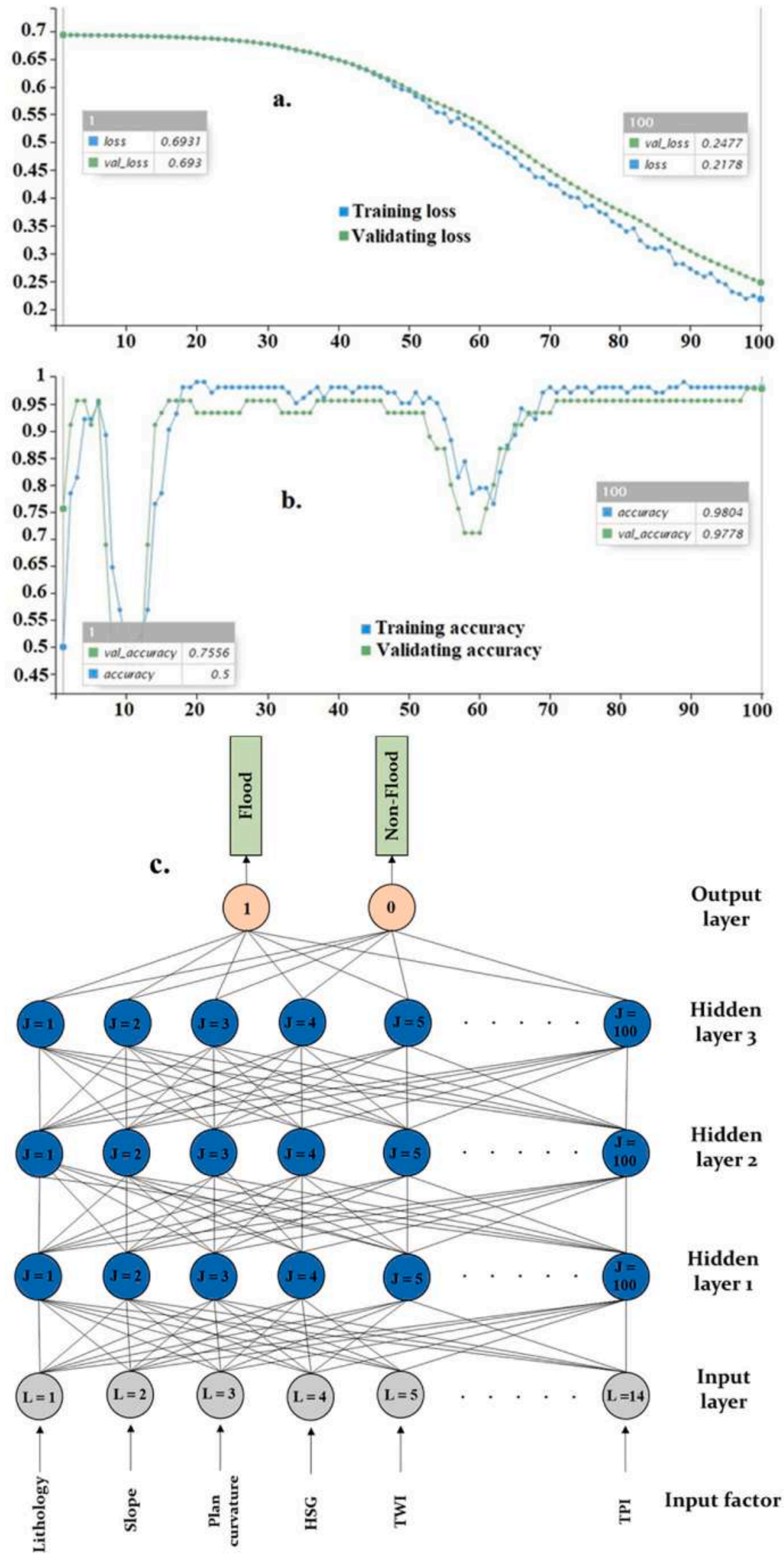

Fig. 6. ICO-DLNN-FR model (a. Loss values; b. Accuracy values; c. Architecture).

established a dropout rate of 0.17, a batch size of 4 and a split validation of 0.4.

The factor importance's of predictors in the ICA-DLNN-FR ensemble were derived following the training procedure. Thus, the highest importance was assigned to Slope (0.22), followed by Land use (0.134), Distance from river (0.13), Elevation (0.123), Convergence Index (0.067), Rainfall (0.065), SPI (0.065), Lithology (0.054), TPI (0.042), TWI (0.036), Plan curvature (0.026), Aspect (0.014), Hydrological Soil Groups (0.014) and Profile curvature (0.01) (Table 2).

The flood susceptibility index was created in Map Algebra using the values of importance for each predictor. Thus, using Natural Breaks, the raster values of FSI ICO-DLNN-FR were partitioned into 5 classes. The very low values are located in the great majority of the mountain area and cover 45.89% of the study zone. The low values are mainly distributed in hilly areas and accounts 26.12% of the entire territory. Medium values are present within the transition areas from hilly to plain zone and also along the main rivers in the mountain region. These values cover around 6.7% of the research area. High and very high values account for 20.3% of the Putna river catchment and are spread on the plain region (Fig. 7a). In Fig. S1 (a.-c.) from the Supplementary file, it can be seen a detailed view regarding the spatial extension of FSI ICO-DLNN-FR across a number of 3 regions from the study area and also the localities that are exposed to flood genesis.

4.3.2. ICO-MLP-FR

The ICO algorithm helped to achieve a very low RMSE value of 0.007 which was obtained taking into account a MLP architecture formed by 32 hidden neurons in the hidden layer. A trial-and-error procedure, with a maximum of 50 neurons, was followed in order to reach the lowest RMSE value. The performance of the ICO-MLP-FR model is highlighted also by the predicted pseudo-probability box-plot (Fig. 8a) which indicates that the majority of flood and non-flood pixels situated in the extreme parts of plot (right and left) are located above 0.5 on y-axis. The ROC Curve, by its AUC (0.989) attests again the very high performance in the classification process (Fig. 8b). The Gain chart is also available in Fig. 8c.

The predictor importance hierarchy shows that Slope (0.236) is again the most influential factor, followed by Distance from river (0.09), Rainfall (0.087), SPI (0.087), Land use (0.083), TPI (0.07), Elevation (0.068), TWI (0.065), Lithology (0.059), Convergence Index (0.051), Plan curvature (0.042), Profile curvature (0.029), Hydrological Soil Groups (0.019) and Aspect (0.016).

The FSI ICO-MLP-FR was obtained also in Map Algebra with the help of determined importance values. Through Natural Breaks algorithm, the raster values of FSI ICO-MLP-FR were split in 5 classes. The very low values cover 30.31% of Putna river basin and most of them are located in the mountain region. The low values, with a percentage of 43.07%, are mainly located in the hilly regions, while medium flood susceptibility is spread on 6.78% of the study zone and its presence is characteristic for

Table 2
Predictor importance in the 3 ensemble models.

Factors	ICA-DLNN-FR	ICA-MLP-FR	ICA-ADT-FR
Aspect	0.014	0.016	0.003
Convergence Index	0.067	0.051	0.105
Distance from river	0.130	0.090	0.185
Elevation	0.123	0.068	0.091
Land use	0.134	0.083	0.062
Lithology	0.054	0.059	0.047
Plan curvature	0.026	0.042	0.032
Profile curvature	0.010	0.029	0.008
Rainfall	0.065	0.087	0.045
Slope	0.220	0.236	0.252
HSG	0.014	0.019	0.035
SPI	0.065	0.087	0.058
TPI	0.042	0.070	0.037
TWI	0.036	0.065	0.040

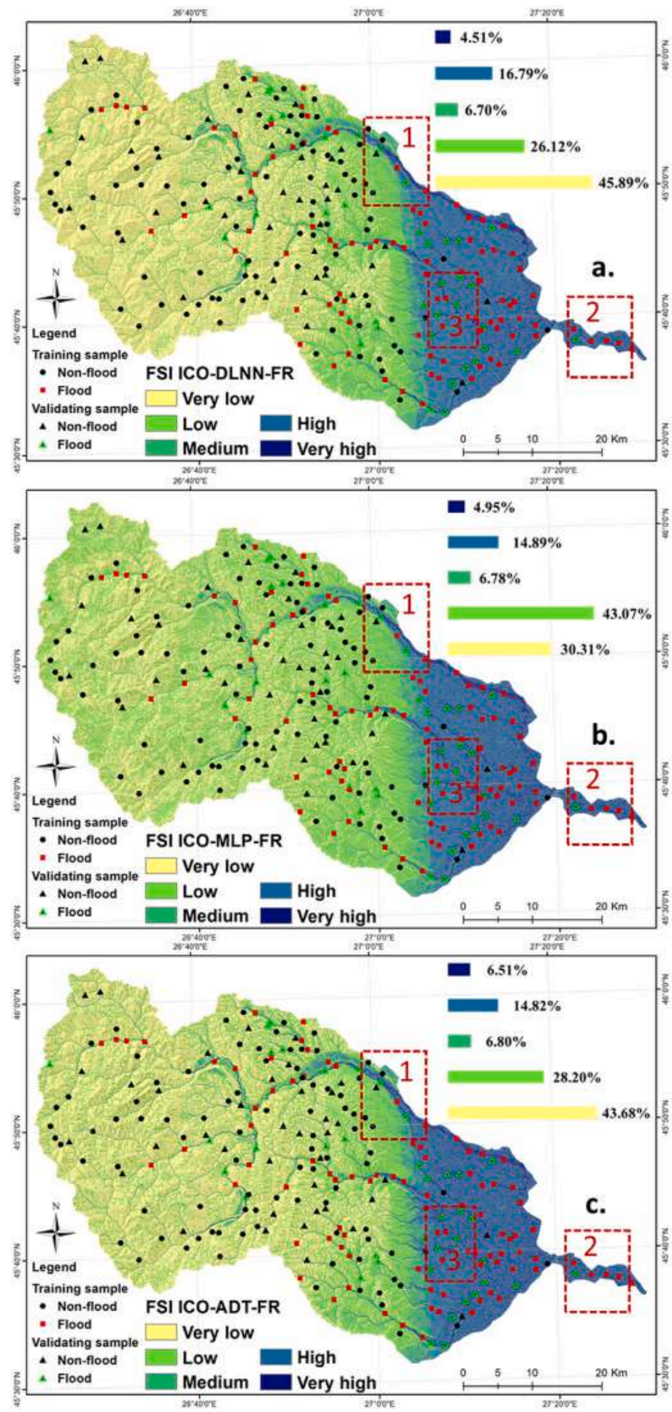

Fig. 7. Flood susceptibility index (a. ICO-DLNN-FR; b. ICO-MLP-FR; c. ICO-ADT-FR).

the transition region from hilly to plain zone. A total of 19.84% of the Putna river catchment is characterized by high and very high values of FSI ICO-MLP-FR these surfaces being distributed on the plain region (Fig. 7b). In Supplementary files in Fig. S1 (d.-f.), it can be observed a zoom with respect to the spatial distribution of FSI ICO-MLP-FR for 3 regions from different corners of the study area.

4.3.3. ICO-ADT-FR

Both training samples and validation samples were subjected to a trial procedure to determine the optimal parameter through which the highest accuracy of ICO-ADT-FR can be obtained. Therefore, the best

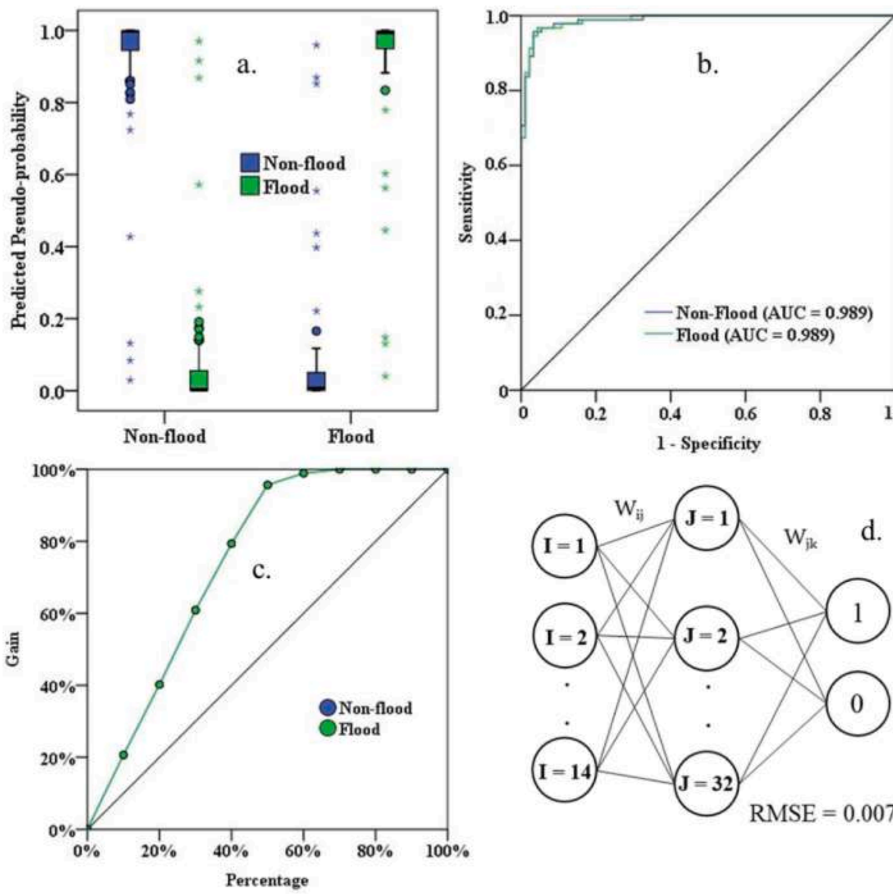

Fig. 8. ICO-MLP-FR model (a. Pseudo-probability; b. ROC Curves; c. Gain chart; d. Architecture).

accuracies (0.941 for training and 0.916 for validating) were obtained after 17 iterations. Also, according to Fig. 9, the optimization algorithm establishes the maximum depth of decision tree to 4. This decision tree was constructed based on the best parameters, and the importance of flood predictors was determined. Again, slope achieved the highest weight (0.252), followed by Distance from river (0.185), Convergence Index (0.105), Elevation (0.091), Land use (0.062), SPI (0.058), Lithology (0.047), Rainfall (0.045), TWI (0.04), TPI (0.037), Hydrological Soil Groups (0.035), Plan curvature (0.032), Profile curvature (0.008) and Aspect (0.003).

The same procedure in Map Algebra, like in the previous 2 cases, was applied to derive the values of FSI ICO-ADT-FR. Also, the Natural Breaks method was used to divide its values into 5 classes. A percentage of 43.68% of the study area is covered by very low flood susceptibility, while 28.2% is characterized by low susceptibility. On around 6.8% of the Putna river basin span the medium susceptibility values, while the high an very high ones total 21.33%. The spatial distribution of the susceptibility values is similar with the 2 previous cases (Fig. 7c). In Fig. S1 (g.-i.) from the Supplementary file, is presented a detailed overview of the spatial extension of FSI ICO-ADT-FR across the 3 regions from the research area and also the localities that are exposed to flood genesis.

4.5. Validation of the established maps

4.5.1. ROC curves

The Success Rate, resulted with the help of training sample, revealed that the highest performance was obtained by ICO-DLNN-FR ensemble (AUC = 0.959), followed by ICO-ADT-FR (AUC = 0.957) and ICO-MLP-FR (0.95) (Fig. 10a). The Prediction Rate, built with validation dataset, shows that the best model was again ICO-DLNN-FR (AUC = 0.911), followed by ICO-ADT-FR (AUC = 0.895) and ICO-MLP-FR (AUC = 0.893) (Fig. 10b).

4.5.2. Statistical metrics

The accuracy estimated taking into account the flood susceptibility values and the locations of flood and non-flood pixels from training sample revealed that ICO-DLNN-FR obtained the highest performance (0.951), being followed by ICO-ADT (0.935) and ICO-MLP-FR (0.929). The same sample utilized for K-index computation showed the next hierarchy: ICO-DLNN-FR (0.902), ICO-ADT (0.87) and ICO-MLP-FR (0.859). In terms of validating sample, the highest accuracy was achieved by ICO-DLNN-FR (0.938), followed by ICO-MLP-FR (0.925) and ICO-ADT-FR (0.9). The same hierarchy was respected also in the case of K-index as following: ICO-DLNN-FR (0.875), ICO-MLP-FR (0.85) and ICO-ADT-FR (0.8) (Table 3).

5. Discussions

Past studies have computed or modeled flood susceptibility maps or models using numerous techniques and algorithms. The flood susceptibility has been predicted by applying a wide variety of statistical and machine-learning methods. There is, however, considered a limitation and a drawback to the results performance the assessment of flood susceptibility using only a stand-alone-algorithm (Cao et al., 2020). As a consequence of poor data representation, the stand-alone-models usually fall short of identifying the best-fit function in the hypothesis space or the true distribution of the sample set (Wang et al., 2021). Therefore, the hybrid or ensemble models are considered more advanced research methods involved in the flood susceptibility prediction (Rahmati et al., 2016). In this regard, it can be mentioned the study of Khosravi et al. (2018) which estimated the flood susceptibility in Haraz river basin

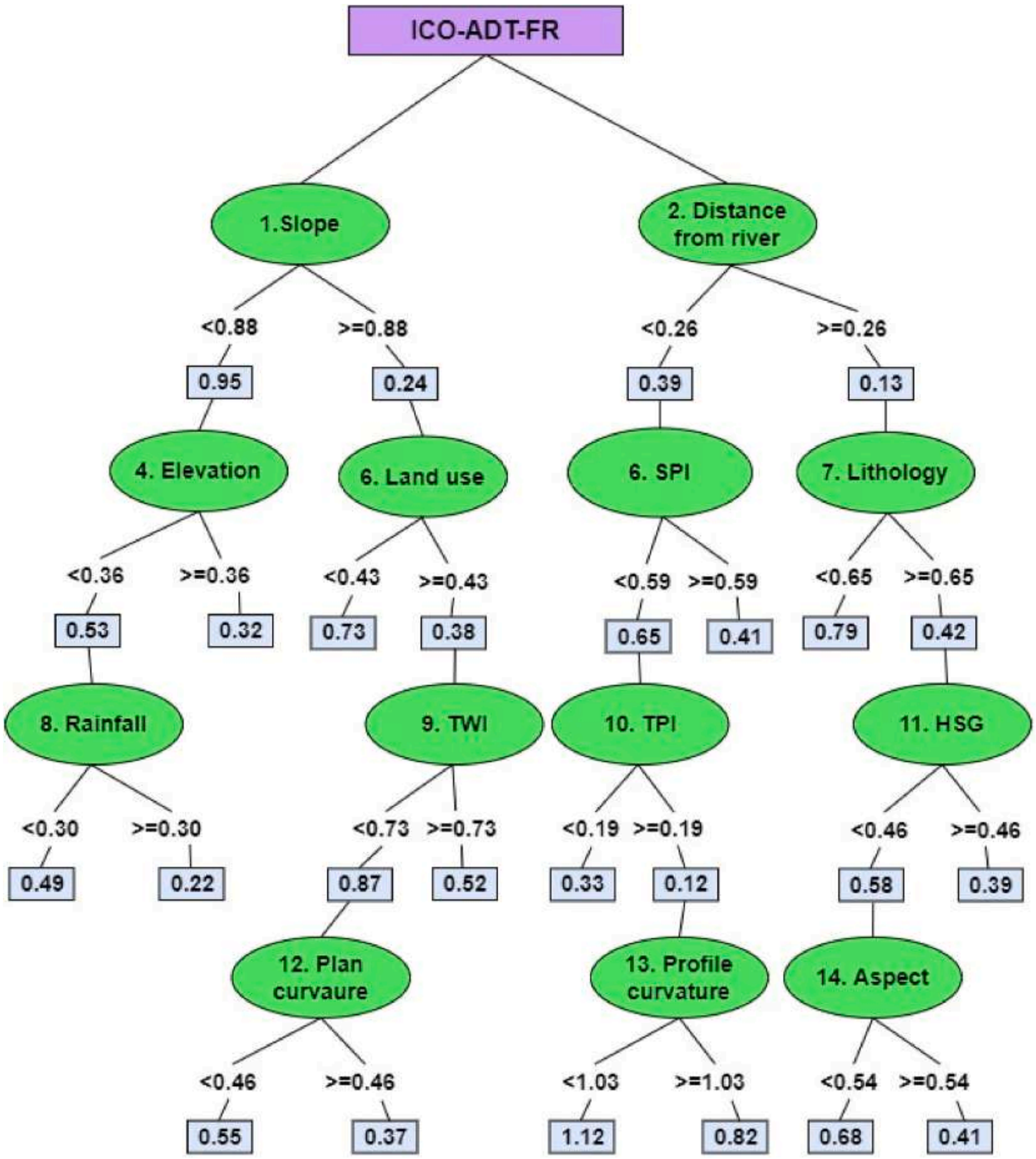

Fig. 9. Optimally pruned Decision Tree Structure for ICO-ADT-FR ensemble.

from Iran, a region with a poor availability of data, using ensemble models built-up from the combination of several decision tree algorithms. In this study, the authors demonstrated that predictors like slope angle, elevation and soil texture have the biggest influence with respect to the flood phenomenon occurrence. Moreover, in his study, developed to estimate the flash-flood susceptibility on Prahova river basin from Romania, Costache (2019a) revealed that the decision tree algorithms obtained a higher performance in combination with a bivariate statistic method than in the case of the application of the stand-alone-models.

In this study, 3 innovative ensemble models were constructed by the combination of Frequency Ratio (FR) and Iterative Classifier Optimizer (ICO) on the one hand, and Deep Learning Neural Network (DLNN), Alternating Decision Tree (ADT) and Multilayer Perceptron (MLP) on the other hand. Firstly, it should be noted that Frequency Ratio has a big advantage, compared to other bivariate statistical models, because it is considered to be a simple algorithm easier to use (Tehrany et al., 2013). This algorithm has the capacity to emphasize the spatial relationship between the location of flood predictors and the characteristics of the flood conditioning factors. Bivariate statistical methods, however, are unable to capture hidden flood features because of the complex mechanism that triggers floods (Wang et al., 2021). Secondly, the Iterative Classifier Optimizer (ICO) helped the three machine learning models to increase their prediction power and finally their accuracy. This fact is demonstrated, for example, in the case of MLP model, by the very low value of RMSE (0.007) achieved after the optimization with ICO algorithm. Also, the ROC Curves carried out with the training and validating sample emphasize very good performances since the AUC is situated above 0.89. Given the very high accuracy of the 3 hybrid models, they will be able to represent very important benchmarks for future studies related to assessing the susceptibility of different areas of the planet to natural hazards in general, and floods in particular. The present study has a high potential to be of particular interest to researchers who want to apply hybrid models based on the ICO algorithm because, in addition to the very high performance it has generated, it is the first time that the ICO algorithm is used in studies related to the estimation of susceptibility to natural hazards. Moreover, the interest may be even higher as in this paper this algorithm has been combined with other 3 state of the art machine learning models like DLNN, MLP and ADT. In terms flood susceptibility results, it is obvious that the plain region with low altitudes and flat surfaces is the most exposed to flood

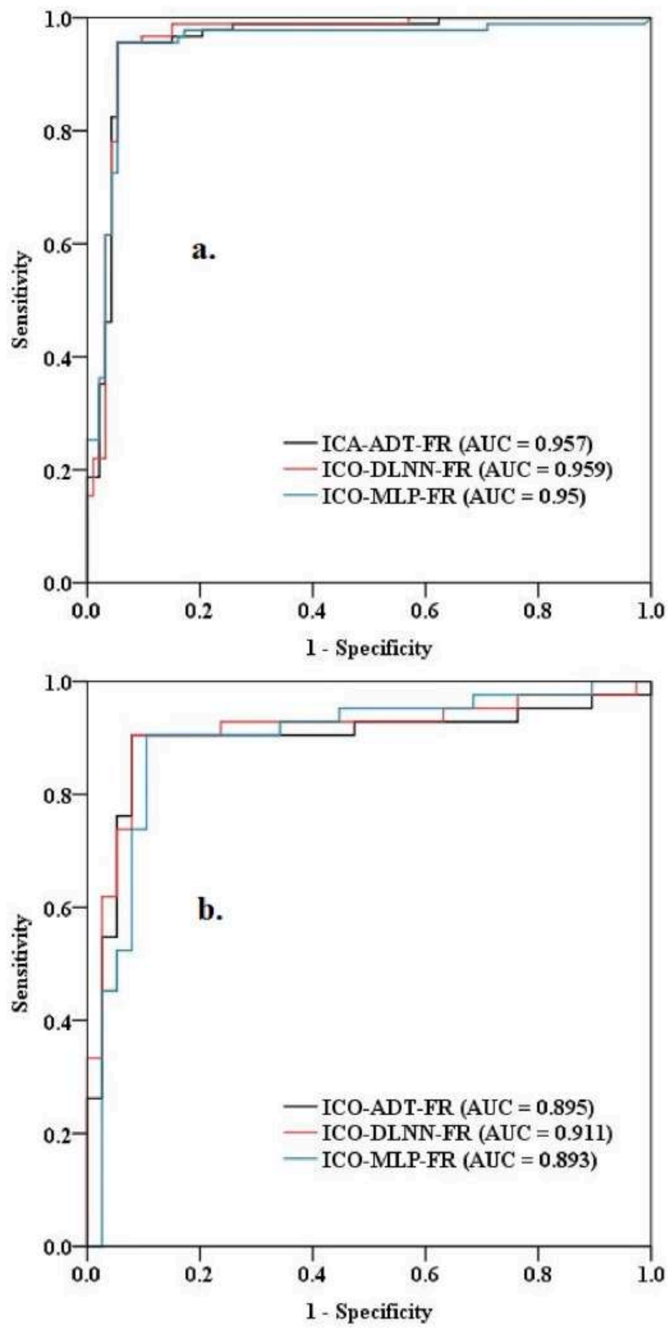

Fig. 10. ROC curve (a. Success rate; prediction rate).

Table 3
Statistical metrics used to validate the flood susceptibility maps.

Metrics	Training sample			Validating sample		
	ICO-ADT-FR	ICO-DLNN-FR	ICO-MLP-FR	ICO-ADT-FR	ICO-DLNN-FR	ICO-MLP-FR
TP	85	87	86	37	38	38
TN	87	88	85	35	37	36
FP	7	5	6	3	2	2
FN	5	4	7	5	3	4
Sensitivity	0.944	0.956	0.925	0.881	0.927	0.905
Specificity	0.926	0.946	0.934	0.921	0.949	0.947
Accuracy	0.935	0.951	0.929	0.9	0.938	0.925
K-index	0.870	0.902	0.859	0.8	0.875	0.85

risk phenomena. The high and very high flood susceptibility is present on around 20% of the Putna river catchment.

6. Conclusions

Within this study, a series of complex geoprocessing and computational operations were proposed for identifying the areas at risk for flooding within one of the most exposed zones from Romania which is the Putna river catchment. The present research was carried out in a period when flood frequency and magnitude have increased exponentially. To calculate the Flood Susceptibility Index for the Putna river catchment, three ensemble models (ICO-DLNN-FR; ICO-MLP-FR; ICO-ADT-FR) were used in this study. It is worthy to note that, in the training process, the three ensemble models involved the use of 14 flood predictors, representing the independent variables, alongside with a sample containing 92 flood and 92 non-flood pixels representing the dependent variable. The results validation was ensured with the help of another sample comprising 40 flood and 40 non-flood pixels. The model with the best performance was ICO-DLNN-FR that achieved an AUC of 0.959 in terms of training sample, and 0.911 in terms of validating sample.

The main novelty of this research resides in the use, for the first time in the literature, of the three ensembles (ICO-DLNN-FR; ICO-MLP-FR; ICO-ADT-FR) to evaluate the susceptibility to a natural hazard. These results will be made available to the competent authorities in order to reduce the flood risk in Putna river basin from Romania.

Funding

This work was supported by a grant of the Romanian Ministry of Education and Research, CNCS – UEFISCDI, project number PN-III-P1-1.1-PD-2019-0424-P, within PNCDI III.

Credit author statement

Conceptualization, R.C., M.S. and B.T.P.; methodology, R.C., A.A., S.I.A., M.S. and I.C.; software, R.C., I.C., and B.T.P.; validation, R.C., I.C., M.A. and B.T.P.; formal analysis, R.C., A.A., A.C. and I.C.; investigation, R.C., A.A. and I.C.; resources, R.C., I.C. and B.T.P.; data curation, R.C., I.C., A.R.M.T.I., S.I.A. and B.T.P.; writing—original draft preparation, R.C., I.C., A.R.M.T.I. and B.T.P.; writing—review and editing, R.C., A.A. and I.C.; visualization, R.C. and B.T.P.; supervision, R.C., A.A. and I.C.; project administration, R.C.; funding acquisition, R.C. and B.T.P. All authors have read and agreed to the published version of the manuscript.

Declaration of competing interest

The authors declare that they have no known competing financial interests or personal relationships that could have appeared to influence the work reported in this paper.

Appendix A. Supplementary data

Supplementary data to this article can be found online at https://doi.org/10.1016/j.jenvman.2022.115316.

References

Abedini, M., Ghasemian, B., Shirzadi, A., Bui, D.T., 2019. A comparative study of support vector machine and logistic model tree classifiers for shallow landslide susceptibility modeling. Environ. Earth Sci. 78, 560.

Ahmadlou, M., Al-Fugara, A., Al-Shabeeb, A.R., Arora, A., Al-Adamat, R., Pham, Q.B., Al-Ansari, N., Linh, N.T.T., Sajedi, H., 2021. Flood susceptibility mapping and assessment using a novel deep learning model combining multilayer perceptron and autoencoder neural networks. J. Flood Risk Manag. 14, e12683.

Ahmadlou, M., Karimi, M., Alizadeh, S., Shirzadi, A., Parvinnejhad, D., Shahabi, H., Panahi, M., 2019. Flood susceptibility assessment using integration of adaptive

network-based fuzzy inference system (ANFIS) and biogeography-based optimization (BBO) and BAT algorithms (BA). Geocarto Int. 34, 1252–1272.
Akay, H., 2021. Flood hazards susceptibility mapping using statistical, fuzzy logic, and MCDM methods. Soft Comput. 25, 9325–9346.
Alfieri, L., Dottori, F., Betts, R., Salamon, P., Feyen, L., 2018. Multi-model projections of river flood risk in Europe under global warming. Climate 6, 6.
Ali, S.A., Parvin, F., Pham, Q.B., Vojtek, M., Vojteková, J., Costache, R., Linh, N.T.T., Nguyen, H.Q., Ahmad, A., Ghorbani, M.A., 2020. GIS-based comparative assessment of flood susceptibility mapping using hybrid multi-criteria decision-making approach, naïve Bayes tree, bivariate statistics and logistic regression: a case of Topľa basin, Slovakia. Ecol. Indicat. 117, 106620. https://doi.org/10.1016/j.ecolind.2020.106620.
Arabameri, A., Pradhan, B., Rezaei, K., Lee, S., Sohrabi, M., 2020. An ensemble model for landslide susceptibility mapping in a forested area. Geocarto Int. 35, 1680–1705.
Arabameri, A., Rezaei, K., Cerdà, A., Conoscenti, C., Kalantari, Z., 2019. A comparison of statistical methods and multi-criteria decision making to map flood hazard susceptibility in Northern Iran. Sci. Total Environ. 660, 443–458.
Bui, D.T., Hoang, N.-D., Martínez-Álvarez, F., Ngo, P.-T.T., Hoa, P.V., Pham, T.D., Samui, P., Costache, R., 2020. A novel deep learning neural network approach for predicting flash flood susceptibility: a case study at a high frequency tropical storm area. Sci. Total Environ. 701, 134413.
Bui, D.T., Hoang, N.-D., Pham, T.-D., Ngo, P.-T.T., Hoa, P.V., Minh, N.Q., Tran, X.-T., Samui, P., 2019. A new intelligence approach based on GIS-based Multivariate Adaptive Regression Splines and metaheuristic optimization for predicting flash flood susceptible areas at high-frequency tropical typhoon area. J. Hydrol. 575, 314–326.
Canbek, G., Sagiroglu, S., Temizel, T.T., Baykal, N., 2017. Binary classification performance measures/metrics: a comprehensive visualized roadmap to gain new insights. In: Presented at the 2017 International Conference on Computer Science and Engineering (UBMK). IEEE, pp. 821–826.
Cao, C., Xu, P., Wang, Y., Chen, J., Zheng, L., Niu, C., 2016. Flash flood hazard susceptibility mapping using frequency ratio and statistical index methods in coalmine subsidence areas. Sustainability 8, 948.
Cao, Y., Jia, H., Xiong, J., Cheng, W., Li, K., Pang, Q., Yong, Z., 2020. Flash flood susceptibility assessment based on geodetector, certainty factor, and logistic regression analyses in fujian province, China. ISPRS Int. J. Geo-Inf. 9, 748.
Chen, W., Li, Y., Xue, W., Shahabi, H., Li, S., Hong, H., Wang, X., Bian, H., Zhang, S., Pradhan, B., 2020. Modeling flood susceptibility using data-driven approaches of naïve bayes tree, alternating decision tree, and random forest methods. Sci. Total Environ. 701, 134979.
Chen, W., Xie, X., Peng, J., Wang, J., Duan, Z., Hong, H., 2017. GIS-based landslide susceptibility modelling: a comparative assessment of kernel logistic regression, Naïve-Bayes tree, and alternating decision tree models. Geomatics, Nat. Hazards Risk 8, 950–973.
Choubin, B., Moradi, E., Golshan, M., Adamowski, J., Sajedi-Hosseini, F., Mosavi, A., 2019. An Ensemble prediction of flood susceptibility using multivariate discriminant analysis, classification and regression trees, and support vector machines. Sci. Total Environ. 651, 2087–2096.
Chowdhuri, I., Pal, S.C., Chakrabortty, R., 2020. Flood susceptibility mapping by ensemble evidential belief function and binomial logistic regression model on river basin of eastern India. Adv. Space Res. 65, 1466–1489.
Costache, R., 2019a. Flash-flood Potential Index mapping using weights of evidence, decision Trees models and their novel hybrid integration. Stoch. Environ. Res. Risk Assess. 33, 1375–1402.
Costache, R., 2019b. Flash-Flood Potential assessment in the upper and middle sector of Prahova river catchment (Romania). A comparative approach between four hybrid models. Sci. Total Environ. 659, 1115–1134.
Costache, R., Arabameri, A., Blaschke, T., Pham, Q.B., Pham, B.T., Pandey, M., Arora, A., Linh, N.T.T., Costache, I., 2021a. Flash-flood potential mapping using deep learning, alternating decision trees and data provided by remote sensing sensors. Sensors 21, 280.
Costache, R., Arabameri, A., Moayedi, H., Pham, Q.B., Santosh, M., Nguyen, H., Pandey, M., Pham, B.T., 2021b. Flash-flood potential index estimation using fuzzy logic combined with deep learning neural network, naïve Bayes, XGBoost and classification and regression tree. Geocarto Int. 1–28.
Costache, R., Bui, D.T., 2020. Identification of areas prone to flash-flood phenomena using multiple-criteria decision-making, bivariate statistics, machine learning and their ensembles. Sci. Total Environ. 712, 136492.
Costache, R., Bui, D.T., 2019. Spatial prediction of flood potential using new ensembles of bivariate statistics and artificial intelligence: a case study at the Putna river catchment of Romania. Sci. Total Environ. 691, 1098–1118.
Costache, R., Ngo, P.T.T., Tien Bui, D., 2020. Novel ensembles of deep learning neural network and statistical learning for flash-flood susceptibility mapping. Water 12, 1549. https://doi.org/10.3390/w12061549.
Costache, R., Zaharia, L., 2017. Flash-flood potential assessment and mapping by integrating the weights-of-evidence and frequency ratio statistical methods in GIS environment–case study: Bâsca Chiojdului River catchment (Romania). J. Earth Syst. Sci. 126, 59.
Dahri, N., Abida, H., 2017. Monte Carlo simulation-aided analytical hierarchy process (AHP) for flood susceptibility mapping in Gabes Basin (southeastern Tunisia). Environ. Earth Sci. 76, 302.
Hall, M., Frank, E., Holmes, G., Pfahringer, B., Reutemann, P., Witten, I.H., 2009. The WEKA data mining software: an update. ACM SIGKDD Explor. Newslett. 11, 10–18.
Hassanien, A.E., Moftah, H.M., Azar, A.T., Shoman, M., 2014. MRI breast cancer diagnosis hybrid approach using adaptive ant-based segmentation and multilayer perceptron neural networks classifier. Appl. Soft Comput. 14, 62–71.
Hong, H., Liu, J., Zhu, A.-X., 2020. Modeling landslide susceptibility using LogitBoost alternating decision trees and forest by penalizing attributes with the bagging ensemble. Sci. Total Environ. 718, 137231.
Islam, A.R.M.T., Talukdar, S., Mahato, S., Kundu, S., Eibek, K.U., Pham, Q.B., Kuriqi, A., Linh, N.T.T., 2021. Flood susceptibility modelling using advanced ensemble machine learning models. Geosci. Front. 12, 101075.
Jenness, J.S., 2000. The Effects of Fire on Mexican Spotted Owls in Arizona and New Mexico.
Jung, W., Bollmann, S., Lee, J., 2020. Overview of quantitative susceptibility mapping using deep learning: current status, challenges and opportunities. NMR Biomed., e4292
Khoirunisa, N., Ku, C.-Y., Liu, C.-Y., 2021. A GIS-based artificial neural network model for flood susceptibility assessment. Int. J. Environ. Res. Publ. Health 18, 1072.
Khosravi, K., Barzegar, R., Golkarian, A., Busico, G., Cuoco, E., Mastrocicco, M., Colombani, N., Tedesco, D., Ntona, M.M., Kazakis, N., 2021. Predictive modeling of selected trace elements in groundwater using hybrid algorithms of iterative classifier optimizer. J. Contam. Hydrol. 103849.
Khosravi, K., Pham, B.T., Chapi, K., Shirzadi, A., Shahabi, H., Revhaug, I., Prakash, I., Bui, D.T., 2018. A comparative assessment of decision trees algorithms for flash flood susceptibility modeling at Haraz watershed, northern Iran. Sci. Total Environ. 627, 744–755.
Kourgialas, N.N., Karatzas, G.P., 2011. Flood management and a GIS modelling method to assess flood-hazard areas—a case study. Hydrol. Sci. J. 56, 212–225.
Lei, X., Chen, W., Avand, M., Janizadeh, S., Kariminejad, N., Shahabi, Hejar, Costache, R., Shahabi, Himan, Shirzadi, A., Mosavi, A., 2020. GIS-based machine learning algorithms for gully erosion susceptibility mapping in a semi-arid region of Iran. Rem. Sens. 12, 2478.
Li, H., Ji, G., Ma, Z., 2007. A nonlinear predictive model based on multilayer perceptron network. In: Presented at the 2007 IEEE International Conference on Automation and Logistics. IEEE, pp. 2686–2690.
Liu, J., Wang, J., Xiong, J., Cheng, W., Li, Y., Cao, Y., He, Y., Duan, Y., He, W., Yang, G., 2022. Assessment of flood susceptibility mapping using support vector machine, logistic regression and their ensemble techniques in the Belt and Road region. Geocarto Int. 1–40.
Meshram, S.G., Safari, M.J.S., Khosravi, K., Meshram, C., 2021. Iterative classifier optimizer-based pace regression and random forest hybrid models for suspended sediment load prediction. Environ. Sci. Pollut. Control Ser. 28, 11637–11649.
Mohammady, M., Pourghasemi, H.R., Pradhan, B., 2012. Landslide susceptibility mapping at Golestan Province, Iran: a comparison between frequency ratio, Dempster–Shafer, and weights-of-evidence models. J. Asian Earth Sci. 61, 221–236.
Nachappa, T.G., Piralilou, S.T., Gholamnia, K., Ghorbanzadeh, O., Rahmati, O., Blaschke, T., 2020. Flood susceptibility mapping with machine learning, multi-criteria decision analysis and ensemble using Dempster Shafer Theory. J. Hydrol. 125275.
Natarajan, L., Usha, T., Gowrappan, M., Palpanabhan Kasthuri, B., Moorthy, P., Chokkalingam, L., 2021. Flood susceptibility analysis in Chennai corporation using frequency ratio model. J. India. Soc. Rem. Sens. 49, 1533–1543.
Pham, B.T., Bui, D.T., Dholakia, M.B., Prakash, I., Pham, H.V., 2016. A comparative study of least square support vector machines and multiclass alternating decision trees for spatial prediction of rainfall-induced landslides in a tropical cyclones area. Geotech. Geol. Eng. 34, 1807–1824.
Pham, B.T., Bui, D.T., Prakash, I., Dholakia, M., 2017. Hybrid integration of Multilayer Perceptron Neural Networks and machine learning ensembles for landslide susceptibility assessment at Himalayan area (India) using GIS. Catena 149, 52–63.
Pham, B.T., Luu, C., Van Phong, T., Trinh, P.T., Shirzadi, A., Renoud, S., Asadi, S., Van Le, H., von Meding, J., Clague, J.J., 2021. Can deep learning algorithms outperform benchmark machine learning algorithms in flood susceptibility modeling? J. Hydrol. 592, 125615.
Prasad, P., Loveson, V.J., Das, B., Kotha, M., 2021. Novel ensemble machine learning models in flood susceptibility mapping. Geocarto Int. 1–23.
Rahmati, O., Darabi, H., Panahi, M., Kalantari, Z., Naghibi, S.A., Ferreira, C.S.S., Kornejady, A., Karimidastenaei, Z., Mohammadi, F., Stefanidis, S., 2020. Development of novel hybridized models for urban flood susceptibility mapping. Sci. Rep. 10, 1–19.
Rahmati, O., Pourghasemi, H.R., Zeinivand, H., 2016. Flood susceptibility mapping using frequency ratio and weights-of-evidence models in the Golastan Province, Iran. Geocarto Int. 31, 42–70.
Romanescu, G., Nistor, I., 2011. The effects of the july 2005 catastrophic inundations in the siret river's lower watershed, Romania. Nat. Hazards 57, 345–368.
Saad, I.A., 2018. An efficient classification algorithms for image retrieval based color and texture features. J. Al Qadisiyah Comput. Sci. Math. 10, 42.
Saha, A., Pal, S.C., Arabameri, A., Blaschke, T., Panahi, S., Chowdhuri, I., Chakrabortty, R., Costache, R., Arora, A., 2021. Flood susceptibility assessment using novel ensemble of hyperpipes and support vector regression algorithms. Water 13, 241.
Saha, S., Paul, G.C., Pradhan, B., Abdul Maulud, K.N., Alamri, A.M., 2021a. Integrating multilayer perceptron neural nets with hybrid ensemble classifiers for deforestation probability assessment in Eastern India. Geomatics, Nat. Hazards Risk 12, 29–62.
Saha, S., Sarkar, D., Mondal, P., 2021b. Efficiency exploration of frequency ratio, entropy and weights of evidence-information value models in flood vulnerabilityassessment: a study of raiganj subdivision, Eastern India. Stoch. Environ. Res. Risk Assess. 1–22.
Shafizadeh-Moghadam, H., Valavi, R., Shahabi, H., Chapi, K., Shirzadi, A., 2018. Novel forecasting approaches using combination of machine learning and statistical models for flood susceptibility mapping. J. Environ. Manag. 217, 1–11.

Sharma, R., Kumar, S., Maheshwari, R., 2015. Comparative analysis of classification techniques in data mining using different datasets. Int. J. Comput. Sci. Mobile Comput. 4, 125–134.
Tang, X., Li, J., Liu, M., Liu, W., Hong, H., 2020. Flood susceptibility assessment based on a novel random Naïve Bayes method: a comparison between different factor discretization methods. Catena 190, 104536.
Tehrany, M.S., Pradhan, B., Jebur, M.N., 2014. Flood susceptibility mapping using a novel ensemble weights-of-evidence and support vector machine models in GIS. J. Hydrol. 512, 332–343.
Tehrany, M.S., Pradhan, B., Jebur, M.N., 2013. Spatial prediction of flood susceptible areas using rule based decision tree (DT) and a novel ensemble bivariate and multivariate statistical models in GIS. J. Hydrol. 504, 69–79. https://doi.org/10.1016/j.jhydrol.2013.09.034.
Vakhshoori, V., Zare, M., 2016. Landslide susceptibility mapping by comparing weight of evidence, fuzzy logic, and frequency ratio methods. Geomatics, Nat. Hazards Risk 7, 1731–1752.
Van Dao, D., Jaafari, A., Bayat, M., Mafi-Gholami, D., Qi, C., Moayedi, H., Van Phong, T., Ly, H.-B., Le, T.-T., Trinh, P.T., 2020. A spatially explicit deep learning neural network model for the prediction of landslide susceptibility. Catena 188, 104451.
Vinke-de Kruijf, J., Kuks, S.M., Augustijn, D.C., 2015. Governance in support of integrated flood risk management? The case of Romania. Environ. Develop. 16, 104–118.
Wang, Y., Fang, Z., Hong, H., Costache, R., Tang, X., 2021. Flood susceptibility mapping by integrating frequency ratio and index of entropy with multilayer perceptron and classification and regression tree. J. Environ. Manag. 289, 112449.
Zaharia, L., Costache, R., Prăvălie, R., Ioana-Toroimac, G., 2017. Mapping flood and flooding potential indices: a methodological approach to identifying areas susceptible to flood and flooding risk. Case study: the Prahova catchment (Romania). Front. Earth Sci. 11, 229–247.
Zaharia, L., Costache, R., Prăvălie, R., Minea, G., 2015. Assessment and mapping of flood potential in the Slănic catchment in Romania. J. Earth Syst. Sci. 124, 1311–1324.

Journal of Hydrology 609 (2022) 127747

Contents lists available at ScienceDirect

Journal of Hydrology

journal homepage: www.elsevier.com/locate/jhydrol

Research papers

Flash-flood hazard using deep learning based on H_2O R package and fuzzy-multicriteria decision-making analysis

Romulus Costache [a,b], Tran Trung Tin [c], Alireza Arabameri [d], Anca Crăciun [b,*], R.S. Ajin [e,f], Iulia Costache [g,*], Abu Reza Md. Towfiqul Islam [h], S.I. Abba [i,j], Mehebub Sahana [k], Mohammadtaghi Avand [l], Binh Thai Pham [m]

[a] *Department of Civil Engineering, Transilvania University of Brasov, 5, Turnului Str, 500152 Brasov, Romania*
[b] *Danube Delta National Institute for Research and Development, 165 Babadag Street, 820112 Tulcea, Romania*
[c] *Department of Information Technology, FPT University, Danang, 550000, Viet Nam*
[d] *Department of Geomorphology, Tarbiat Modares University, Tehran 36581-17994, Iran*
[e] *Kerala State Emergency Operations Centre (KSEOC), Kerala State Disaster Management Authority (KSDMA), Thiruvananthapuram, India*
[f] *Resilience Development Initiative (RDI), Bandung, Indonesia*
[g] *Faculty of Geography, University of Bucharest, Bucharest 010041, Romania*
[h] *Department of Disaster Management, Begum Rokeya University, Rangpur 5400, Bangladesh*
[i] *Interdisciplinary Research Center for Membrane and Water Security, King Fahd University of Petroleum and Minerals, Dhahran 31261, Saudi Arabia*
[j] *Faculty of Engineering, Department of Civil Engineering, Baze University, Abuja, Nigeria*
[k] *Department of Geography, University of Manchester, United Kingdom*
[l] *Department of Forests, Rangelands, and Watershed Management Engineering, Kohgiluyeh & Boyer Ahmad Agricultural and Natural Resources Research and Education Center, AREEO, 75916-11740 Yasouj, Iran*
[m] *University of Transport Technology, 54 Trieu Khuc, Thanh Xuan, Ha Noi, Viet Nam*

A R T I C L E I N F O

This manuscript was handled by Emmanouil Anagnostou, Editor-in-Chief, with the assistance of Giulia Sofia, Associate Editor

Keywords:
Flash-flood susceptibility
Machine learning
H2O package
Suha river basin
Romania

A B S T R A C T

The present study was done in order to simulate the flash-flood susceptibility across the Suha river basin in Romania using a number of 3 hybrid models and fuzzy-AHP multicriteria decision-making analysis. It should be noted that flash-flood events are triggered by heavy rainfall in small river catchments. To achieve the proposed results, a total of 8 flash-flood predictors (slope angle, plan curvature, hydrological soil groups, land use, convergence index, profile curvature, topographic position index, aspect) along with a sample of 111 torrential phenomena points were used as input datasets in the next four algorithms: Fuzzy-Analytical Hierarchy Process (FAHP), Deep Learning Neural Network -Analytical Hierarchy Process (DLNN-AHP), Multilayer Perceptron - Analytical Hierarchy Process (MLP-AHP) and Naïve Bayes - Analytical Hierarchy Process (NB-AHP). The Analytical Hierarchy Process was used to calculate the coefficients for each class/category of flash-flood predictors. The torrential points sample was split into training (70%) and validating samples (30%). The modelling was done in Excel, SPSS and R software (H2O package), while the result mapping was performed in ArcGIS 10.5 software. The analysis revealed that the high and very high susceptibility degrees are spread over a maximum of 35.01% of the study area. The best performances, demonstrated by an AUC-ROC of 0.984, are associated with the Deep Learning Neural Network – Analytical Hierarchy Process model, followed by Naïve Bayes – Analytical Hierarchy Process model (AUC = 0.976), Multilayer Perceptron - Analytical Hierarchy Process model (AUC = 0.882) and Fuzzy-Analytical Hierarchy Process (AUC = 0.807). These results indicates that Deep Learning Neural Network is a promising machine learning model which can provide outcomes with very high precision. Also, according to the present research results the deep learning neural network, having many hidden layers, is able outperform the multilayer perceptron that contains a single hidden layer. The main novelty of the present research is the application of the three ensemble models (DLNN-AHP, MLP-AHP and NB-AHP) and also the use of H2O package for the first time in literature, to evaluate the flash-flood susceptibility in small river catchments.

* Corresponding authors.
E-mail addresses: romulus.costache@icub.unibuc.ro (R. Costache), tintt19@fe.edu.vn (T. Trung Tin), anca.craciun@ddni.ro (A. Crăciun), iulia.elena.costache@gmail.com (I. Costache), mehebub.sahana@manchester.ac.uk (M. Avand), binhpt@utt.edu.vn (B. Thai Pham).

https://doi.org/10.1016/j.jhydrol.2022.127747
Received 12 January 2022; Received in revised form 4 February 2022; Accepted 16 March 2022
Available online 24 March 2022

1. Introduction

A flash flood occurs when heavy rainfall from convective weather has a short duration and highly intensity, and it is often generated in small river basins (less than 200 square kilometers) with a high complex orography (Destro et al., 2018; Wang et al., 2021). As a result of precipitation filling the drainage capacity of the basin slope, flash floods occur when the drainage network is incarcerated, and the basin outlets discharge at extraordinarily high rates (Youssef et al., 2016). Each year, global economic losses are estimated to be around 60 billion USD due to floods and flash-floods (Janizadeh et al., 2019). Storms that produce flash floods can cause severe damage to infrastructures, such as roads, railway tracks, and urban areas. As a result of ongoing urbanization and climate change, many areas are facing many environmental challenges and greater risks of natural disasters (Kjeldsen, 2010). There are many different types of riverine flooding, but the most common are flash floods, which occur when a massive amount of water is released in a short amount of time (three to six hours) due to excessive rainfall, the melting of natural ice, or a dam failure (Janizadeh et al., 2019). The rapid onset of river levels and the high velocity of flash floods make them among the most dangerous types of floods. They cause serious injuries, economic losses, and environmental damage (Destro et al., 2018). Due to the complexity of flash floods, it remains challenging to predict them accurately (Bui et al., 2019). However, it is well-known that weather conditions, soil types, geomorphological structures, and vegetation have a major contribution to flash-flood genesis (Asadi et al., 2019; Youssef et al., 2016). To mitigate the negative effects of flash-floods, it is mandatory to accurately identify the potential zones that can be damaged by these natural hazards.

In order to predict the flash-flood likelihood, a variety of studies were conducted by the researchers. Thus, a part of these studies belongs to the rainfall-runoff modelling approaches (Kratzert et al., 2018; Zhang et al., 2019; Liu et al., 2020). Another type of approach comprises the hydraulic modelling that can be done using some models like Mike, HEC-RAS, TELEMAC-2D or Jflow (Alho and Aaltonen, 2008; Bures et al., 2019; Tamiru and Dinka, 2021). Based on this hydraulic modelling software, the flooded areas corresponding to different discharge return probabilities can be estimated. However, both the rainfall-runoff modelling and hydraulic modelling approaches require a huge amount of measured data and also are time-consuming.

Another category of approach is represented by the flash-flood susceptibility models that are based on the application of various methods having as input data a various number of flash-flood predictors and flash-flood locations (Arabameri et al., 2020). In this regard, we can mention many categories of models like: multicriteria decision-making analysis, bivariate statistical models, and machine learning models (Popa et al., 2019). From the first class of models represented by multicriteria decision-making analysis, the follwing algorithms can be noted: Analytical Hierarchy Process (Handini et al., 2021), Vlse Kriterijuska Optamizacija I Komoromisno Resenje (VIKOR) (Singh and Pandey, 2021), Technique for Order Preference by Similarity to Ideal Solution (TOPSIS) (Rafiei-Sardooi et al., 2021), Analytical Network Process (Chukwuma et al., 2021) and Fuzzy-Analytical Hierarchy Process (Costache et al., 2021a). The bivariate statistical models comprise many algorithms like: frequency ratio (Waqas et al., 2021), weights of evidence (Pham et al., 2021a), index of entropy (Wang et al., 2021), statistical index (Liu et al., 2021a), certainty factor (Costache et al., 2020b) and evidential belief function (Chowdhuri et al., 2020). The third category, represented by the machine learning models contains a large number of algorithms like: decision trees (Khosravi et al., 2018), neural networks (Panahi et al., 2021; Pandey et al., 2021), support vector machine (Xiong et al., 2019), Naive Bayes (Elmahdy et al., 2020), *k*-nearest neighbor (Shahabi et al., 2020a), k-star (Costache et al., 2020c) or deep learning neural network (Chakrabortty et al., 2021). From the category of deep learning algorithms that were used in the literature we also mention the Convolutional Neural Network (Wang et al., 2020), Recurrent Neural Network (Fang et al., 2021) and Autoencoder Neural Network (Ahmadlou et al., 2021). With the intention of improving the results provided by the various models, the researchers resorted to the application of existing optimization models such as: biogeography based optimization (BBO) (Ahmadlou et al., 2019), Particle Swarm Optimization (PSO) (Arora et al., 2021; Ngo et al., 2021) or Harris Hawk Optimization (HHO) (Malik et al., 2021). Moreover, another procedure intended to improve the accuracy of results is the hybridization between two or many models (Arabameri et al., 2020; Islam et al., 2021). However, there is a gap of know knowledge in the literature, in terms of using the advance machine learning models in small river catchments to derive the flash-flood susceptibility.

Taking into account the above considerations, the present research work aims to accurately detect the areas prone to flash-flooding using the following algorithms: hybrid combinations between Deep Learning based on H2O R package and Analytical Hierarchy Process (DLNN-AHP), hybrid combination between Multilayer Perceptron and Analytical Hierarchy Process (MLP-AHP), hybrid combinations between Naive Bayes and Analytical Hierarchy Process (NB-AHP), and Fuzzy-Analytical Hierarchy Process (Fuzzy-AHP). These models were selected to be used for the estimation of flash-flood susceptibility because they belong of the category of state-of-the-art machine learning and multicriteria decision-making algorithms and also, their very high precision was demonstrated in the previous research works related to the natural hazard susceptibility evaluation (Abedini et al., 2019; Bui et al., 2020a; Choubin et al., 2019; Wang et al., 2021). It should be noted that in the present research, the model's accuracy and results validation will be carried out using the ROC Curve method and several statistical metrics. Moreover, in the case of DLNN, their application was highly facilitated by the development of H2O R package. In fact, the use for the first time in the literature of NB-AHP, MLP-AHP and DLNN-AHP hybrid models along with the H2O R package for the application of DLNN model, represents the main elements of novelty that characterize the present research study.

The area, on which the present study is focused, is the Suha river catchment from Romania, a region that was highly affected in the past by flash-floods phenomena and where these hazards caused many damages. Another reason for selecting this area as case study, was the specific relief that is very favorable to the flash-flood genesis. For the present analysis, geospatial data regarding the flash-flood predictors and the presence of torrential areas were used in order to apply the proposed models.

2. Study area

Suha river basin is located in the northern part of Romania (Fig. 1). The elevation ranges between 500 m and 1600 m within the 363 km^2 of land. In spite of the large extent of afforestation, approximately 72% of the basin is covered by forest, the steep slope angles and numerous areas characterized by impassable soils render the Suha catchment susceptible to flash floods (Tîrnovan et al., 2014). A forest's protective role, from a hydrological standpoint, is reduced or wiped out if the precipitation caused by heavy rain exceeds the tree canopy's maximum interception capacity. Throughout the main valleys of the Suha river catchment are built-up areas that have active surface runoff. Other important land use categories are represented by: pastures (12.89%) and agriculture areas (5.25%). The land use category, with the lowest surface across Suha river basin, is represented by the rivers (0.72%). In terms of hydrological soil groups, it should be noted that across the study region all the 4 groups (A, B, C and D) are present (Costache and Bui, 2020).

Within the study area, the most significant flash floods occurred in 1970, 2005, 2010 and 2018. This information was provided by the Romanian National Inspectorate for Emergency Situations. There are a number of socio-economic aspects that were profoundly affected by these phenomena in 2005, including: 32,4 km of road infrastructure, 148 buildings, and more than 267 ha of agricultural land. It was estimated that the economic damage totaled about 260,0000 euros

(Costache and Bui, 2020).

3. Data

3.1. Torrential locations inventory

A thorough inventory of areas that have previously been impacted by natural hazards is the key to predicting future surfaces likely to experience these phenomena (Chen et al., 2018). It was determined that the best method of analysis was to identify areas that had been affected by torrential phenomena (Costache, 2019). Generally, torrential relief sites behave in a way that favors rapid surface runoff events, which in turn lead to flash floods that propagate downslope. We examined aerial imagery from Google Earth to identify areas already affected by torrentiality. These surfaces consist exclusively of the unified presence of torrential microforms, like ravines and gullies, that are formed by surface runoff (Costache, 2019). Approximately 7.5 km^2 of torrential areas were identified across the Suha river basin. A total of 111 points were extracted from the information regarding the presence of torrential phenomena as a part of the methodological workflow. A second dataset representing an equal number of points (1 1 1) with non-torrential phenomena was created by performing this step. A low slope angle is ideal for non-torrential pixels where rapid runoff is virtually impossible (Costache, 2019). The dataset was divided into a training sample (70%) and validation sample (30%) (Fig. 1). This division of the data set was made in order to create the possibility to validate the results offered by the model by using a percentage of 30% of the entire collected data sample. Also, it is very important to note that the split procedure, into 70% for training and 30% for validation, sample is suggested by the vast majority of the previous similar research works (Ahmadlou et al., 2019; Costache et al., 2020c; Islam et al., 2021; Shahabi et al., 2020a).

3.2. Flash-flood predictors

On the basis of Digital Elevation Model (DEM) data extracted from Shuttle Radar Topography Mission (SRTM), 30 m database, six flash flood predictors have been derived. In addition, the hydrological soil groups and land use factors, were extracted from Digital Soil Map of Romania, 1:200000 and Corine Land Cover, 2018 database, respectively. It should be noted that, even if the rainfall is an important factor in the flash-flood genesis, given the small surface of the study area, it was considered that the values of this factor have a low spatial variability across Suha river basin. Therefore, the rainfall was not considered in the present study.

In the next rows, a brief description of each flash-flood predictor will be highlighted.

In general, researchers consider the **slope angle** (Fig. 2a), determined from the Digital Elevation Model (DEM), as the factor with the greatest influence on surface runoff (Ngo et al., 2021; Chao et al., 2021; Wang et al., 2022). According to the morphological analysis, slope angle has a significant impact on flash flood occurrences and manifestations since it controls surface runoff velocity, which, in turn, affects flash flood characteristics (Costache and Bui, 2020; Sahana et al., 2020). The runoff and flash flooding associated with steep slopes are well known, whereas their occurrence on flat surfaces is less likely (Elmahdy et al., 2020). The slope angles of the study area, ranging from 0° and 40.1°, were partitioned into a number of 5 classes through the Natural Breaks classification method. **Plan curvature** (Fig. 2b) represents a second morphometric index achieved by the processing of Digital Elevation Model. Specifically, its values distinguish convergent runoff areas from divergent runoff areas (Minár et al., 2020). The majority of torrential pixels occupy the zones with a plan curvature between 0.1 and 2.5. **Hydrological Soil Groups Surface** (Fig. 2c) runoff is directly controlled by Hydrological Soil Groups, which in turn influence the infiltration

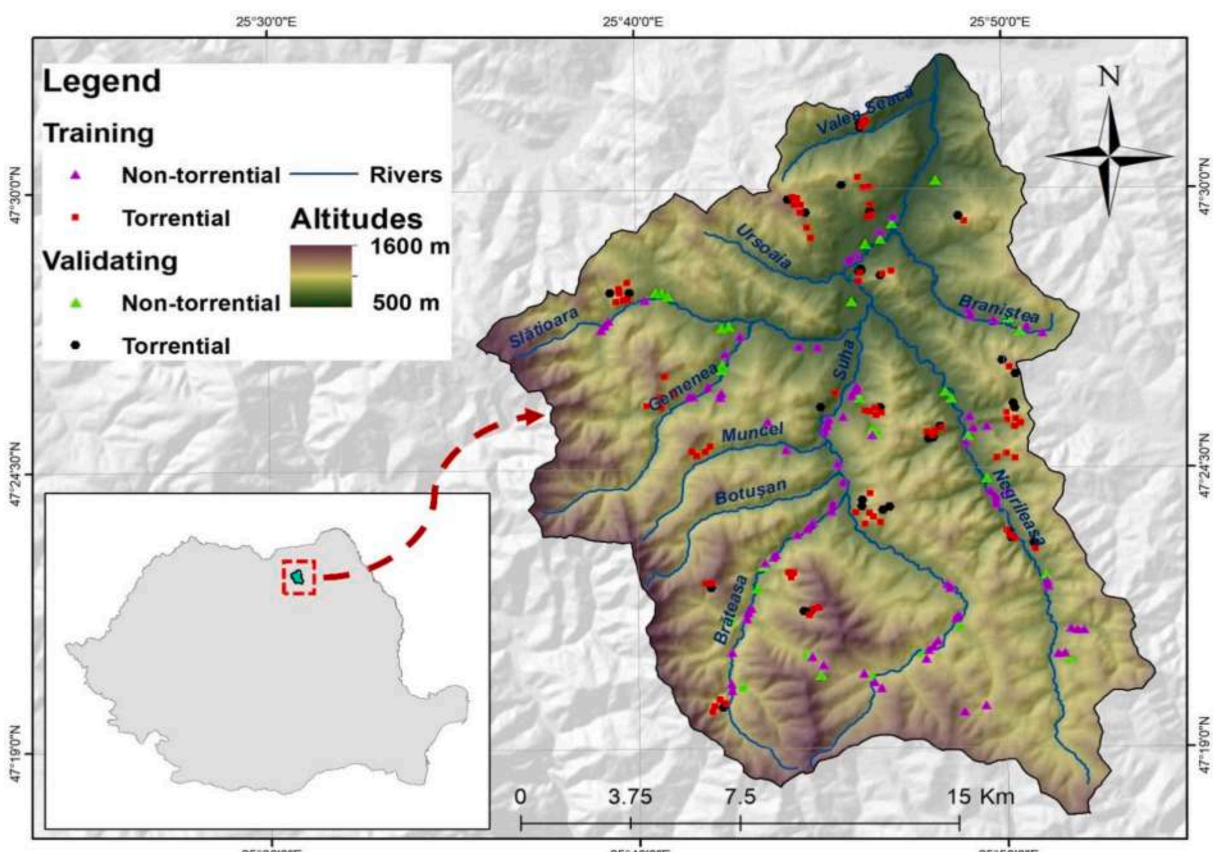

Fig. 1. Study area location within Romania.

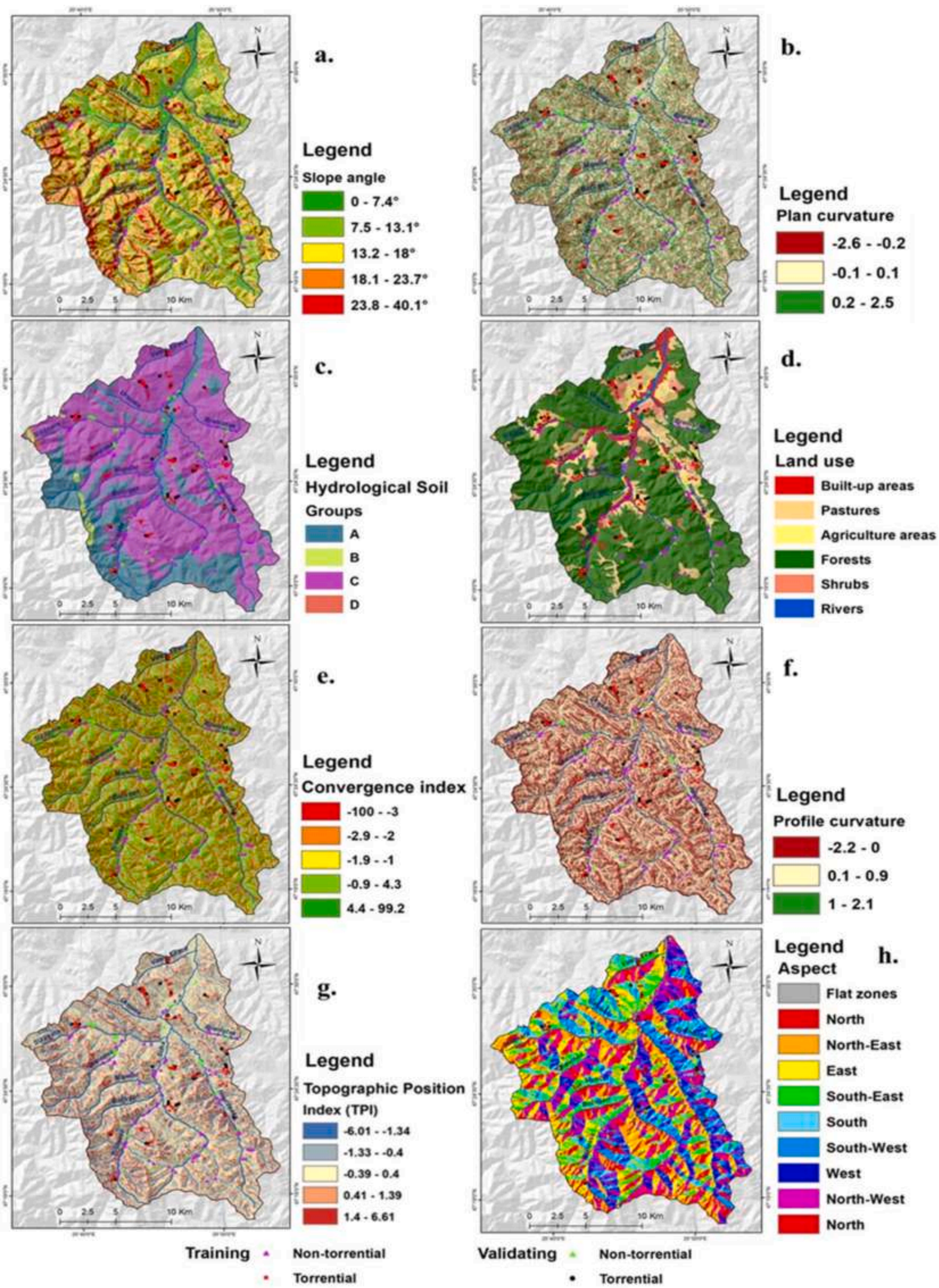

Fig. 2. Flash-flood conditioning factors (a. slope angle; b. plan curvature; c. hydrological soil groups; d. land use; e. convergence index; f. profile curvature; g. topographic position index; h. aspect).

process (Stewart et al., 2011; Lan et al., 2021; Zhao et al., 2021). The soil class C cover approximately 70% of Suha river basin and comprises around 56% of torrential pixels. **Land use** (Fig. 2d) predictor has a widely usage in the research works that are related to the flash-flood susceptibility estimation (Chakrabortty et al., 2021; Xiong et al., 2019). As the first layer of a topographical surface with which raindrops are in contact, the land use plays a vital role in flash floods (Prăvălie and Costache, 2013; Costache and Bui, 2020). Across the study zone a number of 6 different land use categories were identified. The forest has the biggest percentage (72%), while 41% of surfaces with torrential pixels are localized within the pastures. **Convergence Index** (Fig. 2e) is the third predictor derived from DEM. Its main feature is represented by its capacity to highlight the hydrographic convergence degree over a specific zone. Using the Natural Breaks algorithm, the Convergence Index values were classified into 5 different classes. The areas with values from −0.9 to 4.3 have around 40% of the total torrential pixels. The **profile curvature** (Fig. 2f) shows the zones having an accelerated surface runoff and, due to its significance in morphometry, it should be considered in this study. In the present research, the profile curvature was classified into 3 intervals of values and the highest area belongs to

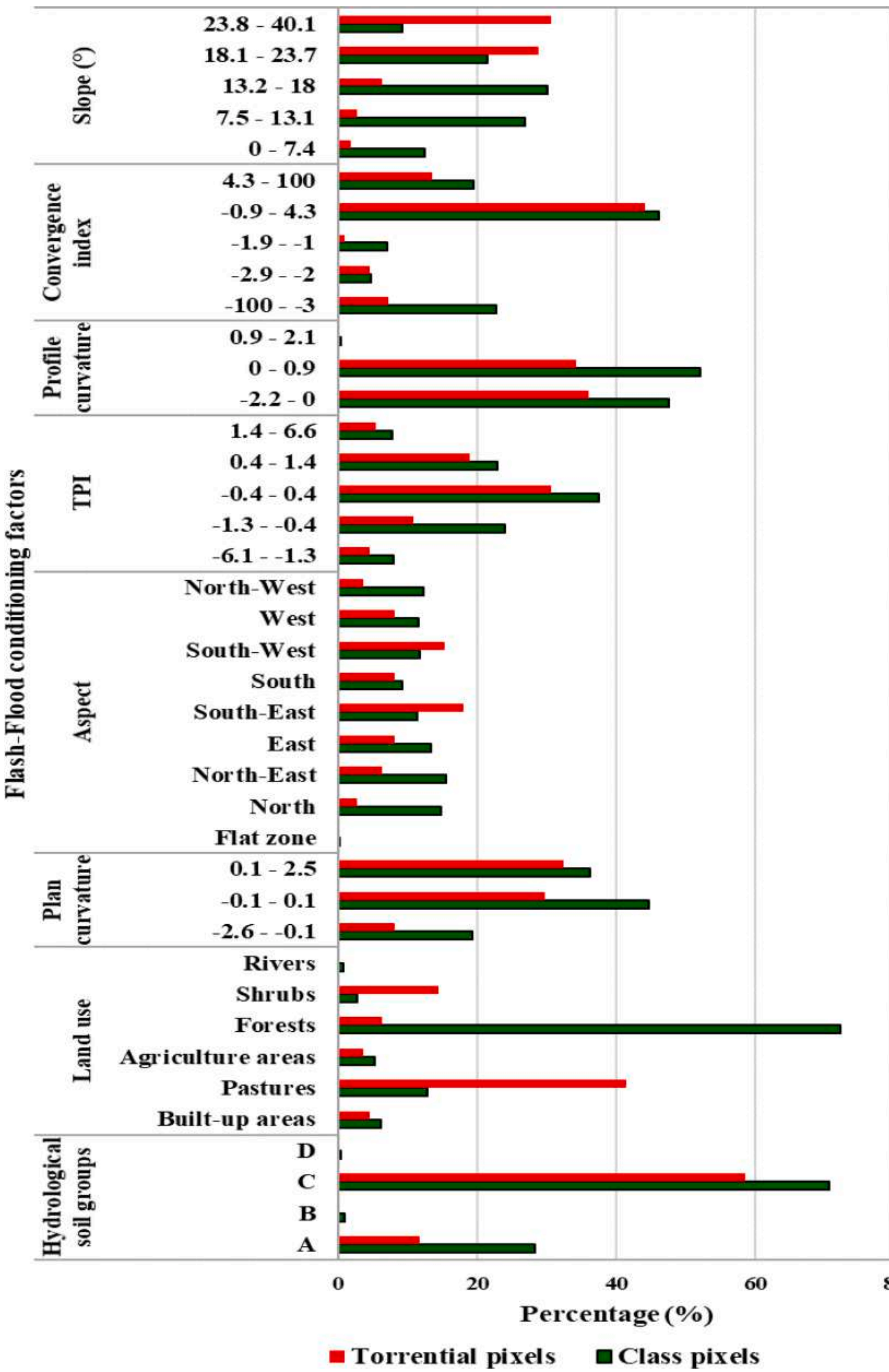

Fig. 3. Percentage of class/categories and torrential pixels.

the values from 0 to 0.9. **Topographic Position Index (TPI)** (Fig. 2g), derived from DEM, indicates the altitude difference between a specific pixel and the pixels from its vicinity. Natural Breaks was also used to divide its values into 5 classes. The middle class with values between −0.4 and 0.4 has the largest surface and contains 30% of torrential pixels. The **Aspect** (Fig. 2h) is the last morphometric predictor taken into account for the flash-flood susceptibility modelling in this research work. The shaded slopes allow the presence of a saturated soil and, therefore, these surfaces could contribute in a more active manner to surface runoff genesis and then to flash-flood occurrence. North-Eastern slopes account 15.47% of the study region and 18% of torrential pixels are located on South-Eastern slopes (Fig. 3).

4. Methods

4.1. Feature selection using ReliefF method

The use of ReliefF algorithm will allow an initial assessment of the predictive capacity of flash-flood predictors. This method have multiple benefits like (Costache et al., 2021b): i) manage to minimize the training process time; ii) help to make the algorithms easier to be analyzed and less complex; ii) increase the models accuracy by selecting the highest predictive variables; iv) minimize the models overfitting. This method can be applied with both discrete and continuous data. In ReliefF algorithm the closest instance of either a different or the same class is considered when evaluating the attribute value (Urbanowicz et al., 2018). Weka 3.9 software was used to apply ReliefF method.

4.2. Deep Learning Neural Network (DLNN)

Deep Learning Neural Network is a type of machine learning model which can efficiently deal with huge amount and unstructured data (Deng et al., 2013; He et al., 2020; Zhan et al., 2022). This model represents a neural network with more than one hidden layer which is widely used in the literature that comprises studies approaching the natural disasters susceptibility (Bui et al., 2020b; Costache et al., 2020a; Shahabi et al., 2020b). These multiple hidden layers will help the transfer of information from the input layer, containing the flash-flood predictors, to the output layer that will have 2 neurons represented by torrential and non-torrential pixels (Panahi et al., 2021). Due to the fact that, in essence, the flash-flood susceptibility estimation is a binary classification procedure, the torrential pixels will be encoded with 1 while the non-torrential pixels will be encoded with 0. At the same time the next sigmoid function will be applied: $E(Y = i/x)$. The approximation of sigmoid function will be provided by the information that is assigned to a single output neuron associated to the class i. In this research, a *softmax* function, having the next form, will be also applied:

$$softmax(a_i) = \frac{\exp(a_i)}{\sum_k \exp(a_i)} \tag{1}$$

where a_i represents the layer of *softmax* function.

The next relations will be used to express a deep neural network containing multiple hidden layers (h):

For $h = 1, \ldots, H$ (hidden layers),

$$a^{(h)}(x) = b^{(h)} + W^{(h)}p^{(h-1)}(x) \tag{2}$$

$$p^{(h)}(x) = \varnothing(a^{(h)}(x)) \tag{3}$$

where, $\varnothing$ is the activation function.

The DLNN algorithm will use as input the AHP coefficients calculated for each class/category of flash-flood predictors. The DLNN model was implemented using H2O package from R programming language.

4.3. Fuzzy Analytical Hierarchy Process (FAHP)

Fuzzy Analytical Hierarchy Process (FAHP) represent an extension of Analytical Hierarchy Process (AHP) multicriteria decision-making model (Roodposhti et al., 2014). This extension is mainly intended to solve several fuzzy problems from the hierarchical point of view (Sun, 2010). By employing fuzzy set theory as well as the analytical hierarchy process can be improved the analysis quality by minimizing the subjectivity when estimating weights criteria. The next steps are required to apply FAHP model for the present research.

The flash-flood predictors mentioned at 3.2 are involved in the construction of pairwise comparison matrices. Further, to calculate the highest important criteria, the linguistic terms will be associated with the pairwise comparisons using the next relation:

$$A' = \begin{bmatrix} 1' & a'_{12} & \cdots & a'_{1n} \\ a'_{21} & 1' & \cdots & a'_{1n} \\ \vdots & \vdots & \ddots & \vdots \\ a'_{n1} & a'_{n2} & \cdots & 1' \end{bmatrix} = \begin{bmatrix} 1' & a'_{12} & \cdots & a'_{1n} \\ 1/a'_{21} & 1' & \cdots & a'_{1n} \\ \vdots & \vdots & \ddots & \vdots \\ 1/a'_{n1} & 1/a'_{n2} & \cdots & 1' \end{bmatrix} \tag{4}$$

where a'_{ij} are pairs of criteria i and j.

In the next phase, the fuzzy weights and geometric mean of each criterion are calculated with the Buckley method (Hategekimana et al., 2018):

$$r'_i = \left(a'_{i1}\ ha'_{i2}\ h \ldots h\ a'_{in}\right)^{\frac{1}{n}}, \tag{5}$$

$$w'_i = r'_i h\ \left(r'_1\ h \ldots h\ r'_n\right)^{-1} \tag{6}$$

where a'_{in} represents the comparison fuzzy value of the pair criterion i and criterion n,r'_1 represents the value of geometric mean of the fuzzy values comparison of criterion i compared to each of the other criteria, and w'_i represents the fuzzy weighting of the i-th criterion, which could be expressed as a TFN, $w'_i = (lw_i, mw_i, uw_i)$, where lw_i, mw_i and uw_i represent the lower, middle and upper values, respectively, of the fuzzy weighting of the ith criterion (Costache et al., 2021a).

The next step was represented by the application of the extent analysis through which the weights of flash-flood predictors will be achieved. The fuzzy triangular comparison matrix was constructed in the first step and has the next form (Hategekimana et al., 2018):

$$A' = (a'_{ij})_{nxn} = \begin{bmatrix} (1,1,1) & (l_{12}, m_{12}, u_{12}) & \cdots & (l_{1n}, m_{1n}, u_{1n}) \\ (l_{21}, m_{21}, u_{21}) & (1,1,1) & \cdots & (l_{2n}, m_{2n}, u_{2n}) \\ \vdots & \vdots & \ddots & \vdots \\ (l_{n1}, m_{n1}, u_{n1}) & (l_{n2}, m_{n2}, u_{n2}) & \cdots & (1,1,1) \end{bmatrix} \tag{7}$$

where $a'_{ij} = (l_{ij}, m_{ij}, u_{ij})anda'^{-1}_{ij} = (1/l_{ij}, 1/m_{ij}, 1/u_{ij})$ for i, j = 1, …, n and $i \neq j$.

Thus, will be done the computation of triangular matrix priority vector. Further, the fuzzy arithmetic function will be applied in order to sum up each row of matrix A':

$$RS_i = \sum_{j=1}^{n} a'_{ij} = \left(\sum_{j=1}^{n} l_{ij}, \sum_{j=1}^{n} m_{ij}, \sum_{j=1}^{n} u_{ij}\right), \quad i = 1, \cdots, n \tag{8}$$

Using the normalized version of equation (8), the fuzzy synthetic extent values for each ith object will be achieved (Roodposhti et al., 2014):

$$S_i^{'} = \sum_j^n a_{ij}^{'} \, h\left[\sum_{k=1}^n \sum_{j=1}^n a_{kj}^{'}\right]^{-1} = \left(\frac{\sum_{j=1}^n l_{ij}}{\sum_{k=1}^n \sum_{j=1}^n u_{kj}}, \frac{\sum_{j=1}^n m_{ij}}{\sum_{k=1}^n \sum_{j=1}^n m_{kj}}, \frac{\sum_{j=1}^n u_{ij}}{\sum_{k=1}^n \sum_{j=1}^n l_{kj}}\right), \ i = 1, \dots, \ n \tag{9}$$

Next, through equation (10) the degree of possibility of $S_i^{'} \geq S_j^{'}$ is computed:

$$V(S_i^{'} \geq S_j^{'}) = \begin{cases} 1, if\, m_i \geq m_j, \\ \frac{u_i - l_j}{(u_i - m_i) + (m_j - l_j)}, l_j \leq u_i, i, j = 1, \cdots, n; j \neq i \\ 0, others \end{cases} \tag{10}$$

where $S_i^{'} = (l_i, m_i, u_i)$ and $S_j^{'} = (l_j, m_j, u_j)$.

Let $w^{'}(a_i) = \min\{V(S_i^{'} \geq S_k^{'})\} \mathrm{k} = 1, 2, \cdots, \mathrm{n}; \quad \mathrm{k} \neq \mathrm{i}$

Then, the weight vector value is determined as following:

$$w^{'}(a_i) = [w^{'}(a_1), w^{'}(a_2), \cdots, w^{'}(a_n)]^T \tag{12}$$

where ai (i = 1, 2, …, n) are n elements. The equation (13) is used after the normalization process, when the weight vectors are computed:

$$w(a_i) = [w(a_1), w(a_2), \cdots, w(a_n)]^T \tag{13}$$

where w is a non-fuzzy number.

4.4. Multilayer Perceptron (MLP)

MLP is a very popular artificial neural network, being characterized by one-way error propagation of the feed-forward network model (Li et al., 2019).Time series prediction, pattern recognition, and so forth can be solved using MLP. The MLP structure contains an input layer, a hidden layer and an output layer (Ke et al., 2021). Each layer's connections to the input and hidden layers and its connections to the output layers will be processed according to the weight values (Li et al., 2019). The back-propagation method is involved in the update process of the weight values (Liu et al., 2021b; Zare et al., 2013). Two stages can be distinguished when this procedure is performed: i) Input and output values are propagated through hidden layers, and the output values are compared with pre-values to determine the difference between them; ii) the connection weights are adjusted in order to achieve the most performant results with the minimum difference. Repeated iteratively, the procedure is continued until a root mean square error of the network is within acceptable limits. In the present study, the input neurons in the input layer are represented by flash-flood predictors, while the output neurons in the output layer are represented by the torrential and non-torrential surfaces. The optimal number of hidden neurons will be established according to the minimum RMSE value (eq. (14)).

$$RMSE = \sqrt{\frac{1}{n}\sum_{i=1}^{n}(c_i - \hat{c}_i)^2} \tag{14}$$

where, n represents the date number, c_i are the measured data, and $\hat{c}_i$ the calculated values.

4.5. Naïve Bayes (NB)

Based on Bayes' Theorem, Naïve Bayes presumes that the dependencies among the predictor attributes do not exists (Jiang et al., 2016). The wide use of NB is due to the fact that it does not require a large volume of training data or a complex workflow for building classification models (Tien Bui et al., 2012). By using the AHP values assigned to each category of flash-flood predictors from the training sample, the NB was involved in the estimation of flash flood within the research zone. If we consider 2 vectors, the first assigned to each predictor having AHP coefficients computed - $g = (g_1, g_2, \dots, g_{10})$, and the second which corresponds to the presence and absence of torrential zones – $f = (f_1, f_2)$, the classification using NB algorithm is based on the next mathematical relation:

$$t_{NB} = \underset{t_i \in [\text{torrential}, \text{no-torrential}]}{\operatorname{argmax}} P(t_i) \prod_{i=1}^{n} P(\frac{f_i}{t_i}) \tag{15}$$

where, $P(t_i)$ is equal to the t_i prior probability which can be computed using the proportion of the observed cases and the output class t_i within the training sample. Moreover, the conditional probability value is calculated using the next equation (Tien Bui et al., 2012):

$$P\left(\frac{f_i}{t_i}\right) = \frac{1}{\sqrt{2\pi\delta}} e^{-(f_i-\mu)^2/2\delta^2} \tag{16}$$

where, μ represents the mean and δ is equal to the x_i-standard deviation.

WEKA v.3.9 software was involved for the application of NB model.

4.6. Results validation

4.6.1. Statistical metrics

The following indices were involved in the results validation process: Sensitivity, Specificity, Kappa Index, F1 score, Accuracy and Precision. Statistical indices are significant if they show a correlation from the spatial point of view between the torrential and non-torrential locations that were observed and the estimated flash-flood susceptible zone (Costache, 2019). The next relations will be applied for statistical metrics derivation (Canbek et al., 2017):

$$\text{Sensitivity} = \frac{\text{TP}}{\text{TP} + \text{FN}} \tag{17}$$

$$\text{Specificity} = \frac{\text{TN}}{\text{FP} + \text{TN}} \tag{18}$$

$$\text{Precision} = \frac{\text{TP}}{\text{TP} + \text{FP}} \tag{19}$$

$$\text{Accuracy} = \frac{\text{TP} + \text{TN}}{\text{TP} + \text{FP} + \text{TN} + \text{FN}} \tag{20}$$

$$\text{k} = \frac{\text{p}_\text{o} - \text{p}_\text{e}}{1 - \text{p}_\text{e}} \tag{21}$$

where P represents the equivalent number of locations with torrential phenomenon, N represents the equivalent number of non-torrential pixels, FP (false positive) and FN (false negative) represents the equivalent number of locations erroneously classified, k is kappa coefficient, p_o is the observed torrential locations, and p_e is equal to the estimated flash-flood susceptibility value.

4.6.2. ROC Curve

In statistics, receiver operating characteristic (ROC) curves are used to determine the predictive value of different statistical or machine learning techniques (Costache et al., 2019; Zhang et al., 2020). A ROC curve is constructed by displaying sensitivity on the Y axis, and false positive rate (1-specificity) on the X axis. Area Under Curve (AUC) is the

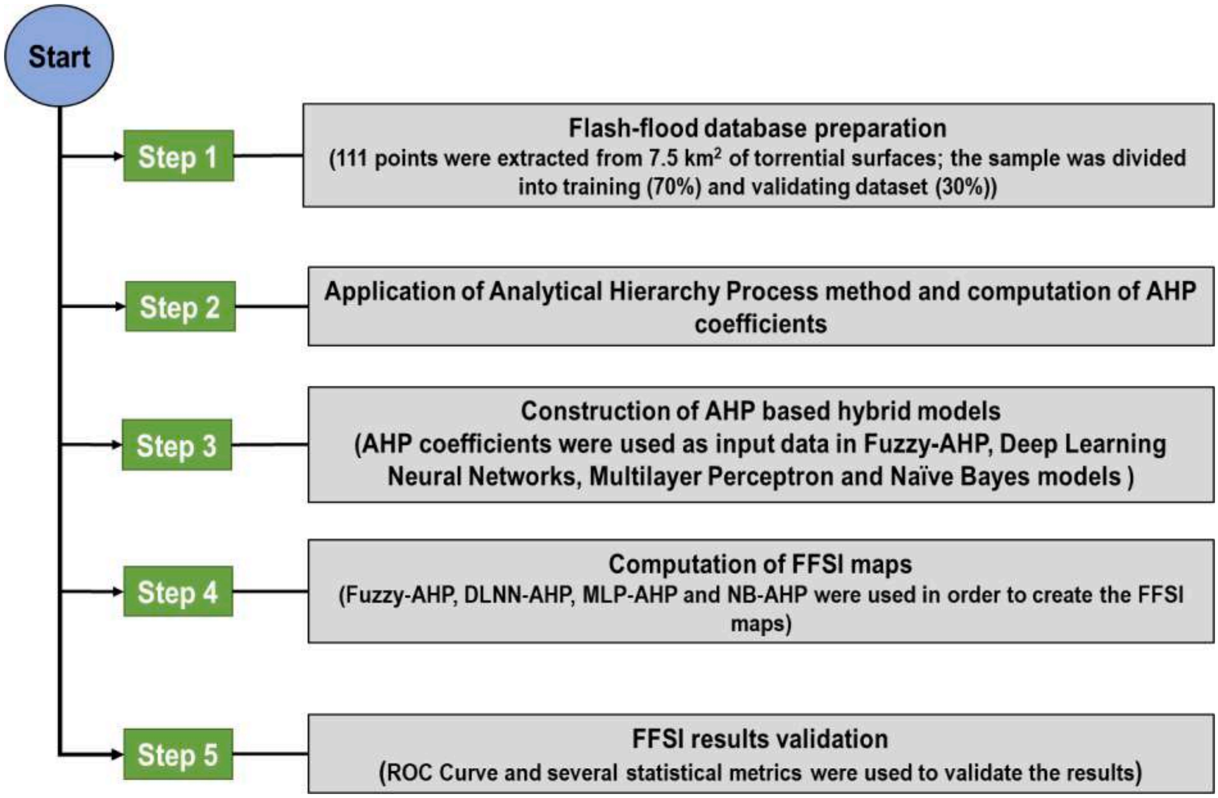

Fig. 4. Flowchart of the methodological steps.

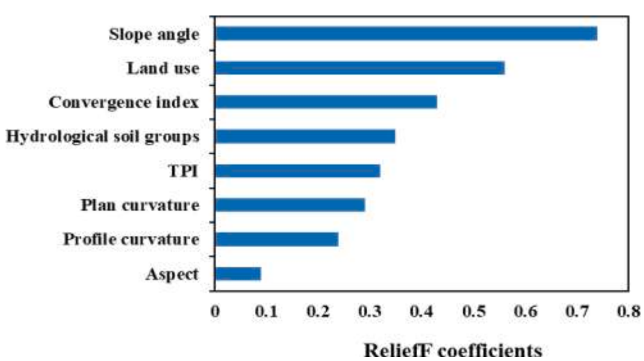

Fig. 5. ReliefF coefficients for feature selection.

essential measure for the model's performance estimated through ROC Curve. The closer AUC to 1 the better the models performance (Hosseini et al., 2020). The following mathematical relationship can be involved for AUC computation:

$$AUC = \frac{(\sum TP + \sum TN)}{(P + N)} \quad (22)$$

The entire workflow is schematically represented in Fig. 4.

5. Results

5.1. Feature selection and correlation analysis

Following the application of the ReliefF method for feature selection, the following results were achieved: Slope angle (0.74), Land use (0.56), Convergence index (0.43), Hydrological soil groups (0.35), TPI (0.32), Plan curvature (0.29), Profile curvature (0.24), Aspect (0.09) (Fig. 5). By analyzing the achieved results, it can be concluded that all the factors are able to influence the flash-flood phenomena and therefore, all of them will be included in the future workflow.

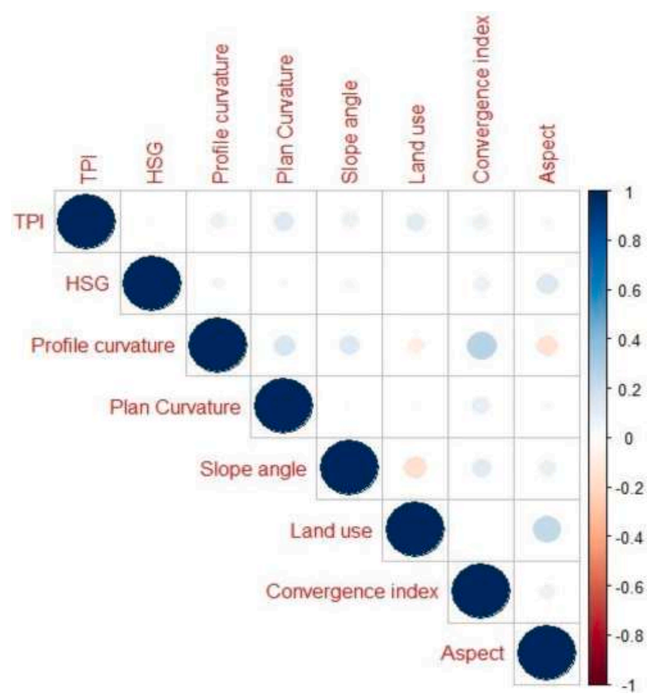

Fig. 6. Correlation matrix among the flash-flood predictors.

To avoid the redundant information among the 8 flash-flood predictors, the correlation matrix, in R software was constructed. It reveals that the highest degree of correlation take place between profile curvature and convergence index, with a value of correlation coefficient

Table 1
Pair-wise comparison matrix and normalized weights for each factor and class/category.

Factor and classes/categories	Pair-wise comparison matrix									Normalized weights
	[1]	[2]	[3]	[4]	[5]	[6]	[7]	[8]	[9]	
Slope angle (°)										
[1] 0 – 7.4	1									0.035
[2] 7.5 – 13.1	3	1								0.072
[3] 13.2 – 18	5	2	1							0.123
[4] 18.1 – 23.7	7	5	3	1						0.263
[5] 23.8 – 40.1	9	7	5	3	1					0.507
TPI										
[1] (-6. 1) – (-1.3)	1									0.442
[2] (-1.3) – (-0.4)	1/2	1								0.257
[3] (-0.3) – 0.4	1/3	1/2	1							0.149
[4] 0.5 – 1.4	1/5	1/3	2/3	1						0.089
[5] 1.4 – 6.61	1/6	1/4	1/3	3/4	1					0.063
Land use										
[1] Built-up areas	1									0.383
[2] Pastures	1/2	1								0.245
[3] Agriculture areas	1/3	1/2	1							0.149
[4] Forests	1/9	1/7	1/5	1						0.040
[5] Shrubs	1/5	1/4	1/3	2	1					0.064
[6] Rivers	1/3	1/2	1	2	2	1				0.119
Profile curvature										
[1] (-2.2) – 0	1									0.633
[2] 0 – 0.9	1/3	1								0.260
[3] 0.9 – 2.1	1/5	1/3	1							0.106
Plan curvature										
[1] (-2.6) – (-0.1)	1									0.128
[2] (-0.1) – 0.1	3	1								0.512
[3] 0.1 – 2.5	4	1/2	1							0.360
Aspect										
[1] Flat surfaces	1									0.034
[2] North	3	1								0.088
[3] North-East	4	2	1							0.109
[4] East	5	3/2	4	1						0.202
[5] South-East	4	3/2	2	3/4	1					0.157
[6] South	4	3/2	3/2	2/3	2/3	1				0.134
[7] South-West	3	4/3	4/3	2/3	2/3	4/5	1			0.116
[8] West	3	5/4	2/3	1/2	3/5	3/5	4/5	1		0.093
[9] North-East	2	1	1/2	1/3	1/2	1/2	1/2	2/3	1	0.067
Convergence index										
[1] 4.3 – 99.2	1									0.057
[2] (-0.9) – 4.3	2	1								0.089
[3] (-1.9) – (-1)	3	2	1							0.143
[4] (-2.9) – (-2)	4	3	2	1						0.227
[5] (−96) – (-3)	6	5	4	3	1					0.485
Hydrological soil groups										
[1] A	1									0.088
[2] B	2	1								0.158
[3] C	3	2	1							0.272
[4] D	5	3	2	1						0.482

equal to 0.327 (Fig. 6).

The Fig. 6 shows that in four cases the correlation coefficient is equal to 0. Thus, it can be seen that no serious correlation is detected between the input variables and, so as, all of them will be involved in the computational workflow.

5.2. AHP coefficients

Table 1 shows the pair-wise comparison between all the classes or categories of flash-flood predictors. According to the outcomes of AHP method, the profile curvature class was between −2.2 and 0, achieved the highest AHP coefficient (0.633), being followed by plan curvature class between −0.1 and 0.1 (AHP = 0.512), slope angle class between 23.8 and 40.1 (AHP = 0.507), convergence index class between −96 and −3 (AHP = 0.485). The lowest values of AHP were achieved by flat surface derived from aspect predictor (AHP = 0.034), slope angle between 0 and 7.4 (AHP = 0.035) and forest surfaces (AHP = 0.04).

The judgment consistency for each matrix was assessed through Consistency Ratio (CR) (Table 2). Given the fact that all values of CR are below to 0.1, all the comparison within the matrices are consistent.

Table 2
Pair-wise comparison matrix properties.

Factors	N	λmax	CI	RI	CR
Slope angle	5	5.196	0.049	1.12	0.044
Land use	6	6.100	0.020	1.24	0.016
Hydrological soil groups	4	5.058	0.014	0.90	0.005
Profile curvature	3	3.039	0.019	0.58	0.033
Plan curvature	3	3.109	0.054	0.58	0.090
TPI	5	5.029	0.007	1.12	0.006
Convergence index	5	5.099	0.025	1.12	0.017
Aspect	9	9.200	0.025	1.45	0.022

Table 3
FAHP evaluation matrix.

	1	2	3	4	5	6	7	8
Profile curvature (1)								
l_1	1	1	1	1	2	1/3	3	1
m_1	1	1	1	2	3	1/2	4	2
u_1	1	1	1	3	4	1	5	3
Plan curvature (2)								
l_2	1	1	1	1	2	1/4	2	1
m_2	1	1	1	2	3	1/3	3	2
u_2	1	1	1	3	4	1/2	4	3
Hydrological Soil Group (3)								
l_3	1	1	1	1	2	1/3	2	1
m_3	1	1	1	2	3	1/2	3	2
u_3	1	1	1	3	4	1	4	3
Land use (4)								
l_4	1/3	1/3	1/3	1	1	1/6	1	1
m_4	1/2	1/2	1/2	1	2	1/5	2	1
u_4	1	1	1	1	3	1/4	3	1
Convergence index (5)								
l_5	1/4	1/4	1/4	1/3	1	1/7	1	1/3
m_5	1/3	1/3	1/3	1/2	1	1/6	2	1/2
u_5	1/2	1/2	1/2	1	1	1/5	3	1
Slope angle (6)								
l_6	1	2	1	4	5	1	5	2
m_6	2	3	2	5	6	1	6	3
u_6	3	4	3	6	7	1	7	4
TPI (7)								
l_7	1/5	1/4	1/4	1/3	1/3	1/7	1	1/3
m_7	1/4	1/3	1/3	1/2	1/2	1/6	1	1/2
u_7	1/3	1/2	1/2	1	1	1/5	1	1
Aspect (8)								
l_8	1/3	1/3	1/3	1	1	1/4	1	1
m_8	1/2	1/2	1/2	1	2	1/3	2	1
u_8	1	1	1	1	3	1/2	3	1

5.3. Flash-flood susceptibility computation

5.3.1. Fuzzy-AHP

Using the Fuzzy-AHP method, the first step to determine the flash-flood susceptibility was to create in Microsoft Excel a fuzzy pair-wise comparison matrix (Table 3). Thus, in this matrix, all 8 flash-flood predictors were included and compared according to their importance in the flash-flood genesis. Based on the results in the comparison matrix, the following equation was used to determine the synthesis values:

Table 4
The ordinate of the highest intersection point, the degree possibility for TFNs, and the wright's landslide predictors.

Profile curvature = 1	Plan curvature = 2	Hydrological Soil Groups = 3
V(S1 ≥ S2) = 1	V(S2 ≥ S1) = 1	V(S3 ≥ S1) = 0.94
V(S1 ≥ S3) = 1	V(S2 ≥ S3) = 0.96	V(S3 ≥ S2) = 1
V(S1 ≥ S4) = 1	V(S2 ≥ S4) = 1	V(S3 ≥ S4) = 1
V(S1 ≥ S5) = 1	V(S2 ≥ S5) = 1	V(S3 ≥ S5) = 1
V(S1 ≥ S6) = 0.54	V(S2 ≥ S6) = 0.43	V(S3 ≥ S6) = 1
V(S1 ≥ S7) = 1	V(S2 ≥ S7) = 1	V(S3 ≥ S7) = 0.49
V(S1 ≥ S8) = 1	V(S2 ≥ S8) = 1	V(S3 ≥ S8) = 1
$\min\{V(S_1 \geq S_k)\} = 0.54$	$\min\{V(S_2 \geq S_k)\} = 0.43$	$\min\{V(S_3 \geq S_k)\} = 0.49$
Weight = 0.19	Weight = 0.155	Weight = 0.175
Land use = 4	**Convergence index = 5**	**Slope angle = 6**
V(S4 ≥ S1) = 0.64	V(S5 ≥ S1) = 0.22	V(S6 ≥ S1) = 1
V(S4 ≥ S2) = 0.6	V(S5 ≥ S2) = 0.18	V(S6 ≥ S2) = 1
V(S4 ≥ S3) = 1	V(S5 ≥ S3) = 0.59	V(S6 ≥ S3) = 1
V(S4 ≥ S5) = 1	V(S5 ≥ S4) = 1	V(S6 ≥ S4) = 1
V(S4 ≥ S6) = 0.09	V(S5 ≥ S6) = 0	V(S6 ≥ S5) = 1
V(S4 ≥ S7) = 1	V(S5 ≥ S7) = 1	V(S6 ≥ S7) = 1
V(S4 ≥ S8) = 0.91	V(S5 ≥ S8) = 0.5	V(S6 ≥ S8) = 1
$\min\{V(S_5 \geq S_k)\} = 0.09$	$\min\{V(S_6 \geq S_k)\} = 0$	$\min\{V(S_7 \geq S_k)\} = 1$
Weight = 0.033	Weight = 0	Weight = 0.354
TPI = 7	**Aspect = 8**	
V(S7 ≥ S1) = 0	V(S10 ≥ S1) = 0.616	
V(S7 ≥ S2) = 0.03	V(S10 ≥ S2) = 0.72	
V(S7 ≥ S3) = 0	V(S10 ≥ S3) = 0.685	
V(S7 ≥ S4) = 0.44	V(S10 ≥ S4) = 1	
V(S7 ≥ S5) = 0.88	V(S10 ≥ S5) = 1	
V(S7 ≥ S6) = 0	V(S10 ≥ S6) = 0.174	
V(S7 ≥ S8) = 1	V(S10 ≥ S7) = 1	
$\min\{V(S_9 \geq S_k)\} = 0.03$	$\min\{V(S_{10} \geq S_k)\} = 0.174$	
Weight = 0	Weight = 0.061	

$$\left[\sum_{k=1}^{n}\sum_{j=1}^{n} a'_{kj}\right]^{-1} = (164.74\ 217.617\ 275.783)^{-1} = (0.0036\ 0.0046\ 0.006) \quad (24)$$

These results were then used to calculate fuzzy numbers that could be assigned to each flash-flood predictor. In the next step, the degree of possibility process was applied based on the fuzzy number (Table 4). Next, the weight of each flash-flood predictor was calculated with the following equations:

$$w(a_i) = \{0.54\ 0.43\ 0.49\ 0.09\ 0\ 1\ 0\ 0.061\}^T \quad (25)$$

$$w(a_i) = \{0.19\ 0.155\ 0.175\ 0.033\ 0\ 0.354\ 0\ 0.061\}^T \quad (26)$$

In addition, the defuzzification process allows TFNs to be converted into crisp weights that are applied to each flash-flood conditioning factor and subsequently multiplied by AHP values to create the $FFSI_{FAHP}$ (Fig. 10a).

The value of $FFSI_{FAHP}$ range from 0.07 to 0.48. The Natural Breaks method was utilized to classify the flash-flood susceptibility values, having the very low class between 0.07 and 0.19 characterized by a percentage of 18.32% (Fig. 9a). The low class is situated between 0.2 and 0.25, having a percentage of 31.59%, while the moderate class between 0.26 and 0.3 occupies a percentage of 32.41%. The high and very high susceptibility values above 0.31 is spread on 17.68%.

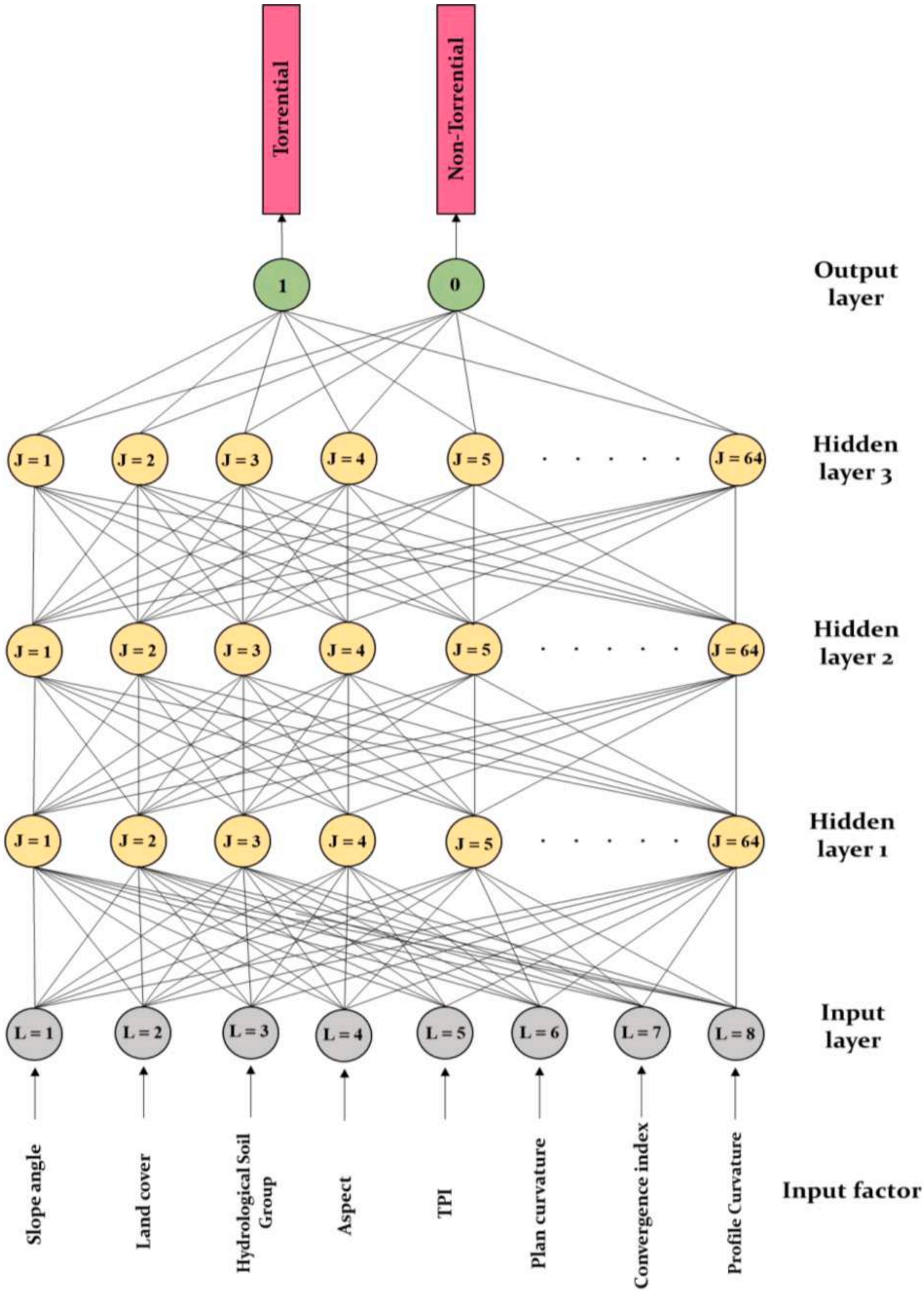

Fig. 7. DLNN-AHP architecture.

5.3.2. DLNN-AHp

The DLNN-AHP model was trained in R environment with the help of tools available in H2O package. The optimum architecture was reached by estimating the loss and accuracy values by after the application of total number of epochs equal to 100. According to the results the maximum accuracy of 0.95 was obtained after 89 epochs while the minimum value of loss (0.042) was reached after 95 epochs. The uniform kernel was used as initializer function, while ReLU was involved as activation function. The batch size was set to 100, validation rate to 0.2, while the dropout rate to 0.1. Thus, the optimal architecture of AHP-DLNN is formed by 8 input neurons, 3 hidden layers with a maximum of 64 neurons and 2 output neurons represented by the presence or absence of torrential pixels (Fig. 7). Finally, the functionalities of H2O R package in terms of Deep Learning Neural Networks algorithm allow to derive the following importance values for each variable: slope angle (0.206), plan curvature (0.114), hydrological soil group (0.114), land use (0.088), convergence index (0.122), profile curvature (0.179), topographic position index (0.111) and aspect (0.066). These values were used to derive in Map Algebra the $FFSI_{AHP\text{-}DLNN}$ within the study zone (Fig. 9b).

Using the Natural Breaks classification method, the $FFSI_{AHP\text{-}DLNN}$ values were divided into 5 classes. The very low class has a percentage of 13.16% and values from 0.09 and 0.19. The low class with a percentage of 29.12%, is situated in the range from 0.2 to 0.23. The moderate susceptibility is spread on 22.7%, while the high and very high values account 35.01% of the study zone.

5.3.3. MLP-AHp

The architecture of MLP-AHP model used in the present research was established according the lowest value achieved by RMSE. Thus, the lowest RMSE equal to 0.013 was achieved with a hidden layer containing 14 hidden neurons (Fig. 8a). Moreover, the pseudoprobability plot exposed in Fig. 8b, confirm that the torrential and non-torrential pixels were correct classified because the majority of values, represented on the left side (in blue) and right side (in green) are situated over the 0.5 of y-axis. The Gain chart (Fig. 8c) and Lift chart (Fig. 8d) prove also the high degree of performance obtained through MLP-AHP model.

The SPSS software permitted the possibility to derive the values of each flash-flood predictor importance in the MLP-AHP ensemble as following: slope angle (0.538), topographic position index (0.109), convergence index (0.096), plan curvature (0.093), hydrological soil group (0.055), aspect (0.052), profile curvature (0.035) and land use (0.022). The factor importance was used to compute the $FFSI_{MLP\text{-}AHP}$ (Fig. 9c).

Again, Natural Breaks algorithm was used to split the susceptibility values into 5 classes. The very low values, between 0.06 and 0.16, span on 31.32% of the study zone, while the low class is spread on 39.09% and is characterized by values from 0.17 to 0.22. Moderate flash-flood susceptibility is characteristic for a percentage of 20.35% of the total territory, while another 9.25% has a high and very high susceptibility.

5.3.4. NB-AHp

Using training data and a 10-fold cross-validation algorithm in the Weka 3.9 environment, the NB-AHP model was built. The cross-validation procedure is designed to minimize over-fitting and reduce

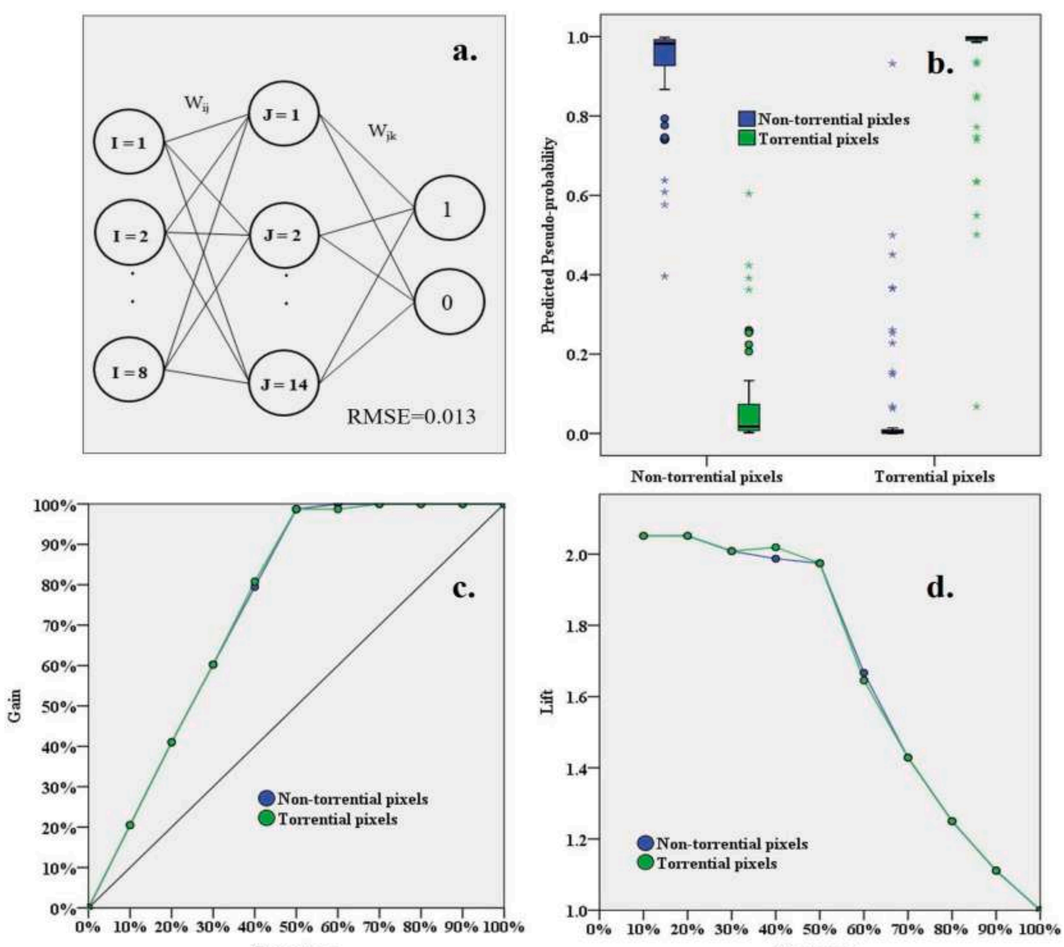

Fig. 8. MLP-AHP model architecture and performances indicators (a. network architecture; b. predicted pseudo-probability; c. gain chart; d. lift chart).

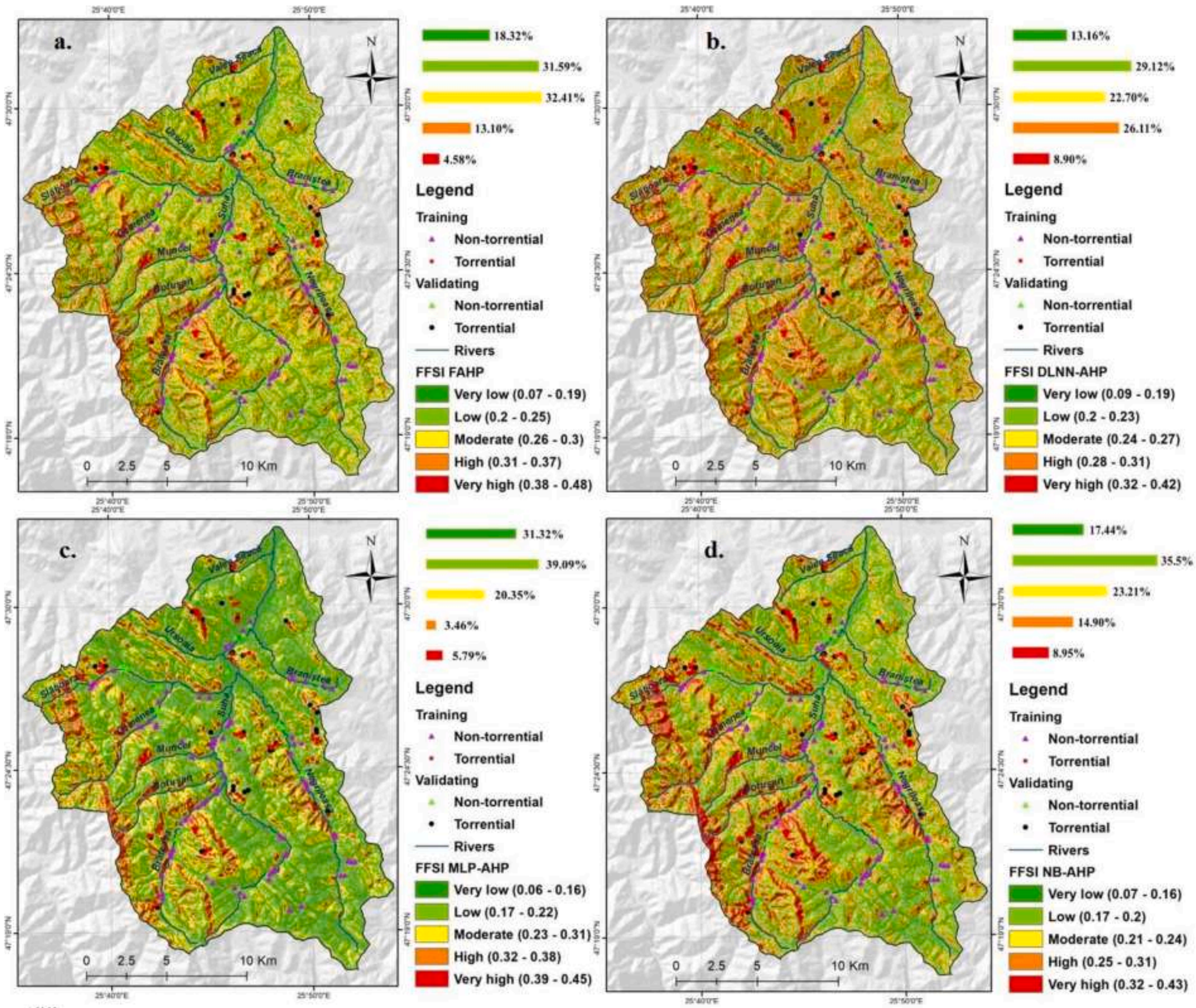

Fig. 9. Flash-Flood Susceptibility Index values (a. FAHP; b. DLNN-AHP; c. MLP-AHP; d. NB-AHP).

data variability as much as possible. Based on the training process, the maximum accuracy reached was 0.926, while the k-index was 0.74. The most important factor was the slope angle (0.427), followed by plan curvature (0.112), topographic position index (0.098), hydrological soil group (0.092), convergence index (0.078), profile curvature (0.066), aspect (0.065) and land use (0.062) (Table 5).

Like in the previous cases, Natural Breaks method helped to split the susceptibility values into 5 classes. The very low values, between 0.07 and 0.16, are spread on 17.44% of the research area, while the low class spans on 35.5% and has values between 0.17 and 0.2. Moderate flash-flood susceptibility is characteristic for a percentage of 23.21% of the total territory, while another 23.85% has a high and very high susceptibility (Fig. 9d).

5.4. Validation and comparison of the models

The results validation part was accomplished using the ROC Curve and a number of 4 statistical metrics.

5.4.1. Analysis of statistical metrics

Basically, the use of training dataset, highlights the following values for the accuracy metric: the highest value was assigned to DLNN-AHP (0.968), followed by NB-AHP (0.942), MLP-AHP (0.885) and FAHP (0.84) (Table 6). The use of validating sample, showed that the best accuracy was associated to DLNN-AHP (0.97), followed by NB-AHP (0.955), MLP-AHP (0.848) and FAHP (0.803).

5.4.2. Analysis of the ROC Curve

In terms of ROC Curves, the Success Rate was constructed with the help of training sample, while the Prediction Rate was designed by taking into consideration the validating dataset. The highest AUC of Success Rate shows was registered by the DLNN-AHP model (0.971), on the second place being NB-AHP (0.945), followed by MLP-AHP (0.888) and FAHP (0.836) (Fig. 10a). The Prediction Rate shows the same hierarchy as follows: DLNN-AHP model (0.984), NB-AHP (0.976), MLP-AHP (0.882) and FAHP (0.807) (Fig. 10b). Since the AUC values were above 0.8, we can state that all applied algorithms have a good performance.

6. Discussions

One of the areas highly affected by flash-floods hazards on the European continent, is the Romanian mountain region (Romanescu et al., 2017), within which is situated also the present research area. In light of the predicted increase in heavy rain frequency (Alfieri et al., 2018), it is crucial to detect promptly areas exposed to flash flood hazards within the Suha river catchment. In order to achieve very high precise results, the mechanisms of flash floods must be understood, and state-of-the-art techniques must be used to evaluate the flash flood susceptibility. To determine which surfaces are prone to rapid surface runoff, we developed four models based on machine learning techniques, fuzzy multi-criteria decision-making, and their ensemble to model the FFSI values from the spatial point of view. In the last 10 years many papers

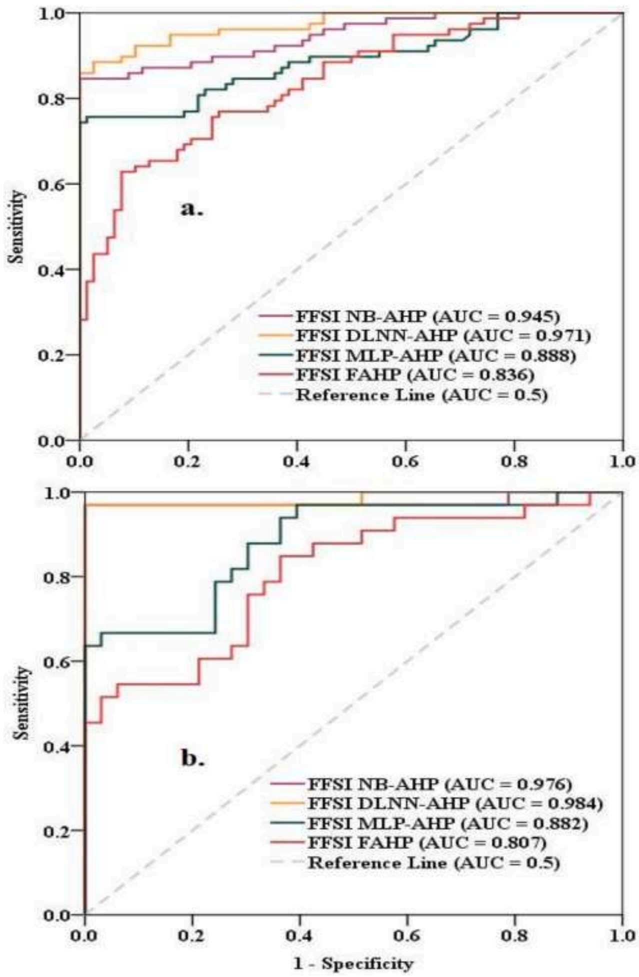

Fig. 10. ROC Curves (a. Success Rate; b. Prediction Rate).

Table 5
Predictor's importance for each of the hybrid model applied.

Predictors	FAHP	DLNN-AHP	MLP-AHP	NB-AHP
Slope angle	0.354	0.206	0.538	0.427
Plan curvature	0.155	0.114	0.093	0.112
Hydrological soil Group	0.175	0.114	0.055	0.092
Land use	0.033	0.088	0.022	0.062
Convergence Index	0	0.122	0.096	0.078
Profile Curvature	0.19	0.179	0.035	0.066
Topographic Position Index	0	0.111	0.109	0.098
Aspect	0.061	0.066	0.052	0.065

(Brewster, 2010; Kruzdlo and Ceru, 2010; Tincu et al., 2018; Zaharia et al., 2015, Zaharia et al., 2012) aimed to evaluate flash-flood susceptibility using the method proposed by Smith (2003). However, the aforementioned studies did not include any methodological considerations regarding surface runoff in the past and/or a statistical approach to determining flash-flood susceptibility within their methodological workflow. Past studies were also subject to a large degree of subjectivity due to the simple overlapping of flash flood predictors, in GIS software. Nonetheless, the training process for the 4 models applied in this paper made use of many flash-flood predictors that have been studied in previous papers. Based on the results of all the models, slope angle was the most significant factor. It has been established in many of the past research works that slope angle has a major influence on runoff genesis and manifestation (Borga et al., 2011; Chakrabortty et al., 2021; Elmahdy et al., 2020). This is explained by the fact that the slope angle affects the surface runoff velocity, which determines how flash floods behave (Fontanine and Costache, 2013). This affirmation is in total agreement with the outputs of the feature selection process that was applied in the present research and which showed that the slope angle has the highest correlation, among all the flash-flood predictors, with the previous torrential phenomena. Land use and convergence index are another 2 flash-flood predictors that resulted to be highly correlated with the historical torrential processes. On the reliability of the models, it becomes evident that the DLNN-AHP ensemble provided the best results, while FAHP was the least reliable. In line with Tehrany et al. (2015) findings, multicriteria decision-making analysis algorithms like FAHP have some disadvantages because this category of methods relies on expert knowledge, without considering the location of the previous areas affected by that hazard. Furthermore, the results of the present study show that the deep learning neural network, due to its complex structure with many hidden layers which are able for an input data deep processing, outperforms the multilayer perceptron with only one hidden layer and also the other three ensemble models used in this research. Thus, the statistical metrics involved in the results validation procedure highlights an accuracy of 0.97 for DLNN-AHP comparing to the lowest accuracy of 0.803 that belongs to the FAHP model. The same difference is also highlighted by the Prediction Rate of ROC Curve, where the AUC of DLNN-AHP was 0.984, meanwhile the AUC of FAHP was 0.807. The very high precision of DLNN model, in terms of flash-flood susceptibility prediction, was also certified in the study carried out by Bui et al. (2020a,b) in the Lao Cai province of Vietnam, where this algorithm reached an accuracy of 0.94. Also, in the same study, the AUC-ROC Curve of DLNN, equal to 0.96, exceeded the AUC-ROC Curve of MLP that was equal to 0.926. Also, in another study done, on the same topic, by Pham et al. (2021b) in Quang Nam province of Vietnam, deep learning neural network algorithm reached an accuracy maximum value of 0.961 and exceeded the performance of the other models like Logistic Regression (accuracy = 0.954), Artificial Neural Network-Radial Basis Function (accuracy = 0.954), Logistic Model Tree (accuracy = 0.954) and Alternating Decision Tree (accuracy = 0.958). Therefore, we can state that the DLNN is a very high performant model that is capable to provide highly accurate results in terms of flood and flash-flood susceptibility prediction.

Table 6
Statistical metrics involved in the evaluation of models' performance.

Metrics	Training sample				Validating sample			
	FAHP	DLNN-AHP	MLP-AHP	NB-AHP	FAHP	DLNN-AHP	MLP-AHP	NB-AHP
TP	65	75	70	73	27	32	29	31
TN	66	76	68	74	26	32	27	32
FP	13	3	8	5	6	1	4	2
FN	12	2	10	4	7	1	6	1
Sensitivity	0.844	0.974	0.875	0.948	0.794	0.970	0.829	0.969
Specificity	0.835	0.962	0.895	0.937	0.813	0.970	0.871	0.941
Accuracy	0.840	0.968	0.885	0.942	0.803	0.970	0.848	0.955
K	0.679	0.936	0.769	0.885	0.606	0.939	0.697	0.909

7. Conclusions

The current study aimed to propose new 3 hybrid algorithms and fuzzy-AHP method to estimate the flash flood susceptibility within the Suha river basin. In each of the hybrid models, pixels associated with torrential areas were used alongside eight flash-flood predictors as input data. As a result of the application of the ReliefF method, all eight flash-flood conditioning factors are reliable and should be incorporated into the analysis. By evaluating the results with ROC curve, all the models achieved good to very good performance, as indicated by area under the curve (AUC) values above 0.807. Furthermore, the accuracy values of over 0.803 indicate the models' robustness. Over 9.25% of the research zone is covered by surfaces with high and high flash flood susceptibility, which are uniformly distributed within the Suha basin.

In this study, there is a significant novelty in that the 3 ensemble models (DLNN-AHP, MLP-AHP and NB-AHP) and H2O R package are used for the first time to predict whether a region is vulnerable to flash-flood phenomena. The results obtained in this study, which have very good accuracy, can be used with a high degree of confidence by the authorities responsible for the mitigation of flash-flood negative effects.

As in any study in which geospatial data is used, a limitation of this study may be the errors that may occur in the spatial representation of the data. Therefore, it should be noted that the focus of the future study will be to obtain data with higher resolution and accuracy and to use them in studies on estimating susceptibility to flash-floods.

Funding

This work was supported by a grant of the Romanian Ministry of Education and Research, CNCS – UEFISCDI, project number PN-III-P1-1.1-PD-2019–0424-P, within PNCDI III.

CRediT authorship contribution statement

Romulus Costache: Conceptualization, Methodology, Software, Validation, Formal analysis, Investigation, Resources, Data curation, Writing – original draft, Writing – review & editing, Visualization, Supervision, Funding acquisition. **Tran Trung Tin:** Conceptualization, Visualization, Funding acquisition. **Alireza Arabameri:** Methodology, Formal analysis, Investigation, Writing – review & editing, Supervision. **Anca Crăciun:** . **R.S. Ajin:** Methodology, Formal analysis, Investigation, Writing – review & editing, Supervision. **Iulia Costache:** Methodology, Software, Validation, Formal analysis, Investigation, Resources, Data curation, Writing – original draft, Writing – review & editing, Supervision. **Abu Reza Md. Towfiqul Islam:** Data curation, Writing – original draft. **S.I. Abba:** Methodology, Data curation. **Mehebub Sahana:** Conceptualization, Methodology. **Mohammadtaghi Avand:** Software, Validation, Resources, Data curation, Writing – original draft. **Binh Thai Pham:** Conceptualization, Software, Validation, Resources, Data curation, Writing – original draft, Visualization, Funding acquisition.

Declaration of Competing Interest

The authors declare that they have no known competing financial interests or personal relationships that could have appeared to influence the work reported in this paper.

References

Abedini, M., Ghasemian, B., Shirzadi, A., Bui, D.T., 2019. A comparative study of support vector machine and logistic model tree classifiers for shallow landslide susceptibility modeling. Environ. Earth Sci. 78, 1–15.

Ahmadlou, M., Karimi, M., Alizadeh, S., Shirzadi, A., Parvinnejhad, D., Shahabi, H., Panahi, M., 2019. Flood susceptibility assessment using integration of adaptive network-based fuzzy inference system (ANFIS) and biogeography-based optimization (BBO) and BAT algorithms (BA). Geocarto Int. 34, 1252–1272.

Ahmadlou, M., Al-Fugara, A., Al-Shabeeb, A.R., Arora, A., Al-Adamat, R., Pham, Q.B., Al-Ansari, N., Linh, N.T.T., Sajedi, H., 2021. Flood susceptibility mapping and assessment using a novel deep learning model combining multilayer perceptron and autoencoder neural networks. J. Flood Risk Manage. 14, e12683.

Alfieri, L., Dottori, F., Betts, R., Salamon, P., Feyen, L., 2018. Multi-model projections of river flood risk in Europe under global warming. Climate 6, 6.

Alho, P., Aaltonen, J., 2008. Comparing a 1D hydraulic model with a 2D hydraulic model for the simulation of extreme glacial outburst floods. Hydrol. Process.: Int. J. 22, 1537–1547.

Arabameri, A., Saha, S., Chen, W., Roy, J., Pradhan, B., Bui, D.T., 2020. Flash flood susceptibility modelling using functional tree and hybrid ensemble techniques. J. Hydrol. 125007.

Arora, A., Arabameri, A., Pandey, M., Siddiqui, M.A., Shukla, U., Bui, D.T., Mishra, V.N., Bhardwaj, A., 2021. Optimization of state-of-the-art fuzzy-metaheuristic ANFIS-based machine learning models for flood susceptibility prediction mapping in the Middle Ganga Plain, India. Sci. Total Environ. 750, 141565.

Asadi, H., Shahedi, K., Jarihani, B., Sidle, R.C., 2019. Rainfall-runoff modelling using hydrological connectivity index and artificial neural network approach. Water 11, 212.

Borga, M., Anagnostou, E., Blöschl, G., Creutin, J.-D., 2011. Flash flood forecasting, warning and risk management: the HYDRATE project. Environ. Sci. Policy 14, 834–844.

Brewster, J., 2010. Development of the flash flood potential index (FFPI) for central NY & Northeast PA. Presented at the Eastern Region Flash Flood Conference, NOAA's National Weather Service, pp. 2–4.

Bui, D.T., Ngo, P.-T.-T., Pham, T.D., Jaafari, A., Minh, N.Q., Hoa, P.V., Samui, P., 2019. A novel hybrid approach based on a swarm intelligence optimized extreme learning machine for flash flood susceptibility mapping. Catena 179, 184–196.

Bui, D.T., Hoang, N.-D., Martínez-Álvarez, F., Ngo, P.-T.-T., Hoa, P.V., Pham, T.D., Samui, P., Costache, R., 2020a. A novel deep learning neural network approach for predicting flash flood susceptibility: a case study at a high frequency tropical storm area. Sci. Total Environ. 701, 134413.

Bui, Q.-T., Nguyen, Q.-H., Nguyen, X.L., Pham, V.D., Nguyen, H.D., Pham, V.-M., 2020b. Verification of novel integrations of swarm intelligence algorithms into deep learning neural network for flood susceptibility mapping. J. Hydrol. 581, 124379 https://doi.org/10.1016/j.jhydrol.2019.124379.

Bures, L., Roub, R., Sychova, P., Gdulova, K., Doubalova, J., 2019. Comparison of bathymetric data sources used in hydraulic modelling of floods. J. Flood Risk Manage. 12, e12495.

Canbek, G., Sagiroglu, S., Temizel, T.T., Baykal, N., 2017. Binary classification performance measures/metrics: A comprehensive visualized roadmap to gain new insights. In: Presented at the 2017 International Conference on Computer Science and Engineering (UBMK). IEEE, pp. 821–826.

Chakrabortty, R., Chandra Pal, S., Rezaie, F., Arabameri, A., Lee, S., Roy, P., Saha, A., Chowdhuri, I., Moayedi, H., 2021. Flash-flood hazard susceptibility mapping in Kangsabati River Basin, India. Geocarto Int. 1–23.

Chao, L., Zhang, K., Wang, J., Feng, J., Zhang, M., 2021. A Comprehensive Evaluation of Five Evapotranspiration Datasets Based on Ground and GRACE Satellite Observations: Implications for Improvement of Evapotranspiration Retrieval Algorithm. Remote Sens. 13 (12), 2414 https://doi.org/10.3390/rs13122414.

Chen, W., Zhang, S., Li, R., Shahabi, H., 2018. Performance evaluation of the GIS-based data mining techniques of best-first decision tree, random forest, and naïve Bayes tree for landslide susceptibility modeling. Sci. Total Environ. 644, 1006–1018.

Choubin, B., Rahmati, O., Tahmasebipour, N., Feizizadeh, B., Pourghasemi, H.R., 2019. Application of fuzzy analytical network process model for analyzing the gully erosion susceptibility, in: Natural Hazards Gis-Based Spatial Modeling Using Data Mining Techniques. Springer, pp. 105–125.

Chowdhuri, I., Pal, S.C., Chakrabortty, R., 2020. Flood susceptibility mapping by ensemble evidential belief function and binomial logistic regression model on river basin of eastern India. Adv. Space Res. 65, 1466–1489.

Chukwuma, E., Okonkwo, C., Ojediran, J., Anizoba, D., Ubah, J., Nwachukwu, C., 2021. A GIS based flood vulnerability modelling of Anambra State using an integrated IVFRN-DEMATEL-ANP model. Heliyon 7, e08048.

Costache, R., 2019. Flash-Flood Potential assessment in the upper and middle sector of Prahova river catchment (Romania). A comparative approach between four hybrid models. Sci. Total Environ. 659, 1115–1134.

Costache, R., Bui, D.T., 2020. Identification of areas prone to flash-flood phenomena using multiple-criteria decision-making, bivariate statistics, machine learning and their ensembles. Sci. Total Environ. 712, 136492.

Costache, R., Hong, H., Wang, Y., 2019. Identification of torrential valleys using GIS and a novel hybrid integration of artificial intelligence, machine learning and bivariate statistics. Catena 183, 104179.

Costache, R., Ngo, P.T.T., Tien Bui, D., 2020a. Novel ensembles of deep learning neural network and statistical learning for flash-flood susceptibility mapping. Water 12, 1549. https://doi.org/10.3390/w12061549.

Costache, R., Pham, Q.B., Avand, M., Linh, N.T.T., Vojtek, M., Vojteková, J., Lee, S., Khoi, D.N., Nhi, P.T.T., Dung, T.D., 2020b. Novel hybrid models between bivariate statistics, artificial neural networks and boosting algorithms for flood susceptibility assessment. J. Environ. Manage. 265, 110485.

Costache, R., Pham, Q.B., Sharifi, E., Linh, N.T.T., Abba, S., Vojtek, M., Vojteková, J., Nhi, P.T.T., Khoi, D.N., 2020c. Flash-flood susceptibility assessment using multi-criteria decision making and machine learning supported by remote sensing and GIS techniques. Remote Sens. 12, 106.

Costache, R., Barbulescu, A., Pham, Q.B., 2021a. Integrated framework for detecting the areas prone to flooding generated by flash-floods in small river catchments. Water 13, 758.

Costache, R., Pham, Q.B., Arabameri, A., Diaconu, D.C., Costache, I., Crăciun, A., Ciobotaru, N., Pandey, M., Arora, A., Ali, S.A., 2021b. Flash-flood propagation

susceptibility estimation using weights of evidence and their novel ensembles with multicriteria decision making and machine learning. Geocarto Int. 1–33.
Deng, L., Hinton, G., Kingsbury, B., 2013. New types of deep neural network learning for speech recognition and related applications: An overview. In: Presented at the 2013 IEEE international conference on acoustics, speech and signal processing. IEEE, pp. 8599–8603.
Destro, E., Amponsah, W., Nikolopoulos, E.I., Marchi, L., Marra, F., Zoccatelli, D., Borga, M., 2018. Coupled prediction of flash flood response and debris flow occurrence: application on an alpine extreme flood event. J. Hydrol. 558, 225–237.
Elmahdy, S., Ali, T., Mohamed, M., 2020. Flash flood susceptibility modeling and magnitude index using machine learning and geohydrological models: A modified hybrid approach. Remote Sensing 12, 2695.
Fang, Z., Wang, Y., Peng, L., Hong, H., 2021. Predicting flood susceptibility using LSTM neural networks. J. Hydrol. 594, 125734.
Fontanine, I., Costache, R., 2013. Using GIS techniques for surface runoff potential analysis in the Subcarpathian area between Buzău and Slănic rivers, in Romania. Cinq Continents 3, 47–57.
Handini, D.R., Hidayah, E., Halik, G., 2021. Flash Flood Susceptibility Mapping at Andungbiru Watershed, East Java Using AHP-Information Weighted Method. Geosfera Indonesia 6, 127–142.
Hategekimana, Y., Yu, L., Nie, Y., Zhu, J., Liu, F., Guo, F., 2018. Integration of multi-parametric fuzzy analytic hierarchy process and GIS along the UNESCO World Heritage: a flood hazard index, Mombasa County, Kenya. Nat. Hazards 92, 1137–1153.
He, Y., Dai, L., Zhang, H., 2020. Multi-Branch Deep Residual Learning for Clustering and Beamforming in User-Centric Network. IEEE Commun. Lett. 24 (10), 2221–2225. https://doi.org/10.1109/LCOMM.2020.3005947.
Hosseini, F.S., Choubin, B., Mosavi, A., Nabipour, N., Shamshirband, S., Darabi, H., Haghighi, A.T., 2020. Flash-flood hazard assessment using ensembles and Bayesian-based machine learning models: application of the simulated annealing feature selection method. Sci. Total Environ. 711, 135161.
Islam, A.R.M.T., Talukdar, S., Mahato, S., Kundu, S., Eibek, K.U., Pham, Q.B., Kuriqi, A., Linh, N.T.T., 2021. Flood susceptibility modelling using advanced ensemble machine learning models. Geosci. Front. 12, 101075.
Janizadeh, S., Avand, M., Jaafari, A., Phong, T.V., Bayat, M., Ahmadisharaf, E., Prakash, I., Pham, B.T., Lee, S., 2019. Prediction success of machine learning methods for flash flood susceptibility mapping in the tafresh watershed, Iran. Sustainability 11, 5426.
Jiang, L., Li, C., Wang, S., Zhang, L., 2016. Deep feature weighting for naive Bayes and its application to text classification. Eng. Appl. Artif. Intell. 52, 26–39.
Ke, B., Nguyen, H., Bui, X.-N., Bui, H.-B., Nguyen-Thoi, T., 2021. Prediction of the sorption efficiency of heavy metal onto biochar using a robust combination of fuzzy C-means clustering and back-propagation neural network. J. Environ. Manage. 293, 112808.
Khosravi, K., Pham, B.T., Chapi, K., Shirzadi, A., Shahabi, H., Revhaug, I., Prakash, I., Bui, D.T., 2018. A comparative assessment of decision trees algorithms for flash flood susceptibility modeling at Haraz watershed, northern Iran. Sci. Total Environ. 627, 744–755.
Kjeldsen, T.R., 2010. Modelling the impact of urbanization on flood frequency relationships in the UK. Hydrol. Res. 41, 391–405.
Kratzert, F., Klotz, D., Brenner, C., Schulz, K., Herrnegger, M., 2018. Rainfall–runoff modelling using long short-term memory (LSTM) networks. Hydrol. Earth Syst. Sci. 22, 6005–6022.
Kruzdlo, R., Ceru, J., 2010. Flash Flood Potential Index for WFO Mount Holly/ Philadelphia. Presented at the Eastern region flash flood conference, poster session, NOAA's National Weather Service, pp. 2–4.
Lan, Z., Zhao, Y., Zhang, J., Jiao, R., Khan, M.N., Sial, T.A., Si, B., 2021. Long-term vegetation restoration increases deep soil carbon storage in the Northern Loess Plateau. Sci. Rep. 11, 13758 https://doi.org/10.1038/s41598-021-93157-0.
Li, D., Huang, F., Yan, L., Cao, Z., Chen, J., Ye, Z., 2019. Landslide susceptibility prediction using particle-swarm-optimized multilayer perceptron: comparisons with multilayer-perceptron-only, bp neural network, and information value models. Appl. Sci. 9, 3664.
Liu, W., Moayedi, H., Nguyen, H., Lyu, Z., Bui, D.T., 2021b. Proposing two new metaheuristic algorithms of ALO-MLP and SHO-MLP in predicting bearing capacity of circular footing located on horizontal multilayer soil. Eng. Comput. 37, 1537–1547.
Liu, J., Wang, J., Xiong, J., Cheng, W., Sun, H., Yong, Z., Wang, N., 2021a. Hybrid models incorporating bivariate statistics and machine learning methods for flash flood susceptibility assessment based on remote sensing datasets. Remote Sens. 13, 4945.
Liu, Y., Zhang, K., Li, Z., Liu, Z., Wang, J., Huang, P., 2020. A hybrid runoff generation modelling framework based on spatial combination of three runoff generation schemes for semi-humid and semi-arid watersheds. J. Hydrol. 590, 125440 https://doi.org/10.1016/j.jhydrol.2020.125440.
Malik, A., Tikhamarine, Y., Sammen, S.S., Abba, S.I., Shahid, S., 2021. Prediction of meteorological drought by using hybrid support vector regression optimized with HHO versus PSO algorithms. Environ. Sci. Pollut. Res. 1–20.
Minár, J., Evans, I.S., Jenčo, M., 2020. A comprehensive system of definitions of land surface (topographic) curvatures, with implications for their application in geoscience modelling and prediction. Earth Sci. Rev. 211, 103414.
Ngo, P.-T.-T., Pham, T.D., Nhu, V.-H., Le, T.T., Tran, D.A., Phan, D.C., Hoa, P.V., Amaro-Mellado, J.L., Bui, D.T., 2021. A novel hybrid quantum-PSO and credal decision tree ensemble for tropical cyclone induced flash flood susceptibility mapping with geospatial data. J. Hydrol. 596, 125682.
Panahi, M., Jaafari, A., Shirzadi, A., Shahabi, H., Rahmati, O., Omidvar, E., Lee, S., Bui, D.T., 2021. Deep learning neural networks for spatially explicit prediction of flash flood probability. Geosci. Front. 12, 101076.
Pandey, M., Arora, A., Arabameri, A., Costache, R., Kumar, N., Mishra, V., Nguyen, H., Mishra, J., Siddiqui, M., Ray, Y., 2021. Flood susceptibility modeling in a subtropical humid low-relief alluvial plain environment: application of novel ensemble machine learning approach. Front. Earth Sci. 9, 659296.
Pham, B.T., Jaafari, A., Van Phong, T., Yen, H.P.H., Tuyen, T.T., Van Luong, V., Nguyen, H.D., Van Le, H., Foong, L.K., 2021a. Improved flood susceptibility mapping using a best first decision tree integrated with ensemble learning techniques. Geosci. Front. 12, 101105.
Pham, B.T., Luu, C., Van Phong, T., Trinh, P.T., Shirzadi, A., Renoud, S., Asadi, S., Van Le, H., von Meding, J., Clague, J.J., 2021b. Can deep learning algorithms outperform benchmark machine learning algorithms in flood susceptibility modeling? J. Hydrol. 592, 125615.
Popa, M.C., Peptenatu, D., Drăghici, C.C., Diaconu, D.C., 2019. Flood hazard mapping using the flood and flash-flood potential index in the Buzău River catchment, Romania. Water 11, 2116.
Prăvălie, R., Costache, R., 2013. The vulnerability of the territorial-administrative units to the hydrological phenomena of risk (flash-floods). Case study: the subcarpathian sector of Buzău catchment. Analele Universităţii din Oradea–Seria Geografie 23 (1), 91–98.
Rafiei-Sardooi, E., Azareh, A., Choubin, B., Mosavi, A.H., Clague, J.J., 2021. Evaluating urban flood risk using hybrid method of TOPSIS and machine learning. Int. J. Disaster Risk Reduct. 66, 102614.
Romanescu, G., Cimpianu, C.I., Mihu-Pintilie, A., Stoleriu, C.C., 2017. Historic flood events in NE Romania (post-1990). J. Maps 13, 787–798.
Roodposhti, M.S., Rahimi, S., Beglou, M.J., 2014. PROMETHEE II and fuzzy AHP: an enhanced GIS-based landslide susceptibility mapping. Nat. Hazards 73, 77–95.
Sahana, M., Pham, B.T., Shukla, M., Costache, R., Thu, D.X., Chakrabortty, R., Satyam, N., Nguyen, H.D., Phong, T.V., Le, H.V., Pal, C.P., Areendran, G., Imdad, K., Prakash, I., 2020. Rainfall induced landslide susceptibility mapping using novel hybrid soft computing methods based on multi-layer perceptron neural network classifier. Geocarto Int. https://doi.org/10.1080/10106049.2020.1837262.
Shahabi, H., Shirzadi, A., Ghaderi, K., Omidvar, E., Al-Ansari, N., Clague, J.J., Geertsema, M., Khosravi, K., Amini, A., Bahrami, S., 2020a. Flood detection and susceptibility mapping using sentinel-1 remote sensing data and a machine learning approach: hybrid intelligence of bagging ensemble based on k-nearest neighbor classifier. Remote Sens. 12, 266.
Shahabi, H., Shirzadi, A., Ronoud, S., Asadi, S., Pham, B.T., Mansouripour, F., Geertsema, M., Clague, J.J., Bui, D.T., 2020b. Flash flood susceptibility mapping using a novel deep learning model based on deep belief network, back propagation and genetic algorithm. Geosci. Front.
Singh, G., Pandey, A., 2021. Spatial prediction of flash floods using susceptibility modeling and geospatial technology: a review. J. Geomatics 15.
Smith, G., 2003. Flash flood potential: Determining the hydrologic response of FFMP basins to heavy rain by analyzing their physiographic characteristics. A white paper available from the NWS Colorado Basin River Forecast Center web site at http://www.cbrfc.noaa.gov/papers/ffp_wpap.pdf.
Stewart, D., Canfield, E., Hawkins, R., 2011. Curve number determination methods and uncertainty in hydrologic soil groups from semiarid watershed data. J. Hydrol. Eng. 17, 1180–1187.
Sun, C.-C., 2010. A performance evaluation model by integrating fuzzy AHP and fuzzy TOPSIS methods. Expert Syst. Appl. 37, 7745–7754.
Tamiru, H., Dinka, M.O., 2021. Application of ANN and HEC-RAS model for flood inundation mapping in lower Baro Akobo River Basin, Ethiopia. J. Hydrol.: Reg. Stud. 36, 100855.
Tehrany, M.S., Pradhan, B., Mansor, S., Ahmad, N., 2015. Flood susceptibility assessment using GIS-based support vector machine model with different kernel types. Catena 125, 91–101.
Tien Bui, D., Pradhan, B., Lofman, O., Revhaug, I., 2012. Landslide susceptibility assessment in vietnam using support vector machines, decision tree, and Naive Bayes Models. Mathematical problems in Engineering 2012.
Tincu, R., Lazar, G., Lazar, I., 2018. Modified flash flood potential index in order to estimate areas with predisposition to water accumulation. Open Geosci. 10, 593–606.
Tîrnovan, A., Cojoc, G.M., Romanescu, G., Obreja, F., 2014. Predicting the potential index of major floods production in the Suha river basin (Suha Bucovineana). Water resources and wetlands.
Urbanowicz, R.J., Meeker, M., La Cava, W., Olson, R.S., Moore, J.H., 2018. Relief-based feature selection: introduction and review. J. Biomed. Inform.
Wang, Y., Fang, Z., Hong, H., Peng, L., 2020. Flood susceptibility mapping using convolutional neural network frameworks. J. Hydrol. 582, 124482.
Wang, Y., Cheng, H., Hu, Q., Liu, L., Jia, L., Gao, S., Wang, Y., 2022. Pore structure heterogeneity of Wufeng-Longmaxi shale, Sichuan Basin, China: Evidence from gas physisorption and multifractal geometries. J. Pet. Sci. Eng. 2 (Part A), 109313 https://doi.org/10.1016/j.petrol.2021.109313.
Wang, Y., Fang, Z., Hong, H., Costache, R., Tang, X., 2021. Flood susceptibility mapping by integrating frequency ratio and index of entropy with multilayer perceptron and classification and regression tree. J. Environ. Manage. 289, 112449.
Wang, S., Zhang, K., Chao, L., Li, D., Tian, X., Bao, H., Chen, G., Xia, Y., 2021. Exploring the utility of radar and satellite-sensed precipitation and their dynamic bias correction for integrated prediction of flood and landslide hazards. J. Hydrol. 603, 126964 https://doi.org/10.1016/j.jhydrol.2021.126964.
Waqas, H., Lu, L., Tariq, A., Li, Q., Baqa, M.F., Xing, J., Sajjad, A., 2021. Flash flood susceptibility assessment and zonation using an integrating analytic hierarchy

process and frequency ratio model for the Chitral District, Khyber Pakhtunkhwa, Pakistan. Water 13, 1650.
Xiong, J., Li, J., Cheng, W., Wang, N., Guo, L., 2019. A GIS-based support vector machine model for flash flood vulnerability assessment and mapping in China. ISPRS Int. J. Geo-Inf. 8, 297.
Youssef, A.M., Pradhan, B., Sefry, S.A., 2016. Flash flood susceptibility assessment in Jeddah city (Kingdom of Saudi Arabia) using bivariate and multivariate statistical models. Environ. Earth Sci. 75, 12.
Zaharia, L., Minea, G., Ioana-Toroimac, G., Barbu, R., Sârbu, I., 2012. Estimation of the areas with accelerated surface runoff in the upper Prahova watershed (Romanian Carpathians). Republic of Macedonia, Balwois.
Zaharia, L., Costache, R., Prăvălie, R., Minea, G., 2015. Assessment and mapping of flood potential in the Slănic catchment in Romania. J. Earth Syst. Sci. 124, 1311–1324.
Zare, M., Pourghasemi, H.R., Vafakhah, M., Pradhan, B., 2013. Landslide susceptibility mapping at Vaz Watershed (Iran) using an artificial neural network model: a comparison between multilayer perceptron (MLP) and radial basic function (RBF) algorithms. Arabian J. Geosci. 6, 2873–2888.
Zhan, C., Dai, Z., Soltanian, M.R., Zhang, X., 2022. Stage-Wise Stochastic Deep Learning Inversion Framework for Subsurface Sedimentary Structure Identification. Geophys. Res. Lett. 49 (1), 10.1029/2021GL095823.
Zhang, Z., Luo, C., Zhao, Z., 2020. Application of probabilistic method in maximum tsunami height prediction considering stochastic seabed topography. Natural hazards (Dordrecht). Nat. Hazard. 104, 2511–2530. https://doi.org/10.1007/s11069-020-04283-3.
Zhang, K., Wang, S., Bao, H., Zhao, X., 2019. Characteristics and influencing factors of rainfall-induced landslide and debris flow hazards in Shaanxi Province, China. Nat. Hazards Earth Syst. Sci. 19 (1), 93–105. https://doi.org/10.5194/nhess-19-93-2019.
Zhao, X., Xia, H., Pan, L., Song, H., Niu, W., Wang, R., Qin, Y., 2021. Drought Monitoring over Yellow River Basin from 2003–2019 Using Reconstructed MODIS Land Surface Temperature in Google Earth Engine. Remote Sens. 13 (18), 3748 https://doi.org/10.3390/rs13183748.

Journal of Hydrology 585 (2020) 124808

Contents lists available at ScienceDirect

Journal of Hydrology

journal homepage: www.elsevier.com/locate/jhydrol

Research papers

Spatial predicting of flood potential areas using novel hybridizations of fuzzy decision-making, bivariate statistics, and machine learning

Romulus Costache[a,b], Mihnea Cristian Popa[c,d,*], Dieu Tien Bui[e,*], Daniel Constantin Diaconu[c,f,*], Nicu Ciubotaru[b,d], Gabriel Minea[b], Quoc Bao Pham[g]

[a] Research Institute of the University of Bucharest, 90-92 Sos. Panduri, 5th District, 050663 Bucharest, Romania
[b] National Institute of Hydrology and Water Management, București-Ploiești Road, 97E, 1st District, 013686 Bucharest, Romania
[c] Centre for Integrated Analysis and Territorial Management, University of Bucharest, Bucharest 010041, Romania
[d] Simion Mehedinți – Nature and Sustainable Development" Doctoral School, University of Bucharest, Bucharest 010041, Romania
[e] Institute of Research and Development, Duy Tan University, Da Nang 550000, Viet Nam
[f] Department of Meteorology and Hydrology, Faculty of Geography, University of Bucharest, Bucharest 010041, Romania
[g] Department of Hydraulic and Ocean Engineering, National Cheng-Kung University, Tainan 701, Taiwan

ARTICLE INFO

This manuscript was handled by A. Bardossy, Editor-in-Chief, with the assistance of Fi-John Chang, Associate Editor

Keywords:
Environmental modeling
Flood
Hybridization
Fuzzy analytical hierarchy process
Index of entropy
Support vector machine

ABSTRACT

The global warming and climate changes determined a considerable increase in the frequency of floods and their related damages. Therefore, the high accuracy prediction of flood susceptible areas plays a key role in flood warnings and risk reduction. The main objective of this study is to propose novel hybridizations of fuzzy Analytical Hierarchy Process (FAHP), Index of Entropy (IoE), and Support Vector Machine (SVM) for predicting the areas susceptible to floods. Buzău river catchment (Romania) was the area on which the present study was focused. In this regard, a database with 205 flooded locations, 205 non-flood locations and 12 flood predictors was established and used to train and validate the flood susceptibility models. The performance of the proposed models was evaluated using the Receiver Operating Characteristic (ROC) Curve and statistical metrics. The results show that all the hybrid models have a high prediction performance and outperform the stand-alone models. Among them, the SVM-IoE model (AUC = 0.979) has the highest performance, followed by the FAHP-IoE (AUC = 0.97), IoE (AUC = 0.969), SVM (AUC = 0.966) and FAHP (AUC = 0.947). These results highlight a very high efficiency of all the applied models. The application of the models mentioned above revealed that a percentage between 12.5% (FPI_{IoE}) and 21.2% (FPI_{FAHP}) of the study area is characterized by high and very high exposure to these hydrological hazards.

1. Introduction

Floods are natural risk phenomena causing severe damages to the environment, loss of human life, determining a slowdown of the economic development of many areas across the world. It is increasingly evident that the overall frequency of major flood events will increase over the next few years, this fact being directly connected with the global climate changes (Spence et al., 2011). This higher frequency and severity of the flood phenomena will inevitably cause exponential growth in terms of economic damage and loss of human life (Jongman, 2018). Globally, each year the floods are responsible for economic losses totaling over $20 billion and more for than 3000 casualties (Nicklin et al., 2019). In Europe, the damages caused by floods are expected to increase five times until the year 2050 and 17 times until the year 2080 (European Environment Agency, 2017). Romania is one of the most flood-affected European countries (Costache, 2019a). Throughout the 20th and early 21st century, numerous areas across Romania were affected by historical floods such as those occurring in the years: 1912, 1932, 1969, 1970, 2005, 2006 and 2010 (Grecu et al., 2017). Annually, in Romania, floods cause material losses of over 100 million euros. With the accession to the European Union in 2007, Romania was forced to align the directives of the European Parliament such as the Directive 2007/60/EC. The activities related to flood risk management are included in this directive. Floods occurrence is difficult to prevent, and their devastating effects are often amplified by certain human activities (Minea et al., 2019) and also by climate changes. However, certain measures undertaken by the responsible authorities can significantly decrease the amount of damage produced

* Corresponding authors at: Institute of Research and Development, Duy Tan University, Da Nang 550000, Viet Nam (D. Tien Bui) and Centre for Integrated Analysis and Territorial Management, University of Bucharest, Bucharest 010041, Romania (M.C. Popa, D.C. Diaconu).
E-mail addresses: mihnea.cristian.popa@drd.unibuc.ro (M.C. Popa), buitiendieu@duytan.edu.vn (D. Tien Bui), daniel.diaconu@unibuc.ro (D.C. Diaconu).

https://doi.org/10.1016/j.jhydrol.2020.124808
Received 1 December 2019; Received in revised form 3 February 2020; Accepted 6 March 2020
Available online 09 March 2020
0022-1694/

by the floods and also can reduce the loss of human life. At the base of all measures intended to reduce the flood vulnerability, is the identification of the areas with a high risk to these types of natural hazards. One of the methods used to quantify the areas susceptible to severe flooding is the hydraulic modeling through which the floodplain extent is directly related to certain discharge values with different probabilities of exceedance. Nevertheless, the hydraulic modeling is time-consuming and also the necessary data, like a Digital Elevation Model at a high resolution, are expensive.

During the last years, many state of the art methods, with the ability to integrate the flood predictors into a GIS environment, were frequently used in the studies related to the flood susceptibility assessment (Ahmadlou et al., 2018; Costache et al., 2019b; Costache and Bui, 2019; Mahmoud and Gan, 2018; Tien Bui et al., 2019; Costache and Prăvălie, 2012). Also, the role of certain flood predictors on the accumulation of water at the soil surface can be quantified. Thus, the most widely used models in the category of bivariate statistics are Statistical Index, Certainty Factor, Frequency Ratio, Index of Entropy and Weights of Evidence (Costache and Zaharia, 2017; Khosravi et al., 2016; Kumar Samanta et al., 2018; Tehrany et al., 2013). Machine Learning algorithms are represented by the models like Artificial Neural Networks, Support Vector Machine, Logistic Regression, Adaptive Neuro-Fuzzy Inference System and Decision Trees (Arabameri et al., 2019; Choubin et al., 2019; Costache, 2019b, 2019c; Dou et al., 2019; Hong et al., 2018; Mojaddadi et al., 2017; Tehrany et al., 2014; Tien Bui et al., 2016; Wang et al., 2019; Wang et al., 2015). The hybrid methods formed by combining two or more stand-alone models are considered more advanced, providing much more accurate results. A key element in using Machine Learning and bivariate statistical models is the use of input data of the points where the flood phenomena already occurred.

In the light of the above considerations, in this study, for detecting the areas prone to floods, five models will be tested which are represented by Index of Entropy (IoE) stand-alone model, Fuzzy Analytical Hierarchy Process (FAHP) stand-alone model, Support Vector Machine (SVM) stand-alone model, FAHP-IoE and SVM-IoE. The entire training process of the five models will be ensured by using 12 flood predictors, 205 flood locations and 205 non-flood locations. The validation of results was performed using the ROC Curve and also several statistical indices. This study was focused on the Buzau river catchment which is one of the most affected regions in Romania by flood phenomena.

2. Study area and data

2.1. The geographical setting of the Buzău river catchment

Buzău river catchment is located in the southeastern part of Romania (Fig. 1), overlapping three landforms, mountains, hills, and plains, respectively. The study area covers a total surface of 5350 km^2 with altitudes ranging from 1 m to 1925 m.

The lithological substrate, in the mountainous and hilly area, mainly consists of limestones, conglomerates, marls, and sandstones. Meanwhile, the plain area overlaps the quaternary sedimentation zones, which include sands, gravels, loess, and clay. Thus, the hard rocks in the mountainous and hilly areas favor the runoff genesis, while the presence of clays in the plains and along the main valleys, creates the premises of flooding phenomena. The low slopes in the plains is another factor which contributes to the increase of the flood potential. On average, the mean annual precipitation is approximately 750 mm, with a maximum of over 1100 mm in the mountainous area and a minimum of less than 500 mm in the lower plains. In terms of land-use, the largest surfaces are covered by forest (40.7%), arable land (30.9%), pastures (16.3%), and built-up areas (4.6%).

The most severe floods within the Buzău river catchment occurred in the years 1970, 2005, 2010, 2016 and 2019 and have affected many localities but also essential infrastructure elements such as the National Road 2 (E85) and the National Road 10.

2.2. Flood inventory

In order to run the flood susceptibility models, we created a database that includes the locations of floods that occurred between 1990 and 2019. In this regard, a correct prediction of surfaces exposed to flood phenomena implies the consideration of the characteristics of the areas affected in the past by flood events. The location of the flood events was determined based on data provided by the General Inspectorate for Emergency Situations (GIES) of Romania, and also, on the data collected from the National Administration of Romanian Waters (NARW). It should be mentioned that were taken into account all the flood events that affected at least one element of infrastructure (buildings, road network etc.). Finally, a total of 205 flood events were located within the study area. It is worth mentioning that the remote sensing techniques were used to validate the 205 flood locations provided by GIES and NARW. Thus, in order to verify the correctness of the data provided by the two institutions, the Normalized Difference Water Index (NDWI) and the Maximum Likelihood method was used for supervised classification of satellite imagery were used. Thus, through the classification of satellite imagery and NDWI, the location affected by floods in the past were identified and were compared with the data provided by the authorities. In order to compute the NDWI, for the period before 2014, Landsat 5, 7, and 8 imagery were used, while for the period after 2014, in addition, were used the Sentinel 1, 2, and 3 imagery.

2.3. Flood conditioning factors

The selection of the flood conditioning factors is an essential step in generating an accurate flood susceptibility map. After a detailed analysis of the literature (Choubin et al., 2019; Costache et al., 2020; Hong et al., 2018; Tehrany et al., 2014; Q. Wang et al., 2015; Z. Wang et al., 2015; Zaharia et al., 2015), the following 12 geographical variables that influence the water accumulation process were initially selected: Elevation, Slope, Slope-aspect, Plan curvature, TPI (Topographic Position Index), TWI (Topographic Wetness Index), Convergence Index (CI), Hydrologic Soil Groups, Land use, Distance from rivers, Rainfall and the Lithology.

A Digital Elevation Model (DEM), for the Buzău river catchment, was obtained from Shuttle Radar Topography Mission (SRTM) 30 m database. The following flood predictors were derived from the DEM at 30 m raster cell size: elevation, slope, convergence index, slope aspect, plan curvature, TPI, and TWI. The hydrological soil groups, lithology, and land use were extracted from vector databases. The distance from rivers was calculated through the Euclidean Distance method using the river network included in the Romanian Water Cadastre, while the rainfall factor was determined based on the data provided by the Meteorological National Administration of Romania. Below are briefly presented the flood conditioning factors.

The slope (Fig. 2a) is the geographical factor characterized by the highest influence on both the runoff and the water accumulation process (Bui et al., 2020; Costache et al., 2014, 2015; Dou et al., 2019; Zaharia et al., 2017; Costache, 2014; Prăvălie and Costache, 2013). This factor was classified into five classes. The class between 0 and 3° occupies 35% of the surface and includes 65% of the flood pixels (Fig. 4a). Approximately 52% of the basin surface is characterized by slopes ranging from 7 to 25°, which are mainly present in the middle and upper part of the study area. The plan curvature (Fig. 2b) is another morphometric factor with a direct influence on flood generation. This factor highlights the areas with divergent and convergent runoff. In the present case, this factor was classified into three classes. The class between −0.09 and 0.1 occupies 71% of the study area and concentrates 83% of the flood pixels (Fig. 4b). An essential flood conditioning factor that has an impact on the water infiltration process is the Hydrological

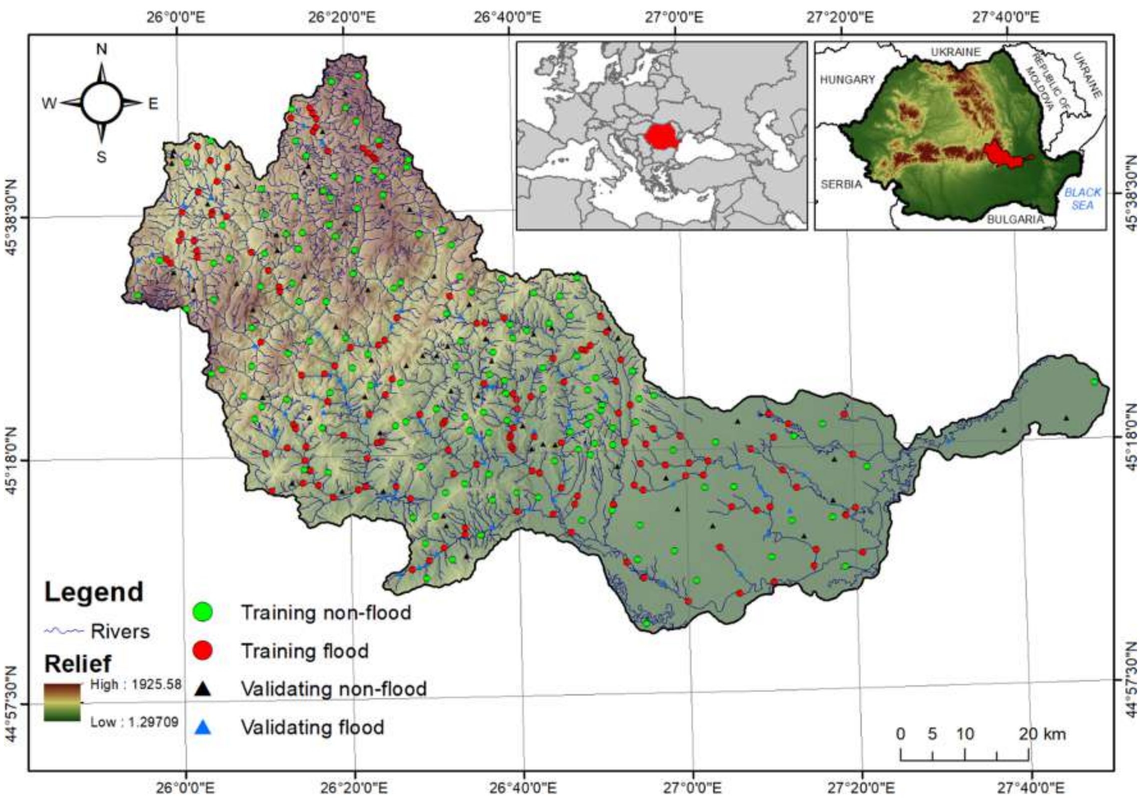

Fig. 1. Study area - Location map.

Soil Group (Fig. 2c). The soil texture plays a vital role in the runoff process. Based on their texture, the hydrological soil groups have been classified into four groups A, B, C, and D. The soil class B is the most predominant soil group that occupies 54% of the study area and 58% of the total flood pixels (Fig. 4c). When saturated, the hydrologic group B has a hydraulic conductivity between 10 and 40 µm/s, which determines a low runoff potential. Taking into account its characteristics, hydrologic soil group A has the lowest runoff potential due to the high rate of infiltration and hydraulic conductivity over 40 µm/s. Group A soils cover 6% of the study area. Group C soils have a hydraulic conductivity between 1 and 10 µm/s and relatively high runoff potential. This group of soils covers 18% of the catchment area. The hydrologic soil group D covers 22% of the area and has the highest runoff potential and the lowest infiltration rate. TPI (Fig. 2d) is a factor showing the differences in altitude between the focused and the neighboring cells (Jenness et al., 2004). This morphometric factor was classified into five classes using the Natural Breaks method as described in Costanzo et al. (2012). The class between (-11.4) – (-10.1) occupies 54% of the area of the Buzău river catchment and 37% of flood pixels, while the class between (-34.1) – (-11.5) has 41% of the total number of flood pixels (Fig. 4d). TWI (Fig. 2e) highlights the tendency of water to accumulate at a certain point in a river catchment. This factor was classified into five classes. The class between 3.06 and 4.8 is the most widespread, occupying 41% of the total area of the catchment, while the class (-0.37) – 3.05 occupies 36% (Fig. 4f). In the class between 4.81 and 7.02, most flood pixels are located (35%). Convergence Index (Fig. 2f) is another conditioning factor used in flood susceptibility analyses. In the present case, this index was classified into five classes according to the previous studies (Zaharia et al., 2017). Over 50% of flood pixels are located in the class (1 0 0) – (-3). The class between 0.1 and 100 accounts 50% of the catchment's surface (Fig. 4f).

The Slope aspect (Fig. 3a) was considered as a flood conditioning factor due to its influence on the regime of soil humidity. Most of the flood pixels (18%) are inside the areas with an eastern orientation, while on the southern slopes are placed about 45% of the flood pixels overlap (Fig. 5a). The Lithology (Fig. 3b) was derived from the Geological Map of Romania (Linzer et al., 1998) and was classified into 12 geological categories (rock groups). Approximately 25% of the catchment is covered by flysch, while almost 49% of the flood events occurred within the areas with sandstones and clays (Fig. 5b). Land use (Fig. 3c) is another predictor that was derived through remote sensing techniques. More specifically, in the present study, the land use was extracted from the CORINE Land Cover 2018 database (Popovici et al., 2013), which was obtained based on supervised classification of satellite imagery. In order to obtain the CORINE Land Cover dataset Sentinel-2 and Landsat 8 satellite imagery was used. For the study area, land use was classified into nine categories. The forests' land use category covers 44% of the catchment area, being followed by the agricultural areas with 31%. Approximately 31% of the flood pixels overlap the agricultural areas (Fig. 5c). Distance from rivers (Fig. 3d) was classified into eight classes. > 56% of the flood pixels are located within a distance shorter than 50 m from the rivers and 18% within a distance between 50 and 100 m (Fig. 5d). The elevation (Fig. 3e), one of the most important factors, was classified in 8 elevation classes. The most spread elevation class in the study area is characterized by altitudes between 2 and 200 m and accounts for 33% of the total surface. About 65% of the flood pixels are located between 2 and 400 m (Fig. 5e). Rainfall is a flood influencing factor with a direct impact on flood genesis (Cao et al., 2016; Costache et al., 2020). For this research, the rainfall map was constructed using the data provided by the National Meteorological Administration. This factor was classified into eight classes. The class ranging from 600 to 700 mm/year, concentrates 30% of the flood pixels (Fig. 5f).

3. Materials and methods

3.1. Linear Support Vector Machine for feature selection

A key step in the given analysis is the assessment of the prediction ability that each flood conditioning factor held in terms of flood

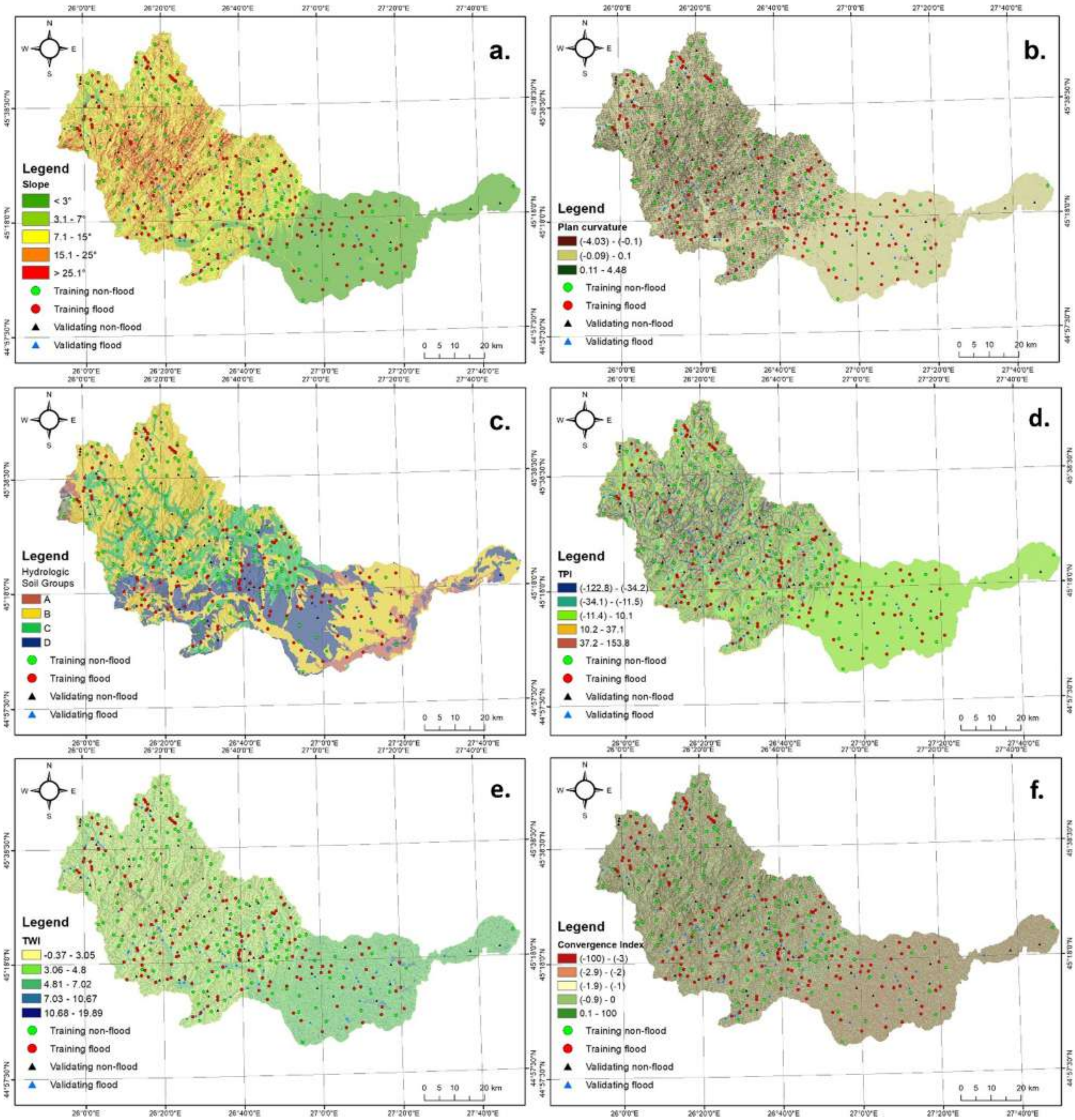

Fig. 2. (a) Slope map; (b) Plan curvature map; (c) Hydrologic soil groups; (d) TPI; (e) TWI and (f) convergence Index map.

susceptibility assessment. This step is beneficial in order to reduce the redundant information and the possible uncertainties associated with the analysis and its results. Linear Support Vector Machine is a potent method used to estimate the prediction capability, as through its results, the irrelevant and unnecessary input variables can be eliminated (Lin, 2002). This method, used for the first time by Guyon and Elisseeff (2003), is involved in assessing the prediction capability of each flood conditioning factor and will be estimated using the following equation (Pham et al., 2017a):

$$f(x) = \mathrm{sign}(w^T * a + b) \tag{1}$$

where f(x) is the mathematical function on which the linear support vector machine is based, w^T is the inverse matrix of weight matrix assigned for each flood factor, a = (a1, a2,…, a12) is the input vector which contains 12 flood conditioning factors, and b is the offset of the origin of the hyper-plane. For the present study, the *Linear Support Vector Machine* model was applied through Weka 9.3 software.

Unquestionably, if a flood conditioning factor holds a weight (w) close to 0, this factor will have a lower prediction rate than a factor with a higher weight (w) value (Chen et al., 2017; Pham et al., 2017b). Also, when the prediction capability of a flood conditioning factor is near to 0, that factor will be considered to remove from further analysis (Hong et al., 2017; Mladenić et al., 2004).

3.2. Fuzzy Analytical Hierarchy process

Fuzzy Analytical Hierarchy Process (FAHP) represents a combination between the fuzzy set theory and the AHP algorithm and is intended to increase the quality of the analysis by reducing the subjectivity in the criteria of weights estimation (Feizizadeh et al., 2014).

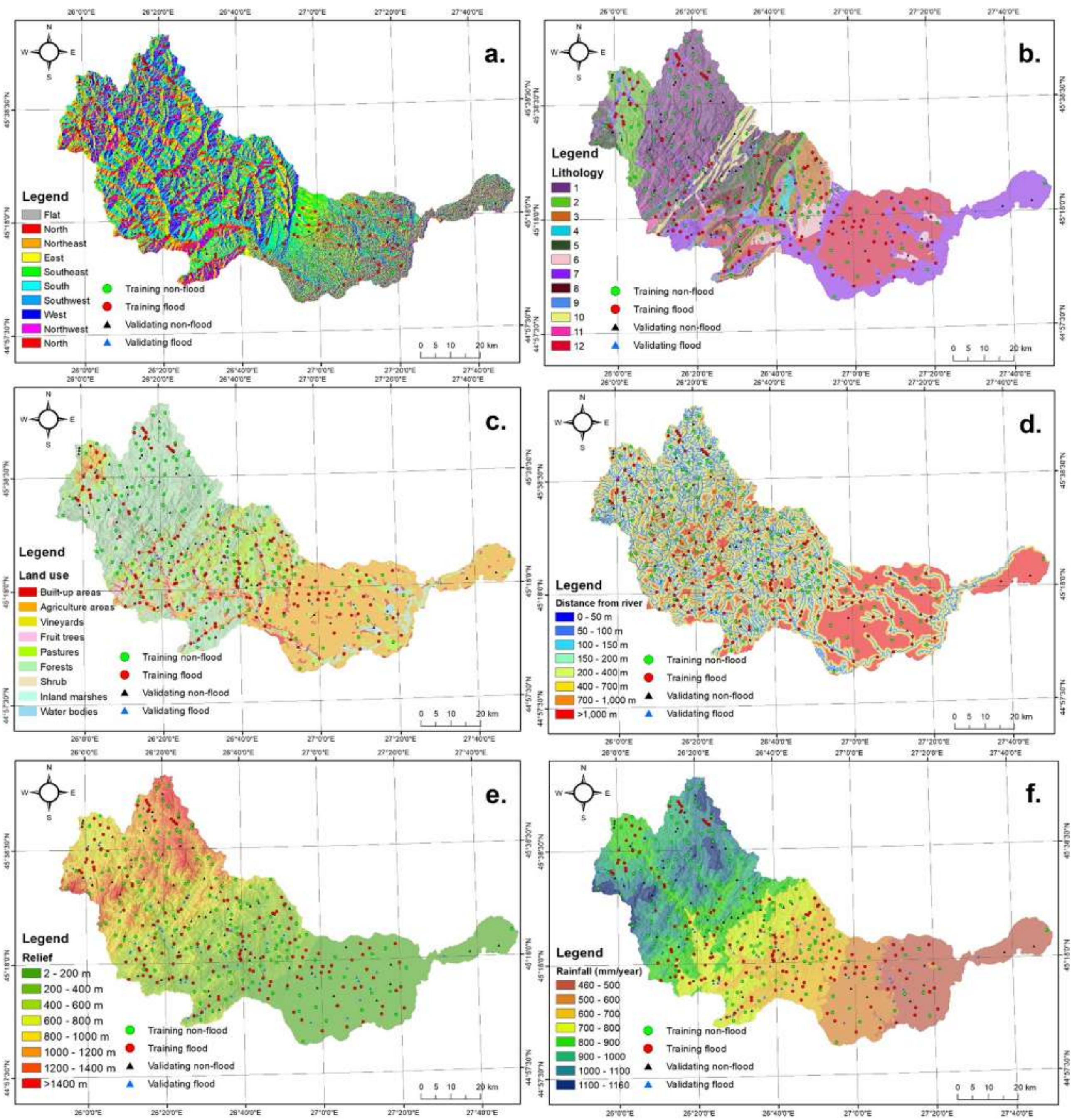

Fig. 3. (a) Slope Aspect map; (b) Lithology map; (c) land use; (d) Distance from river; (e) elevation and (f) rainfall map.

Therefore, we consider that the application of the FAHP model will provide more accurate results than those obtained by the application of the AHP stand-alone model. In the present study, the FAHP model will be used to determine the weights of each flood conditioning factor within the equation of flood potential. The FAHP-IoE models will be run by integrating the IoE coefficients, computed for each factor class/category, into the final equation together with the weights calculated through FAHP.

In the following section, the main aspects of the fuzzy set theory and the AHP algorithm will be presented, as well as how these two models are combined.

3.2.1. Fuzzy set theory

The Fuzzy set theory, introduced by Zadeh (Zadeh, 1965), is mainly used in complex systems that allow the use of imprecise, vague and ambiguous input information (Balezentiene et al., 2013). In the Fuzzy set theory, the degree of membership is reflected by a candidate object that takes on membership values between 0 and 1.

According to (Feizizadeh et al., 2014) a Fuzzy set is described as follows: if Z denotes a space of objects, then the Fuzzy set (A) in (Z) is a set of ordered pairs: $A(x, MF(x))$, $x \in Z$, where the membership function $MF(x)$ is the set A's degree of membership to Z.

A triangular fuzzy number (TFN) M' is denoted by the following three parameters: m_1, m_2, and m_3 (Fig. 6b). The first parameter, m_1, highlights the smallest possible value, m_2 denotes the most promising value, while m_3 indicates the presence of the largest possible value that describes a fuzzy object (Kahraman et al., 2003). Based on the linear representation of TFN on its left and right side, its membership function (9) is defined as follows:

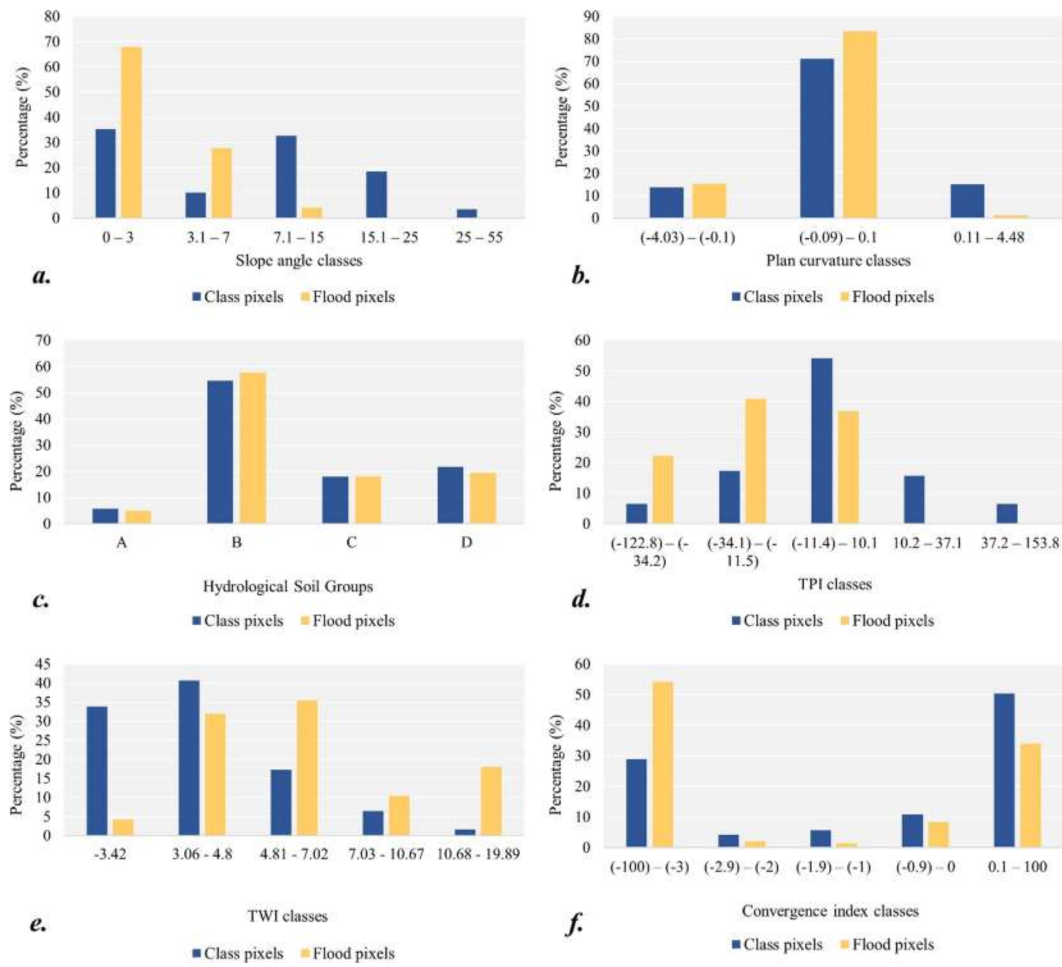

Fig. 4. Relative distribution of flood pixels within the classes of flood conditioning factors (a. Slope; b. Plan curvature; c. Hydrologic soil groups; d. TPI; e. TWI; f. convergence Index).

$$(x|M^{'}) = \begin{cases} 0, & x < m_1 \\ \frac{x - m_1}{m_2 - m_1}, & m_1 \leq x \leq m_2 \\ \frac{m_3 - x}{m_3 - m_2}, & m_2 \leq x \leq m_3 \\ 0, & x > m_3 \end{cases} \tag{2}$$

where $(\boldsymbol{x}|\boldsymbol{M}^{'})$ is the triangular type membership function.

A specific fuzzy number is given by its corresponding left and right representation of each degree of membership (Kahraman et al., 2003):

$$M' = M^{l(x)}, M^{r(x)} = (m_1 + (m_2 - -m_1)x,\ m_3 + (m_2 - -m_3)x).\ x\varepsilon\,[0, 1]$$

where $l(x)$ and $r(x)$ denotes the left-side representation and the right-side representation of a fuzzy number respectively.

3.2.2. Combining AHP algorithm with fuzzy set theory

The Analytical Hierarchy Process (AHP) is a semi-quantitative algorithm frequently used in the assessment of the potential to natural hazards (Gigović et al., 2017). The main aim of the AHP model is to compute the weights of relevant criterion map layers through a pairwise comparison matrix constructed based on expert knowledge. Considering that the conventional AHP algorithm cannot reflect the human thinking style, the FAHP, which is a fuzzy extension of AHP, was applied in order to solve the hierarchical fuzzy problems (Kahraman et al., 2003). The weights of criteria within the FAHP model can be determined through the following two steps:

- All flood conditioning factors were used to construct the pairwise comparison matrices. In order to establish which of the two elements/criteria is more important, linguistic terms were assigned to the pairwise comparison as follows eq.3 (Sun, 2010):

$$A^{'} = \begin{bmatrix} 1' & a'_{12} & \cdots & a'_{1n} \\ a'_{21} & 1' & \cdots & a'_{1n} \\ \vdots & \vdots & \ddots & \vdots \\ a'_{n1} & a'_{n2} & \cdots & 1' \end{bmatrix} = \begin{bmatrix} 1' & a'_{12} & \cdots & a'_{1n} \\ 1/a'_{12} & 1' & \cdots & a'_{2n} \\ \vdots & \vdots & \ddots & \vdots \\ 1/a'_{1n} & 1/a'_{2n} & \cdots & 1' \end{bmatrix} \tag{3}$$

where a'_{ij} measure indicates a pair of criteria i and j, let $1'$ be (1,1,1), when i is equal to j (i.e. $i = j$); if $1', 2', 3', 4', 5', 6', 7', 8', 9'$ measure that variable i has a higher relative importance in comparison with the variable j and whereas $1/1', 1/2', 1/3', 1/4', 1/5', 1/6', 1/7', 1/8', 1/9'$ measure that variable j is relatively more critical (Chen et al., 2013).

The pairwise comparison between the fuzzy parameters was based on the triangular number of linguistic variables that are defined in Fig. 6b.

- The fuzzy geometric mean and the fuzzy weight of each criterion can be calculated through the Buckley method (Buckley, 1985) as follows:
  $r_i' = (a'_{i1} \otimes\ \ a'_{i2} \otimes\ \ ...\otimes a'_{in})^{\frac{1}{n}}$, and then
  $w_i' = r_i' \otimes\ \ (r_1' \otimes\ \ ...\otimes r_n')^{-1}$

where $a_{in}^{'}$ is the fuzzy comparison value between the pair criterion i and criterion n, $r_1^{'}$ is the geometric mean of the fuzzy comparison values for criterion i compared to each of the other criteria, and $w_i^{'}$ is the fuzzy weighting of the i-th criterion, that can also be represented by a TFN, $w_i^{'} =\ (lw_i,\ mw_i,\ uw_i)$, where lw_i, mw_i and uw_i are the lower, middle and

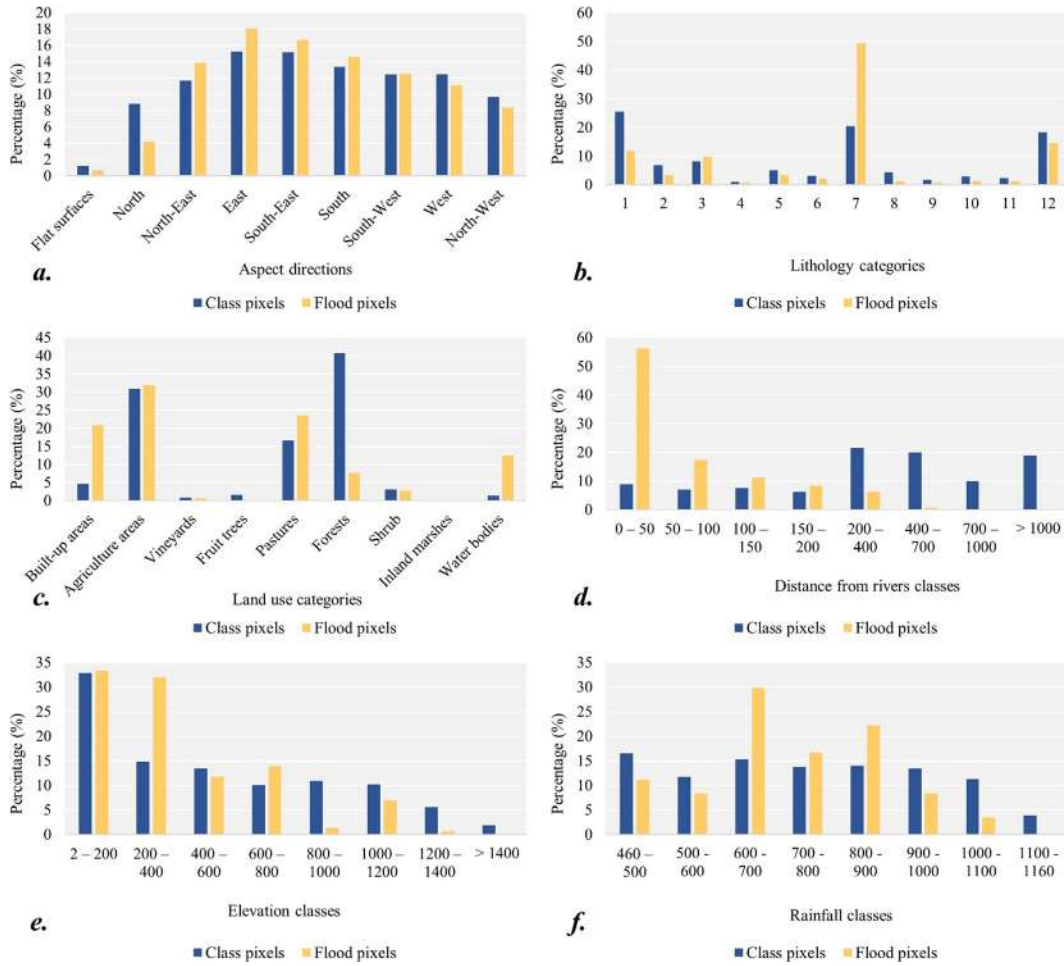

Fig. 5. Relative distribution of flood pixels within the classes of flood conditioning factors (a. Slope Aspect; b. Lithology; c. land use; d. Distance from river; e.Elevation; f. Rainfall).

upper values, respectively, of the fuzzy weighting of the ith criterion (Feizizadeh et al., 2014; Sun, 2010).

3.2.3. FAHP extent method

In order to determine the final values of the corresponding flood predictor weights, the extent analysis algorithm was computed. The first step of this algorithm is the construction of a fuzzy triangular comparison matrix form (4) (Wang and Chen, 2008):

$$A^{'} = (a_{ij}^{'})_{nxn} = \begin{bmatrix} (1,\,1,\,1) & (l_{12}, m_{12},\, u_{12}) & \cdots & (l_{1n}, m_{1n},\, u_{1n}) \\ (l_{21}, m_{21},\, u_{21}) & (1,\,1,\,1) & \cdots & (l_{2n}, m_{2n},\, u_{2n}) \\ \vdots & \vdots & \ddots & \vdots \\ (l_{n1}, m_{n1},\, u_{n1}) & (l_{n2}, m_{n2},\, u_{n2}) & \cdots & (1,\,1,\,1) \end{bmatrix} \quad (4)$$

where $a_{ij}^{'} = (l_{ij}, m_{ij},\, u_{ij})anda_{ij}^{'-1} = (1/l_{ij}, 1/m_{ij},\, 1/u_{ij})$ for $i, j = 1, \ldots, n$ and $i \neq j$.

The extent analysis method and the priority vector of the triangular matrix will be calculated. Thus, in a first stage, the fuzzy arithmetic function will be employed, to sum up each row of matrix $A^{'}$:

$$RS_i = \sum_{j=1}^{n} a_{ij}^{'} = \left(\sum_{j=1}^{n} l_{ij},\, \sum_{j=1}^{n} m_{ij},\, \sum_{j=1}^{n} u_{ij}\right),\ i = 1,\ \cdots, n \quad (5)$$

Fig. 6 a. The degree of possibility of $S_i^{'} \geq S_j^{'}$; b. The triangular fuzzy number corresponding to linguistic variables according to the level of preference.

Through the normalization of the above relation, the value of the fuzzy synthetic extent in terms of the ith object can be obtained as follows (Roodposhti et al., 2014):

$$S_i' = \sum_{j}^{n} a_{ij}' \otimes \left[\sum_{k=1}^{n} \sum_{j=1}^{n} a_{kj}'\right]^{-1} = \left(\frac{\sum_{j=1}^{n} l_{ij}}{\sum_{k=1}^{n}\sum_{j=1}^{n} u_{kj}},\, \frac{\sum_{j=1}^{n} m_{ij}}{\sum_{k=1}^{n}\sum_{j=1}^{n} m_{kj}},\, \frac{\sum_{j=1}^{n} u_{ij}}{\sum_{k=1}^{n}\sum_{j=1}^{n} l_{kj}}\right),\ i = 1,\ \ldots, n. \quad (6)$$

The computation of the degree of possibility of $S_i^{'} \geq S_j^{'}$ (Fig. 6a) represents the third step of the FAHP extent method. Thus, by comparing the fuzzy numbers, the degree of possibility can be obtained for each pairwise comparison according to the following relation (Eq.7) (Ahmed and Kilic, 2016):

$$V(S_i^{'} \geq S_j^{'}) = \mu_{S_i^{'}}(d) = \begin{cases} 1,\ if m_i \geq m_j, \\ \frac{u_i - l_j}{(u_i - m_i) + (m_j - l_j)},\ l_j \leq u_i,\ i, j = 1, \cdots, n;\ j \neq i \\ 0,\ others \end{cases} \quad (7)$$

where $S_i^{'} = (l_i,\, m_i,\, u_i)$, $S_j^{'} = (l_j,\, m_j,\, u_j)$ and d is the crossover point's abscissa of $S_i^{'}$and$S_j^{'}$ according to Fig. 6a.

Considering that:

$$w^{'}(a_i) = \min\{V(S_i^{'} \geq S_k^{'})\},\quad k = 1,\, 2,\, \cdots, n;\ k \neq i \quad (8)$$

Then, the value of weight vector will be calculated as:

$$w^{'}(a_i) = [w^{'}(a_1),\, w^{'}(a_2), \cdots, w^{'}(a_n)]^T \quad (9)$$

where a_i $(i = 1,\, 2,\, \ldots,\, n)$ are n elements. After the normalization process, the weight vectors can be obtained using the following relation (Eq.10):

$$w(a_i) = [w(a_1),\, w(a_2), \cdots, w(a_n)]^T \quad (10)$$

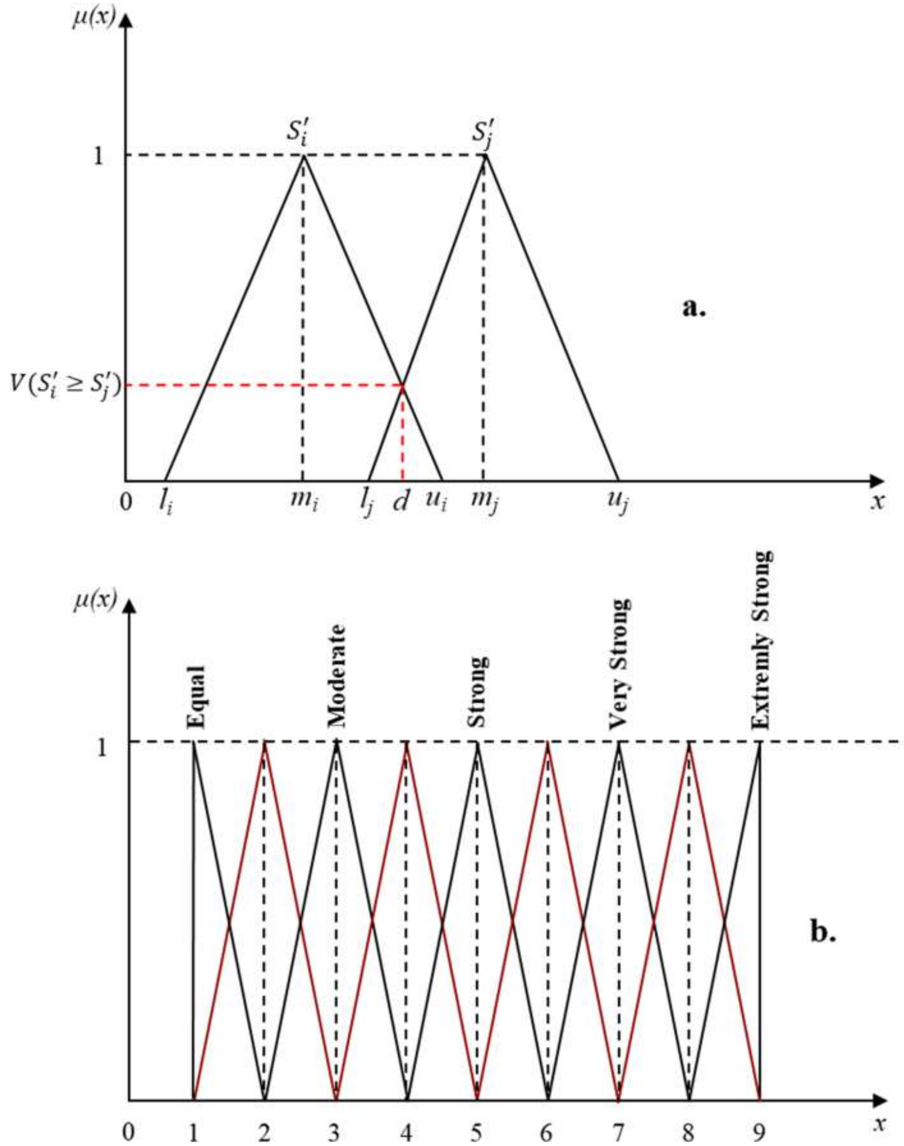

Fig. 6. The degree of possibility of $S_i^{'} \geq S_j^{'}$; b. Triangular fuzzy number corresponding to linguistic variables according to the level of preference.

where w is a non-fuzzy number.

3.3. Index of Entropy

The Index of Entropy (IoE) is a bivariate statistical method, widely used in studies focusing on the assessment of natural hazards potential (Khosravi et al., 2016). The selection of IoE to model the flood susceptibility within the study area is recommended by the highly accurate results provided by these methods in the previous studies related to the computation of susceptibility to natural hazards (Siahkamari et al., 2018; Tien Bui et al., 2018; Costache and Tien Bui, 2020). The entropy measures the disorders, instability, and uncertainty of a given system. By using the Index of Entropy in the present study, we consider that the entropy of a flood event represents the extent to which various factors determine the flood occurrence. Thus, in the Index of Entropy the weight that each flood conditioning holds in flood potential index computation will be used. The final weight for each variable (W_j) can be determined as follows (Chen et al., 2015):

$$P_{ij} = \frac{FR_{ij}}{\sum_{i=1}^{S_j} FR_{ij}} \tag{11}$$

where FR_{ij} is the frequency ratio coefficient for each class/category i of parameter j, S_j is the number of classes and P_{ij} is the probability density. Thus, the probability P_{ij} is calculated for each class/category of factor as the ratio between the FR value of that class/category and the sum of frequency ratio values within a factor (Wang et al., 2015). The FR_{ij} is calculated as the ratio between the percentage of flood locations, located in class/category, from the total number of flood locations and the percentage of a specific class/category within the entire study area.

$$H_j = -\sum_{i=1}^{S_j} (P_{ij})log_2(P_{ij}), \quad j = 1, 2, \cdots, n \tag{12}$$

$$H_{jmax} = log_2(S_j) \tag{13}$$

$$I_j = \frac{H_{jmax} - H_j}{H_{jmax}}, I = (0, 1), \quad j = 1, \cdots, n \tag{14}$$

$$P_j = \frac{1}{S_j}\sum_{i=1}^{S_j} FR_{ij} \tag{15}$$

$$W_j = I_j * P_j \tag{16}$$

where H_j and H_{jmax} represent the entropy values, I_j is the information coefficient, P_j is the empirical probability and W_j is the resultant

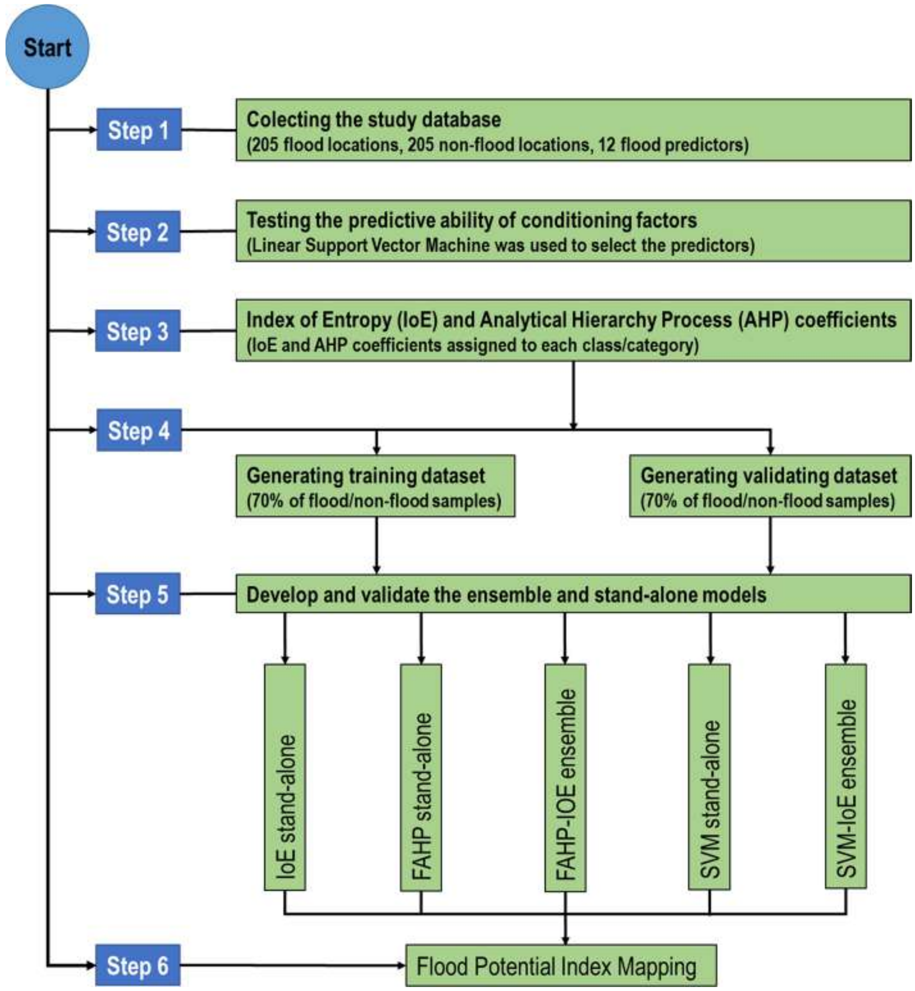

Fig. 7. Scheme of the workflow developed within the present research.

Table 1
Descriptive statistics of training/validating sample in terms of numerical variable.

		Convergence Index	TPI	TWI	Plan Curvature	Altitude	Slope	Rainfall	Distance from river
Training sample	Mean	−5.28	−7.00	5.07	0.00	526.34	9.68	564.53	314.99
	S.E.	1.21	1.52	0.21	0.01	22.80	0.58	2.67	32.63
	Median	−0.10	−4.64	4.10	0.00	431.23	4.07	562.19	127.28
	S.D.	20.55	25.75	3.54	0.18	386.86	9.84	45.28	553.73
	S.V.	422.45	663.12	12.52	0.03	149659.6	96.85	2050.01	306,615
	Kurtosis	3.51	0.82	3.18	16.12	−0.77	−0.60	−0.85	21.21
	Skewness	−0.38	0.12	1.85	1.44	0.59	0.81	0.10	4.04
	Range	167.21	160.86	19.04	2.19	1469.30	38.91	198.53	4747.49
	Minimum	−67.21	−87.23	0.80	−0.76	4.59	0.00	473.60	0.00
	Maximum	100.00	73.62	19.85	1.43	1473.89	38.91	672.13	4747.49
	Count	288	288	288	288	288	288	288	288
Validatingsample	Mean	−4.62	−6.99	5.06	−0.01	496.25	9.48	562.60	434.45
	S.E.	1.63	2.39	0.29	0.02	33.39	0.90	4.04	85.30
	Median	−0.37	−5.36	4.02	0.00	401.65	3.44	559.36	120.00
	S.D.	17.97	26.40	3.18	0.18	368.84	9.97	44.65	942.18
	S.V.	322.90	696.93	10.09	0.03	136043.2	99.5	1993.96	887694.2
	Kurtosis	3.37	0.70	0.97	11.97	−0.49	−0.66	−0.53	38.28
	Skewness	−1.01	0.14	1.26	−1.11	0.67	0.86	0.03	5.48
	Range	126.35	162.72	13.38	1.70	1433.48	34.22	202.77	8109.47
	Minimum	−75.84	−85.76	0.92	−1.10	7.98	0.10	474.41	0.00
	Maximum	50.51	76.96	14.30	0.60	1441.46	34.32	677.17	8109.47
	Count	122	122	122	122	122	122	122	122

*S.E. – Standard Error; S.D. – Standard Deviation; S.V. – Sample Variance

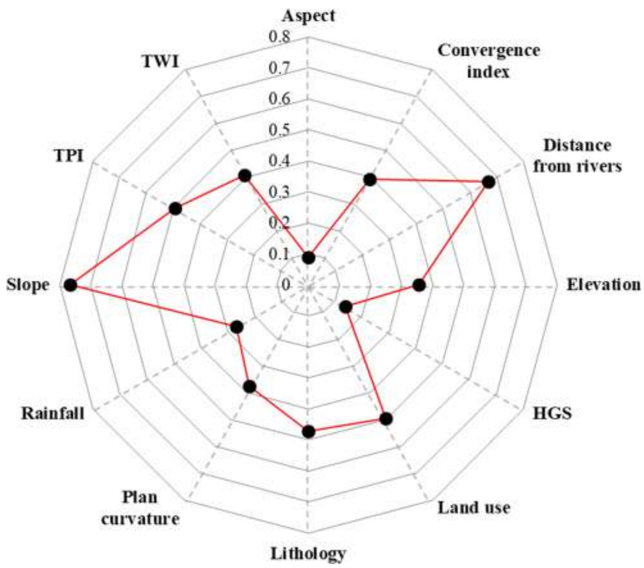

Fig. 8. Average Merit of the flood conditioning factors.

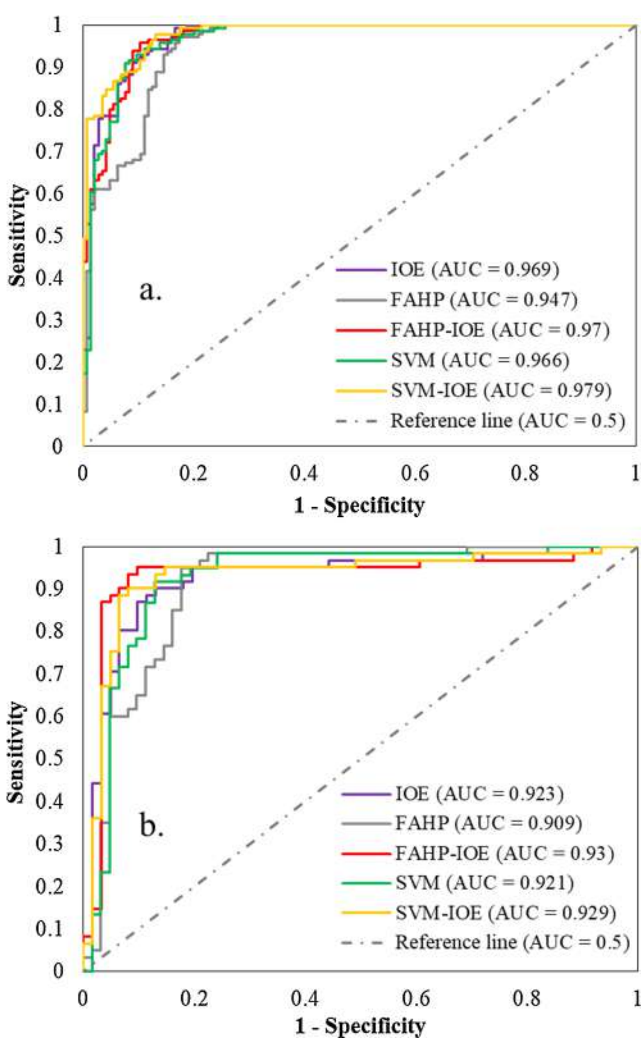

Fig. 9. ROC Curves and AUC: a. Success Rate; b. Prediction Rate.

weight value given to each flood factor.

The final values of the flood potential index were obtained through the IoE stand-alone model by implementing the Eq. (17) in GIS environments (Devkota et al., 2013):

$$FSI_{IOE} = \sum_{i=1}^{n} \frac{Z}{m_i} * C * W_j \tag{17}$$

where i is the total number of flood conditioning factors, Z is the number of classes of the factor that owns the most classes, m_i is the number of classes of each specific factor, C is the value of class after secondary classification and W_j is the final weight of each factor.

Table 2
Statistical measures assigned to FPI models.

Sample	Metrics	IoE	FAHP	FAHP-IoE	SVM	SVM-IoE
Training data	TP	135	132	136	134	138
	TN	133	131	135	133	136
	FP	9	12	8	10	6
	FN	11	13	9	11	8
	PPV (%)	93.8	91.7	94.4	93.1	95.8
	NPV (%)	92.4	91.0	93.8	92.4	94.4
	Sensitivity (%)	92.5	91.0	93.8	92.4	94.5
	Specificity (%)	93.7	91.6	94.4	93.0	95.8
	Accuracy (%)	93.1	91.3	94.1	92.7	95.1
	Kappa	0.861	0.826	0.882	0.854	0.903
Validating data	TP	54	51	56	53	57
	TN	56	53	55	52	56
	FP	7	10	5	8	4
	FN	5	8	6	9	5
	PPV (%)	88.5	83.6	91.8	86.9	93.4
	NPV (%)	91.8	86.9	90.2	85.2	91.8
	Sensitivity (%)	91.5	86.4	90.3	85.5	91.9
	Specificity (%)	88.9	84.1	91.7	86.7	93.3
	Accuracy (%)	90.2	85.2	91.0	86.1	92.6
	Kappa	0.803	0.705	0.820	0.721	0.852

3.4. Support Vector Machine

Being used in classification and regression problems, Support vector machine (SVM) represents a machine learning model based on statistical learning theory and the structural risk minimization principle (Suykens and Vandewalle, 1999). SVM is one of the most powerful machine learning methods whose efficiency in flood susceptibility mapping was demonstrated within the studies carried out during the last years (Choubin et al., 2019; Naghibi et al., 2017; Sachdeva et al., 2017). The training data used in the SVM model is divided using an optimal hyper-plane. It is to be noted that in a binary classification, the optimal hyper-plane is designed to widen the margin between classes (Pourghasemi et al., 2013). The new data will be classified as soon as the hyper-plane is obtained. In this phase, the original input space is being mapped into a high-dimensional feature space (Tien Bui et al., 2012).

In the present study, we will take into account the pair (x_i, y_i) with $x_i \in R^m$, $y_i \in \{1, 0\}$ and i = 1, …, m, where × is a vector of the input space containing the altitude, the distance from rivers, land-use, soil classes, NDVI, slope angle, sti, lithology, twi, rainfall, plan curvature and the slope aspect, whilst y = 1 represent the flood pixels presence and non-flood pixels presence when y = 0. The SVM algorithm will be used to highlight the line which divides the most precise way that the flood and non-flood pixels are located in a 2-D space.

If the training of the training data can be linearly separated, the hyper-plane could be defined as follows (Tien Bui et al., 2012):

$$y_i(w * x_i + b) \geq 1 - \xi_i \tag{18}$$

where $\boldsymbol{w}$ is a coefficient vector that determines the orientation of the hyper-plane in the feature space, $\boldsymbol{b}$ represents the offset of the hyper-plane from the origin and ξi is the positive slack variable (Tien Bui et al., 2012).

The optimal hyperplane can be obtained by using the Lagrange multipliers, as follows (Tien Bui et al., 2012):

Table 3
Frequency ratio and Index of Entropy coefficients value distribution within flood conditioning factors classes/category.

Factor	Class	Flood pixels	Class pixels	FR_{ij}	(P_{ij})	W_j
Plancurvature	(−4.03) – (−0.1)	22	813,760	1.12	0.47	0.61
	(−0.09) – 0.1	120	4,229,391	1.17	0.49	
	0.11 – 4.48	2	902,090	0.09	0.04	
Slope (°)	0 – 3	98	2,096,422	1.93	0.40	0.82
	3.1 – 7	40	606,526	2.72	0.57	
	7.1 – 15	6	1,946,782	0.13	0.03	
	15.1 – 25	0	1,093,638	0.00	0.00	
	25 – 55	0	201,873	0.00	0.00	
TPI	(−122.8) – (−34.2)	32	389,408	3.39	0.53	1.06
	(−34.1) – (−11.5)	59	1,025,382	2.38	0.37	
	(−11.4) – 10.1	53	3,214,449	0.68	0.11	
	10.2 – 37.1	0	935,266	0.00	0.00	
	37.2 – 153.8	0	380,736	0.00	0.00	
C.I.	(−1 0 0) – (−3)	78	1,721,674	1.87	0.46	0.60
	(−2.9) – (−2)	3	247,790	0.50	0.12	
	(−1.9) – (−1)	2	336,023	0.25	0.06	
	(−0.9) – 0	12	644,210	0.77	0.19	
	0.1 – 100	49	2,995,542	0.68	0.17	
Hydrological Soil Group	A	7	341,746	0.85	0.22	0.66
	B	83	3,242,969	1.06	0.28	
	C	26	1,071,383	1.00	0.26	
	D	28	1,289,141	0.90	0.24	
Aspect	Flat surfaces	1	72,784	0.57	0.08	0.64
	North	6	524,887	0.47	0.06	
	North-East	20	694,741	1.19	0.16	
	East	26	903,945	1.19	0.16	
	South-East	24	899,875	1.10	0.15	
	South	21	793,016	1.09	0.15	
	South-West	18	737,885	1.01	0.13	
	West	16	742,253	0.89	0.12	
	North-West	12	575,855	0.86	0.11	
Land use	Built-up areas	30	273,759	4.52	0.26	1.69
	Agriculture areas	46	1,840,323	1.03	0.06	
	Vineyards	1	53,415	0.77	0.04	
	Fruit trees	0	90,234	0.00	0.00	
	Pastures	34	983,962	1.43	0.08	
	Forests	11	2,421,852	0.19	0.01	
	Shrub	4	186,818	0.88	0.05	
	Inland marshes	0	11,138	0.00	0.00	
	Water bodies	18	83,580	8.89	0.50	
Distance from river (m)	0 – 50	81	526,369	6.35	0.53	1.22
	50 – 100	25	416,254	2.48	0.21	
	100 – 150	16	454,203	1.45	0.12	
	150 – 200	12	367,919	1.35	0.11	
	200 – 400	9	1,285,190	0.29	0.02	
	400 – 700	1	1,185,694	0.03	0.00	
	700 – 1000	0	593,507	0.00	0.00	
	> 1000	0	1,115,667	0.00	0.00	
Elevation (m)	2 – 200	48	1,951,514	1.02	0.16	0.60
	200 – 400	46	884,762	2.15	0.34	
	400 – 600	17	803,057	0.87	0.14	
	600 – 800	20	602,552	1.37	0.22	
	800 – 1000	2	647,751	0.13	0.02	
	1000 – 1200	10	611,209	0.68	0.11	
	1200 – 1400	1	332,459	0.12	0.02	
	> 1400	0	111,937	0.00	0.00	
Rainfall (mm/year)	460 – 500	16	985,015	0.67	0.09	0.67
	500–600	12	695,309	0.71	0.10	
	600–700	43	909,395	1.95	0.28	
	700–800	24	818,862	1.21	0.17	
	800–900	32	832,149	1.59	0.22	
	900–1000	12	801,234	0.62	0.09	
	1000–1100	5	668,968	0.31	0.04	
	1100–1160	0	233,051	0.00	0.00	
Lithology	1	17	1,517,652	0.46	0.05	0.55
	2	5	404,793	0.51	0.06	
	3	14	484,363	1.19	0.13	
	4	1	57,639	0.72	0.08	
	5	5	302,091	0.68	0.07	
	6	3	194,118	0.64	0.07	
	7	71	1,218,884	2.40	0.26	
	8	2	260,019	0.32	0.03	
	9	1	98,442	0.42	0.05	
	10	2	178,269	0.46	0.05	
	11	2	141,858	0.58	0.06	
	12	21	1,087,113	0.80	0.09	
TWI	−0.37–3.05	6	2,013,896	0.12	0.01	2.51
	3.06–4.8	46	2,421,166	0.78	0.05	
	4.81–7.02	51	1,023,282	2.06	0.13	
	7.03–10.67	15	386,558	1.60	0.10	
	10.68–19.89	26	100,339	10.7	0.70	

$$Minimize \sum_{i=1}^{n} \alpha_i - \frac{1}{2} \sum_{i,j=1}^{n} \alpha_i \alpha_j y_i y_j (x_i, x_j \tag{19}$$

$$\text{Subjectto} \sum_{i=1}^{n} \alpha_i y_i = 00 \le \alpha i \le C \tag{20}$$

where α_i represents the Lagrange multipliers and C is the penalty parameter that controls the trade-off between the complexity of the decision function and the number of misclassified training examples (Costache, 2019a).

The new data can be classified when the linear hyper-plane is being used. The classification can be obtained through the following relation:

$$f(x) = \text{sign}\left(\sum_{i=1}^{n} y_i \alpha_i x_i, +b\right) \tag{21}$$

In the case when a non-linear separable hyper-plane is being required, the original input will move into a high-dimensional feature space, therefore a non-linear kernel function will be used. The following relation will be used in order to classify the new data (Osuna and Girosi, 1998):

$$f(x) = \sum_{i=1}^{n} (\alpha_i - \alpha_i^*) K(x_i, x) + b \tag{22}$$

Therefore the α_i and α_i* represent the Lagrange multipliers ($\alpha_i \ge 0$, $\alpha_i^* \le C$) and $K(x_i, x_j)$ represents the kernel function.

The open-source machine learning Weka software will be used for the training process of the SVM-FR and SVM-WOE hybrid models. For the calculation of the SVM based hybrid models, we will use the Radial Basis Function, one of the most efficient functions (Kavzoglu et al., 2014; Wechsler, 2000). The following formulae represent the mathematical expression of the Radial Basis Function (Tehrany et al., 2015):

$$K(X_i, X_j) = exp(-\gamma ||X_i - X_j||), \gamma > 0 \tag{23}$$

in which γ is the gamma term in the kernel function for all kernel types except the linear ones.

4. The proposed methodology for predicting potential flood areas

A sophisticated workflow including the use of 3 stand-alone and 2 hybrid models was developed in order to estimate the flood potential across the study area. The workflow is graphically described in Fig. 7.

4.1. Establishment of the flood database for the Buzău river catchment

It can be noted that the database required for the present research was constructed with the help of the ArcCatalog application. Thus,

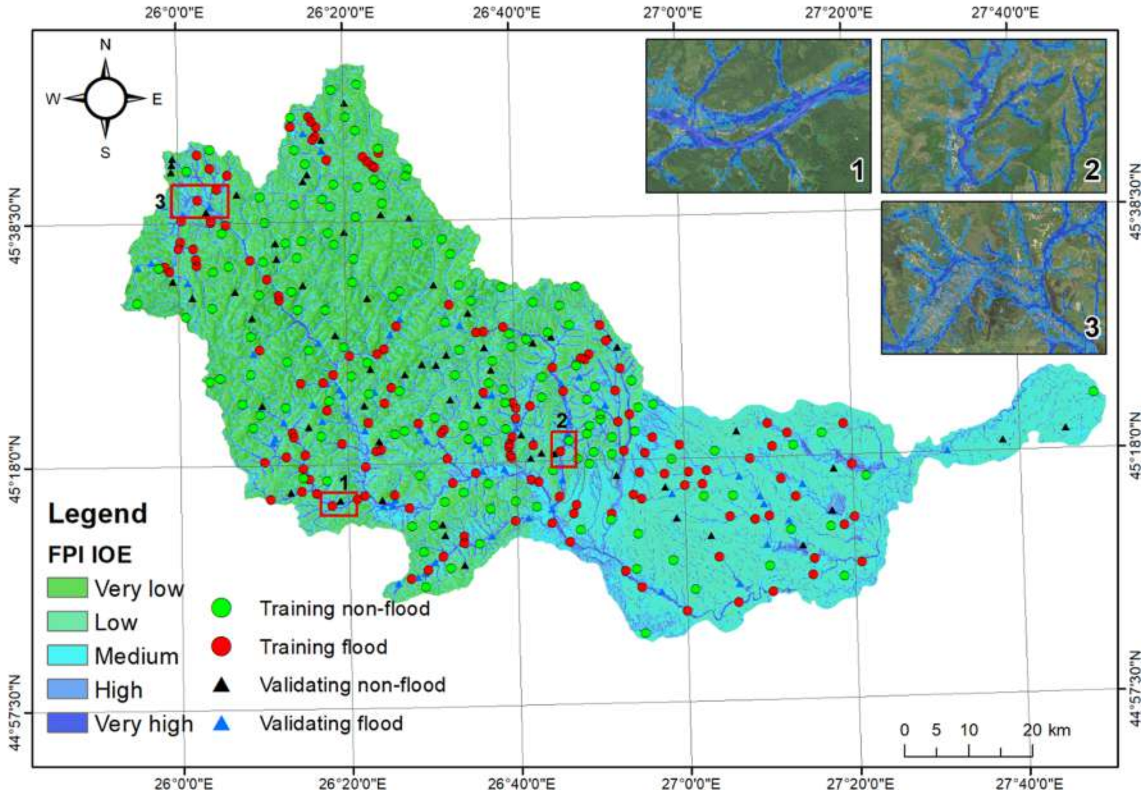

Fig. 10. FPI_{IOE} spatial distribution across the Buzău river basin.

along with the 12 flood conditioning factors, the database comprises 205 flood locations. In order to be more easily processed, the data regarding the flood influencing factors were converted in raster format with a cell size of 30 × 30 m. According to other studies (Tehrany et al., 2014), a new sample with the absence of flood phenomena (non-flood locations) has been generated. This sample also contains 205 points, which are placed in areas with high slopes or at high distances from the rivers where floods are less likely to occur.

4.2. Training data, validation data, and feature selection

Another essential step of the present analysis is the establishment of training and validating data. Thus, the data used to train the flood potential models consists of the 12 flood influencing factors in raster format along with a specific percentage of the flood and non-flood locations. Thus, according to Tehrany et al. (2015), a percentage equal to 70% of the flood and non-flood locations were used as the training sample, while the other 30% of flood and non-flood locations were used for results validation. The training and validating samples were divided through the *Subset Features* tool implemented in GIS software. Therefore, a total number of 288 locations (144 floods and 144 non-floods) were included in the training sample, while the other 122 locations (61 floods and 61 non-floods) was involved in the validation process. It should be mentioned also that the flood locations were encoded with 1 and non-flood locations were encoded with 0. In addition, for a number of 8 flood predictors, that are characterized by numerical values, several descriptive statistics were computed (Table 1). It should be mentioned that the descriptive statistics were computed by using the flood and non-flood points within the training and validating samples.

Further, as was stated at 3.1, the Linear Support Vector Machine algorithm was employed for feature selection. Thus, in this step, the entire flood and non-flood sample together with the flood conditioning factors were used in Weka software in order to determine the predictive ability for each geographical variable.

4.3. Configuration and training of flood models

In terms of the IoE stand-alone model, the assessment of flood potential requires the calculation of the probability density (P_{ij}) for each factor class/categories and the weights of flood conditioning factors. In this regard, the flood locations from the training sample were used. In the first stage, the (P_{ij}) and weights of flood conditioning factors were calculated using the eq. 11 and 16. Further, the flood potential index was calculated by using the eq. 17.

In order to derive the flood potential index through the FAHP stand-alone model, the Analytical Hierarchy Process was used in the first step in order to calculate the weights of each factor class/category. Thus, the AHP weights were computed with the help of 12 comparison matrices that were generated in Microsoft Excel 2013 software. The comparison matrix were constructed based on the human expert opinions. It should be mentioned that a survey was sent by email to a number of 23 experts from the Romanian Waters National Administration. The experts provided their opinion regarding the hierarchy of the importance of the factor classes/categories in terms of flood potential. The entire procedure of AHP algorithm is presented in many scientific works (Pourghasemi et al., 2013; Yalcin, 2008; Yoshimatsu and Abe, 2006). All the AHP weights were assigned to each factor class/category in GIS environment. The second step consisted in the construction of the Fuzzy Analytical Hierarchy Process evaluation matrix which was used in order to calculate the weights of each flood conditioning factor. The final step in the computation of flood potential index through the FAHP model was the multiplication of the flood conditioning factors raster, having the AHP weights assigned, with the weights derived from FAHP model. In terms of FAHP-IoE, the flood potential was derived by the multiplication of IoE coefficients with the FAHP weights.

The configuration of SVM stand-alone and SVM-IoE models was ensured through ArcGIS 10.5 and Weka 9.3 software. Thus, in the first step, the information regarding the normalized values of flood conditioning factors and the IoE coefficients was extracted in GIS environment for each flood and non-flood location from the training

Table 4
AHP Pair-wise comparison matrix.

Factor and classes/categories	*Pair-wise comparison matrix*												*Normalizedweights*
	[1]	[2]	[3]	[4]	[5]	[6]	[7]	[8]	[9]	[10]	[11]	[12]	
Classes in each factor													
Slope angle													
[1] less than 3°	1												0.439
[2] 3 – 7°	1/2	1											0.246
[3] 7 – 15°	1/4	1/2	1										0.181
[4] 15 – 25°	1/5	1/3	1/3	1									0.089
[5] > 25°	1/6	1/5	1/6	1/3	1								0.045
TPI													
[1] (−2 0) – (−3.8)	1												0.458
[2] (−3.7) – (−1.1)	1/2	1											0.258
[3] (−1) – 1.3	1/4	1/2	1										0.158
[4] 1.4 – 4.5	1/6	1/4	1/3	1									0.082
[5] 4.6 – 20	1/7	1/5	1/3	1/3	1								0.045
TWI													
[1] −9.7 – 4.5	1												0.408
[2] 4.6 – 8.4	1/2	1											0.299
[3] 8.5 – 12	1/3	1/2	1										0.159
[4] 13–15	1/4	1/5	1/2	1									0.084
[5] 16 – 25	1/6	1/6	1/4	1/2	1								0.049
Land use													
[1] Built-up areas	1												0.241
[2] Agriculture zone	1/3	1											0.116
[3] Vineyards	1/5	1/2	1										0.076
[4] Fruit trees	1/3	1/3	1/5	1									0.067
[5] Pastures	1/2	3	4	2	1								0.203
[6] Forest	1/8	1/5	1/4	1/5	1/5	1							0.023
[7] Natural grassland	1/3	1/3	2	2	1/3	5	1						0.070
[8] Moors and heatland	1/3	1/3	1/2	1/2	1/4	2	1	1					0.051
[9] Transitional woodland-shrub	1/2	3	4	1/3	1/3	4	2	2	1				0.152
Lithology													
[1] 1	1												0.031
[2] 2	1/2	1											0.076
[3] 3	1	1/3	1										0.094
[4] 4	1/4	2	3	1									0.128
[5] 5	1/8	1/4	1	1/4	1								0.042
[6] 6	1/7	1/4	1	1/3	2	1							0.074
[7] 7	1/6	1	2	1/2	3	1	1						0.064
[8] 8	1/2	6	8	6	9	8	6	1					0.194
[9] 9	1/3	3	5	4	8	6	4	1/3	1				0.095
[10] 10	1/6	2	3	2	4	4	3	1/5	1/2	1			0.084
[11] 11	1/7	1/3	1/2	1/3	1	1/2	1/3	1/9	1/7	1/4	1		0.062
[12] 12	1/9	1/	1/2	1/3	1	1/2	1/3	1/9	1/7	1/4	1	1	0.057
Rainfall													
[1] 460 – 500	1												0.023
[2] 500–600	2	1											0.027
[3] 600–700	3	3	1										0.048
[4] 700–800	4	4	2	1									0.063
[5] 800–900	5	5	3	2	1								0.091
[6] 900–1000	6	6	4	4	2	1							0.132
[7] 1000–1100	7	7	5	6	5	4	1						0.253
[8] 1100–1160	8	9	7	8	6	5	2	1					0.362
Plan curvature													
[1] −11.8 – 0	1												0.089
[2] 0.1 – 0.5	4	1											0.324
[3] 0.6 – 8.5	6	2	1										0.587
Slope aspect													
[1] Flat surfaces	1												0.032
[2] North	5	1											0.072
[3] North-East	4	3	1										0.104
[4] East	4	4	5	1									0.218
[5] South-East	4	3	3	4/5	1								0.164
[6] South	5	2	2	5/7	2/3	1							0.144
[7] South-West	2	4	2/3	3/8	3/4	4/5	1						0.113
[8] West	3	5/4	4/3	4/9	2/3	3/5	4/5	1					0.090
[9] North-East	3	1/2	1/3	1/2	1/2	1/3	4/9	2/3	1				0.063
Convergence index													
[1] (−1 0 0) – (−3)	1												0.489
[2] (−2.9) – (−2)	1/3	1											0.272
[3] (−1.9) – (−1)	1/4	1/3	1										0.122
[4] (−1) – 0	1/6	1/4	1/2	1									0.074
[5] 0 – 100	1/8	1/7	1/3	1/2	1								0.044
HGS													

(*continued on next page*)

Table 4 (*continued*)

Factor and classes/categories	*Pair-wise comparison matrix*												*Normalizedweights*
	[1]	[2]	[3]	[4]	[5]	[6]	[7]	[8]	[9]	[10]	[11]	[12]	
[1] A	1												0.072
[2] B	2	1											0.145
[3] C	3	2	1										0.201
[4] D	7	3	5	1									0.582
Distance from river (m)													
0 – 50	1												0.319
50 – 100	1/2	1											0.226
100 – 150	1/3	1/2	1										0.156
150 – 200	1/4	1/3	1/2	1									0.108
200 – 400	1/5	1/4	1/3	1/2	1								0.068
400 – 700	1/6	1/5	1/4	1/3	1/2	1							0.062
700 – 1000	1/7	1/6	1/5	1/4	1/3	1/4	1						0.038
> 1000	1/7	1/8	1/7	1/6	1/3	1/5	1/4	1					0.022
Elevation (m)													
2 – 200	1												0.310
200 – 400	1/2	1											0.208
400 – 600	1/3	1/2	1										0.171
600 – 800	1/4	1/3	1/3	1									0.107
800 – 1000	1/5	1/3	1/4	1/2	1								0.088
1000 – 1200	1/6	1/5	1/5	1/3	1/3	1							0.058
1200 – 1400	1/6	1/6	1/5	1/5	1/4	1/3	1						0.038
> 1400	1/8	1/7	1/6	1/7	1/8	1/7	1/5	1					0.019

sample. Further, these data in CSV tabular format were imported in Weka software where the weights of each flood predictor were calculated by Support Vector Machine algorithm. It should be remarked that for both SVM stand-alone and SVM-IoE models the Radial Basis Function was used. It is very important to mention that the performance of the SVM model will heavily depends on the correctness of estimation of the C and γ parameters. Cross-Validation was implied to establish the best values of these parameters (C and γ) for each of the two models. Therefore, in terms of SVM stand-alone, the C parameter obtained a value of 1.5 and the γ was equal to 0.16, while in terms of SVM-IoE, the C parameter achieved a value of 1.8 whereas the γ parameter received a value of 0.13.

4.4. Performance evaluation of the flood models

The ROC Curve model was involved in the results validation procedure within the majority of studies related to the assessment of potential to a natural hazard for a specific area (Khosravi et al., 2018; Razavi Termeh et al., 2018; Siahkamari et al., 2018). The ROC Curve graph is a technique for visualizing, organizing and selecting classifiers based on their performance (Fawcett, 2006). The ROC Curve is mainly used to judge the discrimination ability of the statistical models that combine different test results for predictive purposes (Hanley and Mcneil, 1982). The Area Under Curve (AUC) represent the main statistical indicator of ROC Curve. The AUC is used to measure the accuracy and the performance of the applied models (Bradley, 1997). In the present research, the ROC Curve will describe the capacity of the models to correctly predict the occurrence of the flood phenomena. The graphical representation will be possible by plotting the sensitivity on Y-axis against the specificity on X-axis. The closer the value of AUC gets to 1, the better the model is (Pallant, 2016). The following equation can be used to calculate the AUC values (Chen et al., 2018):

$$\mathrm{AUC} = \frac{(\sum TP + \sum TN)}{(\mathrm{P} + \mathrm{N})} \tag{23}$$

where TP (true positive) represent the correctly classified flood pixels, TN (true negative) represent the correctly classified non-flood pixels, P is the total number of flood pixels and N is the total number of non-flood pixels.

In the present study, both the Succes Rate and the Prediction Rate were constructed. The Success Rate is a type of ROC Curve plot which highlights the model fitting rate and indicates how the Flood Potential Index separates the flood locations within the susceptibility zones. The Prediction Rate is also a type of ROC Curve plot which reveal the model performance in terms of the prediction of the future flood events (Vakhshoori and Zare, 2018). For the Success Rate, the flood and non-flood points from the training dataset were used, while for the Prediction Rate the flood and non-flood points from validating dataset along were involved.

In addition to the ROC curve and AUC, the next statistical metrics were computed: specificity, sensitivity, accuracy, kappa index. The specificity represents a statistical indicator which measures the proportion of non-flood pixels that are correctly classified as non-flood pixles (Baratloo et al., 2015). The sensitivity represents a statistical index which measures the proportion of flood pixels that are classified as flood pixels (Baratloo et al., 2015). The accuracy represents the ability of test to differentiate the flood and non-flood pixels (Baratloo et al., 2015). Kappa index (k) is a statistical indicator that measures the agreement between two raters who each classify the total number of flood and non-flood pixels into two exclusive categories, flood and non-flood respectively. Through the below-written equation the aforementioned statistical measures could be determined:

$$\mathrm{k} = \frac{\mathrm{p_o} - \mathrm{p_e}}{1 - \mathrm{p_e}},\quad \mathrm{Sensitivity} = \frac{\mathrm{TP}}{\mathrm{TP} + \mathrm{FN}},\quad \mathrm{Specificity} = \frac{\mathrm{TN}}{\mathrm{FP} + \mathrm{TN}},$$
$$\mathrm{Accuracy} = \frac{\mathrm{TP} + \mathrm{TN}}{\mathrm{TP} + \mathrm{FP} + \mathrm{TN} + \mathrm{FN}} \tag{24}$$

where FP (false positive) are the number of flood pixels erroneously classified and FN (false negative) are the number of non-flood pixels erroneously classified; k is kappa coefficient, p_o is the observed flood pixels, and p_e is the estimated flood pixels.

According to Queiroz et al. (2016), if the values of the above indices exceed the threshold of 0.81 it is considered that there is almost a perfect agreement between the observed and the predicted values.

5. Results

5.1. Predictiveness of the flood conditioning factors

By using the Linear Support Vector Machine model, the hierarchy of flood predictors in terms of the Average Merit (AM) values were established. In the present case, the AM is used as a conventional term in

Table 5
FAHP evaluation matrix.

	1	2	3	4	5	6	7	8	9	10	11	12
Elevation (1)												
l_1	1	1	1	1	2	0.33	3	1	2	2	4	9
m_1	1	1	1	2	3	0.5	4	2	3	3	5	9
u_1	1	1	1	3	4	1	5	3	4	4	6	9
Distance from river (2)												
l_2	1	1	1	1	2	0.25	2	1	2	2	3	7
m_2	1	1	1	2	3	0.33	3	2	3	3	4	8
u_2	1	1	1	3	4	0.5	4	3	4	4	5	9
Land use (3)												
l_3	1	1	1	1	2	0.33	2	1	3	2	3	7
m_3	1	1	1	2	3	0.5	3	2	4	3	4	8
u_3	1	1	1	3	4	1	4	3	5	4	5	9
HGS (4)												
l_4	0.33	0.33	0.33	1	1	0.16	1	1	1	1	2	5
m_4	0.5	0.5	0.5	1	2	0.2	2	1	2	2	3	6
u_4	1	1	1	1	3	0.25	3	1	3	3	4	7
TPI (5)												
l_5	0.25	0.25	0.25	0.33	1	0.14	1	0.33	1	1	1	2
m_5	0.33	0.33	0.33	0.5	1	0.16	2	0.5	1	1	2	3
u_5	0.5	0.5	0.5	1	1	0.2	3	1	1	1	3	4
Slope angle (6)												
l_6	1	2	1	4	5	1	5	2	4	3	6	9
m_6	2	3	2	5	6	1	6	3	5	4	7	9
u_6	3	4	3	6	7	1	7	4	6	5	8	9
Convergence index (7)												
l_7	0.2	0.2	0.2	0.33	0.33	0.14	1	0.33	1	1	1	2
m_7	0.25	0.25	0.25	0.5	0.5	0.16	1	0.5	1	1	2	3
u_7	0.33	0.33	0.33	1	1	0.2	1	1	1	1	3	4
Lithology (8)												
l_8	0.33	0.33	0.33	1	1	0.25	1	1	1	2	3	5
m_8	0.5	0.5	0.5	1	2	0.33	2	1	2	3	4	6
u_8	1	1	1	1	3	0.5	3	1	3	4	5	7
TWI (9)												
l_9	0.25	0.25	0.2	0.33	1	0.16	1	0.33	1	1	1	3
m_9	0.33	0.33	0.25	0.2	1	0.2	1	0.5	1	1	2	4
u_9	0.5	0.5	0.33	1	1	0.25	1	1	1	1	3	5
Rainfall (10)												
l_{10}	0.25	0.25	0.25	0.33	1	0.2	1	0.25	1	1	2	4
m_{10}	0.33	0.33	0.33	0.5	1	0.25	1	0.33	1	1	3	5
u_{10}	0.5	0.5	0.5	1	1	0.33	1	0.5	1	1	4	6
Plan curvature (11)												
l_{11}	0.16	0.2	0.2	0.25	0.33	0.12	0.33	0.33	0.33	0.25	1	2
m_{11}	0.2	0.25	0.25	0.33	0.5	0.14	0.5	0.5	0.5	0.33	1	3
u_{11}	0.25	0.33	0.33	0.5	1	0.16	1	1	1	0.5	1	4
Aspect (12)												
l_{12}	0.11	0.11	0.11	0.14	0.25	0.11	0.25	0.14	0.2	0.16	0.25	1
m_{12}	0.11	0.12	0.12	0.16	0.33	0.11	0.33	0.16	0.25	0.2	0.33	1
u_{12}	0.11	0.14	0.14	0.2	0.5	0.11	0.5	0.2	0.33	0.25	0.5	1

order to express the weights of factors calculated by Linear Support Vector Machine (LSVM) using Weka software 9.3. Thus, the AM values are equal to the weights calculated through LSVM. This measure (AM), highlights the level of the predictive ability of each flash-flood predictor in terms of flood susceptibility. The slope angle obtained the highest AM (0.766) being followed by distance from rivers (0.668), land use (0.497), TPI (0.495), lithology (0.473), TWI (0.41), convergence index (0.393), plan curvature (0.377), altitudes (0.356), rainfall (0.266), hydrological soil group (0.138) and aspect (0.089) (Fig. 8).

According to the results presented above all the flood conditioning factors have AM values higher than 0. It should be noted that within the literature there is no general consensus regarding a specific threshold below which the variables should be removed from the analysis. Therefore, since all the variables have a certain influence on flood genesis, all the flood conditioning factors will be used in the analysis in order to determine the flood potential. Moreover, we consider that in order to have a complete overview on the flood susceptibility across a specific region it is very important to take into consideration all the variables that has an influence on flood genesis however small that influence is.

5.2. Performance of the flood models

The Success Rate and the Prediction Rate (Fig. 9a and b) were employed to test the reliability and the accuracy of the proposed models. 70% of the flood location (training data) was used to prepare the Success Rate, while the other 30% (validating data) was involved in the construction of the Prediction Rate. It can be noted that larger values of AUC indicate a higher performance of the algorithms. In terms of the Success Rate, the results highlight that SVM-IoE, with an AUC = 0.979, was the best model, while FAHP stand-alone methods achieved the lowest performance (AUC = 0.947) (Fig. 9a). Further, the results of Prediction Rate, indicate that FAHP-IoE has the highest predictive ability (AUC = 0.93), while the FAHP method was again the weakest algorithm (AUC = 0.909) (Fig. 9b).

In the second stage, the reliability of the results was verified by several statistical measures. The use of the training data to calculate the indices mentioned above highlights the fact that the SVM-IoE model is the most performant of all. This model achieved a value of 94.5%, in the case of Sensitivity, which is higher than 93.8% obtained by FAHP-IoE, also higher than 92.5% in the case of IoE stand-alone. The same

Table 6
The ordinate of the highest intersection point, the degree possibility for TFNs and the wrights of flood predictor.

Altitude = 1	Distance from rivers = 2	Land use = 3	HGS = 4
$V(S_1 \geq S_2) = 1$	$V(S_2 \geq S_1) = 0.9$	$V(S_3 \geq S_1) = 0.94$	$V(S_4 \geq S_1) = 0.52$
$V(S_1 \geq S_3) = 1$	$V(S_2 \geq S_3) = 0.96$	$V(S_3 \geq S_2) = 1$	$V(S_4 \geq S_2) = 0.64$
$V(S_1 \geq S_4) = 1$	$V(S_2 \geq S_4) = 1$	$V(S_3 \geq S_4) = 1$	$V(S_4 \geq S_3) = 0.6$
$V(S_1 \geq S_5) = 1$	$V(S_2 \geq S_5) = 1$	$V(S_3 \geq S_5) = 1$	$V(S_4 \geq S_5) = 1$
$V(S_1 \geq S_6) = 0.53$	$V(S_2 \geq S_6) = 0.43$	$V(S_3 \geq S_6) = 0.49$	$V(S_4 \geq S_6) = 0.09$
$V(S_1 \geq S_7) = 1$	$V(S_2 \geq S_7) = 1$	$V(S_3 \geq S_7) = 1$	$V(S_4 \geq S_7) = 1$
$V(S_1 \geq S_8) = 1$	$V(S_2 \geq S_8) = 1$	$V(S_3 \geq S_8) = 1$	$V(S_4 \geq S_8) = 0.91$
$V(S_1 \geq S_9) = 1$	$V(S_2 \geq S_9) = 1$	$V(S_3 \geq S_9) = 1$	$V(S_4 \geq S_9) = 1$
$V(S_1 \geq S_{10}) = 1$	$V(S_2 \geq S_{10}) = 1$	$V(S_3 \geq S_{10}) = 1$	$V(S_4 \geq S_{10}) = 1$
$V(S_1 \geq S_{11}) = 1$	$V(S_2 \geq S_{11}) = 1$	$V(S_3 \geq S_{11}) = 1$	$V(S_4 \geq S_{11}) = 1$
$V(S_1 \geq S_{12}) = 1$	$V(S_2 \geq S_{12}) = 1$	$V(S_3 \geq S_{12}) = 1$	$V(S_4 \geq S_{12}) = 1$
$\min\{V(S_1 \geq S_k)\} = 0.53$	$\min\{V(S_2 \geq S_k)\} = 0.43$	$\min\{V(S_3 \geq S_k)\} = 0.49$	$\min\{V(S_4 \geq S_k)\} = 0.09$
Weight = 0.196	Weight = 0.157	Weight = 0.179	Weight = 0.033
TPI = 5	**Slope angle = 6**	**Convergence index = 7**	**Lithology = 8**
$V(S_5 \geq S_1) = 0.08$	$V(S_6 \geq S_1) = 1$	$V(S_7 \geq S_1) = 0.04$	$V(S_8 \geq S_1) = 0.61$
$V(S_5 \geq S_2) = 0.21$	$V(S_6 \geq S_2) = 1$	$V(S_7 \geq S_2) = 0.03$	$V(S_8 \geq S_2) = 0.71$
$V(S_5 \geq S_3) = 0.18$	$V(S_6 \geq S_3) = 1$	$V(S_7 \geq S_3) = 0.05$	$V(S_8 \geq S_3) = 0.68$
$V(S_5 \geq S_4) = 0.59$	$V(S_6 \geq S_4) = 1$	$V(S_7 \geq S_4) = 0.44$	$V(S_8 \geq S_4) = 1$
$V(S_5 \geq S_6) = 0.05$	$V(S_6 \geq S_5) = 1$	$V(S_7 \geq S_5) = 0.88$	$V(S_8 \geq S_5) = 1$
$V(S_5 \geq S_7) = 1$	$V(S_6 \geq S_7) = 1$	$V(S_7 \geq S_6) = 0.06$	$V(S_8 \geq S_6) = 0.16$
$V(S_5 \geq S_8) = 0.5$	$V(S_6 \geq S_8) = 1$	$V(S_7 \geq S_8) = 0.34$	$V(S_8 \geq S_7) = 1$
$V(S_5 \geq S_9) = 1$	$V(S_6 \geq S_9) = 1$	$V(S_7 \geq S_9) = 0.88$	$V(S_8 \geq S_9) = 1$
$V(S_5 \geq S_{10}) = 0.88$	$V(S_6 \geq S_{10}) = 1$	$V(S_7 \geq S_{10}) = 0.74$	$V(S_8 \geq S_{10}) = 1$
$V(S_5 \geq S_{11}) = 1$	$V(S_6 \geq S_{11}) = 1$	$V(S_7 \geq S_{11}) = 1$	$V(S_8 \geq S_{11}) = 1$
$V(S_5 \geq S_{12}) = 1$	$V(S_6 \geq S_{12}) = 1$	$V(S_7 \geq S_{12}) = 1$	$V(S_8 \geq S_{12}) = 1$
$\min\{V(S_5 \geq S_k)\} = 0.05$	$\min\{V(S_6 \geq S_k)\} = 1$	$\min\{V(S_7 \geq S_k)\} = 0.03$	$\min\{V(S_8 \geq S_k)\} = 0.16$
Weight = 0.018	Weight = 0.367	Weight = 0.011	Weight = 0.058
TWI = 9	**Rainfall = 10**	**Plan curvature = 11**	**Aspect = 12**
$V(S_9 \geq S_1) = 0.09$	$V(S_{10} \geq S_1) = 0.05$	$V(S_{11} \geq S_1) = 0.03$	$V(S_{12} \geq S_1) = 0.07$
$V(S_9 \geq S_2) = 0.1$	$V(S_{10} \geq S_2) = 0.2$	$V(S_{11} \geq S_2) = 0.06$	$V(S_{12} \geq S_2) = 0.04$
$V(S_9 \geq S_3) = 0.05$	$V(S_{10} \geq S_3) = 0.16$	$V(S_{11} \geq S_3) = 0.04$	$V(S_{12} \geq S_3) = 0.02$
$V(S_9 \geq S_4) = 0.51$	$V(S_{10} \geq S_4) = 0.63$	$V(S_{11} \geq S_4) = 0.23$	$V(S_{12} \geq S_4) = 0.03$
$V(S_9 \geq S_5) = 0.99$	$V(S_{10} \geq S_5) = 1$	$V(S_{11} \geq S_5) = 0.62$	$V(S_{12} \geq S_5) = 0.05$
$V(S_9 \geq S_6) = 0.07$	$V(S_{10} \geq S_6) = 0.04$	$V(S_{11} \geq S_6) = 0.03$	$V(S_{12} \geq S_6) = 0.03$
$V(S_9 \geq S_7) = 1$	$V(S_{10} \geq S_7) = 1$	$V(S_{11} \geq S_7) = 0.73$	$V(S_{12} \geq S_7) = 0.04$
$V(S_9 \geq S_8) = 0.41$	$V(S_{10} \geq S_8) = 0.53$	$V(S_{11} \geq S_8) = 0.1$	$V(S_{12} \geq S_8) = 0.08$
$V(S_9 \geq S_{10}) = 0.85$	$V(S_{10} \geq S_9) = 1$	$V(S_{11} \geq S_9) = 0.6$	$V(S_{12} \geq S_9) = 0.02$
$V(S_9 \geq S_{11}) = 1$	$V(S_{10} \geq S_{11}) = 1$	$V(S_{11} \geq S_{10}) = 0.45$	$V(S_{12} \geq S_{10}) = 0.13$
$V(S_9 \geq S_{12}) = 1$	$V(S_{10} \geq S_{12}) = 1$	$V(S_{11} \geq S_{12}) = 1$	$V(S_{12} \geq S_{11}) = 0.17$
$\min\{V(S_9 \geq S_k)\} = 0.07$	$\min\{V(S_{10} \geq S_k)\} = 0.04$	$\min\{V(S_{11} \geq S_k)\} = 0.03$	$\min\{V(S_{12} \geq S_k)\} = 0.02$
Weight = 0.025	Weight = 0.146	Weight = 0.011	Weight = 0.007

situation can be observed in the case of Specificity where the value of 95.8%, achieved by SVM-IoE, is higher than 94.4% (FAHP-IoE) and also higher than 93.7% (IoE). It can be noted that SVM-IoE achieved very good performances also in terms of Accuracy (95.1%) and Kappa index (0.903) (Table 2). The use of the validating data revealed that SVM-IoE was the most performant model in the case of all statistical measures. The SVM-IoE obtained the following results: Sensitivity = 91.9%, Specificity = 93.3%, Accuracy = 92.6% and Kappa index = 0.852.

5.3. Flood modeling with index of Entropy

The first step of the application of IoE model consisted into calculating the Frequency Ratio (FR) values for each class/category of factors. The highest value of 10.7 FR coefficients was attributed to the TWI class between 10.68 and 19.89, followed by the water bodies land-use category (FR = 8.89), the distance from rivers between 0 and 50 m (FR = 6.35) and the built-up areas land use category (FR = 4.52). It can be noted that 10 classes/categories achieved FR value equal to 0 (Table 3). The FR values were employed to obtain the probability density (Pij). The highest value of 0.7 was achieved by the TWI class between 10.68 and 19.89, followed by the slope class between 3.1 and 7 ((Pij) = 0.57) (Table 3) and the distance from rivers between 0 and 50 m ((Pij) = 0.53). As in the case of the FR coefficients, the same classes/categories obtained a probability density equal to 0. After 5 following successive steps, which implied the use of the probability density, the weights of each flood conditioning factor were obtained. The highest weight was held by the TWI (2.51), followed by the Land-use (1.69), Distance from rivers (1.22), TPI (1.06), Slope (0.82), Rainfall (0.67), Hydrological Soil Groups (0.66), Aspect (0.64), Plan Curvature (0.61), Convergence Index (0.6), Elevation (0.6) and Lithology (0.55). Finally, the FPI_{IoE} was obtained by multiplying the weights of the flood predictors with the IoE coefficients assigned to each class/category.

The FPI_{IoE} (Fig. 10) values, ranging from 0.38 to 5.65, have been grouped into 5 classes defined by the Natural Breaks method. The first class, between 0.38 and 1.17, occupies 25.43% of the total study area and indicates the surfaces with very low flood potential. The class, between 1.17 and 1.68, covers about 32.13% of the total surface of the Buzău river basin and emphasizes surfaces with low flood potential. The medium values of FPI_{IoE} are distributed especially in the plainregion and represent about 30%. The high and very high values of the FPI_{IoE} occupy about 12.5% of the Buzău river basin and occur mainly along the main rivers of the study area.

5.4. Flood modeling with the FAHP stand-alone and FAHP-IoE

The estimation of AHP weights for each class/category of flood conditioning was the first step in the application of FAHP stand-alone model. The AHP weights included in Table 4, were obtained by constructing 12 pair-wise comparison matrices for each flood conditioning factors. The highest values of AHP weights (0.587) were assigned to Plan curvature class between 0.11 and 0.48 (Table 4), followed by

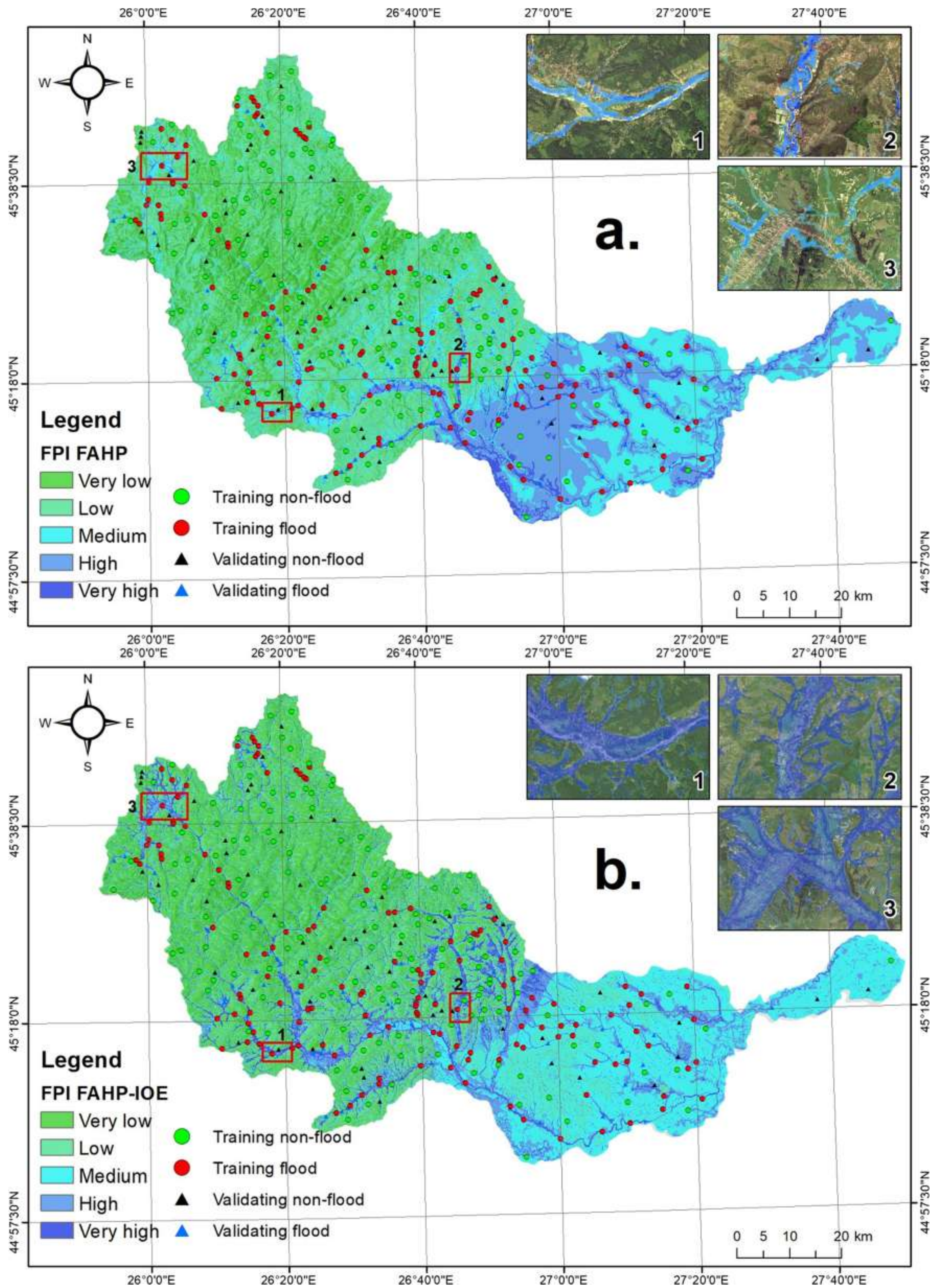

Fig. 11. FPI spatial distribution across the Buzău river basin: a. FPI_{FAHP}; b. $FPI_{FAHP\text{-}IOE}$.

hydrological soil group D (0.582), convergence index class between (−1 0 0) and (-3), etc.

The construction of the fuzzy pairwise comparison matrix (Table 5) was the second step of the workflow developed through the FAHP model. Thus, the 12 criteria (flood conditioning factors) were compared within the matrix.

Further, the synthetic fuzzy values, derived according to the methodology described at 4.3.3, were computed in order to be included in the calculation process of the final weights of flood predictors. In this regard, the analysis was performed according to the following steps:

$$\left[\sum_{k=1}^{n}\sum_{j=1}^{n} a_{kj}^{'}\right]^{-1} = (194.17254.\ 58323.77)^{-1} = (0.0030.\ 0040.005) \tag{25}$$

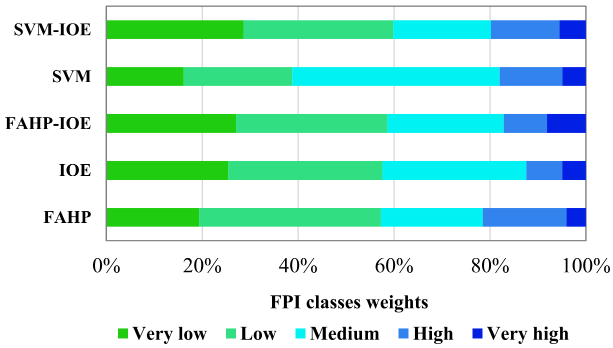

Fig. 12. Weights of the FPI classes.

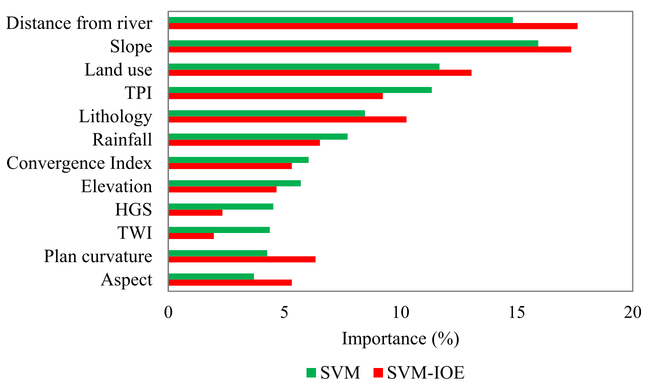

Fig. 13. Flood conditioning factors importance in SVM stand-alone and SVM-IOE.

Further, the fuzzy number were compared by mean of the degree of possibility procedure.

The results of these comparisons are inserted in Table 6, and were further used to determine the weight vector according to eq. 26 and 27:

$$w'(a_i) = \{0.53\ 0.43\ 0.49\ 0.09\ 0.05\ 1\ 0.03\ 0.16\ 0.07\ 0.04\ 0.03\ 0.02\}^T \tag{26}$$

$$w(a_i) = \{0.196\ 0.157\ 0.179\ 0.033\ 0.018\ 0.367\ 0.011\ 0.058\ 0.025\ 0.146\ 0.011\ 0.007\}^T \tag{27}$$

Thus, through the defuzzification process, the TFNs were converted into the values of the crisp weights which will later be assigned for each flood conditioning factor in order to estimate the flood potential. As mentioned before within the methodology, the FPI_{FAHP} and $FPI_{FAHP\text{-}IOE}$ values will be obtained by the multiplication of the crisp weight's values with the AHP and IoE coefficients.

FPI_{FAHP} (Fig. 11**a**) values ranging from 0.07 and 0.37, were split into 5 classes through *Natural Breaks* method. The first class, between 0.07 and 0.13, covers approximately 19.35% of the Buzău river basin, while the low values included in the second class are distributed on around 37.9% of the study area. Medium flood potential is encountered on 21.2%, while the high and very high FPI_{FAHP} values are spread over 21.5% of the entire study area.

The $FPI_{FAHP\text{-}IoE}$ model (Fig. 11**b**) with the values between 0.04 and 0.8, was classified into 5 classes using *Natural Breaks* method. The first class, ranging between 0.04 and 0.19, covers almost 27% of the study area, especially in the mountainous areas, whereas the small values of the $FPI_{FAHP\text{-}IoE}$, ranging between 0.19 and 0.35, cover 31.55% of the research area (Fig. 12). The average values of the $FPI_{FAHP\text{-}IoE}$ occupy about 25% of the study area, while the IVth and Vth classes of FPI cover a total surface of 17%. Unlike in the FPI_{IoE}, the high and very high values of $FPI_{FAHP\text{-}IoE}$ occur in the transitioning areas from hilly region to the plain region.

5.5. Flood modeling with the SVM stand-alone and SVM-IoE

In the first stage, the SVM stand-alone model was used to determine the flood potential across the study area. In this regard, the values of flood conditioning factors and the flood and non-flood points from the training samples were used as input data. The determination of the weights for each flood predictor was optimized by the use of the two parameters represented by C (1.5) and γ (0.16). The slope angle was the most important factor (15.93%), followed by distance from river (14.84%), land use (11.68%), tpi (11.35%), lithology (8.47%), rainfall (7.72%), convergence index (6.04%), elevation (5.71%), hydrological soil group (4.52%), twi (4.37%), plan curvature (4.26%) and aspect (3.69%) (Fig. 13). The application of SVM-IoE assumed the use of IoE coefficients as input data and a new estimation of the two parameters C (1.8) and γ (0.13). In this case, the distance from rivers achieved the highest relative importance (17.63%), followed by the slope angle (17.35%), land-use (13.06%), lithology (10.26%), TPI (9.24%), rainfall (6.53%), plan curvature (6.34%), aspect (5.32%), convergence index (5.32%), elevation (4.66%), hydrological soil groups (2.33%) and the TWI (1.96%) (Fig. 14).

FPI_{SVM} values, ranging from 0.06 to 0.33, were divided into five classes using the *Natural Breaks* method. The very low flood potential is encountered on 16.13% of the study area, while the low value of FPI_{SVM} can be found on 22.6%. A percentage of 43.28% of the study area is covered by medium values of FPI_{SVM}, while the high and very high flood potential appears on approximately 18% of Buzău river basin. Further the $FPI_{SVM\text{-}IoE}$ values between 0.28 and 5.31, were divided into five classes using the same method like in the case of the previous four flood potential indices. It is noted that from the total surface of the basin, around 28.62% of the area is represented by the very low flood potential class and 31.23% of those with low potential. The average values of the FPIFAHP-IoE are present around 20% of the Buzau river basin.

6. Discussion and conclusions

The Flood Potential Index for the Buzău river catchment has been computed in past researches and has been done through various techniques that have shown different results. The past researches have been based on a simpler analysis which involved the overlay of the conditioning factors, without taking into account the locations of the historical floods. It should be noted that the historical floods provide essential data in the detection of the areas prone to floods and their spread. Previous researches, conducted by Costache et al. (2015) and Zaharia et al. (2017) have not attempted to validate the results through various validation methods, as was made in the present study. The results validation methods confirmed the high performance of the models which were employed to compute the Flood Potential Index in the present research. Therefore, we consider that the models could be used at a national scale for flood hazard mapping.

The idea that global climate change causes an increase in flood frequency is unanimously accepted by the international scientific world. Taking into account this consideration, the assessment of certain territories from the flood susceptibility point of view represent a mandatory activity that should be included in the flood risk management. The main result of the present study is represented by the values of flood potential index which were spatially modeled across the Buzău river basin. In order to derive the FPI values a number of three stand-alone models (Index of Entropy, Fuzzy Analytical Hierarchy Process, Support Vector Machine) and two hybrids (FAHP-IoE and SVM-IoE) were used. The models were trained by using 144 flood and 144 non-flood points, which represent the dependent variables, and 12 flood predictors representing the independent variables. During the application of the methodological workflow, there were achieved some auxiliary results represented by the AHP and IoE coefficients assigned to each factor class/category, or by the weight values of the flood

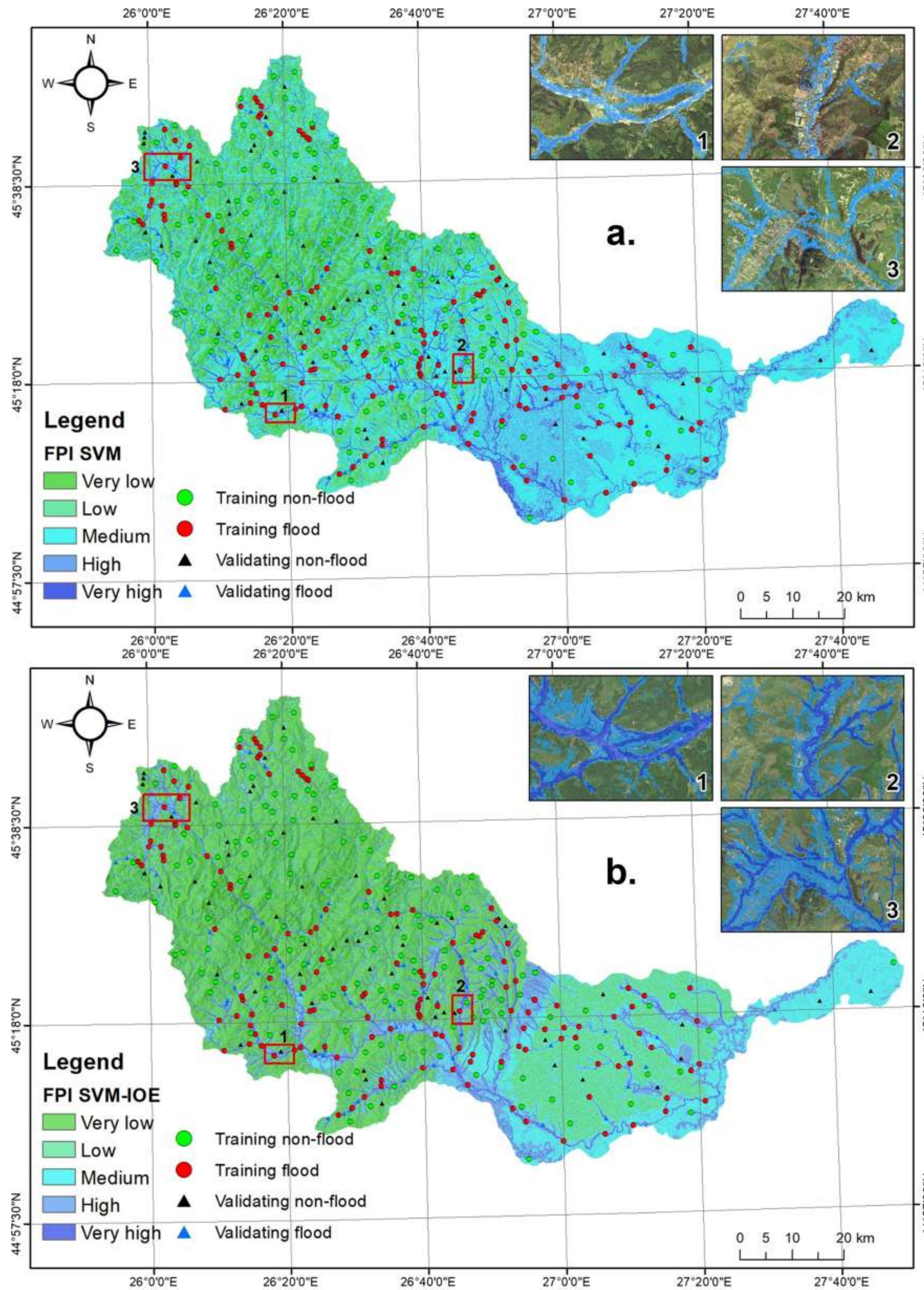

Fig. 14. FPI spatial distribution across the Buzău river basin: a. FPI_{SVM}; b. $FPI_{SVM\text{-}IOE}$.

predictors calculated through FAHP, and SVM models. These auxiliary results contributed to the achievement of the main result of the analysis.

It should be noted that seven flood conditioning factors were derived from databases that were obtained by applying remote sensing techniques, so it should be noted the essential role which remote sensing holds in assessment of potential to different natural hazards. It should be mentioned that after an initial evaluation of the predictive ability of the conditioning factors through the Linear Support Vector Machine method, all 12 factors were further considered into the analysis. The results of the analysis highlighted that the areas with a high and very high flood potential, occupy between 13% (FPI_{IoE}) and 21.5%

(FPI_{FAHP}) of the study area. The most prone areas are located near watercourses, and also in the plain region where the slope is low. The validation process shows that, in terms of the Success Rate, the hybrid SVM-IoE was the most performant model (AUC = 0979), while in terms of Prediction Rate, FAHP-IoE obtained the highest performance (AUC = 0.93).

Given the fact that the Buzau river basin is one of the most affected regions by floods in Romania, the results can be useful to the local authorities responsible for the management of emergency situations. Also, since the methods used in this study have had a high-performance rate, they can represent a strong benchmark for future studies.

CRediT authorship contribution statement

Romulus Costache: Conceptualization, Investigation, Data curation, Visualization, Methodology, Formal analysis, Writing - original draft, Supervision, Writing - review & editing. **Mihnea Cristian Popa:** Conceptualization, Investigation, Data curation, Visualization, Methodology, Formal analysis, Writing - original draft. **Dieu Tien Bui:** Conceptualization, Investigation, Data curation, Visualization, Methodology, Formal analysis, Writing - original draft, Supervision, Writing - review & editing. **Daniel Constantin Diaconu:** Conceptualization, Investigation, Data curation, Visualization, Methodology, Formal analysis, Writing - original draft. **Nicu Ciubotaru:** Conceptualization, Investigation, Data curation, Visualization. **Gabriel Minea:** Conceptualization, Investigation, Data curation, Visualization. **Quoc Bao Pham:** Conceptualization, Investigation, Data curation, Visualization.

Declaration of Competing Interest

The authors declare that they have no known competing financial interests or personal relationships that could have appeared to influence the work reported in this paper.

References

Ahmadlou, M., Karimi, M., Alizadeh, S., Shirzadi, A., Parvinnejhad, D., Shahabi, H., Panahi, M., 2018. Flood susceptibility assessment using integration of adaptive network-based fuzzy inference system (ANFIS) and biogeography-based optimization (BBO) and BAT algorithms (BA). Geocarto Int. 1–21. https://doi.org/10.1080/10106049.2018.1474276.
Ahmed, F., Kilic, K., 2016. Comparison of Fuzzy Extent Analysis Technique and its Extensions with Original Eigen Vector Approach. Presented at the ICEIS 2, 174–179.
Arabameri, A., Pradhan, B., Rezaei, K., Lee, C.-W., 2019. Assessment of Landslide Susceptibility Using Statistical- and Artificial Intelligence-Based FR–RF Integrated Model and Multiresolution DEMs. Remote Sens. 11, 999. https://doi.org/10.3390/rs11090999.
Balezentiene, L., Streimikiene, D., Balezentis, T., 2013. Fuzzy decision support methodology for sustainable energy crop selection. Renew. Sustain. Energy Rev. 17, 83–93. https://doi.org/10.1016/j.rser.2012.09.016.
Baratloo, A., Hosseini, M., Negida, A., El Ashal, G., 2015. Part 1: simple definition and calculation of accuracy, sensitivity and specificity.
Bradley, A.P., 1997. The use of the area under the ROC curve in the evaluation of machine learning algorithms. Pattern Recognit. 30, 1145–1159.
Buckley, J.J., 1985. Fuzzy hierarchical analysis. Fuzzy Sets Syst. 17, 233–247. https://doi.org/10.1016/0165-0114(85)90090-9.
Bui, D.T., Hoang, N.-D., Martínez-Álvarez, F., Ngo, P.-T.T., Hoa, P.V., Pham, T.D., Samui, P., Costache, R., 2020. A novel deep learning neural network approach for predicting flash flood susceptibility: A case study at a high frequency tropical storm area. Sci. Total Environ. 701, 134413.
Cao, C., Xu, P., Wang, Y., Chen, J., Zheng, L., Niu, C., 2016. Flash flood hazard susceptibility mapping using frequency ratio and statistical index methods in coalmine subsidence areas. Sustainability 8, 948. https://doi.org/10.3390/su8090948.
Chen, W., Li, W., Hou, E., Bai, H., Chai, H., Wang, D., Cui, X., Wang, Q., 2015. Application of frequency ratio, statistical index, and index of entropy models and their comparison in landslide susceptibility mapping for the Baozhong Region of Baoji, China. Arab. J. Geosci. 8, 1829–1841.
Chen, W., Xie, X., Peng, J., Shahabi, H., Hong, H., Tien Bui, D., Duan, Z., Li, S., Zhu, A.-X., 2018. GIS-based landslide susceptibility evaluation using a novel hybrid integration approach of bivariate statistical based random forest method. Catena 164. https://doi.org/10.1016/j.catena.2018.01.012.
Chen, W., Xie, X., Wang, J., Pradhan, B., Hong, H., Bui, D.T., Duan, Z., Ma, J., 2017. A comparative study of logistic model tree, random forest, and classification and regression tree models for spatial prediction of landslide susceptibility. Catena 151, 147–160.
Chen, Y., Yu, J., Khan, S., 2013. The spatial framework for weight sensitivity analysis in AHP-based multi-criteria decision making. Environ. Model. Softw. 48, 129–140. https://doi.org/10.1016/j.envsoft.2013.06.010.
Choubin, B., Moradi, E., Golshan, M., Adamowski, J., Sajedi-Hosseini, F., Mosavi, A., 2019. An ensemble prediction of flood susceptibility using multivariate discriminant analysis, classification and regression trees, and support vector machines. Sci. Total Environ. 651, 2087–2096. https://doi.org/10.1016/j.scitotenv.2018.10.064.
Costache, R., 2014. Using GIS techniques for assessing lag time and concentration time in small river basins. Case study: Pecineaga river basin, Romania. Geographia Tech. 9 (1), 31–38.
Costache, R., 2019a. Flood susceptibility assessment by using bivariate statistics and machine learning models – a useful tool for flood risk management. Water Resour. Manag. 33, 3239–3256. https://doi.org/10.1007/s11269-019-02301-z.
Costache, R., 2019b. Flash-Flood Potential assessment in the upper and middle sector of Prahova river catchment (Romania). A comparative approach between four hybrid models. Sci. Total Environ. 659, 1115–1134. https://doi.org/10.1016/j.scitotenv.2018.12.397.
Costache, R., 2019c. Flash-flood Potential Index mapping using weights of evidence, decision Trees models and their novel hybrid integration. Stoch. Environ. Res. Risk Assess. 33, 1375–1402. https://doi.org/10.1007/s00477-019-01689-9.
Costache, R., Bui, D.T., 2019. Spatial prediction of flood potential using new ensembles of bivariate statistics and artificial intelligence: A case study at the Putna river catchment of Romania. Sci. Total Environ. 691, 1098–1118.
Costache, R., Fontanine, I., Corodescu, E., 2014. Assessment of surface runoff depth changes in Sărăţel River basin, Romania using GIS techniques. Open Geosci. 6, 363–372.
Costache, R., Hong, H., Pham, Q.B., 2020. Comparative assessment of the flash-flood potential within small mountain catchments using bivariate statistics and their novel hybrid integration with machine learning models. Sci. Total Environ. 711, 134514.
Costache, R., Hong, H., Wang, Y., 2019b. Identification of torrential valleys using GIS and a novel hybrid integration of artificial intelligence, machine learning and bivariate statistics. Catena 183, 104179.
Costache, R., Tien Bui, D., 2020. Identification of areas prone to flash-flood phenomena using multiple-criteria decision-making, bivariate statistics, machine learning and their ensembles. Sci. Total Environ. 712, 136492. https://doi.org/10.1016/j.scitotenv.2019.136492.
Costache, R., Zaharia, L., 2017. Flash-flood potential assessment and mapping by integrating the weights-of-evidence and frequency ratio statistical methods in GIS environment - case study: Bâsca Chiojdului River catchment (Romania). J. Earth Syst. Sci. 126, 59. https://doi.org/10.1007/s12040-017-0828-9.
Costache, R., Pham, B.P., Sharifi, E., Linh, N.T.T., Abba, S.I., Vojtek, M., Vojtek, J., Nhi, P.T.T., 2020. Flash-flood susceptibility assessment using multi-criteria decision making and machine learning supported by remote sensing and GIS techniques. Remote Sens. 12, 106. https://doi.org/10.3390/rs12010106.
Costache, R., Prăvălie, R., 2012. The use of GIS techniques in the evaluation of the susceptibility of the floods genesis in the hydrographical basin of Bâsca Chiojdului river. Analele Universităţii din Oradea, Seria Geografie 22 (2), 284–293.
Costache, R.-D., Prăvălie, R., Mitof, I., Popescu, C., 2015. Flood vulnerability assessment in the low sector of sărăţel catchment. Case study: Joseni village. Carpathian J. Earth Environ. Sci. 10, 161–169.
Costanzo, D., Rotigliano, E., Irigaray, C., Jiménez-Perálvarez, J.D., Chacón, J., 2012. Factors selection in landslide susceptibility modelling on large scale following the gis matrix method: application to the river Beiro basin (Spain). Nat. Hazards Earth Syst. Sci. 12, 327–340. https://doi.org/10.5194/nhess-12-327-2012.
Devkota, K., Regmi, A., Pourghasemi, H.R., Yoshida, K., Pradhan, B., Chang Ryu, I., Dhital, M., Althuwaynee, O., 2013. Landslide susceptibility mapping using certainty factor, index of entropy and logistic regression models in GIS and their comparison at Mugling-Narayanghat road section in Nepal Himalaya. Nat. Hazards 65, 135–165. https://doi.org/10.1007/s11069-012-0347-6.
Dou, J., Yunus, A.P., Tien Bui, D., Sahana, M., Chen, C.-W., Zhu, Z., Wang, W., Thai Pham, B., 2019. Evaluating GIS-Based Multiple Statistical Models and Data Mining for Earthquake and Rainfall-Induced Landslide Susceptibility Using the LiDAR DEM. Remote Sens. 11, 638. https://doi.org/10.3390/rs11060638.
European Environment Agency, 2017. Climate change, impacts and vulnerability in Europe 2016: an indicator-based report (No. 1/2017). European Environment Agency, Copenhagen.
Fawcett, T., 2006. An introduction to ROC analysis. Pattern Recognit. Lett. 27, 861–874.
Feizizadeh, B., Shadman Roodposhti, M., Jankowski, P., Blaschke, T., 2014. A GIS-based extended fuzzy multi-criteria evaluation for landslide susceptibility mapping. Comput. Geosci. 73, 208–221. https://doi.org/10.1016/j.cageo.2014.08.001.
Gigović, L., Pamučar, D., Bajić, Z., Drobnjak, S., 2017. Application of GIS-Interval Rough AHP Methodology for Flood Hazard Mapping in Urban Areas. Water 9, 360. https://doi.org/10.3390/w9060360.
Grecu, F., Zaharia, L., Ioana-Toroimac, G., Armaș, I., 2017. Floods and Flash-Floods Related to River Channel Dynamics, in: Radoane, M., Vespremeanu-Stroe, A. (Eds.), Landform Dynamics and Evolution in Romania, Springer Geography. Springer International Publishing, Cham, pp. 821–844. https://doi.org/10.1007/978-3-319-32589-7_33.
Guyon, I., Elisseeff, A., 2003. An Introduction to Variable and Feature Selection. J. Mach. Learn. Res. 3, 1157–1182.
Hanley, J.A., Mcneil, B., 1982. The Meaning and Use of the Area Under a Receiver Operating Characteristic (ROC) Curve. Radiology 143, 29–36. https://doi.org/10.1148/radiology.143.1.7063747.
Hong, H., Liu, J., Zhu, A.-X., Shahabi, H., Pham, B.T., Chen, W., Pradhan, B., Bui, D.T.,

2017. A novel hybrid integration model using support vector machines and random subspace for weather-triggered landslide susceptibility assessment in the Wuning area (China). Environ. Earth Sci. 76, 652.
Hong, H., Panahi, M., Shirzadi, A., Ma, T., Liu, J., Zhu, A.-X., Chen, W., Kougias, I., Kazakis, N., 2018. Flood susceptibility assessment in Hengfeng area coupling adaptive neuro-fuzzy inference system with genetic algorithm and differential evolution. Sci. Total Environ. 621, 1124–1141. https://doi.org/10.1016/j.scitotenv.2017.10.114.
Jenness, J., Beier, P., Ganey, J., 2004. Associations between Forest Fire and Mexican Spotted Owls. For. Sci. 50, 765–772.
Jongman, B., 2018. Effective adaptation to rising flood risk. Nat. Commun. 9, 1–3. https://doi.org/10.1038/s41467-018-04396-1.
Kahraman, C., Cebeci, U., Ulukan, Z., 2003. Multi-criteria supplier selection using fuzzy AHP. Logist. Inf. Manag. 16, 382–394. https://doi.org/10.1108/09576050310503367.
Kavzoglu, T., Sahin, E.K., Colkesen, I., 2014. Landslide susceptibility mapping using GIS-based multi-criteria decision analysis, support vector machines, and logistic regression. Landslides 11, 425–439. https://doi.org/10.1007/s10346-013-0391-7.
Khosravi, K., Nohani, E., Maroufinia, E., Pourghasemi, H.R., 2016. A GIS-based flood susceptibility assessment and its mapping in Iran: a comparison between frequency ratio and weights-of-evidence bivariate statistical models with multi-criteria decision-making technique. Nat. Hazards. J. Int. Soc. Prev. Mitig. Nat. Hazards 83, 947–987.
Khosravi, K., Pham, B., Chapi, K., Shirzadi, A., Shahabi, H., Revhaug, I., Prakash, I., Tien Bui, D., 2018. A Comparative Assessment of Decision Trees Algorithms for Flash Flood Susceptibility Modeling at Haraz Watershed. Northern Iran. Sci. Total Environ. 627, 744–755. https://doi.org/10.1016/j.scitotenv.2018.01.266.
Kumar Samanta, R., Bhunia, G., Shit, P., Pourghasemi, H.R., 2018. Flood susceptibility mapping using geospatial frequency ratio technique: a case study of Subarnarekha River Basin, India. Model. Earth Syst. Environ. https://doi.org/10.1007/s40808-018-0427-z.
Lin, Y., 2002. Support Vector Machines and the Bayes Rule in Classification. Data Min. Knowl. Discov. 6, 259–275. https://doi.org/10.1023/A:1015469627679.
Linzer, H.-G., Frisch, W., Zweigel, P., Girbacea, R., Hann, H.-P., Moser, F., 1998. Kinematic evolution of the Romanian Carpathians. Tectonophysics 297, 133–156. https://doi.org/10.1016/S0040-1951(98)00166-8.
Mahmoud, S.H., Gan, T.Y., 2018. Multi-criteria approach to develop flood susceptibility maps in arid regions of. Middle East.
Minea, G., Gabriela, I.-T., Gabriela, M., 2019. The dominant runoff processes on grassland versus bare soil hillslopes in a temperate environment - An experimental study. J. Hydrol. Hydromech. 67. https://doi.org/10.2478/johh-2019-0018.
Mladenić, D., Brank, J., Grobelnik, M., Milic-Frayling, N., 2004. Feature selection using linear classifier weights: interaction with classification models. In: Presented at the Proceedings of the 27th annual international ACM SIGIR conference on Research and development in information retrieval, pp. 234–241.
Mojaddadi, H., Pradhan, B., Nampak, H., Ahmad, N., Ghazali, A.H., bin,, 2017. Ensemble machine-learning-based geospatial approach for flood risk assessment using multi-sensor remote-sensing data and GIS. Geomat. Nat. Hazards Risk 8, 1080–1102. https://doi.org/10.1080/19475705.2017.1294113.
Naghibi, S.A., Ahmadi, K., Daneshi, A., 2017. Application of support vector machine, random forest, and genetic algorithm optimized random forest models in groundwater potential mapping. Water Resour. Manag. 31, 2761–2775.
Nicklin, H., Leicher, A.M., Dieperink, C., Van Leeuwen, K., 2019. Understanding the Costs of Inaction–An Assessment of Pluvial Flood Damages in Two European Cities. Water 11, 801. https://doi.org/10.3390/w11040801.
Osuna, E., Girosi, F., 1998. Reducing the run-time complexity of. Support Vector Machines.
Pallant, 2016. SPSS Survival Manual, 6 edition. ed. Open University Press, Maidenhead New York.
Pham, B.T., Bui, D.T., Pourghasemi, H.R., Indra, P., Dholakia, M., 2017a. Landslide susceptibility assesssment in the Uttarakhand area (India) using GIS: a comparison study of prediction capability of naïve bayes, multilayer perceptron neural networks, and functional trees methods. Theor. Appl. Climatol. 128, 255–273.
Pham, B.T., Bui, D.T., Prakash, I., 2017b. Landslide susceptibility assessment using bagging ensemble based alternating decision trees, logistic regression and J48 decision trees methods: a comparative study. Geotech. Geol. Eng. 35, 2597–2611.
Popovici, E.-A., Bălteanu, D., Kucsicsa, G., 2013. assessment of changes in land-use and land-cover pattern in romania using corine land cover database. Carpathian J. Earth Environ. Sci. 8, 195–208.
Pourghasemi, H.R., Moradi, H.R., Fatemi Aghda, S.M., 2013. Landslide susceptibility mapping by binary logistic regression, analytical hierarchy process, and statistical index models and assessment of their performances. Nat. Hazards 69, 749–779. https://doi.org/10.1007/s11069-013-0728-5.
Prăvălie, R., Costache, R., 2013. The vulnerability of the territorial-administrative units to the hydrological phenomena of risk (flash-floods). Case study: the subcarpathian sector of Buzău Catchment. Analele Universităţii din Oradea, Seria Geografie 23 (1), 91–98.
Queiroz, G.V., Rino Neto, J., de Paiva, J.B., Capelozza Filho, L., 2016. Analysis of reliability, accuracy, sensitivity and predictive value of a subjective method to classify facial pattern in adults. Dent. Press J. Orthod. 21, 58–66.
Razavi Termeh, S.V., Kornejady, A., Pourghasemi, H.R., Keesstra, S., 2018. Flood susceptibility mapping using novel ensembles of adaptive neuro fuzzy inference system and metaheuristic algorithms. Sci. Total Environ. 615, 438–451. https://doi.org/10.1016/j.scitotenv.2017.09.262.
Roodposhti, M.S., Rahimi, S., Beglou, M.J., 2014. PROMETHEE II and fuzzy AHP: an enhanced GIS-based landslide susceptibility mapping. Nat. Hazards 73, 77–95. https://doi.org/10.1007/s11069-012-0523-8.
Sachdeva, S., Bhatia, T., Verma, A., 2017. Flood susceptibility mapping using GIS-based support vector machine and particle swarm optimization: A case study in Uttarakhand (India). Presented at the 2017 8th International conference on computing, communication and networking technologies (ICCCNT), IEEE, pp. 1–7.
Siahkamari, S., Haghizadeh, A., Zeinivand, H., Tahmasebipour, N., Rahmati, O., 2018. Spatial prediction of flood-susceptible areas using frequency ratio and maximum entropy models. Geocarto Int. 33, 927–941. https://doi.org/10.1080/10106049.2017.1316780.
Spence, A., Poortinga, W., Butler, C., Pidgeon, N.F., 2011. Perceptions of climate change and willingness to save energy related to flood experience. Nat. Clim. Change 1, 46–49. https://doi.org/10.1038/nclimate1059.
Sun, C.-C., 2010. A performance evaluation model by integrating fuzzy AHP and fuzzy TOPSIS methods. Expert Syst. Appl. 37, 7745–7754. https://doi.org/10.1016/j.eswa.2010.04.066.
Suykens, J.A.K., Vandewalle, J., 1999. Least Squares Support Vector Machine Classifiers. Neural Process. Lett. 9, 293–300. https://doi.org/10.1023/A:1018628609742.
Tehrany, M.S., Pradhan, B., Jebur, M.N., 2015. Flood susceptibility analysis and its verification using a novel ensemble support vector machine and frequency ratio method. Stoch. Environ. Res. Risk Assess. 29, 1149–1165. https://doi.org/10.1007/s00477-015-1021-9.
Tehrany, M.S., Pradhan, B., Jebur, M.N., 2014. Flood susceptibility mapping using a novel ensemble weights-of-evidence and support vector machine models in GIS. J. Hydrol. 512, 332–343. https://doi.org/10.1016/j.jhydrol.2014.03.008.
Tehrany, M.S., Pradhan, B., Jebur, M.N., 2013. Spatial prediction of flood susceptible areas using rule based decision tree (DT) and a novel ensemble bivariate and multivariate statistical models in GIS. J. Hydrol. 504, 69–79. https://doi.org/10.1016/j.jhydrol.2013.09.034.
Tien Bui, D., Khosravi, K., Shahabi, H., Daggupati, P., Adamowski, J.F., Melesse, A.M., Thai Pham, B., Pourghasemi, H.R., Mahmoudi, M., Bahrami, S., Pradhan, B., Shirzadi, A., Chapi, K., Lee, S., 2019. Flood Spatial Modeling in Northern Iran Using Remote Sensing and GIS: A Comparison between Evidential Belief Functions and Its Ensemble with a Multivariate Logistic Regression Model. Remote Sens. 11, 1589. https://doi.org/10.3390/rs11131589.
Tien Bui, D., Pradhan, B., Löfman, O., Revhaug, I., 2012. Landslide susceptibility assessment in vietnam using support vector machines, decision tree, and naïve bayes models. Math. Probl. Eng. 2012, 26. https://doi.org/10.1155/2012/97/46/38.
Tien Bui, D., Pradhan, B., Nampak, H., Bui, Q.-T., Tran, Q.-A., Nguyen, Q.-P., 2016. Hybrid artificial intelligence approach based on neural fuzzy inference model and metaheuristic optimization for flood susceptibilitgy modeling in a high-frequency tropical cyclone area using GIS. J. Hydrol. 540, 317–330. https://doi.org/10.1016/j.jhydrol.2016.06.027.
Tien Bui, D., Shahabi, H., Shirzadi, A., Chapi, K., Alizadeh, M., Chen, W., Mohammadi, A., Ahmad, B., Panahi, M., Hong, H., 2018. Landslide detection and susceptibility mapping by airsar data using support vector machine and index of entropy models in cameron highlands, malaysia. Remote Sens. 10, 1527.
Vakhshoori, V., Zare, M., 2018. Is the ROC curve a reliable tool to compare the validity of landslide susceptibility maps? Geomat. Nat. Hazards Risk 9, 249–266.
Wang, Q., Li, W., Chen, W., Bai, H., 2015a. GIS-based assessment of landslide susceptibility using certainty factor and index of entropy models for the Qianyang County of Baoji city. China. J. Earth Syst. Sci. 124, 1399–1415.
Wang, T.-C., Chen, Y.-H., 2008. Applying fuzzy linguistic preference relations to the improvement of consistency of fuzzy AHP. Inf. Sci. 178, 3755–3765. https://doi.org/10.1016/j.ins.2008.05.028.
Wang, Y., Hong, H., Chen, W., Li, S., Panahi, M., Khosravi, K., Shirzadi, A., Shahabi, H., Panahi, S., Costache, R., 2019. Flood susceptibility mapping in Dingnan County (China) using adaptive neuro-fuzzy inference system with biogeography based optimization and imperialistic competitive algorithm. J. Environ. Manage. 247, 712–729.
Wang, Z., Lai, C., Chen, X., Yang, B., Zhao, S., Bai, X., 2015b. Flood hazard risk assessment model based on random forest. J. Hydrol. 527, 1130–1141. https://doi.org/10.1016/j.jhydrol.2015.06.008.
Wechsler, H., 2000. Learning from Data: Concepts, Theory and Methods, Vladimir Cherkassky and Filip Mulier, John Wiley, New York, 1998. Int. J. Robust Nonlinear Control 10, 747–748. https://doi.org/10.1002/1099-1239(20000730)10:9<747::AID-RNC507>3.0.CO;2-5.
Yalcin, A., 2008. GIS-based Landslide Susceptibility Mapping Using Analytical Hierarchy Process and Bivariate Statistics in Ardesen (Turkey): Comparisons of Results and Confirmations. Catena 72, 1–12. https://doi.org/10.1016/j.catena.2007.01.003.
Yoshimatsu, H., Abe, S., 2006. A review of landslide hazards in Japan and assessment of their susceptibility using an analytical hierarchic process (AHP) method. Landslides 3, 149–158. https://doi.org/10.1007/s10346-005-0031-y.
Zadeh, L.A., 1965. Fuzzy sets. Inf. Control 8, 338–353. https://doi.org/10.1016/S0019-9958(65)90241-X.
Zaharia, L., Costache, R., Prăvălie, R., Ioana-Toroimac, G., 2017. Mapping flood and flooding potential indices: a methodological approach to identifying areas susceptible to flood and flooding risk. Case study: the Prahova catchment (Romania). Front. Earth Sci. 11, 229–247. https://doi.org/10.1007/s11707-017-0636-1.
Zaharia, L., Costache, R., Prăvălie, R., Minea, G., 2015. Assessment and mapping of flood potential in the Slănic catchment in Romania. J. Earth Syst. Sci. 124, 1311–1324.

Science of the Total Environment 711 (2020) 134514

Contents lists available at ScienceDirect

Science of the Total Environment

journal homepage: www.elsevier.com/locate/scitotenv

Comparative assessment of the flash-flood potential within small mountain catchments using bivariate statistics and their novel hybrid integration with machine learning models

Romulus Costache [a,b], Haoyuan Hong [c,d,e,*], Quoc Bao Pham [f,*]

[a] Research Institute of the University of Bucharest, 36-46 Bd. M. Kogalniceanu, 5th District, 050107 Bucharest, Romania
[b] National Institute of Hydrology and Water Management, București-Ploiești Road, 97E, 1st District, 013686 Bucharest, Romania
[c] Key Laboratory of Virtual Geographic Environment (Nanjing Normal University), Ministry of Education, Nanjing 210023, China
[d] State Key Laboratory Cultivation Base of Geographical Environment Evolution (Jiangsu Province), Nanjing 210023, China
[e] Department of Geography and Regional Research, University of Vienna, Universitätsstraße 7, 1010 Vienna, Austria
[f] Department of Hydraulic and Ocean Engineering, National Cheng-Kung University, Tainan 701, Taiwan

HIGHLIGHTS

- Flash-flood susceptibility was calculated within a small river basin.
- SI and 5 ensembles were used to calculate the flash-flood potential.
- Pixels with torrential phenomena were employed as dependent variables.
- A number of 8 flash-flood predictors were used to train the models.
- MLP-SI ensemble was the most performant applied algorithms.

GRAPHICAL ABSTRACT

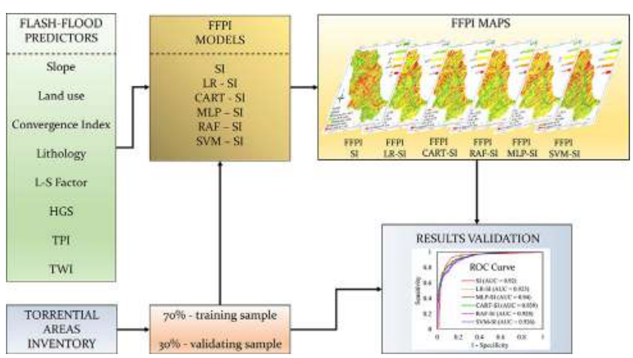

ARTICLE INFO

Article history:
Received 20 July 2019
Received in revised form 10 September 2019
Accepted 16 September 2019
Available online 8 October 2019

Keywords:
Flash-flood potential index
Bâsca Chiojdului catchment
Statistical index
Machine learning models
Ensemble models

ABSTRACT

The present study is carried out in the context of the continuous increase, worldwide, of the number of flash-floods phenomena. Also, there is an evident increase of the size of the damages caused by these hazards. Bâsca Chiojdului River Basin is one of the most affected areas in Romania by flash-flood phenomena. Therefore, Flash-Flood Potential Index (FFPI) was defined and calculated across the Bâsca Chiojdului river basin by using one bivariate statistical method (Statistical Index) and its novel ensemble with the following machine learning models: Logistic Regression, Classification and Regression Trees, Multilayer Perceptron, Random Forest and Support Vector Machine and Decision Tree CART. In a first stage, the areas with torrentiality were digitized based on orthophotomaps and field observations. These regions, together with an equal number of non-torrential pixels, were further divided into training surfaces (70%) and validating surfaces (30%). The next step of the analysis consisted of the selection of flash-flood conditioning factors based on the multicollinearity investigation and predictive ability estimation through Information Gain method. Eight factors, from a total of ten flash-floods predictors, were selected in order to be included in the FFPI calculation process. By applying the models represented by Statistical Index and its ensemble with the machine learning algorithms, the weight of each conditioning factor and of each factor class/category in the FFPI equations was established. Once the weight values were derived, the FFPI values across the Bâsca Chiojdului river basin were calculated by overlaying the flash-flood

* Corresponding authors at: Department of Geography and Regional Research, University of Vienna, Universitätsstraße 7, 1010 Vienna, Austria (H. Hong).
E-mail addresses: romulus.costache@hidro.ro (R. Costache), hong_haoyuan@outlook.com, 171301013@stu.njnu.edu.cn (H. Hong), N88057033@ncku.edu.tw, pbquoc92@gmail.com (Q.B. Pham).

https://doi.org/10.1016/j.scitotenv.2019.134514

predictors in GIS environment. According to the results obtained, the central part of Bâsca Chiojdului river basin has the highest susceptibility to flash-flood phenomena. Thus, around 30% of the study site has high and very high values of FFPI. The results validation was carried out by applying the Prediction Rate and Success Rate. The methods revealed the fact that the Multilayer Perceptron – Statistical Index (MLP-SI) ensemble has the highest efficiency among the 3 methods.

1. Introduction

Climate changes occurred during the last decades, worldwide, are becoming more and more evident. These changes are highlighted by a rapid increase in the frequency of extreme weather phenomena such as heat waves, droughts, periods with excess of humidity, or torrential rains (Rojas et al., 2012; Sampson et al., 2015). It also can be noted that over the last years, extreme phenomena have succeeded with a great rapidity. When these phenomena occur in areas with a high population density, they may represent a risk for the settlements. Frequently, in areas where terrain features are favourable, heavy rainfall leads to devastating flash-floods. In the literature there exist many definitions of flash-floods. Collier (2007) defines the flash-floods as those floods which are characterized by their rapid occurrence resulting in a very limited opportunity for warnings to be prepared and issued. According to Toukourou et al. (2011), the flash-floods is a flood triggered by a heavy rainfall, with a period of manifestation generally <6 h. Another definition of flash-floods is given by Archer and Fowler (2018) which defined the flash-floods as a phenomenon with a rapid speed of response that may causes severe flooding of land and properties far from rivers. Therefore, we can state that the flash-floods are generated by heavy rainfalls which determine a rapid increase of the river discharge and level that may cause severe damages due to the floods occurred in the areas with a low slope angles.

The available data reveals that in 2016, across the globe, floods affected more than 78 million persons (Guha-sapir et al., 2011) and generated material losses of about $56 billion (Karamouz and Fereshtehpour, 2019). Therefore, floods and flash-floods rank the first in terms of damages caused by natural hazards, exceeding the damages caused by earthquakes, volcanic eruptions and landslides. Romania is one of the most affected European country by flash-floods occurrence (Romanescu et al., 2017). This aspect is certified by the large number of flash-flood warnings issued over the last 3 years by the National Institute of Hydrology and Water Management of Romania. Thus, in 2015, 114 yellow code, 11 orange code flash-floods warnings and 4 red code flash-floods warnings were issued, while in the next year (2016), 295 yellow code were issued along with 75 orange code and 7 red code. In 2017, 193 yellow code, 18 orange code and 1 red code were issued, while in 2018, 243 yellow code, 75 orange code and 8 red code were submitted to the local authorities. In order to mitigate the flash-floods damages, the issuance of these warnings is extremely important (Bubeck et al., 2012). In order to support the flash-flood warning activity, in addition to the accuracy of precipitation data estimation by meteorological radar, a comprehensive analysis of the flash-flood potential given by terrain surface features is necessary. This kind of analysis is also useful to streamline the territory planning in order to diminish the potential damage generated by flash-floods.

The Flash-Flood Potential Index (FFPI) is a well-known method used in the international literature to evaluate the flash-flood potential in a specific area. This index was initially introduced by Smith (2003) which calculates the flash-flood potential across the Colorado river basin by considering several flash-flood conditioning factors such as: slope angle, soil type, vegetation and land use/land cover. In order to calculate the FFPI, the author used the values of the reclassified rasters, between 1 and 10, into a simple map algebra operation. It should be mentioned that the conditioning factors received equal weights. The same approach was used by Kruzdlo and Ceru (2010) in order to determine the spatial variability of the flash-flood potential index for Weather Forecast Office (WFO) Mount Holly/Philadelphia. In terms of FFPI equation, two new variables, represented by profile curvature and lithology, were introduced by Zaharia et al. (2012) in an analysis intended to calculate the FFPI within a small mountain catchment in Romania. Another study focused on a mountain catchment in Romania was carried out by Minea (2013) that used also the simple map algebra to represent the spatial variability of FFPI. Tincu et al. (2018) included the flow accumulation factor in the equation designated to calculate a Modified Flash-Flood Potential Index on Trotuş river basin (Romania). In this study, besides the weights assigned to each class and category of factors, the authors established also different weights for each flash-flood predictor. The major drawback of the previous methods is that the weights of the flash-flood predictors are assigned in a subjective manner without taking into account the location of the surfaces with torrential phenomena. A first attempt to consider the areas with torrential phenomena in the FFPI computation, was made by Costache and Zaharia (2017), which tried to evaluate the flash-flood susceptibility, across Bâsca Chiojdului river basin (Romania), by using two bivariate statistical methods (Frequency Ratio and Weights of Evidence). The aforementioned methods along with other machine learning models were widely used, in the literature, to identify the areas prone to flood and flash-floods. Thus, (Shafapour Tehrany et al., 2017), in a study on Jianxi Province (China), revealed the fact that weights of evidence and logistic regression achieved the same performances in terms of flood susceptibility prediction. In other four studies, (Costache, 2019a; Costache et al., 2019; Hong et al., 2018; Shafizadeh-Moghadam et al., 2018) tried to evaluate the susceptibility to floods and flash-floods by using many ensemble models resulted by the combination of bivariate statistical models, such as Frequency Ratio, Weights of Evidence, Evidential Belief Function and Certainty Factor, and machine learning models like Logistic Regression, Random Forest, Support Vector Machine, Multilayer Perceptron and Naïve Bayes. The results obtained revealed the fact that the ensemble models are characterized by high performances, with a prediction accuracy higher than 85%. (Khosravi et al., 2018) performed a comparative analysis regarding the results of different decision trees with respect to flash-flood susceptibility. They concluded that Naïve Bayes Tree, Logistic Model Tree and Alternating Decision Tree were almost perfect, with an Area Under Curve close to 1.

To complete the results achieved by Costache and Zaharia (2017), the present paper has the main objective the assessment of flash-flood potential using more advanced analysis techniques. Therefore, the flash-flood susceptibility across Bâsca Chiojdului river catchment will be calculated by using a bivariate statistical method (Statistical Index (SI)) and another 5 ensemble models derived by the hybrid integration of SI with the following 5 machine learning models: Logistic Regression (LR), Classification and Regression Tree (CART), Multilayer Perceptron (MLP), Random Forest (RAF) and Support Vector Machine (SVM). The performance of the hybrid models will be assessed through several statistical measures represented by Sensitivity, Specificity, Accuracy and Kappa Index, while the validation of the FFPI values will be carried out through the ROC Curve.

2. Materials and methods

Given the fact that in this study a spatial evaluation of the degree of susceptibility to flash-floods is desired, all the data used are geospatial. It should be noted also that for data processing and analysis many software were used. Thus, in a first stage for geospatial data collection and processing ArcGIS 10.5, ArcGIS Pro 2.2 and SAGA GIS 2.1.4 were used. The data resulted from the geoprocessing workflow was used in Microsoft Excel 2016 in order to derive the Statistical Index coefficients. In the next step, the machine learning training procedure were carried using the following software: SPSS 21 software for Logistic Regression and Multilayer Perceptron models, Salford Predictive Modeler 8.2 software for Classification and Regression Tree model, ArcGIS Pro 2.2 software for Random Forest model, and Weka 9.3 software for Support Vector Machine. All the cartographic materials were obtained using ArcGIS 10.5, while the graphics were designed mainly in Microsoft Excel using also the results provided also by the others software.

2.1. Study area and data collection

In this sub-section will be presented the main characteristics of Bâsca Chiojdului catchment with a special view on the flash-flood conditioning factors and the inventory of areas with torrential phenomena.

2.1.1. Study area general characteristics

The present study will be carried out within the perimeter of Bâsca Chiojdului river basin, placed in the central south-eastern region of Romania (Fig. 1). The study area overlaps both Carpathian (mountainous) region (44%), and Subcarpathian (hilly) region (56%).

The small surface of the basin (340 km^2) corroborates with an average slope of 12°, and also with a circularly catchment shape, generates favourable conditions for surface runoff and flash-floods occurrence. Others geographically factors that influence the surface runoff are the forest cover degree (50%), which was determined based on Corine Land Cover 2018 dataset (Costache and Popescu, 2013; Kucsicsa et al., 2019), and the hydrological soil group (predominantly group B), which was extracted from Digital Soil Map of Romania, 1:200,000 (Arghiuş and Arghiuş, 2011; Costache and Pravalie, 2012). According to (Costache and Zaharia, 2017) the average lag time of Bâsca Chiojdului catchment is equal to 4.36 h while the concentration time is around 7.27 h. The small values of the two parameters, Tlag and Tc, indicate, also, the fact

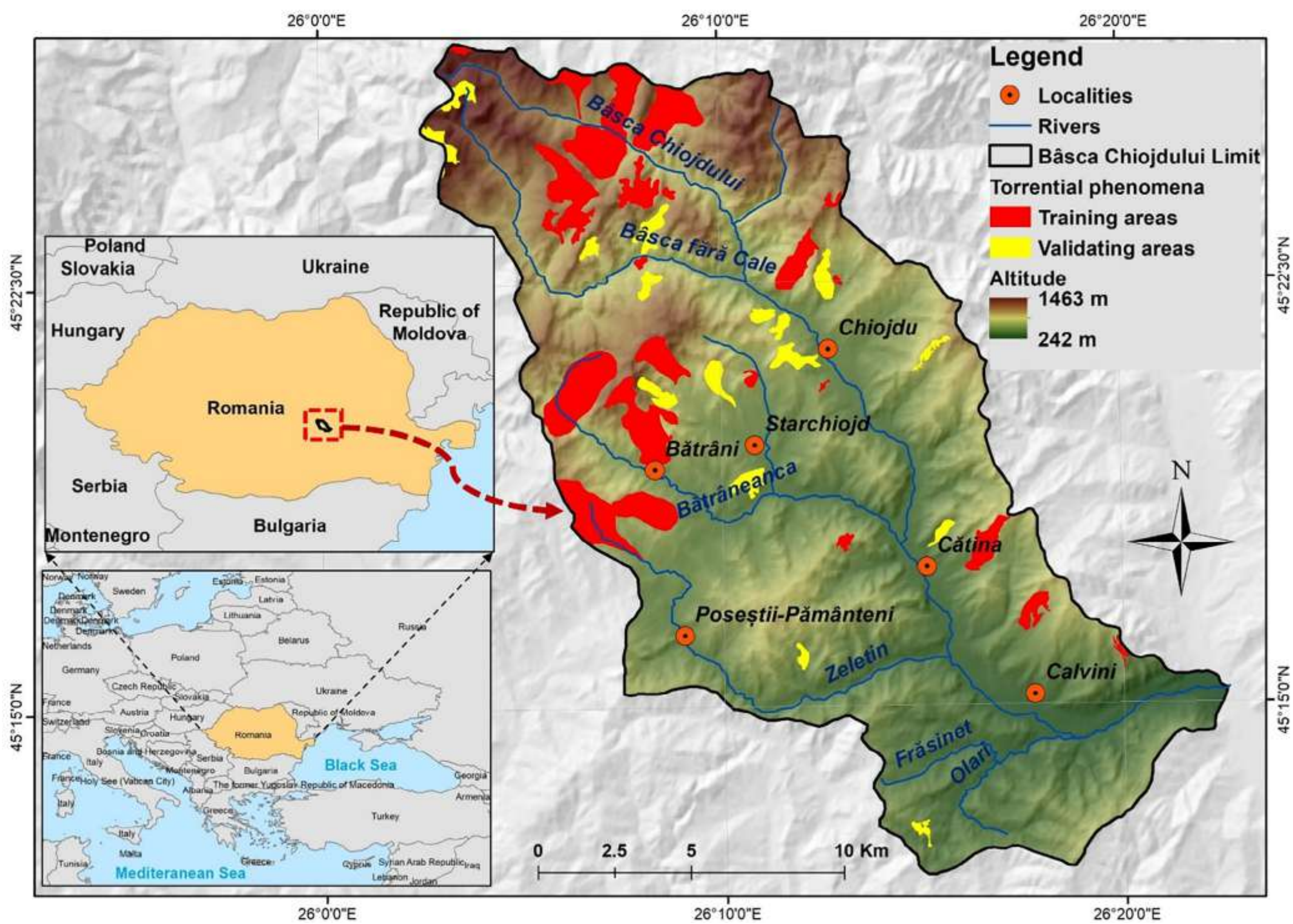

Fig. 1. Location of the study area.

that Bâsca Chiojdului catchment is susceptible to flash-floods occurrence.

Within the perimeter of Bâsca Chiojdului catchment can be found many socio-economic objectives exposed to the flash-floods occurrence. These objectives are located in the following 6 localities which quantifies a total number of 25,417 inhabitants: Calvini, Poseștii-Pământeni, Bătrâni, Starchiojd, Chiojdu and Cătina. Within the perimeter of these localities are also located 331 km of roads from which the most important are: National Road 10 (DN 10) with a total length of 1.3 km, County Road 102B (DJ 102B) with a total length of 21.3 km, County Road 103P (DJ 103P) with a total length of 907 m, County Road 102L (DJ 102L) with a total length of 20.7 km and County Road 100 M (DJ 100 M) with a total length of 720 m. During the time, these socio-economic elements were affected by many severe flash-flood phenomena. The most devastating flash-flood events occurred in 1975, when the discharge of Bâsca Chiojdului reached the historical maximum value of 300 m^3/s, in 1990 when the discharge was equal to 170 m^3/s, and in 2005 when the discharge values was 236 m^3/s. Important flash-flood were manifested also, during the last years (2016, 2018 and 2019) when, according to the General Inspectorate of Emergency Situations of Romania, almost 350 peoples were affected, and>120 houses and 5.3 km of roads were destroyed by these natural risks. It should be noted also, that, according to the National Administration of Romanian Waters, almost 27 km belonging to Bâsca Chiojdului river situated downstream of Chiojdu locality is a sector with a high potential for floods which are triggered by the flash-floods propagated from the upper areas.

2.1.2. Flash-flood conditioning factors

In order to understand the manner in which the flash-flood phenomena occur, the analysis and selection of flash-floods predictors is a very important step. Therefore, in a first step, ten flash-flood predictors were considered into the analysis. From a total number of ten predictors, the following seven variables are morphometric factors which were derived from the Digital Elevation Model: slope relief, L-S Factor, convergence index of hydrographic network, Stream Power Index (SPI), Topographic Wetness Index (TWI), profile curvature and Topographic Position Index (TPI). The others three predictors, extracted from vector geodatabase, are the following: land use, hydrological soil group, lithology. A short description of each of flash-flood causative factor is presented in the following rows.

Slope relief is one of the factors computed with the help of Digital Elevation Model (DEM) extracted from Shuttle Radar Topographic Mission (SRTM) database at 30 m spatial resolution (Mamede da Silva et al., 2018). The values of this morphometric index are directly related to the velocity of the surface runoff (Fontanine and Costache, 2013b; Fontanine and Costache, 2013a; Costache et al., 2014, 2015; Costache, 2019b; Costache, 2014). The higher the slope angle, the active the surface runoff. In order to obtain the spatial distribution of slope values across the study area, the *Slope tool* from *Spatial Analyst* extension of ArcGIS 10.5 software. The DEM was used as input data in the aforementioned tool. In the case of the present study the slope map was carried out by dividing its values into the following five classes according to the literature (Pravalie and Costache, 2013; Pravalie and Costache, 2014): <3°, 3–7°, 7.1–15°, 15.1–25°, >25° (Fig. 2a). L-S factor is a morphometric index that was widely used to estimate the combined effect of the slope length and the slope steepness on surface runoff manifestation (Costache, 2019c; Zaharia et al., 2017, 2015). The derivation of L-S factor is based on the following formula (Moore and Wilson, 1992):

$$LS = \left(\frac{A_s}{22.13}\right)^m \left(\frac{sin(\theta)}{0.0896}\right)^n \quad (1)$$

where A_s is the unit contributing area (m^2), θ is the slope value in radians, m (0.4–0.56) and n (1.2–1.3) are exponents. Regarding the Bâsca Chiojdului catchment, the L-S factor was computed by using the DEM as input in the *Basic Terrain Analysis* module of SAGA GIS 2.1.4. The values of m and n exponents were automatically optimized by the GIS software according to the characteristics of DEM used as input data. The L-S factor values were classified into the following classes based on Natural Breaks method: 0–3.75, 3.76–7.17, 7.18–10.75, 10.76–15.33, 15.34–41.49 (Fig. 2e). Another factor whose values were calculated using the Digital Elevation Model (DEM) is Topographic Wetness Index (TWI). The high values of TWI highlight the areas with an important potential for runoff concentration. The application of the following formula allows the computation of TWI values:

$$TWI = ln\left(\frac{\alpha}{\tan\beta}\right) \quad (2)$$

where α represents the total upslope region draining through a point (per unit contour length) and tan β represents the slope angle value measured at the point. By implementing the previous formula (2) in Map Algebra of ArcGIS software the TWI values were determined. The raster for the catchment area or upslope region (α) was derived in SAGA GIS by using the DEM as input data, while for the slope value (β) was taken into the raster already derived in ArcGIS 10.5. As in the case of L-S factor, the Natural Breaks method was also used to divide the TWI values as following: 3.15–6.1, 6.11–7.78, 7.79–10.21, 10.22–14.5, 14.51–24.59 (Fig. 2i). The Topographic Position Index (TPI), derived in SAGA GIS 2.1.4 (Conrad et al., 2015) from DEM, is a flash-flood conditioning factor used to compare the altitude of a point with the mean altitude of the neighbouring surface (Costache, 2019b). The positive values of TPI indicate a higher altitude for that specific point comparing to the adjacent areas (Mieza et al., 2016). It should be mentioned that, within the SAGA GIS 2.1.4, there exists a dedicated tool for TPI computation which was used also in the present research. Along with the input data represented by the DEM at 30 m cell size, the TPI computation required the establishment of a neighbourhood size. Given the fact that in the present study is analysed the susceptibility to flash-floods which requires a high detailed representation of relief landforms, a circular neighbourhood with a small radius should be selected (Skentos, 2018). Therefore, in order to take into account, the first cells located near the cell on which the TPI is calculated a radius of 65 m was selected. It should be mentioned that the radius is calculated from the centre of cell on which the TPI is calculated. The classification of TPI values was done through the Natural Breaks method as following: (−20)–(−3.8), (−3.7)–(−1.1), (−1.1)–1.3, 1.4–4.5, 4.6–20 (Fig. 2h). The *Natural Breaks* method was used to classify the values of L-S Factor, TWI, and TPI flash-flood predictors because it is considered a clustering method that creates one of the best arrangement of values into different classes and determines the minimization of variance for objects from the chosen subsets and maximization of variance between the subsets (Rosati et al., 2010). Another morphometric index used as causative factor for flash-flood phenomena is the Profile Curvature. The values of this variable allow to differentiate the surfaces characterized by accelerated runoff from those with a decelerated runoff. The negative values represent the areas characterized by an accelerated runoff while the positive values indicate the surfaces with a decelerated runoff. The Profile curvature raster was obtained based on DEM which was used as input data in *Curvature* tool from Spatial Analyst extension of ArcGIS 10.5 software. The profile curvature map was created by dividing its values into three classes according to the literature (Minea, 2013): (−3)–0, 0.1–0.9, 1–2 (Fig. 2j). Given the fact that through its values the areas with a high degree of drainage convergence are identified, Convergence index is a very important flash-flood causative factor (Costache and Bui, 2019). Due to

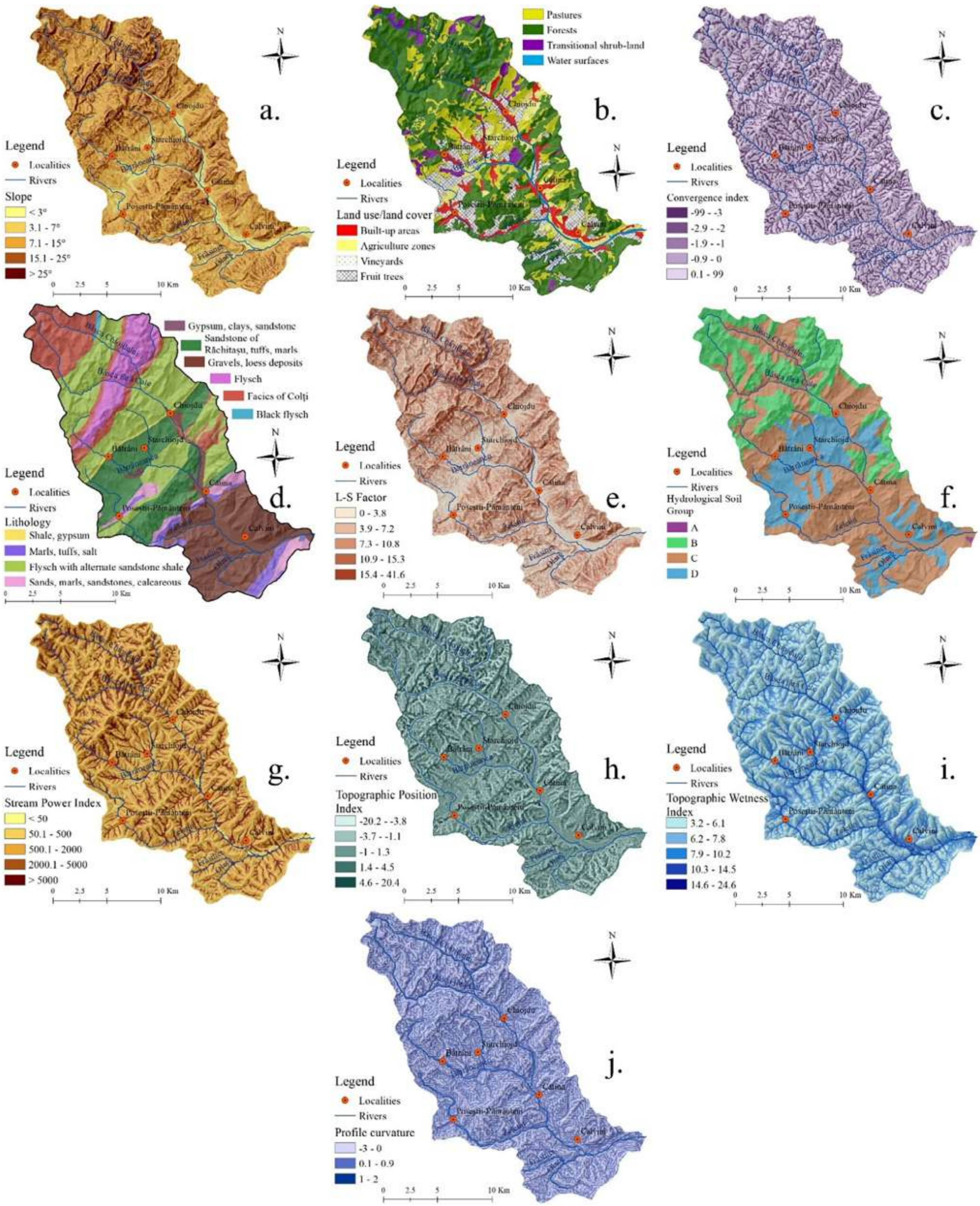

Fig. 2. Flash-flood conditioning factors (a. slope, b. land use/land cover, c. convergence index, d. lithology, e. L-S Factor, f. hydrological soil group, g. Stream Power Index, h. Topographic Position Index, i. Topographic Wetness Index, j. Profile Curvature).

the low concentration time of the runoff, the areas highlighted by negative values of Convergence Index, are the most favourable to flash-flood phenomenon. In fact, the negative values of Convergence Index indicate the presence of the valleys, while the positive ones indicate the presence of the interfluvial areas. As in the case of L-S Factor and TWI, the Convergence Index was derived in SAGA GIS

2.1.4. with the help of *Basic Terrain Analysis* module in which the DEM was the only input data. The classes of Convergence Index were established according to the literature (Costache et al., 2019): (−99)–(−3), (−2.9)–(−2), (−1.9)–(−1), (−0.9)–0, 0–99 (Fig. 2c). Stream Power Index (SPI), derived from DEM, highlights the capacity of the flowing water to transport the sediments along a river valley (Moore et al., 1991). Its computation is based on the following formula:

$$SPI = \alpha \times \tan\beta \tag{3}$$

where α represents the total up slope region draining through a point (per unit contour length) and tan β represents the slope angle value measured at the point. As in the case of TWI factor, the SPI values were determined by implementing the Eq. (3) in Map Algebra of ArcGIS software. The upslope region (α) and slope value (β) are the same parameters as in the case of TWI. SPI values were divided into the following classes: <50, 50–500, 501–2000, 2001–5000, >5000 (Fig. 2g). Due to its influence on the runoff velocity, land use/land cover, extracted in the present case from Corine Land Cover, 2018 dataset (Kucsicsa et al., 2019), is considered a very important flash-flood causative factor (Wang et al., 2019b; Tien Bui et al., 2020). Thus, the built-up areas are the most favourable to runoff occurrence, while the forest areas are the most restrictive. Across the research zone the following 8 land use category were identified: built-up areas, agriculture zones, vineyards, fruit trees, pastures, forests, transitional shrub-land, and water bodies (Fig. 2b). Hydrological soil group is a geographical factor that controls the water infiltration process (Costache, 2019c). In order to establish the hydrological groups in a first step the soil texture was extracted from the Digital Soil Map of Romania, 1:200,000. Further was realized the association between the soil texture and the hydrological soil group according to (Chendeş, 2011). In terms of Bâsca Chiojdului river basin, all the 4 hydrological soil groups are present (Fig. 2f). Another factor that exerts an important influence on water infiltration process is the lithology. Within the research area a number of 10 lithological groups were mapped (Fig. 2d).

In order to be employed in the present workflows, the following flash-floods conditioning factors were transformed from a polygon vector format to a raster format with the cell size of 30 m: land use/land cover, hydrological soil group and lithology.

2.1.3. Inventory of the surfaces affected by torrential phenomena and creation of training and validating dataset

The detection and mapping of the surfaces affected by torrentiality in Bâsca Chiojdului Catchment was the first stage of the present study. The usefulness of integrating this information in the present research is explained by the fact that flash-floods are more likely to produce in the areas with similar features as those where have already occurred. Further, it is necessary to understand the spatial relationship between the presence of torrential processes and flash-flood predictors. Therefore, the areas affected by torrentiality were digitized based on aerial imagery and field measurements. Were considered the surfaces with a unified presence of the torrential microforms such as ravines and gullies (Costache and Zaharia, 2017). After this step, a number of 36 polygons, with a total area of approximately 34 km^2, were identified as affected by torrentiality. These surfaces accounts for 10% of the study area. 70% of the total digitized areas were used as training dataset, while 30% were used to validate the results. In order to divide these areas into training and validating dataset the *Generate Subset Polygons* tool from ArcGIS Pro 2.2 was used. In order to be used in the present study, the surfaces affected by torrential phenomena were transformed from polygon shapefile format to raster with a cell size of 30 m. This spatial resolution was chosen because it is equal to the cell size of the Digital Elevation Model (DEM) extracted from Shuttle Radar Topography Mission (SRTM) database (Mamede da Silva et al., 2018). The DEM represents the data source for a number of 7 morphometric factors taken into account in the present analysis which were presented at 2.1.2. Therefore, a total number of 37,723 pixels were identified as being affected by torrential phenomena. Further, a number of 26,406 pixels were included in training data, and the other 11,317 were included in validating data set. Due to the fact that the flash-flood potential mapping is based on a binary classification of pixels, another dataset, representing the areas not affected by torrential phenomena, was created. This data set contains the same number of pixels (37,723) as torrential areas dataset and was created through a random selection of pixels located in general on surfaces with a low slope angle, close to 0°, where the surface runoff is almost impossible. It should be mentioned that the non-torrential dataset was divided also in training (70%) and validating samples (30%). Due to the fact that training and validating areas will be used as a binary dataset, value 1 was assigned to regions with torrential processes, while the value 0 was assigned to areas characterized by the absence of torrential phenomena.

2.2. Methods used

In order to estimate the flash-flood susceptibility for Bâsca Chiojdului catchment the collected data, presented above, were included in many methodological processing steps. The scheme of the entire methodological workflow is graphically represented in Fig. 3.

2.2.1. Variance inflation (VIF) and tolerance (TOL) for multicollinearity assessment

In this study, multi-collinearity analysis was used to evaluate the inter-associations or correlation between the flash-flood predictors. Multi-collinearity occurs when the predictors have a high correlation with each other. It can causes the mistake description of relevant factors in the statistical models and thus can affects the models' results (Dou et al., 2019). Therefore, the variance inflation factor (VIF) and tolerance (TOL) were used to detect the multicollinearity among the predictors in this study. This two indicators are commonly used for multi-collinearity examination (Dou et al., 2019; Garosi et al., 2019; Wang et al., 2019a). Let X = {$X_1, X_2, \ldots, X_N$} define independent predictors and R_j^2 indicates the coefficient of determination when the jth independent predictor X_j is regressed on all other predictors in the model. The VIF is calculated as follows:

$$VIF = \frac{1}{1 - R_j^2} \tag{4}$$

If the VIF value >10 or the TOL value <0.1, the corresponding predictors are collinear and need be removed from the prediction models (Dou et al., 2019; Wang et al., 2019a).

2.2.2. Information Gain (IG) for feature selection

Due to the fact that certain geographical factors, from those taken into account for the present analysis, have a low influence on surface runoff, a selection of the flash-flood predictors, based on a statistical model, was realized. Information Gain (IG) is one of the most popular method in this type of research (Dai and Ji, 2014; Gao et al., 2017; Javidi and Mansoury, 2017) and, therefore, was also used in the present study. IG method, proposed by Hunt et al. (1966), is very useful in order to assess an attribute of quality. The value of IG for each flash-flood predictor, was estimated using the following formula (6) (Chen et al., 2018):

$$IG(Y_i X_i) = H(Y) - H(Y|X_i) \tag{5}$$

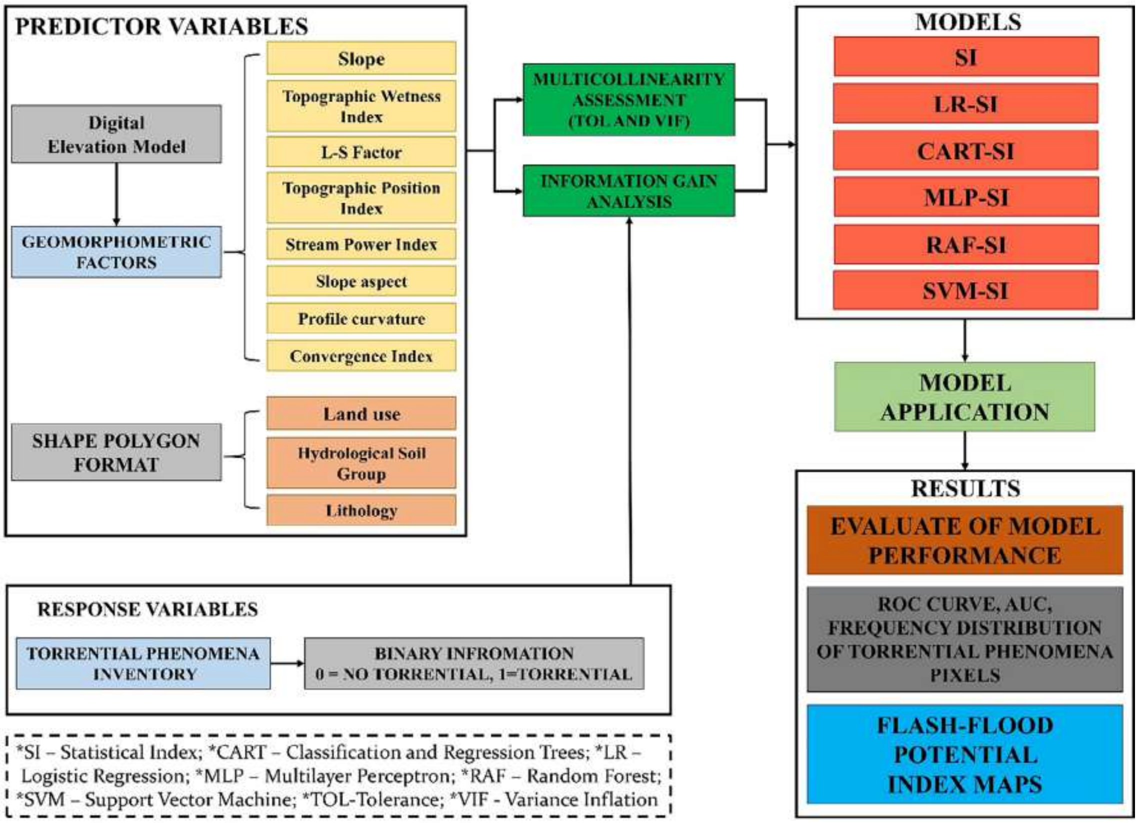

Fig. 3. The scheme of the workflow implemented for Flash-Flood Potential calculation.

where *H(Y)* is the entropy value of *Yi* and *H(Y|Xi)* is the entropy of *Y* after associating the values of the flash-flood conditioning factor *Xi* (Chen et al., 2018).

In a first step, the calculation of IG values assumed the preparation of the data regarding the presence and absence of the torrential phenomena in the ArcGIS 10.5 software. The data was processed in the same attribute table, along with the data regarding the conditioning factors. Subsequently, the resulting attribute table was processed in Microsoft Excel 2016 software. These data was further imported in WEKA v. 3.9.2 software developed by The University of Waikato, Hamilton, New Zeeland (Hall et al., 2009). Using this software, dedicated mainly to machine learning applications, IG values for each flash-floods conditioning factor were calculated.

2.2.3. Statistical index (SI)

This method was used for the first time in a research regarding natural risks by (van Westen, 1997). In this method, the weight of a class or category of factor in the final result (FFPI SI) considered to be the natural logarithm of the density of the torrential phenomena within that class or category of factor divided by the density of the torrential phenomena throughout the entire study area (Rautela and Lakhera, 2000). Statistical Index weights for each class/category of factors were calculated by using the following formula, by Van Westen et al. (1997):

$$W_{ij} = \ln\left(\frac{f_{ij}}{f}\right) = \ln\left(\frac{\frac{Npix(S_i)}{Npix(N_i)}}{\frac{\sum Npix(S_i)}{\sum Npix(N_i)}}\right) \tag{6}$$

where: W_{ij} – is the weight given to a certain class/category *i* of parameter *j*; f_{ij} – is the torrential pixels density within the class *i* of parameter *j*, *f* – is the torrential pixels density within the entire map, *Npix(Si)* is the number of torrential pixels in parameter class i, and *Npix(Ni)* is the total number of pixels in the same parameter class.

In order to apply the Statistical Index Model, a workflow that involved the use of ArcGIS 10.5 software as well as Microsoft Excel 2016 software, was developed. Therefore, in a first step, the rasters corresponding to flash-flood conditioning factors and the surfaces with torrential processes, were imported in GIS environment. Further, in order to quantify the number of torrential pixels within each class/category of factor, each raster corresponding to a single flash-flood conditioning factor was combined with the raster corresponding to the regions with torrential processes. After this step, in order to determine the final weights of a class/category of factors, the data were processed in Microsoft Excel 2016. The weights already obtained were assigned to each factor class/category in ArcGIS 10.5 software. Once the weight values were assigned to each class/category, the FFPISI was computed through the sum operation implemented in Map Algebra. Positive weights highlight a class/category that is favourable to flash-flood phenomenon, while a negative weight value highlights a class/category that reduces the potential of flash-flood occurrence.

2.2.4. Logistic regression (LR)

The main aim of the logistic regression method is to determine the best fitting model which describes the relationship between the dependent binary variable (Y) and a set of independent (explanatory) variables (Kavzoglu et al., 2014; Lee and Pradhan, 2007; Pradhan, 2010; Pradhan and Lee, 2010). In the logistic regression model, a dependent variable is formed only by two classes / categories (presence and absence). Therefore, the logistic regression model is mainly useful to predict the presence or the absence of a certain phenomenon, prediction based on the values of the independent variables and also based on the relationship between the dependent and independent variables. The variables considered in the Logistic Regression model could be continuous, discrete or a combination of both.

The generalized linear model of the logistic regression method can be calculated by using the following equation (Bui et al., 2011; Kavzoglu et al., 2014; Pradhan, 2011):

$$p = \frac{1}{1 + e^{-Z}} \tag{7}$$

where p is the probability of an event, Z is a value from $-\infty$ to $+\infty$, defined by the following equation:

$$Z = \beta_0 + \beta_1 x_1 + \beta_2 x_2 + \cdots + \beta_n x_n \tag{8}$$

where b_0 is the intercept of the model, the β_i (i = 0, 1, 2, ..., n) are the slope coefficients of the logistic regression model, and the x_i (i = 0, 1, 2, ..., n) are the independent variables.

When predictor variables are highly correlated in a logistic model, it can be assumed that there exists a multicollinearity between independent variables (Midi et al., 2010). The multicollinearity can cause inaccurate estimates and may also affect the hypothesis tests and the confidence intervals (Midi et al., 2010). In the present paper, the multicollinearity diagnosis between independent variables will be assessed according to the procedure described at 2.2.1.

2.2.5. Classification and regression tree (CART)

The machine learning technique was used especially in studies regarding landslide susceptibility (Felicísimo et al., 2013; Hong et al., 2015; Pradhan, 2013; Yeon et al., 2010; Youssef et al., 2016). CART is a method based on rules that presents the information in an intuitive and easy to visualize way. Three types of independent variables could be included into the analysis (number, binary and categorical), this fact being another advantage of this technique. In order to construct the trees, each predictor is selected so as to reduce data errors. The measure to which a predictor is preferred in relation to another is the entropy value.

A missing value of a particular predictor will not be used to determine the optimal ramification of a tree. If CART is used to predict new data, missing values are handled by substitutes (surrogates) (Breiman et al., 1984). The predicted values of a terminal node represent the average of the response values in that node (Breiman et al., 1984). In CART algorithm, there is an optimal sampling rule named modified towing that is based on a direct comparison of target attribute in two child nodes. This process is performed according to the Eq. (9):

$$I(Split) = \left[0.25(q(1-q))^u \sum_k |PL(k) - PR(k)|\right]^2 \tag{9}$$

where: k is the index of the target classes, PL(k) and PR(k) represent the probability distributions of the target in the left and right child nodes, respectively, and the power term u embeds a user-trollable penalty on splits that create child nodes with unequal sizes (Wu et al., 2008).

The result of CART algorithm is a complex decision tree that needs to be pruned in order to keep only the most important information.

2.2.6. Multilayer perceptron (MLP)

MLP is one of the most commonly used artificial neural networks. It is an effective technique that could capture the complex non-linear relationship between predictors and a specific phenomenon (Jahani and Mohammadi, 2019). This model has been used in many fields like spatial prediction of flood (Costache and Bui, 2019) and landslide susceptibility assessment (Pham et al., 2017). Through the back-propagation algorithm weights of feed-forward network structure are updated and optimized (Costache and Bui, 2019). Therefore it can be distinguished a forward training stage and backward training stage (Costache and Bui, 2019). In the forward stage, the inputs are propagated forward through the hidden layer to compute the output classes which are compared to the observed values in order to estimate the difference between them. In the backward stage, the connection weights were adjusted in order to improve the output with the root mean square error (RMSE, Eq. (10)) (Pham et al., 2017). In order to achieve an acceptable value of RMSE the process already described will be iteratively repeated.

$$RMSE = \sqrt{\frac{1}{n}\sum_{i=1}^{n}(c_i - \hat{c}_i)^2} \tag{10}$$

where n is the number of the torrential pixels, c_i and $\hat{c}_i$ are the observed flash-flood potential values and the computed flash-flood potential values, respectively.

2.2.7. Random forest (RAF)

Random forests (RAF), developed by Breiman (2001), are very flexible and powerful ensemble learning method based on decision trees which can be used for both classification and prediction. Recently, RAF was applied in different areas to solve classification problems (Ibarra-Berastegi et al., 2011; Arabameri et al., 2019; Dou et al., 2019; Pham et al., 2019a,b; Woznicki et al., 2019).

RAF can be defined as a bunch of random trees (decision trees). The RAF is based on the fundamental idea to grow several decision trees on random subsets in the following steps: i) take the training data and re-sample the data several times; ii) select a set of random features for each re-sample; iii) determine a decision tree for the given re-sample and a random set of features; iv) aggregate the set of determined decision trees to get a single decision tree. Each decision tree contributing one vote, then the class which received the most votes is the final prediction class (Woznicki et al., 2019). In this study, RF was implemented to categorize two classes including the value of "0″ which was assigned to areas characterized by the absence of torrential phenomena, and the value of "1" which was assigned to regions with torrential processes.

2.2.8. Support vector machine (SVM)

The SVM is a machine learning method based on the principle of the structural risk minimization from statistical learning theory. In a binary classification, the main objective of the SVM algorithm is to find a hyper-plane which can divide the training data in an optimally manner. The hyper-plane is constructed by transforming the original input space into a higher-dimensional feature space (Naghibi et al., 2017). Once the optimal hyper-plane is delineated, the support vectors located closest to the hyper-plane can be identified (Pham et al., 2019a,b). Having the support vectors identified and the optimal hyper-plane defined, a specific kernel function will be employed to transform the input data into two distinct classes (Choubin et al., 2019). According to Naghibi et al. (2017), if the points of the classes are located above the hyper-plane they will be classified as positives (torrential pixels = 1), while if they are located below the hyper-plane the points will be classified as negatives (non-torrential pixels = -1). In terms of kernel function, in the present research the Radial Basis Function will be employed because it outperforms others kernel function suc as: linear, polynomial and sigmoid (Choubin et al., 2019; Tien Bui et al., 2012).

2.3. Configuration of hybrid models for FFPI computation

In order to configure the five hybrid models used for FFPI computation the SI coefficients determined following the procedure described at 2.2.3. were used as input data in the machine learning models. According to the literature (Cherukuri et al., 2019), the data used as input in machine learning algorithms should be rescaled in the same range of values. Therefore, the SI coefficients were normalized between 0.1 and 0.9 by using the following equation (Costache, 2019a):

$$y = \frac{(x - min(d)) * (max(n) - min(n))}{max(d) - min(d)} + min(n) \quad (11)$$

where: y – standardized value of x; x – current value of variable; d-range value limits; n – standardization range limits.

It is important also to mention that the training sample, which represents 70% of the total torrential areas, was further split into another training sample (70%) used to run the models, and a testing sample used to test the performances of the models (30%). Thus the new training sample will contain 18,482 torrential pixels and 18,482 non-torrential pixels, while the testing sample will contain 7922 torrential pixels and 7922 non-torrential pixels.

2.3.1. LR-SI

In the present analysis, the areas with presence/absence of torrential phenomena, across Bâsca Chiojdului river basin, represent the binary variable. In order to be included in the analysis, the value of 1 was assigned to the areas affected by torrential phenomena, and the value of 0 was assigned to areas without torrential phenomena. Further, the next step of the analysis consisted of the combination of each raster representing flash-flood conditioning factors, having SI coefficient assigned, with the raster representing presence or absence of torrential phenomena. The resulted data in tabular format was further used in SPSS software where logistic regression analysis was carried out. A very important parameter used in the Logistic Regression (LR) modelling is the classification cut-off value which usually is set to 0.5 by default. Though, in the present analysis, in order to establish the best cut-off value, the LR modelling was repeated by using a number of eleven cut-off values (0.01, 0.1, 0.2, 0.3, 0.4, 0.5, 0.6, 0.7, 0.8, 0.9 and 0.99) according to the literature (Soureshjani and Kimiagari, 2013). Finally, will be chosen the cut-off value which allows the achievement of the best performances demonstrated by the highest value of sum between Specificity and Sensitivity of the model. Additionally, in order to assess the significance of input data, the quality of the applied model and also to analyse the overdispersion, the following parameters were also computed: standard error (S.E.), Wald x^2 with p-value, residual deviance (RD), degree of freedom (DF) and Akaike Information Criteria (AIC). Specifically, the presence of overdispersion, which may affect the logistic regression results, is indicated by a high difference between RD with DF values (Aitkin, 1996). The final weight of each independent variable will be equal to the logistic regression coefficients (βi) value. According to Eq. (9), Z values of each raster cell will be derived in GIS environment by summing the constant value of the intercept of the model (β_0), and the rasters of flash-flood predictors (x_i), each of them being multiplied with (β_i) coefficient. It should be taken into account that the rasters of flash-flood predictors will have assigned the SI values. Further, in order to derive the FFPI values in map algebra, the raster having the values of cells equal to Z, will be used in Eq. (8).

2.3.2. CART-SI

The construction of decision tree trough CART algorithm was possible by using the input data represented by SI coefficients and absence/presence of torrential areas in Salford Predictive Modeler v 8.2 software (Fitriani and Siahaan, 2016). Some specific parameters, used to train the CART model, has been optimized after a trial process through which the best values of AUC was determined. The optimization of the parameters was performed with the help of testing sample which accounts a number of 15,844 pixels. Thus, the minimum cases of parent nodes was established at 28, the number of minimum cases of terminal nodes was set at 13, the sample size is equal to the number of torrential and non-torrential pixels in training data (approximately 37,000), and the tree depth was automatically established by the software after the application of the aforementioned parameters.

2.3.3. MLP-SI

The SI coefficients were also used as input data in Multilayer Perceptron (MLP) model which was run in SPSS 21 software. In the present case the architecture of MLP-SI ensemble consists of the following elements: i) one input layer which includes eight neurons represented by the flash-flood predictors; ii) one hidden layer with a specific number of neurons; iii) one output layers with 2 neurons represented by the presence and absence of torrential phenomena. A very important step in the configuration and training MLP-SI ensemble is the establishment of the optimum number of hidden neurons within hidden layer. According to (Sheela and Deepa, 2013), most of the researchers used a trial-error process in order to select the optimum number of hidden neurons. Therefore, in the present case was selected the number of hidden neurons which determined the achievement of the lowest Root Mean Square Error (RMSE).

The lowest error indicates the highest stability of the model, while a higher error highlights a worst stability (Sheela and Deepa, 2013).

2.3.4. RAF-SI

Like in the case of the three ensembles analysed above, the computed SI values were used as input data in RAF model. The RAF-SI ensemble was run with the help of *Forest-based Classification and Regression* tool from ArcGIS Pro 2.2 software. A very important output of the RAF modelling process is the out-of-bag (OOB) error which is directly related with the stability and the accuracy of the model. The OOB error is calculated by using the cases that were unselected by the RAF algorithm during the random selection of training data set (Trigila et al., 2015). In order to reach the minimum OOB error the RAF model was automatically run in ArcGIS Pro 2.2 software for 300 times with a number of trees from 1 to 300. Finally, for FFPI computation was selected the RAF model characterized by the minimum OBB error with a minimum trees number. The model outputs contain also the importance of each flash-flood predictor in terms of FFPI computation. It should be mentioned that the final raster of FFPI was automatically derived in ArcGIS Pro 2.2 software, without applying an additional weighted sum in Map Algebra.

2.3.5. SVM-SI

The SVM-SI ensemble was implemented by using the SI coefficients as input data in SVM model, together with the pixels representing the torrential and non-torrential areas. The configuration and training of SVM-SI was carried out through Weka 9.3 software where the data obtained from GIS workflows was processed. An essential step in the application of SVM model with Radial Basis Function (RBF) is represented by the selection of penalty parameter C and γ term. The values of these indicators have a crucial influence on the accuracy of the model because they prevent the model's over-fitting (C penalty) and the degree of nonlinearity (γ term). In order to optimize the values of the two parameters a cross-validation procedure was applied. Thus, many pairs (C, γ) were tested until the best accuracy of the model was achieved. Finally, for C parameter a value of 2.1 was attributed, while the optimum value of γ term was established at 0.12.

2.4. Models performance assessment and results validation

The models performance assessment represents an essential step within the workflow developed in order to identify areas susceptible to flash-floods (Chen et al., 2017).

2.4.1. Statistical measures

In order to test the performances of the applied models the following statistical metrics will be used: specificity, sensitivity, accuracy, kappa index. These statistical indices can be determined using the following relations:

$$k = \frac{p_o - p_e}{1 - p_e} \tag{12}$$

$$Sensitivity = \frac{TP}{TP + FN} \tag{13}$$

$$Specificity = \frac{TN}{FP + TN} \tag{14}$$

$$Accuracy = \frac{TP + TN}{TP + FP + TN + FN} \tag{15}$$

where FP (false positive) and FN (false negative) are the numbers of pixels erroneously classified; k is kappa coefficient, p_o is the observed torrential pixels, and p_e is the estimated torrential pixels.

2.4.2. ROC curve

ROC Curve and Area Under Curve (AUC) represent the second method used in order to validate the results and to test the model performance. Area Under Curve (AUC) is the most important indicator of ROC Curve. Its value is sub-unitary and highlights the performance degree of the applied models. The closer value gets to 1, the better the model is. Training areas pixels were used in order to construct the success rate, meanwhile validating areas pixels are used to construct prediction rate. Success rate shows how well the results match the training areas, while the prediction accuracy of the models was assessed through the prediction rate. By using the number of pixels representing the areas affected by torrentiality, and the calculated values of FFPI, ROC Curve was constructed. In order to assess the ability of the models to predict the presence or the absence of flash-flood potential, the Area Under Curve (AUC) values were used. The AUC can be calculated as follows:

$$AUC = \frac{(\sum TP + \sum TN)}{(P + N)} \tag{16}$$

where TP (true positive) and TN (true negative) are the number of pixels that are correctly classified, P is the total number of pixels with torrential phenomena and N is the total number of pixels without torrential phenomena.

3. Results

3.1. Multicollinearity assessment and feature selection

The results obtained after the modelling in SPSS 21 software show that the TOL values for the independent variables considered for this study, are within the range between 0.459 (TWI) and 0.923 (Land use/land cover). In terms of VIF values, it can be noted a range between 1.01 (TPI) and 3.332 (Convergence Index) (Table 1). Following the analysis of the VIF and TOL values, there are no serious multi-collinearity conditions between the variables. Further the predictive ability of the flash-flood conditioning factors was tested.

The computed Information Gain (IG) values offer some useful information regarding the influence that flash-floods conditioning factors have on flash-floods phenomena. The highest value (IG = 0.0775) was assigned to slope relief factor (Table 1). Thus, according to the IG analysis, the slope relief has the highest importance on flash-flood occurrence process. On the second position is the land use/land cover (IG = 0.0564), followed by L-S Factor (IG = 0.0491), topographic wetness index (TWI) (IG = 0.0441), topographic position index (TPI) (IG = 0.0391), hydrological soil group (IG = 0.0379), lithology (IG = 0.0334) and convergence index (IG = 0.0290). On the last two position, with IG = 0, are profile curvature and aspect. It should be noted that even if the morphometric factors have as data source the Digital Elevation Model, their IG values are different. The main explanation is that the IG values are estimated based on the spatial relationships between the values of each flash-flood conditioning factor and the presence/absence of the torrential areas. Due to the fact that the last two factors, with IG = 0, have no predictive ability in terms of flash-floods occurrence process, these will be removed from the analysis.

Table 1
The predictive ability and multicollinearity analysis for independent variables.

Factor	TOL	VIF	IG
Slope	0.463	2.083	0.0775
TPI	0.595	1.010	0.0391
TWI	0.459	3.272	0.0441
Land use/land cover	0.923	1.045	0.0564
Lithology	0.894	1.118	0.0334
Convergence index	0.515	3.332	0.0290
L-S Factor	0.489	2.875	0.0491
Hydrological Soil Groups	0.849	1.177	0.0379
Aspect	0.721	2.561	0
Profile curvature	0.612	1.813	0

3.2. Statistical index computation

The weight values corresponding to the statistical index coefficients were assigned to each class/category of flash-flood conditioning factors considered for the analysis. For the slope relief factor, weights values range from −1.17 (slope class between 0–3°) and 0.5 (slope class >25°). Regarding TPI factor, the highest value of Statistical Index weights was 0.32, being assigned to the range class between 4.6 and 20. The middle-class interval of TWI (7.79–10.21) contains the highest value of SI weight (0.12). Land use/land cover category represented by built-up areas has the highest SI weight value (3.09) from the entire data set used in the present study (Table 2). Regarding land-use, it can be noted that with the decrease of the Manning roughness coefficients, the SI weight values increase for each category. This relationship between Manning roughness coefficients and SI weight value could be explained by the fact that flash-flood occurrence is more likely on the surfaces with lower roughness coefficient, such as built-up areas. From the lithology point of view, the highest SI weight was assigned to Sandstone of Rachitașu, the hardest rock in the study area. The L-S Factor values are directly proportional to the SI weight values, while regarding the convergence index situation is inverse. Thus, the highest values of SI weights are assigned to convergence index negative values located in river valleys areas. Regarding the hydrologic soil groups, the lowest value of SI weight value (−0.64) was assigned to class C, while the highest value is specific to class D.

Table 2 Normalized SI values and weights of flash-floods conditioning factors.

3.3. Performances of the modelling process

After the calculation of Statistical Index coefficients, the normalized values corresponding to each factor class/category were

Table 2
Normalized classes of flash-floods conditioning factors used.

Factor	Class	*Pp (%)	*Pt(%)	SI	SI_N	LR-SI (β_i)	CART-SI	MLP-SI	RAF-SI	SVM-SI
Slope	0–3°	5.84	1.80	−1.17	0.10	3.06	0.18	0.23	0.2	0.25
	3.1–7°	14.38	14.22	−0.01	0.66					
	7.1–15°	47.99	58.09	0.19	0.75					
	15.1–25°	28.52	23.91	−0.17	0.58					
	>25°	3.27	1.99	0.5	0.90					
TPI	(−20)–(−3.8)	18.19	19.31	0.05	0.28	0.37	0.07	0.11	0.08	0.06
	(−3.7)–(−1.1)	23.65	22.92	−0.03	0.10					
	(−1)–1.3	26.39	19.40	0.3	0.85					
	1.4–4.5	21.07	23.56	0.11	0.42					
	4.6–20	10.70	14.81	0.32	0.90					
TWI	3.15–6.1	12.78	13.09	0.02	0.73	1.63	0.09	0.1	0.11	0.12
	6.11–7.78	28.43	30.58	0.07	0.82					
	7.79–10.21	24.81	28.01	0.12	0.90					
	10.22–14.5	22.08	20.07	−0.09	0.55					
	14.51–24.59	11.90	8.25	−0.36	0.10					
Landuse	Forest	49.46	27.48	−0.5	0.36	2.69	0.21	0.17	0.23	0.18
	Fruit trees, Shrub	21.35	24.98	0.15	0.46					
	Agricole areas, Vineyards	6.95	0.73	−2.2	0.10					
	Pastures	15.81	46.53	1.07	0.59					
	Built areas	6.42	0.29	3.09	0.90					
Lithology	Sands, Gravels, Loess	5.65	2.32	−0.88	0.10	1.01	0.16	0.12	0.13	0.15
	Marls, clay	29.80	18.13	−0.49	0.23					
	Gypsum, Limestone	38.57	49.14	0.24	0.46					
	Sandstone, Tuffs, Schysts	22.17	29.65	0.29	0.48					
	Sandstone of Rachitașu	3.80	0.71	1.6	0.90					
L-S Factor	0–3.75	21.85	14.91	−0.3	0.10	1.73	0.11	0.13	0.09	0.08
	3.76–7.17	29.74	37.42	0.22	0.73					
	7.18–10.76	26.30	30.12	0.13	0.62					
	10.77–15.33	16.63	13.76	−0.18	0.25					
	15.34–41.59	5.47	3.79	0.36	0.90					
Convergence index	0.1–99	16.84	13.62	−0.21	0.10	−0.46	0.03	0.05	0.04	0.06
	(−0.9)–0	46.20	44.34	−0.04	0.49					
	(−1.9)–(−1)	9.62	10.50	0.08	0.76					
	(−2.9)–(−2)	7.14	8.27	0.14	0.90					
	(−99)–(−3)	20.21	23.28	0.14	0.90					
Hydrological soil groups	A	0.08	0.00	0.19	0.50	2.48	0.15	0.09	0.12	0.1
	B	25.32	30.71	0.11	0.46					
	C	52.40	58.59	−0.64	0.10					
	D	22.20	10.70	1.03	0.90					

* Pp(%) – percentage of class pixels; Pt(%) – percentage of torrential pixels.

used in order to train the five hybrid models proposed for the computation of flash-flood potential within Bâsca Chiojdului catchment. The performances of the five hybrid models were assessed through several statistical measures for both training and testing sample. In terms of *Sensitivity* the MLP-SI hybrid model achieved the highest value for both training (91.7%) and validating sample (89.9%), while the SVM-SI hybrid model obtained the lowest performances for training areas (88.1%) and LR-SI for validating areas (87.2%) samples (Table 3). If we discussed about the *Specificity*, we can observe that the MLP-SI obtained the highest performances, 93.1% for training areas and 93.2% for validating sample, while the RAF-SI has the lowest performance in terms of training areas (89.4%) and LR-SI has the lowest performance in terms of validating areas (89.3%). The *Accuracy* indicator revealed that the MLP-SI has the highest values for training (92.4%) and validating (91.5%) areas, while the lowest performances were achieved by SVM-SI for training sample (89%) and LR-SI for validating sample (88.2%). Regarding the Kappa index, it can be observed that the highest val-

Table 3
Statistical measures values.

Metrics	Training sample					Testing sample				
	LR-SI	CART-SI	MLP-SI	RAF-SI	SVM-SI	LR-SI	CART-SI	MLP-SI	RAF-SI	SVM-SI
TP	16,906	17,061	17,234	16,514	16,696	7095	7240	7400	7316	7165
TN	16,408	16,680	16,913	16,613	16,220	6882	7050	7095	6960	6966
FP	1576	1421	1248	1968	1786	824	682	521	606	757
FN	2074	1802	1569	1870	2262	1040	872	827	962	956
PPV (%)	91.5	92.3	93.2	89.4	90.3	89.6	91.4	93.4	92.4	90.4
NPV (%)	88.8	90.3	91.5	89.9	87.8	86.9	89.0	89.6	87.9	87.9
Sensitivity (%)	89.1	90.4	91.7	89.8	88.1	87.2	89.3	89.9	88.4	88.2
Specificity (%)	91.2	92.2	93.1	89.4	90.1	89.3	91.2	93.2	92.0	90.2
Accuracy (%)	90.1	91.3	92.4	89.6	89.0	88.2	90.2	91.5	90.1	89.2
Kappa	0.803	0.826	0.848	0.792	0.781	0.764	0.804	0.830	0.802	0.784
AUC	0.915	0.929	0.942	0.903	0.894	0.889	0.913	0.928	0.904	0.897

ues for training (0.848) and for validating (0.83) samples were assigned to MLP-SI, while the lowest values were attributed to SVM-SI for training areas (0.781) and to LR-SI for validating areas (0.764). The same situation is present also in the case of AUC values, with MLP-SI being the most performant model and SVM-SI and LR-SI having the lowest performances.

Overall, we can state that all the models obtained very good performances in terms of statistical measures.

3.4. Flash-flood potential Index mapping

Once established that all the models obtained very good results, as well as the fact that the results are statistically significantly different, the Flash-flood Potential Index was determined by means of the mentioned models.

3.4.1. Statistical Index stand-alone model

After assigning SI weight values for each class/category of flash-flood conditioning factor, the resulted rasters were summed up in ArcGIS 10.5 software, so the FFPI SI was obtained. FFPI SI values ranging between −1.72 and 7.63 were normalized between 0.1 and 0.9 in order to have the same range as the results provided by the other models. Further these values were classified in five intervals using the following 4 classification methods available in ArcGIS software: *Natural Breaks, Quantile, Equal Intervals* and *Geometrical Intervals.* In order to establish the best classification method, the frequency of all torrential pixels was determined for each of the five classes. In this regard, will be taken into account the percentage of torrential pixels located in the Very High class. The highest percentage of torrential pixels within the very high class the better the classification method is. In case of SI model, the highest percentage of torrential pixels in the fifth class of FFPI was established for the classification performed through *Natural Breaks* method (62.32%), followed by *Geometrical Intervals* (58.43%), *Quantile* (53.75%) and *Equal Intervals* (50.23%) (Fig. S1a). Therefore, for the classification of FFPI-SI values in the final map, the *Natural Breaks* method was selected (Fig. 4a). Very low values of FFPI SI cover approximately 14.1% of the Bâsca Chiojdului river basin. These areas have a relatively homogeneous distribution across the study area, excepting the central part where they are absent. Low FFPI SI values cover approximately 27% of the study area. Medium FFPI SI values are spread relatively uniformly throughout the Bâsca Chiojdului River basin, and are spread on approximately 27.3% of Bâsca Chiojdului River basin. Approximately 20% of study area is covered with high FFPI SI values, while very high values are extended on 10.7%. High and very high values of flash-flood potential are specific to the central part of Bâsca Chiojdului River basin especially.

3.4.2. LR-SI hybrid model

As was mentioned at 2.3.1, the best cut-off value used in the final LR-SI model was established after the repeated application of LR modelling with eleven different values between 0.01 and 0.99. According to the results provided in Table S1, the highest sum of Sensitivity (89.1) and Specificity (91.2) was obtained by using a cut-off value equal to 0.7. Therefore, this cut-off was used in order to perform the LR-SI model. In order to investigate the statistical significance of the flash-floods conditioning factors, the Wald x^2 statistical test, Residual Deviance (RD) and Akaike Information Criteria (AIC) were used (Table S2). The results of three aforementioned indicators revealed the fact that all the variables and factor categories have a significant contribution in the training of LR-SI ensemble (Table S2). The value of RD, estimated as a goodness-of-fit parameter for the logistic regression model, was compared with the degrees of freedom (DF) in order to analyse the overdispersion. According to the results, RD value of 1113.43 is very close to the DF value of 1106. Their ratio value of 1.006 is very close to 1. Therefore, we can state that no overdispersion was detected in the present case. Following the training of LR-SI hybrid model the intercept of the model (β_0 = 1.82) and the regression coefficients (β_i) were determined for each flash-flood conditioning factor (Table 2). If we analyse the values of regression coefficients (β_i) we can see that the highest value was assigned to slope angle (3.06), followed by land use (2.69), hydrological soil group (2.48), L-S Factor (1.73), twi (1.63), lithology (1.01), tpi (0.3) and convergence index (−0.46). In can be observed that seven predictors obtained positive values, while another one achieved a negative regression coefficient. Positive values highlight the fact that a certain flash-flood conditioning factor has a positive influence on flash-floods occurrence process, while negative values show restrictive conditions for flash-floods occurrence.

Finally, the FFPI LR-SI was computed by implementing the Eq. (8) in ArcGIS 10.5, according to the workflow described at 3.4.2.

After the computation of FFPI LR-SI, its values were normalized between 0.1 and 0.9. As in the case of FFPI-SI, the same four methods were used to classify the FFPI LR-SI values into five intervals. In terms of percentage of torrential pixels located in the very high class, the *Quantile* methods achieved the highest value (71.44%), followed by *Geometrical Intervals* (68.43%), *Natural Breaks* (66.33%), *Equal Intervals* (53.11%) (Fig. S1b). Therefore, the *Quantile* method was used to carry out the final FFPI LR-SI map (Fig. 4b). Very low values represent approximately 5.8% of Bâsca Chiojdului River Catchment and are especially located on interfluvial lines where surface runoff is less probably to occur (Fig. 4b). 23.6% of the study area is characterized by low flash-flood potential index values, these areas being relatively homogeneously distributed in the southern half of Bâsca Chiojdului River catchment. The largest areas are characterized by a medium potential for flash-flood occurrence. Medium values of FFPI LR cover approximately 44.3% of the study area. Due to the fact that high and very high FFPI LR values cover approximately 26.7% of the study area, Bâsca Chiojdului River catchment is considered to be very exposed to flash-flood phenomena.

3.4.3. CART-SI hybrid model

The result of the training process applied for CART-SI hybrid consisted of a very complex decision tree which was pruned in order to select that part containing the most important information (McKenney and Pedlar, 2003). Therefore, the tree whose terminal nodes have recorded the highest values of the success parameters, presented in Table 3, was selected.

The optimal pruned regression tree for the study area has a number of 11 terminal nodes (Fig. S2). As it can be noted, all flash-floods conditioning factors were considered in the decision tree construction process.

According to the scheme of the optimally pruned regression tree for the study area, the most important factor that influences flash-flood occurrence is the land use (0.21), followed by slope (0.18), lithology (0.16), hydrological soil groups (0.15), L-S factor (0.11), twi (0.09), tpi (0.07) and convergence index (0.03).

In order to determine the FFPI CART-SI values within the study area, the relative weights of flash-flood conditioning factors were used in GIS environment.

In terms of normalized values of FFPI CART-SI, the best classification was attributed to *Natural Breaks* method, with 73.21% of torrential pixels in the very high class, followed *Geometric Intervals* (69.31%), *Quantile* (68.43%) and *Equal Intervals* (54.4%) (Fig. S1c). In this case, the FFPI CART-SI values were mapped with the help of *Natural Breaks* method. Very low values of Flash-Flood Potential Index were estimated for approximately 5.5% of Bâsca Chiojdului River catchment (Fig. 4c). These are located especially within the interfluvial areas where runoff occurrence is less likely to occur.

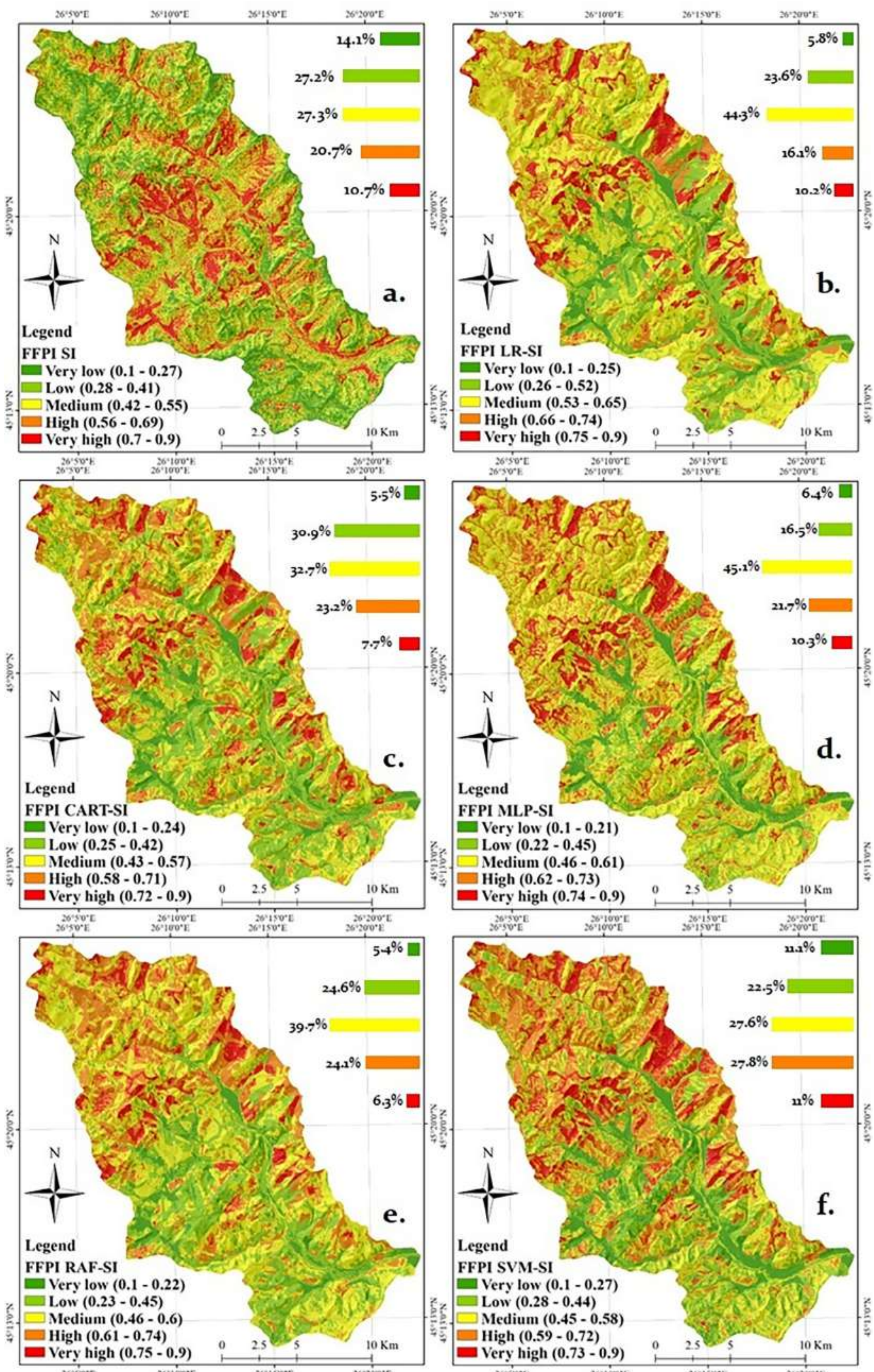

Fig. 4. Spatial distribution of FFPI values (a. FFPI SI; b. FFPI LR-SI; c. FFPI CART-SI; d. FFPI RAF-SI; e. FFPI MLP-SI; f. FFPI SVM-SI).

Around 30.9% of the study is covered by the second class of FFPI CART-SI, which indicate a low potential for flash-flood occurrence. As well as FFPI LR-SI, the FFPI CART-SI medium values cover the largest part of Bâsca Chiojdului River catchment, being present on 32.7% of the study area. Generally, these values are spread homogenously across the entire research area. The areas covered with high and very high values of FFPI CART-SI are spread on approximately 31% of the Bâsca Chiojdului River catchment.

3.4.4. MLP-SI hybrid model

As it was mention at sub-section 2.3.4 the number of hidden neurons was established following a trial-error process intended to determine the MLP architecture with the lowest RMSE value. In the present case the RMSE value was estimated for a number of 50 MLP architectures (Fig. S3). According to the results obtained the RMSE value decrease continuously from 0.473, obtained with a single hidden neuron, to 0.014 which was achieved by applying an architecture with 19 hidden neurons. From 19 to 50 hidden neurons the RMSE value has stabilized at 0.014. It should be mentioned that the excessive number of hidden neurons can cause the over fitting (Sheela and Deepa, 2013). Therefore, in order to compute the FFPI, was chosen the MLP architecture with a number of 19 hidden neurons (Fig. S4). Further, the weight of each flash-flood predictor, obtained after the MLP-SI training, were used in a weighted sum operation in order to derive the Flash-Flood Potential Index values.

In order to map the FFPI MLP-SI values, the same procedure as in the previous cases was applied. Thus, the most performant was the *Geometric Intervals* classification method, with 74.23% of torrential pixels in the fifth class of FFPI MLP-SI, followed by *Quantile* (69.23%), *Natural Breaks* (64.22%) and *Equal Intervals* (59.35%) (Fig. S1d). Using the *Geometrical Intervals*, the normalized values of FFPI MLP-SI, between 0.1 and 0.9, were spatially represented. The first class, between 0.1 and 0.21, covers approximately 5.6% of the Bâsca river catchment, while the second accounts around 16.5%. The medium values, between 0.46 and 0.61, are spread on approximately 45% of the total, while the high and very high FFPI is encountered on 32% of the research area (Fig. 4d).

3.4.5. RAF-SI hybrid model

By running the RAF-SI model it was observed that the increase in the number of trees generates a decrease in the OOB error. This tendency is maintained until 234 trees from this point the OOB becoming stable at 0.0831 (Fig. S5). Therefore, in order to derive the FFPI the RAF-SI model applied was characterized by a structure with 234 trees. The flash-flood predictor with the highest influence in RAF-SI model was the land use (0.23), followed by slope (0.2), lithology (0.13), hydrological soil groups (0.12), twi (0.11), L-S factor (0.09), tpi (0.08) and convergence index (0.04).

In terms of FFPI RAF-SI values, the best classification was obtained by applying the *Geometrical Intervals* method (71.52%), followed by *Natural Breaks* (67.32%), *Quantile* (65.4%) and *Equal Intervals* (59.32%) (Fig. S1e). The *Geometrical Intervals* method used to represent the spatial distribution of MLP-SI, revealed that the first class of flash-flood potential cover only 5.4% of the study area, while the low values are present on approximately 24.6% of the total surface (Fig. 4e). The largest areas (39.7%) are occupied by the medium values of FFPI MLP-SI, while around 30% of the research zone has a high and very high flash-flood potential.

3.4.6. SVM-SI hybrid model

Following the training procedure of SVM-SI hybrid model the weights of each flash-flood predictor was derived. Thus, the slope obtained the highest weight (0.25), followed by land use (0.18), lithology (0.15), twi (0.12), hydrological soil groups (0.1), L-S Factor (0.08), tpi (0.06) and convergence index (0.06).

After the application of weighted sum which involved the use of SI coefficients and the weights of each flash-flood predictors, the values of FFPI SVM-SI was derived. Further the four classification methods were applied in order to establish the which is the most performant. The *Geometric Intervals* provides again the best classification, with a percentage of 68.32% of torrential pixels within the very high class. This method was followed by *Quantiles* (64.29%), *Equal Intervals* (61.3%) and *Natural Breaks* (59.3%) (Fig. S1e). By analysing the results of the *Geometric Intervals* classification, it can be noted that the very low values of FFPI SVM-SI are spread on 11.1% of the Bâsca Chiojdului catchment, while low values occupy 22.5%. The surfaces located on a medium flash-flood potential has an weight of 27.6%, while the high and very high values cover a total percentage of 38.8%.

3.5. Results validation (ROC Curve)

According to Fig. 5a, the most performant model in terms of training areas pixels, is the MLP-SI (AUC = 0.94), followed by CART-SI (AUC = 0.939), RAF-SI (AUC = 0.933), SVM-SI (AUC = 0.929), LR-SI (AUC = 0.925) and SI (AUC = 0.92). AUC values higher than 0.85 in all three cases highlight a very high efficiency of all the models used to determine the areas with flash-flood potential. In terms of Prediction Rate, the MLP-SI was also the first with AUC = 0.927, followed by CART-SI (AUC = 0.922), SVM-SI (AUC = 0.918), RAF-SI (AUC = 0.914), SI (AUC = 0.91) and LR-SI (AUC = 0.901) and (Fig. 5b).

The significance of the differences between AUC values was evaluated through the Wilcoxon signed-rank test. Usually, if p-value exceeds 0.05 and z-value ranges between −1.96 to +1.96,

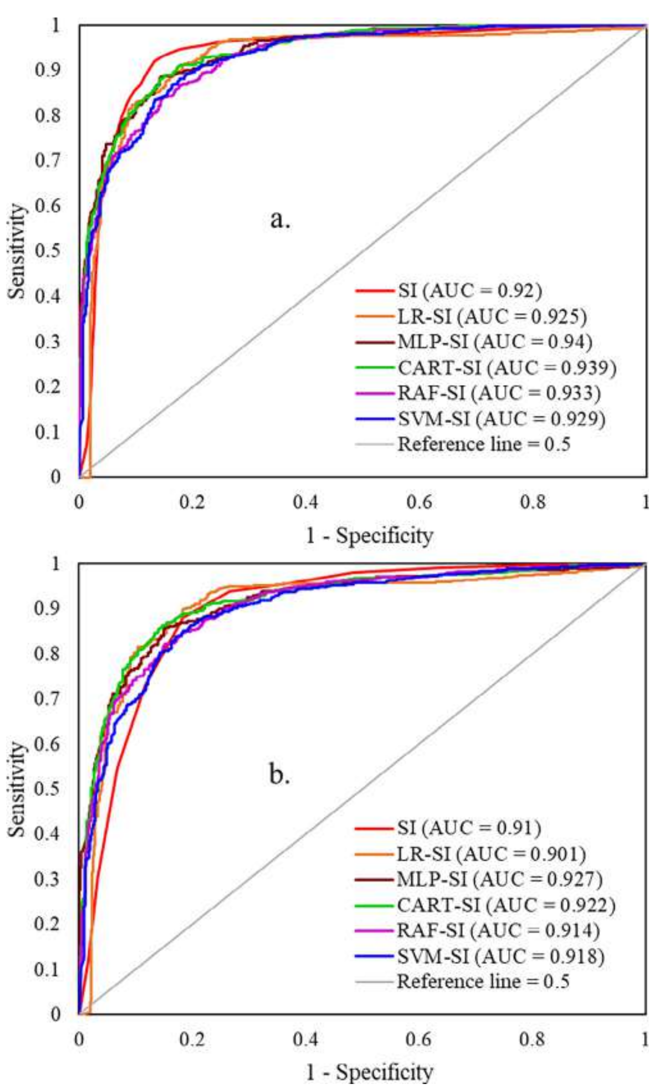

Fig. 5. ROC Curve (a. Success Rate; b. Prediction rate).

then we can state that the differences between AUC values are not significant from the statistical point of view. In terms of Success Rate, the highest statistical difference, highlighted by a z-value equal to -12.084, was recorded in the case of the comparison between SI and MLP-SI models (Table S3). For the Prediction Rate, the highest statistical difference (z-value = -10.322) was estimated after the comparison between LR-SI and MLP-SI models. However according to the results of Wilcoxon signed-rank test the p-values resulted from all the comparison are <0.05. Therefore, we can state that all the differences between the AUC values are statistically significant.

4. Discussion

The determination of FFPI values across Bâsca Chiojdului river catchment was already performed in other researches from the international literature. The first attempt to calculate the FFPI values across Bâsca Chiojdului river catchment, based on a simple overlaying of flash-flood conditioning factors in GIS environment without considering the areas already affected by torrential phenomena, was carried out by Pravalie and Costache (2014). By comparing with the results of the present study it can be observed that the weights of 28% of the surfaces with high and very high FFPI values obtained by Pravalie and Costache (2014) are close to the weights achieved by applying LR-SI (26.3%), RAF-SI (30.4%), CART-SI (30.9%), SI (31.4%) and MLP-SI (32%). This fact occurs even if the methods used to determine the spatial variability of FFPI values were different. Another attempt to determine the FFPI values across Bâsca Chiojdului river catchment was done by (Costache and Zaharia, 2017). In the mentioned study, the calculation of FFPI values was carried out by using two statistical models: Weights of Evidence and Frequency Ratio. In this case, the application of Weights of Evidence highlighted a weight of 33% for high and very high FFPI values, while the application of Frequency Ratio revealed a weight of 39% which is similar to the weights achieved in the case of SVM-SI (38.8%). It can be noted the fact that in the present study, as well as in the case of the previous two studies, the high and very high values of flash-flood potential index are located in the central part of Bâsca Chiojdului river catchment. It is also important to note that the application of ROC Curve provides more accurate results in the present study, in which the minimum AUC value of Success Rate was 0.92 (SI), comparing to the 0.73 (Weights of Evidence) that was obtained in the previous study performed by Costache and Zaharia (2017). Moreover, the accurate results achieved in the present study recommend the involvement of the methods and the eight flash-flood conditioning in computation of FFPI on other areas. In fact, these flash-flood predictors, which can be considered relevant for FFPI determination, were used in the past, together with others predictors, in order to assess the flash-flood susceptibility on other areas. Thus, Costache (2019a) tried to calculate the FFPI on Prahova river catchment (Romania) through a number of 4 hybrid models resulted from the combination of LR and SVM models on the one hand with the Frequency Ratio (FR) and Weights of Evidence (WoE) on the other hand. The results obtained by Costache (2019a) revealed that the high and very high FFPI values cover between 31% (SVM-WoE) and 45% (LR-WoE) of the study area. Instead the performances of the models, estimated through ROC Curve were slightly lower than the performances achieved in the present research using also ROC Curve. Many decision trees based models were used in other study by Costache (2019c) in order to estimate the FFPI on Prahova river catchment. In this case also the performances of the models in terms of ROC Curve were slightly lower than the performance achieved in the present research. The SI stand-alone model provides very good results in the assessment of flash-flood susceptibility on Haraz river catchment (Iran). Thus, Khosravi et al. (2016) showed that SI stand-alone model can reach to an accuracy of 99.71% in terms of flash-flood susceptibility evaluation.

The use of such modern methods characterized by high accuracy in predicting areas potentially affected by flash-floods and floods is of high importance in the context of predictions regarding global climate change. Thus, in the future, an increase in the frequency of flash-floods will be expected due to the changes in the manifestation of rainfalls which will have a more pronounced torrential character (Maghsood et al., 2019). It should be noted that the magnitude of the flash-floods is expected to increase in the future due to the deforestation activities that are carried out on large areas in the mountainous area of Romania (Petrişor, 2015), and also due to the extension of urbanized surfaces that causes the conversion of more surfaces into impervious areas. The deforestation activities and the increase in the severity and frequency of flash-floods will have a direct impact also in the woody and bedload transport which will be more actively in the future (Hooke, 2019). In Bâsca Chiojdului river catchment, the bedload transport has a high influence on riverbed dynamics which can further influence the characteristics of floods and flash-floods (Murărescu et al., 2012). During the flash-flood events, the sediment dynamics and woody transport can be very dangerous for the buildings and infrastructure elements which are affected by this phenomenon. Therefore, it is very important, in the future research works, to identify across the Bâsca Chiojdului river basin, those torrential catchments which are susceptible to sediment and woody transport.

5. Conclusions

Nowadays, a very important part of the researcher's activity is represented by the study of the flash-flood susceptibility. In the present study, the flash-flood potential (FFPI) was calculated by using one bivariate statistical method (SI) and other five ensembles (LR-SI, CART-SI, MLP-SI, RAF-SI, SVM-SI). These models were trained through a number of 8 flash-flood predictors along with a sample representing the presence/absence of areas affected by torrential phenomena. According to the applied algorithms, a percentage between 26.3% and 38.8% of the research zone is covered with high and very high values of FFPI. The application of ROC Curve in the results validation process, revealed that MLP-SI model has the highest efficiency among the applied models (AUC = 0.94 – training areas; AUC = 0.927 – validating areas).

As any other research, the results obtained in the present study could be subject to errors and uncertainties due to certain factors such as: possible errors occurred in the digitization of the areas affected by torrential phenomena; errors that could occur due to inexact spatial representation of flash-flood conditioning factors.

We can state that the main novelty of the present study is represented by the use of the five hybrid models to calculate the FFPI values for a small river catchment.

In order to increase the accuracy of flash-flood forecast and warning, the results of the present study could successfully be used by the National Institute of Hydrology and Water Management from Romania. In terms of policy implications, the results of the present study can represent a useful tool for central and local authorities which should prioritize the interventions in the areas which are more susceptible to flash-floods occurrence than other regions. These interventions could consist in measures taken before flash-flood events, which are intended to reduce the susceptibility to these hazards, and post flash-flood events, which should refer to the increase of the resilience of the affected environment, the restoration of the socio-economic elements affected and to the help of the affected population. Interdiction of deforestation in the susceptible areas, by legislation changes, the afforestation and the correct management of torrential areas are the most important measures taken to reduce the flash-flood susceptibility.

Declaration of Competing Interest

The authors declare that they have no known competing financial interests or personal relationships that could have appeared to influence the work reported in this paper.

Appendix A. Supplementary data

Supplementary data to this article can be found online at https://doi.org/10.1016/j.scitotenv.2019.134514.

References

Aitkin, M., 1996. A general maximum likelihood analysis of overdispersion in generalized linear models. Stat. Comput. 6, 251–262. https://doi.org/10.1007/BF00140869.
Arabameri, A., Yamani, M., Pradhan, B., Melesse, A., Shirani, K., Bui, D.T., 2019. Novel ensembles of COPRAS multi-criteria decision-making with logistic regression, boosted regression tree, and random forest for spatial prediction of gully erosion susceptibility. Total Environ. Sci. 688, 903–916. https://doi.org/10.1016/j.scitotenv.2019.06.205.
Archer, D., Fowler, H., 2018. Characterising flash flood response to intense rainfall and impacts using historical information and gauged data in Britain. J. Flood Risk Manag. 11, S121–S133. https://doi.org/10.1111/jfr3.12187.
Arghiuş, C., Arghiuş, V., 2011. The quantitative estimation of the soil erosion using USLE type ROMSEM model: case-study-the Codrului ridge and Piedmont (Romania). Carpathian J. Earth Environ. Sci. 6, 59–66.
Breiman, L., 2001. Random forests. Mach. Learn. 45, 5–32.
Breiman, L., Friedman, J.H., Olshen, R.A., Stone, C.J., 1984. Classification and Regression Trees. Wadsworth Int. Group 432, Belmont, CA, pp. 151–166.
Bubeck, P., Botzen, W.J., Aerts, J.C., 2012. A review of risk perceptions and other factors that influence flood mitigation behavior. Risk Anal. Int. J. 32, 1481–1495. https://doi.org/10.1111/j.1539-6924.2011.01783.x.
Bui, D.T., Lofman, O., Revhaug, I., Dick, O., 2011. Landslide susceptibility analysis in the Hoa Binh province of Vietnam using statistical index and logistic regression. Nat. Hazards 59, 1413. https://doi.org/10.1007/s11069-011-9844-2.
Chen, W., Xie, X., Wang, J., Pradhan, B., Hong, H., Bui, D.T., Duan, Z., Ma, J., 2017. A comparative study of logistic model tree, random forest, and classification and regression tree models for spatial prediction of landslide susceptibility. Catena 151, 147–160. https://doi.org/10.1016/j.catena.2016.11.032.
Chen, W., Peng, J., Hong, H., Shahabi, H., Pradhan, B., Liu, J., Zhu, A.-X., Pei, X., Duan, Z., 2018. Landslide susceptibility modelling using GIS-based machine learning techniques for Chongren County, Jiangxi Province, China. Sci. Total Environ. 626, 1121–1135. https://doi.org/10.1016/j.scitotenv.2018.01.124.
Chendeş, V., 2011. Water resources in Curvature Subcarpathians. Geospatial assessments – In Romanian. Evaluări Geospaţiale Ed Acad. Rom. Bucureşti.
Cherukuri, H., Perez-Bernabeu, E., Selles, M., Schmitz, T., 2019. Machining chatter prediction using a data learning model. J. Manuf. Mater. Process. 3, 45. https://doi.org/10.3390/jmmp3020045.
Choubin, B., Moradi, E., Golshan, M., Adamowski, J., Sajedi-Hosseini, F., Mosavi, A., 2019. An Ensemble prediction of flood susceptibility using multivariate discriminant analysis, classification and regression trees, and support vector machines. Sci. Total Environ. 651, 2087–2096. https://doi.org/10.1016/j.scitotenv.2018.10.064.
Collier, C., 2007. Flash flood forecasting: what are the limits of predictability? Q. J. R. Meteorol Soc. J. Atmospheric Sci. Appl. Meteorol. Phys. Oceanogr. 133, 3–23. https://doi.org/10.1002/qj.29.
Conrad, O., Bechtel, B., Bock, M., Dietrich, H., Fischer, E., Gerlitz, L., Wehberg, J., Wichmann, V., Böhner, J., 2015. System for automated geoscientific analyses (SAGA) v. 2.1. 4. Geosci. Model Dev. 8, 1991–2007. https://doi.org/10.5194/gmd-8-1991-2015.
Costache, R., 2014. Using GIS techniques for assessing lag time and concentration time in small river basins. Case study: Pecineaga river basin, Romania. Geographia Technica 9 (1), 31–38.
Costache, R., 2019a. Flash-flood Potential assessment in the upper and middle sector of Prahova river catchment (Romania). A comparative approach between four hybrid models. Sci. Total Environ. 659, 1115–1134. https://doi.org/10.1016/j.scitotenv.2018.12.397.
Costache, R., 2019b. Flood susceptibility assessment by using bivariate statistics and machine learning models-a useful tool for flood risk management. Water Resour. Manag. 33, 3239–3256. https://doi.org/10.1007/s11269-019-02301-z.
Costache, R., 2019c. Flash-flood Potential Index mapping using weights of evidence, decision Trees models and their novel hybrid integration. Stoch. Environ. Res. Risk Assess. 33, 1375–1402. https://doi.org/10.1007/s00477-019-01689-9.
Costache, R., Bui, D.T., 2019. Spatial prediction of flood potential using new ensembles of bivariate statistics and artificial intelligence: a case study at the Putna river catchment of Romania. Sci. Total Environ. 691, 1098–1118. https://doi.org/10.1016/j.scitotenv.2019.07.197.
Costache, R., Fontanine, I., Corodescu, E., 2014. Assessment of surface runoff depth changes in Sărăţel River basin, Romania using GIS techniques. Open Geosci. 6, 363–372. https://doi.org/10.2478/s13533-012-0181-0.
Costache, R., Zaharia, L., 2017. Flash-flood potential assessment and mapping by integrating the weights-of-evidence and frequency ratio statistical methods in GIS environment–case study: Bâsca Chiojdului River catchment (Romania). J. Earth Syst. Sci. 126, 59. https://doi.org/10.1007/s12040-017-0828-9.
Costache, R., Popescu, C., 2013. The touristic accessibility in the Hunedoara County in terms of road network. Geographia Technica 8 (2), 1–12.
Costache, R., Pravalie, R., 2012. The use of GIS techniques in the evaluation of the susceptibility of the floods genesis in the hydrographical basin of Bâsca Chiojdului river. Analele Universităţii din Oradea. Seria Geografie 22 (2), 284–293.
Costache, R., Pravalie, R., Mitof, I., Popescu, C., 2015. Flood vulnerability assessment in the low sector of Saratel Catchment. Case study: Joseni Village. Carpathian J. Earth Environ. Sci. 10, 161–169.
Costache, R., Hong, H., Wang, Y., 2019. Identification of torrential valleys using GIS and a novel hybrid integration of artificial intelligence, machine learning and bivariate statistics. Catena 183,. https://doi.org/10.1016/j.catena.2019.104179 104179.
Dai, W., Ji, W., 2014. A mapreduce implementation of C4. 5 decision tree algorithm. Int. J. Database Theory Appl. 7, 49–60. https://doi.org/10.14257/ijdta.2014.7.1.05.
Dou, J., Yunus, A.P., Bui, D.T., Merghadi, A., Sahana, M., Zhu, Z., Chen, C.-W., Khosravi, K., Yang, Y., Pham, B.T., 2019. Assessment of advanced random forest and decision tree algorithms for modeling rainfall-induced landslide susceptibility in the Izu-Oshima Volcanic Island, Japan. Sci. Total Environ. 662, 332–346. https://doi.org/10.1016/j.scitotenv.2019.01.221.
Felicísimo, Á.M., Cuartero, A., Remondo, J., Quirós, E., 2013. Mapping landslide susceptibility with logistic regression, multiple adaptive regression splines, classification and regression trees, and maximum entropy methods: a comparative study. Landslides 10, 175–189. https://doi.org/10.1007/s10346-012-0320-1.
Fitriani, W., Siahaan, A.P.U., 2016. Comparison between WEKA and Salford Systemin data mining software. Int. J. Mob. Comput. Appl. 3, 1–4.
Fontanine, I., Costache, R., 2013a. Using GIS techniques for surface runoff potential analysis in the Subcarpathian area between Buzău and Slănic rivers. Cinq Continents 3 (7), 47–57.
Fontanine, I., Costache, R., 2013b. The potential for water diffuse pollution with heavy metals in Arieş river basin. Analele stiintifice ale Universitatii" Alexandru Ioan Cuza" din Iasi-seria Geografie 59 (2), 59–72.
Gao, L., Ye, M., Lu, X., Huang, D., 2017. Hybrid method based on information gain and support vector machine for gene selection in cancer classification. Genomics Proteomics Bioinformatics 15, 389–395. https://doi.org/10.1016/j.gpb.2017.08.002.
Garosi, Y., Sheklabadi, M., Conoscenti, C., Pourghasemi, H.R., Van Oost, K., 2019. Assessing the performance of GIS-based machine learning models with different accuracy measures for determining susceptibility to gully erosion. Sci. Total Environ. 664, 1117–1132. https://doi.org/10.1016/j.scitotenv.2019.02.093.
Guha-sapir, D., Hoyois, P., Below, R., 2011. Annual Disaster Statistical Review 2016: The Numbers and Trends. Université catholique de Louvain, Centre for Research on the Epidemiology of Disasters (CRED). Zugänglich unter, Brussels.
Hall, M., Frank, E., Holmes, G., Pfahringer, B., Reutemann, P., Witten, I.H., 2009. The WEKA data mining software: an update. ACM SIGKDD Explor. Newsl. 11, 10–18.
Hong, H., Pradhan, B., Xu, C., Bui, D.T., 2015. Spatial prediction of landslide hazard at the Yihuang area (China) using two-class kernel logistic regression, alternating decision tree and support vector machines. Catena 133, 266–281. https://doi.org/10.1016/j.catena.2015.05.019.
Hong, H., Tsangaratos, P., Ilia, I., Liu, J., Zhu, A.-X., Chen, W., 2018. Application of fuzzy weight of evidence and data mining techniques in construction of flood susceptibility map of Poyang County, China. Sci. Total Environ. 625, 575–588. https://doi.org/10.1016/j.scitotenv.2017.12.256.
Hooke, J., 2019. Extreme sediment fluxes in a dryland flash flood. Sci. Rep. 9, 1686. https://doi.org/10.1038/s41598-019-38537-3.
Hunt, E.B., Marin, J., Stone, P.J., 1966. Experiments in induction.**
Ibarra-Berastegi, G., Saénz, J., Ezcurra, A., Elías, A., Diaz Argandoña, J., Errasti, I., 2011. Downscaling of surface moisture flux and precipitation in the Ebro Valley (Spain) using analogues and analogues followed by random forests and multiple linear regression. Hydrol. Earth Syst. Sci. 15, 1895–1907. https://doi.org/10.5194/hess-15-1895-2011.
Jahani, B., Mohammadi, B., 2019. A comparison between the application of empirical and ANN methods for estimation of daily global solar radiation in Iran. Theor. Appl. Climatol. 137, 1257–1269. https://doi.org/10.1007/s00704-018-2666-3.
Javidi, M.M., Mansoury, S., 2017. Diagnosis of the disease using an ant colony gene selection method based on information gain ratio using fuzzy rough sets. J. Part. Sci. Technol. 3, 175–186. https://doi.org/10.22104/JPST.2018.2649.1102.
Karamouz, M., Fereshtehpour, M., 2019. Modeling DEM errors in coastal flood inundation and damages: a spatial non-stationary approach. Water Resour. Res. https://doi.org/10.1029/2018WR024562.
Kavzoglu, T., Sahin, E.K., Colkesen, I., 2014. Landslide susceptibility mapping using GIS-based multi-criteria decision analysis, support vector machines, and

logistic regression. Landslides 11, 425–439. https://doi.org/10.1007/s10346-013-0391-7.
Khosravi, K., Pourghasemi, H.R., Chapi, K., Bahri, M., 2016. Flash flood susceptibility analysis and its mapping using different bivariate models in Iran: a comparison between Shannon's entropy, statistical index, and weighting factor models. Environ. Monit. Assess. 188, 656. https://doi.org/10.1007/s10661-016-5665-9.
Khosravi, K., Pham, B.T., Chapi, K., Shirzadi, A., Shahabi, H., Revhaug, I., Prakash, I., Bui, D.T., 2018. A comparative assessment of decision trees algorithms for flash flood susceptibility modeling at Haraz watershed, northern Iran. Sci. Total Environ. 627, 744–755. https://doi.org/10.1016/j.scitotenv.2018.01.266.
Kruzdlo, R., Ceru, J., 2010. Flash Flood Potential Index for WFO Mount Holly/Philadelphia. In: Presented at the Eastern region Flash Flood Conference, poster session. NOAA's National Weather Service, pp. 2–4.
Kucsicsa, G., Popovici, E.-A., Bălteanu, D., Grigorescu, I., Dumitraşcu, M., Mitrică, B., 2019. Future land use/cover changes in Romania: regional simulations based on CLUE-S model and CORINE land cover database. Landsc. Ecol. Eng. 15, 75–90. https://doi.org/10.1007/s11355-018-0362-1.
Lee, S., Pradhan, B., 2007. Landslide hazard mapping at Selangor, Malaysia using frequency ratio and logistic regression models. Landslides 4, 33–41. https://doi.org/10.1007/s10346-006-0047-y.
Maghsood, F.F., Moradi, H., Bavani, M., Reza, A., Panahi, M., Berndtsson, R., Hashemi, H., 2019. Climate change impact on flood frequency and source area in Northern Iran under CMIP5 scenarios. Water 11, 273. https://doi.org/10.3390/w11020273.
Mamede da Silva, P., de Miranda, F.P., Landau, L., 2018. Mapping the Brazilian Amazon fluvial sensitivity index to oil spills with Shuttle Radar Topography Mission (SRTM) data. Geocarto Int. 33, 555–572. https://doi.org/10.1080/10106049.2016.1273399.
McKenney, D.W., Pedlar, J.H., 2003. Spatial models of site index based on climate and soil properties for two boreal tree species in Ontario, Canada. For. Ecol. Manag. 175, 497–507. https://doi.org/10.1016/S0378-1127(02)00186-X.
Midi, H., Sarkar, S.K., Rana, S., 2010. Collinearity diagnostics of binary logistic regression model. J. Interdiscip. Math. 13, 253–267. https://doi.org/10.1080/09720502.2010.10700699.
Mieza, M.S., Cravero, W.R., Kovac, F.D., Bargiano, P.G., 2016. Delineation of site-specific management units for operational applications using the topographic position index in La Pampa, Argentina. Comput. Electron. Agric. 127, 158–167. https://doi.org/10.1016/j.compag.2016.06.005.
Minea, G., 2013. Assessment of the flash flood potential of Bâsca River Catchment (Romania) based on physiographic factors. Open Geosci. 5, 344–353. https://doi.org/10.2478/s13533-012-0137-4.
Moore, I.D., Grayson, R., Ladson, A., 1991. Digital terrain modelling: a review of hydrological, geomorphological, and biological applications. Hydrol. Process. 5, 3–30. https://doi.org/10.1002/hyp.3360050103.
Moore, I.D., Wilson, J.P., 1992. Length-slope factors for the Revised Universal Soil Loss Equation: simplified method of estimation. J. Soil Water Conserv. 47, 423–428.
Murărescu, O., Zarea, R., Turloiu-Firică, R., Pehoiu, G., 2012. Bâsca Chiojdului riverbed dynamics (Romania) and its impact on the environment. Case study: sector area. Present Environ. Sustain. Dev, 6.
Naghibi, S.A., Ahmadi, K., Daneshi, A., 2017. Application of support vector machine, random forest, and genetic algorithm optimized random forest models in groundwater potential mapping. Water Resour. Manag. 31, 2761–2775. https://doi.org/10.1007/s11269-017-1660-3.
Petrişor, A.-I., 2015. Using CORINE data to look at deforestation in Romania: distribution & possible consequences. Urban. Arhit. Construcţii 6, 83–90.
Pham, B.T., Bui, D.T., Pourghasemi, H.R., Indra, P., Dholakia, M., 2017. Landslide susceptibility assessment in the Uttarakhand area (India) using GIS: a comparison study of prediction capability of naïve bayes, multilayer perceptron neural networks, and functional trees methods. Theor. Appl. Climatol. 128, 255–273. https://doi.org/10.1007/s00704-015-1702-9.
Pham, B.T., Jaafari, A., Prakash, I., Bui, D.T., 2019a. A novel hybrid intelligent model of support vector machines and the MultiBoost ensemble for landslide susceptibility modeling. Bull. Eng. Geol. Environ. 78, 2865–2886. https://doi.org/10.1007/s10064-018-1281-y.
Pham, Q.B., Yang, T.C., Kuo, C.M., Tseng, H.W., Yu, P.S., 2019b. Combing random forest and least square support vector regression for improving extreme rainfall downscaling. Water 11 (3), 451. https://doi.org/10.3390/w11030451.
Pradhan, B., 2010. Remote sensing and GIS-based landslide hazard analysis and cross-validation using multivariate logistic regression model on three test areas in Malaysia. Adv. Space Res. 45, 1244–1256. https://doi.org/10.1016/j.asr.2010.01.006.
Pradhan, B., 2011. Manifestation of an advanced fuzzy logic model coupled with Geo-information techniques to landslide susceptibility mapping and their comparison with logistic regression modelling. Environ. Ecol. Stat. 18, 471–493. https://doi.org/10.1007/s10651-010-0147-7.
Pradhan, B., 2013. A comparative study on the predictive ability of the decision tree, support vector machine and neuro-fuzzy models in landslide susceptibility mapping using GIS. Comput. Geosci. 51, 350–365. https://doi.org/10.1016/j.cageo.2012.08.023.
Pradhan, B., Lee, S., 2010. Delineation of landslide hazard areas on Penang Island, Malaysia, by using frequency ratio, logistic regression, and artificial neural network models. Environ. Earth Sci. 60, 1037–1054. https://doi.org/10.1007/s12665-009-0245-8.
Pravalie, R., Costache, R., 2014. The analysis of the susceptibility of the flash-floods' genesis in the area of the hydrographical basin of Bāsca Chiojdului river/Analiza susceptibilitatii genezei viiturilor īn aria bazinului hidrografic al rāului Bāsca Chiojdului. Presented at the Forum Geografic, University of Craiova, Department of Geography, p. 39. https://doi.org/10.5775/fg.2067-4635.2014.089.i.
Pravalie, R., Costache, R., 2013. The vulnerability of the territorial-administrative units to the hydrological phenomena of risk (flash-floods). Case study: the subcarpathian sector of Buzău catchment. Analele Universităţii din Oradea–Seria Geografie 23 (1), 91–98.
Rautela, P., Lakhera, R.C., 2000. Landslide risk analysis between Giri and Tons rivers in Himachal Himalaya (India). Int. J. Appl. Earth Obs. Geoinformation 2, 153–160. https://doi.org/10.1016/S0303-2434(00)85009-6.
Rojas, R., Feyen, L., Bianchi, A., Dosio, A., 2012. Assessment of future flood hazard in Europe using a large ensemble of bias-corrected regional climate simulations. J. Geophys. Res. Atmos. 117, D17109. https://doi.org/10.1029/2012JD017461.
Romanescu, G., Cimpianu, C.I., Mihu-Pintilie, A., Stoleriu, C.C., 2017. Historic flood events in NE Romania (post-1990). J. Maps 13, 787–798. https://doi.org/10.1080/17445647.2017.1383944.
Rosati, L., Fipaldini, M., Marignani, M., Blasi, C., 2010. Effects of fragmentation on vascular plant diversity in a Mediterranean forest archipelago. Plant Biosyst. 144, 38–46. https://doi.org/10.1080/11263500903429213.
Sampson, C.C., Smith, A.M., Bates, P.D., Neal, J.C., Alfieri, L., Freer, J.E., 2015. A high-resolution global flood hazard model. Water Resour. Res. 51, 7358–7381. https://doi.org/10.1002/2015WR016954.
Shafapour Tehrany, M., Shabani, F., Neamah Jebur, M., Hong, H., Chen, W., Xie, X., 2017. GIS-based spatial prediction of flood prone areas using standalone frequency ratio, logistic regression, weight of evidence and their ensemble techniques. Geomat. Nat. Hazards Risk 8, 1538–1561.
Shafizadeh-Moghadam, H., Valavi, R., Shahabi, H., Chapi, K., Shirzadi, A., 2018. Novel forecasting approaches using combination of machine learning and statistical models for flood susceptibility mapping. J. Environ. Manage. 217, 1–11. https://doi.org/10.1016/j.jenvman.2018.03.089.
Sheela, K.G., Deepa, S., 2013. Neural network based hybrid computing model for wind speed prediction. Neurocomputing 122, 425–429. https://doi.org/10.1016/j.neucom.2013.06.008.
Skentos, A., 2018. Topographic Position Index based landform analysis of Messaria (Ikaria Island, Greece). Acta Geobalcanica 4, 7–15.
Smith, G., 2003. Flash flood potential: Determining the hydrologic response of FFMP basins to heavy rain by analyzing their physiographic characteristics. White Pap. Available NWS Colo. Basin River Forecast Cent. Web Site Httpwww Cbrfc Noaa Govpapersffpwpap Pdf.
Soureshjani, M.H., Kimiagari, A.M., 2013. Calculating the best cut off point using logistic regression and neural network on credit scoring problem-A case study of a commercial bank. Afr. J. Bus. Manag. 7, 1414–1421.
Tien Bui, D., Hoang, N.-D., Martínez-Álvarez, F., Ngo, P.-T.T., Hoa, P.V., Pham, T.D., Samui, P., Costache, R., 2020. A novel deep learning neural network approach for predicting flash flood susceptibility: A case study at a high frequency tropical storm area. Science of The Total Environment 701, 134413. https://doi.org/10.1016/j.scitotenv.2019.134413.
Tien Bui, D., Pradhan, B., Lofman, O., Revhaug, I., 2012. Landslide susceptibility assessment in Vietnam using support vector machines, decision tree, and Naive Bayes Models. Math. Probl. Eng. 2012. https://doi.org/10.1155/2012/974638.
Tincu, R., Lazar, G., Lazar, I., 2018. Modified flash flood potential index in order to estimate areas with predisposition to water accumulation. Open Geosci. 10, 593–606. https://doi.org/10.1515/geo-2018-0047.
Toukourou, M., Johannet, A., Dreyfus, G., Ayral, P.-A., 2011. Rainfall-runoff modeling of flash floods in the absence of rainfall forecasts: the case of "Cévenol flash floods". Appl. Intell. 35, 178–189. https://doi.org/10.1007/s10489-010-0210-y.
Trigila, A., Iadanza, C., Esposito, C., Scarascia-Mugnozza, G., 2015. Comparison of logistic regression and random forests techniques for shallow landslide susceptibility assessment in Giampilieri (NE Sicily, Italy). Geomorphology 249, 119–136. https://doi.org/10.1016/j.geomorph.2015.06.001.
van Westen, C., 1997. Statistical Landslide Hazards Analysis, ILWIS 2.1 for Windows Application Guide. ITC Publication.
Van Westen, C.J., Rengers, N., Terlien, M., Soeters, R., 1997. Prediction of the occurrence of slope instability phenomenal through GIS-based hazard zonation. Geol. Rundsch. 86, 404–414.
Wang, Y., Fang, Z., Hong, H., 2019a. Comparison of convolutional neural networks for landslide susceptibility mapping in Yanshan County, China. Sci. Total Environ. 666, 975–993. https://doi.org/10.1016/j.scitotenv.2019.02.263.
Wang, Y., Hong, H., Chen, W., Li, S., Panahi, M., Khosravi, K., Shirzadi, A., Shahabi, H., Panahi, S., Costache, R., 2019b. Flood susceptibility mapping in Dingnan County (China) using adaptive neuro-fuzzy inference system with biogeography based optimization and imperialistic competitive algorithm. J. Environ. Manage. 247, 712–729. https://doi.org/10.1016/j.jenvman.2019.06.102.
Woznicki, S.A., Baynes, J., Panlasigui, S., Mehaffey, M., Neale, A., 2019. Development of a spatially complete floodplain map of the conterminous United States using random forest. Sci. Total Environ. 647, 942–953. https://doi.org/10.1016/j.scitotenv.2018.07.353.
Wu, X., Kumar, V., Quinlan, J.R., Ghosh, J., Yang, Q., Motoda, H., McLachlan, G.J., Ng, A., Liu, B., Philip, S.Y., 2008. Top 10 algorithms in data mining. Knowl. Inf. Syst. 14, 1–37. https://doi.org/10.1007/s10115-007-0114-2.

Yeon, Y.-K., Han, J.-G., Ryu, K.H., 2010. Landslide susceptibility mapping in Injae, Korea, using a decision tree. Eng. Geol. 116, 274–283. https://doi.org/10.1016/j.enggeo.2010.09.009.

Youssef, A.M., Pourghasemi, H.R., Pourtaghi, Z.S., Al-Katheeri, M.M., 2016. Landslide susceptibility mapping using random forest, boosted regression tree, classification and regression tree, and general linear models and comparison of their performance at Wadi Tayyah Basin, Asir Region, Saudi Arabia. Landslides 13, 839–856. https://doi.org/10.1007/s10346-015-0614-1.

Zaharia, L., Minea, G., Ioana-Toroimac, G., Barbu, R., Sârbu, I., 2012. Estimation of the areas with accelerated surface runoff in the upper Prahova watershed (Romanian Carpathians). Balwois Repub, Maced.

Zaharia, L., Costache, R., Prăvălie, R., Minea, G., 2015. Assessment and mapping of flood potential in the Slănic catchment in Romania. J. Earth Syst. Sci. 124, 1311–1324.

Zaharia, L., Costache, R., Prăvălie, R., Ioana-Toroimac, G., 2017. Mapping flood and flooding potential indices: a methodological approach to identifying areas susceptible to flood and flooding risk. Case study: the Prahova catchment (Romania). Front. Earth Sci. 11, 229–247. https://doi.org/10.1007/s11707-017-0636-1.

Science of the Total Environment 659 (2019) 1115–1134

Contents lists available at ScienceDirect

Science of the Total Environment

journal homepage: www.elsevier.com/locate/scitotenv

Flash-Flood Potential assessment in the upper and middle sector of Prahova river catchment (Romania). A comparative approach between four hybrid models

Romulus Costache *

Research Institute of the University of Bucharest, 36-46 Bd. M. Kogalniceanu, 5th District, 050107 Bucharest, Romania
National Institute of Hydrology and Water Management, Bucureşti-Ploieşti Road, 97E, 1st District, 013686 Bucharest, Romania

HIGHLIGHTS

- One of the first attempts to calculate Flash-Flood Potential using hybrid models
- Areas affected by torrential phenomena were considered into the analysis.
- 10 flash-flood conditioning factors were selected based on statistical analysis.
- Areas with high flash-flood susceptibility were identified.
- By using three methods the results' validation was carried out.

GRAPHICAL ABSTRACT

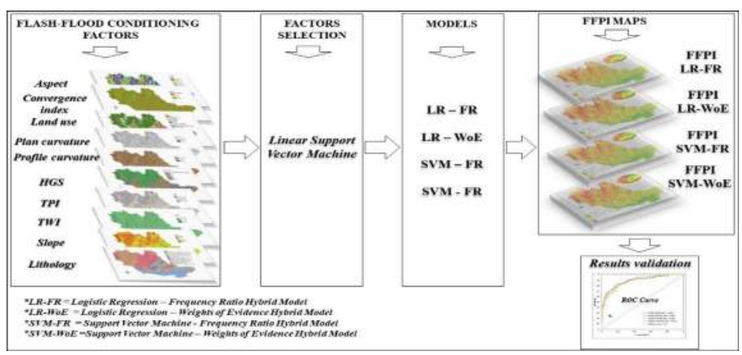

ARTICLE INFO

Article history:
Received 11 September 2018
Received in revised form 13 December 2018
Accepted 25 December 2018
Available online 27 December 2018

Editor: Ralf Ludwig

Keywords:
Flash-Flood Potential Index
Prahova river catchment
Frequency Ratio
Logistic Regression
Support Vector Machine
Hybrid models

ABSTRACT

An accurate assessment of Flash-Flood Potential for certain areas is mandatory for the improvement of flash-flood forecast and warnings. The main aim of the present study is represented by the calculation of Flash-Flood Potential Index within the upper and the middle sector of Prahova river catchment (Romania) by using 4 hybrid models: Logistic Regression-Frequency Ratio (LR-FR) model, Logistic Regression-Weights of Evidence (LR-WoE) model, Support Vector Machine-Frequency Ratio (SVM-FR) model and Support Vector Machine-Weights of Evidence (SVM-WoE). The identification of areas affected by torrential phenomena represents the first step performed in the present research. These areas with a total surface of 260 km^2 were divided into training areas (70%) and validating areas (30%). By the mean of Linear Support Vector Machine (LSVM) model, 10 flash-flood conditioning factors were selected and further used for the Flash-Flood Potential assessment. Based on the spatial relationship between areas affected by torrential phenomena and flash-floods conditioning factors characteristics, the FR and WoE coefficients were calculated. In order to be integrated into Logistic Regression and Support Vector Machine (RBF) analysis, these values were standardized. According to the results of the 4 hybrid models used for FFPI calculation, the high and very high Flash-Flood Potential are spread over 33% of the study area. The model performance assessment and results validation were carried out by the mean of the three different methods: i) relative frequency distribution of torrential phenomena pixels within FFPI classes; ii) ROC Curve (Success Rate and Prediction Rate) and AUC value; iii) statistical measures represented by Sensitivity, Specificity and Accuracy.

* Research Institute of the University of Bucharest, 36-46 Bd. M. Kogalniceanu, 5th District, 050107 Bucharest, Romania.
E-mail address: romuluscostache2000@yahoo.com.

https://doi.org/10.1016/j.scitotenv.2018.12.397
0048-9697/

1. Introduction

Worldwide, many regions are frequently affected by water excess related natural hazards. When these phenomena occur suddenly, they become very dangerous for human communities. Flash-floods are natural phenomena characterized by a very high occurrence velocity. In the last decades, climate changes led to an increase in the frequency and severity of these phenomena. At the same time, the large damages generated annually by floods and flash-floods reveal the high vulnerability of many regions to these widespread hazards (Costache and Zaharia, 2017). Given this situation, the study of flash-flood characteristics and occurrence conditions, as well as the identification of flash-flood susceptible areas, occupies an increasingly important part in the natural hazards research field. The most important components of an efficient flash-flood forecast and warning system are represented by the rainfall estimation based on radar data and flash-flood susceptibility assessment for a certain area of interest. By analyzing the flash-flood susceptibility, at the same rainfall intensity, for an area highly susceptible to flash-flood occurrence, it can be decided to issue a flash-flood warning, while for a less exposed area it can be decided to not issue a flash-flood warning. European Flash-Flood Awareness System (EFAS) is the first operational European system that provides flood warning, with a flash-flood component (Bartholmes et al., 2009; Thielen et al., 2009). Nonetheless, the flash-flood component of EFAS estimates the hazard to these phenomena only based on rainfall data and river size catchment. An accurate estimation of the possibility of flash-flood occurrence in a given region requires, alongside with rainfall data, a detailed analysis of the main flash-flood conditioning factors such as: slope angle, land use, lithology, hydrological soil group etc. The identification and analysis of the areas affected by torrential phenomena in the past is also recommended for flash-flood susceptibility studies. According to other studies focused on natural hazard research, the information regarding the past events represent the key for predicting future events (Tehrany et al., 2014; Cao et al., 2016; Rahmati et al., 2016; Youssef et al., 2016a, 2016b). In this regard, in order to determine the susceptibility of certain areas to different natural risk phenomena, different methods were proposed: Weights of Evidence, Frequency Ratio, Logistic Regression, Support Vector Machine, artificial neural network, decision tree etc. (Tehrany et al., 2013; Regmi et al., 2014; Demir et al., 2015; Youssef et al., 2016a, 2016b; Khosravi et al., 2018; Le et al., 2018; Samanta et al., 2018). The application of these models in the susceptibility research has a positive effect in growing the objectivity of final results.

In order to increase the results quality, the integrated use of statistical techniques with those specific to machine learning field is recommended (Goetz et al., 2015; Althuwaynee et al., 2016). In order to identify the surfaces with a high potential for flash-flood occurrence, in the past studies Flash-Flood Potential Index (FFPI) was used (Davis, 2002; Kruzdlo and Ceru, 2010; Ceru, 2012; Prăvălie & Costache; Minea, 2013; Zaharia et al., 2015; Costache and Zaharia, 2017). The main drawback of the methods applied in these studies is that the models designed to estimate the flash-flood susceptibility do not consider the location of the past events, the calculation of Flash-Flood Potential Index being carried out by using a simple overlay process of flash-flood conditioning factors in GIS environment (Wahid et al., 2016; Shehata and Mizunaga, 2018). For this reason, we consider that an analysis based on statistical methods and machine learning techniques, which also takes into account the past events, is necessary. In this type of research, the assessment of the model's performance and the results validation process are also mandatory. Therefore, the main purpose of the present paper is represented by the estimation of Flash-Flood Potential across the upper and middle sector of Prahova river catchment, Romania, by using four hybrid models: Logistic Regression-Frequency Ratio (LR-FR) model, Logistic Regression-Weights of Evidence (LR-WoE) model, Support Vector Machine-Frequency Ratio (SVM-FR) model and Support Vector Machine-Weights of Evidence (SVM-WoE). The assessment of model performance and results validation will be performed by the mean of three methods: i) relative frequency distribution of torrential phenomena pixels within FFPI classes; ii) ROC Curve (Success Rate and Prediction Rate) and AUC value; iii) statistical measures represented by Sensitivity, Specificity and Accuracy.

The results of present analysis could be successfully used in order to improve the flash-flood forecast and warnings issued for regions located within the study area.

2. Study area

The upper and the middle sector of Prahova river catchment are located in the central-southern part of Romania (Fig. 1). These areas occupy 2600 km^2 and record altitudes ranging between 128 m a.s.l. and 2500 m a.s.l.

The study area is characterized by a variety of landforms. The drainage density values decrease from Carpathian sector (North) to Subcarpathian sector (South), from over 0.7 km/km^2 to <0.5 km/km^2. The slope angle values range between 0° and 73° with a mean of 12.43°. Considering the total area of the upper and the middle sector of Prahova river catchment, it is obvious that the mean slope value is very high. The average value of afforestation coefficient of the study area is around of 52%, while from the pedological point of view, the hydrological soil group A prevails (801 km^2), followed by the hydrological soil group B (727 km^2) and the hydrological soil group D (682 km^2).

Annual precipitation amount ranges between 600 and 1000 mm, being considerably influenced by altitudes. The rainfalls have a torrential regime, especially in May–July, when approximately 15% from the total annual amount is recorded, leading often to flash-floods occurrence. According to Zaharia et al. (2017), the most important flash-floods across the study area were recorded in the following years: 1970, 1975, 1998, 2001, 2002 and 2005 (Table 1). It is noteworthy the fact that these events were recorded at the outlets of several catchments with surfaces <100 km^2 which are most susceptible to flash-flood occurrence.

As reported by the Ministry of Environment and Water Management of Romania (MEHWM, 2006), the flash-floods events in 2005 caused important damages within the study area, on many infrastructure elements as follows: 3000 houses and household annexes, 59 socio-economic units, 490 bridges and culverts, approximately 5000 km of roads and around 1500 ha of agricultural surfaces. The total economic losses were estimated at 27 million euros (Zaharia et al., 2017).

From the economic point of view, the upper and the middle sector of Prahova river catchment are one of the most developed regions from Romania. The Carpathian region of the study area is well known for the tourist activities. There are tourist centers such as Sinaia, Busteni, Azuga and Predeal. According to the Romanian National Institute of Statistics (2018), in the study area is located 12 cities with 152,000 inhabitants. In terms of transport infrastructure, the study area is crossed by the most circulated road from Romania with a continental importance (European Road 60-E60). The railway infrastructure is also very well represented within the study area.

Taking into the account the high population density, the economic development and the past flash-floods events, we can assume the fact that the study area has a high vulnerability to floods and flash-floods.

3. Materials and methods

Regarding the methodology developed in the present study, geospatial data represented by Digital Elevation Model, the areas affected by torrential phenomena, land use, hydrological soil groups and lithology were exclusively used. The data sources will be mentioned bellow.

The applied methodology is presented schematically in Fig. 2 and consists of the following main steps: i) inventory and mapping of areas affected by torrential phenomena; ii) flash-flood conditioning

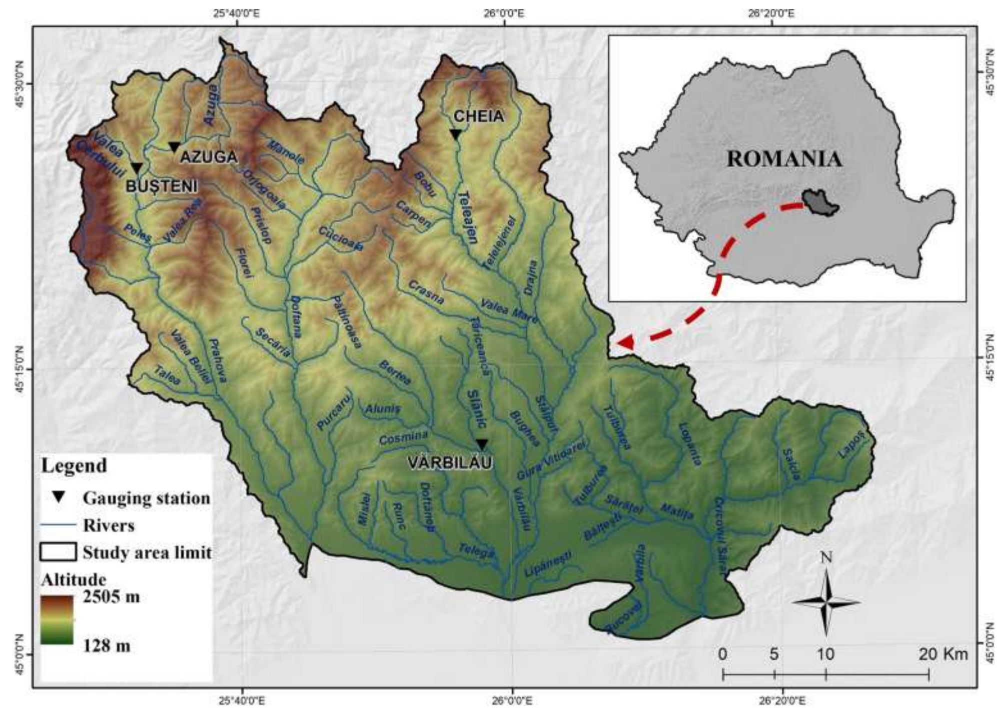

Fig. 1. Study area location in Romania.

factors selection using statistical methods; iii) integrated use of statistical techniques (Frequency Ratio and Weights of Evidence) with those specific to machine learning field (Logistic Regression and Support Vector Machine) for estimating the Flash-Flood Potential Index (FFPI) values within the study area.

3.1. Inventory and mapping of areas affected by torrential phenomena

In order to calculate the flash-flood susceptibility for a given region, the identification of the areas affected by torrential phenomena in the past is an essential step. Performing this stage is mandatory in the perspective of correct conclusions, regarding the relationship between environmental variables and natural risk phenomena. The inventory of areas with torrential phenomena was carried out by using the orthorectified aerial imagery provided by NACREA (2016), these surfaces being validated by field surveys. The areas affected by torrential phenomena were considered those that are characterized by the unified presence of torrential microform of relief such as ravines and gullies which are generated by surface runoff (Costache and Zaharia, 2017) (Fig. 3). The areas affected by torrential phenomena are spread on approximately 10% of the upper and middle sector of Prahova river catchment. Therefore, a total number of 288,121 pixels were identified as affected by torrentiality. 70% of areas affected by torrentiality were randomly selected as training sample, while the other 30% were used for results validation. In order to be incorporated into the analysis, the areas characterized by the presence of torrentiality were converted from polygon format into raster format. The areas without torrential phenomena were also converted in raster format. Value of 1 was assigned to areas affected by torrentiality, while 0 was assigned to areas without torrential phenomena.

Table 1
The main flash-floods events within the study area (adapted after Zaharia et al., 2017).

River	Gauging station	Catchment surface (km^2)	Qmax (m^3/s)	Date (month/year)
Azuga	Azuga	83	94	July 1975
			92.4	September 2001
			81.5	March 2007
			74.6	July 1988
			53.8	May 1984
Valea Cerbului	Buşteni	26	62.3	June 2001
			54.2	July 1988
			24.7	August 1999
			22.2	July 1969
			22.2	June 1981
Slănic	Vărbilău	42	175	July 2002
			158	July 1975
			130	June 1998
			127	August 2005
			106	July 1979
Teleajen	Cheia	41	85	August 1970
			66.2	July 1975
			57.8	July 1969
			51.7	May 1984
			46.4	June 1985

Qmax = peak flow of flash-flood event.

3.2. Flash-flood conditioning factors

In some of the previous studies, a number of maximum 5 flash-flood conditioning factors were considered for FFPI calculation (Brewster, 2009; Zaharia et al., 2012; Fontanine and Costache, 2013). In order to increase the degree of accuracy of the final results, in this study, 10 factors that influence the surface runoff, were included in the analysis. Therefore, the following 10 environmental variables were considered: slope angle, land use, lithology, hydrological soil group, convergence index, topographic wetness index (TWI), topographic position index (TPI), aspect, plan curvature and profile curvature. A number of 7 morphometric factors, from the total of 10, were derived from the Digital Elevation Model retrieved from the SRTM, 30 databases (NASA Earth Data, 2018). Thus, the factors such as slope angle, aspect, profile curvature and plan curvature were obtained in ArcGIS 10.5 software, while the values of the other 3 factors (convergence index, tpi and twi) were calculated in SAGA GIS 2.0.1 software. The cell size for raster of all the above-mentioned factors was established at 30 m. Flash-flood conditioning factors such as land use, lithology and hydrological soil group were extracted from vector datasets. In order to be included in the

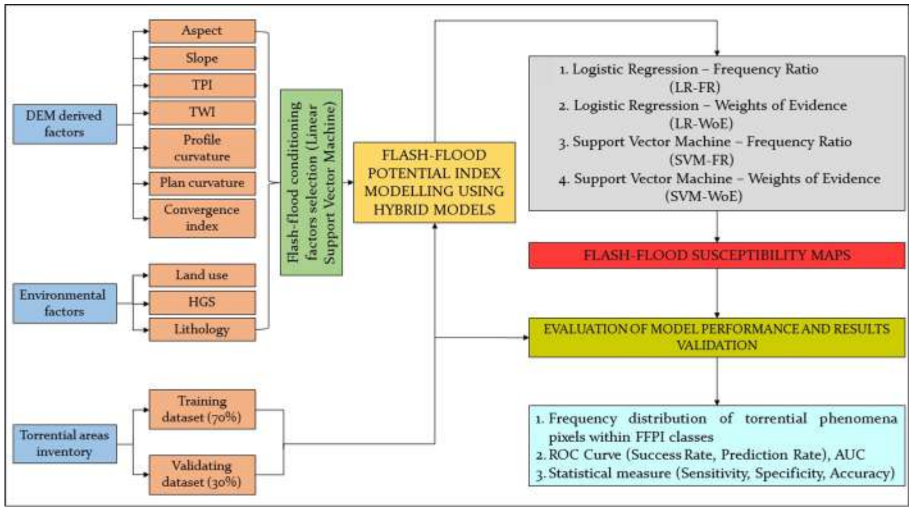

Fig. 2. Flowchart of the methodology.

analysis, these factors were converted to raster format with the same cell size as the morphometric factors.

Slope angle is considered the factor that has the most significant influence on surface runoff process (Costache et al., 2015; Tehrany et al., 2015; Termeh et al., 2018). According to the international literature, slope values were grouped into five classes as following: <3°, 3–7°, 7–15°, 15–25°, >25° (Fig. 4a). Unlike low slope values that favor flooding phenomenon, flash-floods are more likely in areas with high slopes where surface runoff occurs. From the analyze of the frequency distribution of torrential areas within slope classes, it can be noted that approximately 92% areas are spread on slopes higher than 15° (Fig. 6a). A percent of 42% of study area is characterized by slopes ranging between 7° and 15°.

Land use is another flash-flood conditioning factor with a great influence on surface runoff process and consequently on flash-floods occurrence. In order to carry out the land use map for the study area, Corine Land Cover database (EEA, 2006) was used. The forest is one of the land use category with an essential hydrological role that diminishes the runoff and minimize the possibility of flash-floods occurrence (Calder, 2002; Carvalho-Santos et al., 2014; Costache et al., 2014; Cojoc et al., 2015; Romanescu et al., 2018). Approximately 52% of the upper and middle sector of Prahova river catchment is covered by forests (Fig. 4b). Given the fact that, in the last decades, the deforestation rate in Romania has rapidly intensified (Andronache et al., 2017) and the forest coverage percentage at national level is around 30,2% (Stăncioiu et al., 2018), we can state that the afforestation percentage of the study area is relatively high and has a significant role in reducing the potential damages caused by flash-floods. The fact that around 5% of the areas affected by torrential phenomena are located within forests' perimeter is also remarkable (Fig. 6). The pastures and natural grasslands include the largest area affected by torrential phenomena - 70% of the total torrential areas. Alongside with built-up areas, these land use categories are characterized by the lowest values of Manning roughness coefficients.

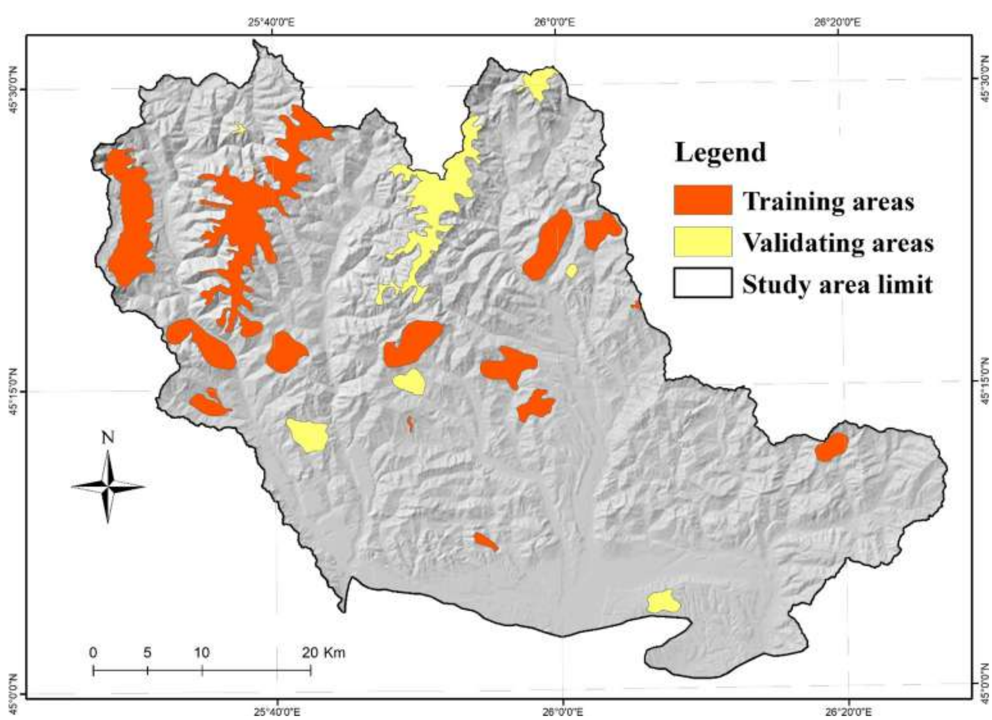

Fig. 3. The spatial distribution of the areas with torrential phenomena within the upper and middle zone of Prahova river catchment.

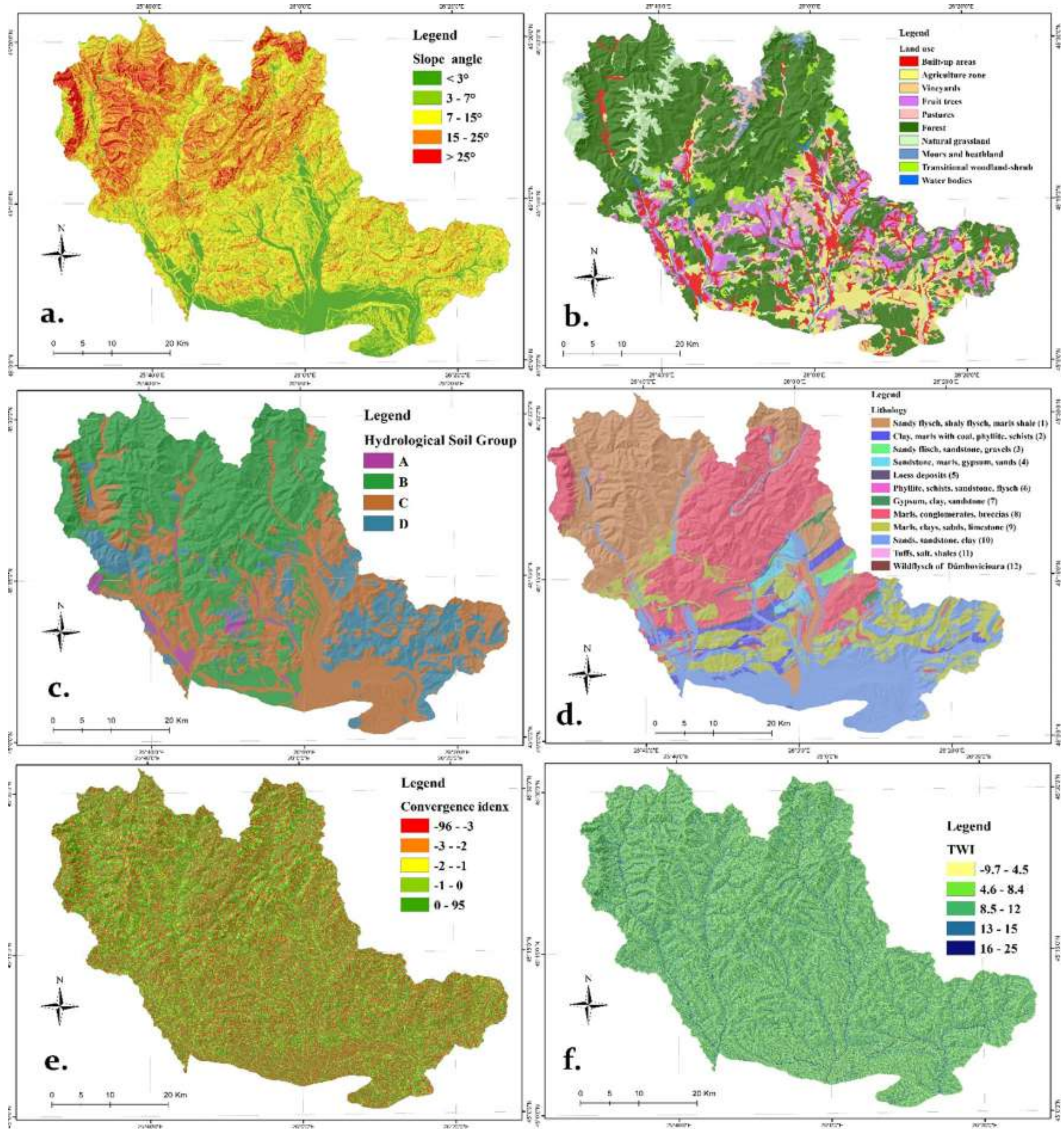

Fig. 4. Flash-flood conditioning factors (a. Slope; b. Land use; c. Hydrological Soil Group; d. Lithology; e. Convergence index; f. Topographic Wetness Index).

Profile curvature is the morphometric factor that highlights the curvature of surfaces in vertical plan on the slope direction (Duman et al., 2006). Due to the influence on surface runoff velocity, this morphometric factor is very important for Flash-Flood Potential assessment. For the study area the profile curvature values range between −8.2–9.7 (Fig. 5a). The negative values of this parameter highlight the areas with accelerated runoff, while the positive values indicate the presence of surfaces with low runoff velocity. Areas with torrential phenomena are mainly distributed over negative values of profile curvature (Fig. 7a).

Plan curvature is another morphometric factor that influences the surface runoff. This parameter shows the contour line formed by the intersection of a horizontal plane with the soil surface. In fact, its values make the difference between the areas with divergent runoff and those with convergent runoff. Plan curvature values ranging between 0.1 and 0.5 are distributed on approximately 50% of study area (Fig. 5b). Most torrential phenomena are spread on positive values of plan curvature (Fig. 7b).

The Aspect of slopes (Fig. 5b) has an indirect influence to flash-flood occurrence by imposing a specific regime to soil humidity. For example, on the shaded slopes, the soil moisture and therefore the water infiltration in the soil are diminished and the surface runoff becomes more intense. During the winter, due to the long-lasting snow cover, shaded slopes are less favorable to flash-flood occurrence, while during spring, due to the snow melt process which is very intense on sunny slopes, flash-floods are more likely to occur. In the present study, 20% of the areas affected by torrential phenomena are located on the eastern slopes (Fig. 7d).

The Topographic Position Index (TPI) is one of the factors derived in SAGA GIS 2.0.1. The values of this morphometric index reflect the altitude difference between a focused cell and the neighbor cells (Jenness, 2000). TPI values were grouped in five classes by using Natural Breaks method, according to the classification procedure used by Costanzo et al. (2012) (Fig. 5c). The Natural Breaks method is highly recommended for certain indicators with spatial distribution for which specific classes intervals were not established before, so that the similar

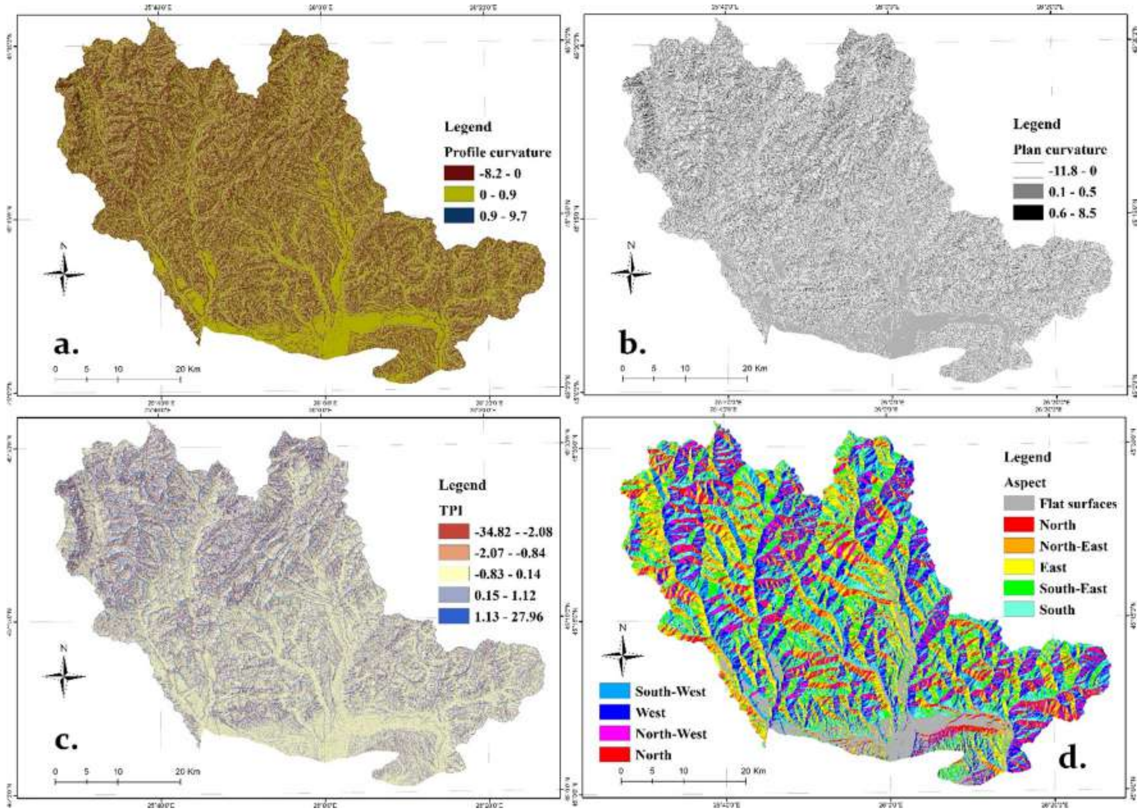

Fig. 5. Flash-flood conditioning factors (a. Profile curvature; b. Plan curvature; c. Topographic Position Index; d. Aspect).

values are best grouped and the differences between classes are maximized (Chen et al., 2013). The Over 40% of the study area is characterized by TPI values ranging between −0.8 and 0.1. Approximately 80% of the areas affected by torrentiality are located within the surfaces with positive values of TPI (Fig. 7c).

Topographic Wetness Index (TWI) values were calculated in SAGA GIS 2.0.1 software, based on the following Eq. (1) (Moore et al., 1991):

$$\mathrm{TWI} = \ln\left(\frac{\alpha}{\tan\beta}\right), \tag{1}$$

where α is the cumulative up slope area draining through a point (per unit contour length) and $\tan\beta$ is the slope angle at the point.

This index highlights the water accumulation tendency to a given point of hydrographic basin. For the study area, TWI values range between −9.7–25 (Fig. 4f). The highest values are specific to valleys. Around 35% of torrential areas are spread within the middle-class values of TWI (8.5–12) (Fig. 6f).

The Lithology layer used in the present study was extracted from Digital Geological Map of Romania, 1:200,000 (NGIR, 2002). By influencing the pedological characteristics and also the water infiltration process, this factor has an important influence to surface runoff (Prăvălie and Costache, 2013). Across the upper and middle sector of Prahova river catchment, a number of 12 rocks group were identified (Fig. 5d). Marls, flysch and conglomerates cover the largest areas from the study zone. Sand and gravels are specific to valleys perimeter. Almost 90% of the torrential areas are found on sedimentary rocks mentioned above.

According to the National Engineering Handbook (2007), hydrological soil groups (Fig. 4c) were established for the study area. Over 60% of torrential phenomena are located in areas characterized by the presence of hydrological soil group B (Fig. 6c).

Convergence Index is a morphometric factor which was used in previous flash-flood susceptibility studies (Zaharia et al., 2015). According to the international literature, five classes were used in order to group convergence index values (Costache and Zaharia, 2017) (Fig. 4e). Negative values highlight a high degree of hydrological network convergence, while the positive values indicate the presence of interfluvial zones. Around 50% of the areas affected by torrential phenomena are spread over surfaces with positive values of convergence index (Fig. 6e).

3.3. Selection of flash-flood conditioning factors

In a study whose main purpose is the assessment of susceptibility to a specific phenomenon, it is very important to analyze the factors which influence the hazard and a carefully selection of these factors, based on a statistical analysis, is also recommended. Due to the fact that the considered variables have a different influence on flash-flood occurrence the factors selection process in the present study is mandatory.

In studies related to the estimation of susceptibility to different natural hazards the selection of conditioning factors is a widely used process. Here are some of the many selection methods that have been proposed in the literature: Gain Ratio (Pham et al., 2016a, 2016b; Bui et al., 2012), consistency (Dash and Liu, 2003); Information Gain (Bui et al., 2016a, 2016b), Symmetrical uncertainty (Senthamarai Kannan and Ramaraj, 2010), fuzzy rough set (Dai and Xu, 2013); PSO-based feature selection (Ajit Krisshna et al., 2014), chi-square statistic (Chen et al., 2009). In the present study, for flash-flood conditioning factors selection and for the assessment of their predictive capability, Linear Support Vector Machine (LSVM) method, proposed for the first time by Guyon and Elisseeff (2003), was employed. By using the results of LSVM method, the irrelevant and unnecessary input variables could be removed (Lin et al., 2008; Bui et al., 2017).

By considering the training areas and using the Eq. (1), specific to LSVM model, prediction capabilities of ten flash-flood conditioning factors were assessed (Eq. (2)):

$$f(x) = \mathrm{sign}(w^T * a + b), \tag{2}$$

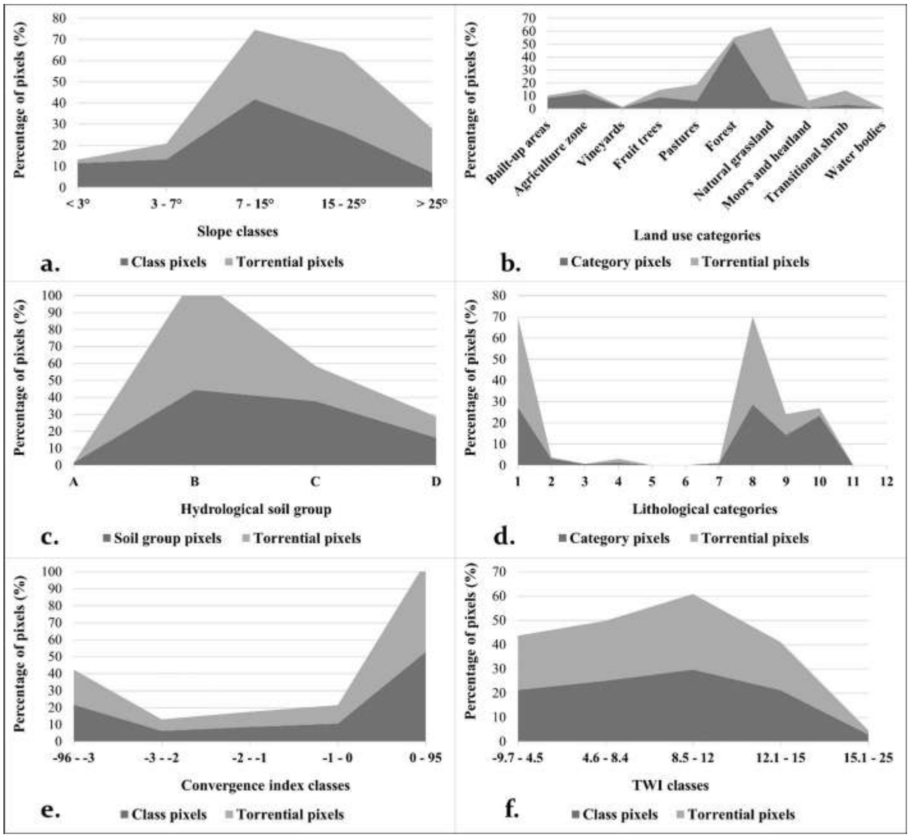

Fig. 6. Relative frequency distribution of torrential phenomena pixels within flash-flood conditioning factors classes/category (a. Slope; b. Land use; c. Hydrological Soil Group; d. Lithology; e. Convergence index; f. Topographic Wetness Index).

where w^T is the inverse matrix of weight matrix assigned in each landslide conditioning factor, a = (a1, a2, ..., a11) is the vector of inputs that contains eleven landslide conditioning factors, b is the offset from the origin of the hyper-plane (Bui et al., 2017).

According to Mladenić et al. (2004) an flash-flood conditioning factor with a weight (w) value close to 0 has a smaller predictive capability than other flash-flood conditioning factor with a higher weight (w) value.

3.4. FFPI calculation method

In order to calculate FFPI values within the present study area, several steps were followed.

Thus, in a first stage, for each factor class/category Frequency Ratio (FR) and Weights of Evidence (WoE) weights were determined. The weights value will be the results of the spatial relationships between

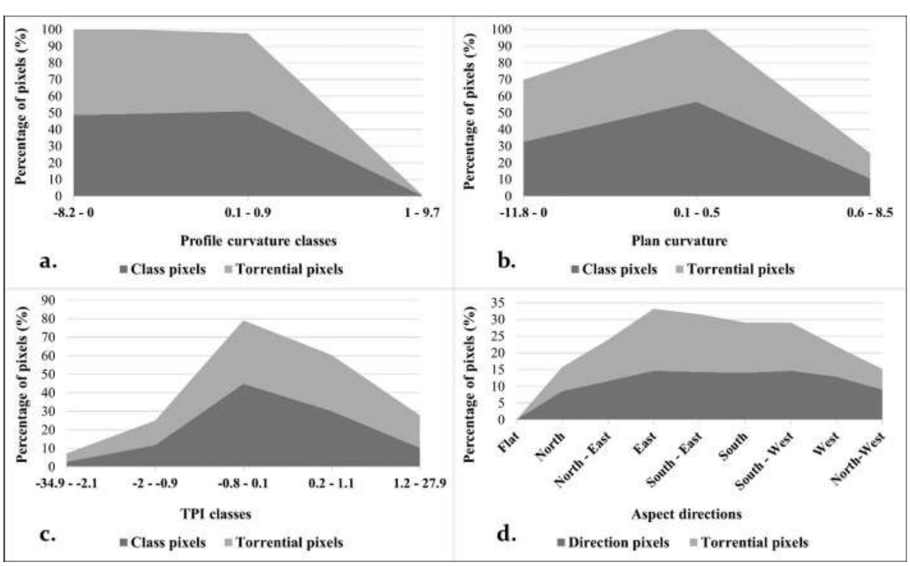

Fig. 7. Relative frequency distribution of torrential phenomena pixels within flash-flood conditioning factors classes/category (a. Profile curvature; b. Plan curvature; c. Topographic Position Index; d. Aspect).

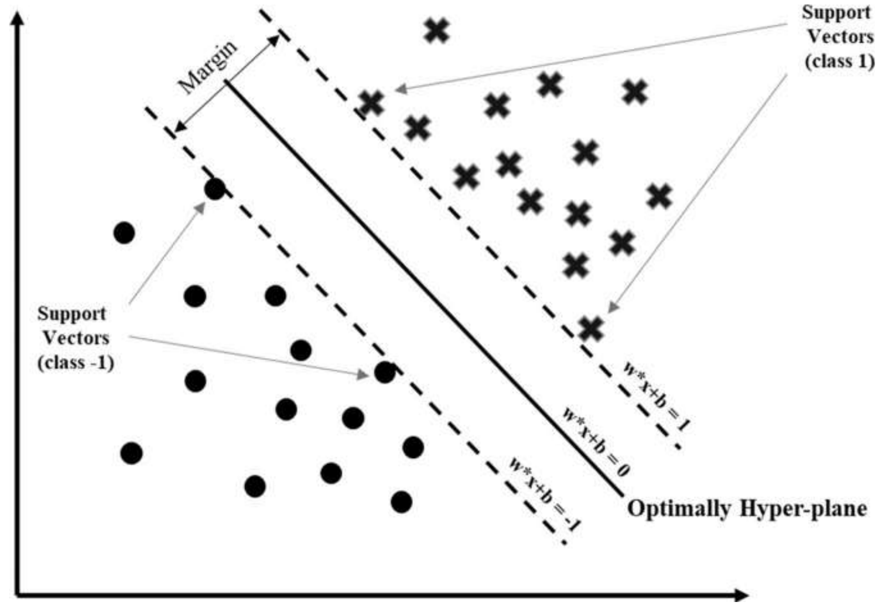

Fig. 8. Optimally hyper-plane for a linearly separable data.

the areas affected by torrential phenomena and each factor class/category. Once computed the FR and WoE weights for each factor class/category, a new raster of flash-flood conditioning factors was created in GIS environment. By incorporating the new rasters into the Logistic Regression (LR) and Support Vector Machine (SVM) analysis, FFPI values were calculated across the study area.

3.4.1. Frequency Ratio (FR) model

FR is an easy to use and understanding bivariate statistical model (Pradhan and Lee, 2009). The FR weights were assessed by applying the ratio between the number of pixels with torrential phenomena inside a factor's class and the total number of pixels with torrential phenomena over the whole study area (Eq. (3)) (Lee and Pradhan, 2007; Youssef et al., 2015a, 2015b; Costache and Zaharia, 2017):

$$FR = \frac{\frac{Np(LXi)}{\sum_{i=1}^{m} Np(LXi)}}{\frac{Np(Xj)}{\sum_{j=1}^{m} Np(Xj)}}, \tag{3}$$

where: FR-the Frequency Ratio of class i of factor j, Np(LXi) – the number of pixels with torrentiality within class i of factor variable X, Np(Xj) is the number of pixels within factor variable Xj, m is the number of classes in the factor variable Xi, and n is the number of factors in the study area.

In order to estimate FR weights, the combination of each flash-flood conditioning factor raster with the raster corresponding to areas affected by torrential phenomena, was performed. The combination results in tabular format were imported in Excel 2016 and the calculus was carried out. Once established, FR weights were assigned to each corresponding factor class/category.

3.4.2. Weights of Evidence (WoE) model

WoE is a bivariate Bayesian statistical model widely used in studies regarding the assessment of natural hazards susceptibility (Youssef et al., 2015a, 2015b). This data-driven method developed initially for geological studies (Agterberg, 1992; Bonham-Carter, 2002) was taken over by other researchers and used in studies related to the analysis of susceptibility to different hazards such as: landslides, flood and flash-flood (Kayastha et al., 2012; Tehrany et al., 2014; Khosravi et al., 2016a.; Khosravi et al., 2016b.; Rahmati et al., 2016; Youssef et al., 2016a, 2016b). By applying WoE method in the present study, the data was prepared to be incorporated in SVM and LR models for FFPI calculation. The WoE coefficients values were estimated based on the relationship between the absence and the presence of torrential areas, and each factor class/category. The calculation of each coefficient value requires the computation of the positive weight (W^+) and the negative weight (W^-). Positive weights reflect the presence of areas affected by torrential phenomena while negative weights show the absence of areas affected by torrential phenomena. The following equations are used in order to compute the two types of

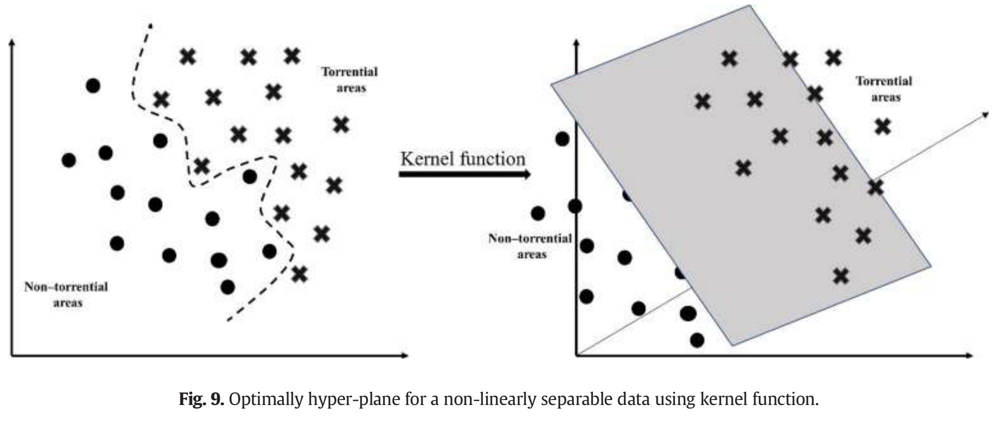

Fig. 9. Optimally hyper-plane for a non-linearly separable data using kernel function.

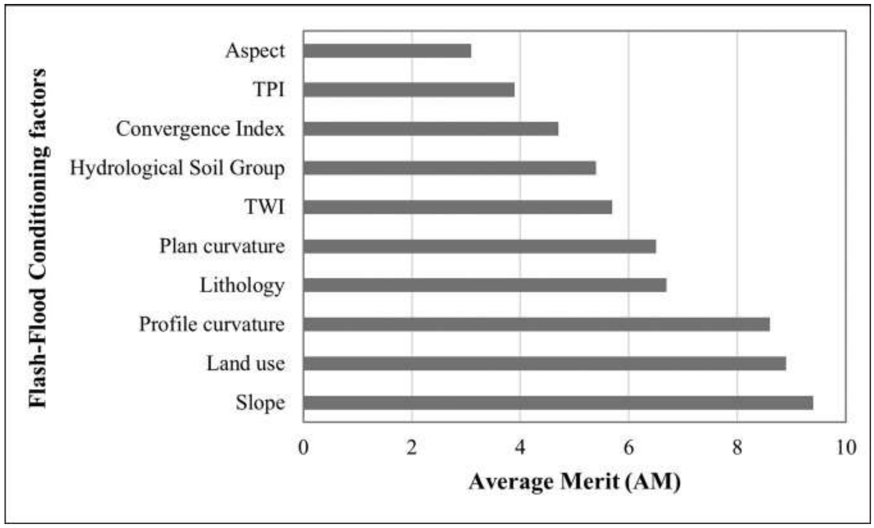

Fig. 10. Prediction capability of the flash-flood conditioning factor.

weights (Bonham-Carter, 1994):

$$W^+ = \ln \frac{P\{B/S\}}{P\left\{B/\overline{S}\right\}} \tag{4}$$

and

$$W^- = \ln \frac{P\{\overline{B}/S\}}{P\left\{\overline{B}/\overline{S}\right\}}, \tag{5}$$

where: W^+ – positive weight, W^- – negative weight, P – the probability, B – the presence of runoff predictive factor, $\overline{B}$ – the absence of a runoff predictive factor, S – the presence of torrentiality, $\overline{S}$ – the absence of torrentiality.

The results of the combination process performed on the previous point were used in order to implement the Eqs. (4) and (5) in ArcGIS 10.5 software environment. Therefore, these two equations can be rewritten as (Van Westen et al., 2003):

$$W^+ = \ln \frac{\dfrac{Npix_1}{Npix_1 + Npix_2}}{\dfrac{Npix_3}{Npix_3 + Npix_4}} \tag{6}$$

and

$$W^- = \ln \frac{\dfrac{Npix_2}{Npix_1 + Npix_2}}{\dfrac{Npix_4}{Npix_3 + Npix_4}} \tag{7}$$

where: $Npix_1$ - number of pixels with torrentiality in the class; $Npix_2$ number of pixels with torrentiality from outside of the class; $Npix_3$ - number of pixels in the class without torrentiality; $Npix_4$ - number of pixels without torrentiality from outside of the class; W^+ - positive weight, W^- - negative weight.

The factors' final weighting (Wf) was obtained with the formula (Van Westen et al., 2002; Costache and Zaharia, 2017):

$$Wf = Wplus + W\ \mathrm{min}total - Wwin, \tag{8}$$

where: Wplus – positive weight of a class factor, Wmin – negative weight of a class factor, Wmintotal – the total of all negative weights in a multiclass map.

3.4.3. Support Vector Machine (SVM)

Support Vector Machine (SVM) is a classification model based on statistical learning theory, this method being applied both in classification and regression problems with large amount of data (Vapnik, 1995;

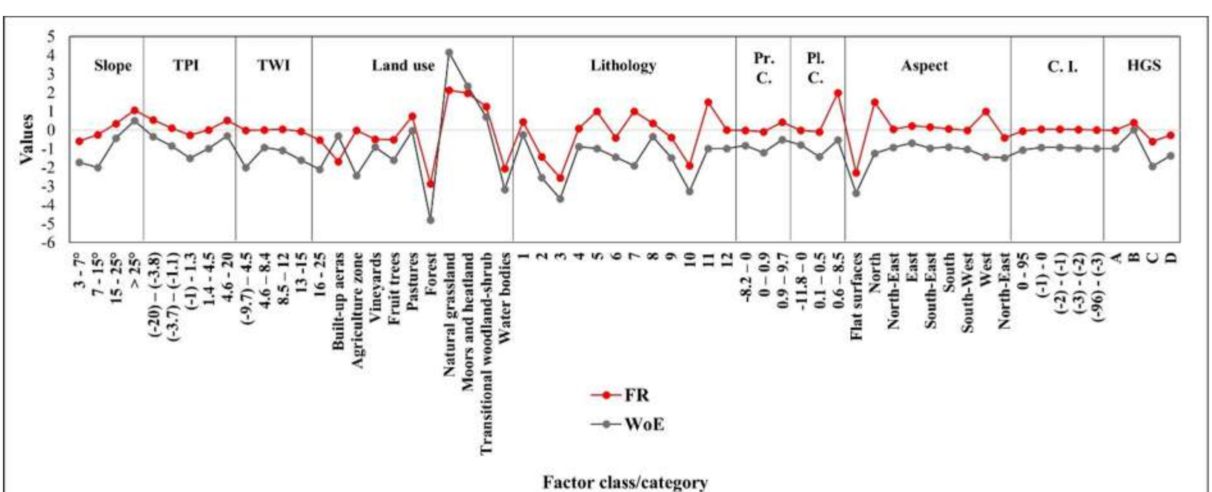

Fig. 11. Frequency Ratio and Weights of Evidence coefficients value distribution within flash-flood conditioning factors classes/category.

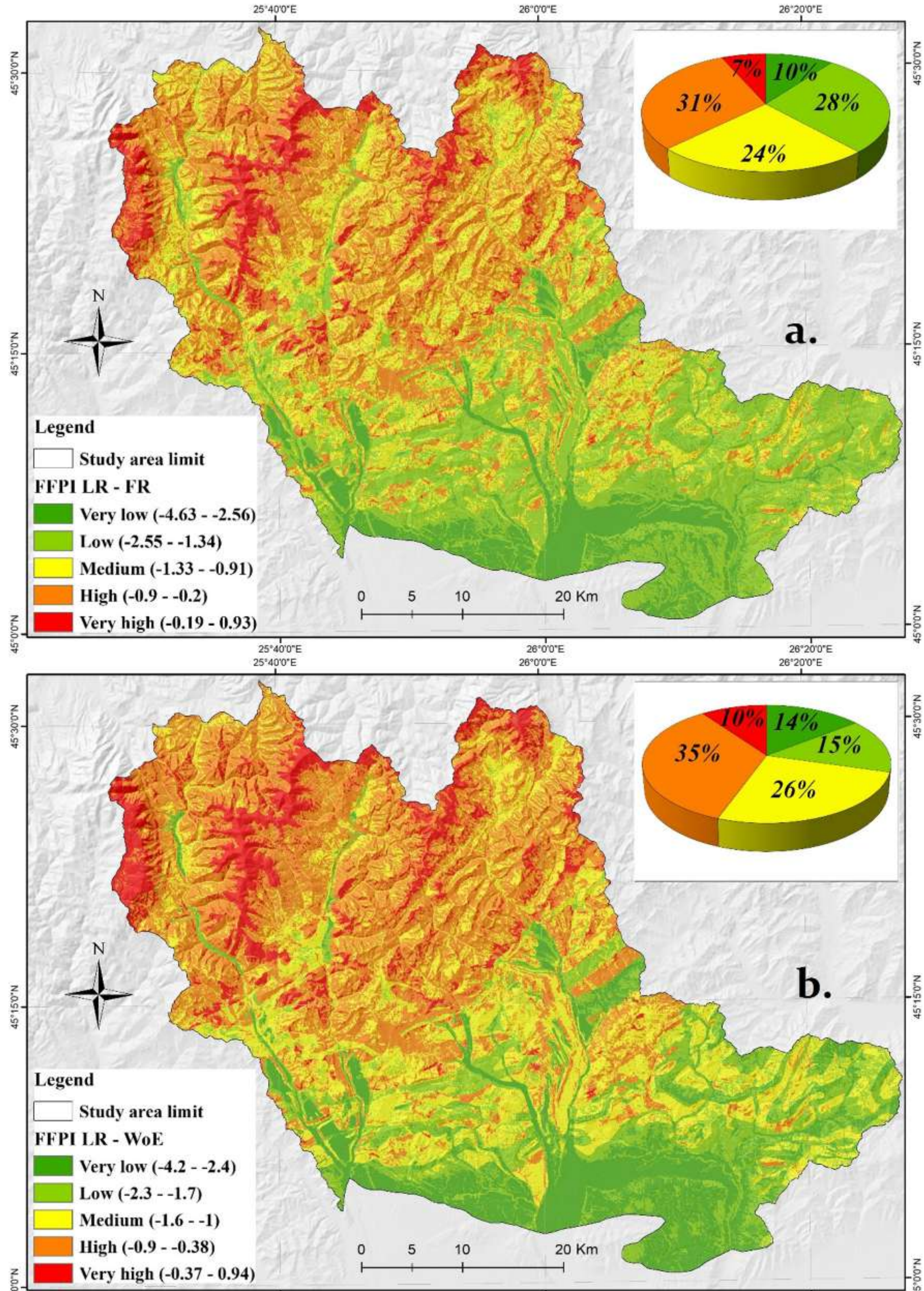

Fig. 12. Spatial distribution of FFPI values (a. FFPI LR-FR and b. FFPI LR-WoE).

Hua and Sun, 2001; Pourghasemi et al., 2013). The main objective of the algorithm is to identify a hyper-plane that optimally divides the training data (Fig. 8). The closest data to the hyper-plane are called support vectors and represent essential elements of training data. Once the optimum surface of hyper-plane obtained, it can be used for classifying the new data.

By adapting to the present study, we consider the pair (x_i, y_i) cu $x_i \in R^m$, $y_i \in \{1,-1\}$ and $i = 1, \ldots, m$, where x is a vector of the input

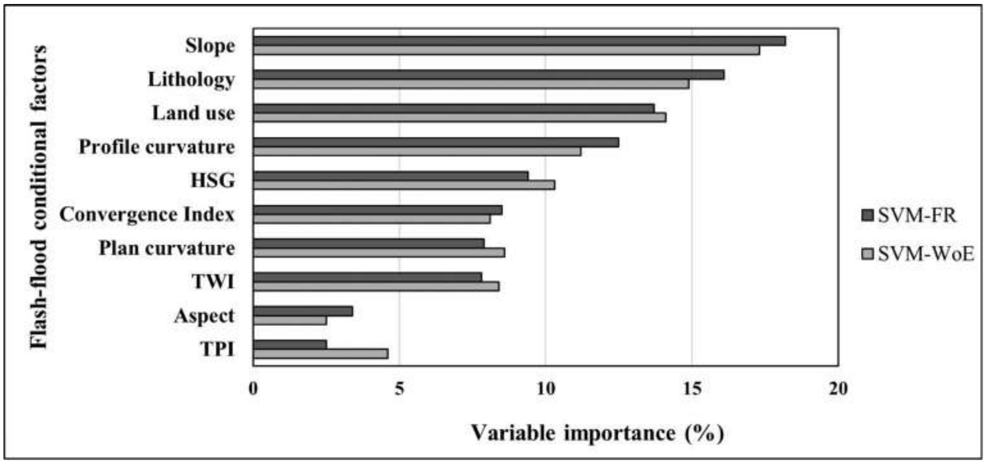

Fig. 13. Flash-flood conditional factors importance.

space containing the slope angle, profile curvature, lithology, land use, aspect, twi, tpi, convergence index, plan curvature and hydrological soil group, while y represent the areas affected by torrential phenomena when $y = 1$, and areas without torrential phenomena when $y = -1$. In a two-dimensional space, SVM algorithm seeks to solve the problems by identifying a line which most efficiently separates the points inside the positive class (areas affected by torrentiality) from those inside the negative class (areas without torrentiality).

If training data are linear separable, the hyper-plane is defined by the following relation (Eq. (9)) (Bui et al., 2012):

$$y(w * x_i + b) \geq 1 - \xi_i, \tag{9}$$

where w is a coefficient vector that determines the orientation of the hyper plane in the feature space, b is the offset of the hyper plane from the origin, and ξ_i is the positive slack variables (Bui et al., 2012).

In order to find the optimally hyper-plane the following problem need to be solved:

$$\text{Minimize} \sum_{i=1}^{n} \alpha_i - \frac{1}{2} \sum_{i,j=1}^{n} \alpha_i \alpha_j y_i y_j (x_i, x_j), \tag{10}$$

$$\text{Subject to } \sum_{i=1}^{n} \alpha_i y_i = 0 \; 0 \leq \alpha i \leq C, \tag{11}$$

where α_i are Lagrange multipliers, C is the penalty parameter that controls the trade-off between the complexity of the decision function and the number of training examples misclassified (Hong et al., 2016).

The function necessary for new data classification by using a linear hyper-plane can be written as (Bui et al., 2012):

$$f(x) = \text{sign}\left(\sum_{i=1}^{n} y_i \alpha_i x_i, +b\right). \tag{12}$$

In practice, there are many situations in which a non-linear separable hyper-plane is needed to be used, and therefore the original input data may be transferred into a high-dimension feature space (Fig. 9). In these cases when a nonlinear kernel function should be applied, the Eq. (12) will be rewritten as follows (Kavzoglu et al., 2014):

$$f(x) = \sum_{i=1}^{n} (\alpha_i - \alpha_i^*) K(x_i, x) + b, \tag{13}$$

where α_i and α_i^* are Lagrange multipliers ($\alpha_i \geq 0$, $\alpha_i^* \leq C$) and $K(x_i, x_j)$ is the kernel function.

The application of SVM model in the present study for FFPI calculation has been facilitated through Weka Software v. 3.9.2 2, developed within The University of Waikato Hamilton, New Zealand. From a total of 4 types of kernel functions usually used in SVM models, Radial Basis Function is considered one of most efficient in this type of research (Cherkassky and Mulier, 2007; Kavzoglu et al., 2014), and, therefore, was selected to be applied in the present study also.

The mathematical representation of Radial Basis Function (RBF) is reproduced below (Pourghasemi et al., 2013):

$$K(X_i, X_j) = (-\gamma \|X_i - X_j\|), \gamma > 0, \tag{14}$$

where γ is the gamma term in the kernel function for all kernel types except linear.

The accuracy of SVM model results depends both on the correct selection of kernel function and on the estimation of C and γ (Tehrany et al., 2015). Therefore, a careful determination of the 2 parameters is required. According to Hong et al. (2015) a high value of C may lead to over fit while a small value of C factor will lead to under fitting. One of the most common methods used for estimating SVM parameters is represented by the grid search method on C and γ by using cross-validation (Kavzoglu and Colkesen, 2009; Chang and Lin, 2011). This method was also applied in the present study, in which many pairs (C, γ) where tested until the pair with the best cross-validation parameters was selected ($C = 2.5$, $\gamma = 0.1$).

Beside the SVM parameters (C, γ), the input model data consisted of the areas affected by torrential phenomena as well as flash-flood conditioning factors with FR and WoE weights assigned for each class/category.

3.4.4. Logistic Regression

A very popular multivariate statistical analysis method, the Logistic Regression is used for analyzing the relationship between a dependent binary variable (Y) and several independent variables (X_i) which can explain the spatial distribution of independent variable (Kavzoglu et al., 2014). The dependent variable in the Logistic Regression is binary, its two classes being characterized by the presence (1) or absence (0) of the analyzed phenomenon. Depending on the spatial relationships between the phenomenon and the factors classes/categories, the Logistic Regression model performs a spatial prediction of the susceptibility to this phenomenon. In terms of independent variables within the Logistic Regression model, both continuous data (slope angle, profile curvature, plan curvature etc.) and discrete data (land use, lithology, hydrological soil group) could be incorporated. In the present study, the value of 1 has been attributed to areas affected by torrential phenomena and a value of 0 has been attributed to areas without torrential phenomena. In order to be able to perform the analysis, the raster corresponding to the binary variable will be combined in GIS environment with the rasters associated with all flash-flood conditioning factors obtained after

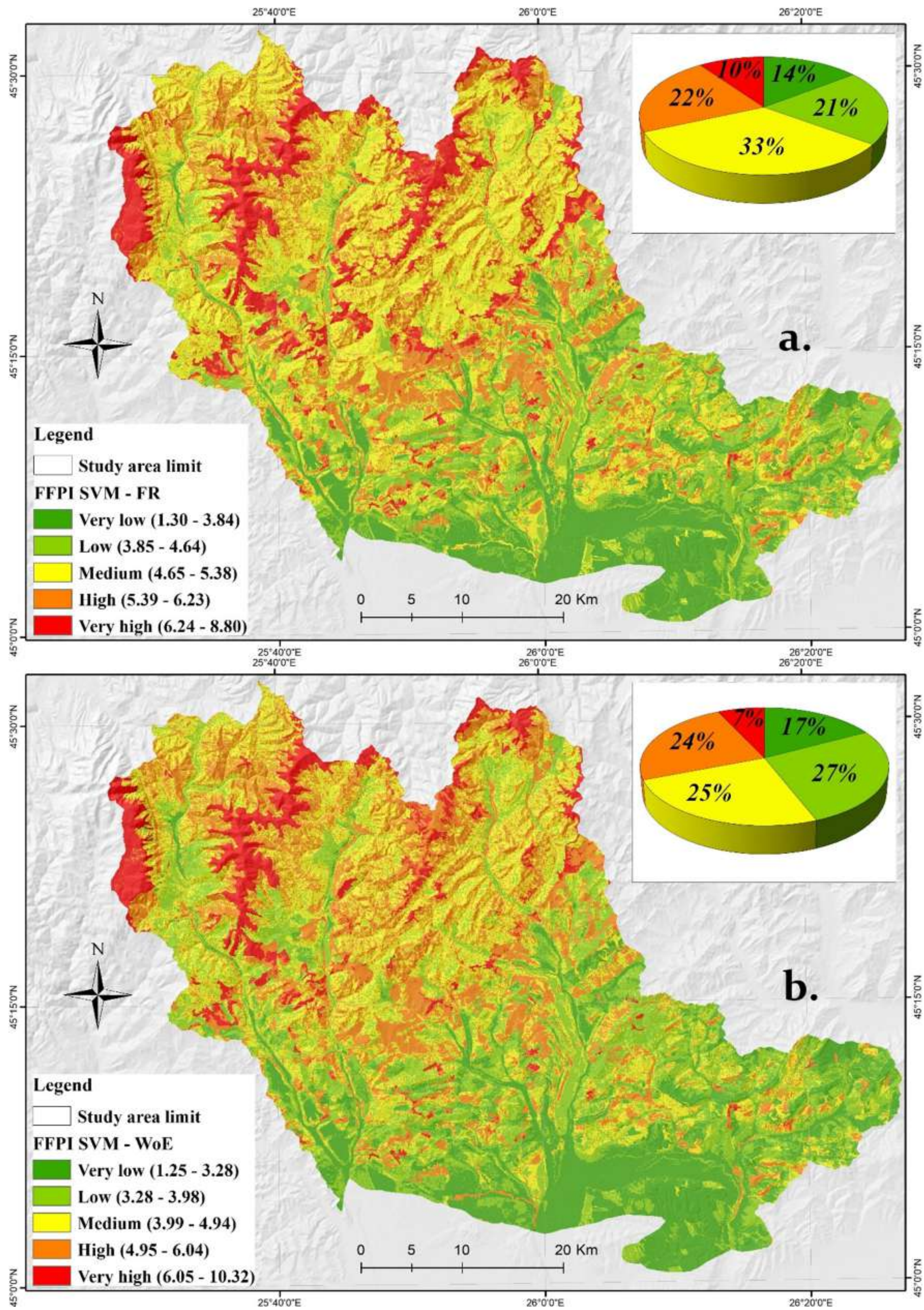

Fig. 14. Spatial distribution of FFPI values (a. $FFPI_{SVM\text{-}FR}$ and b. $FFPI_{SVM\text{-}WoE}$).

the application of FR and WoE models. Subsequently, the table associated to the new resulted raster, will be exported in a format specific to SPSS 21 software. By using SPSS 21, the weight of each independent variable expressed by the value of the Logistic Regression coefficients will be calculated.

By using the following equation the generalized linear model of the Logistic Regression method can be calculated (Kavzoglu et al., 2014):

$$p = \frac{1}{1 + e^{-z}}, \tag{15}$$

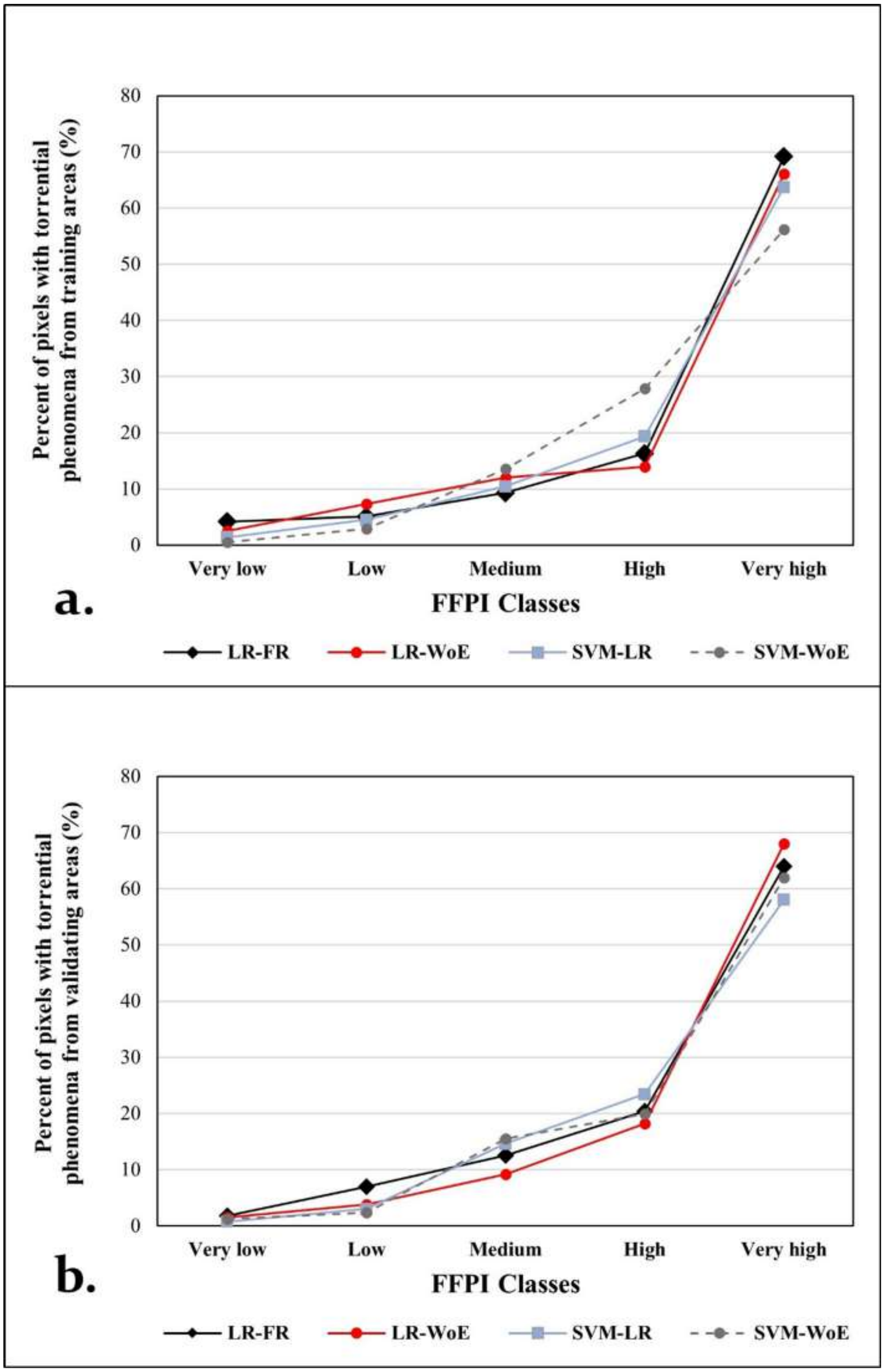

Fig. 15. Relative distribution of torrential pixels within FFPI classes (a. training dataset; b. validating dataset).

where p is the probability of an event. Z is a value from $-\infty$ to $+\infty$, defined by the following equation:

$$z = b_0 + b_1x_1 + b_2x_2 + \ldots + b_nx_n, \tag{16}$$

where b_0 is the intercept of the model, the b_i ($i = 0, 1, 2, \ldots, n$) are the slope coefficients of the Logistic Regression model, and the x_i ($i = 0, 1, 2, \ldots, n$) are the independent variables (Lee and Sambath, 2006).

Due to the fact that Logistic Regression model is sensitive to collinearities among the independent variables, the multicollinearity analysis is mandatory (Hosmer and Lemeshow, 1989). In the present study, by using SPSS 21 software, Tolerance (TOL) and Variance Inflation Factor (VIF), which are two of the most important indicators of a possible multicollinearity among the independent variables, will be calculated. Values <0.2 of TOL indicate the possibility of multicollinearity existence, as well as in case of values higher than 4 of VIF (Menard, 1995; Dou et al., 2018).

3.5. Results validation and model performance assessment

3.5.1. Relative distribution of training and validating areas within FFPI classes

Relative distribution of training and validating areas within FFPI classes was the first method used for results validation and for

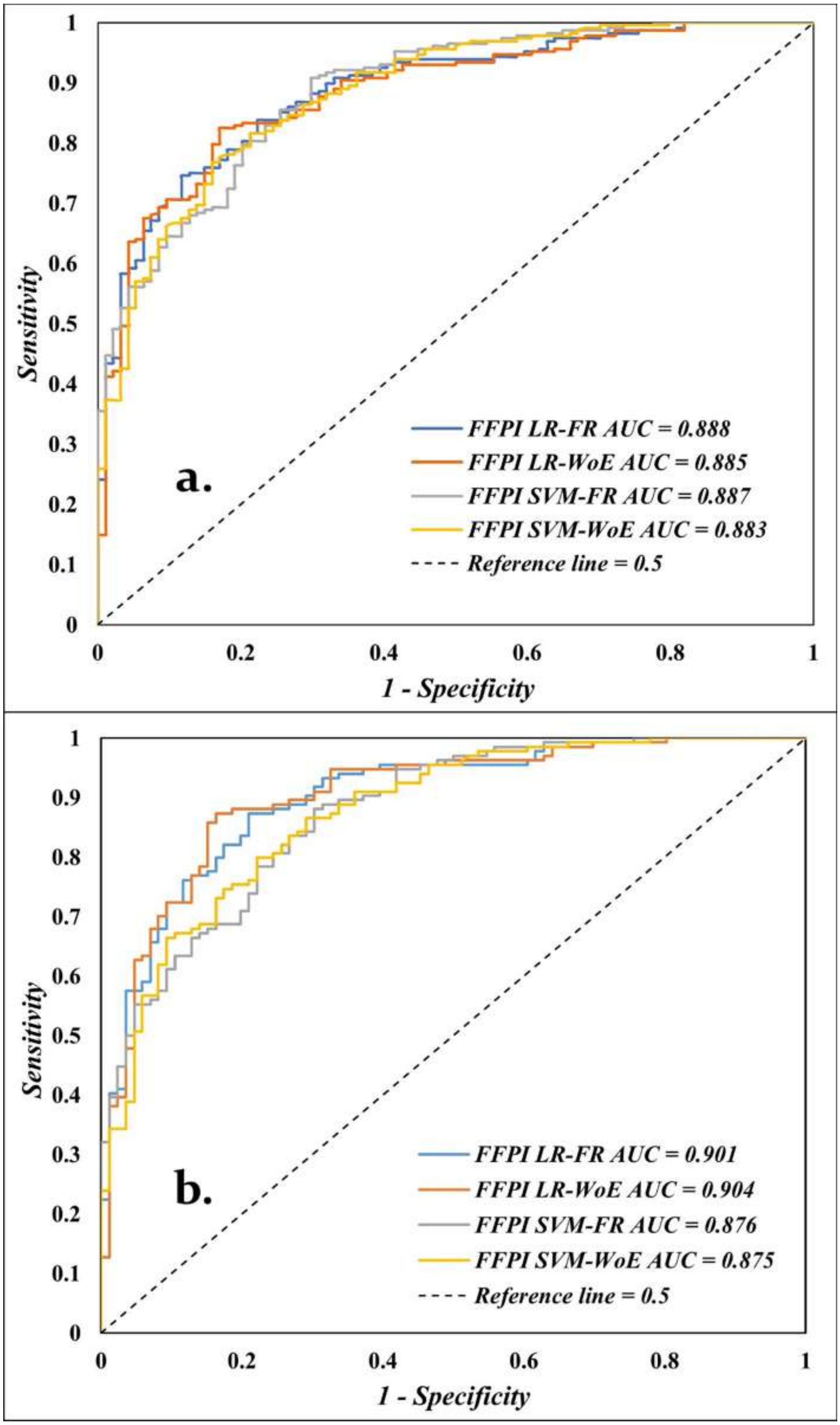

Fig. 16. ROC curves with associated AUC values computed from training samples (a. Success Rate) and validation samples (b. Prediction Rate).

assessment of the model performance. Training areas were considered in order to assess the model performance, while validating areas were used for results validation. This method is widely used within the studies regarding the assessment of susceptibility to different natural hazards (Hong et al., 2018a, 2018b). A good efficiency of the models is highlighted by a consistent presence of areas with torrential phenomena inside the High and Very High values of FFPI

3.5.2. Receiver operating characteristics (ROC)

The second method used for assessing the model performance and results validation is represented by the ROC Curve and AUC (Area Under Curve). ROC Curve is mainly used to judge the discrimination ability of the statistical models that combine different test results for predictive purposes (Hanley and McNeil, 1982). This method describes the capacity of a system to correctly predict the occurrence of an event.

By the mean of ROC Curve, the connection/trade-off between sensitivity and specificity is represented in a graphical way. Therefore, the ROC Curve graphic can be constructed by representing sensitivity on Y axis and specificity on X axis (Chen et al., 2018). This graphic model is widely used in order to assess the performance of the various methods applied in the analysis of the surfaces susceptibility to natural hazards (Youssef et al., 2015a, 2015b; Bui et al., 2016a, 2016b; Chapi et al., 2017; Termeh et al., 2018). The effectiveness measure of a model is given by the AUC value. The closer value gets to 1, the better the model is (Pallant, 2013).

The equation underlying the AUC calculation has the following form (Hong et al., 2018a.):

$$\mathrm{AUC} = \frac{(\sum \mathrm{TP} + \sum \mathrm{TN})}{(\mathrm{P} + \mathrm{N})}, \tag{17}$$

where TP (true positive) and TN (true negative) are number of pixels that are correctly classified, P is the total number of pixels with torrential phenomena and N is the total number of pixels without torrential phenomena.

The success rate, constructed by the mean of training areas, will assess the models performance, while prediction rate constructed by the mean of the validating areas will be used to validate the results.

3.5.3. Statistical measures

In the susceptibility studies that incorporate into the analysis the presence and absence of the phenomenon, the model assessment and results validation through statistical method has a crucial role (Hong et al., 2018a). In the present research, specificity and accuracy, were used as statistical indices. In the previous studies, these parameters were especially used in landslide susceptibility models assessment (Bui et al., 2016a, 2016b; Chen et al., 2017; Chen et al., 2018). By the mean of the following equations, the three indicators were calculated:

$$\mathrm{Sensitivity} = \frac{\mathrm{TP}}{\mathrm{TP} + \mathrm{FN}}, \tag{18}$$

$$\mathrm{Specificity} = \frac{\mathrm{TN}}{\mathrm{FP} + \mathrm{TN}}, \tag{19}$$

$$\mathrm{Accuracy} = \frac{\mathrm{TP} + \mathrm{TN}}{\mathrm{TP} + \mathrm{FP} + \mathrm{TN} + \mathrm{FN}}, \tag{20}$$

where FP (false positive) and FN (false negative) are the numbers of pixels erroneously classified.

4. Results and discussion

4.1. Predictive capability of flash-flood conditioning factors

By applying LSVM method, described at Section 3.3, the predictive capability for each flash-flood conditioning factors, expressed as Average Merit (AM) values, was determined (Fig. 10).

As it can be observed in Fig. 10, slope angle has the highest predictive capability with an AM value of 9.4. The result agrees with other research papers that consider the slope angle as the factor with the highest influence on surface runoff process (Tehrany et al., 2015; Dai et al., 2017; Abdulkareem et al., 2018).

On the next position, in terms of predictive capability, is land use factor with an AM value of 8.9. This is explained by the fact that the large variety of land use types generates very different surface runoff behaviors in a given area (Niehoff et al., 2002; Hundecha and Bárdossy, 2004).

Considering the AM values, land use factor is followed by the profile curvature (AM = 8.6), lithology (AM = 6.7), plan curvature (AM = 6.5), twi (AM = 5.7), hydrological soil group (AM = 5.4), convergence index (AM = 4.7), tpi (AM = 3.9) and aspect (AM = 3.1).

As it can be seen, the AM values of flash-flood conditioning factors range between 3.1 and 9.4. Even if the AM value specific to slope angle, exceeds about 3 times the AM value of aspect, all 10 variables initially considered in the present study show a significant contribution to the flash-flood occurrence and therefore will be further included into the analysis.

4.2. Application of hybrid models LR-FR and LR-WoE

According to the methodological approach described at Section 3.4, in a first stage of the workflow FR and WoE coefficients were estimated for each factor class/category. A total number of 61 values were established for both FR and WoE coefficients. Minimum and maximum FR values in the entire dataset were estimated for two land use categories. The Natural Grasslands category is the most favorable to flash-flood occurrence (FR = 2.13), while Forest surfaces represent the most restrictive category for this phenomenon (FR = −2.86) (Fig. 11). The surfaces with slopes exceeding 25° have also a high potential for flash-flood occurrence (FR = 1.07).

A similar situation is also applicable to Weights of Evidence coefficients, the maximum value being assigned to Natural Grassland (WoE = 5.17), followed by Moors and Heatland (WoE = 3.36), Transitional wood-land shrub (WoE = 1.71) and slopes higher than 25 ° (WoE = 1.51). It is also noted that forest areas are characterized by the smallest WoE coefficient value (−3.8) (Table 2).

In order to be included in the Logistic Regression and Support Vector Machine models, FR and WoE coefficient were standardized, in range 0.1–0.9, by using the following equation (Pradhan and Lee, 2010):

$$y = \frac{(x - \min(d)) * (\max(n) - \min(n))}{\max(d) - \min(d)} + \min(n), \tag{21}$$

where: y – standardized value of x; x – current value of variable; d – range value limits; n – standardization range limits.

The multicollinearity analysis was performed before the application of Logistic Regression model. The results of the analysis show that there is no serious multicollinearity between flash-flood conditioning factors. The lowest value of TOL belongs to Slope factor (0.87), while the Aspect (0.99) recorded the highest value (Table 3). In terms of VIF values the situation has reversed, Aspect (1.01) having the lowest value, while Slope (1.15) recorded the highest value (Table 2).

Further, by integrating FR and WoE values into the Logistic Regression model, the $\mathrm{FFPI}_{\mathrm{LR\text{-}FR}}$ and $\mathrm{FFPI}_{\mathrm{LR\text{-}WoE}}$ values were computed. Following the analysis performed in SPSS 21, Logistic Regression coefficients for the both two applied models (LR-FR and LR-WoE), were calculated. In terms of $\mathrm{FFPI}_{\mathrm{LR\text{-}FR}}$ computing equation, the highest value of LR coefficients (0.2) was attributed to slope factor, followed by lithology (0.19), aspect (0.152), land use (0.11), twi (0.031), hydrological soil group (0.024), profile curvature (0.017), plan curvature (0.006), tpi (−0.005) and convergence index (−0.045). The equation underlying the $\mathrm{FFPI}_{\mathrm{LR\text{-}FR}}$ calculation has the following form:

$$\begin{aligned} Z_{\mathrm{FR}} = {} & 0.2^{*}\,[\mathrm{Slope}] + 0.19^{*}\,[\mathrm{Lithology}] + 0.152^{*}\,[\mathrm{Aspect}] + 0.11^{*}\,[\mathrm{Land\ use}] \\ & + 0.031^{*}\,[\mathrm{TWI}] + 0.024^{*}\,[\mathrm{HSG}] + 0.017^{*}\,[\mathrm{Profile\ curvature}] \\ & + 0.006^{*}\,[\mathrm{Plan\ curvature}] - 0.005^{*}\,[\mathrm{TPI}] - 0.045^{*}\,[\mathrm{Convergence\ Index}] \\ & - 4.347 \end{aligned} \tag{22}$$

Regarding the $\mathrm{FFPI}_{\mathrm{LR\text{-}WoE}}$ computation, the highest value of β calculated by Logistic Regression model was assigned to lithology factor (0.189), followed by slope (0.149), aspect (0.127), land use (0.113), twi (0.041), hydrological soil group (0.02), profile curvature (0.015), plan curvature (0.005), tpi (−0.011) and convergence index (−0.037).

Table 2
Standardized classes FR and WoE values of flash-flood conditioning factors.

Factor	Class	FR coefficients	FR standardized coefficients	WoE coefficients	WoE standardized coefficients
Slope	<3°	−1.93	0.10	−2.15	0.10
	3–7°	−0.58	0.46	−0.71	0.42
	7–15°	−0.24	0.55	−0.43	0.48
	15–25°	0.35	0.71	0.58	0.70
	>25°	1.07	0.90	1.51	0.90
TPI	(−20)–(−3.8)	0.54	0.90	0.66	0.88
	(−3.7)–(−1.1)	0.11	0.48	0.15	0.53
	(−1)–1.3	−0.27	0.10	−0.50	0.10
	1.4–4.5	0.01	0.38	0.01	0.45
	4.6–20	0.52	0.87	0.69	0.90
TWI	−9.7–4.5	0.05	0.90	−0.01	0.80
	4.6–8.4	0.01	0.83	0.08	0.90
	8.5–12	0.05	0.90	−0.08	0.71
	13–15	−0.06	0.76	−0.59	0.10
	16–25	−0.53	0.10	0.07	0.89
Landuse	Built-up areas	−1.68	0.29	−1.86	0.27
	Agriculture zone	−1.26	0.36	−1.44	0.31
	Vineyards	−0.49	0.48	−0.53	0.39
	Fruit trees	−0.50	0.48	−0.59	0.39
	Pastures	0.75	0.68	0.97	0.53
	Forest	−2.86	0.10	−3.80	0.10
	Natural grassland	2.13	0.90	5.17	0.90
	Moors and heatland	1.97	0.87	3.36	0.74
	Transitional woodland-shrub	1.26	0.76	1.71	0.59
	Water bodies	−2.05	0.23	−2.16	0.25
Lithology	1	0.44	0.90	0.76	0.90
	2	−1.42	0.40	−1.53	0.37
	3	−2.56	0.10	−2.67	0.10
	4	0.10	0.81	0.12	0.75
	5	0.01	0.78	0.01	0.72
	6	−0.40	0.68	−0.44	0.62
	7	−0.82	0.56	−0.89	0.51
	8	0.37	0.88	0.65	0.87
	9	−0.38	0.68	−0.48	0.61
	10	−1.90	0.28	−2.26	0.20
	11	0.01	0.78	0.01	0.72
	12	0.01	0.78	0.01	0.72
Profile curvature	−8.2–0	0.08	0.36	0.18	0.53
	0–0.9	−0.09	0.1	−0.19	0.10
	0.9–9.7	0.42	0.9	0.49	0.90
Plan curvature	−11.8–0	0.08	0.36	0.22	0.67
	0.1–0.5	−0.09	0.1	−0.41	0.10
	0.6–8.5	0.42	0.9	0.47	0.90
Aspect	Flat surfaces	−2.27	0.10	−2.37	0.10
	North	−0.20	0.76	−0.24	0.74
	North-East	0.06	0.84	0.07	0.83
	East	0.23	0.90	0.32	0.90
	South-East	0.18	0.88	0.04	0.82
	South	0.07	0.85	0.09	0.83
	South-West	−0.01	0.82	−0.02	0.80
	West	−0.34	0.72	−0.42	0.68
	North-East	−0.40	0.70	−0.47	0.67
Convergence index	0–95	−0.05	0.10	−0.07	0.10
	(−1)–0	0.05	0.90	0.07	0.89
	(−2)–(−1)	0.06	0.90	0.07	0.90
	(−3)–(−2)	0.03	0.67	0.03	0.69
	(−96)–(−3)	0.01	0.48	0.01	0.50
HGS	A	0.00	0.58	0.01	0.48
	B	0.41	0.90	1.04	0.90
	C	−0.60	0.10	−0.93	0.10
	D	−0.27	0.36	−0.35	0.34

Thus, the $FFPI_{LR\text{-}WoE}$ computation equation has the following form:

$$\begin{aligned}Z_{WoE} = {} & 0.149^{*}\,[\text{Slope}] + 0.189^{*}\,[\text{Lithology}] + 0.127^{*}\,[\text{Aspect}] \\ & + 0.113^{*}\,[\text{Land use}] + 0.041^{*}\,[\text{TWI}] + 0.02^{*}\,[\text{HSG}] \\ & + 0.015^{*}\,[\text{Profile curvature}] + 0.005^{*}\,[\text{Plan curvature}] - \\ & + 0.011^{*}\,[\text{TPI}] - 0.037^{*}\,[\text{Convergence Index}] - 4.682\end{aligned} \tag{23}$$

In order to find out the statistical significance of β coefficients assigned to each flash-flood conditioning factor considered into Logistic Regression analysis, Wald x^2 statistical test was employed. The Wald x^2 values increase with significance of β coefficients (Kavzoglu et al., 2014). Among the variables considered, slope is the most effective flash-flood conditioning factor ($Wald_{FR} = 43.285$, $Wald_{WoE} = 29.75$), while aspect is the less effective ($Wlad_{FR} = 4.482$, $Wald_{WoE} = 2.521$) (Table 4).

$FFPI_{LR\text{-}FR}$ and $FFPI_{LR\text{-}WoE}$ were calculated and mapped by implementing the Logistic Regression Eqs. (22) and (23) in the Map Algebra tool from ArcGIS 10.5 software.

The resulting $FFPI_{LR\text{-}FR}$ values for the upper and middle sector of Prahova river catchment range from (−4.63) to 0.93, and were grouped in 5 classes, by using the Natural Breaks classification method (Fig. 12a). The areas with very low values of Flash-Flood Potential are located especially in the southern part of study area. These surfaces are spread on

Table 3
The multicollinearity analysis for independent variables.

Variables	Collinearity statistics	
	TOL	VIF
Aspect	0.99	1.01
Convergence index	0.94	1.06
Land use	0.97	1.03
Lithology	0.89	1.12
Slope	0.87	1.15
Plan curvature	0.97	1.03
Profile curvature	0.98	1.02
TWI	0.95	1.05
HSG	0.94	1.07
TPI	0.93	1.08

approximately 10% of the upper and middle sector of Prahova river catchment being characterized by $FFPI_{LR\text{-}FR}$ values ranging from (−4.63) to (−2.56). The second $FFPI_{LR\text{-}FR}$ value class ranges between (−2.55) and (−1.34) and totals 28% of the study area. Within these areas the potential of flash-flood occurrence is low, these phenomena being possible in case of very heavy rainfall. The surfaces included in the second $FFPI_{LR\text{-}FR}$ class of values are located only in the southern half of the research area. The $FFPI_{LR\text{-}FR}$ class value corresponding to the medium Flash-Flood Potential ranges between (−1.33) and (−0.91) and is spread on a quarter of study area. The high and very high $FFPI_{LR\text{-}FR}$ values, ranging from (−0.9) to 0.93, are located in the mountain sector of the northern part of study area, and occur mainly on slopes higher than 15° that characterize the areas with Naturals grasslands. Within these areas, that cover approximately 38% of study area, the main touristic mountain resorts from Romania are located (Sinaia, Buşteni, Azuga, Predeal).

By applying the LR-WoE hybrid model $FFPI_{LR\text{-}WoE}$, values ranging between (−4.2) and 0.94, were calculated and mapped. The resulting values were grouped in five classes by the Natural Breaks classification method. The first $FFPI_{LR\text{-}WoE}$ value class (very low) ranges from (−4.2) to (−2.4) and covers about 14% of study area. Similar to $FFPI_{LR\text{-}FR}$, these surfaces are present especially in the southern part of the upper and middle sector of Prahova river basin. The areas that belong to low Flash-Flood Potential are present on approximately 15% of the study area, being spread as fragmented surfaces in the southern half of research area. Medium values of $FFPI_{LR\text{-}WoE}$ included in the range between (−1.6) and (−1), are spatially distributed on 26% of study area. These values are mainly located, as compact surfaces, in the central part of research area and, in a fragmented manner, in the northern part. $FFPI_{LR\text{-}WoE}$ values higher than (−0.9), highlighting the surfaces with high and very high Flash-Flood Potential, are spread on 45% of study area, and are located especially in the Carpathian region.

Table 4
The outputs of the Logistic Regression model.

Factor	β		Std. error		Wald x^2	
	FR	WoE	FR	WoE	FR	WoE
Slope	0.200	0.149	0.003	0.003	43.285	29.75
TPI	−0.005	−0.011	0.002	0.002	15.23	11.13
TWI	0.031	0.041	0.004	0.004	7.714	11.26
Land use	0.110	0.113	0.002	0.005	33.22	27.77
Lithology	0.190	0.189	0.003	0.002	12.08	14.20
Profile curvature	0.017	0.015	0.004	0.003	4.789	2.819
Plan curvature	0.006	0.005	0.002	0.004	6.980	6.655
Aspect	0.152	0.127	0.006	0.002	7.063	4.967
Convergence index	−0.045	−0.037	0.002	0.004	4.482	2.521
HGS	0.024	0.020	0.002	0.003	2.241	12.26

4.3. Application of hybrid models SVM-FR and SVM-WoE

As in the case of Logistic Regression analysis, FR and WoE coefficients values, established for flash-flood conditioning factors, were incorporated into the SVM modeling. The estimation of the values of the two SVM essential parameters ($C = 2.5$, $\gamma = 0.1$) offered the possibility to calculate the weights held by each flash-flood conditioning factor in the $FFPI_{SVM\text{-}FR}$ and $FFPI_{SVM\text{-}WoE}$ computation process. The value estimation of the two SVM parameters ($C = 2.5$, $\gamma = 0.1$), gave the possibility to derive the weights held by each flash-flood conditioning factor in the $FFPI_{SVM\text{-}FR}$ and $FFPI_{SVM\text{-}WoE}$ computation process (Fig. 13). According to the results of SVM-FR model, the highest importance is assigned to slope angle (18%), followed by lithology (16.1%), land use (13.7%), hydrological soil group (9.4%), convergence index (8.5%), plan curvature (7.9%), twi (7.8%), aspect (3.4%) and tpi (2.5%). Further, in the case of SVM-WoE, the hierarchy of the most important factors is unchanged, slope angle being the most important (17.3%), followed by lithology (14.9%), land use (14.1%), profile curvature (11.2%), hydrological soil group (10.3%), plan curvature (8.6%), twi (8.4%), convergence index (8.1%), tpi (4.6%) and aspect (4.6%) (Fig. 13).

By considering the weights of flash-flood conditioning factors resulted after the application of SVM model, a weighted sum operation in GIS environment was performed in order to compute $FFPI_{SVM\text{-}FR}$ and $FFPI_{SVM\text{-}WoE}$ rasters.

$FFPI_{SVM\text{-}FR}$ values ranging between 1.3 and 8.8 (Fig. 14a) were grouped in 5 classes by using the Natural Breaks classification method. The lowest $FFPI_{SVM\text{-}FR}$ values cover approximately 14% of the study area and range between 1.3 and 3.84. The second $FFPI_{SVM\text{-}FR}$ value class, which highlights a low Flash-Flood Potential is mainly presented in the southern region of research area being spread on around 21% of upper and middle sector of Prahova river catchment. The largest part of the study area, around 33%, is occupied by the medium values of $FFPI_{SVM\text{-}FR}$. The areas with high and very high flash-flood ($FFPI_{SVM\text{-}FR} > 5.39$) potential cover nearly 32% of the research area and are mainly located in the Carpathian region.

In the case of $FFPI_{SVM\text{-}WoE}$, the spatial distribution of the five Flash-Flood Potential classes is largely similar to the $FFPI_{SVM\text{-}FR}$. Nonetheless, there are some differences in terms of value range limits and regarding the weights of each value class. Therefore, $FFPI_{SVM\text{-}WoE}$ values range from 1.25 to 10.32 (Fig. 14a). The areas with very low Flash-Flood Potential, ranging between 1.25 and 3.28, occupy about 17% of research area. The $FFPI_{SVM\text{-}WoE}$ second value class is spread on approximately 27% of study area, while the medium value class covers a quarter of the total surface of the upper and middle sector of Prahova river catchment. Around 31% of study area presents a high and very high potential to flash-flood occurrence.

It can be observed that the high and very high values of $FFPI_{SVM\text{-}FR}$ and $FFPI_{SVM\text{-}WoE}$ have a more compact spatial distribution than those obtained by the $FFPI_{LR\text{-}FR}$ and $FFPI_{LR\text{-}WoE}$ computation.

4.4. Results validation and accuracy assessment

In Fig. 15a and b the relative distribution of torrential areas pixels, within the FFPI classes for each of the 4-hybrid model applied, is represented. This method quantifies the measure in which the areas affected by torrential phenomena overlap the surfaces with high and very high Flash-Flood Potential. In the present study, the percentage of training areas that are located within areas with high and very Flash-Flood Potential, ranges between 79.04% ($FFPI_{LR\text{-}WoE}$) and 84.21% ($FFPI_{LR\text{-}FR}$) (Fig. 15a). In terms of validating areas, the highest percentage is held by $FFPI_{SVM\text{-}WoE}$ (82.91%) while $FFPI_{LR\text{-}FR}$ (79.48%) is on the last position. It can be observed that there are small differences between the models in terms of percentage of torrential areas located within the high and very high FFPI value classes. Therefore, from this point of view, the models present a high accuracy of the results as well as a high efficiency of the way in which the results were grouped into five value classes.

Table 5
ROC Curve parameters using training dataset for success rate and prediction rate.

Models	Training dataset				Validating dataset			
	95% confidence interval				95% confidence interval			
	AUC	S.E.	Lower bound	Upper bound	AUC	S.E.	Lower bound	Upper bound
FFPI LR-FR	0.888	0.023	0.849	0.927	0.901	0.021	0.86	0.941
FFPI LR-WoE	0.885	0.021	0.846	0.924	0.904	0.021	0.863	0.945
FFPI SVM-FR	0.887	0.022	0.848	0.926	0.876	0.023	0.831	0.921
FFPI SVM-WoE	0.883	0.020	0.844	0.922	0.875	0.023	0.830	0.921

The second method designed for the model performance assessment and results validation is represented by the ROC Curve for which both Success Rate and Prediction Rate were constructed. In order to graphically represent ROC Curve and to calculate the AUC, the values of the 4 FFPI and the number of pixels with torrentiality (training data and validating data) were used. The parameters represented by 95% - Confidence Interval and Standard Error, were determined as well (Table 5).

In terms of Success Rate, designed by using training areas, the highest AUC value belongs to LR-FR hybrid model (0.888), followed by SVM-FR (AUC = 0.887), LR-WoE (AUC = 0.885) and SVM-WoE (AUC = 0.883) (Fig. 16a). In the case of Prediction Rate, the highest AUC value was assigned to LR-WoE hybrid model (0.904), followed by LR-FR (AUC = 0.901), SVM-FR (AUC = 0.876) and SVM-WoE (AUC = 0.875) (Fig. 16b).

AUC values for both Success Rate and Prediction Rate indicate a high performance of the models applied as well as a good accuracy of the results obtained.

The third stage in results validation and model performance assessment process consists of the estimation of several statistical indices.

By using the training dataset, the best performance in terms of the classification of pixels with torrential phenomena was established for LR-FR model (sensitivity = 0.719), followed by SVM-FR (sensitivity = 0.719), SVM-WoE (sensitivity = 0.713) and LR-WoE (sensitivity = 0.700). Regarding the classification of pixels without torrential phenomena, the best performance was associated to SVM-FR (specificity = 0.825) model, followed by LR-WoE (specificity = 0.821), SVM-WoE (specificity = 0.820) and LR-FR (specificity = 0.789) (Table 5). The highest value of accuracy was obtained by SVM-FR model (0.724), followed by SVM-WoE (0.723), LR-FR (0.721) and LR-WoE (0.708).

The use of validating dataset highlights the SVM-WoE (sensitivity = 0.78) as the model with the best performance regarding the classification of pixels corresponding to torrential phenomena. On the following positions, there are the models: SVM-FR (sensitivity = 0.77), LR-FR (sensitivity = 0.742) and LR-WoE (sensitivity = 0.723). For pixels without torrential phenomena the best classification was performed by SVM-FR (specificity = 0.825) model, followed by LR-WoE (specificity = 0.821), SVM-WoE (specificity = 0.820) and LR-FR (specificity = 0.789). The highest results accuracy was attributed to SVM-WoE (0.801) model, followed by SVM-FR (0.797), LR-WoE (0.772) and LR-FR (0.766) (Table 6).

5. Conclusions

In the context of rapid increase of flash-floods frequency, the activity represented by the identification of areas susceptible to these phenomena becomes very important, being, at the same time, the central subject of many research papers from the international literature. In order to increase the accuracy of flash-flood forecasts and warnings, the assessment of areas susceptible to these phenomena, is an essential step. The use of new statistical and machine learning techniques and especially combining them, in order to obtain hybrid models, leads to a significant increase in the accuracy of the results obtained. In the present study, the potential for flash-floods occurrence was calculated by integrating 10 flash-flood conditioning factors into a 4 hybrid models (LR-FR, LR-WoE, SVM-FR and SVM-WoE). The importance of the present study is also given by the high development degree of the research area, the upper and middle sectors of Prahova river catchment being the main tourist areas of Romania and one of the most important industrial regions of the country. An attempt to determine FFPI values across the study area was performed by Zaharia et al. (2017). In order to carry out the analysis, the authors of the mentioned study didn't consider the presence of the areas previously affected by torrential phenomena, FFPI values being calculated by using a simple overlapping of the flash-floods conditioning factors in GIS environment. The authors conclude that 35% of study area is characterized by a high and very high Flash-Flood Potential, this percentage being close to those obtained in the present study by applying the following models SVM-WoE (31%), SVM-WoE (32%) and LR-FR (38%). Instead, by applying the LR-WoE model, 45% of study area resulted to be affected by a high and very high Flash-Flood Potential.

The great advantage of this study is given by the possibility to test the performance of the applied models and to validate the results obtained, through several methods. In this regard, three methods were employed for the present analysis. Thus, by performing the relative distribution of torrential pixels within FFPI classes, FR-LR was highlighted to be the most effective model in terms of FFPI value classification, while SVM-WoE was indicated as the best model regarding the accuracy of the results. In case of Success Rate constructed by mean of ROC Curve procedure, LR-FR model (AUC = 0.888) was the most effective, while LR-WoE model (AUC = 0.904) was the most effective in terms of Prediction Rate. The results of the third method used highlight the SVM-FR (accuracy = 0.724) for training areas and the SVM-WoE (accuracy = 0.801) for validating areas as being the most accurate models.

The possibility to evaluate the applied models performance as well as to validate the obtained results, by considering the surfaces previously affected by torrential phenomena gives a high degree of objectivity for the present study comparing to others.

Table 6
Model performance using training and validating datasets.

Parameters	FFPI LR-FR		FFPI LR-WoE		FFPI SVM-FR		FFPI SVM-WoE	
	Training	Validating	Training	Validating	Training	Validating	Training	Validating
True positive	141,830	62,298	136,997	62,547	139,873	64,578	137,293	65,372
True negative	139,853	66,543	135,901	70,320	137,853	69,224	136,534	71,349
False positive	55,232	17,767	53,784	15,336	50,983	14,678	49,832	15,672
False negative	53,987	21,678	58,654	23,987	54,783	19,335	55,231	18,394
Sensitivity	0.724	0.742	0.700	0.723	0.719	0.770	0.713	0.780
Specificity	0.717	0.789	0.716	0.821	0.730	0.825	0.733	0.820
Accuracy	0.721	0.766	0.708	0.772	0.724	0.797	0.723	0.801

As in any other research work, the results of the present study are subject to errors mainly due to the errors occurred in the delineation process of the areas affected by torrential phenomena and the errors occurred in the spatial representation of flash-flood conditioning factors.

In order to issue flash-flood forecast and warning, the results of the present research could be successfully used by the National Institute of Hydrology and Water Management from Romania.

Acknowledgements

This study was funded by the Research Institute of the University of Bucharest.

References

Abdulkareem, J.H., Pradhan, B., Sulaiman, W.N.A., Jamil, N.R., 2018. Quantification of runoff as influenced by morphometric characteristics in a rural complex catchment. Earth Syst. Environ. 2 (1), 145–162.

Agterberg, F.P., 1992. Combining indicator patterns in weights of evidence modeling for resource evaluation. Nat. Resour. Res. 1 (1), 39–50.

Ajit Krisshna, N.L., Deepak, V.K., Manikantan, K., Ramachandran, S., 2014. Face recognition using transform domain feature extraction and PSO-based feature selection. Appl. Soft Comput. 22, 141–161. https://doi.org/10.1016/j.asoc.2014.05.007.

Althuwaynee, O.F., Pradhan, B., Lee, S., 2016. A novel integrated model for assessing landslide susceptibility mapping using CHAID and AHP pair-wise comparison. Int. J. Remote Sens. 37 (5), 1190–1209.

Andronache, I., Fensholt, R., Ahammer, H., Ciobotaru, A.M., Pintilii, R.D., Peptenatu, D., Drăghici, C., Diaconu, D., Radulović, M., Pulighe, G., Azihou, A.F., Toyi, M.S., Sinsin, B., 2017. Assessment of textural differentiations in forest resources in Romania using fractal analysis. Forests 8 (3), 54.

Bartholmes, J.C., Thielen, J., Ramos, M.H., Gentilini, S., 2009. The European Flood Alert System EFAS – part 2: statistical skill assessment of probabilistic and deterministic operational forecasts. Hydrol. Earth Syst. Sci. 13, 141–153.

Bonham-Carter, G.F., 1994. Geographic information systems for geoscientists-modeling with GIS. Computer methods in the geoscientists 13, 398.

Bonham-Carter, G.F., 2002. Geographic Information Systems for Geoscientist: Modeling With GIS. Pergamon, New York, pp. 302–334.

Brewster, J., 2009. Development of the flash flood potential index. A Microsoft PowerPoint presentation available at. http://www.erh.noaa.gov/bgm/research/ERFFW/presentations/june_02_2010/Brewster_Jim_Development_of_FFPI.ppt.

Bui, T.D., Pradhan, B., Lofman, O., Revhaug, I., 2012. Landslide susceptibility assessment in Vietnam using support vector machines, decision tree, and Naive Bayes Models. Math. Probl. Eng. 2012.

Bui, D.T., Pradhan, B., Nampak, H., Bui, Q.T., Tran, Q.A., Nguyen, Q.P., 2016a. Hybrid artificial intelligence approach based on neural fuzzy inference model and metaheuristic optimization for flood susceptibilitgy modeling in a high-frequency tropical cyclone area using GIS. J. Hydrol. 540, 317–330.

Bui, D.T., Ho, T.C., Pradhan, B., Pham, B.T., Nhu, V.H., Revhaug, I., 2016b. GIS-based modeling of rainfall-induced landslides using data mining-based functional trees classifier with AdaBoost, Bagging, and MultiBoost ensemble frameworks. Environ. Earth Sci. 75 (14), 1101.

Bui, D.T., Tuan, T.A., Hoang, N.D., Thanh, N.Q., Nguyen, D.B., Van Liem, N., Pradhan, B., 2017. Spatial prediction of rainfall-induced landslides for the Lao Cai area (Vietnam) using a hybrid intelligent approach of least squares support vector machines inference model and artificial bee colony optimization. Landslides 14 (2), 447–458.

Calder, I.R., 2002. Forests and hydrological services: reconciling public and science perceptions. Land Use Water Resour. Res. 2 (2), 1–12.

Cao, C., Xu, P., Wang, Y., Chen, J., Zheng, L., Niu, C., 2016. Flash flood hazard susceptibility mapping using frequency ratio and statistical index methods in coalmine subsidence areas. Sustainability 8 (9), 948.

Carvalho-Santos, C., Honrado, J.P., Hein, L., 2014. Hydrological services and the role of forests: conceptualization and indicator-based analysis with an illustration at a regional scale. Ecol. Complex. 20, 69–80.

Ceru, J., 2012. The flash flood potential index for Pennsylvania. 2012 ESRI Federal GIS Conference http://proceedings.esri.com/library/userconf/feduc12/papers/user/JoeCeru.pdf.

Chang, C., Lin, C., 2011. LIBSVM: a library for support vector machines. ACM Trans. Intell. Syst. Technol. 2 (3), 1–27.

Chapi, K., Singh, V.P., Shirzadi, A., Shahabi, H., Bui, D.T., Pham, B.T., Khosravi, K., 2017. A novel hybrid artificial intelligence approach for flood susceptibility assessment. Environ. Model. Softw. 95, 229–245.

Chen, H., Liu, H., Han, J., Yin, X., He, J., 2009. Exploring optimization of semantic relationship graph for multi-relational Bayesian classification. Decis. Support. Syst. 48, 112–121.

Chen, J., Yang, S., Li, H., Zhang, B., Lv, J., 2013. Research on geographical environment unit division based on the method of natural breaks (Jenks). International Archives of the Photogrammetry, Remote Sensing and Spatial Information Sciences XL-4 (W3), p. 47.

Chen, W., Panahi, M., Pourghasemi, H.R., 2017. Performance evaluation of GIS-based new ensemble data mining techniques of adaptive neuro-fuzzy inference system (ANFIS) with genetic algorithm (GA), differential evolution (DE), and particle swarm optimization (PSO) for landslide spatial modelling. Catena 157, 310–324.

Chen, W., Xie, X., Peng, J., Shahabi, H., Hong, H., Bui, D.T., Duan, Z., Li, S., Zhu, A.X., 2018. GIS-based landslide susceptibility evaluation using a novel hybrid integration approach of bivariate statistical based random forest method. Catena 164, 135–149.

Cherkassky, V., Mulier, F., 2007. Learning From Data: Concepts, Theory and Methods. 2nd ed. John Wiley & Sons, New Jersey.

Cojoc, G.M., Romanescu, G., Tirnovan, A., 2015. Exceptional floods on a developed river: case study for the Bistrita River from the Eastern Carpathians (Romania). Nat. Hazards 77 (3), 1421–1451.

Costache, R., Zaharia, L., 2017. Flash-flood potential assessment and mapping by integrating the weights-of-evidence and frequency ratio statistical methods in GIS environment–case study: Bâsca Chiojdului River catchment (Romania). J. Earth Syst. Sci. 126 (4), 59.

Costache, R., Fontanine, I., Corodescu, E., 2014. Assessment of surface runoff depth changes in Sărăţel River basin, Romania using GIS techniques. Cent. Eur. Geosci. 6 (3), 363–372.

Costache, R., Prăvălie, R., Mitof, I., Popescu, C., 2015. Flood vulnerability assessment in the low sector of Sărăţel Catchment. Case study: Joseni Village. Carpath. J. Earth Environ. Sci. 10 (1), 161–169.

Costanzo, D., Rotigliano, E., Irigaray Fernández, C., Jiménez-Perálvarez, J.D., Chacón Montero, J., 2012. Factors selection in landslide susceptibility modelling on large scale following the gis matrix method: application to the river Beiro basin (Spain). Nat. Hazards Earth Syst. Sci. 12, 327–340.

Dai, J., Xu, Q., 2013. Attribute selection based on information gain ratio in fuzzy rough set theory with application to tumor classification. Appl. Soft Comput. 13, 211–221. https://doi.org/10.1016/j.asoc.2012.07.029.

Dai, Q., Peng, X., Yang, Z., Zhao, L., 2017. Runoff and erosion processes on bare slopes in the Karst Rocky Desertification Area. Catena 152, 218–226.

Dash, M., Liu, H., 2003. Consistency-based search in feature selection. Artif. Intell. 151, 155–176.

Davis, R.S., 2002. The flash flood (FF) index: estimating flash flood severity. Proceedings of the Symposium on Managing the Extremes, Floods and Droughts.

Demir, G., Aytekin, M., Akgun, A., 2015. Landslide susceptibility mapping by frequency ratio and logistic regression methods: an example from Niksar–Resadiye (Tokat, Turkey). Arab. J. Geosci. 8 (3), 1801–1812.

Dou, J., Yamagishi, H., Zhu, Z., Yunus, A.P., Chen, C.W., 2018. TXT-tool 1.081-6.1 A comparative study of the Binary Logistic Regression (BLR) and Artificial Neural Network (ANN) models for GIS-based spatial predicting landslides at a regional scale. Landslide Dynamics: ISDR-ICL Landslide Interactive Teaching Tools. Springer, Cham, pp. 139–151.

Duman, T.Y., Can, T., Gokceoglu, C., Nefeslioglu, H.A., Sonmez, H., 2006. Application of logistic regression for landslide susceptibility zoning of Cekmece Area, Istanbul, Turkey. Environ. Geol. 51 (2), 241–256.

EEA, 2006. European Environment Agency – CORINE land cover 2012 raster data. at. http://www.eea.europa.eu/data-and-maps/data/corineland-cover-2012-raster, Accessed date: 8 September 2018.

Fontanine, Iulia, Costache, R., 2013. Using GIS techniques for surface runoff potential analysis in the Subcarpathian area between Buzău and Slănic rivers, in Romania. Cinq Continents 3 (7), 201–214.

Goetz, J.N., Brenning, A., Petschko, H., Leopold, P., 2015. Evaluating machine learning and statistical prediction techniques for landslide susceptibility modeling. Comput. Geosci. 81, 1–11.

Guyon, I., Elisseeff, A., 2003. An introduction to variable and feature selection. J. Mach. Learn. Res. 3, 1157–1182.

Hanley, J.A., McNeil, B.J., 1982. The meaning and use of the area under a receiver operating characteristic (ROC) curve. Radiology 143 (1), 29–36.

Hong, H., Pradhan, B., Xu, C., Bui, D.T., 2015. Spatial prediction of landslide hazard at the Yihuang area (China) using two-class kernel logistic regression, alternating decision tree and support vector machines. Catena 133, 266–281.

Hong, H., Pradhan, B., Jebur, M.N., Bui, D.T., Xu, C., Akgun, A., 2016. Spatial prediction of landslide hazard at the Luxi area (China) using support vector machines. Environ. Earth Sci. 75 (1), 40.

Hong, H., Liu, J., Bui, D.T., Pradhan, B., Acharya, T.D., Pham, B.T., Zhu, A.-X., Chen, W., Ahmad, B.B., 2018a. Landslide susceptibility mapping using J48 Decision Tree with AdaBoost, Bagging and Rotation Forest ensembles in the Guangchang area (China). Catena 163, 399–413.

Hong, H., Tsangaratos, P., Ilia, I., Liu, J., Zhu, A.X., Chen, W., 2018b. Application of fuzzy weight of evidence and data mining techniques in construction of flood susceptibility map of Poyang County, China. Sci. Total Environ. 625, 575–588.

Hosmer, D.W., Lemeshow, S., 1989. Applied Regression Analysis. Wiley, New York (307 p).

Hua, S., Sun, Z., 2001. Support vector machine approach for protein subcellular localization prediction. Bioinformatics 17 (8), 721–728.

Hundecha, Y., Bárdossy, A., 2004. Modeling of the effect of land use changes on the runoff generation of a river basin through parameter regionalization of a watershed model. J. Hydrol. 292 (1–4), 281–295.

Jenness, J.S., 2000. The Effects of Fire on Mexican Spotted Owls in Arizona and New Mexico. (MSc thesis). Northern Arizona University, p. 137.

Kavzoglu, T., Colkesen, I., 2009. A kernel functions analysis for support vector machines for land cover classification. Int. J. Appl. Earth Obs. Geoinf. 11, 352–359.

Kavzoglu, T., Sahin, E.K., Colkesen, I., 2014. Landslide susceptibility mapping using GIS-based multi-criteria decision analysis, support vector machines, and logistic regression. Landslides 11 (3), 425–439.

Kayastha, P., Dhital, M.R., De Smedt, F., 2012. Landslide susceptibility mapping using the weight of evidence method in the Tinau watershed, Nepal. Nat. Hazards 63 (2), 479–498.

Khosravi, K., Nohani, E., Maroufinia, E., Pourghasemi, H.R., 2016a. A GIS-based flood susceptibility assessment and its mapping in Iran: a comparison between frequency ratio and weights-of-evidence bivariate statistical models with multi-criteria decision-making technique. Nat. Hazards 83 (2), 947–987.
Khosravi, K., Pourghasemi, H.R., Chapi, K., Bahri, M., 2016b. Flash flood susceptibility analysis and its mapping using different bivariate models in Iran: a comparison between Shannon's entropy, statistical index, and weighting factor models. Environ. Monit. Assess. 188 (12), 656.
Khosravi, K., Pham, B.T., Chapi, K., Shirzadi, A., Shahabi, H., Revhaug, I., Bui, D.T., 2018. A comparative assessment of decision trees algorithms for flash flood susceptibility modeling at Haraz watershed, northern Iran. Sci. Total Environ. 627, 744–755.
Kruzdlo, R., Ceru, J., 2010, June. Flash flood potential index for WFO Mount Holly/Philadelphia. Eastern Region Flash Flood Conference, Poster Session. NOAA's National Weather Service, pp. 2–4.
Le, Q.H., Van Nguyen, T.H., Do, M.D., Le, T.C.H., Nguyen, H.K., Luu, T.B., 2018. TXT-tool 1.084-3.1: landslide susceptibility mapping at a regional scale in Vietnam. Landslide Dynamics: ISDR-ICL Landslide Interactive Teaching Tools. Springer, Cham, pp. 161–174.
Lee, S., Pradhan, B., 2007. Landslide hazard mapping at Selangor, Malaysia using frequency ratio and logistic regression models. Landslides 4 (1), 33–41.
Lee, S., Sambath, T., 2006. Landslide susceptibility mapping in the Damrei Romel area, Cambodia using frequency ratio and logistic regression models. Environ. Geol. 50 (6), 847–855.
Lin, S.-W., Lee, Z.-J., Chen, S.-C., Tseng, T.-Y., 2008. Parameter determination of support vector machine and feature selection using simulated annealing approach. Appl. Soft Comput. 8, 1505–1512.
Menard, S., 1995. Applied logistic regression analysis. Sage Publications, Thousand Oaks, CA.
MEWM, 2006. Ministry of Environment and Water Management – Report on the Effects of Flooding and Dangerous Meteorological Phenomena in 2005, Implemented Measures, Actions Taken to Repair Affected Units and to Diminish or Prevent Future Damages (in Romanian) (40 p, Bucharest, Romania).
Minea, G., 2013. Assessment of the flash flood potential of Bâsca River Catchment (Romania) based on physiographic factors. Open Geosci. 5 (3), 344–353.
Mladenić, D., Brank, J., Grobelnik, M., Milic-Frayling, N., 2004. Feature selection using linear classifier weights: interaction with classification models. Proceedings of the 27th Annual International ACM SIGIR Conference on Research and Development in Information Retrieval. ACM, pp. 234–241.
Moore, I.D., Grayson, R.B., Ladson, A., 1991. Digital terrain modeling: a review of hydrological, geomorphological, and biological applications. Hydrol. Process. 5, 3–30.
NASA Earth Data, 2018. Earth Observing System Data and Information System (EOSDIS). Available at:. https://worldview.earthdata.nasa.gov/, Accessed date: 15 August 2018.
National Engineering Handbook, 2007. Chapter 7 – Hydrologic Soil Groups, United States Department of Agriculture – National Resources Conservation Service.
National Geological Institute of Romania (NIGR), 2002. Digital Geological Map of Romania, 1:200.000 Scale.
Niehoff, D., Fritsch, U., Bronstert, A., 2002. Land-use impacts on storm-runoff generation: scenarios of land-use change and simulation of hydrological response in a meso-scale catchment in SW-Germany. J. Hydrol. 267 (1–2), 80–93.
Pallant, J., 2013. SPSS Survival Manual. McGraw-Hill Education, UK.
Pham, B.T., Bui, D., Prakash, I., Dholakia, M., 2016a. Evaluation of predictive ability of support vector machines and naive Bayes trees methods for spatial prediction of landslides in Uttarakhand state (India) using GIS. J. Geom. 10, 71–79.
Pham, B.T., Pradhan, B., Bui, D.T., Prakash, I., Dholakia, M.B., 2016b. A comparative study of different machine learning methods for landslide susceptibility assessment: a case study of Uttarakhand area (India). Environ. Model. Softw. 84, 240–250.
Pourghasemi, H.R., Jirandeh, A.G., Pradhan, B., Xu, C., Gokceoglu, C., 2013. Landslide susceptibility mapping using support vector machine and GIS at the Golestan Province, Iran. J. Earth Syst. Sci. 122 (2), 349–369.
Pradhan, B., Lee, S., 2009. Landslide risk analysis using artificial neural network model focusing on different training sites. J. Phys. Sci. 3 (11), 1–15.
Pradhan, B., Lee, S., 2010. Landslide susceptibility assessment and factor effect analysis: backpropagation artificial neural networks and their comparison with frequency ratio and bivariate logistic regression modelling. Environ. Model. Softw. 25 (6), 747–759.
Prăvălie, R., Costache, R., 2013. The vulnerability of the territorial-administrative units to the hydrological phenomena of risk (flash-floods). Case study: the subcarpathian sector of Buzău catchment. An. Univ. Oradea Ser. Geogr. 23 (1), 91–98.
Rahmati, O., Pourghasemi, H.R., Zeinivand, H., 2016. Flood susceptibility mapping using frequency ratio and weights-of-evidence models in the Golastan Province, Iran. Geocarto Int. 31 (1), 42–70.
Regmi, A.D., Devkota, K.C., Yoshida, K., Pradhan, B., Pourghasemi, H.R., Kumamoto, T., Akgun, A., 2014. Application of frequency ratio, statistical index, and weights-of-evidence models and their comparison in landslide susceptibility mapping in Central Nepal Himalaya. Arab. J. Geosci. 7 (2), 725–742.
Romanescu, G., Mihu-Pintilie, A., Stoleriu, C.C., Carboni, D., Paveluc, L.E., Cimpianu, C.I., 2018. A comparative analysis of exceptional flood events in the context of heavy rains in the summer of 2010: Siret Basin (NE Romania) case study. Water 10 (2), 216.
Romanian National Institute for Statistics, 2018. Romania. Statistical Yearbook Bucharest.
Samanta, R.K., Bhunia, G.S., Shit, P.K., Pourghasemi, H.R., 2018. Flood susceptibility mapping using geospatial frequency ratio technique: a case study of Subarnarekha River Basin, India. Model. Earth Syst. Environ. 4 (1), 395–408.
Senthamarai Kannan, S., Ramaraj, N., 2010. A novel hybrid feature selection via symmetrical uncertainty ranking based local memetic search algorithm. Knowl.-Based Syst. 23, 580–585.
Shehata, M., Mizunaga, H., 2018. Flash flood risk assessment for Kyushu Island, Japan. Environ. Earth Sci. 77 (3), 76.
Stăncioiu, P.T., Niţă, M.D., Lazăr, G.E., 2018. Forestland connectivity in Romania—implications for policy and management. Land Use Policy 76, 487–499.
Tehrany, M.S., Pradhan, B., Jebur, M.N., 2013. Spatial prediction of flood susceptible areas using rule based decision tree (DT) and a novel ensemble bivariate and multivariate statistical models in GIS. J. Hydrol. 504, 69–79.
Tehrany, M.S., Pradhan, B., Jebur, M.N., 2014. Flood susceptibility mapping using a novel ensemble weights-of-evidence and support vector machine models in GIS. J. Hydrol. 512, 332–343.
Tehrany, M.S., Pradhan, B., Mansor, S., Ahmad, N., 2015. Flood susceptibility assessment using GIS-based support vector machine model with different kernel types. Catena 125, 91–101.
Termeh, S.V.R., Kornejady, A., Pourghasemi, H.R., Keesstra, S., 2018. Flood susceptibility mapping using novel ensembles of adaptive neuro fuzzy inference system and metaheuristic algorithms. Sci. Total Environ. 615, 438–451.
The National Agency of Cadaster and Real Estate Advertising (NACREA), 2016. Orthorectified Aerial Images, 1:5000 Scale.
Thielen, J., Bartholmes, J., Ramos, M.-H., de Roo, A., 2009. The European flood alert system - part 1: concept and development. Hydrol. Earth Syst. Sci. 13, 125–140.
Van Westen, C.J., Montoya, L., Boerboom, L., Badilla Coto, E., 2002. Multi-hazard risk assessment using GIS in urban areas: a case study for the city of Turrialba, Costa Rica. Proc. Regional workshop on Best Practise in Disaster Mitigation, Bali, pp. 120–136.
Van Westen, C.J., Rengers, N., Soeters, R., 2003. Use of geomorphological information in indirect landslide susceptibility assessment. Nat. Hazards 30 (3), 399–419.
Vapnik, V.N., 1995. The Nature of Statistical Learning Theory. Springer Verlag, New York.
Wahid, A., Madden, M., Khalaf, F., Fathy, I., 2016. Geospatial analysis for the determination of hydro-morphological characteristics and assessment of flash flood potentiality in arid coastal plains: a case in southwestern Sinai, Egypt. Earth Sci. Res. J. 20 (1), 1–9.
Youssef, A.M., Al-Kathery, M., Pradhan, B., 2015a. Landslide susceptibility mapping at AlHasher area, Jizan (Saudi Arabia) using GIS-based frequency ratio and index of entropy models. Geosci. J. 19 (1), 113–134.
Youssef, A.M., Pradhan, B., Jebur, M.N., El-Harbi, H.M., 2015b. Landslide susceptibility mapping using ensemble bivariate and multivariate statistical models in Fayfa area, Saudi Arabia. Environ. Earth Sci. 73 (7), 3745–3761.
Youssef, A.M., Pradhan, B., Sefry, S.A., 2016a. Flash flood susceptibility assessment in Jeddah city (Kingdom of Saudi Arabia) using bivariate and multivariate statistical models. Environ. Earth Sci. 75 (1), 12.
Youssef, A.M., Pourghasemi, H.R., Pourtaghi, Z.S., Al-Katheeri, M.M., 2016b. Landslide susceptibility mapping using random forest, boosted regression tree, classification and regression tree, and general linear models and comparison of their performance at Wadi Tayyah Basin, Asir Region, Saudi Arabia. Landslides 13 (5), 839–856.
Zaharia, L., Minea, G., Toroimac, G.I., Barbu, R., Sârbu, I., 2012. Estimation of the Areas With Accelerated Surface Runoff in the Upper Prahova Watershed (Romanian Carpathians). Balwois, Republic of Macedonia.
Zaharia, L., Costache, R., Prăvălie, R., Minea, G., 2015. Assessment and mapping of flood potential in the Slănic catchment in Romania. J. Earth Syst. Sci. 124 (6), 1311–1324.
Zaharia, L., Costache, R., Prăvălie, R., Ioana-Toroimac, G., 2017. Mapping flood and flooding potential indices: a methodological approach to identifying areas susceptible to flood and flooding risk. Case study: the Prahova catchment (Romania). Front. Earth Sci. 11 (2), 229–247.

Stochastic Environmental Research and Risk Assessment
https://doi.org/10.1007/s00477-019-01689-9

ORIGINAL PAPER

Flash-flood Potential Index mapping using weights of evidence, decision Trees models and their novel hybrid integration

Romulus Costache[1,2]

Abstract

Flash-floods are among the natural risk phenomena that annually cause important material damages and losses of human lives worldwide. One of the main activities for mitigating the negative effects of these phenomena consist of the identification and spatial representation of the surfaces prone to surface runoff occurrence. *Flash-Flood Potential Index (FFPI)* is the common method used to assess the degree of susceptibility to flash-floods of a certain surface. The main drawback of the aforementioned method is represented by the fact that, in the majority of the studies, the geographical factors considered for *FFPI* calculation received equal weights, even if they do not influence in the same measure the surface runoff process. Moreover, within the methodologies developed in the previous studies, the areas affected by torrential phenomena have not been considered for FFPI computation. To address these shortcomings, in the present study, *FFPI* values are estimated by using a number of 4 stand-alone models (Alternating Decision Tree (ADT), Rotation Forest, Weights of Evidence (WOE), Logistic Model Tree) and 3 hybrid models generated by the integration of WOE model with each of the other decision tree-based algorithms. The first stage of the study consisted of the inventory of the areas where torrential phenomena occurred in the past, 70% of them being included in the training sample, while the others 30% in the validating sample. Further, 12 flash-flood conditioning factors, selected through the correlation-based feature selection algorithm, were used to train the 7 models applied for *FFPI* calculation. The results of the 7 models revealed that the surfaces with a high and very high flash-flood susceptibility occupy between 23.3 and 43.7% of the entire study zone. The ROC Curve method was involved in the models performance assessment and in the results validation procedure. From this point of view, the best results were obtained by the *ADT-WOE* hybrid model.

Keywords FFPI · Weights of evidence · Decision trees models · Prahova river catchment · Hybrid integration

1 Introduction

During the last years, the studies whose main aim was the evaluation of susceptibility to different natural disasters have increased both in number and complexity. Moreover, there is also an increase in the number of modern methods used for this purpose. In terms of susceptibility assessment, the most studied phenomena are: floods, flash-floods and landslides (Lee 2005; Yesilnacar and Topal 2005; Pradhan and Youssef 2011; Tehrany et al. 2015; Khosravi et al. 2016; Youssef et al. 2016). Floods and flash-floods are one of the most widespread risk phenomena, causing the most economic damage and loss of human life (Glas et al. 2017; Arrighi et al. 2018). In this context, the measures taken to prevent and mitigate the negative effects of these phenomena on human communities are extremely important. Many non-structural measures adopted in emergency situations are based on the flash-flood forecasting and early warning activity. The previous assessment of areas susceptible to these phenomena is extremely important for the flash-flood warning activity. In the literature, the flash-flood susceptibility or severity was evaluated by using several indices such as: Flash-Flood Potential Index (FFPI) (Smith 2003), Flashiness (Saharia et al. 2017) or Flash-

✉ Romulus Costache
romuluscostache2000@yahoo.com

1 Research Institute of the University of Bucharest, 36-46 Bd. M. Kogălniceanu, 5th District, 050107 Bucharest, Romania

2 National Institute of Hydrology and Water Management, Bucureşti-Ploieşti Road, 97E, 1st District, 013686 10 Bucharest, Romania

Published online: 25 May 2019

Flood Guidance (FFG) (Georgakakos 2006). Generally, the assessment of flash-flood susceptibility through FFPI method is performed in GIS environment by overlapping several physiographic factors that influence the surface runoff intensity. The FFPI results are qualitative, in raster format, the highest values indicating the areas prone to flash-flood occurrence. The Flashiness index method estimates the severity of rapid floods based on the difference between the peak discharge and action stage discharge normalized by the flooding rise time and catchment area (Saharia et al. 2017). Thus, the initial results of Flashiness method are estimated individually for each gauging station, being then extrapolated for a given zone, in format raster, by correlating the initial Flashiness values with those of several factors such as slope index, curve number or mean annual precipitation. Therefore, the quality of the results provided by Flashiness method will depend on the gauging stations density, discharge measurements accuracy and the spatial resolution of the conditioning factors, unlike FFPI results whose accuracy is influenced only by the spatial resolution of the geographical factors. FFG method estimates the amount of rainfall of duration required to produce bank full conditions at the outlet of a small river basin. Therefore, along with Flashiness index, the FFG is another method whose results are influenced by the accuracy of the data measured at gauging stations or provided by the weather radar. Given the manner in which each index can be computed, we can state that the FFPI method is more accessible in terms of method complexity and required data, being therefore easier to be implemented, comparing to the other two indices. The utility of this method was initially demonstrated by Smith (2003), which calculated, for the first time, the FFPI values across the Colorado river catchment. At that time, in order to determine FFPI, the author integrated in GIS software a number of 4 variables that influence the surface runoff process (slope, soil type, vegetation and land use). The same method was taken over by other researchers and adapted for other areas in the US (Kruzdlo and Ceru 2010), or for other countries (Prăvalie and Costache 2014; Costache and Zaharia 2017; Zaharia et al. 2017). The equal weights assigned for flash-floods conditioning factors in the FFPI calculation process is the main drawback of the initially proposed method. Moreover, in the initial method, the areas affected in the past by the torrential phenomena were not considered. The weighting of the conditioning factors and the consideration of the areas already affected by a certain phenomenon are exemplified in many research studies whose central subject is the evaluation of susceptibility to the occurrence of various natural phenomena such as: floods (Chapi et al. 2017) and landslides (Conforti et al. 2014; Regmi et al. 2014; Demir et al. 2015; Dou et al. 2015; Goetz et al. 2015). The most commonly used methods in these studies are: frequency ratio (Cao et al. 2016; Youssef et al. 2016; Siahkamari et al. 2018), weights of evidence (Wang et al. 2016; Ding et al. 2017; Shafapour Tehrany et al. 2017; Hong et al. 2018a, b), logistic regression (Althuwaynee et al. 2014; Kavzoglu et al. 2014; Lombardo et al. 2015), decision trees (Bui et al. 2013; Tsangaratos and Ilia 2016; Pham et al. 2017a, b), artificial neural network (Bui et al. 2016; Chen et al. 2017a, b, c; Dou et al. 2018), naïve bayes etc. (Pham et al. 2016a, b; Hong et al. 2017; Chen et al. 2018).

Due to the fact that Romania is one of the countries most affected by flash-floods phenomena in Europe (Hanger et al. 2018; Romanescu et al. 2018), the studies that investigate the susceptibility to these natural disasters are extremely useful in drawing up flood risk management plans as well as in the forecasting and warning activity. Regarding the Romanian territory, one of the most exposed areas to flash-floods phenomena is Prahova river catchment. The flash-floods occurred in the last years have caused major material damage especially to the infrastructure from the study area. The present research aims to evaluate the potential of flash-floods occurrence across the upper and middle zone of Prahova river catchment. In this respect, techniques specific to machine learning, bivariate statistics and their novel hybrid integration will be used. As machine learning techniques, three decision tree models (Rotation Forest, Logistic Model Tree and Alternating Decision Tree) have been selected, while as bivariate statistic method, the Weights of Evidence model was chosen. Because it is considered that hybrid techniques provide more accurate results than stand-alone models (Shirzadi et al. 2017), a hybrid integration of the 3 machine learning techniques with Weights of Evidence model was performed. It is for the first time in the literature when FFPI values are calculated by using 3 decision tree models and also by the mean of their hybrid integration with WOE model. In order to calculate the FFPI through the aforementioned models, a number of 12 flash-flood predictors along with the surfaces affected in the past by torrential processes, were included in the analysis. The results validation process was carried out by 2 methods: density of torrential areas inside the FFPI classes and ROC Curve.

2 Study area

The study area is part of the Romanian territory and lies between 45°32′21.85″N and 45°00′23.33″N latitude, and 25°27′32.00″E and 26°27′10.19″E longitude (Fig. 1).

The altitudes range from 128 m, in the southern part of the research area, to 2505 m in the north-western part, near the most important tourist localities of Romania: Sinaia, Busteni, Azuga and Predeal. On a total area of 2600^2 km,

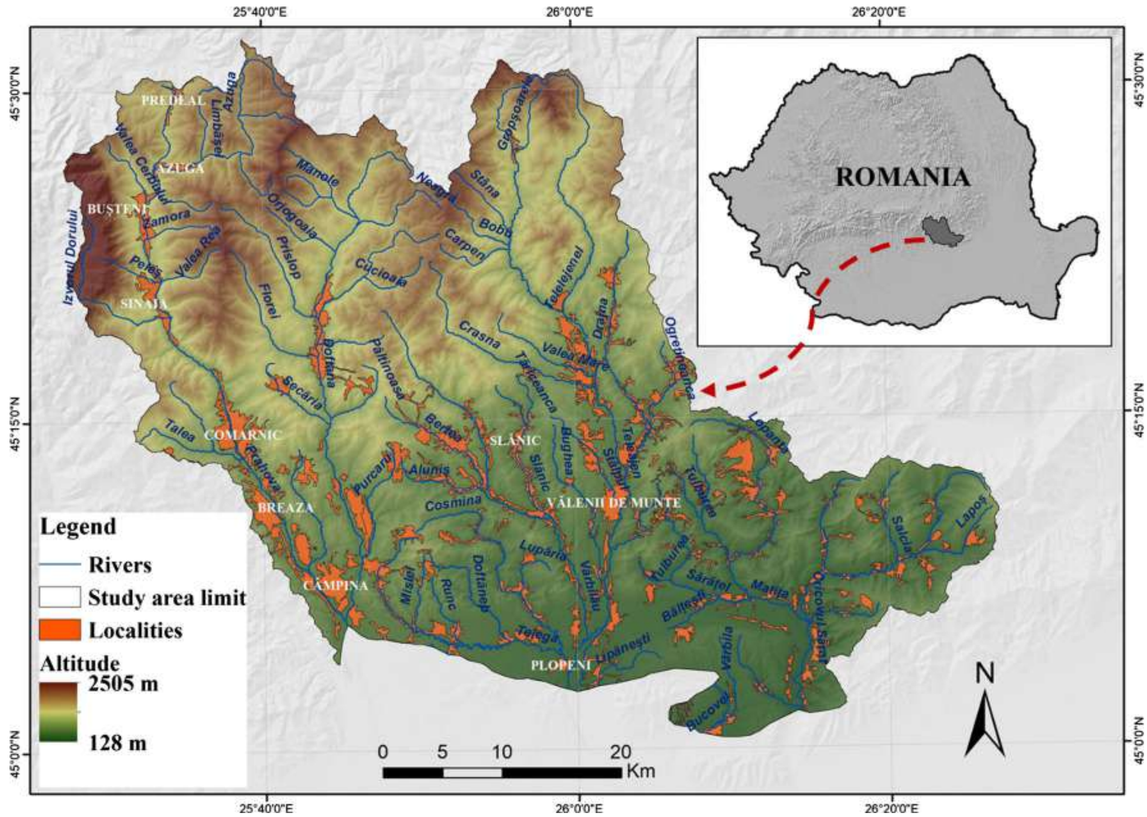

Fig. 1 Location of the study area

approximately 1000 km of rivers, included in the Romanian River Cadastre, are located. Valea Cerbului and Valea Rea, situated in the upper part of the research area, are two examples of river basins that were affected by severe flash-floods events during the last years. An extremely important factor for the potential of flash-floods triggering is the slope angle of relief. Across the study area the average slope angle value is 12.43°. It could be considered a relatively high value, taking into account the total surface of the basin on which this study is focused. The highest slope angle values occur in the mountain sector of the research area where the annual precipitation average records approximately 1000 mm. Hard rocks, such as sandstones and conglomerates, along with the impermeable soils and deforested surfaces, also contribute to the flash-floods occurrence especially in the summer season when convective rain is more likely. The main socio-economic elements threatened by flash-floods are the tourist cities located in the North-Western part, as well as the National Road 1 (E60), which is the main road in Romania of high importance at European level. Taking into account the economic development of the study area, as well as the high frequency of flash-floods, we believe that carrying out detailed flash-floods susceptibility studies is of major importance for the considered area.

The study area has a relatively large extent on the perimeter of the Carpathian and Subcarpathian Curvature, with many sub-catchments characterized by a high variety in terms of morphometry (slope values, altitude values), climatic elements (precipitation values), lithology, vegetation and soil. Therefore, given all the aforementioned elements, it can be assumed that the present paper and the research area are representative especially for the mountainous and hilly areas of the entire Carpathian Chain. The presence of human settlements across the study area is another element that makes the upper and middle sector of Prahova river catchment a representative one for other areas of the Carpathian Chain characterized by a large number of socio-economic elements. From a methodological point of view, we can state that the representativeness of the present study is also due to the fact that all variables and models taken into account for FFPI computation can be reproduced in any region of the globe.

3 Data and methods

In order to identify the zones prone to surface runoff, geospatial and meteorological data were used. The data are referring to the Digital Elevation Model, land use, soil, lithology, rainfall data and areas affected in the past by torrential phenomena. The aforementioned data were used in the following steps of the methodological workflow: (i) torrential areas inventory; (ii) estimation of predictive ability of flash-flood predictors and their selection based on statistical principles; (iii) application of stand-alone and hybrid models for the estimation of FFPI variability across the research area; (iv) flash-flood susceptibility assessment and FFPI maps creation; (v) results validation and the assessment of models performance. The workflow developed in the present study is synthetically presented in the Fig. 2.

3.1 Torrential areas inventory

Mapping the areas affected in the past by flash-floods is an essential step towards an accurate evaluation of the relationships between flash-flood predictors and FFPI values (Tehrany et al. 2015). In the present research, the identification of torrential area, covering approximately 260 km^2, was performed by using the aerial imagery, these surfaces being validated in the field, where a GSP Trimble GeoXH 2008 Series device was used, for a high measurement accuracy. Those surfaces having as characteristic the unitary presence of microforms, such as ravines and guiles, have been considered to be areas affected by torrentiality (Costache and Zaharia 2017). The smallest zone with torrential phenomena has an area of 0.35 sq. km, while the largest is of 71.1^2 km. In order to be involved in the methodological workflow, these surfaces have been randomly split into training sample (70%) and validating sample (Fig. 3). A number of 289,000 pixels, which is approximately equivalent to the surface covered by

Fig. 2 The scheme of the methodological workflow

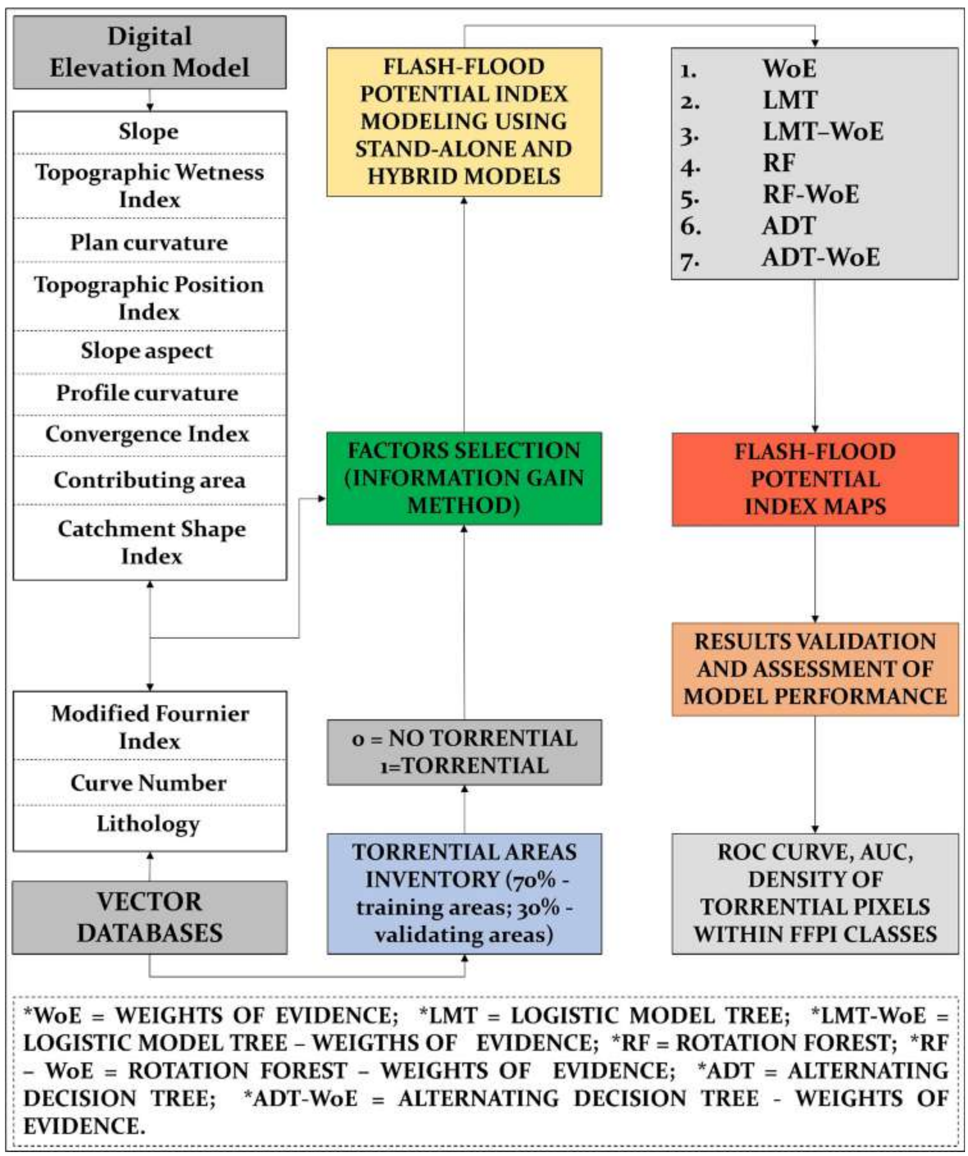

torrential pixels (260 km^2), were included in the analysis as non-torrential areas. It should be noted that the non-torrential pixels were randomly selected from those characterized by slope angles lower than 5°, where it was considered that runoff is less likely to be generated. As in the case of torrential areas, the non-torrential pixels were included into training sample (70%) and validating sample (30%). Therefore, the training sample comprises a number of 202,300 torrential pixels and 202,300 non-torrential pixels, while the validating sample contains a number of 86,700 torrential pixels and 86,700 non-torrential pixels.

3.2 Flash-flood influencing factors

The next step of the workflow was represented by the selection and mapping of flash-flood predictors. Thus, a number of 12 geographical variables has been considered for FFPI estimation. The land use and hydrological soil groups influence in a great measure the characteristics of the runoff process (Costache 2014; Vaezi et al. 2017). For a better characterization of the study area in terms of runoff potential, the land use factor extracted from Corine Land Cover, 2012 database, and hydrological soil group factor which was obtained based on the Digital Soil Map of Romania, 1:200000, were combined in order to derive the Curve Number (CN) index. The CN is an empirical parameter widely used in hydrology in order to estimate the direct runoff from a rainfall event (Saharia et al. 2017). The CN values, ranging from 0 to 100, are influenced only by the land use type and the hydrological soil group. It should be mentioned that the CN values close to 100 indicate a very high potential for runoff occurrence (Ryu et al. 2016). Regarding the study area, the *Natural Breaks* method was employed to divide the CN values into the following six classes: 0–43, 43–52, 52–69–69–80, 80–89, 88–100 (Fig. 5e). The CN values ranging from 43 to 80 cover more than 70% of the research zone (Fig. 7). Lithology has, also, a crucial role in terms of runoff manifestation due to its major influence on water infiltration process. The mapping of lithological categories, within the Prahova basin, was based on the Geological Map of Romania, 1:200000. The lithological categories represented by marls, flysch and conglomerates are spread on approximately 40% of the research area (Fig. 5f). Taking into account their classes and categories, the 2 factors mentioned above were transformed from vector dataset into raster dataset with a 30 m cell size, which is equal to the spatial resolution of the Digital Elevation Model. The Modified Fournier Index (MFI), proposed by Arnoldus (1980), is another flash-flood conditioning factor that was used to highlight the spatial

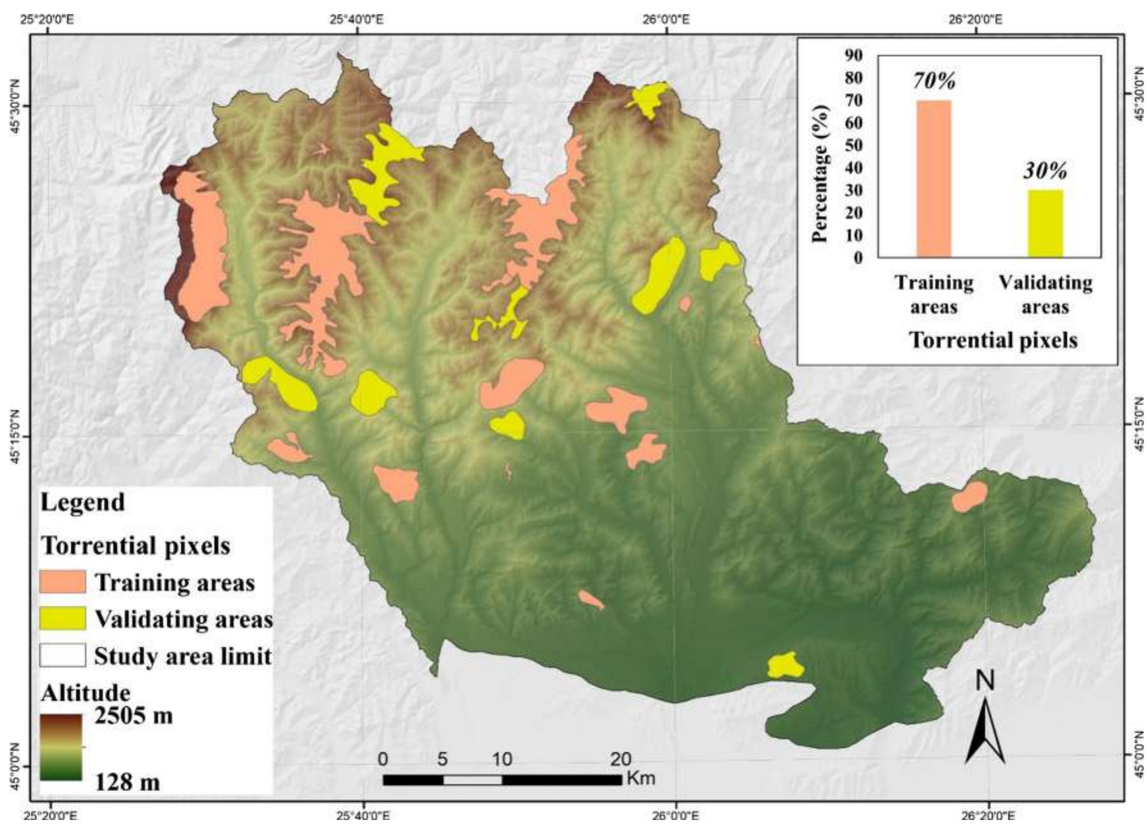

Fig. 3 The location of torrential areas within the study area

variability of rainfall intensity across the study area (Kazakis et al. 2015; Zaharia et al. 2015). Its computation was possible by using the following formula (Kourgialas and Karatzas 2011):

$$MFI = \sum_{i=1}^{12} \frac{P_i^2}{P}, \quad (1)$$

where P_i is the mean monthly precipitation (mm), and P—is the mean annual precipitation.

In order to derive the raster data corresponding to each of the 12 months of the year, the average monthly rainfall data (1980–2015) was used. This data was collected from a number of 23 weather stations located in the upper and middle basin of Prahova river, and in its surrounding area. The Spline method, considered to be the most appropriate for this type of analysis with a relatively small number of points (Kourgialas and Karatzas 2011), was employed to interpolate the data from the weather stations. Once obtained, the raster data related to the average monthly rainfall amount were used as input in Eq. 1. Using the *Natural Breaks* method, the MFI values calculated in GIS environment at a cell size of 30 m, were classified into the following 5 classes: 53.56–57.43, 57.44–62.83, 62.84–68.69, 68.7–75.14, 75.15–83.46 (Fig. 5d). The largest surfaces, quantifying about 28% of the study area, are covered by the first class (53.56–57.43) and the third class (62.84–68.89) of MFI values. Areas characterized by the presence of MFI values ranging from 68.7 to 75.14, include the highest percentage of torrential pixels (36.65%). The values of the other morphometric variables, involved in the analysis, were calculated based on the Digital Elevation Model (SRTM, 30 m). The first one, considered to be the most important factor on the surface runoff process, is slope angle (Wu et al. 2017). Slope angle is a morphometric factor that influences water infiltration rate and controls the velocity of runoff (Rahmati and Pourghasemi 2017). Steep slopes are favourable to rapid surface runoff occurrence, while flat surfaces are prone to inundation phenomena due to water stagnation process. Across the upper and middle basin of Prahova river, slope angle values were divided into 5 classes according to the international literature (Zaharia et al. 2015): $< 3°$, 3–7°, 7–15°, 15–25°, $> 25°$ (Fig. 5a). Almost 41% of the study area has slopes ranging from 7° to 15°. 37% of the torrential areas belongs to the slope class between 15° and 25° (Fig. 7). Because it highlights the areas with accelerated surface runoff, profile curvature is an extremely important factor in generating an overview regarding the flash-flood potential that exists within a specific area. Profile curvature values were calculated by using the following formula applied to a moving window (Alkhasawneh et al. 2013) (Fig. 4):

$$Profile\ curvature = \frac{((Z_2 + Z_8)/2 - Z_5)}{2\omega}, \quad (2)$$

where: Z—altitude value of a grid cell, ω—cell size.

The profile curvature map was produced by dividing its values in three classes as following: − 8.2–0, 0.1–0.9, 0.6–9.7 (Fig. 6d).

The plan curvature is another morphometric factor considered in the present analysis. The values of this variable highlight the difference between the convex, flat and concave surfaces. As in the case of profile curvature, the plan curvature values were derived based on a formula applied to a moving window:

$$Plan\ curvature = \frac{((Z_4 + Z_6)/2 - Z_5)}{2\omega}. \quad (3)$$

The plan curvature map was produced by classifying its values in three groups as following: 11.8–0, 0.1–0.5, 0.6–8.5 (Fig. 6c).

The convergence index (CI) was involved in several of the previous attempts to calculate the Flash-Flood Potential Index (Zaharia et al. 2015, 2017). According to Costache and Zaharia (2017), in order to classify the CI values 5 classes were established: (− 99)–(− 3), (− 3)–(− 2), (− 2)–(− 1), (− 1)–0, 0–99 (Fig. 5b). The values of the Topographic Position Index (TPI) can be calculated by using the difference between the altitude of a certain cell and the altitude of the neighboring cells. (Jenness 2000). According to Fig. 6a, the TPI map was created by diving its values into the following five classes using the *Natural Breaks* method: (− 34.82)–(− 2.08), (− 2.07)–(− 0.84), (− 0.83)–0.14, 0.15–1.12, 1.13–27.96. The topographic wetness index (TWI) is a widely used factor that shows the flow water accumulation tendency in certain point of hydrographic catchment. Using the Eq. (4) the values of

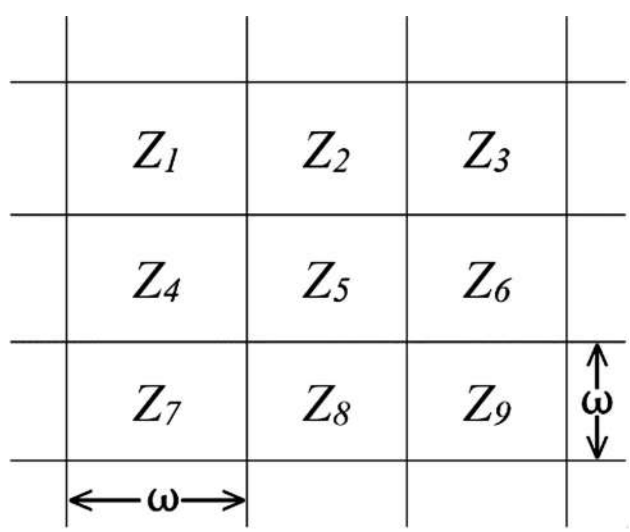

Fig. 4 3 × 3 moving window

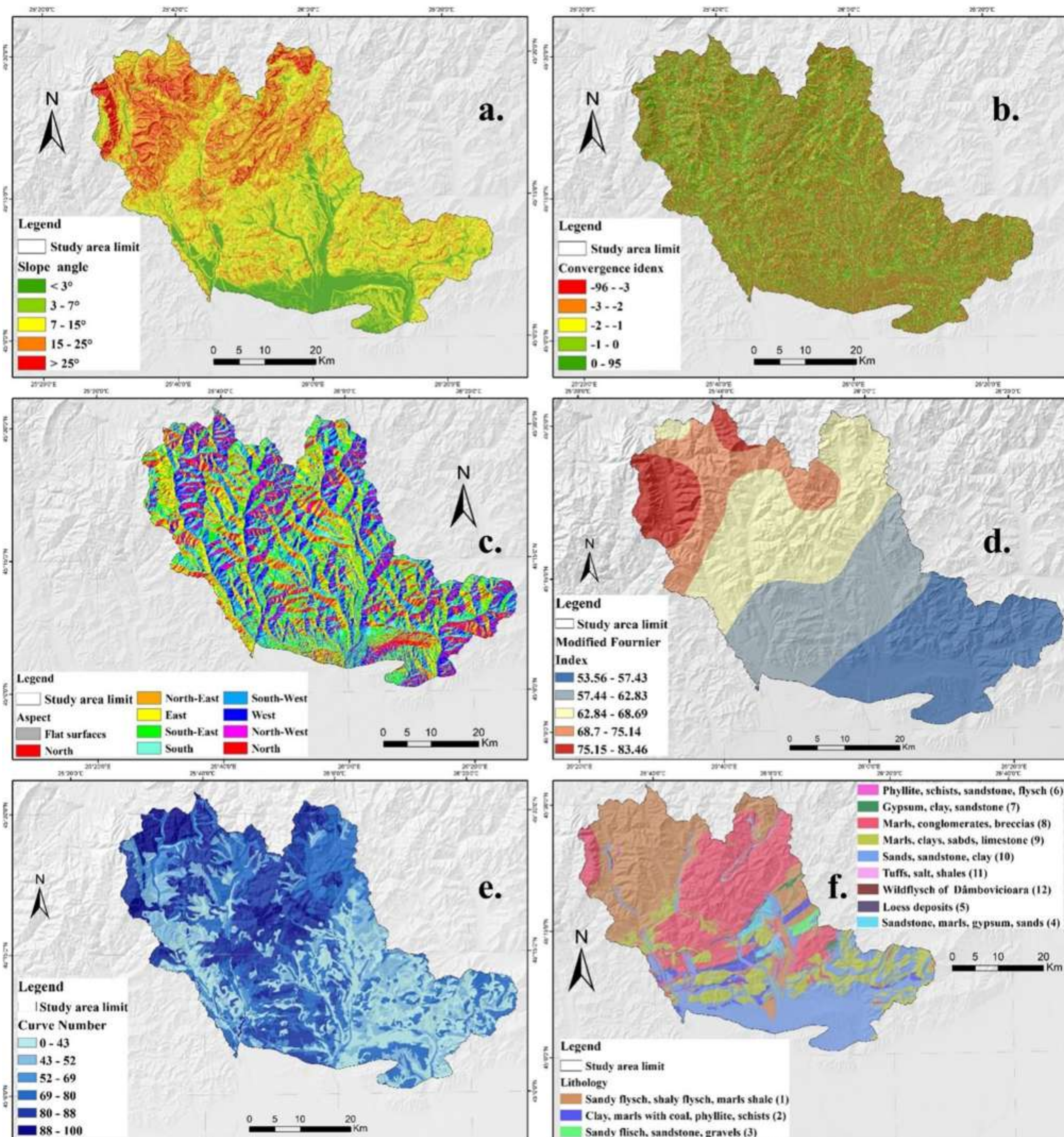

Fig. 5 Flash-flood conditioning factors (**a**. Slope; **b**. Convergence index; **c**. Aspect; **d**. Modified Fournier Index; **e**. Curve Number; **f**. Lithology)

this morphometric factor were calculated (Moore et al. 1991):

$$TWI = \ln\left(\frac{\alpha}{\tan\beta}\right), \quad (4)$$

where α is the area of upslope catchment that drains into a point (per unit contour length) and tan β is the average slope angle of the upslope catchment measured in that point. As in the case of TPI, TWI values were reclassified by using the *Natural Breaks* method: (− 9.7)–4.5, 4.6–8.4, 8.5–12, 13–15, 16–25 (Fig. 6b). Slope aspect is a variable that influences the physiographic characteristics which can affect runoff regime and soil moisture. Within the upper and middle basin of Prahova river, the largest areas are covered by the eastern and south-western slopes. The catchment shape is another morphometric factor that

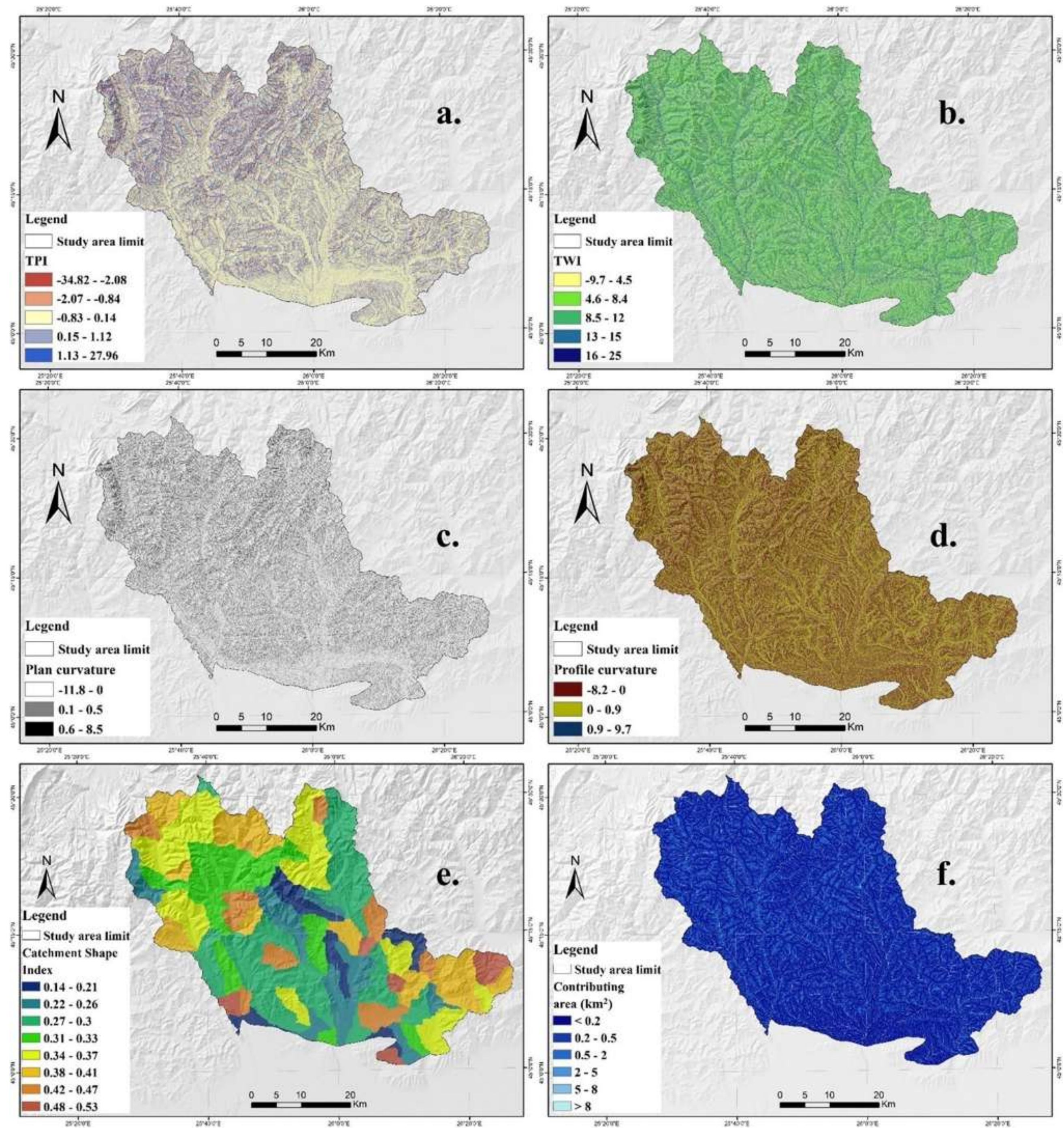

Fig. 6 Flash-flood conditioning factors (**a**. TPI; **b**. TWI; **c**. Plan curvature; **d**. Profile curvature; **e**. Catchment Shape Index; **f**. Contributing area)

controls the flash-floods potential within a hydrographic basin. Its main influence is related to the value of concentration time of a catchment. Generally, a circular-shaped watershed will have a lower concentration time than a watershed with a long narrow shape (Musy and Higy 2010). The sub-catchments of the study area were delineated based on a GIS workflow which implied the use of the Digital Elevation Model. In the present study, the Catchment Shape Index was expressed with the help of the circularity ratio (R_c) formula (Zaharia et al. 2017):

$$R_c = \frac{4\pi A}{P^2}, \tag{5}$$

where A is the area of the catchment (in km^2) and P is the perimeter of the catchment (in km). A circular catchment shape is indicated by an Rc value close to 1 (Zaharia et al.

2017). In the present research, the Catchment Shape Index values were divided into following the 8 classes, by using the *Natural Breaks* method: 0.14–0.21, 0.22–0.26, 0.27–0.3, 0.31–0.33, 0.34–0.37, 0.38–0.41, 0.42–0.47, 0.48–0.53. The largest areas are covered by catchments characterized by values between 0.27 and 0.3, while the highest percentage of torrential pixels (27%) are located inside the class between 0.34 and 0.37 (Fig. 6e).

The contributing area is a morphometric factor which has a great influence on flash-floods occurrence process (Diakakis et al. 2016; Samela et al. 2018). In order to compute the upslope contributing area (km^2) across the study area, the flow accumulation raster, obtained from the DEM, was multiplied with the value of a raster cell surface (900 m^2) and then divided by 1.000.000. The final map of contributing area was obtained by grouping its values into the following 6 classes: < 0.2 km^2, 0.2–0.5 km^2, 0.5–2 km^2, 2–5 km^2, 5–8 km^2, > 8 km^2 (Fig. 6f). Over 98% of the study has an upslope contributing area lower than 0.2 km^2 (Fig. 7).

The classes and categories adopted for each flash-flood influencing factor were used in the computation of the weights of evidence coefficients according to the methodology described at 3.4. Instead, in order to be included in the Correlation-based Feature Selection model described at 3.3., the values of the continuous variables were normalized within the range between 0 and 1. This transformation was carried out for all the conditioning factors, excepting aspect and lithology, which are the only categorical variables taken into account in the present analysis. Even if the normalization process has no impact in the performance of the decision tree-based algorithms, the normalized values, aspect directions and lithological categories were also involved in the training process of the decision tree stand-alone models applied in the present study.

3.3 Factor selection using correlation-based feature selection (CFS)

According to Ozcift and Gulten (2011), a factor is of a major importance for a model if it is highly correlated to the presence of the analyzed phenomena, and uncorrelated to any of the other factors. Thus, a high correlation between each flash-flood conditioning factor and areas with torrentiality demonstrate a good predictive capability of that factor compared to the others. Correlation-based Feature Selection (CFS) model identifies very fast and displays the information that are irrelevant, redundant and noisy (Hall 1999). Usually, a factor is redundant if it is highly correlated with other factors. Therefore, the greatest CFS scores will be assigned to flash-flood conditioning factors which are highly correlated with torrential phenomena location. The scores are defined by the following equation (Ozcift and Gulten 2011):

$$CFS = \frac{\mathrm{k}r_{cf}}{\sqrt{\mathrm{k} + \mathrm{k}(\mathrm{k}-1)r_{ff}}}, \tag{6}$$

where *CFS* is the correlation between each flash-flood predictor and the presence/absence of torrential areas, k is the number of flash-flood predictor, r_{cf} is the average correlation between flash-flood conditioning factor and areas with torrentiality, and r_{ff} is the average intercorrelation between flash-flood predictors.

The determination of *CFS* scores will be performed by integrating the normalized and categorical values of flash-flood influencing factors, and the torrential/non-torrential areas in Weka 9.3.2 software.

3.4 Weights of evidence

Proposed for the first time in geological studies (Agterberg 1992), the Weights of Evidence (WOE) model was used by many researchers to assess the susceptibility of the surfaces to different disasters, such as: landslides, floods and flash-floods (Kayastha et al. 2012; Tehrany et al. 2014; Costache and Zaharia 2017). This data-driven method represents a Bayesian bivariate statistical model widely used in the geoscience research field.

In this paper, the Weights of Evidence was used as a stand-alone model for the computation of FFPI across the study area, and also, as a method for the derivation of input data involved in the training process of the ensemble models resulted from the hybrid integration of the WOE on the one hand and the decision tree models (Rotation Forest (RF), Logistic Model Tree (LMT) and Alternating Decision Tree (ADT)) on the other hand.

Since flash-flood conditioning factors, within WOE model, are constant in time, the weights of each factor class/category will be estimated based on the spatial relationships between them and the presence/absence of torrential phenomena. In fact, the calculation of weights assigned to each class/category of flash-flood conditioning factors, is based on Bayes' conditional probability theorem which is described by the following relation (Regmi et al. 2014):

$$P\left\{\frac{A}{B}\right\} = \ln\frac{P\left(\frac{B}{A}\right)\mathrm{X}\ P(A)}{P(B)}, \tag{7}$$

where P is the probability, B is the presence of flash-flood conditioning factor and A is the presence of torrential areas.

The estimation of WOE coefficients requires, in a first stage, the calculation of negative weights (W^-) and positive weights (W^+). The negative weights highlight the

Fig. 7 The percentage of class pixels and torrential pixels within the classes/categories of flash-flood conditioning factors

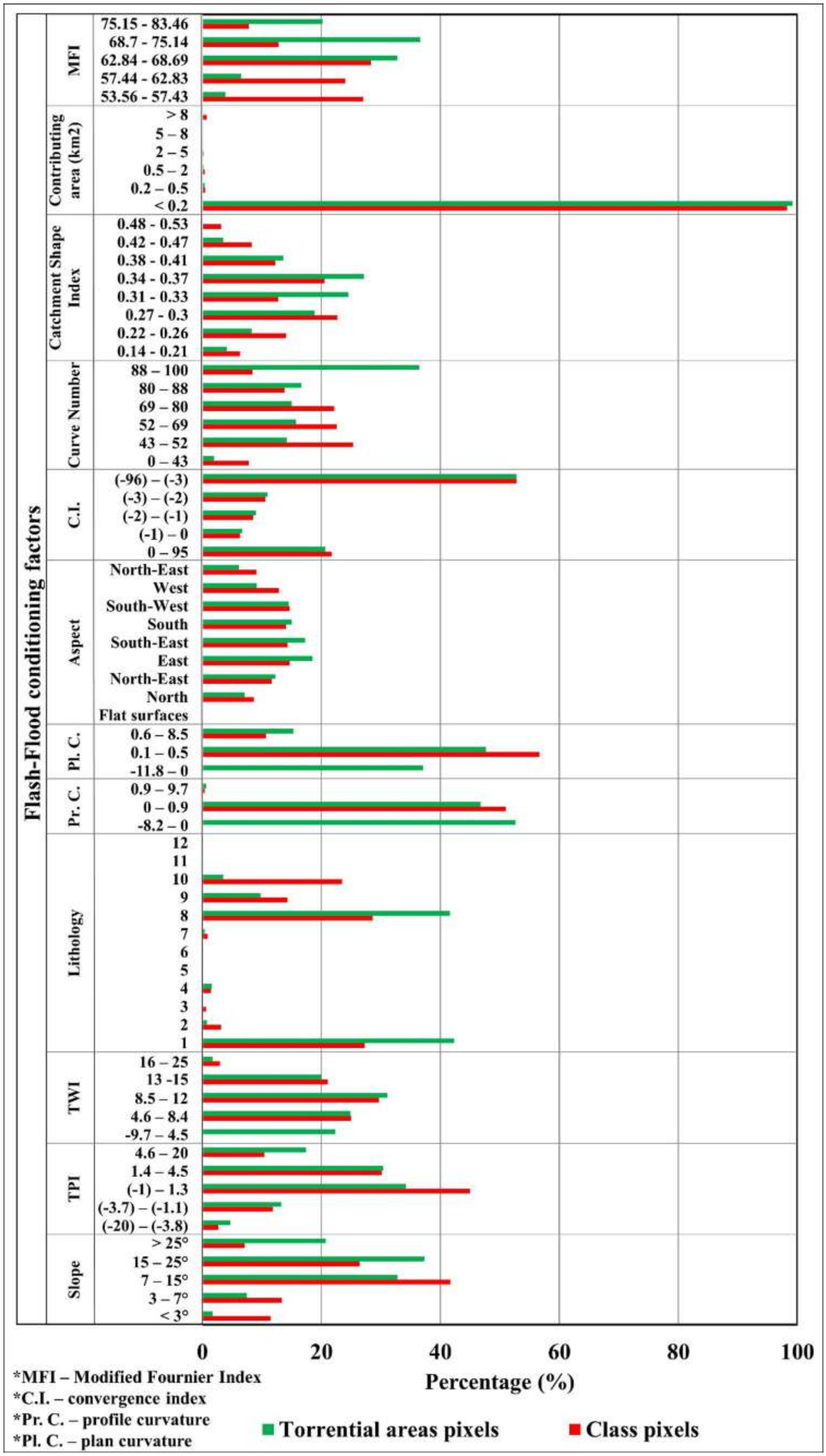

overlay between a class/category of a predictor and an area characterized by the absence of torrential phenomenon, while the positive weights indicate the overlay between a class/category and an area with torrential phenomena (Van Westen 2002).

According to Bonham-Carter et al. (1994), the values of negative and positive weights can be derived using the formulas:

$$W^{+} = \ln\frac{P\{B|S\}}{P\{B|\bar{S}\}} \tag{8}$$

and

$$W^{-} = \ln\frac{P\{\bar{B}|S\}}{P\{\bar{B}|\bar{S}\}}, \tag{9}$$

were W^{+} is the positive weight, W^{-} is the negative weight, P is the probability, B is the presence of a flash-flood influencing factor, $\bar{B}$ is the absence of a flash-flood influencing factor, S represents the presence of torrential phenomena, $\bar{S}$ represents the absence of torrential phenomena.

For an easy implementation in GIS environment, the form of the above equations can be changes as following (Van Westen et al. 2003):

$$W^{+} = \ln\frac{\frac{Npix_1}{Npix_1+Npix_2}}{\frac{Npix_3}{Npix_3+Npix_4}} \tag{10}$$

and

$$W^{-} = \ln\frac{\frac{Npix_2}{Npix_1+Npix_2}}{\frac{Npix_4}{Npix_3+Npix_4}}, \tag{11}$$

where $Npix_1$ is the number of pixels with phenomena inside a factor class/category; $Npix_2$ is the number of pixels with torrential phenomena outside the factor class/category; $Npix_3$ is the number of pixels without torrential phenomena inside a factor class/category; $Npix_4$ is the number of pixels without torrential phenomena outside a factor class/category; W^{+} is the value of positive weight and W^{-} is the value of negative weight.

The last step is represented by the calculation of the final weights of evidence coefficients assigned to each factor class/category. In this regard the following relation will be used (Costache and Zaharia 2017):

$$Wf = Wplus + W\mathrm{min}total - Wmin, \tag{12}$$

where Wplus is the positive weight of a class factor, Wmin is the negative weight of a class factor, Wmintotal is the total of all negative weights in a multiclass map. Further, the $\mathrm{FFPI_{WOE}}$ will be calculated as following:

$$FFPI_{WOE} = \sum_{j=1}^{n} Wfij, \tag{13}$$

where $Wfij$ is the final weight of class i in parameter $_j$ and n is the numbers of variables.

Instead, when the WOE coefficients are used to train the hybrid models designed for FFPI calculations, their values will be normalized through the formula (Pradhan and Lee 2010):

$$y = \frac{(Wf - \min(d)) * (\max(n) - \min(n))}{\max(d) - min(d)} + min(n), \tag{14}$$

where: y—standardized value of Wf; Wf—current value of variable; d—limits of Wfrange values within a flash-flood conditioning factor; n—standardization range limits. The standardization range was considered between 0.1 and 0.9.

3.5 Rotation forest (RF)

Rotation Forest (RF) is a relatively new and powerful classification method (Rodriguez et al. 2006). In the recent years, the RF model was used also to evaluate the susceptibility to different natural risk phenomena (Pham et al. 2016a, b; Chen et al. 2017a, b, c; Pham et al. 2017a, b; Hong et al. 2018a, b). Being an ensemble method, it is considered that RF model provides more accurate results compared to a single-based classifier method (Ozcift and Gulten 2011). In the RF method, the classifier ensembles are generated through the feature extraction process. In order to create the training dataset required by a base classifier, the feature set is randomly split into many K subsets (K is a model parameter), and a Principal Component Analysis (PCA) is subsequently applied for each subset (Rodriguez et al. 2006). The main steps of RF procedure are described in the next rows.

Let g = [g_1,..., g_{10}] be the vector of flash-flood conditioning factors described by n classes/categories, let G the dataset containing the conditioning factors in a form of N x n matrix and let T = [t_1,t_2] be a vector of torrential areas, where t_1—the presence of torrential phenomena and t_2—the absence of torrential phenomena. Presuming that the dataset (F) is randomly divided into K subsets and L decision trees of the RF algorithm denoted by {D_1,..., D_L}, the following steps will be required to construct the training data set:

(i) Divide F randomly into many K feature subsets, where an individual subset contains M = n/K features.
(ii) If we consider F_{ij} as the jth subset of features to train the classifier D_i, and G_{ij} as the dataset for G, then a bootstrap resampling procedure with 75% of the dataset will be used in order to create a new training dataset. Subsequently a linear transformation is applied to G_{ij} to calculate the coefficients of the matrix C_{ij}. The matrix will contain

the coefficients $a_{i,j}^{(1)} \ldots, a_{i,j}^{(M_j)}$, each of them with a size of M × 1.

(iii) Derive the sparse rotation matrix R_i containing the obtained vectors with the related coefficients as following:

$$R_i = \begin{bmatrix} a_{i,1}^{(1)}, a_{i,1}^{(2)}, \ldots, a_{i,1}^{(M_1)} & 0 & \cdots & 0 \\ 0 & a_{i,1}^{(1)}, a_{i,1}^{(2)}, \ldots, a_{i,1}^{(M_2)} & \cdots & 0 \\ \vdots & \vdots & \ddots & \vdots \\ 0 & 0 & \cdots & a_{i,K}^{(1)}, a_{i,K}^{(2)}, \ldots, a_{i,K}^{(M_K)} \end{bmatrix} \quad (15)$$

The matrix obtained is rearranged with the coefficients that correspond to each class, their values being derived by using the average combination in the given test sample which is described by the following equation (Chen et al. 2017a, b, c):

$$m_j(g) = \frac{1}{L} + \sum_{i=1}^{L} d_{ij}\left(gR_i^a\right), j = 1, \ldots, c, \quad (16)$$

where $d_{ij}\left(xR_i^a\right)$ is the probability given by the classifier D_i for the hypothesis that x belongs to the class j.

In order to derive the FFPI values, RF model will be applied both as stand-alone model, as well in a hybrid combination with WOE statistical model. In both situations the application of the models will be performed using Weka 9.3.2 software.

3.6 Logistic model tree (LMT)

Logistic Model Tree represents a combination between Logistic Regression method and decision tree machine learning algorithm (Landwehr et al. 2005; Chen et al. 2017b). LMT model has the following advantages (Eristi and Demir 2012): is a fast learning algorithm; the different sensitive parameters do not need adjustment; is a simple model with a very high learning efficiency. According to Landwehr et al. (2005), the LMT structure is formed by non-terminal nodes N (set of inner) and terminal nodes T (set of leaves). The regression function is applied to the results provided by decision tree algorithm at each leaves level, while the CART algorithm is used for tree pruning and information gain method for splitting (Chen et al. 2017b). The *LogitBoost* algorithm, employed in order to apply the *Logistic Regression* function for each class C_i (torrential areas and non-torrential areas), is described by the following relation (Bui et al. 2016):

$$L_C(x) = \sum_{i=1}^{F} \beta_i x_i + \beta_0, \quad (17)$$

where F is the number of flash-flood influencing factors and β_i is the coefficient assigned to the i-th component in the input vector x.

In the LMT model, the posterior probability for each leaf node, is estimated by using the linear logistic regression model (Landwehr et al. 2005; Chen et al. 2017b):

$$p(C|x) = \frac{\exp(L_C(x))}{\sum_{C'}^{F} \exp(L_{C'}(x))}, \quad (18)$$

where F is the number of classes.

Weka software was used for the implementation of both LMT stand-alone model and LMT-WOE hybrid models.

3.7 Alternating decision tree

Alternating Decision Tree (ADT), proposed for the first time by Freund and Manson (1999), provides a mechanism which combines boosting algorithm with decision tree. Unlike other decision tree algorithms, like CART and Random Forest, ADT produce simpler structures of decision tree and classification rules easier-to-interpret (Liu et al. 2005; Hong et al. 2015). This method is a natural extension of voted-stumps and decision tree algorithms, and it consists of alternating layers of prediction and decision nodes (Freud and Manson 1999). According to Hong et al. (2015), the prediction nodes are made of a single number, meanwhile the predicate condition is specified by the decision nodes. Therefore, the ADT structure is formed by decision paths, where a path corresponding to a decision node continues with the specific offspring node and other path that corresponding to a prediction node will continue with all of the offspring nodes (Liu et al. 2005).

If we consider x_1 as precondition, x_2 as a base condition, and two real numbers f and g, the values of f and g can be calculated as following (Khosravi et al. 2018):

$$f = 0.5 * \ln \frac{W_+(x_1 \cap x_2)}{W_-(x_1 \cap x_2)}, \quad g = 0.5 * \ln \frac{W_+(x_1 \cap \overline{x_2})}{W_-(x_1 \cap \overline{x_2})}, \quad (19)$$

where W denotes the sum of the values from any prediction node, and the best x_1 and x_2 are estimated by minimizing the $Z_t(x_1, x_2)$, determined as following:

$$z_t(x_1 x_2) = 2\sqrt{W_+(x_1 \cap x_2) * W_-(x_1 \cap x_2)} + \sqrt{W_+(x_1 \cap \overline{x_2}) * W_-(x_1 \cap \overline{x_2})} + W(\overline{x_2}) \quad (20)$$

In the present study, the ADT with AdaBoost boosting algorithm was used to estimate the *Flash-Flood Potential Index* based on the information related to the 12 flash-flood influencing factors and to the presence and absence of torrential phenomena. Considering the ADT structure, *FFPI* value for a certain pixel will be calculated as the sum of the values which are assigned to each prediction node and which occur at the transition of the pixel through all the applicable branches.

Within the entire ADT procedure, a number of 20 boosting iteration was applied. By using the training sample and validating sample, the classification accuracy was estimated for each iteration.

FFPI values were estimated both by the individual use of ADT model, and by the hybrid integration with the WOE model. ArcGIS 10.5 and Weka software were used in this regard.

3.8 Evaluation of the model's performance and results validation

3.8.1 Density of torrential pixels inside the classes of FFPI

The first method used to assess the model's performance and to validate the results, is represented by the estimation of torrential pixels density inside the classes of FFPI resulted by applying the aforementioned models. This widely used method in other studies related to natural hazards susceptibility assessment (Costache and Zaharia 2017; Hong et al. 2018a, b), highlights a good performance of the models when a large part of the torrential areas in the training sample is located over the surfaces with a high and very high flash-flood potential. The accurate results are indicated by a high density of torrential areas in the validating sample within the FFPI classes characterized by high and very high values.

3.8.2 Receiver operating characteristics curve (ROC Curve)

This method is used to evaluate the capacity of the model to correctly predict an event. In order to construct the ROC Curve, the sensitivity will be represented on Y axis against the 1-specificity that will be represented on X axis with various cut-off thresholds (Chen et al. 2017a, b, c). Area Under Curve (AUC) is the quantitative indicator that shows the measure in which a model is assessed as effective or not. An efficient model is indicated by a value of AUC close to 1, while a weak model is highlighted by an AUC values close to 0 (Youssef et al. 2015; Costache and Zaharia 2017). The AUC values could be calculated through the relation (Hong et al. 2018a, b):

$$\mathrm{AUC} = \frac{\left(\sum TP + \sum TN\right)}{(\mathrm{P} + \mathrm{N})}, \tag{21}$$

where TP (true positive) and TN (true negative) indicate the sum of pixels correctly classified, P is the number of torrential pixels and N is the number of non-torrential pixels.

4 Results and discussions

4.1 Predictive capability of flash-flood influencing factors

The predictive capability of the 12 flash-flood influencing factors was estimated through the *CFS* method described at 3.3. The predictive capability was expressed in Average Merit values (AM) (Fig. 8).

The application of *CFS* methods demonstrate that the highest predictive capability was assigned to slope angle with an AM value of 0.294. This result is in agreement with the majority of the studies related to surface runoff manifestation process, in which the slope angle is considered the most important influencing factor (Douvinet et al. 2015; Bathrellos et al. 2016; Ozturk et al. 2018). Regarding the Average Merit values, slope angle is followed by curve number (0.258), lithology (0.193), profile curvature (0.182), Modified Fournier Index (0.175), TWI (0.169), plan curvature (0.151), catchment shape index (0.144), convergence index (0.125), contributing area (0.083), aspect (0.078) and TPI (0.035).

Since the average merit computed for each flash-flood conditioning factor is higher than 0, all the variables will be employed into the analysis.

4.2 Application of weights of evidence stand-alone model

The first stage accomplished within the FFPI estimation process through WOE model, consisted of the calculation of WOE coefficients for each factor class/category. These values were determined according to the methodology

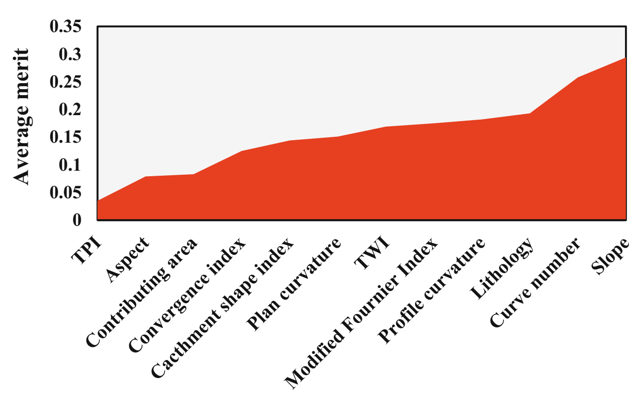

Fig. 8 Average Merit assigned to the flash-flood conditioning factor using CFS method

described at 3.4. The highest *Wf* value (2.38) pertain to *Curve Number* class ranging from 88 to 100 (Table 1). Given the fact that the value of *Curve Number* is determined by the intersection of land use type with the hydrological soil group, we can state that the these high values of *Wf* are mainly explained on the one hand by the presence of a land use type characterized by low values of Manning roughness coefficients which are favorable to an intense manifestation of surface runoff, and on the other hand by the presence of a hydrological soil group characterized by a low degree of permeability (Costache 2014). The analysis showed that high values of *Wf* were also recorded by *MFI* class between 68.7 and 75.14 (1.65), *Slope angles* higher than 25° (1.51), *MFI* class between 75.15 and 83.46 (1.32), and *Catchment Shape Index* class between 0.31 and 0.33 (0.94). It can be observed that the *Slope angles* higher than 25°, are related to the highest value of positive weights (W^+) (1.87) (Fig. 9). The lowest values of *Wf*, among the 72 factors classes/categories, have been estimated for the *Slope angles* lower than 3° (− 2.15), lithological group 10 (− 2.26), *MFI* class ranging from 53.56 to 57.43 (− 2.35), flat surfaces (− 2.37) and lithological group 3 (− 2.67). The lowest negative weight (W^-) of − 0.77, was established for the class of *Contributing area* lower than 0.2 km^2.

Once calculated, *Wf* values were attributed to the corresponding factor classes/categories in GIS environment. Subsequently, flash-flood conditioning factors in raster format were summed up in order to compute $FFPI_{WOE}$ values (Fig. 10). $FFPI_{WOE}$ values, ranging from (− 25.35) to 9.84 were grouped into 5 classes (very low; low; medium; high; very high) through *Natural Breaks* method available in *ArcGIS 10.5*. The first class, which denotes very low $FFPI_{WOE}$ values, occupies approximately 12.6% of study area and ranges between (− 25.35) and (− 6.27). Within these areas, located mainly in the southern region of the upper and middle basin of Prahova river, the flash-floods occurrence is almost impossible due to the small slope angle. Low $FFPI_{WOE}$ values ranging from (− 6.26) to (− 2.18), are characteristic to 28.3% of research area while the medium values cover around 35.7% of total. $FFPI_{WOE}$ values included in the IVth and Vth classes characterize 23.3% of the study area, being located on compact areas situated mainly in the north-western region. In case of heavy rainfall, the presence of these large compact surfaces, with a very high susceptibility degree, leads to severe flash-flood events.

4.3 Application of *LMT* stand-alone model and *LMT-WOE* hybrid model

The analysis of the multicollinearity among flash-flood conditioning factors, was realized by computing two parameters represented by the tolerance (TOL) and variance inflation factor (VIF) (Table 2). Since the smallest *TOL* value is of 0.79 (*Contributing area*) and the highest *VIF* values is of 1.19 (*Convergence Index*), it can be concluded that there is not a serious collinearity among the variables included in the analysis.

Additionally, a cross-validation procedure was employed in order to establish the optimal number of iterations used to assess the classification performance. In this regard, *LMT* and *LMT-WOE* models were compared with the other stand-alone and hybrid models considered in the present research (Fig. 11). Of all models, the highest accuracy was obtained by *RF* stand-alone model (93.4%) after 18 iterations. In terms of *LMT* stand-alone model the highest accuracy (92.1%) resulted after 18 iterations, while for *LMT-WOE* hybrid model, the highest accuracy has been reached after 19 iterations (Table 3).

Following the training process of *LMT* stand-alone model and *LMT-WOE* hybrid model, the importance of each flash-flood conditioning factor was determined (Fig. 15). Therefore, in the case of *LMT* stand-alone algorithm the slope angle (15.78%) was the most important factor, followed by curve number (14.68%), lithology (11.84%), plan curvature (10.57%),mfi (9.63%), twi (7.45%), convergence index (7.1%), profile curvature (6.17%), contributing area (5.52%), tpi (5.05%), aspect (3.8%) and catchment shape index (2.41%). According to the *LMT-WOE* hybrid model, the highest importance was also recorded by slope angle (15.73%), followed by curve number (14.48%), lithology (13.07%), plan curvature (8.82%), mfi (8.17%), convergence index (7.56%), contributing area (7.23%), tpi (6.78%), twi (5.68%), profile curvature (4.73%), catchment shape index (4.73%) and aspect (3%). Using the variables importance, $FFPI_{LMT}$ and $FFPI_{LMT\text{-}WOE}$ were calculated in ArcGIS 10.5.

Therefore, considering the *Natural Breaks* classification method, $FFPI_{LMT}$ values, ranging from 0.11 to 0.89, were grouped into 5 classes (Fig. 12a). The first class of values, between 0.11 and 0.23, is characteristic to 6.4% of the upper and middle basin of Prahova river and highlights the regions with a very low flash-flood susceptibility degree. The next class that ranges between 0.23 and 0.34, covers 19.6% of the upper and middle basin of Prahova river. The highest weight, in terms of area, is held by the medium values of $FFPI_{LMT}$. Thus, the surfaces included in the medium class are spread on around 30.3% of the total, a slightly more than the high values of $FFPI_{LMT}$ which cover 27.5% of study area. The values that characterize a very high potential for flash-floods occurrence are encountered on about 16.2% of the entire study area, and range between 0.69 and 0.89.

By including the WOE coefficients values in the training process of *LMT* model, the results of *LMT-WOE* hybrid

Table 1 Standardized classes WOE values of flash-flood conditioning factors

Factor	Class	Class pixels (%)	Torrential areas pixels (%)	WOE coefficients	WOE standardized coefficients
Slope	< 3°	11.46	1.66	− 2.15	0.10
	3–7°	13.32	7.46	− 0.71	0.42
	7–15°	41.72	32.83	− 0.43	0.48
	15–25°	26.42	37.35	0.58	0.70
	> 25°	7.09	20.70	1.51	0.90
TPI	(− 20)–(− 3.8)	2.71	4.67	0.66	0.88
	(− 3.7)–(− 1.1)	11.82	13.25	0.15	0.53
	(− 1)–1.3	44.96	34.26	− 0.50	0.10
	1.4–4.5	30.14	30.41	0.01	0.45
	4.6–20	10.38	17.42	0.69	0.90
TWI	− 9.7–4.5	21.30	22.33	− 0.01	0.80
	4.6–8.4	24.98	24.89	0.08	0.90
	8.5–12	29.70	31.13	− 0.08	0.71
	13 − 15	21.09	19.93	− 0.59	0.10
	16–25	2.93	1.72	0.07	0.89
Lithology	1	27.28	42.31	0.76	0.90
	2	3.08	0.75	− 1.53	0.37
	3	0.65	0.05	− 2.67	0.10
	4	1.43	1.59	0.12	0.75
	5	0.10	0.00	0.01	0.72
	6	0.05	0.04	− 0.44	0.62
	7	0.89	0.39	− 0.89	0.51
	8	28.62	41.59	0.65	0.87
	9	14.30	9.77	− 0.48	0.61
	10	23.45	3.52	− 2.26	0.20
	11	0.07	0.00	0.01	0.72
	12	0.08	0.00	0.01	0.72
Profile curvature	− 8.2–0	48.62	52.61	0.18	0.53
	0–0.9	50.97	46.77	− 0.19	0.10
	0.9–9.7	0.40	0.62	0.49	0.90
Plan curvature	− 11.8–0	32.68	37.05	0.22	0.67
	0.1–0.5	56.65	47.66	− 0.41	0.10
	0.6–8.5	10.66	15.29	0.47	0.90
Aspect	Flat surfaces	0.08	0.01	− 2.37	0.10
	North	8.64	7.10	− 0.24	0.74
	North–East	11.62	12.30	0.07	0.83
	East	14.69	18.54	0.32	0.90
	South–East	14.34	17.24	0.04	0.82
	South	14.06	15.07	0.09	0.83
	South–West	14.66	14.49	− 0.02	0.80
	West	12.84	9.15	− 0.42	0.68
	North–East	9.07	6.11	− 0.47	0.67
Convergence index	0–95	21.72	20.65	− 0.07	0.10
	(− 1)–0	6.34	6.70	0.07	0.89
	(− 2)–(− 1)	8.51	8.99	0.07	0.90
	(− 3)–(− 2)	10.62	10.89	0.03	0.69
	(− 96)–(− 3)	52.81	52.77	0.01	0.50

Table 1 (continued)

Factor	Class	Class pixels (%)	Torrential areas pixels (%)	WOE coefficients	WOE standardized coefficients
Curve Number	0–43	7.78	1.97	− 1.53	0.10
	43–52	25.32	14.19	− 0.79	0.25
	52–69	22.57	15.72	− 0.49	0.31
	69–80	22.14	15.05	− 0.52	0.31
	80–88	13.80	16.61	0.25	0.46
	88–100	8.39	36.46	2.38	0.90
Catchment Shape Index	0.14–0.21	6.34	4.12	− 0.50	0.79
	0.22–0.26	14.04	8.24	− 0.65	0.78
	0.27–0.3	22.70	18.81	− 0.26	0.81
	0.31–0.33	12.73	24.53	0.94	0.90
	0.34–0.37	20.50	27.13	0.10	0.83
	0.38–0.41	12.26	13.61	0.14	0.84
	0.42–0.47	8.29	3.46	0.22	0.75
	0.48–0.53	3.14	0.09	− 1.26	0.10
Contributing area (km^2)	< 0.2	98.26	99.15	0.78	0.90
	0.2–0.5	0.43	0.40	− 0.08	0.65
	0.5–2	0.33	0.19	− 0.62	0.50
	2–5	0.17	0.09	− 0.70	0.47
	5–8	0.10	0.07	− 0.41	0.56
	> 8	0.71	0.10	− 2.02	0.10
Modified Fournier Index	53.56–57.43	27.03	3.88	− 2.35	0.10
	57.44–62.83	23.99	6.46	− 1.63	0.24
	62.84–68.69	28.32	32.78	0.24	0.62
	68.7–75.14	12.81	36.65	1.65	0.90
	75.15–83.46	7.84	20.22	1.32	0.83

model were spatially modelled (Fig. 12b). Very low values of $FFPI_{LMT\text{-}WOE}$ are characteristic for an area of 260 km^2, having a weight of 10.7% of the upper and middle basin of Prahova river. The surfaces characterized by a low flash-flood susceptibility cover around 24.6% of research area and correspond to $FFPI_{LMT\text{-}WOE\text{-}}$ ranging between 0.22 and 0.39. The next class of values ranges between 0.39 and 0.59 and is distributed on about 34.4% of the upper and middle basin of Prahova river. Together, the high and very high flash-flood susceptibility occupy around 30.3% of the total.

4.4 Application of *RF* stand-alone model and *RF-WOE* hybrid model

The application of *RF* stand-alone model and *RF-WOE* hybrid model for *FFPI* calculation within the study area, requires, in a first stage, an optimization process, this operation having a large influence on the results accuracy provided by the two methods. The parameters obtained after the optimization process are presented in Table 3. In the same table are presented the optimal parameters corresponding to the other applied models.

As it was aforementioned, the accuracy of *RF* stand-alone model (93.4%), was obtained after 18 iterations, while for *RF-WOE* hybrid model the highest accuracy of 92.4% resulted after 16 iterations.

After the training process of *RF* and *RF-WOE* models, the weight of each flash-flood conditioning factor was derived. Similar to the previous models, the slope angle obtained the highest importance both for *RF* and *RF-WOE* model (Fig. 15). The variable weigths were further used to calculate the FFPI values.

In both situations, the Natural Breaks method was applied to classify the FFPI's value range. Therefore, in terms of $FFPI_{RF}$ the first class of values, which indicates a very low flash-flood susceptibility, covers around 8.9% of the upper and middle basin of Prahova river, and range between 0.13 and 0.22 (Fig. 13a). The next class of values, ranging from 0.22 to 0.37, is present on around 20.1%,

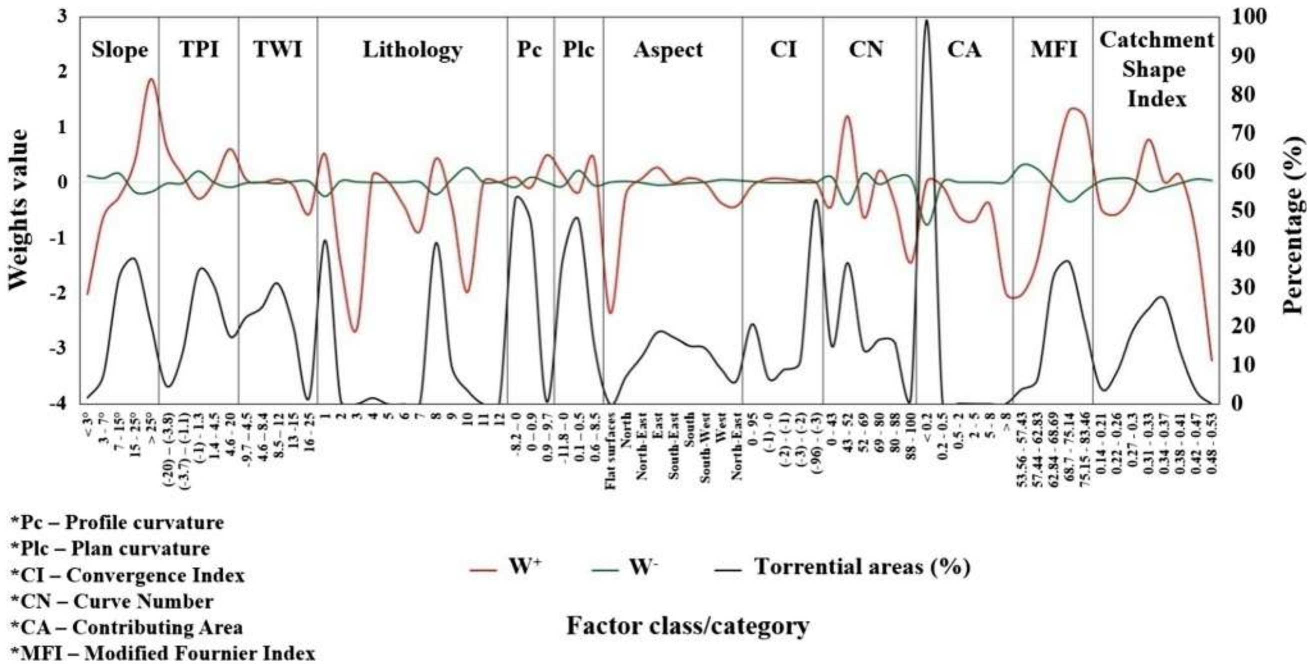

Fig. 9 Positive (W +) and negative weights (W −) computed for each flash-flood conditioning factors classes/category through WOE model

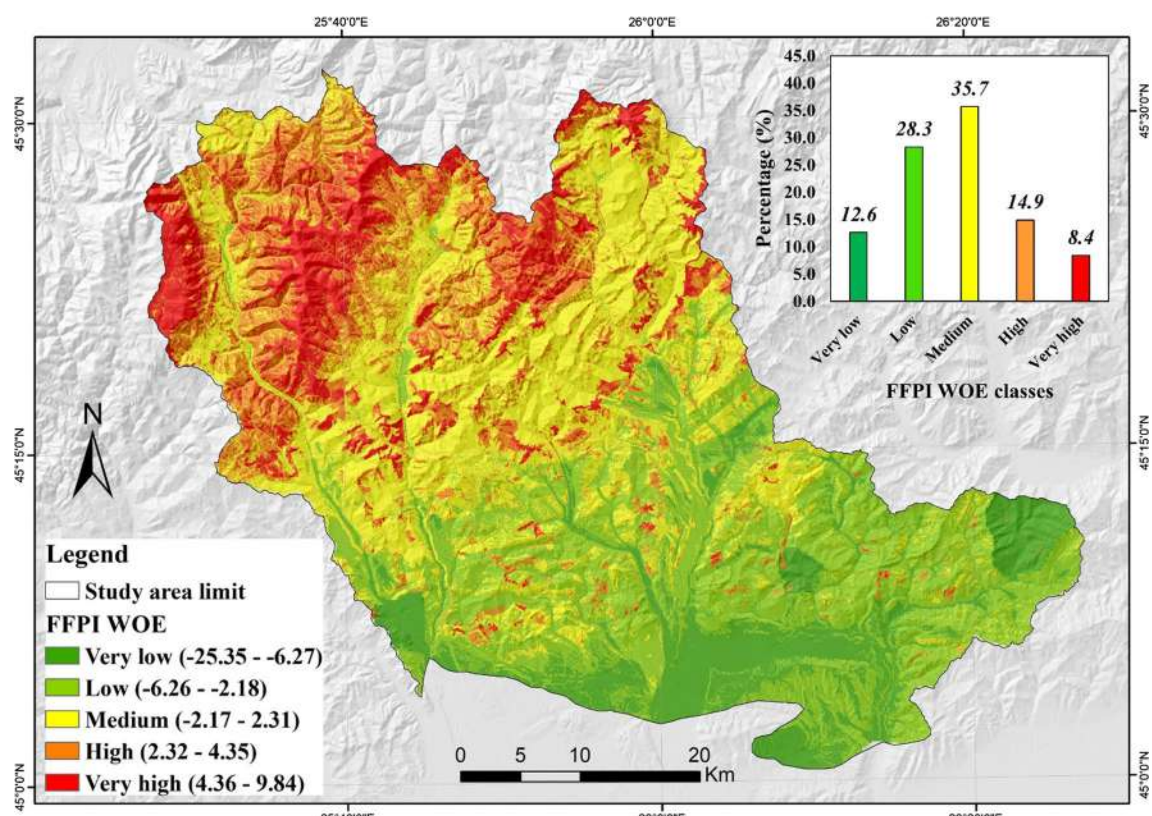

Fig. 10 FFPI values – WoE model

while the medium $FFPI_{RF}$ values are encountered on approximately 28.8% of the research zone. Over 42% of the upper and middle basin of Prahova river is characterized by high and very high values of $FFPI_{RF}$. The most compact areas with such surfaces are located in the North-Western part.

Table 2 The multicollinearity analysis for independent variables

Variables	Collinearity statistics	
	TOL	VIF
Aspect	0.93	1.03
Convergence Index	0.83	1.19
Curve number	0.97	1.02
Lithology	0.94	1.01
Slope	0.85	1.11
Plan curvature	0.87	1.14
Profile curvature	0.84	1.18
TWI	0.81	1.13
TPI	0.85	1.02
Modified Fournier Index	0.95	1.03
Contributing area	0.79	1.17
Catchment Shape Index	0.97	1.01

Table 3 The optimal parameters of models applied in the present study

Models	No. iterations	Seed	Accuracy (%)
RF	18	4	93.4
RF-WOE	16	3	92.4
LMT	18	2	92.1
LMT-WOE	19	5	92.5
ADT	19	3	93.1
ADT-WOE	17	2	92.9

By using the WOE coefficients in the training process of the *RF* model, the spatially distribution of $FFPI_{RF\text{-}WOE}$ values, across the study area, was represented. This time, the very low values are spread on around 9.4% of the total, while the low flash-flood potential covers about 20.5% of the study area. The medium $FFPI_{RF\text{-}WOE}$ values, ranging from 0.36 to 0.53, are distributed on about 29.6% of the total research area. According to the results obtained, the high and very high flash-flood susceptibility can be encountered on around 40.4% of study area. Unlike $FFPI_{RF}$, the high and very high values of $\mathrm{FFPI}_{RF\text{-}WOE}$ have a higher degree of compaction, which would increase the possibility of severe flash-floods.

4.5 Application of *ADT* stand-alone model and *ADT-WOE* hybrid model

For the *ADT* stand-alone model, the highest accuracy of 93.1% was reached after 19 iterations, while the *ADT-WOE* hybrid model achieved the highest accuracy (92.9%) after 17 iterations. The optimally pruned decision trees used in the present analysis are represented in Fig. 14a, b.

The training process of *ADT* and *ADT-WOE* models allows to estimate the weights that each flash-flood influencing factor will have in the *FFPI* calculation procedure. In this regard, the slope angle, curve number and lithology were ranked on the first places (Fig. 15).

The $FFPI_{ADT}$ values range between 0.14 and 0.86 (Fig. 16a). Further, the *Natural Breaks* method was used to group the $FFPI_{ADT}$ values into 5 classes. Very low class covers approximately 9.7% of study area, while the second class is distributed on around 19.7%. Medium values of $FFPI_{ADT}$, ranging from 0.33 to 0.46, have the largest weight among the five classes. The IVth and Vth classes are spread on around 36.7% of the total area, and characterize the surfaces with a high and very high potential for flash-flood occurrence. High and very high values of $FFPI_{ADT}$ appear uniformly in all the regions of the upper and middle basin of Prahova river.

The application of *ADT-WOE* hybrid model led to *FFPI* values ranging from 0.07 to 0.89 (Fig. 16b). A total of 34.8% of the study area is covered by very low and low $FFPI_{ADT\text{-}WOE}$ values. The largest areas (30.2%) are occupied by $FFPI_{ADT\text{-}WOE}$ values included in the medium class.

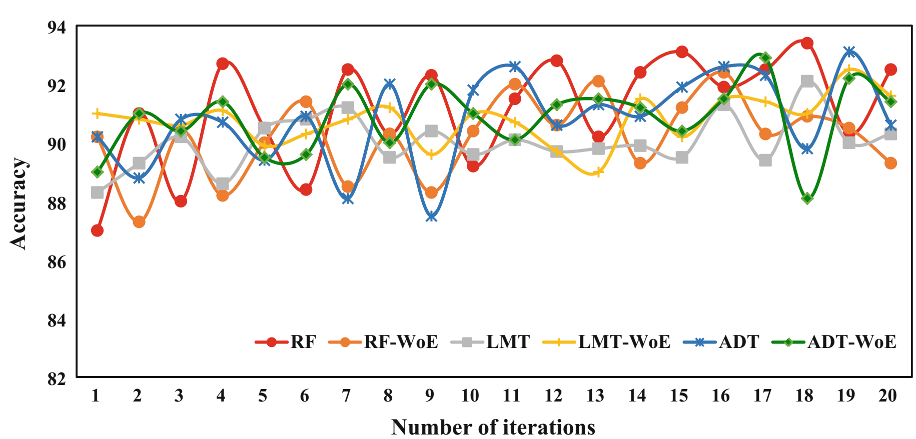

Fig. 11 Correlation between the number of iteration and models accuracy

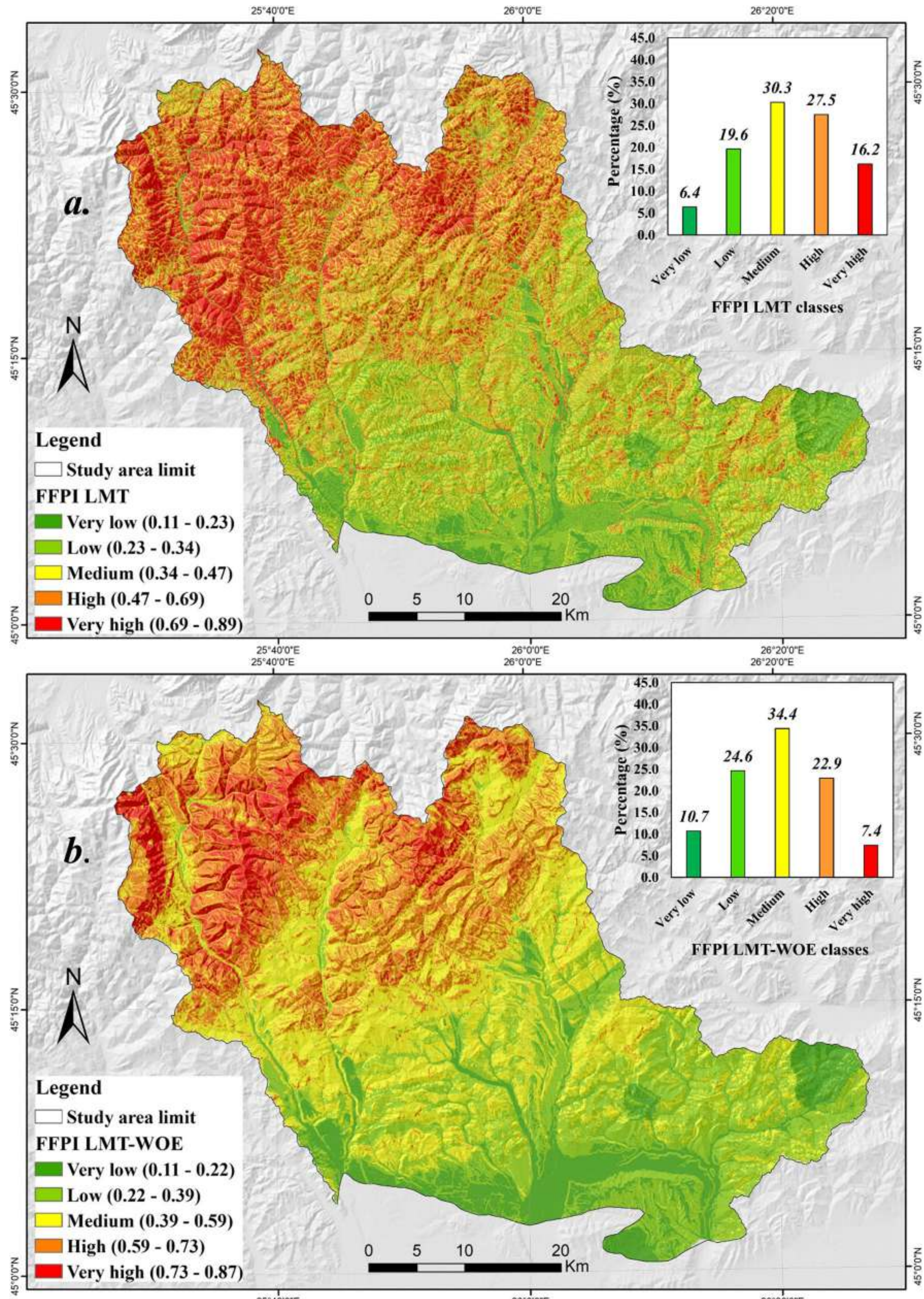

Fig. 12 FFPI values (**a**. LMT model and **b**. LMT-WOE model)

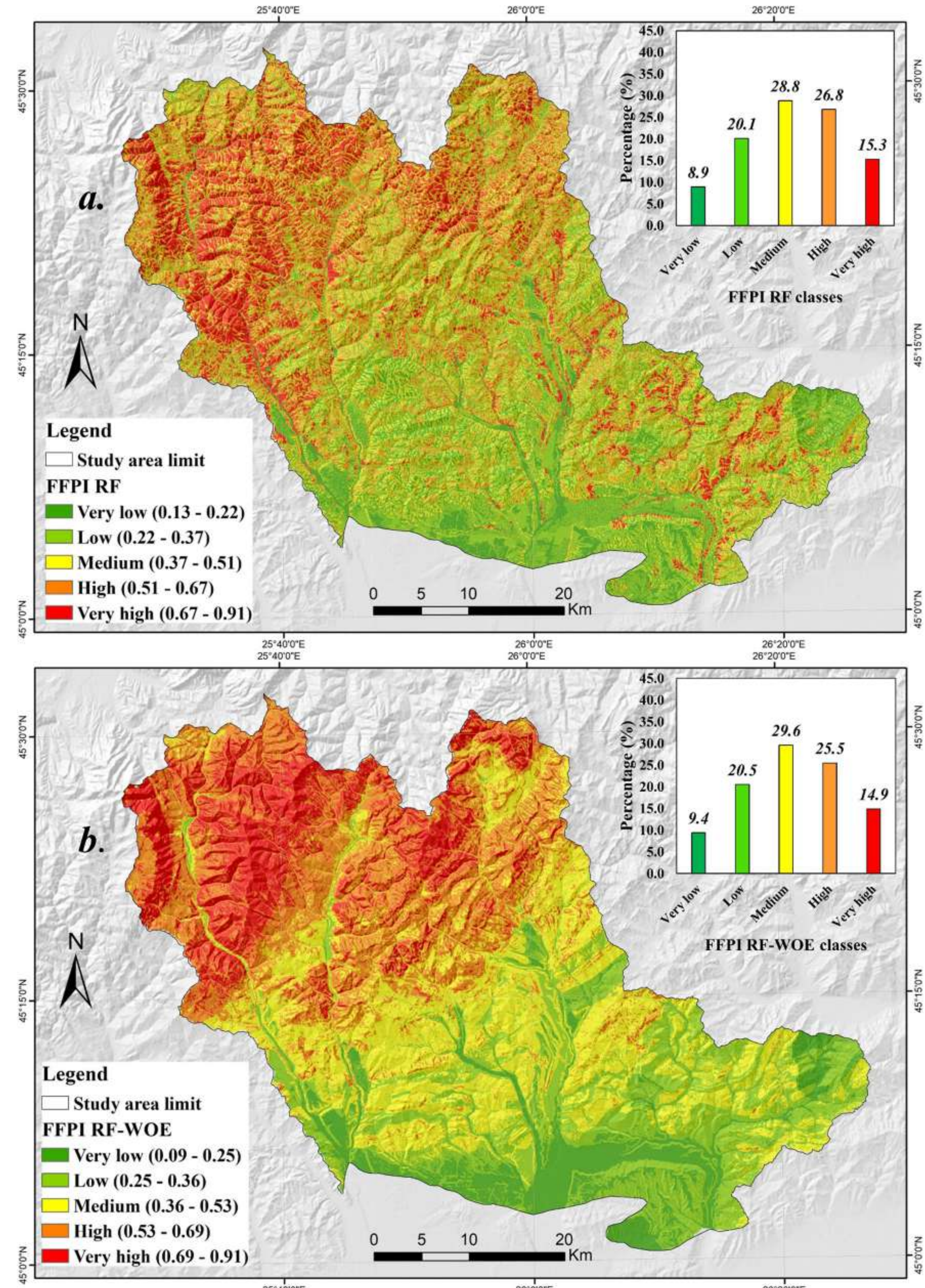

Fig. 13 FFPI values (**a**. RF model and **b**. RF-WOE model)

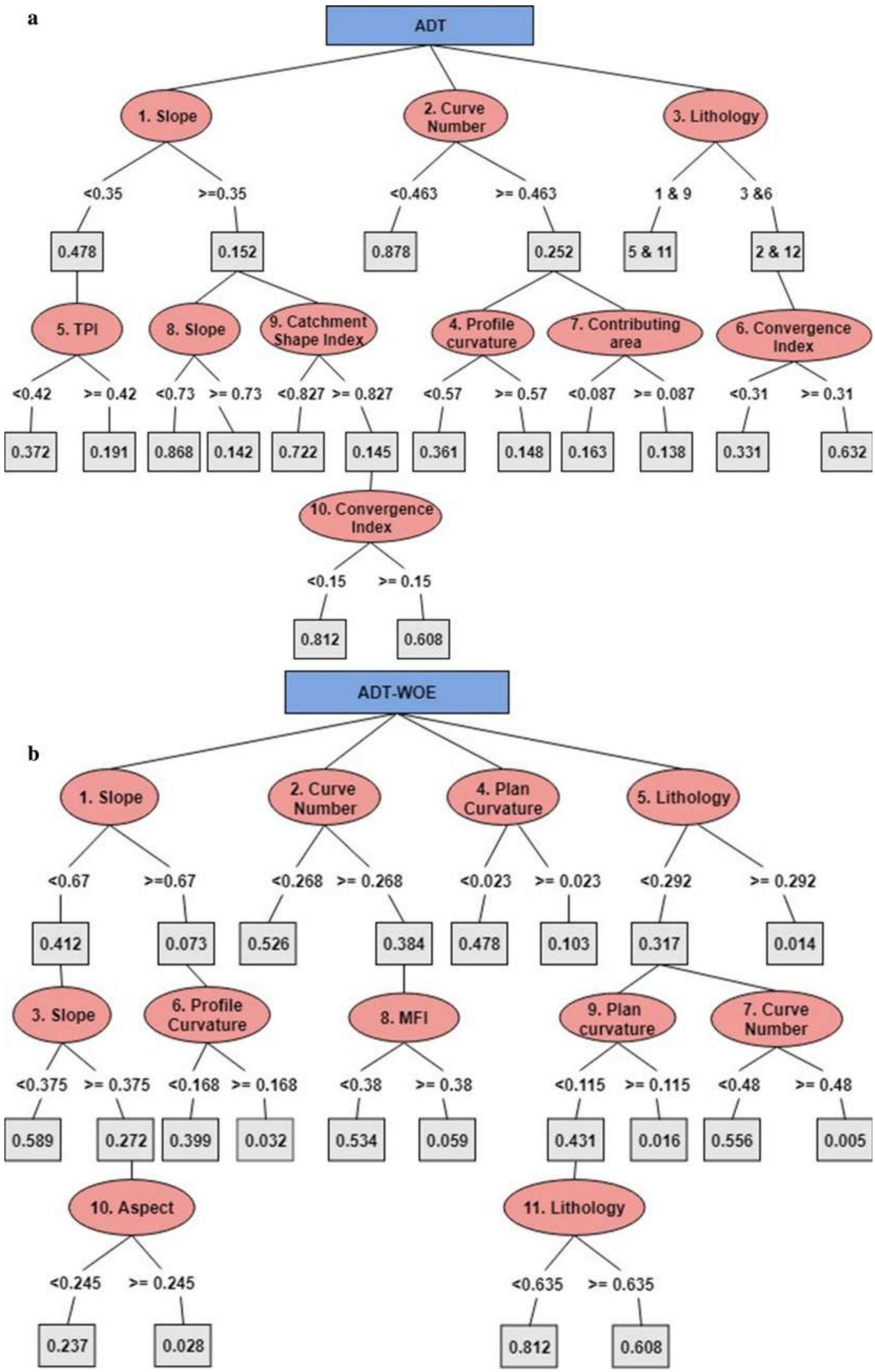

Fig. 14 The optimally pruned decision tree used in **a**. ADT model and **b**. ADT-WOE model

About 35% of the research zone has high and very high values of $FFPI_{ADT-WOE}$, these surfaces being located especially in the northern half area.

4.6 Model performance assessment and results validation

4.6.1 Density of torrential areas within FFPI classes

In terms of torrential pixels belonging to the training sample, the best performance was achieved by the *ADT-WOE* hybrid model (Fig. 17a). By applying this model, around 88.24% of the training areas are situated inside the IVth and Vth classes of $FFPI_{ADT-WOE}$. The -*ADT-WOE* hybrid model was followed by: *RF* (84%), *LMT-WOE* (82.29%), *RF-WoE* (80.82%), *LMT* (80.26%), *WOE* (79.37%), and *ADT* (72.73%). In order to demonstrate the efficiency of the application of bivariate statistics and machine learning techniques in the process of FFPI calculation, the present results were compared with those obtained by Zaharia et al. (2017) which calculated the same index on the same study area. The FFPI values derived by Zaharia et al. (2017), were calculated based on a Weighted Sum (*WS*) operation, in which the importance of each flash-flood conditioning factor was established in a subjective manner. Thus, the results obtained in the aforementioned work revealed that only 64.91% of the torrential pixels from the training sample are located inside the IVth and Vth classes of $FFPI_{WS}$.

As it was stated in the methodology section, validating areas were considered for results validation. In this regard, it can be seen that *ADT-WOE* is the best model with a percentage of 79.76% of the total torrential pixels (validating sample) included into the IVth and Vth classes of $FFPI_{ADT-WoE.}$ The order of the other models in terms of their accuracy is the following: *LMT-WOE* (76.92%), *RF* (75.51%), *LMT* (75%), *RF-WOE* (71.43%), *WOE* (69.57%) and *ADT* (68.09%) (Fig. 17b). All the 7 models performed better than $FFPI_{WS}$ (Zaharia et al. 2017) whose IVth and Vth classes include only 58.33% of the torrential pixels (validating sample).

4.6.2 ROC Curve

ROC Curve represents the second method used to evaluate the performances of the applied models and to validate the obtained results. Additionally, *Standard Error* (*S.E.*) and *95%—Confidence Interval* ($CI_{95\%}$) limits were defined (Table 4).

The training area pixels were employed in order to construct the *Success Rate* used to assess the model's performances (Fig. 18a). *Success Rate* demonstrates the capacity of the models to correctly classify the areas prone to flash-flood occurrence by comparison with training areas. The best performance was assigned to *ADT-WOE* ensemble (*AUC = 0.917*), followed by *RF* model (*AUC = 0.91*), *LMT* (*AUC = 0.909*), *LMT-WOE* model (*AUC = 0.906*), *WOE* model (*AUC = 0.903*), *RF-WOE* model (*AUC = 0.893*) and *ADT* model (*AUC = 0.889*) (Fig. 18a). It can be observed that all the 7 models applied for *FFPI* estimation in the present study perform better than the *Weighted Sum* method used by Zaharia et al. (2017), for which an AUC value of 0.745 was obtained.

The validation of the results obtained by the seven stand-alone and hybrid models, was done with the help of the *Prediction Rate*. This graphic representation, constructed through the validation areas, highlights the agreement between the observed and the predicted values of FFPI (Tehrany et al. 2015). This time also, *ADT-WoE* hybrid model was ranked first (*AUC = 0.886*), followed by *LMT-WOE* model (*AUC = 0.881*), *LMT* model (*AUC =*

Fig. 15 Flash-flood influencing factors importance

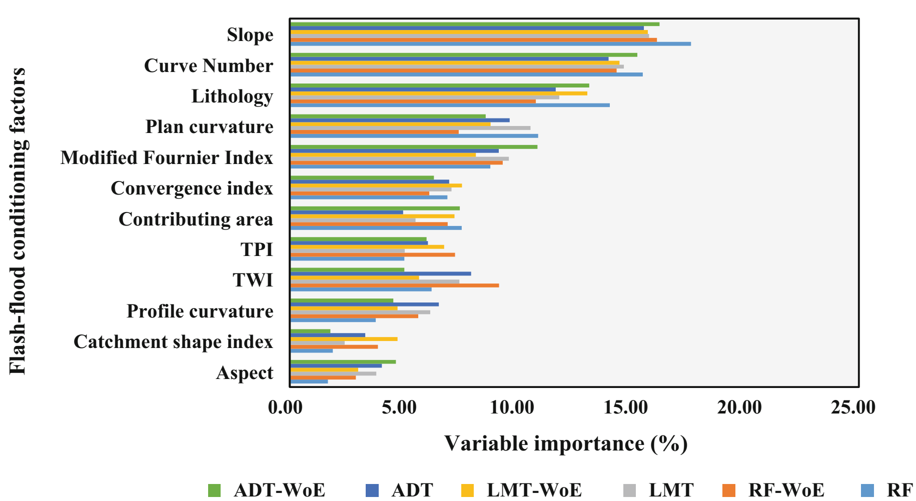

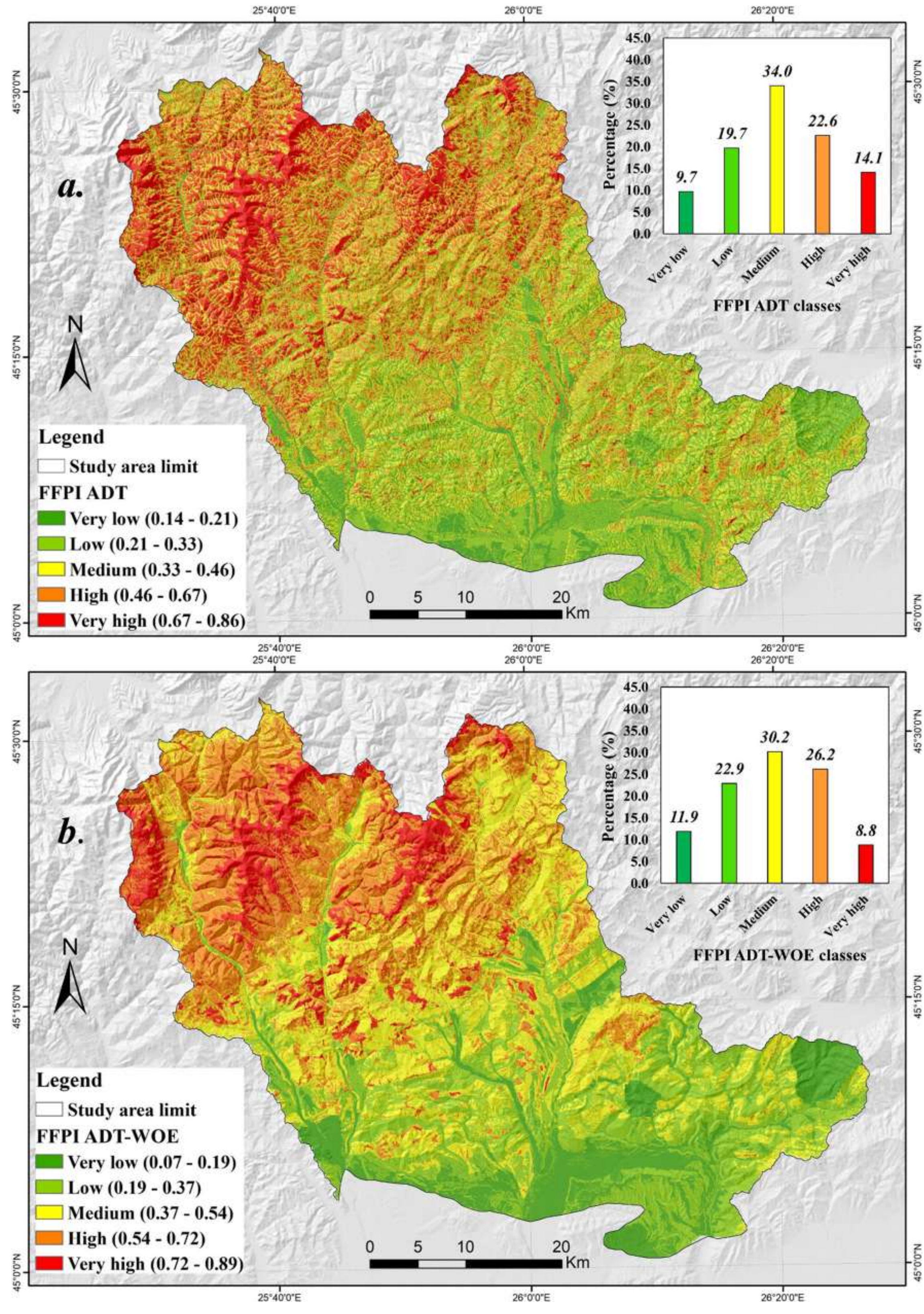

Fig. 16 FFPI values (**a**. ADT model and **b**. ADT-WOE model)

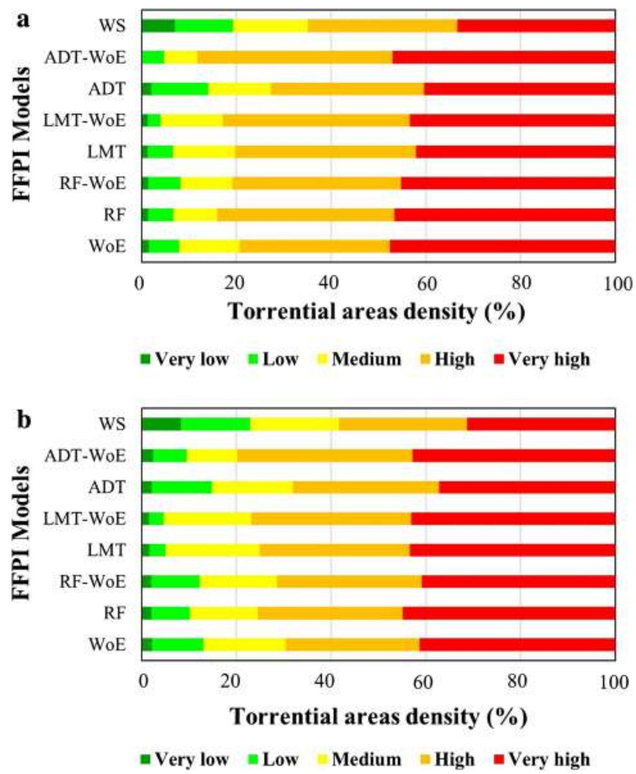

Fig. 17 Density of torrential areas within FFPI classes (**a**. Training areas; **b**. Validating areas)

0.876), *RF-WOE* model (*AUC = 0.872*), *ADT* model (*AUC = 0.863*), *WOE* model (*AUC = 0.841*), and *RF* model (*AUC = 0.825*) (Fig. 18b). Also, in this situation, all the models applied in the present analysis have higher performances than the *Weighted Sum* method (AUC = 0.711).

It should be noted that the ADT model performs better when its capabilities are combined with those specific to WOE method than in the case when it is used as a stand-alone model. Therefore, it can be assumed that, at least in

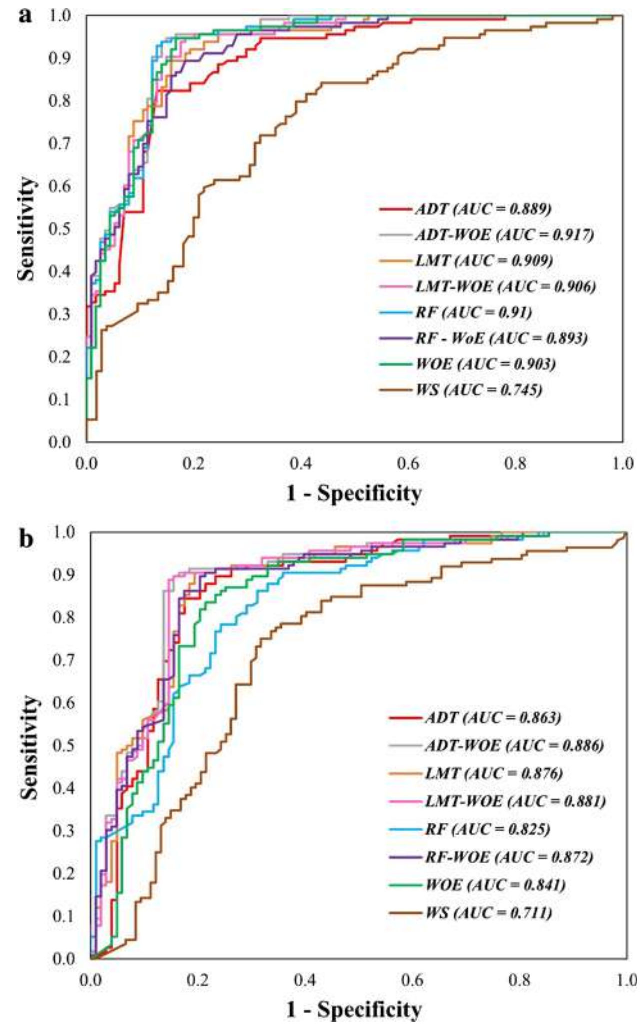

Fig. 18 ROC curves graphics (**a**. Success Rate; **b**. Prediction Rate)

the present situation, the ADT model has a higher performance when the input data is represented by the weights of evidence coefficients assigned to each class/category of flash-flood conditioning factors.

Table 4 The values of ROC Curve parameters (Standard Error and 95%—Confidence Interval)

Models	Training dataset				Valitdating dataset			
	AUC	S.E.	$CI_{95\%}$		AUC	S.E.	$CI_{95\%}$	
			Lower bound	Upper bound			Lower bound	Upper bound
FFPI ADT	0.889	0.017	0.846	0.931	0.863	0.027	0.810	0.916
FFPI ADT-WOE	0.917	0.017	0.882	0.946	0.886	0.024	0.839	0.933
FFPI LMT	0.909	0.016	0.875	0.943	0.876	0.023	0.828	0.925
FFPI LMT-WOE	0.906	0.018	0.872	0.941	0.881	0.025	0.833	0.930
FFPI RF	0.910	0.018	0.877	0.943	0.825	0.028	0.770	0.881
FFPI RF-WOE	0.893	0.022	0.856	0.929	0.872	0.025	0.823	0.921
FFPI WOE	0.903	0.017	0.869	0.937	0.841	0.029	0.785	0.897

Table 5 Statistical significance of differences between AUC values

Pair-wise comparison of AUC	Success rate			Prediction rate		
	z-value	*p*-value	Significance	z-value	*p*-value	Significance
ADT vs ADT-WOE	− 39.89	< 0 .0001	YES	− 18.26	< 0.0001	YES
ADT vs LMT	− 27.92	< 0.0001	YES	− 10.13	< 0.0001	YES
ADT vs LMT-WOE	− 23.56	< 0.0001	YES	− 14.16	< 0.0001	YES
ADT vs RF	− 29.39	< 0.0001	YES	+ 27.23	< 0.0001	YES
ADT vs RF-WOE	− 5.37	< 0.0001	YES	− 6.96	< 0.0001	YES
ADT vs WOE	− 19.26	< 0.0001	YES	+ 16.15	< 0.0001	YES
ADT-WOE vs LMT	+ 12.02	< 0.0001	YES	− 7.83	< 0.0001	YES
ADT-WOE vs LMT-WOE	+ 16.39	< 0.0001	YES	− 11.86	< 0.0001	YES
ADT-WOE vs RF	+ 10.55	< 0.0001	YES	+ 29.51	< 0.0001	YES
ADT-WOE vs RF-WOE	+ 34.54	< 0.0001	YES	− 4.66	< 0.0001	YES
ADT-WOE vs WOE	+ 20.69	< 0.0001	YES	+ 18.44	< 0.0001	YES
LMT vs LMT-WOE	+ 4.37	< 0.0001	YES	− 4.03	< 0.0001	YES
LMT vs RF	− 1.47	0.07	NO	+ 37.31	< 0.0001	YES
LMT vs RF-WOE	+ 22.56	< 0.0001	YES	+ 3.17	0.0013	YES
LMT vs WOE	+ 8.67	< 0.0001	YES	+ 26.25	< 0.0001	YES
LMT-WOE vs RF	− 5.87	< 0.0001	YES	+ 41.31	< 0.0001	YES
LMT-WOE vs RF-WOE	+ 18.19	< 0.0001	YES	+ 7.21	< 0.0001	YES
LMT-WOE vs WOE	+ 4.31	< 0.0001	YES	+ 30.27	< 0.0001	YES
RF vs RF-WOE	+ 24.03	< 0.0001	YES	− 34.16	< 0.0001	YES
RF vs WOE	+ 10.15	< 0.0001	YES	− 11.1	< 0.0001	YES
RF-WOE vs WOE	− 13.89	< 0.0001	YES	+ 23.09	< 0.0001	YES

Another remarkable aspect is that the AUC values of the 7 models are very close, with a maximum difference of 0.028 in the case of *Success Rate* and 0.061 in terms of *Prediction Rate*. Although the AUC values obtained for the 7 models are very close, it is very important to analyse whether there exists a statistically significant difference between them. The statistical significance of the difference between the AUC values related to each of the seven models was tested using the methodology proposed by Hanley and McNeil (1982). As a brief characterization, in order to estimate the statistical significance of the difference between AUC values, this method takes into consideration the following elements: the AUC values, the standard error, and the number of positive (torrential pixels) and negative (non-torrential pixels) cases used to construct the ROC Curve. The main outcomes of this method are the z statistic value and the significance level (p value). If p is less than 0.05, the difference between two compared AUC values is statistically significant (Hanley and McNeil 1982).

According to the results presented in Table 5, in terms of Success Rate, the pair-wise comparison revealed a significant difference between almost all the AUC values. Among all the 21 pair-wise comparisons, the only difference which is not significant (p = 0.07) is between LMT (AUC = 0.909) and RF (AUC = 0.91) stand-alone models. The comparisons between the values of Prediction Rate, show that all the differences between the AUC values are statistically significant, the high p-value of 0.0013 being obtained following the comparison between LMT and RF-WOE models.

5 Conclusions

Over the last period of time, there has been an exponential growth in the frequency of high-risk hydrological phenomena, such as flash-floods, having a direct effect on the increase of material damage and loss of human lives. The mitigation of the negative effects requires first of all the identification of the surfaces with a high potential for the surface runoff manifestation. Until now, the most commonly used method for determining the potential to flash-floods is represented by the *Flash-Flood Potential Index* (*FFPI*). The main goal of the present study was to calculate the *FFPI* values across the upper and middle basin of Prahova river, by combining the GIS techniques with those specific to bivariate statistics (*Weights of Evidence*) and machine learning fields (*Rotation Forest, Logistic Model Tree* and *Alternating Decision Tree*). Three hybrid models were formed by the combination of *WOE* model with each of the three decision tree-based models. In order to train the models, it was necessary to identify the areas with torrential phenomena occurred in the study area, as well as to select a number of 12 flash-flood conditioning factors, whose predictive ability was tested through the correlation-based feature selection (CFS) method. According to CFS model, slope angle recorded the highest predictive ability. The evaluation of results accuracy and models' performances was carried out by estimating the relative distribution of torrential areas within FFPI classes and by using the ROC Curve model. *ADT-WOE* hybrid model obtained the best performances for both results classification ($AUC = 0.917$) and results validation ($AUC = 0.886$). The lowest performance regarding the results classification was assigned to *ADT* stand-alone model ($AUC = 0.889$), while in terms of results accuracy *RF* stand-alone model was the weakest ($AUC = 0.825$). Nevertheless, all the models used in this study proved to be more efficient than the subjective *WS* method applied by Zaharia et al. (2017) in order to calculate the FFPI on the same study area.

All the seven models have highlighted the north-western part of the study area as the most exposed to the flash-flood occurrence. Together, high and very high *FFPI* values had total weights ranging from 23.3% (*WOE* model) to 43.7% (*LMT* stand-alone model) of the study area.

The main novelty of the present study consists of the use of three hybrid models and the consideration of the areas affected in the past by torrentiality for FFPI calculation.

The results of this study can be used in the activity of flash-flood forecasting which take place within the National Institute of Hydrology and Water Management of Romania. The present analysis can be also used by the local authorities in order to prevent the construction of new buildings in the areas prone to flash-floods phenomena. Also, the high performance that characterises all the models employed in FFPI computation recommends the use of these methods and the flash-flood influencing factors on other areas for which the assessment of flash-flood susceptibility should be done. The way in which each flash-flood conditioning factor was classified, and at least the weights of the most important flash-flood conditioning factors may represent a benchmark for studies carried out within other catchments including those outside of Romania.

Acknowledgements The author would like to thank the two anonymous reviewers of the Stochastic Environmental Research and Risk Assessment journal, for their critical and valuable comments that helped to improve the article. This study was financially supported by the Research Institute of the University of Bucharest.

References

Agterberg FP (1992) Combining indicator patterns in weights of evidence modeling for resource evaluation. Nat Res Res 1(1):39–50

Alkhasawneh MS, Ngah UK, Tay LT, Isa M, Ashidi N, Al-batah MS (2013) Determination of important topographic factors for landslide mapping analysis using MLP network. Sci World J 2013:1–12. https://doi.org/10.1155/2013/415023

Althuwaynee OF, Pradhan B, Park HJ, Lee JH (2014) A novel ensemble bivariate statistical evidential belief function with knowledge-based analytical hierarchy process and multivariate statistical logistic regression for landslide susceptibility mapping. Catena 114:21–36

Arnoldus HM (1980) An approximation of the rainfall factor in the universal soil loss equation. In: de Boodts M, Gabriels D (eds) Assessments of erosion. Wiley, Chichester, pp 127–132

Arrighi C, Rossi L, Trasforini E, Rudari R, Ferraris L, Brugioni M, Castelli F (2018) Quantification of Flood risk mitigation benefits: a building-scale damage assessment through the RASOR platform. J Environ Manag 207:92–104

Bathrellos GD, Karymbalis E, Skilodimou HD, Gaki-Papanastassiou K, Baltas EA (2016) Urban flood hazard assessment in the basin of Athens Metropolitan city, Greece. Environ Earth Sci 75(4):319

Bui DT, Ho TC, Revhaug I, Pradhan B, Nguyen DB (2013) Landslide susceptibility mapping along the national road 32 of Vietnam using GIS-based J48 decision tree classifier and its ensembles. In: Cartography from pole to pole: selected contributions to the XXVIth internationalconference of the ICA. Springer, Dresden, p 303

Bui DT, Tuan TA, Klempe H, Pradhan B, Revhaug I (2016) Spatial prediction models for shallow landslide hazards: a comparative assessment of the efficacy of support vector machines, artificial neural networks, kernel logistic regression, and logistic model tree. Landslides 13(2):361–378

Cao C, Xu P, Wang Y, Chen J, Zheng L, Niu C (2016) Flash flood hazard susceptibility mapping using frequency ratio and statistical index methods in coalmine subsidence areas. Sustainability 8(9):948

Chapi K, Singh VP, Shirzadi A, Shahabi H, Bui DT, Pham BT, Khosravi K (2017) A novel hybrid artificial intelligence approach for flood susceptibility assessment. Environ Model Softw 95:229–245

Chen W, Xie X, Wang J, Pradhan B, Hong H, Bui DT, Ma J (2017a) A comparative study of logistic model tree, random forest, and classification and regression tree models for spatial prediction of landslide susceptibility. Catena 151:147–160

Chen W, Shirzadi A, Shahabi H, Ahmad BB, Zhang S, Hong H, Zhang N (2017b) A novel hybrid artificial intelligence approach based on the rotation forest ensemble and naïve Bayes tree classifiers for a landslide susceptibility assessment in Langao County, China. Geomat Nat Hazards Risk 8(2):1955–1977

Chen W, Pourghasemi HR, Zhao Z (2017c) A GIS-based comparative study of Dempster-Shafer, logistic regression and artificial neural network models for landslide susceptibility mapping. Geocarto Int 32(4):367–385

Chen W, Yan X, Zhao Z, Hong H, Bui DT, Pradhan B (2018) Spatial prediction of landslide susceptibility using data mining-based kernel logistic regression, naive Bayes and RBFNetwork models for the Long County area (China). Bull Eng Geol Environ 78:1–20

Conforti M, Pascale S, Robustelli G, Sdao F (2014) Evaluation of prediction capability of the artificial neural networks for mapping landslide susceptibility in the Turbolo River catchment (northern Calabria, Italy). Catena 113:236–250

Costache R (2014) Using GIS techniques for assessing lag time and concentration time in small river basins. Case study: Pecineaga river basin, Romania. Geogr Techn 9(1):31–38

Costache R, Zaharia L (2017) Flash-flood potential assessment and mapping by integrating the weights-of-evidence and frequency ratio statistical methods in GIS environment–case study: BâscaChiojdului River catchment (Romania). J Earth Syst Sci 126(4):59

Demir G, Aytekin M, Akgun A (2015) Landslide susceptibility mapping by frequency ratio and logistic regression methods: an example from Niksar-Resadiye (Tokat, Turkey). Arab J Geosci 8(3):1801–1812

Diakakis M, Deligiannakis G, Pallikarakis A, Skordoulis M (2016) Factors controlling the spatial distribution of flash flooding in the complex environment of a metropolitan urban area. The case of Athens 2013 flash flood event. Int J Disaster Risk Reduct 18:171–180

Ding Q, Chen W, Hong H (2017) Application of frequency ratio, weights of evidence and evidential belief function models in landslide susceptibility mapping. Geocarto Int 32(6):619–639

Dou J, Yamagishi H, Pourghasemi HR, Yunus AP, Song X, Xu Y, Zhu Z (2015) An integrated artificial neural network model for the landslide susceptibility assessment of Osado Island, Japan. Nat Hazards 78(3):1749–1776

Dou J, Yamagishi H, Zhu Z, Yunus AP, Chen CW (2018) TXT-tool 1.081-6.1 A comparative study of the binary logistic regression (BLR) and artificial neural network (ANN) models for GIS-based spatial predicting landslides at a regional scale. In Sassa K et al (eds) Landslide dynamics: ISDR-ICL landslide interactive teaching tools. Springer, Cham, pp 139–151. https://doi.org/10.1007/978-3-319-57774-6_10

Douvinet J, Van De Wiel MJ, Delahaye D, Cossart E (2015) A flash flood hazard assessment in dry valleys (northern France) by cellular automata modelling. Nat Hazards 75(3):2905–2929

Eristi H, Demir Y (2012) The feature selection based power quality event classification using wavelet transform and logistic model tree. PrzeglądElektrotechniczny 88(7a):43–48

Georgakakos KP (2006) Analytical results for operational flash flood guidance. J Hydrol 317(1–2):81–103

Glas H, Jonckheere M, Mandal A, James-Williamson S, De Maeyer P, Deruyter G (2017) A GIS-based tool for flood damage assessment and delineation of a methodology for future risk assessment: case study for Annotto Bay, Jamaica. Nat Hazards 88(3):1867–1891

Goetz JN, Brenning A, Petschko H, Leopold P (2015) Evaluating machine learning and statistical prediction techniques for landslide susceptibility modeling. Comput Geosci 81:1–11

Hall MA (1999) Correlation-based feature selection for machine learning. Deptartment of Computer Science, Doctoral dissertation, University of Waikato

Hanger S, Linnerooth-Bayer J, Surminski S, Nenciu-Posner C, Lorant A, Ionescu R, Patt A (2018) Insurance, public assistance, and household flood risk reduction: a comparative study of Austria, England, and Romania. Risk Anal 38(4):680–693

Hanley JA, McNeil BJ (1982) The meaning and use of the area under a receiver operating characteristic (ROC) curve. Radiology 143(1):29–36

Hong H, Pradhan B, Xu C, Bui DT (2015) Spatial prediction of landslide hazard at the Yihuang area (China) using two-class kernel logistic regression, alternating decision tree and support vector machines. Catena 133:266–281

Hong H, Liu J, Zhu AX, Shahabi H, Pham BT, Chen W, Bui DT (2017) A novel hybrid integration model using support vector machines and random subspace for weather-triggered landslide susceptibility assessment in the Wuning area (China). Environ Earth Sci 76(19):652

Hong H, Liu J, Bui DT, Pradhan B, Acharya TD, Pham BT, Ahmad BB (2018a) Landslide susceptibility mapping using J48 decision tree with adaboost, bagging and rotation forest ensembles in the Guangchang area (China). Catena 163:399–413

Hong H, Tsangaratos P, Ilia I, Liu J, Zhu AX, Chen W (2018b) Application of fuzzy weight of evidence and data mining techniques in construction of flood susceptibility map of Poyang County, China. Sci Total Environ 625:575–588

Jenness JS (2000) The effects of fire on Mexican spotted Owls in Arizona and New Mexico. MSc thesis. Northern Arizona University, p 137

Kavzoglu T, Sahin EK, Colkesen I (2014) Landslide susceptibility mapping using GIS-based multi-criteria decision analysis, support vector machines, and logistic regression. Landslides 11(3):425–439

Kayastha P, Dhital MR, De Smedt F (2012) Landslide susceptibility mapping using the weight of evidence method in the Tinau watershed, Nepal. Nat hazards 63(2):479–498

Kazakis N, Kougias I, Patsialis T (2015) Assessment of flood hazard areas at a regional scale using an index-based approach and analytical hierarchy process: application in Rhodope-Evros region, Greece. Sci Total Environ 538:555–563

Khosravi K, Nohani E, Maroufinia E, Pourghasemi HR (2016) A GIS-based flood susceptibility assessment and its mapping in Iran: a comparison between frequency ratio and weights-of-evidence bivariate statistical models with multi-criteria decision-making technique. Nat Hazards 83(2):947–987

Khosravi K, Pham BT, Chapi K, Shirzadi A, Shahabi H, Revhaug I, Bui DT (2018) A comparative assessment of decision trees algorithms for flash flood susceptibility modeling at Haraz watershed, northern Iran. Sci Total Environ 627:744–755

Kourgialas NN, Karatzas GP (2011) Flood management and a GIS modelling method to assess flood-hazard areas—a case study. Hydrol Sci J-J des Sci Hydrol 56(2):212–225

Kruzdlo R, Ceru J (2010) Flash Flood Potential Index for WFO Mount Holly/Philadelphia. In: Eastern region flash flood conference, poster session, NOAA's National Weather Service, pp 2–4)

Landwehr N, Hall M, Frank E (2005) Logistic model trees. Machine learning 59(1–2):161–205

Lee S (2005) Application of logistic regression model and its validation for landslide susceptibility mapping using GIS and remote sensing data. Int J Remote Sens 26(7):1477–1491

Liu KY, Lin J, Zhou X, Wong ST (2005) Boosting alternating decision trees modeling of disease trait information. In: BMC genetics, vol 6(1). BioMed Central, p S132

Lombardo L, Cama M, Conoscenti C, Märker M, Rotigliano E (2015) Binary logistic regression versus stochastic gradient boosted decision trees in assessing landslide susceptibility for multiple-occurring landslide events: application to the 2009 storm event in Messina (Sicily, southern Italy). Nat Hazards 79(3):1621–1648

Musy A, Higy C (2010) Hydrology: a science of nature. CRC Press, Boca Raton

Ozcift A, Gulten A (2011) Classifier ensemble construction with rotation forest to improve medical diagnosis performance of machine learning algorithms. Comput Methods Programs Biomed 104(3):443–451

Ozturk U, Wendi D, Crisologo I, Riemer A, Agarwal A, Vogel K, Korup O (2018) Rare flash floods and debris flows in southern Germany. Sci Total Environ 626:941–952

Pham BT, Bui DT, Prakash I, Dholakia MB (2016a) Rotation forest fuzzy rule-based classifier ensemble for spatial prediction of landslides using GIS. Nat Hazards 83(1):97–127

Pham BT, Bui D, Prakash I, Dholakia M (2016b) Evaluation of predictive ability of support vector machines and naive Bayes trees methods for spatial prediction of landslides in Uttarakhand state (India) using GIS. J Geomat 10:71–79

Pham BT, Bui DT, Dholakia MB, Prakash I, Pham HV, Mehmood K, Le HQ (2017a) A novel ensemble classifier of rotation forest and Naïve Bayer for landslide susceptibility assessment at the Luc Yen district, Yen Bai Province (Viet Nam) using GIS. Geomat Nat Hazards Risk 8(2):649–671

Pham BT, Bui DT, Prakash I (2017b) Landslide susceptibility assessment using bagging ensemble based alternating decision trees, logistic regression and J48 decision trees methods: a comparative study. Geotech Geol Eng 35(6):2597–2611

Pradhan B, Youssef AM (2011) A 100-year maximum flood susceptibility mapping using integrated hydrological and hydrodynamic models: Kelantan River Corridor, Malaysia. J Flood Risk Manag 4(3):189–202

Rahmati O, Pourghasemi HR (2017) Identification of critical flood prone areas in data-scarce and ungauged regions: a comparison of three data mining models. Water Resour Manag 31(5):1473–1487

Regmi AD, Devkota KC, Yoshida K, Pradhan B, Pourghasemi HR, Kumamoto T, Akgun A (2014) Application of frequency ratio, statistical index, and weights-of-evidence models and their comparison in landslide susceptibility mapping in Central Nepal Himalaya. Arab J Geosci 7(2):725–742

Rodriguez JJ, Kuncheva LI, Alonso CJ (2006) Rotation forest: a new classifier ensemble method. IEEE Trans Pattern Anal Mach Intell 28(10):1619–1630

Romanescu G, Mihu-Pintilie A, Stoleriu CC, Carboni D, Paveluc LE, Cimpianu CI (2018) A comparative analysis of exceptional flood events in the context of heavy rains in the summer of 2010: Siret Basin (NE Romania) Case Study. Water 10(2):216

Ryu J, Jung Y, Kong DS, Park BK, Kim YS, Engel BA, Lim KJ (2016) Approach of land cover based asymptotic curve number regression equation to estimate runoff. Irrig Drain 65:94–104

Saharia M, Kirstetter PE, Vergara H, Gourley JJ, Hong Y, Giroud M (2017) Mapping flash flood severity in the United States. J Hydrometeorol 18(2):397–411

Samela C, Albano R, Sole A, Manfreda S (2018) A GIS tool for cost-effective delineation of flood-prone areas. Comput Environ Urban Syst 70:43–52

ShafapourTehrany M, Shabani F, NeamahJebur M, Hong H, Chen W, Xie X (2017) GIS-based spatial prediction of flood prone areas using standalone frequency ratio, logistic regression, weight of evidence and their ensemble techniques. Geomat Nat Hazards Risk 8(2):1538–1561

Shirzadi A, Bui DT, Pham BT, Solaimani K, Chapi K, Kavian A, Revhaug I (2017) Shallow landslide susceptibility assessment using a novel hybrid intelligence approach. Environ Earth Sci 76(2):60

Siahkamari S, Haghizadeh A, Zeinivand H, Tahmasebipour N, Rahmati O (2018) Spatial prediction of flood-susceptible areas using frequency ratio and maximum entropy models. Geocarto Int 33(9):927–941

Smith G (2003) Flash flood potential: determining the hydrologic response of ffmp basins to heavy rain by analyzing their physiographic characteristics. A white paper available from the NWS Colorado Basin River Forecast Center web site at http://www.cbrfc.noaa.gov/papers/ffp_wpap.pdf

Tehrany MS, Lee MJ, Pradhan B, Jebur MN, Lee S (2014) Flood susceptibility mapping using integrated bivariate and multivariate statistical models. Environ Earth Sci 72(10):4001–4015

Tehrany MS, Pradhan B, Jebur MN (2015) Flood susceptibility analysis and its verification using a novel ensemble support vector machine and frequency ratio method. Stoch Environ Res Risk Assess 29(4):1149–1165

Tsangaratos P, Ilia I (2016) Landslide susceptibility mapping using a modified decision tree classifier in the Xanthi Perfection, Greece. Landslides 13(2):305–320

Vaezi AR, Zarrinabadi E, Auerswald K (2017) Interaction of land use, slope gradient and rain sequence on runoff and soil loss from weakly aggregated semi-arid soils. Soil Tillage Res 172:22–31

Van Westen CJ (2002) Use of weights of evidence modeling for landslide susceptibility mapping. International Institute for Geoinformation Science and Earth Observation: Enschede, The Netherlands

Van Westen CJ, Rengers N, Soeters R (2003) Use of geomorphological information in indirect landslide assessment. Nat Hazards 30(3):399–419

Wang LJ, Guo M, Sawada K, Lin J, Zhang J (2016) A comparative study of landslide susceptibility maps using logistic regression, frequency ratio, decision tree, weights of evidence and artificial neural network. Geosci J 20(1):117–136

Wu S, Yu M, Chen L (2017) Nonmonotonic and spatial-temporal dynamic slope effects on soil erosion during rainfall-runoff processes. Water Resour Res 53(2):1369–1389

Yesilnacar E, Topal T (2005) Landslide susceptibility mapping: a comparison of logistic regression and neural networks methods in a medium scale study, Hendek region (Turkey). Eng Geol 79(3–4):251–266

Youssef AM, Al-Kathery M, Pradhan B (2015) Landslide susceptibility mapping at AlHasher area, Jizan (Saudi Arabia) using GIS-based frequency ratio and index of entropy models. Geosci J 19(1):113–134

Youssef AM, Pradhan B, Sefry SA (2016) Flash flood susceptibility assessment in Jeddah city (Kingdom of Saudi Arabia) using bivariate and multivariate statistical models. Environ Earth Sci 75(1):12

Zaharia L, Costache R, Prăvălie R, Minea G (2015) Assessment and mapping of flood potential in the Slănic catchment in Romania. J Earth Syst Sci 124(6):1311–1324

Zaharia L, Costache R, Prăvălie R, Ioana-Toroimac G (2017) Mapping flood and flooding potential indices: a methodological approach to identifying areas susceptible to flood and flooding risk. Case study: the Prahova catchment (Romania). Front Earth Sci 11(2):229–247